PIERS 2010 Cambridge

Progress In Electromagnetics Research Symposium

Abstracts

July 5–8, 2010
Cambridge, USA

www.emacademy.org
www.piers.org

PIERS 2010 Cambridge Abstracts

Published by

The Electromagnetics Academy
777 Concord Avenue, Suite 207
Cambridge, MA 02138

www.emacademy.org
www.piers.org

ISSN: 1559-9450
ISBN: 978-1-934142-13-4

Progress In Electromagnetics Research Symposium

July 5–8, 2010

Cambridge, USA

PIERS 2010 CAMBRIDGE ORGANIZATION

PIERS Founding Chair

J. A. Kong, MIT, USA

PIERS Chair

L. Tsang, University of Washington, USA

PIERS 2010 Cambridge General Chair and Co-Chair

T. Habashy, Schlumberger-Doll Research, Cambridge, Massachusetts, USA

A. Abubakar, Schlumberger-Doll Research, Cambridge, Massachusetts, USA

PIERS 2010 Cambridge Technical Chairs

A. Abubakar, Schlumberger-Doll Research, Cambridge, Massachusetts, USA

T. Habashy, Schlumberger-Doll Research, Cambridge, Massachusetts, USA

PIERS 2010 Cambridge Organizing Committee Chair

B.-I. Wu, MIT, Cambridge, Massachusetts, USA

PIERS 2010 Cambridge International Advisory Committee

S. Barmada
L. C. Botten
J. Brady
C.-H. Chan
W.-C. Chew
C-K. Chou
H.-T. Chuah
S.-T. Chun
N. Engheta
A. K. Fung
Z.-H. Gu
L. Gurel
M. Hallikainen
Y. Hara
H.-C. Huang
A. Ishimaru
E. Jakeman
K. Kobayashi
L.-W. Li
I. V. Lindell
S.-G. Liu
K.-M. Luk
S. Mano
G. D. McNeal
K. K. Mei
Y. Miyazaki
P. Pampaloni
A. Priou
K. Senne
R. Shin
E. Slob
M. Tateiba
P. van den Berg
D. Watts
K. Yasumoto
W.-X. Zhang

PIERS 2010 Cambridge Technical Program Committee

S. J. Anderson
A. Baghai-Wadji
G. Berginc
W. M. Boerner
H. Braunisch
C.-T. Chan
H. W. Chang
H.-S. Chen
K.-S. Chen
Y.-H. Chen
T.-J. Cui
V. Druskin
Y. Du
A. Elsherbeni
H. T. Ewe
H. C. Fernandes
J. Goswami
S. He
W. Hong
Y.-Q. Jin
M. Li
L. Liang
J. Liu
Q.-H. Liu
S. Lucyszyn
J. T. Lue
R. Mackie
A. Massa
E. L. Miller
M. Moghaddam
Z.-P. Nie
Y. Okuno
D. Omeragic
M. Oristaglio
G. Pan
J. Pribetich
R. Ramer
L.-X. Ran
C. M. Rappaport
A. K. Sarychev
C. Seo
X.-Q. Sheng
Y. V. Shestopalov
J.-C. Shi
A. Sihvola
S. Tjuatja
M.-S. Tong
D. P. Tsai
J. Vrba
B.-I. Wu
C. J. Wu
M. Y. Xia
G. Xie
T. S. Yeo
M. Zaslavsky
X.-M. Zhang
J. Zhou

PIERS 2010 Cambridge Organizing Committee

A. Abubakar
R. H. Ding
Q. Jiang
J. G. Liu
M. Zaslavsky
X. Chang
I. Ehrenberg
S. Lee
G. D. Pan
B. J. Zhang
Y.-H. Chen
T. Habashy
M. K. Li
B. I. Wu
B. L. Zhang
K.-H. Ding
S. Y. Huang
L. Liang
X. L. Xu

PIERS 2010 CAMBRIDGE SESSION ORGANIZERS

A. Abubakar
H. T. Chuah
R. Doebbelin
S. Foteinopoulou
E. O. Kamenetskii
J. Lettl
R. Mackie
M. Moghaddam
M. Oristaglio
V. Ramos
G. Shvets
J. Vrba
T.-J. Yang
S. Zvanovec
H. Braunisch
B. K. Chung
V. L. Druskin
E. Gescheidtová
K. Kobayashi
J. Li
P. Marin
J. Ojeda-Castañeda
F. Papoff
P. Rocca
R. Suaya
C.-J. Wu
M. Zaslavsky
B. D. F. Casse
G. Cohen
M. D'Urso
T. M. Habashy
R. V. Kohn
M. Li
A. R. McGurn
G. Oliveri
K. Radhakrishnan
A. D. Rosen
V. Subramanian
G. Xie
H. Zhang
X. Chen
L. Daniel
X. Ferrieres
J. T. Johnson
S.-C. Kong
X. Lu
P. M. Meaney
D. Omeragic
R. Ramer
Y. V. Shestopalov
A. J. Terzuoli
S. J. Xu
I. Zhang

PIERS 2010 CAMBRIDGE SPONSORS

- ☐ Schlumberger-Doll Research (SDR)
- ☐ MIT Center for Electromagnetic Theory and Applications/Research Laboratory of Electronics
- ☐ The Electromagnetics Academy at Zhejiang University
- ☐ Zhejiang University
- ☐ The Electromagnetics Academy

PIERS 2010 SESSIONS

Session 1A1
Electromagnetic Modeling, Inversion and Applications 1

Electromagnetic and Economic Security Cloak

Jianhua Li[1], **Feng Xie**[1], **Qian Hao**[1], **Lee Xie**[1], **Ganquan Xie**[1], **and Xianwei Zhou**[2]

[1]GL Geophysical Laboratory, USA
[2]University of Science and Technology in Beijing, China

Abstract— In this paper, we propose a economic electromagnetic GL double layer ECEM cloak to protect market, bank and economic system. A global economic and local economic relationship and develop approaching process is constructed by GL EM EC inversion. The inner ECEM cloak prevents the inner economic information can not leak to out. The outer ECEM cloak prevent exterior economic to interfere the local economic concealment in which some market and bank are staying safety. The GL double layer EMEC cloak can control the inner-outer information exchange. The GL double layer ECEM cloak system will be designed by software and hardware.

Rapid Bounds on Electrostatic Energies Using Diagonal Approximations of Boundary-integral Equations

J. P. Bardhan
Rush University Medical Center, USA

Abstract— Electrostatic interactions between molecules in solution are often studied using macroscopic continuum models, particularly linear models. Such studies typically treat the molecules as regions of homogeneous low permittivity and the solvent as a region of different permittivity. One approach to calculate these electrostatic energies is a boundary-integral equation long known in many communities. The numerical solution of boundary-integral equations (or, for that matter, of the PDE form of the problem) is of course a numerically challenging problem, which has motivated the development of faster, approximate methods. In this contribution I will describe one such method, called BIBEE (for boundary-integral based electrostatics estimation). The BIBEE method has focused on the somewhat curious result that two diagonal approximations to the boundary-integral operator give (under circumstances suitable to molecular systems) easily proved upper and lower bounds for the electrostatic energy of the system. Even more surprisingly, BIBEE preserves to an excellent degree the eigenstructure of what is called the reaction-potential matrix (the i, j entry of the matrix being the reaction potential induced at point i by a charge at point j due to polarization of the solvent region). Thus, in essence this represents a fast method for approximating the Green's function of the system in question. The BIBEE method is a novel result in molecular electrostatics, but it seems implausible that the basic idea is new to the general electromagnetics community. I hope that the PIERS audience can offer their expertise to help shed light on numerous open questions regarding the approximation's properties.

When PML Isn't P: The Failure of Perfectly Matched Layers

Po-Ru Loh, **Ardavan F. Oskooi**, **Mihai Ibanescu**, **Maksim Skorobogatiy**, **Lei Zhang**, **Yehuda Avniel**, **and Steven G. Johnson**
Massachusetts Institute of Technology, Cambridge, MA 02139, USA

Abstract— Although perfectly matched layers (PMLs) have been widely used to truncate numerical simulations of electromagetism and other wave equations, we point out an important case in which any PML approach inevitably causes exponential growth rather than decay of fields. Specifically, we consider the case of backward-wave guided modes (with opposite phase and group velocity) that arise in certain non-index-guided waveguides, especially those using

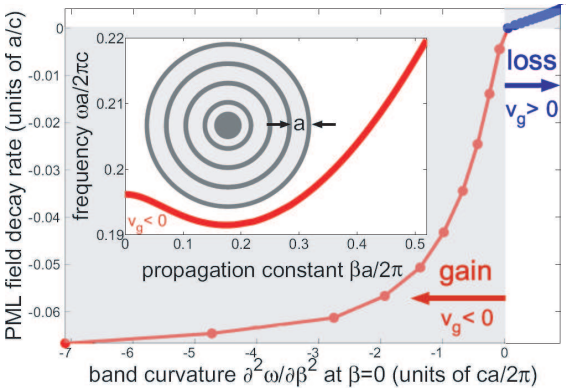

Figure 1: Field decay rate within the PML vs. curvature of the dispersion relation at $\beta = 0$, showing onset of gain for $v_g < 0$ and loss for $v_g > 0$. *Inset.* Dispersion relation (of the first TE band) with $v_g < 0$ region at $\beta = 0$, and cross-section of the Bragg fiber.

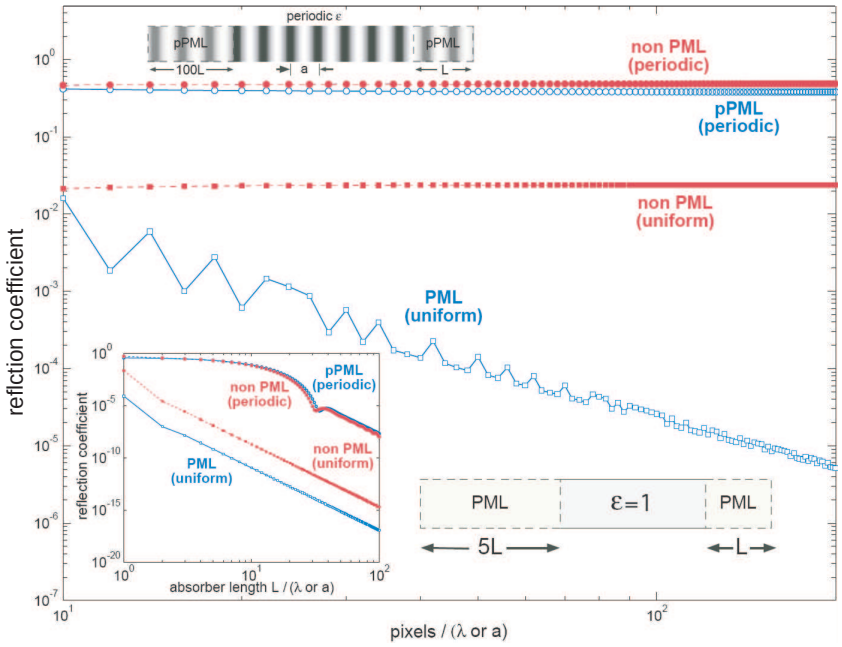

Figure 2: Reflection coefficient as a function of discretization resolution for both a uniform medium and a periodic medium with PML and non-PML absorbing boundaries (insets). For the periodic medium, PML fails to be reflectionless even in the limit of high resolution, and does no better than a non-PML absorber. Inset: reflection as a function of absorber thickness L for fixed resolution $\sim 50\text{pixels}/\lambda$: as the absorber becomes thicker and the absorption is turned on more gradually, reflection goes to zero via the adiabatic theorem; PML for the uniform medium only improves the constant factor.

metals or photonic crystals. We show that PML acts as a gain medium for backward-wave modes in constant cross-section waveguides, leading to field divergence in the PML regions [1]. This exponential growth can be seen from the complex coordinate-stretching view of PML, but we also explain this behavior on the physical grounds of PML being an (artificial) anisotropic absorber: backward waves have mostly longitudinal fields, hence see gain. More precisely, we identify a simple yet little-known relation between group and phase velocity and the orientation of the electromagnetic field:

$$v_g = v_p(f_t - f_z),$$

where f_t and f_z are the fractions of the electromagnetic (EM) field energy in the transverse (xy) and longitudindal (z) directions, respectively. Applying this relation and first-order perturbation theory to PML, we find that introducing a low-strength PML leads to an additional time-dependent exponential factor with rate constant proportional to $-v_p/v_g$, which in particular is positive — implying gain — for backward-wave modes.

The case of backward waves is not unique in causing complete and irrecoverable failure of PML; in fact, PML also fails to be reflectionless — even in the limit of infinite resolution — in structures such as photonic crystals where the material is not analytic in the direction perpendicular to the boundary. However, any absorber, turned on slowly enough, is asymptotically reflectionless, providing a fallback when PML fails — and also explaining why published claims of e.g., "photonic crystal PML" have appeared to work. Indeed, for adiabatic absorbers, the asymptotic scaling relationship between reflectivity and absorber length is determined by the smoothness of turn-on of the absorber [2].

REFERENCES

1. Loh, P.-R., A. F. Oskooi, M. Ibanescu, M. Skorobogatiy, and S. G. Johnson, "A fundamental relation between phase and group velocity, and application to failure of PML in backward-wave structures," *Physical Review E*, Vol. 79, 065601, 2009.
2. Oskooi, A. F., L. Zhang, Y. Avniel, and S. G. Johnson, "The failure of perfectly matched layers, and towards their redemption by adiabatic absorbers," *Optics Express*, Vol. 16, 11376–11392, 2008.

ISAR Simulations of Complex Objects and Verification with Measurements at TUBITAK MRC

Uğur Saynak[1], **Alper Çolak**[1], **Harun Cetinkaya**[2], **Mustafa Tekbas**[2], **I. Hakki Tayyar**[1, 3], **Deniz Bölükbas**[1], **Caner Ozdemir**[1, 4], **and Alexey Vertiy**[2]

[1]Information Technologies Institute (ITI), TÜBİTAK MRC, Gebze, Kocaeli, Turkey
[2]Material Institute, International Laboratory for High Technology (ILHT)
TUBITAK-MRC, Gebze, Kocaeli, Turkey
[3]GYTE, Dept. of Electronics Engineering, Gebze, Kocaeli
[4]Mersin University, Dept. of Electrical-Electronics Engineering, Mersin, Turkey

Abstract— Two-dimensional (2-D) inverse synthetic aperture radar (ISAR) imaging is a powerful tool in analyzing the scattering from targets such that it can be used for identification and classification of different objects [1]. Recently, there has been an increasing interest for ISAR research in Marmara Research Center of Scientific and Technological Research Council of Turkey (TUBITAK-MRC). A 2-D ISAR imaging algorithm has been developed to provide the ISAR image of any target in a simulation environment The required electromagnetic field scattering are calculated by a Shooting and Bouncing Ray based code that can also estimate and add the diffracted field contributions for the selected target.

In this paper, the validation of the ISAR imaging algorithm together with the EM simulator are demonstrated by measurements conducted at TUBITAK-MRC facilities We have designed ISAR experimental setup with 100 GHz anechoic chamber. All measurements have been supplied by Sub THz vector network analyzer (ELMIKA S4403). The mm wave band set up used for ISAR study is presented and the millimeter wave measuring capabilities and limitations are given in detail. For validation, the F-16 type scaled model has been selected as the target with the maximum dimension of 26 cm. The 2-D ISAR measurements have been performed at the center frequency of 90 GHz. The comparison of the simulated ISAR image of the CAD model of the target and the measured ISAR image of the scaled model provides a good match.

REFERENCES

1. Bhalla, R. and H. Ling, *IEEE Trans. Antennas Propagat.*, Vol. 44, No. 11, 1445, 1996.

Investigating Energetic and Impedance Relations of Microwave Transmission Line Filled with Dielectric Material

Attila Gollei, A. Magyar, and M. Gerzson
Department of Electrical Engineering and Information Systems, Faculty of Information Technology
University of Pannonia, Hungary

Abstract— During microwave treatment, microwave energy is transferred to a material sample placed in an applicator of given geometric parameters. As a result of the energy transfer, the sample absorbs energy from the microwave space depending on its dielectric properties. The degree of energy absorption is directly proportional to the dielectric loss and proportional to the square root of the dielectric constant. The temperature of the sample continuously increases due to the energy transfer and its dielectric properties also change with the rising temperature. For the microwave generator the transmission line acts as an impedance terminator whose value depends on the wavelength and on the geometric properties of the transmission line. The impedance of transmission line also depends on the dielectric properties of the material which are either partially or fully filling the transmission line. Since the temperature of the sample changes due to the energy impact, the value of the impedance terminator represented by parameters the transmission line also changes together with the sample properties. During the energy impact the varying dielectric properties of the sample change the axial distribution of the microwave energy in the transmission line, therefore the amount of energy absorbed in the sample also changes. To avoid this case, the automatic tuning mechanism changes the position of the shortcut at the end of the transmission line so that the field intensity be always maximal in the sample. The tuning mechanism manipulates the position in accordance with the changing dielectric properties of the sample. The changes in the dielectric properties of the sample and the position of the shortcut change the impedance of the microwave transmission line at the given wavelength as well. The change of the impedance terminator has an influence on the reflection factor of the transmission line, which makes an effect on the standing wave ratio developed in the transmission line. The developed standing wave ratio determines the amount of microwave energy which enters the transmission line, i.e. the way impedance of the transmission line is matched to that of supplying generator.

Although the microwave energy supply is constant, time and temperature dependent energy impedance and dielectric relations are developed. A part of them is measurable e.g., the temperature, the position of the shortcut and axial distribution of the microwave energy measured by microwave detectors placed at the suitable position along the waveguide. The other part of them not be directly measured, they can only be computed from the previously measured ones. In a closed model which contains the parameters of the sample and the waveguide, the continuously chancing parameters can be determined in relation of the temperature. These parameters are as fallows: attenuation of the transmission line, temporal change of the sample temperature, dielectric properties of the sample, loss factor of the sample, penetration depth, impedance of the transmission line, standing wave ratio reflection factor. The above parameters can be modeled as a function of sample temperature or as a function of time.

Electromagnetic Field Analysis in Permanent Magnet Retarder Based on Finite Element Method

L. Z. Ye, **D. S. Li**, **B. F. Jiao**, **and Y. Z. Wang**
School of Mechanical Engineering and Applied Electronics Technology
Beijing University of Technology, China

Abstract— Eddy current retarder for vehicle generates a large number of heats when it works continuously, and it leads to serious decline in braking torque. This paper proposes a novel permanent magnet retarder (PMR) for vehicle, whose cooling system is connecting with engine cooling-water. A 3-dimensional finite element model is developed to model the electromagnetic behavior of permanent magnet retarder under constant speed operation. Magnetic field and eddy current field in PMR are numerically solved by finite element method. By accounting for non-linear permeability of rotor and weaken effect in magnetic field generated by eddy current magnetic field, the calculation accuracy of air-gap magnetic field and retarder brake torque are enhanced. Experiment shows that temperature of retarder is below 150°C, and the braking torque keep hard characteristic curve. The calculated air-gap magnetic flux density is fairly good agreement with measured one.

Simulation of 3D Laser Imaging

Gerard Berginc and Michel Jouffroy
THALES, 2 avenue Gay Lussac, 78995 Elancourt Cedex, France

Abstract— This paper addresses modeling of new optical non-conventional imaging with laser systems. The availability of near infrared lasers and near infrared focal plane arrays can make laser systems practical and cost efficient. The eye-safe property of wavelengths around 1.5 µm is perfectly suited to laser imagery applications. Laser systems provide high-resolution day and night imaging. These systems have several distinct technological and practical advantages over thermal imaging systems making them attractive alternatives, or at the very least, complementary components to existing infrared imaging technology. An interesting feature of laser imagery is the capability to provide depth position of a target with respect to the background. Optical non-conventional imaging explores the advantages of laser imaging to form a three-dimensional image of the scene. 3D laser imaging can be used for three-dimensional medical imaging, topography, surveillance, robotic vision because of ability to detect and recognize objects hidden behind porous occluders, such as foliage or camouflage. In this paper, we present the 3D laser imaging simulation of a large scale scene. For the inversion method, we use a cone-beam algorithm, which is a convolution-backprojection algorithm deduced from the Radon transform. The first step of the simulation process is the generation of a scene of interest which consists of many types of objects: buildings, trees, vehicles. The vehicles are often obscured by other objects. A CAD model of the scene is generated. The second step contains the simulation of the receiver, the transmitter and the optics system. For the receiver, we simulate the response of the different types of detectors we can use: detection and false alarm probabilities, detector response function, noise sources. The blurring caused by the optics of the system is simulated. The third step is the modeling of the electromagnetic scattering from the different objects of the scene. The physics based model, we present in this paper, is designed to provide accurate results but to also include all of the electromagnetic interaction mechanisms. The surfaces of the different vehicles or hard targets are considered as randomly rough surfaces and we compute the laser signature (laser cross-section) of the vehicles. To model the laser interaction with the randomly rough surfaces, we use the second-order Small-Slope Approximation method. Because the problem, we consider in this paper, is three-dimensional, all the scattering coefficients (coherent and incoherent components of the electromagnetic field) are functions of the azimuth angles, and the cross-polarized terms do not vanish. We define, in this case, the Mueller matrix, which gives all the combinations of the polarization states of the scattered electromagnetic waves. The randomly rough surfaces of the complex object are characterized by electromagnetic parameters (permittivity...) and roughness parameters (standard deviation of rough surface height and autocorrelation function). Our model addresses also transparent structures. Buildings and trees are modeled by polarized reflectance applied to the different facets generated by the CAD model. The fourth step contains the absorption and scattering of the laser wave by the components of the atmosphere, the simulation of the atmospheric turbulence effects: scintillation, beam spreading, beam wandering. The last step of the simulation contains the development of three-dimensional reconstruction algorithm to obtain a high-resolved three-dimensional image. This computer model can help predict 3D imaging performance and it is used to develop reconstruction algorithms. We also give comparison between experimental data and simulation of 3D laser images.

Studying the Effects of Wind Farms on a Terrain to the Scattered Field by Utilizing the ISAR Concept

Deniz Bölükbas[1], **Uğur Saynak**[1], **Alper Çolak**[1], **I. Hakki Tayyar**[1, 2], **and Caner Özdemir**[1, 3]

[1]Information Technologies Institute (ITI), TÜBITAK MRC, Gebze, Kocaeli, Turkey
[2]Department of Electronics Engineering, GYTE, Gebze, Kocaeli, Turkey
[3]Department of Electrical-Electronics Engineering, Mersin University, Mersin, Turkey

Abstract— There has been a growing public and private sector interest on Wind Turbines (WTs) for generating electrical power. Beside the many advantages of wind energy, the WTs have their own drawbacks that must be taken into account. First, the turbines are physically large structures, typically 70 meters in height or more. Therefore, they are in the coverage of the radar even at long ranges in most cases. Furthermore, the WTs have rotating blades whose direction and the rotation speed are dependent on the wind direction and power, respectively. It is clear that the rotating large blades will generate the Doppler Effect such that the radar echo appears as a moving target on the radar operator's screen. In addition, a large number of WTs are generally constructed on a very limited field in most wind farms; therefore, the adverse impacts to the radar echo become even much worse.

There are a number of works in the literature that study the analysis the impacts of WT on radar parameters [1] including radar cross section (RCS) analysis from a WT. However, it is clear that such an analysis will not be adequate to understand the full scattering phenomena from a wind farm that have many WTs. Moreover, the strong electromagnetic interaction between the terrain and the other WTs must be taken into account as well.

In this paper, the RCS value of the WT is simulated and presented depending on the material of the blades and the tower, if they are metal, concrete, fiberglass or RAM coated. The two dimensional (2-D) inverse synthetic aperture radar (ISAR) images of a wind farm are formed with 5 WTs. A terrain data adopted from a Digital Terrain Elevation Data (DTED) map and used in the analysis. The polarization effects of the incident field are observed clearly at the scattered field. To analyze the effects of the terrain, different terrain specifications are used such as soil, sea or concrete. All 2-D ISAR images are constructed by the help of a Shooting and Bouncing Ray based simulator [2] that can scattered and diffracted fields from complex bodies at high frequencies.

REFERENCES

1. Kent, B. M., K. C. Hill, A. Buterbaugh, G. Zelinski, R. Hawley, L. Cravens, C. Vogel, and T. Coveyou, "Dynamic radar cross section and radar doppler measurements of commercial general electric windmill power turbines, Part 1: Predicted and measured radar signatures," *IEEE Trans. Antennas Propag.*, Vol. 50, No. 2, 211–219, 2008.
2. Saynak, U., et al., *Electromagnetic Wave Scattering Conference 2008*, 127, Antalya, Turkey, 2008.

FDTD Analysis in a PCB Stripline Structure

E. Y. S. Lutif[1], **M. R. F. Gontijo**[1], **A. J. F. Orlando**[1], **and A. C. C. Migliano**[1, 2]

[1]Aerospace Technological Institute (ITA), CTA, Brazil
[2]Advanced Study Institute (IEAv), CTA, Brazil

Abstract— An FDTD analyses is reported in changes in the permittivity and permeability and also in the dimensions in a PCB stripline structure of stripline-dielectric-ground plane as the dielectric thickness are fixed and these distributions of electromagnetic waves are described graphically. Extensive computation is performed in the spectral domain and the sample shows sensitivity in the work area in the PCB stripline structure. An electromagnetic wave is formatted of the type TEM $12.0 \times 0.64\,\mathrm{mm}^2$. The derivation of ε_r and μ_r as a function of S_{11} and S_{21} is included, as well a practical design for a stripline sample holder.

The exact knowledge of material permittivity ε^* and permeability μ^* is essential in the study of physical phenomena which govern interactions between electromagnetic waves and matter. The accurate electromagnetic analysis of discontinuities in a stripline device, used for the broad band measurement of complex permittivity and permeability of materials, is presented.

In this paper, we will first describe the electromagnetic analysis of the stripline treated by the FDTD software approach then we will focus our attention on the study of the cell discontinuities based on the transmission line methods. We will analyses two w/h relations 0.86 and 1.3 and two materials permittivity. The sample shows two works areas between 5.7 GHz–6.7 GHz for the relation $w/h = 0.86$ and 6.7 GHz–7.4 GHz for the relation $w/h = 1.3$ for air permittivity. The work area increased for the relation $w/h = 1.3$ when we use the dielectric material with permittivity 3. In particular, there were resonant-like peaks at 13–15 GHz in both permittivity analyzed.

A General Method for FDTD Modeling of Scattering by Isotropic and Anisotropic Frequency-dispersive Media

Bing Wei, **De-Biao Ge**, **Fei Wang**, **and Yuqiang Zhang**
Department of Physics, Xi'dian University, Xi'an 710071, China

Abstract— The finite difference time-domain (FDTD) method has been widely used in electromagnetic numerical algorithm due to its excellent characteristics such as ability to deal with non-uniform, dispersive and anisotropic media. Some algorithms in FDTD such as RC-FDTD, DI-FDTD, JEC-FDTD and ADE-FDTD etc. dedicating to dispersive media, including isotropic and anisotropic, were developed. A disadvantage of the inhere algorithms is the requirement of deducing formulations in particular for different kind of dispersion model. Furthermore, it is difficult to deal with a magnetized plasma/ferrite problem while an external dc magnetic field of arbitrary direction exerted because of both the dispersiveness and anisotropy.

In 2002, Ge etc. introduced the shift operator FDTD (SO-FDTD) method to deal with the non-magnetized plasma problem [1]. It is found now that the SO-FDTD can be extended to treat the EM problem for different kind of dispersion model in a unified form for both isotropic and anisotropic dispersive media that is of practical interest in programming. In this paper, we first prove that the complex permittivity in three kinds of dispersive model, i.e., Debye, Lorentz and Drude model, can be described by a rational polynomial fraction in $j\omega$. By replacing $j\omega$ by the partial derivative operator $\partial/\partial t$ we may obtain the constitutive equation relating D and E in time domain. A shift operator z_t is then introduced to deduce the constitutive equation in discretised time domain and the formulation for D and E available for FDTD computation is derived. For magnetized plasma/ferrite, it is figured out that the elements of the relative permittivity/permeability tensor can also be formulated by a rational polynomial fraction in $j\omega$. By the same manner the SO-FDTD is used to the analyses of EM problem of magnetized plasma/ferrite subject to an external dc magnetic field with arbitrary direction. The extended SO-FDTD proposed is of conciseness in deduction and generality in treatment of a variety of dispersive media. In addition a digital filtering technique in DSP is applied to reduce the computer storage requirement in SO-FDTD programming.

The proposed SO-FDTD is exemplified by the scattering of non-magnetized and magnetized plasma/ferrite and a PEC object covered with plasma, demonstrating the feasibility of presented scheme.

ACKNOWLEDGMENT

Project supported by the National Natural Science Foundation of China (Grant No. 60871071).

REFERENCES

1. *Chinese Journal of Radio Science*, Vol. 18, No. 4, 359–362, Aug. 2003.

Magnetic Field Distribution of a Novel Variable Inductor Based on Orthogonal Magnetization

Zhengrong Jiang[1], **Zhengxi Li**[1], **and Jianye Chen**[2]

[1]Department of Electrical & Mechanical Engineering, North China University of Technology Beijing 100144, China

[2]Department of Electrical Engineering, Tsinghua University, Beijing 100084, China

Abstract— A computation method for the magnetic field distribution of a novel variable inductor based on orthogonal magnetization is presented. The inductor includes two windings, one is an ac winding for exciting ac field, another is a dc winding for creating dc bias field, the latter is perpendicular to the former. The vector combination results in a semi-rotating field in the core and make the hysteresis "shearing". This feature makes the variable inductor safely and have linearly characteristic in case application on HVDC. The effect on material magnetic characteristic caused by orthogonal bias field is explained and the field distribution is computed, the calculated results are consistent with the experimental data well.

Session 1A2
Remote Sensing and Polarimetry, SAR, GPR, Imaging

Polarimetric UHF Calibration for SETHI

H. Oriot[1], **C. Coulombeix**[1], **and P. Dubois-Fernandez**[2]

[1]ONERA, Chemin de la Hunière, F-91761 Palaiseau cedex, France
[2]ONERA, Base aérienne 701, 13661 Salon AIR, France

Abstract— The SETHI sensor from ONERA is an airborne radar equipped with different bands (UHF-VHF, L, X) on a Falcon 20. The UHF-VHF band is fully polarimetric and can operate between 225 MHz up to 460 MHz. In August 2009, this system was used in French Guiana for the TROPISAR experiment. This experiment was conducted to provide ESA and CNES with measurements of temporal coherence at P- and L-band over tropical forests for time intervals compatible with spaceborne missions (typically 20–30 days). In this paper we present the methodology used to calibrate the UHF data.

Data were acquired from 20° incidence angle up to 65° incidence angle and a swath of about 4500 m. The UHF antenna is located under the left wing of the Falcon 20. For this experiment, it was pointing with an incident angle of 45°. The antenna pattern being quite large, this configuration induced a secondary reflection of the incident wave with the wing leading to an antenna pattern deformation (in intensity, phase and frequency). Therefore, the calibration procedure was performed in two steps: Crosstalk estimation and removal, antenna pattern estimation and compensation.

The crosstalk estimation was based on the Quegan's algorithm. The crosstalk parameters vary with both range and frequency. As a consequence, the Quegan's estimation procedure was adapted and the crosstalk removed. A study of the Quegan parameters also showed that the parameters were depending on the aircraft attitude. The data acquisition geometry was shown to be responsible for this behavior and after the necessary geometric correction step, this dependency was removed so that the crosstalk parameters could be estimated once for all images.

Then, the antenna pattern compensation was performed using known corner refelctors that had been placed along the swath on a calibration area.

Finally calibrated images are shown and evaluated.

Towards a Polarimetric SAR Processor for Airborne Sensor

H. M. J. Cantalloube[1], B. Fromentin-Denoziere[1], and C. E. Nahum[2]

[1]ONERA (Office National d'Études et Recherches Aérospatiales), Palaiseau, France
[2]DGA (Direction Génŕale pour l'Armement), Bagneux, France

Abstract— ONERA recently added an UHF/VHF (222 to 470 MHz) component to its airborne SAR system Sethi (the replacement of the former RAMSES system). The antenna is made of two dipole pairs (for polarimetric measurements) with a cylindrical reflector on a pod suspended under the aircraft wing. Due to the proximity of the wing and the long wavelength, the antenna pattern is highly distorted from that of the naked antenna. Furthermore, as we wish azimuth resolutions similar to attainable range resolution (60 cm), a wide integration angle (around 30 degrees) is required.

Finite element modelling of the antenna with the surrounding aircraft with the program ELSEM3D allowed to compute the far field radiation of the antenna in its operating position. Simulations showed that the "center of phase" approximation does not hold to the accuracy required by SAR processing, hence the phase variation with squint during integration must be corrected for (in a similar manner to motion compensation). They also showed that the radiated waves from each of the two antenna feeds could not be approximated as a linear polarised light with axis in the direction of the excited antenna axis.

Previously, polarimetric images were computed by computing 16 single look complex images (combined later into the 4 polarimetric single look complex images). Each image is computed for one transmit and one receive antenna ports and during the azimuth integration, its signal was multiplied by the cosinus or sinus of the angle between the antenna axes and the terrain vertical. This angle varies during integration due to both attitude fluctuations and motion nonlinearities of the aircraft trajectory. Due to the difficulty of including this time-varying factor in the frequency domain processor, this polarimetric processing was done in time domain (2-stage factored, but still slow compared to frequency domain processing).

We shall here describe advances in frequency domain SAR processing that allows to include such a time-varying polarimetric factor in the azimuth integration and describe how we can convert the measures with two non orthogonal elliptically polarised channel (at a given point in the azimuth integration) into two vertical and horizontal (with respect to the terrain) linear polarised component in a computationally efficient way in a SAR processor (both time-domain and frequency-domain types).

With such a SAR processor and with the system calibrating procedure derived from Sarabandi approach but including antenna axis motion during integration (described in 2005 at PoInSAR) it will be possible to compute airborne SAR images that really measure polarimetric responses along vertical and horizontal axis with respect to the terrain, and not contaminated by polarmetric axes (and ellipticity) fluctuation during integration.

We should the assert the interest of this approch by comparing images obtained by direct use of the 4 polarimeric signal, images obtained by the earlier axis rotation technique and the images obtained by a taking into account the antenna off-axis depolarizing.

Polarimetric SAR Image Classification Using Radial Basis Function Neural Network

Turker Ince
Izmir University of Economics, Izmir, Turkey

Abstract— This paper presents a robust radial basis function (RBF) network based classifier for polarimetric synthetic aperture radar (SAR) images. The proposed feature extraction process utilizes the covariance matrix, the gray level co-occurrence matrix (GLCM) based texture features, and the backscattering power (SPAN) combined with the $H/\alpha/A$ decomposition, which are projected onto a lower dimensional feature space using principal component analysis. For the pattern recognition unit, an RBF network is employed, and for the classifier training two popular techniques are explored: conventional backpropagation (BP) and particle swarm optimization (PSO). Recently, neural network based approaches for classification of polarimetric SAR data have been shown to outperform other well-known techniques including Wishart maximum likelihood and wavelet-based methods. In this study, the RBF neural network classifier is chosen due to their superior performance with simpler network architectures and robustness to noise and outliers. By using both polarimetric covariance matrix and decomposition based pixel values and textural information (contrast, correlation, energy, and homogeneity) in the feature set, classification accuracy is improved. An experimental study is performed using the fully polarimetric San Francisco Bay and Flevoland data sets acquired by the NASA/Jet Propulsion Laboratory Airborne SAR (AIRSAR) at L-band to evaluate the performance of the proposed method. The results demonstrate that the RBF network classifier trained by the global PSO algorithm achieves superior classification results while maintaining robustness and efficiency.

A Radar Scattering and Analysis Model for Time-series InSAR (T-SAR)

Howard Zebker and Piyush Shanker Agram
Depts. of Geophysics and Electrical Engineering, Stanford University, USA

Abstract— InSAR measurements of Earth topography, displacement, and volume structure are now commonly used for static descriptions of surface geophysical properties. Over the past 20 years the community has developed many capabilities to exploit single interferograms for the above and other applications. The repeating nature of orbital geometries for spaceborne radars permits the next logical step in InSAR capability — extending the measurement modality from three dimensions to four, and presenting the temporal variability of surface change. Here we present a radar scattering model supporting two existing time series techniques, persistent scattering (PS) and small baseline subset analysis (SBAS). We begin with a model for the probability that a given pixel is persistent over time and InSAR baseline, which gives us the PS spatial density, and relate this to the spatial sampling needed to represent geophysical processes. The multiple persistent scatter and SBAS implementations in use today all use different algorithms to identify and connect the stable scattering pixels and areas over time, so each must be modeled by a slightly different system architecture. Yet the basic probability density functions are common to each, so we derive a generic system model that can be suitably altered to accommodate a given specific algorithm and implementation. Our goal here is a model accurately describing the scattering process over time and resulting radar performance based on system parameters, and orbital and imaging geometries. This allows us to properly choose between the several radar systems now in use for a given application, and perhaps more importantly, design new spaceborne systems to enable specific studies and uses. We present several data sets collected by the various instruments in orbit today, and find that the accuracy of the radar image time series varies from several mm to cm in radar line-of-sight measurements. Finally, we examine several possible designs for the proposed NASA DESDynI mission and tabulate the expected level of performance for various surface conditions.

A Fully Polarimetric Borehole Radar Based Numerical Modeling: Fully Polarimetric Response to Synthetic Natural Fractures

J. G. Zhao[1, 2] and M. Sato[3]

[1]State Keylab of Petroleum Resource & Prospecting
China University of Petroleum, Beijing, China
[2]Keylab of Geophysical Prospecting, CNPC, China
[3]Center for Northeast Asian Studies, Tohoku University, Japan

Abstract— A fully polarimetric borehole radar system with four combinations of dipole and cylindrical slot antennas was developed to acquire fully polarimetric data sets in drilled boreholes. The system in conjunction with a methodology of radar polarimetry analysis, proposed in previous research, has proved to be a potential tool for physical characterization and classification of subsurface fractures.

Despite of such progress, current polarimetric research on subsurface targets like fractures is restricted to qualitative analysis. This motivates us to explore more quantitative approaches to characterize the fractures in real world environmental engineering projects by using fully polarimetric borehole radar signal properties. To achieve this goal, in this work, we utilize a procedure of computer numerical modeling to systematically investigate fully polarimetric radar response to fractures with different conditions. First, synthetic fractures with different roughness are generated on a computer via fractal theory based simulation techniques. Quantitative assessment for the roughness of synthetic fractures is possible by use of three main parameters: the fractal dimension, the rms roughness at a reference length, and a length scale describing the degree of mismatch between the two fracture surfaces, allowing future detailed study of mechanical and transport properties of fractures and fully polarimetric radar response on them. Next, a 3D subgrid FDTD numerical simulation is used to synthesize both constant-offset and multiple-offset fully polarimetric data sets with synthetic fractures as primary reflectors. Based on the synthetic data sets, it is possible to relatively quantitatively evaluate the applicability of different radar polarimetry analysis approaches to physical characterization of subsurface fractures.

We conclude that synthetic fully polarimetric data sets through computer forward modeling allows us to quantitatively investigate polarimetric scattering mechanism from synthetic natural subsurface fractures with known roughness parameters. The simulation research is conducive to practical field data processing and interpretation.

Flaw Detection in a Concrete Medium Using Acoustic Synthetic Aperture Imaging Technique

A. Ganguli[1], **D. Abramo**[1], **S. Wadia-Fascetti**[1], **and C. Rappaport**[2]

[1]Department of Civil & Environmental Engineering, Northeastern University, Boston, MA, USA
[2]Department of Electrical & Computer Engineering, Northeastern University, Boston, MA, USA

Abstract— This paper investigates the performance of the acoustic Synthetic Aperture Imaging (SAI) technique, which uses signals received at different locations to focus on occlusions, for the detection of defects inside a concrete medium typical for a bridge deck. A Finite Difference in Time Domain (FDTD) scheme in two dimensions is used to simulate elastic wave propagation generated by the Impact-Echo method. The FDTD scheme is used to generate waveforms on the surface of the concrete medium that are then used by the SAI technique to form an interior image of the concrete medium.

Imaging results show that planar air voids of larger sizes, embedded in various locations inside the concrete, scatter the acoustic field more than the steel reinforcement bars. Therefore, they appear as brighter regions in the image of the medium, as shown in Fig. 1. A case depicting a severe loss of structural integrity is investigated where a crack surrounds some of the steel bars, and a bright area near the anomaly is observed. This indicates that the SAI technique can provide a first estimate on the existence of structural damage. However, cracks located close to the surface, cannot be identified very well due to layer resonances excited between the crack and the surface, which creates misleading diagnostic information, if prior knowledge of the defect location is not known.

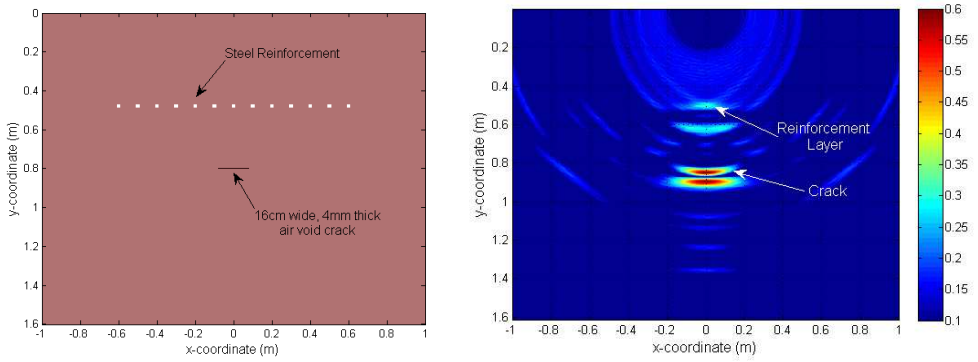

(a) (b)

Figure 1: (a) Defect location relative to steel reinforcement layer; (b) reconstructed image.

Accurate Modeling of Ground-coupled Ground Penetrating Radar with 2-D FDTD Using Observed Calibration Measurements

Christopher Wright, **Carey Rappaport**, **Kimberly Belli**, **and Sara Wadia-Fascetti**
Northeastern University, Stearns 11, 360 Huntington Ave Boston, MA 02115, USA

Abstract— Ground Penetrating Radar (GPR) has emerged as a valuable tool to evaluate and prioritize maintenance needs for transportation infrastructure. The use of software for modeling heterogeneous subsurface environments and simulating GPR responses plays an important role in the advancement of the technology. Simulated responses are generated using a 2-D finite difference time domain (FDTD) scheme with an arbitrary excitation. The problem at hand is to determine what excitation of the FDTD scheme is needed to obtain a simulated response that is comparable to the field response for some subsurface environment.

The proposed method, which has produced promising results (See Figure 1), uses calibration measurements from the GPR antenna and simulated data from an arbitrary excitation to calculate a new excitation signal. For this work the calibration measurements were collected using a 1.5 GHz ground coupled GPR antenna to capture the responses to several metal plates buried in dry sand. Multiple metal plates allowed for the calculation of the permittivity of the sand so that the environment could be modeled using software. Simulated data were collected for the modeled environment using a modulated Gaussian excitation pulse. A filtering algorithm was used to produce a new excitation, that, when used in the FDTD scheme, produced a response that compared closely to the calibration measurements.

Several challenges must be resolved before this work can be successfully concluded. Differences in the rate of signal attenuation between the 3-D sand pit environment and the 2-D FDTD environment must be accounted for. In addition, the antenna itself appears to be a source of ringing in the data that must be included in the model.

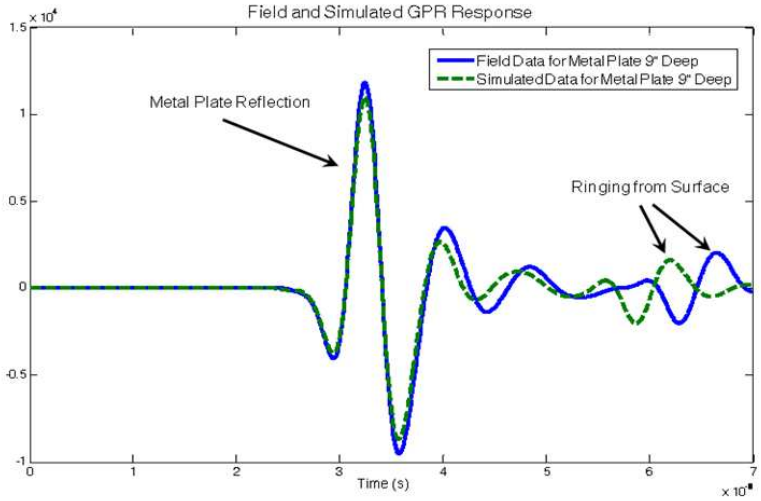

Figure 1: Comparison of field and simulated data for a metal plate buried 9 inches in dry sand. Differences between the signals such as the amplitude of the metal plate reflection and time of the ringing showcase some of the challenges encountered.

A New Method of Near-field Three Dimensional Synthetic Aperture Radar Imaging

Nan-Jing Li[1], **Chu-Feng Hu**[1], **Yong-Xin Zhao**[2], **and Jianjun Wei**[3]

[1]National Key Laboratory of UAV Specialty Technique
Northwestern Polytechnic University, Xi'an, China
[2]The 46th Middle School of Xi'an, Shaanxi, China
[3]Shaanxi Qiangde Technology Co., Ltd., Shaanxi, China

Abstract— A fully 3-D image reconstruction algorithm that quasi-monostatic mode is used and the transmitting and receiving systems working in stepped-frequency was developed. The algorithm is not restricted by far field as the traditional imaging algorithm. Through synthetic aperture processing for radar data, the resolutions of the image and detecting ability of radar are improved. A new back-project method, which can increase accuracy of interpolation, was presented. 3-D image of the objects can be achieved through fast Fourier transform and integrating after interpolation. Several imaging results from simulations and experiment were presented. These results show that the algorithm for 3-D image reconstruction based on this back-project method can produce a microwave 3-D image with high resolutions.

Impact of Soil Roughness in Underground Focusing SAR Images

Fernando Quivira, José A. Martínez Lorenzo, and Carey M. Rappaport
The Gordon CenSSIS, Northeastern University, 360 Huntigton Ave., Suite 302 Stearns Center
Boston, MA 02115, USA

Abstract— Underground tunnels present both military and homeland security threats since smugglers can turn them into transit routes for trafficking weapons, explosives, people, drugs, and other illicit materials. Detecting and imaging the presence of tunnels in any given region of ground is possible because the air that fills them is materially quite different from anything else underground. The Spotlight Synthetic Aperture Radar (SL-SAR) has been used due to its ability to scan large areas of terrain in a short amount of time, which is ideal for tunnel detection. In order to obtain strong and distinct target signals, Underground Focusing based on ray refraction at the ground surface was used (UF). This presents a challenge since this technique requires an estimation of the ground characteristics. The random roughness of the soil surface tends to distort the reconstructed image of the analyzed geometry.

This work explores the impact of the surface roughness in Underground Focusing SAR imaging for tunnel detection applications. The study starts by simulating incident plane waves from 19 angles (-45 to 45 degrees) at 128 different frequencies (55 to 550 MHz) with 2-D Finite Difference Frequency Domain (FDFD) analysis on 2 different types of soil: non-dispersive sandy soil and lossy clay loam soil.

The next part of the study involves the Underground Focusing reconstruction and the SAR imaging. In order to generate a focused image, the algorithm takes into account the constitutive parameters of both media and the wave refraction at the air/ground surface interface. The image is then generated using the differential phase associated with the wave refraction and the scattered fields received by the 19 antennas in the farfield (Fig. 1).

Increased surface roughness degrades the quality of the reconstructed image, thus making the tunnel more difficult to detect. By examining cases with varying degrees of roughness for each type of soil, it is possible to quantify the performance of Underground Focusing SAR tunnel imaging.

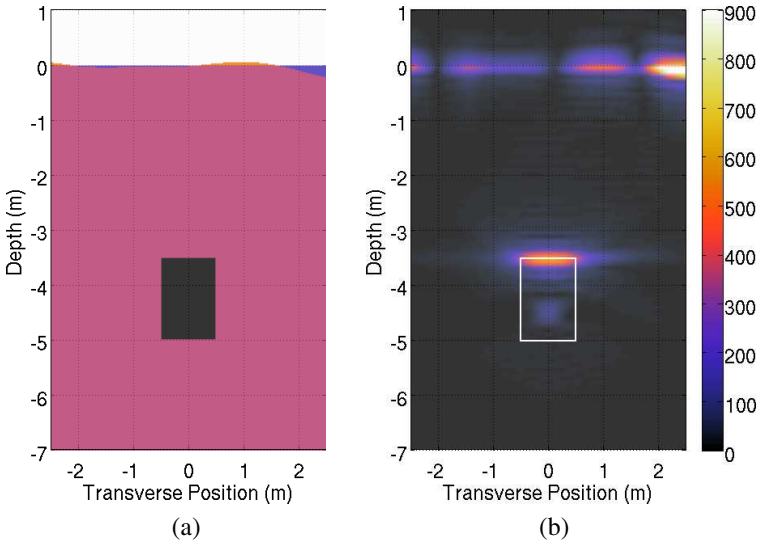

Figure 1: Geometry and underground focusing reconstruction for non-dispersive sandy soil ($\epsilon_g = 2.55(1 + 0.01i)\epsilon_0$): (a) Geometry with roughness = 0.1. (b) Tunnel reconstruction at 100 m from ground..

Wide Band Radar with Detecting and Tracing Corona Arc around Any High Speed and Anti Radar Aircraft

Milad Johnny and Maryam Johnny
Iran University of Science and Technology, Narmak, Tehran, Iran

Abstract— As we know, radar is an electromagnetic system for detecting and tracing any target. The base of this machine is to transfer some electromagnetic waveforms (like a square wave with sinusoidal modulator) and to analyze its echoes. Simple radar consists of a transmitter and receiver antenna and an electromagnetic detector. Transmitter antenna generates and emits electromagnetic waves. Some parts of these transmitted signals reflected from the body of target scatter and therefore; the receiver can detect the target and its features such as velocity and position of it.

In this paper, we are suggesting a new system that can detect any flying object without transmitting any electromagnetic wave. It can detect the object by analyzing the received signals that are generated by corona arc. It can be a revolution in the new radar systems and their usual and military application. At the end of the article, we briefly discuss the detecting and tracing the corona signals.

Session 1A3
RF and Wireless Communication

Matrix Calculation and Compensation of Multiple CFO Interferences in the OFDMA Uplink Communication System

Heung-Gyoon Ryu
Department of Electronic Engineering, Chungbuk National University, CheongJu 361-763, Korea

Abstract— OFDMA (Orthogonal Frequency Division Multiple Access) technique has been widely used in digital communication system to achieve very high data rate. However, like other OFDM-based systems, OFDMA system is very sensitive to frequency synchronization errors, especially in the uplink channel where many mobile users have individually different CFOs (Carrier Frequency Offset). When many different CFOs exist, the orthogonality between the subcarriers will be lost so that ICI (Inter Carrier Interference) as well as MAI (Multi-Access Interference) will be generated to disturb the received signal. Therefore, the system BER performance will be seriously degraded. Thus, research on the suppression to the interference caused by many different CFOs is of great importance. In this paper, we firstly analyze the interferences, including ICI and MAI, caused by multiple CFOs in the uplink channel of OFDMA system. Next, the suppression method based on block type pilots is proposed to overcome this interference simultaneously. From the simulation results, it can be seen that the multiple CFOs will make serious degradation to the system performance. However, by the proposed suppression processing method, the system performance can be significantly improved.

Threshold Power-based Radiation Pattern Measurement of Passive UHF RFID Tags

Leena Ukkonen and Lauri Sydänheimo
Department of Electronics, Rauma Research Unit, Tampere University of Technology, Finland

Abstract— Measuring the radiation pattern of passive ultra-high frequency (UHF) radio frequency identification (RFID) tags is challenging due to the special characteristics of RFID systems. Traditional antenna measurements where cables and matching circuits are attached to antennas are not feasible because attaching cables affects the properties of tag antennas. In addition, these kinds of measurements do not give proper information about the functioning of the tag. Therefore, novel and contactless radiation pattern measurement systems have been proposed to be used in RFID tag antenna radiation pattern measurement [1–3]. In this paper, we will measure tag's radiation pattern with threshold-power based method in active mode, i.e., when the tag is characterized in operation with the microchip. Reliability of this method is further analyzed.

Radiation pattern measurement of RFID tags is important in characterization of tag functioning. Similarly as the traditional antenna radiation pattern measurement, it gives information about the best radiation directions of the tag. More importantly, radiation pattern of a tag can be measured when the tag has been attached to the identified object. This way the effect of the identified material on the radiation pattern of the tag can be verified.

The operation abilities of passive UHF RFID systems depend mainly on two fundamental operational principles of passive UHF tags [3]:

1. The capability of the tag for wireless energy collection from the reader, i.e., tag's energy harvesting. This depends on the impedance matching between the tag's antenna and the IC and the IC sensitivity. The energy harvesting information provides factors that define a minimum transmission power level for the reader unit to turn the tag on over a certain reading distance, i.e., tag's threshold power.

2. The strength and clarity of desired backscattered signal from the tag, i.e., the radar cross section (RCS) properties of the tag.

The radiation pattern of an RFID tag can be measured based on these two fundamental operational principles analyzing the forward and reverse communication links. In practice, the forward link limits the read range of passive UHF RFID systems. Therefore, in this paper we concentrate on threshold-power based radiation pattern measurement of passive UHF RFID tags. Threshold power-based technique is demonstrated in measuring E and H plane radiation patterns of different tags in air and on material.

REFERENCES

1. Ritamäki, M., A. Ruhanen, V. Kukko, J. Miettinen, and L. H. Turner, "Contactless radiation pattern measurement method for UHF RFID transponders," *IEE Electronics Letters*, Vol. 41, No. 13, June 2005.
2. Lao, R.-R., W.-T. Shay, J. C. Hsu, and J.-H. Tarng, "Optically modulated scatterer technique for radiation pattern measurement of small antennas and RFID tags," *IEEE Antennas and Wireless Propagation Letters*, Vol. 8, 76–79, April 2009.
3. Ukkonen, L. and L. Sydänheimo, "Radiation pattern measurement of passive UHF RFID tags," *Proc. Antenna Measurement Techniques Association 31st Annual Symposium (AMTA 2009)*, 369–374, Salt Lake City, UT, USA, November 1–6, 2009.

Energy Efficient Fuzzy Logic Based Intelligent Wireless Sensor Network

Malay Ranjan Tripathy[1], **Kunal Gaur**[2], **Sonam Sharma**[3], **and G. S. Virdi**[1]

[1]Department of Electronics and Communication Engineering
Jind Institute of Engineering and Technology (JIET), Jind, Haryana, India
[2]Department of Electrical and Electronics Engineering
Jind Institute of Engineering and Technology (JIET), Jind, Haryana, India
[3]Department of Information Technology, Jind Institute of Engineering and Technology (JIET)
Jind, Haryana, India

Abstract— Rapid growth of wireless sensor network (WSN) [1–3] is becoming possible because of the availability of recent advanced technologies in the areas of sensors, VLSI, Microelectromechanical systems (MEMS), computations and wireless communication systems. In WSN, a large number of low cost specially distributed sensor nodes [4] with real time embedded systems based on limited computation, energy and memory resources are used to monitor the environment of interest. To make these sensor networks intelligent enough a control mechanism like fuzzy logic based control system [5] is being used widely for many WSN applications. Fuzzy logic is basically the extension of dual logic (crisp logic) that includes the intermediate value between absolutely true and absolutely false. It improves the accuracy in taking a decision about a system that has vague information. It has the efficiency to solve the system uncertainties when mathematical models fail to describe the system. Due to its numerous applications fuzzy logic based WSN is a topic of prime interest to many researchers.

Energy efficient WSN is the main concern of this paper. To achieve this purpose we have considered various issues like fuzzy control system based sensor nodes and optimized networking and routing protocols.

Sensor nodes in general powered by small batteries that are hard to replace or recharge. Therefore energy constraint is a major challenge for wide and remote applications [6, 7]. In a typical wireless enabled sensor system energy consumption occurs in three domains: Sensing, data processing and communication. During sensing the least possible of energy is consumed by the sensing circuits. In this paper we propose to use fuzzy logic control mechanism to activate rest of the sensing circuits (i.e., data processing and communication) only when the event of interest in the environment is available. So that WSN empowered by Fuzzy logic control mechanism will work as an intelligent and power efficient sensing network.

Apart from this we have considered an optimal network topology to reduce the energy requirement and processing time. We are using hybrid network topology [8] and clustering nodes so that WSN can be stable and reliable throughout the life of the node and also providing other way to improve network performance. In order to explore the node behavior we have used network simulator and found the usefulness of the proposed network. Towards the end we have mentioned about the use of a location-based routing protocol called GEAR (Geographical and Energy Aware Routing) [9] which is based on energy efficient geographic packet forwarding techniques.

REFERENCES

1. Akyildiz, I. F., W. Su, Y. Sankarasubramaniam, and E. Cayirci, "Wireless sensor networks: A survey," *Computer Networks*, Vol. 38, No. 4, 393–422, March 2002.
2. Zhang, Q. and Y. Zhang, "Cross layer design for QoS supporting multi hop wireless network," *Proceeding of the IEEE*, Vol. 96, No. 1, 64–76, 2008.
3. Zhang, J., P. V. Orlik, Z. Sahinoglu, A. F. Molisun, and P. Kinney, "UWB system for wireless sensor network," *Proceeding of the IEEE*, Vol. 97, No. 2, 313–331, 2009.
4. Jain, E. and Q. Liang, "Sensor placement and lifetime of wireless sensor networks: Theory and performance analysis," *Sensor Network Operations*, S. Phoha, T. F. LaPorta, and C. Griffin, Eds., Wiley, New York, 2005.
5. Mendel, J. M., "Fuzzy logic systems for engineering: A tutorial," *Proceeding of the IEEE*, Vol. 83, No. 3, 345–377, March 1995.
6. Shu, H., Q. Liang, and J. Gao, "Wireless sensor network lifetime analysis using interval type-2 fuzzy logic systems," *IEEE Transaction on Fuzzy Systems*, Vol. 16, No. 2, 416–427, April 2008.

7. Estrin, D. and R. Govindan, "Next century challenges; scalable coordination in sensor networks," *Mobicon'99*, 263–270, Seattle, WA, August 1999.
8. Kim, S.-Y., O. Guzide, and S. Cook, "Towards an optimal network topology in wireless sensor networks," *SUJUR*, Vol. 1, 2009.
9. Yu, Y., R. Govindan, and D. Estrin, "Geographical and energy aware routing: A recursive data dissemination protocol for wireless sensor networks," *UCLA Computer Science Department Technical Report*, UCLA/CSD-TR-01-0023, May 2001.

Ground-to-ground Radio Frequency (RF) Propagation in Desert Environments in the 30–2500 MHz Frequency Range

Julia Andrusenko, Jacob A. Gilbert, Jack L. Burbank, William T. Kasch, John R. Ward, and Leah C. Lewis
The Johns Hopkins University Applied Physics Laboratory, Laurel, MD 20723-6099, USA

Abstract— Radio Frequency (RF) propagation modeling is a technical area that has and continues to receive much attention from the communications research and wireless service provider communities. Consequently, there is a rich set of existing models that predict the propagation characteristics in various environments and frequency bands. However, one area that has received little attention to date is the ground-to-ground propagation, which is of obvious interest to ground-based war fighters. This is primarily driven by the nature of commercial-based communications and the inherent need for tower-based infrastructural nodes. This issue is exacerbated by the lack of attention paid to many frequency bands of interest to the military community, such as those in the Very High Frequency (VHF) band, which is a band with particularly poor support from existing propagation models. As a result, The Johns Hopkins University Applied Physics Laboratory (JHU/APL) has conducted extensive measurements of the characteristics of RF propagation in the 30–2500 MHz frequency bands for both surface-based transmitter and receiver. This paper presents results obtained for an open desert environment, as a function of transmission frequency, transmitter-receiver separation, and antenna height. Empirical measurements from Ft. Huachuca, AZ are presented and compared versus predictions made by the Free Space Path Loss Model, Two-Ray Ground Reflection Model, and Remcom, Inc.'s Wireless InSite software suite for modeling the effects of terrain, foliage, and man-made structures on the propagation of electro-magnetic waves.

Rain Fade Modelling Using Hidden Markov Model for Tropical Area

Baso Maruddani[1, 2], **Adit Kurniawan**[2], **Sugihartono**[2], **and Achmad Munir**[2]

[1]Electrical Engineering Department, State University of Jakarta
Jl. Rawamangun Muka, Jakarta 13220, Indonesia
[2]Radio Telecommunication and Microwave Laboratory
School of Electrical Engineering and Informatics, ITB
Jl. Ganesha 10, Bandung, West Java 40132, Indonesia

Abstract— Rain affects a transmission of an electromagnetic signal in three ways: (1) It attenuates the signal; (2) it increases the system noise temperature; and (3) it changes the polarization. All three of these mechanisms cause degradation in the received signal quality and become increasingly significant as the carrier frequency increases. At C-band, the effects are minor. At Ku-band, while they are noticeable, the effect can be accommodated. But at higher frequencies, such as Ka-band, the degradation can be so great that it simply cannot be compensated at the level of availability usually expected for lower frequencies. This paper proposes a propagation channel model caused by rain in tropical area using hidden Markov model approach.

In wireless communication systems using millimeter wave above 10 GHz, rain fade is one of the problems that has to mitigate for better availability. Indonesia as a tropical area has more rain rate compared to non-tropical area. Rain events can be modeled as a random process. The Hidden Markov Models (HMM) are widely used for modeling random processes. Drawbacks in a standard HMM for modeling state occupancy have often been pointed out. In HMM, Markov chain parameters (initial matrices probability, transition matrices probability, set of output distribution and emission matrices probability) obtained from rain rate measurement in Bandung, Indonesia for 6 months.

The HMM uses four states to model the rain events and every state has unique rain rate values. For tropical area, rain rate above 120 mm/hour is always happen. From the HMM parameter, we simulated the rain event to get the channel model. To compare the measurement result and simulation result, cumulative distribution function (CDF) can be used and can be seen in Fig. 1. The CDF of rain events simulation has similarity about 98% compared to measurement result. Fig. 2 shows the channel modeling result which shows the attenuation for signal caused by rain in tropical area.

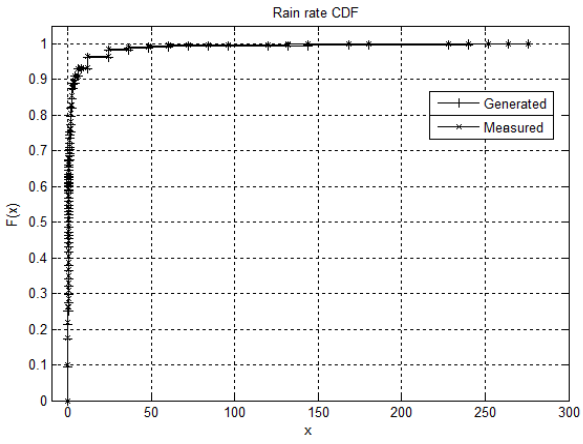

Figure 1: Rain rate CDF.

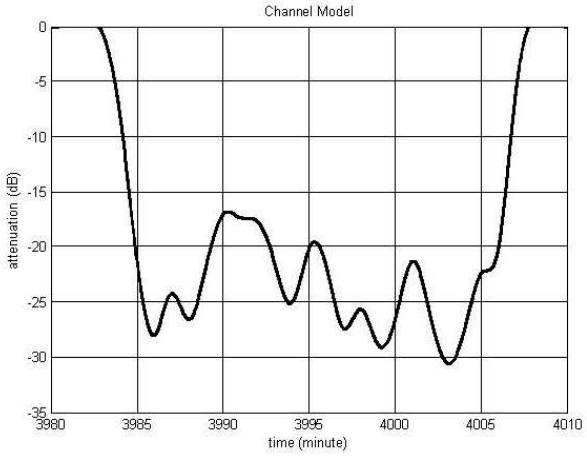

Figure 2: Simulation result for channel modelling.

Power Control and Diversity Performance Analysis in CDMA Systems

Baso Maruddani[1, 2] and Adit Kurniawan[2]

[1]Electrical Engineering Department, State University of Jakarta, Indonesia
[2]School of Electrical Engineering and Informatics, Bandung Institute of Technology, Indonesia

Abstract— In wireless communication, fading is one of problems since it causes the signal fluctuation so it may cause degradation signal level at receiver. Code Division Multiple Access (CDMA) as one of wireless communication types also experience fading. But another problem that CDMA system faced is signal interference from other user because all users in CDMA system use the same frequency. One of the solutions to mitigate fading is diversity. Diversity can improve the quality of accepted signal in receiver. Power control also improves the CDMA system performance because power control can minimize the interference among users.

Power control has an important role in CDMA system. The use of power control is indispensable to combat near-far effect and fading problem. Power control, however, fails to combat deep fading, because of its limitation in tracking fast and deep fades. On the other hand, diversity is one technique to alleviate the deep fading that experienced by signals. This paper investigates the performance of CDMA system when the power control and antenna diversity technique are combined at base station. From simulations, we can see the difference between the effect of diversity antenna on power control performance. The ratio of fading rate to the control rate ($f_D T_p$) is set for the same value (i.e., 0.011, 0.044, and 0.078), the performance of bit error rate (BER) as a function of the ratio of energy per bit to interference density (E_b/I_o) of power control improves significantly when it is combined with diversity antenna.

From the picture, CDMA system using power control combined with antenna diversity (blue and green curve) gives more improvement for performance than CDMA with power control only (red line). But the performance improves significantly from 1-antenna (not using diversity) to 2-antenna diversity compared than from 2-antenna diversity to 3-antenna diversity. To achieve BER of 10^{-3}, the required E_b/I_o for 3-antenna diversity system is 5 dB higher than for AWGN channel. To achieve BER of 10^{-3}, the required E_b/I_o for 2-antenna diversity system is 5.5 dB higher than for AWGN channel. And to achieve BER of 10^{-3}, the required E_b/I_o for no diversity system is 10.2 dB higher than for AWGN channel.

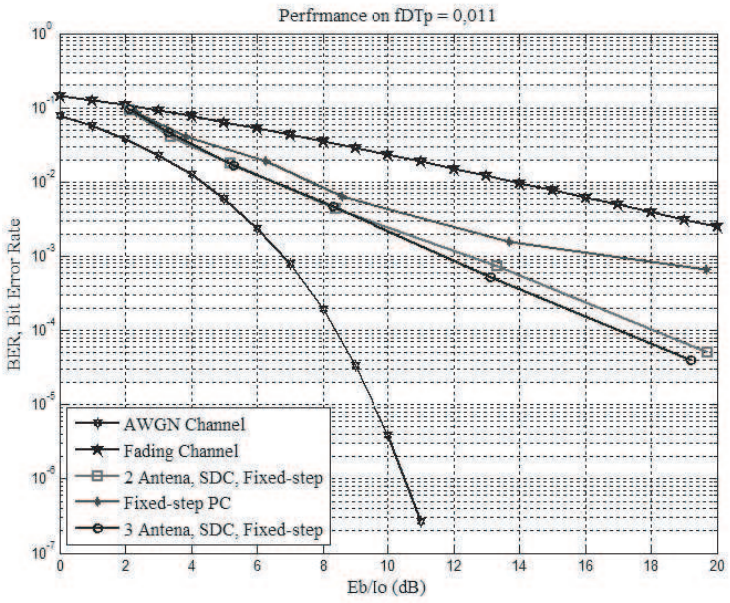

Parameter Analysis in Indoor Wireless Radiopropagation Simulation Environments

Victor Torres, **Fermin Esparza**, **Miguel Navarro**, **Miguel Beruete**, **and Francisco Falcone**
Universidad Pública de Navarra, Spain

Abstract— Recent advances in wireless communication technology enable services, such as sensor networks or high speed packet access. To achieve such a goal, adaptive modulation schemes are employed, strongly influenced by interference in the environment. This leads to coverage-capacity issues, where the coverage radius is dynamic and time varying. Due to the fact that user speed is variable, the sensitivity of the receivers is dynamic, leading to different degradation values depending on the effective value of interference within the complete scenario.

In this paper, parameters regarding simulation of indoor wireless systems is evaluated. An in-house three dimensional ray tracing code has been programmed and tested with complex indoor scenarios, taking into account morphology of the scenario (details such as wall postion, furniture, ventilation ducts, etc.) as well as material properties (loss tangent and dielectric constant). Different parameters regarding the simulation, such as ray density or reflection/refraction conditions are analyzed, in order to seek the optimal simulation configuration. Several type of technologies are presented, such as ZigBee, second generation GSM and future Long Term Evolution 3GPP systems. The results are applicable to the design of future large scale indoor wireless system deployments in heterogeneous configurations and are aimed to aid in the radio planning and optimization phases of such deployments.

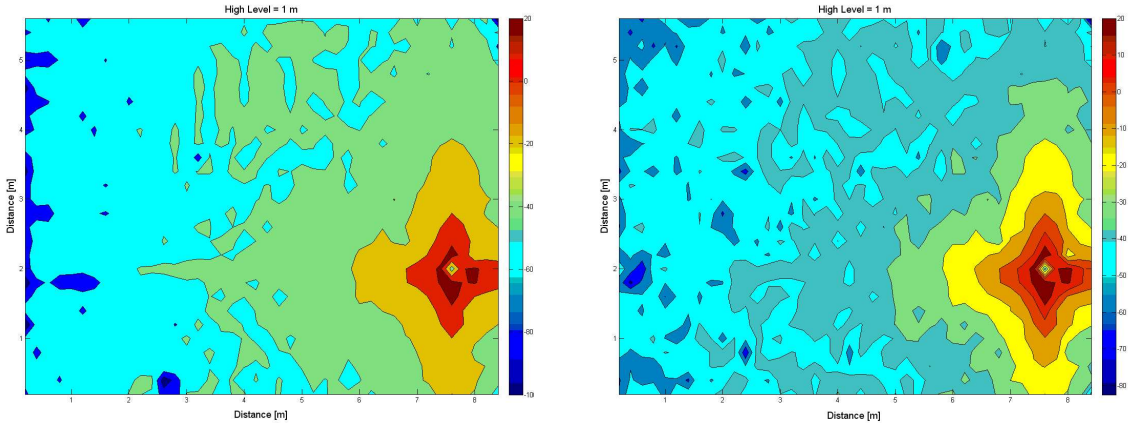

Figure 1: Simulation results for an indoor second generation GSM power density coverage plot. The left hand side takes into account three reflected ray components, whereas the plot at the right hand side takes into account seven components.

A Novel Power Controller of Wireless Sensor Network Node Circuit for Energy Saving

Shi-Sheng Jin[1], **Wei-Wei Cheng**[2], **Shun Yuan**[1], **Jun-Yong Wang**[1], **and Jue Li**[1]

[1]Guizhou Meteorological Information Center, Guiyang, Guizhou 550002, China
[2]Institute of Microelectronics and Optoelectronics, Zhejiang University
Hangzhou, Zhejiang 310027, China

Abstract— A novel power controller of wireless sensor network node circuit for energy saving are designed, fabricated and tested. In fact, autonomous sensors play a very important role in the environmental, structural, and medical fields [1–3]. The use of this kind of systems can be expanded for several applications, for example in implantable devices inside the human body where it is impossible to use wires [4–6]. Furthermore, they enable measurements in harsh or hermetic environments, such as under extreme heat, cold, humidity or corrosive conditions. The use of batteries as a power supply for these devices represents one solution, but the size, and sometimes the cost and unwanted maintenance burdens of replacement are important drawbacks [7–10].

In this paper, a novel power controller of wireless sensor network node circuit for energy saving are discussed. Their general architectures are presented. Sensing strategies, communication techniques and power management are analyzed. Then, general building blocks of an autonomous sensor are presented and the design guidelines that such a system must follow are given. Furthermore, this paper reports different proposed applications of autonomous sensors applied in harsh or hermetic environments: two examples of passive autonomous sensors that use telemetric communication are proposed, the first one for humidity measurements and the second for high temperatures. Other examples of self-powered autonomous sensors that use a power harvesting system from electromagnetic fields are proposed for temperature measurements and for airflow speeds.

Reduction in size and power consumption of consumer electronics has opened up many opportunities for low power wireless sensor networks. One of the major challenges is in supporting battery operated devices as the number of nodes in a network grows [11, 12]. The two main alternatives are to utilize higher energy density sources of stored energy, or to generate power at the node from local forms of energy [13, 14]. This paper mentions the state-of-the art technology in the field of both energy storage and energy harvesting for sensor nodes. The options discussed for energy storage include batteries, capacitors, fuel cells, heat engines and beta-voltaic systems. The field of energy harvesting is discussed with reference to photo-voltaic, temperature gradients, fluid flow, pressure variations and vibration harvesting.

Considering other aspects, accuracy and stabilization of measurement are disturbed by the temperature, humidity, pressure and other factors of environment, so dual-path architecture and application of programmable logic circuit compensate the error and process the data of measurement results precisely and in high speed. Moreover, the radio frequency transmitter sends the data to a receiver wirelessly and the receiver displays a visual value which represents the resonant frequency of sensor which corresponds to the mass to be measured to remote users.

A resonant frequency f_s which is set by Equation (1) and a parallel resonant frequency f_p which is determined by Equation (2) [4],

$$f_s = \frac{1}{2\pi\sqrt{L_m C_m}} \tag{1}$$

$$f_p = \frac{1}{2\pi\sqrt{L_m \frac{C_m C_0}{C_m + C_0}}} \tag{2}$$

where L_m is the motional inductance, C_m is the motional capacitance, C_0 is the clamped capacitance, and R_m is the motional resistance of resonant network.

On account of the advantages above, a novel power controller of wireless sensor network node circuit for energy saving is designed, which is shown in Fig. 1. It consists of LF antenna (low frequency antenna), RF antenna (radio frequency antenna), wakeup circuit, logic control switch, battery which is composed of three power supply modules, power switch array which is composed of three power array modules, duplexer, monitor circuit which is composed of detector, filter and comparator, radio frequency transmitting circuit which is composed of PA (power amplifier),

gain amplifier and modulator, DSP (digital signal processing), and data sampling circuit which is composed of A/D (analogue to digital converter) and sensor.

We develop the extensive applications of the a novel power controller of wireless sensor network node circuit for energy saving based the above circuit, shown in Fig. 2. It consists of LF antenna (low frequency antenna), RF antenna (radio frequency antenna), wakeup circuit, logic control switch, battery which is composed of four power supply modules, power switch array which is composed of four power array modules, duplexer, RF switch (radio frequency switch), monitor circuit which is composed of detector, filter and comparator, radio frequency receiving circuit which is composed of LNA (low noise amplifier), AGC amplifier (automatic gain control amplifier) and demodulator, radio frequency transmitting circuit which is composed of PA (power amplifier), gain amplifier and modulator, DSP (digital signal processing), and data sampling circuit which is composed of A/D (analogue to digital converter) and sensor. And Fig. 3 is the photo of the above circuit system.

REFERENCES

1. Akyildiz, I. F., et al., "Wireless mesh networks: A survey," *Computer Networks — The International Journal of Computer and Telecommunications Networking*, Vol. 47, 445–487, Mar. 2005.
2. Anastasi, G., et al., "Energy conservation in wireless sensor networks: A survey," *Ad Hoc Networks*, Vol. 7, 537–568, May 2009.
3. Baronti, P., et al., "Wireless sensor networks: A survey on the state of the art and the 802.15.4 and ZigBee standards," *Computer Communications*, Vol. 30, 1655–1695, May 2007.
4. Buratti, C., et al., "An overview on wireless sensor networks technology and evolution," *Sensors*, Vol. 9, 6869–6896, Sep. 2009.
5. Huang, G. Q., et al., "Wireless manufacturing: A literature review, recent developments, and case studies," *International Journal of Computer Integrated Manufacturing*, Vol. 22, 579–594, Jul. 2009.
6. Joshi, C. V., et al., "A review of the challenges in the implementation of next-generation ZigBee networking," *Iete Technical Review*, Vol. 25, 161–167, Jul.–Aug. 2008.
7. Knight, C., et al., "Energy options for wireless sensor nodes," *Sensors*, Vol. 8, 8037–8066, Dec. 2008.
8. Lopez, T. S., et al., "Integrating wireless sensors and RFID tags into energy-efficient and dynamic context networks," *Computer Journal*, Vol. 52, 240–267, 2009.
9. Oweis, R. and M. Minarik, "Design, simulation and realization of a dual-mode oscillator with distributed RC structure," *Radioengineering*, Vol. 8, 17–21, 1999.
10. Rhee, I. K., et al., "Clock synchronization in wireless sensor networks: An overview," *Sensors*, Vol. 9, 56–85, Jan. 2009.
11. Sardini, E. and M. Serpelloni, "Passive and self-powered autonomous sensors for remote measurements," *Sensors*, Vol. 9, 943–960, Feb. 2009.
12. Willig, A., "Recent and emerging topics in wireless industrial communications: A selection," *IEEE Transactions on Industrial Informatics*, Vol. 4, 102–124, May 2008.
13. Xiao, R. Y. and G. Z. Wu, "A survey on routing in wireless sensor networks," *Progress in Natural Science*, Vol. 17, 261–269, Mar. 2007.
14. Yick, J., et al., "Wireless sensor network survey," *Computer Networks*, Vol. 52, 2292–2330, Aug. 2008.

A UHF and HF RFID Integration System for Access Control Application

Wei He, **Yinlong Huang**, **and Weihua Sun**
Anti-counterfeit Information Department, The Third Research Institute of MPS, China

Abstract— In this paper, a novel RFID (Radio Frequency Identification) application integration system for UHF (ultra high frequency) and HF (high frequency) operation is presented. This system is at UHF and HF band operation, and consists of UHF reader, circular polarization antenna, HF reader, HF loop antenna, computer and LED touching display, etc. In this design, UHF reader complies with standard of ISO 18000-6B, 6C and HF reader complies with standard of ISO 15693. Designing this system make it a suitable candidate for RFID application in access control for some importance meetings and sporting contests etc.

Session 1A4
Robust and Efficient Electromagnetic Solutions for Large-scale Problems

On the Frequency Barrier of Surface Integral Equations from a Circuit Point of View

Lijun Jiang[1] **and Albert E. Ruehli**[2]

[1]Department of EEE, The University of Hong Kong, China
[2]Department of EMC, The Missouri University of Science and Technology
Rolla, Missouri, USA

Abstract— The failure to provide an accurate low frequency and even DC solution has been a key issue of research for integral equation based formulations. Loop-star techniques were conceived to extend the low frequency limit of SIEs such as EFIE methods. It has successfully improved the low frequency conditioning, but requires complicated graph oriented algorithm. In addition, this approach does not work for DC.

At the same time, the Partial Element Equivalent Circuit (PEEC) approach has been used to solve similar electromagnetic problems for packaging and interconnect applications. It uses the Modified Nodal Analysis (MNA) circuit solver formulation, which is employed in most of Spice circuit solvers. PEEC+MNA not only provide a well conditioned low frequency solution, but also a dc solution. The attached figure shows an equivalent circuit for this simplest PEEC model. Both PEEC and EFIE approaches separates the MoM impedance Z_{ij} into a separate inductance and a capacitance part for the electromagnetic solution. In fact, most important low frequency issues can be observed from this simple circuit. The capacitances will represent open circuits at low frequencies such that the MoM impedances will go to infinity. EFIE mixes the capacitance contribution with that of the inductance, which causes the underflow of the inductance effects. The PEEC method uses Kirchoff's Current Law (KCL) in MNA to enforce the continuity of the current. Both nodal potentials and currents are included as unknowns in PEEC. Hence, PEEC demonstrates much better conditioning than EFIE at the low frequency regime (not DC).

For a meaningful DC solution, two conditions are necessary. First, the losses must be included in the model. This is symbolized by the resistance in series to the inductances. Clearly, at DC, the inductances will become short circuits and the remaining circuit only consists of resistive losses. Second, the solver formulation must be separate the capacitive and inductive circuit such that a solution can be found in spite of the open circuited capacitances. It corresponds the Helmholtz decomposition between the electric field and the magnetic field. For this reason, PEEC use the MNA approach in solving the equations. Again, the key issue is that both the currents and the potentials must be included as unknowns. EFIE completely breaks at DC due to the decomposition.

In the presentation we will include example solutions and matrix condition numbers to support the discussion. Also, we consider the use of RWG basis functions to show that the popular approach can be formulated such that some of the properties of the PEEC method can be inherited to improve EFIE, such as the Augmented EFIE developed by Qian and Chew.

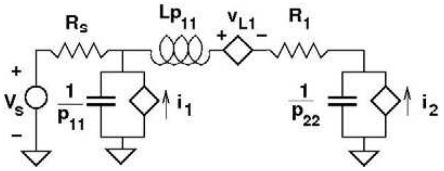

Fast Integral Equation Solution Techniques for Planar-3D Structures in Multilayered Media

Thomas Vaupel
Fraunhofer Institute for High Frequency Physics and Radar Techniques FHR
Wachtberg, Germany

Abstract— For the analysis and design process of (M)MIC structures and printed antenna systems, electromagnetic simulators based on the Method of Moments (MoM) combined with the Green's function of the multilayered environment are widely used due to their high accuracy and good modeling capabilities which have been accomplished over the last years.

To overcome the computational burden of the standard Method of Moments (MoM), a diagonalized translation operator on the Cartesian wavenunmer plane is constructed combined with a group decomposition of the structure, allowing efficient matrix vector multiplications in context with the used Krylov subspace methods without the need of generating the explicit system matrix for sufficiently separated groups [1].

Besides of planar electric and magnetic surface currents for the modeling of microstrip/stripline and slotline/aperture components, volume currents with vertical direction are employed for the modeling of vertical interconnects and via-holes as well as finite dielectric regions, where arbitrary vertical discretizations in combination with arbitrary crossings of layer interfaces are possible. Thus, the characterization of complex Planar-3D structures with large vertical extensions is possible (e.g., LTCC structures). For the interactions of the vertical currents with the planar components, extended Green's functions are derived by analytical space domain integrations. Finally, all Green's functions and translation operators depend only on the Cartesian wavenumbers, allowing a consistent group coupling computation during the matrix vector multiplications by efficient numerical spectral domain integrations. For this goal Legendre-Filon and extented Laguerre quadrature techniques are used with different kind of complex integration path deformations. These techniques are also used for the generation of the explicit parts of the system matrix in case of near-field interactions or for situations where the standard MoM has advantages over an iterative solution.

For a decisive convergence acceleration of the Krylov subspace solvers (mainly a Generalized Minimum Residual approach (GMRES)), a diakoptic preconditioner is used based on the group decomposition in combination with a Reversed Cuthill McKee algorithm applied to the group ordering. With the latter strategy, the generation of matrix fill-ins during the necessary sparse Cholesky or LU-decompositions can be minimized or avoided.

The method is currently applied to antenna arrays with feed network as well as frequency selective structures and metamaterials.

REFERENCES

1. Vaupel, T., "A fast spectral domain solver for the characterization of larger microwave structures in multilayered environments," *ACES Journal*, Vol. 24, No. 5, 493–503, Oct. 2009.

A Surface Absorber Approach with the Boundary Element Method to Terminate Nanophotonic Devices

Lei Zhang[1], **Steven G. Johnson**[2], **and Jacob K. White**[1]

[1]Research Laboratory of Electronics
Department of Electrical Engineering and Computer Science, MIT, USA
[2]Research Laboratory of Electronics, Department of Mathematics, MIT, USA

Abstract— In this paper we present the decay rate results from using the surface conductive absorber technique [1]. The technique developed for terminating optical waveguides using the surface integral equation (SIE) method addresses the difficulties with waveguides and surfaces extending to infinity. In order to attenuate waves reflected from truncated waveguides, a region with surface absorption is appended to the truncated ends of the waveguide (See Fig. 1). The transition between the non-absorbing and absorbing regions will generate reflections that can be minimized by making the transition as smooth as possible and we show this smoothness can be achieved by smoothly changing the surface conductivity. Numerical experiments demonstrate that the reflections of our method are orders of magnitude smaller than those generated by straightforward approaches, for instance, adding a volume absorptivity to the waveguide interior. In addition, the asymptotic power-law behavior of the transition reflection as a function of the length of the surface absorber and the power law is determined by the smoothness of the transition [2].

The longitudinal section of a dielectric waveguide with an attached surface absorber is shown in Fig. 1. In Fig. 2 we show the complex magnitude of the electric field inside the waveguide with an absorber of a quadratically varying surface conductivity. The flat curve of the complex magnitude in the absorber region indicates that reflections have been successfully eliminated.

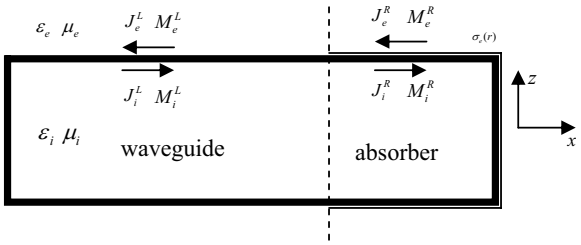

Figure 1: 2-D longitudinal section of a 3-D rectangular waveguide with a surface absorber. $\sigma(r)$ is the varying conductivity on the absorber surface. The dashed line indicates the position of the interface.

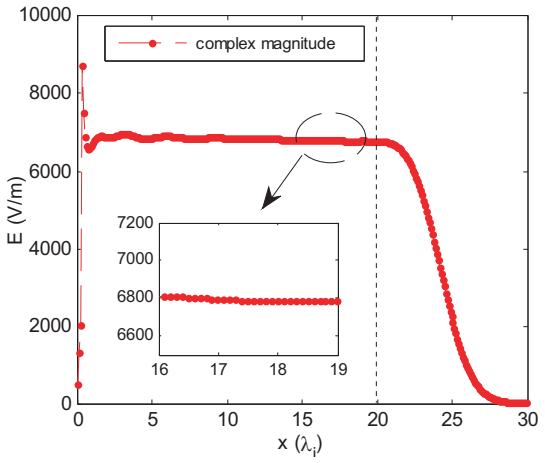

Figure 2: The complex magnitude of electric field along the longitudinal direction inside the waveguide and the absorber.

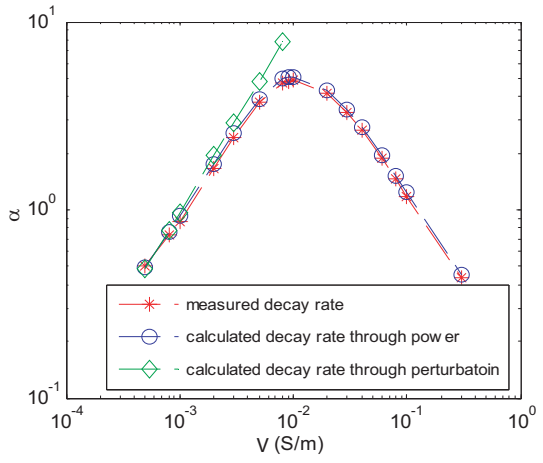

Figure 3: Decay rate due to surface conductivity.

Moreover, we show a quasi quadratic-log behavior of the decay rate due to surface conductivity by exponential curve fitting in Fig. 3. We further confirm this behavior using a first-order perturbation method, which is accurate for small conductivity, and with a power conservation method using Poynting's theorem. Note that the power method agrees with the fitted decay rate for the entire conductivity range.

REFERENCES

1. Zhang, L., J. H. Lee, A. Farjadpour, J. White, and S. Johnson, "A novel boundary element method with surface conductive absorbers for 3-D analysis of nanophotonics," *2008 IEEE MTT-S International Microwave Symposium Digest*, 523–536, 2008.
2. Oskooi, A. F., L. Zhang, Y. Avniel, and S. G. Johnson, "The failure of perfectly matched layers, and towards their redemption by adiabatic absorbers," *Optics Express*, Vol. 16, 11376–11392, 2008.

A Hybrid PMM-MOM Method for Analyzing Electrically Large and Finite Frequency Selective Surface

Jianxun Su and Xiaowen Xu
Department of Electronic Engineering, Beijing Institute of Technology, Beijing 100081, China

Abstract— A hybrid PMM-MOM (periodic MOM and exact MOM) method is proposed for the analysis of electrically large and finite frequency selective surfaces (FSS).

Surface waves are unique for finite and curved arrays, which will not appear in infinite one, and the surface waves and Floquet currents in this case will interfere with each other, resulting in strong variations of the current amplitudes. Therefore, if modeling finite or curved FSS by PMM, it will cause significant errors or even lead to wrong results sometimes. The exact full-wave model is employed in the analysis of finite FSS, including both planar and curved structures. However, the strict model takes up a great deal of memory, especially for large finite periodic structure. Therefore, a new method to save memory and to obtain sufficient accuracy is presented for the analysis of a finite FSS. The new method divides the finite FSS into two parts. The inner part with approximate periodic boundary is analyzed by PMM, the outer boundary part is analyzed by the exact full-wave model (MOM + MLFMA). The most important thing is to ensure the current continuity of the boundary of the two parts. The new method can obtain sufficient accuracy, and save memory. As an example, consider a planar array with 50×50 or more cross-dipoles, the transmission and reflection coefficients and RCS are studied. The accuracy and efficiency of three methods, including periodic method of moments, exact full-wave model and new proposed hybrid PMM-MOM method, are compared. As for accuracy, new method is more accurate than the PMM, and is almost the same as the exact full-wave model. As for memory, PMM apply the periodic conditions to limited the calculate domain on just one unite, of course, it take up the least memory. However, compared to the exact full-wave model, new method save more memory. The new method not only can be used to analyze the finite frequency selective surfaces, in fact, it can be used to analyze arbitrary electrically large and finite periodic structures, including large phased array.

In this paper, we describe an efficient new method to analyze the large finite FSS array. To the best of our knowledges, this method has not yet described in public. A hybrid PMM-MOM method is used to analyze electrically large and finite frequency selective surfaces (FSS). New method is more accurate and save more memory. Numerical examples are given to demonstrate the accuracy and efficiency of the new proposed method.

ACKNOWLEDGMENT

This work is supported by the National Natural Science Foundation of China under Grant 60871003.

The Discontinuous Galerkin Method for Highly Inhomogeneous Media

Christoph Schwarzbach and Eldad Haber
University of British Columbia, Vancouver, Canada

Abstract— The simulation of geophysical measurements involves a physical description of the earth's interior by spatially varying constitutive parameters. In particular, these parameters may be discontinuous and have jumps by orders of magnitude. We address the problem of solving Maxwell's equations for that case by a discontinuous approach also for the fields. The Discontinuous Galerkin (DG) method allows us to enforce the interface conditions explicitly by adding appropriate penalty or Lagrange multiplier terms to the variational formulation. We restrict ourselves to the case of time-harmonic fields and derive a symmetric discretization for the first order Maxwell system. In spite of potential savings in storage for a second order formulation we prefer to discretize the first order form as it results in accuracy for both the electric and magnetic fields; both needed for geophysical applications. The main challenge in the DG method is the solution of the linear system. We propose and experiment with a number of preconditioning techniques. In particular, we use a preconditioner based on the potentials formulation to Maxwell's equations. We show that using our approach we are able to obtain significant accuracy even for very challenging problems.

Multi-region Pseudospectral Time Domain (MR/PSTD) Modeling of Electromagnetic Wave Propagation

Lanbo Liu[1, 2], **Benjamin Barrowes**[2], **Zhao Zhao**[1], **and Zijian Liu**[1]

[1]Dept. of Civil & Environmental Engineering, University of Connecticut
Storrs, CT 06269-2037, USA
[2]USACE Engineers Engineering Research and Development Center
Cold Regions Research and Engineering Laboratory
Hanover, NH 03755, USA

Abstract— For a wide breadth of engineering problems involving with electromagnetic (EM) wave simulations, the EM wave actually propagates through a substantial portion of the domain occupied by very uniform medium such as air. A hybrid approach of using more analytical solution in the uniform region and more advanced (hence more computationally intensive) numerical algorithms in the complicated sub-regions will essentially improve the computation efficiency. One of this hybrid approaches in known as multi-region finite difference time domain (MR/FDTD) method. MR/FDTD uses the Kirchhoff integration to account for EM wave propagation in the uniform region, and FDTD for the sub-regions containing complicated scatterers or EM devices. We have extended MR/FDTD to the so called MR/PSTD, i.e., the computation of the EM wave propagation in the sub-regions is handled by the pseudospectral time domain (PSTD) method. By this combination we improved further of the computational efficiency with larger grids and hence larger time steps to save memory and computation time. Our approach will be illustrated by a case study of through-wall detection of life signals of human breath and heart beat.

Simplified Integral Equation Modeling of Low-frequency Electromagnetic Scattering from a Resistive Underground Target

Shaaban A. Bakr[1] **and Trond Mannseth**[2]

[1]Centre for Integrated Petroleum Research, University of Bergen, Norway
[2]Centre for Integrated Petroleum Research, Department of Mathematics, University of Bergen, Norway

Abstract— We consider solving three-dimensional electromagnetic (EM) problems within geophysics where the target body (petroleum reservoir, CO_2 deposition aquifer) is buried deeply underground. Such applications are characterized by use of low source frequencies, a resistive target body, and a large number of grid cells in the discretized model of the target.

The large number of grid cells puts extra emphasis on computational cost and complexity. With finite difference (FD) methods the computational domain is much larger than the target itself, increasing the number of grid cells further. An advantage, however, is that the corresponding coefficient matrix is sparse. With integral equation (IE) methods only the target needs to be discretized. A disadvantage is that the corresponding coefficient matrix is dense. Recently, a novel approximate hybrid method, simplified IE (SIE) modeling, has shown excellent accuracy in modeling the low-frequency EM response from a resistive target in a 2D setting.

The method consists of solving a finite volume problem in a localized region containing the target, and using IE method to obtain the field outside that region. The hybrid method thus replaces the dense-matrix part of the rigorous IE method by sparse-matrix calculations based on an approximation of Maxwell's equations. The accuracy of SIE modeling is confirmed in 3D. Our concern is, however, to quantify the computational cost and complexity of SIE modeling and compare its computational performance to IE modeling when computing the low-frequency EM response from a resistive target with a large number of grid cells. It is shown that the theoretical number of floating point operations per iteration with SIE modeling is orders of magnitude smaller than that with IE modeling. The computational advantage of SIE over IE is confirmed by numerical simulations. It is also found that the computational complexity of SIE is much smaller than that of FD.

A Three-dimensional Inversion Approach for Cross-well Electromagnetic Field Data

J. Liu, G. Pan, A. Abubakar, T. M. Habashy, M. Zaslavsky, and V. L. Druskin
Schlumberger-Doll Research, Cambridge, MA, USA

Abstract— Electromagnetic (EM) methods have been one of the important tools for the appraisal of a reservoir because of their sensitivity to the conductivity which is a function of the fluid saturation. One of the well-known EM techniques is the single-well induction logging measurement. This induction logging measurement has a sensitivity of up to a few meters from the well and is a function of the separation between the transmitter and the receiver, the frequency of operation and the resistivity distribution. To reach deeper into the reservoir, a cross-well EM technology was developed. The system operates very similar to the single-well logging tool however with transmitters (magnetic dipoles) and receivers (magnetic fields) deployed in separate wells and at a lower frequency of operation. After the data set has been collected, an inversion process is applied to convert the EM signals to a conductivity distribution map of the region between the wells using a non-linear inversion algorithm.

In this presentation, we present a rigorous three-dimensional (3D) inversion algorithms where a Gauss-Newton minimization approach with a multiplicative cost function is employed. The Gauss-Newton approach is well-known to have higher convergence rates than the non-linear conjugate gradient or quasi-Newton methods. On the other hand the Gauss-Newton method can be more expensive than the non-linear conjugate gradient since in this approach one is required to invert the Hessian matrix. By using the multiplicative cost function we do not need to determine the so-called regularization parameter in the optimization process, hence the algorithm is fully automated. Further, the algorithm is equipped with two different regularization functions to produce either a smooth (by using a standard L_2-norm function) or a blocky (by using a weighted L_2-norm function) conductivity distribution. Further in order to enhance the robustness of the algorithm we incorporated a non-linear transform procedure for constraining the minimum and the maximum values of the conductivity distribution and a line-search procedure for enforcing the error reduction in the cost function in the optimization process.

In this talk, in addition to the synthetic data, we will discuss the application of this inversion approach to field data sets. Through the case study of field data sets, we will show the pros and cons our 3D inversion approach.

Computation of Casimir Forces in Arbitrary Geometries and Materials via the Finite-difference Time-domain Method

Alejandro W. Rodriguez[1], **Alexander P. McCauley**[1], **John D. Joannopoulos**[1], **and Steven G. Johnson**[2]

[1]Department of Physics, Massachusetts Institute of Technology, Cambridge, MA 02139, USA
[2]Department of Mathematics, Massachusetts Institute of Technology, Cambridge, MA 02139, USA

Abstract— Casimir forces between neutral objects arise due to quantum fluctuations of the electromagnetic field [1, 2]. In addition to being theoretically interesting, recent experiments also indicate that Casimir forces (which are usually attractive and increasing with decreasing object separation) may contribute significantly to "stiction" or friction in microelectromechanical systems (MEMS). In order to gain a better understanding of this effect, scientists have begun to explore new theoretical methods capable of computing the force in complex geometries (beyond simple parallel-plate geometries or similar approximations thereof), where interesting effects have been recently demonstrated [1, 2]. In what follows, we introduce a simple and general theoretical framework for computing Casimir forces in arbitrary geometries and for arbitrary materials using the finite-difference time-domain (FDTD) method [1, 2]. Our approach allows researchers to exploit powerful, widely available and *parallel* FDTD software that can be used to compute forces in large three-dimensional geometries, *anisotropic* dielectrics and even periodic media, without requiring any modification.

The computation of Casimir forces via FDTD involves the evolution of Maxwell's equations in response to short dipole current pulses [1]. This approach is based on a standard formulation in which the Casimir force is expressed as a contour integral of the frequency-domain Maxwell stress tensor, which is in turn expressed in terms of the electromagnetic Green's function (GF) via the fluctuation-dissipation theorem. The passage to the time domain is *conceptually* simple: the GF is simply the electromagnetic response to a short dipole current source, which yields the entire frequency spectrum in a single time-domain calculation [1]. Previous numerical frequency-domain formulations, however, require that the force integrand be evaluated over imaginary frequencies, where the integrand is known to be a smooth and decaying function of frequency (the alternative, computing the real-frequency GF, yields a highly oscillatory and infinite-bandwidth integrand, which is undesirable for numerical evaluation). Unfortunately, a direct implementation of imaginary-time deformations or Wick rotations in FDTD is impossible, since they lead to exponentially growing fields in time. Thankfully, imaginary-time deformations are not the only suitable contours over which to evaluate Green's functions, and in particular, we exploit a recently derived equivalence between complex contour deformations and material deformations that allows us to express the GF of any geometry evaluated over some suitable complex contour in terms of the

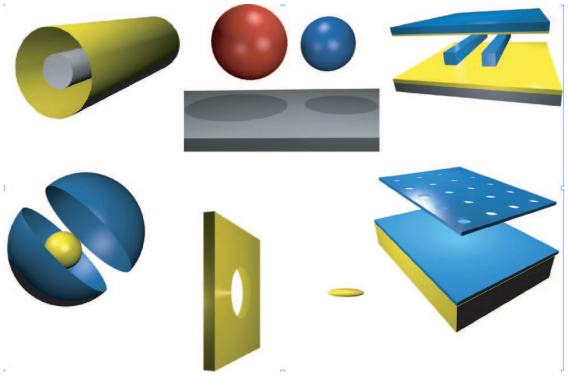

Figure 1: Illustration of various geometries exhibiting unusual Casimir physics and studied using FDTD. These include: stable suspension of eccentric objects, multi-body stable configurations (two-sphere diclusters), non-monotonic features in piston-like geometries, and repulsion between perfectly-metallic, plane-separated objects. Many of these challenging geometries are either periodic (translationally symmetric) or have cylindrical symmetry, allowing us to exploit off-the-shelf FDTD features that greatly reduce the computational costs.

real-time response of a short current pulse in a transformed (dissipative) dielectric medium. From this perspective, one need only identify a suitable dispersive medium (simple to implement in FDTD), and check that the corresponding complex contour has the desired numerical properties. One such medium, common to many FDTD solvers, corresponds to a constant DC conductivity, which we use to validate our approach. To conclude, we illustrate the flexibility and generality of FDTD by performing calculations (using a freely available FDTD code [3]) in a number of interesting and challenging geometries [2], depicted schematically in Fig. 1.

REFERENCES

1. Rodriguez, A. W., A. P. McCauley, J. D. Joannopoulos, and S. G. Johnson, "Theoretical ingredients of a casimir anaolog computer," arXiv:0903.0599, 2009.
2. Rodriguez, A. W., A. P. McCauley, J. D. Joannopoulos, and S. G. Johnson, "Computing casimir forces in the time domain: Theory," *PRA*, Vol. 80, 012115, 2009.
3. Rodriguez, A. W., A. P. McCauley, J. D. Joannopoulos, and S. G. Johnson, "Computing casimir forces in the time domain: Applications," arXiv:0906.5170, 2009.
4. http://ab-initio.mit.edu/wiki/index.php/Casimir_calculations_in_Meep.

Spectral Element Method for 2-D and 3-D Photonic Crystals with Dispersive and Anisotropic Materials

Ma Luo and Qing Huo Liu
Department of Electrical and Computer Engineering, Duke University, Durham, NC, USA

Abstract— Two- and three-dimensional photonic crystals (PCs) are very important artificial materials that can be designed to possess novel properties, such as complete band gaps, and ultra-high or ultra-low density of states. The band structures of photonic crystals are essential to understanding their physical phenomena and engineering application. Efficient computational tools are important for rapid prototyping of PCs for various applications.

We develop one such efficient and highly accurate tool based on the spectral element method (SEM) to calculate the band structures of 2-D and 3-D PCs consisting of dispersive and anisotropic materials. The SEM basis functions in the reference domain are constructed by Gauss-Lobatto-Legendre (GLL) polynomials. Mixed order vector basis functions are used in order to suppress spurious modes. The basis functions in the reference domain are mapped to the physical space by contravariant mapping, so the tangential component remains continuous at all interfaces between different elements. By using the variation principle, the wave equation is converted into a matrix equation, with the solution of a column vector representing electric field at nodal points. When the materials are non-dispersive, the matrix equation is linear, which can be solved for the eigenvalues and eigenvectors by an iterative solver.

However, when the materials are dispersive, the matrix eigenvalue equation is nonlinear because the coefficient in front of the mass matrix depends of the eigenvalue. A self-consistent method for solving this nonlinear eigenvalue equation is strongly dependent on the initial guess of the solution. To overcome this difficulty, we propose an alternative method using a polynomial factoring method to transform the nonlinear matrix eigenvalue equation into a linear matrix eigenvalue equation. This is based on the fact that the permittivity of the dispersive materials can be expressed by Drude model and (or) Lorentz models, which are rational polynomial functions of frequency. Numerical results show that the errors converge exponentially with the order of the SEM basis functions. The high efficiency and high accuracy properties exist for both isotropic and anisotropic materials. Our SEM solver consumes a CPU time about 80 times smaller than a commonly used software package, MPB, and the memory about 17 times less for nondispersive materials PCs.

In this presentation, we will show the efficiency and accuracy of the 2-D and 3-D spectral element method for the simulation of photonic crystals. We will further demonstrate the applications of this method to simulate the extraordinary light transmission and absorption by sub-wavelength metallic slits in periodic structures. It is expected that the spectral element method can be a highly valuable tool for design simulation of photonic crystals and other periodic structures.

Session 1A5a
Recent Advances in Numerical Methods for Maxwell's Equations

Staggered Grid Pseudo-spectral Time-domain Method for Light Scattering Analysis

Y. Ohmura and Y. Okamura
Graduate School of Engineering Science, Osaka University, Japan

Abstract— A pseudo-spectral time-domain (PSTD) method [1] has been widely used in a light scattering in a random medium because of its efficiency to compute electromagnetic fields in a large scale structure. However, artifacts appear when simulating a small particle scattering problem with the PSTD method. Particle size must be large enough compared to a cell size to reduce the appearance of the artifacts. In this paper, we propose a staggered grid PSTD (we call SPSTD) method to overcome this problem. Being different from the PSTD method reported so far, electric and magnetic fields are sampled on a Yee's lattice [2]. We found that the artifacts are caused by removing a Nyquist spatial frequency component in spatial differentiation and can be eliminated by using the staggered grid.

Figure 1 shows a configuration we consider in this paper to demonstrate the method proposed. The cell size is 0.1 μm×0.1 μm. S is an incident pulse plane wave with the center wavelength of 660 nm. P is a particle with the dimension of 0.1 μm×0.1 μm and the permittivity of $4\varepsilon_0$, where ε_0 is the permittivity in vacuum. Beranger's PML is used as an absorbing boundary. Fig. 2 shows an electric filed at the observation point D in Fig. 1 with the PSTD and SPSTD methods. An incident wave and a scattered wave appear at around 10 fs and 60 fs for both cases, respectively. An artifact appears at around 40 fs for the PSTD method; on the other hand it disappears for the SPSTD method. This artifact may cause a crucial error in simulating the wave propagation in a random medium. We are now working on simulating the wave propagation in a multi-scattering system.

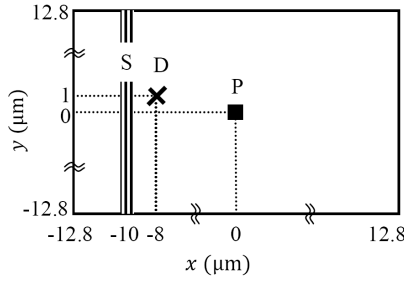

Figure 1: Configuration to demonstrate the SPSTD method.

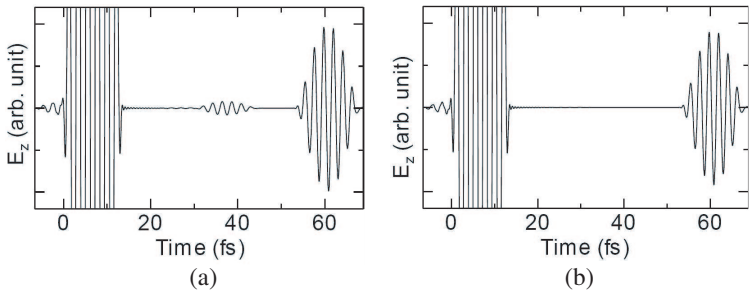

Figure 2: Electric field at point D. (a) PSTD and (b) SPSTD.

REFERENCES

1. Liu, Q. H., "The PSTD algorithm: A time-domain method requiring only two cells per wavelength," *Microwave and Optical Technology Letters*, Vol. 15, No. 3, 158–165, June 1997.
2. Kunz, K. S. and R. J. Luebbers, *The Finite Difference Time Domain Method for Electromagnetics*, CRC Press, 1993.

Application of Alternating Direction Implicit (ADI) Algorithm to Staggered-grid PSTD Modeling of Electromagnetic Waves

Zijian Liu[1], **Lanbo Liu**[1, 2], **and Benjamin Barrowes**[2]

[1]Department of Biomedical Engineering, University of Connecticut, Storrs, CT 06269-2037, USA
[2]USACE Engineering Research and Development Center
Cold Regions Research and Engineering Laboratory, Hanover, NH 03755, USA

Abstract— Due to stability constraints, small spatial discretization is strictly required for the explicit finite-difference time domain (FDTD) method when directly solving Maxwell's equations. By applying the fast Fourier transform and inverse transform to represent the spatial derivatives, the pseudo-spectral time-domain (PSTD) method has achieved a spatial gridding of only two points per wavelength while maintaining a high accuracy. However, similar to any explicit time marching algorithm, the computation speed same of the FDTD method is still limited by the Courant-Friedrich-Levy (CFL) condition, which sets an upper bound for the size of the time steps. Recently, some successful applications of the alternating-direction implicit (ADI) method have been developed with the FDTD method to efficiently ensure the stability and convergence of the calculation, even though the time step exceeds the maximum time step allowed under the CFL condition. We have developed the staggered-grid ADI/PSTD by extending current ADI/FDTD. We apply the staggered-grid approach in our algorithms by shifting the spatial derivatives halfway between 2 adjacent nodes and making the Nyquist wave number a non-zero pure real value of $-\pi/\Delta x$, thereby enhancing the stability of the differentiation operators. We discuss the staggered-grid ADI/PSTD method in detail and apply it to the simulation of a uniform space/half-space model. We then present an analysis of the results and discuss its possible advantages and further potential.

Analysis of Fractal Patch Antennas through Conformal FDTD Algorithms

B. Camps-Raga[1], **N. E. Islam**[1], **and S. Joe Yakura**[2]

[1]Department of Electrical and Computer Engineering, University of Missouri, Columbia, MO, USA
[2]Air Force Research Lab, Kirtland AFB, NM, USA

Abstract— Direct implementation of the finite-difference time-domain (FDTD) method with structured uniform grids, specifically for complex geometries with local discontinuities, can produce inaccurate field values in the vicinity of discontinuous stair-cased uniform grids [3]. One factor that contributes to this inaccuracy is the result of the staircase mesh generation, which is inherent in the structured FDTD method. These anomalies have been addressed through various compensation techniques. For example, creating finer grids can provide higher accuracy, however, at the cost of computer time and memory, especially at higher frequencies. Other techniques, such as sub-gridding and contour path finite-difference time-domain (CPFDTD) schemes have also been proposed [2, 4], but their implementation often requires an accurate interpolation of the field values from neighboring cells, and they are subject to instability problems. Additionally, static mesh refinement techniques are well suited only when structures involving Euclidean geometries and grids are chosen to conform to the outer boundaries. For fractals, since the structure may become highly resonant at higher frequencies, complex adaptive mesh refinement (AMR) techniques may be required [1].

A simpler approach, which accurately models perfect electric conductor (PEC) surfaces without sub- gridding, makes use of conformal finite-difference time-domain (CFDTD) algorithms with locally- conformal grids [7]. These techniques have been applied to improve temporal resolutions without requiring the finer grids. One specific advantage of our approach is seen in modeling of the feed in complex structures where the traditional coaxial feed typically requires a large number of time steps for stable numerical calculations.

In this paper, we apply the CFDTD algorithm, combined with improved feed and thin wire models [5, 6], to study the radiation of iterated designs of a Minkowski patch mounted on a $50 \times 50 \times 0.795$ mm dielectric substrate with a dielectric constant of 2.2. The good agreement between our simulation technique and the time-consuming sub-gridding technique suggests that the proposed approach is very efficient in studying the fractal antennas. Figs. 1(a) and (b), respectively, show the frequency response of a 30×30 mm patch (canonical structure) and the first Minkowski iteration (M1) derived from our technique. In the final presentation we will show results of the third iteration, including far-field parameters.

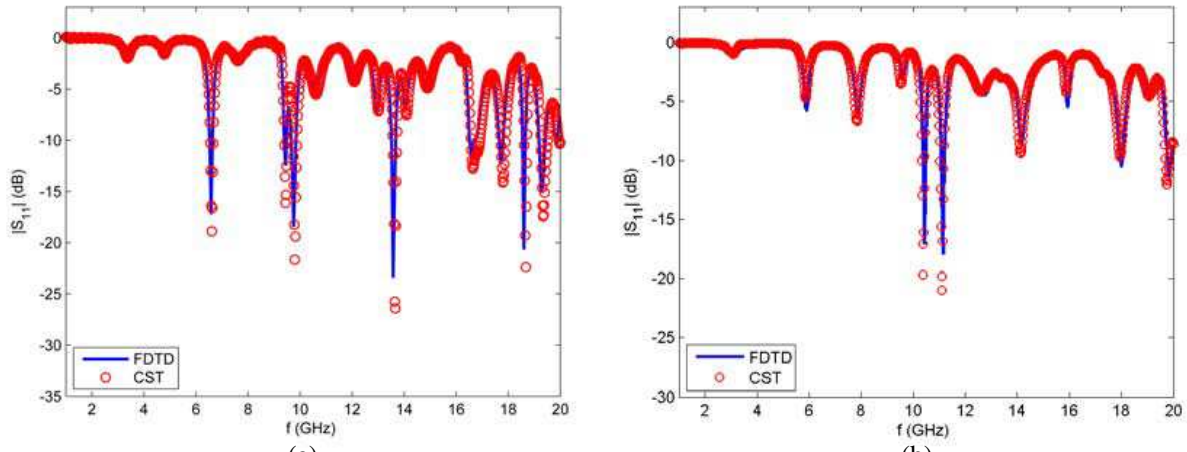

Figure 1: Return loss (dB) for two iterations of the Minkowski fractal patch. (a) Return loss for a square patch with a side length of 30 mm on a 50×50 mm, 0.795 mm thick dielectric substrate with $\epsilon_r = 2.2$. (b) Return loss for the M1 patch on a 50×50 mm, 0.795 mm thick dielectric substrate with $\epsilon_r = 2.2$.

REFERENCES

1. Dey, S. and R. Mittra, "A locally conformal finite-difference time-domain (fdtd) algorithm for modeling three-dimensional perfectly conducting objects," *IEEE Microwave and Guided Wave Letters*, Vol. 7, No. 9, 273–275, Sep. 1997.
2. Jurgens, T. G. and A. Taflove, "Three-dimensional contour fdtd modeling of scattering from single and multiple bodies," *IEEE Transactions on Antennas and Propagation*, Vol. 41, No. 12, 1703–1708, Dec. 1993.
3. Kim, I. S. and W. J. R. Hoefer, "A local mesh refinement algorithm for the time domain-finite difference method using maxwell's curl equations," *IEEE Transactions on Microwave Theory and Techniques*, Vol. 38, No. 6, 812–815, Jun. 1990.
4. Kunz, K. S. and L. Simpson, "A technique for increasing the resolution of finite-difference solutions of the maxwell equation," *IEEE Transactions on Electromagnetic Compatibility*, Vol. 23, No. 4, 419–422, Nov. 1981.
5. Makinen, R. M., J. S. Juntunen, and M. A. Kivikoski, "An improved thin-wire model for fdtd," *IEEE Transactions on Microwave Theory and Techniques*, Vol. 50, No. 5, 1245–1255, May 2002.
6. Maloney, J. G., K. L. Shlager, and G. S. Smith, "A simple fdtd model for transient excitation of antennas by transmission lines," *IEEE Transactions on Antennas and Propagation*, Vol. 42, No. 2, 289–292, Feb. 1994.
7. Mittra, R. and W. H. Yu, "A conformal fdtd algorithm for modeling perfectly conducting objects with curve-shaped surfaces and edges," *Microwave and Optical Technology Letters*, Vol. 27, No. 2, 136–138, 2000.

FEMGD: An Efficient Discontinuous Galerkin Approach on Hybrid Meshes for Time Domain Maxwell's Equations

Gary Cohen[1], **Xavier Ferrieres**[2], **and Bernard Pecqueux**[3]

[1]INRIA, Domaine de Voluceau, Rocquencourt, BP 105, 78153 Le Chesnay Cedex, France
[2]ONERA, France
[3]CEG, France

Abstract— Mixed spectral element methods are based on first-order formulations and mass-lumping techniques using Gauss-like quadrature formulas on hexahedra. These are proved very efficient tools to solve acoustic and elastic wave equations in terms of storage and computational time. They were extended to time domain Maxwell's equations by using discontinuous Galerkin methods (DGM) on hexahedra. The use of a mass-lumping technique provides a 3×3 block-diagonal mass matrix which is easy to invert and the mixed formulation ensures a local definition of the curl matrix, which induces a dramatical gain of storage [1].

Unfortunately, it is very difficult to mesh any geometry by hexahedra and, from a practical point of view, very few pure hexahedral mesh generators can be found on the market. In a first step, FEMGD used split tetrahedral meshes. However, this solution leads to highly distorted meshes which require to have three more degrees of freedom to get the same accuracy as a regular mesh. A palliative to this difficulty is to allow the mesh to use, besides hexahedra, elements of other shapes, i.e., tetrahedral, wedges and pyramids. Such a mesh is call hybrid mesh. This technique was integrated to FEMGD in a second step.

Tetrahedra are defined as in Hesthaven's approach and wedges are the product of Hesthaven's triangles [2] and 1D spectral elements based on Gauss-Lobatto rules. Pyramids use high-order rational function basis as described in [3]. The degrees of freedom of the different kinds of elements locations can correspond on the faces of the elements in order to define the jump terms in an easy way.

Moreover, local order definition and recursive local time-stepping methods adapted to our DG approach are included to speed-up the performance of our software. The first strategy enables to increase the minimum time-step and to reduce the number of degrees of freedom. The second one allows the use of much larger time-steps on most of the elements, which considerably reduces the computing time.

Numerical experiments will show the efficiency of our approach.

REFERENCES

1. Cohen, G., X. Ferrieres, and S. Pernet, "A spatial high-order hexahedral discontinuous galerkin method to solve maxwell equations in time domain," *J. of Comp. Phys.*, Vol. 217, 340–363, 2006.
2. Hesthaven, J. S. and T. Warburton, *Nodal Discontinuous Galerkin Methods*, Series: Texts in Applied Mathematics, Vol. 54, Springer-Verlag, 2008.
3. Bergot, M., G. Cohen, and M. Duruflé, "Higher-order finite elements for hybrid meshes using new nodal pyramidal elements," *J. of Sci. Comp.*, to appear.

A Maxwell-Vlasov Method Based on a New Discontinuous Galerkin Scheme: Application to High Power Microwave Source

L. Pebernet[1], **V. Mouysset**[1], **F. Rogier**[1], **X. Ferrieres**[1], **and R. Vezinet**[2]

[1]ONERA, France
[2]DGA, France

Abstract— This paper describes a Maxwell-Vlasov method based on a Discontinuous Galerkin scheme well- suited for solving Maxwells equations in time domain. The aim of this work consists in modeling weak density plasmas by using a Particle In Cell (PIC) method. In particular, we look for an efficient numerical method to simulate high power microwave sources generated by cavity ge- ometries. In this context, high order spatial approximation methods as DG scheme are good candidates to obtain accurate solutions for long time simulation. Indeed, this kind of method allows us to decrease significally numerical dispersive and dissipative errors, by taking into account a high degree of approximation. This point is very important for plasma applications, where the physical phenomena require large simulations in time in comparison with usual Maxwells problems.

In a first part of this paper, we describe the Discontinuous Galerkin approach chosen to solve the Maxwell equations and the advantages offered by this method in terms of accuracy, CPU time and memory storage. Some examples about cavity simulations are given to show the advantages of the method with respect to others such as FDTD for instance. Next, we present the introduction of a PIC model inside the method and the resulting modified system of equations. In particular, to guarantee the continuity equation $\Delta \cdot J = \frac{\partial \rho}{\partial t}$ or $\Delta \cdot E = \frac{\rho}{\varepsilon}$, a hyperbolic corrective formulation is studied. Then, the motion equations related to the particles and strategies to obtain a fast location of the particles inside the unstructured mesh and to evaluate fields and currents at these positions are presented. Concerning this second point, several interpolations between the locations of the fields and the particles in the mesh are examinated. Some comparisons between two approaches close to a Nearest Grid Point and a Cloud In Cell methods are given.

In a last part, some 3D examples concerning transmission lines and diodes configurations are presented to validate and to quantify the performance of our method. With these results, we also deal with the interest of a high order approximation in space to solve the Maxwell-Vlasov equations. Some comparisons on time CPU, memory storage and accuracy solutions are performed in order to illustrate this purpose for various meshes and orders of approximation in space.

Session 1A5b
Optical Properties of Semiconductors and Nanostructures 1

Interaction between BN Nanotubes and Molecules by Optical Spectra

Chunyi Zhi, **Yoshio Bando**, **Chengchun Tang**, **and Dmitri Golberg**
World Premier International Center for Materials Nanoarchitectonics (MANA)
National Institute for Materials Science, Namiki1-1, Tsukuba, Ibaraki 305-004, Japan

Abstract— We report optical spectrum investigations to interaction between BN nanotubes and organic molecules. Grams level of BN nanotubes were synthesized by a chemical vapor deposition method. To improve their dispersibility and processiblity, various molecules were used to interact with them and the interactions were investigated by optical spectra.

Poly (m-phenylenevinylene-co-(2,5-dioctoxy-p-phenylenevinylene)) (PmPV), a conjugated conducting polymer was used to wrap BN nanotubes, the wrapped nanotubes were found to be well dispersed in many organic solvents. The hybrid system was investigated by cathodoluminescence and UV-vis absorption, and the obvious peak shift observed indicates that the strong π-π interaction between BN nanotubes and PmPV molecules induces strong charge transfer between them. In the other experiment, a dye named perylene-3,4,9,10-tetracarboxylic acid tetrapotassium salt (PTAS) was used to functionalized BN nanotubes, similar optical spectrum change was observed. Based on these observation, it was proposed that BN nanotubes can interact with aromatic molecules intensively due to their localized π electronic structure and polarized surface. Another experiment actually proves this deduction, in which BN nanotubes have been functionalized with zinc phthalocyanines (ZnPc) and complementary steadystate absorption and fluorescence spectroscopies revealed prominent electronic transfer in these hybrids. Furthermore, upon photoexcitation of a ZnPc/BN nanotubes nanohybrid, in the presence of MV^{2+} and a hole-trap, the MV^{+} species accumulated in an aqueous solvent. The present findings may not only broaden the chemical horizon of smart BNNT utilization, but also stimulate research on these unique nanotubular materials in the photochemistry field.

The Color Emissions of ZnO Single Crystals Implanted by Different Ions

Y. N. Chen, **S. J. Xu**, **C. C. Zheng**, **J. Q. Ning**, **X. M. Dai**, **and C. C. Ling**
Department of Physics, The University of Hong Kong, Pokfulam Road, Hong Kong, China

Abstract— The color emissions of ZnO single crystals upon ion implantation and thermal annealing has been studied by means of low-temperature photoluminescence. The ZnO samples studied in the present work are pressured melt grown single crystals which shows negligible color emission before any treatment. After the nitrogen and copper implantation, a red broad emission peaked at 620 nm and the characteristic structured green emission were recorded respectively.

In both the unimplanted sample and the nitrogen implanted one, the characteristic structured green emission start to emerge after annealing treatment at 750°C and 900°C. As for the copper implanted sample, the characteristic structure green emission is suppressed after the annealing treatment at 500°C and 650°C, and the emission emerges again upon annealing treatment at 750°C and 900°C. We have also recorded the characteristic structured green emission in samples of ZnO grown by hydrothermal and flux method.

Our study shows that the structured green emission stems from one characteristic defect of ZnO. Its optical activity can be simply activated upon annealing above a certain temperature. The result also suggests that this structured green emission is copper related.

ZnO Tetrapods: Radiative Recombination and Exceptionally Long Exciton Lifetime

Kam Sing Wong
Department of Physics, Hong Kong University of Science and Technology
Clear Water Bay, Kowloon, Hong Kong, China

Abstract— In this work, we show that the material quality of ZnO tetrapods, indicated by the absence of defect emission and long PL lifetime, is strongly dependent on growth temperature. The tetrapods with exceptional optical properties, i.e., intense UV emission, no defect emission, and photoluminescence (PL) lifetime in the range of tens of nanoseconds at room temperature, could be grown within a very narrow temperature range only. A reduction in the PL lifetime and an increase in the defect emission are observed both for higher and lower growth temperatures. The obtained PL lifetime for optimal growth temperature is an order of magnitude higher than the best results achieved in epilayers and single crystals. Temperature dependence of the PL lifetime of high quality tetrapod samples indicates that the dominant recombination processes are radiative.

The absolute quantum efficiencies of ZnO tetrapod grown at different temperatures were also studied using integrating sphere. Our studies showed good correlation of absolute quantum efficiency and PL lifetime of ZnO tetrapods grow at different temperatures. The sample grown in optimal temperature exhibited the largest absolute quantum efficiency and longest PL decay lifetimes among all the samples. Samples with high quantum efficiencies having longer PL lifetimes are consistent with the theoretical predication. More details of our time-resolved PL exciton lifetime and absolute quantum efficiency measurements of assemble average and individual ZnO tetrapods will be presented in the conference.

ACKNOWLEDGMENT

The work is supported by Research Grants Council of Hong Kong (project number 604405).

Polarization of Emission from Self-assembled Quantum Dots and Its Application to the Optical Characterization of Structure

Weidong Sheng
Department of Physics, Fudan University, Shanghai 200433, China

Abstract— Optical anisotropy originates from the spatial anisotropy in the probability density of electrons. In natural atoms, the symmetry of the electron states conforms with that of the spherically shaped confining potential and the emission from the transitions between these states is isotropic. Semiconductor self-assembled quantum dots are three-dimensional nanostructures in which carriers are confined by the band gap difference between the dot and barrier materials or passivated surface. Unlike their counterparts in nature, these artificial atoms can take anisotropic shapes. The luminescence from these structures exhibits anisotropic linear polarization, believed to be caused by the structural anisotropy.

Here we report on a theoretical study of optical anisotropy in the emission from self-assembled quantum dots by using an empirical tight-binding method. The mechanisms how shape anisotropy and strain field lead to linearly polarized emission from interband transitions are identified. The anisotropic structure of quantum dots is shown to impose stronger confinement for the localized p-like orbitals aligning along the short axis, as a result, the valence-band electrons prefer to occupy the orbitals aligning along the long axis, which leads to stronger optical emission polarized along that direction. Due to very little difference in the dielectric constants between the quantum dot and barrier materials, we find that the local field or depolarization effect contribute only a small proportion of the overall linear polarization of the emission.

The polarization of intersubband transitions from the ground electronic state in elongated quantum dots is, however, shown to have a different origin from that of interband transitions. The multiband tight-binding approach presents a different picture of the electronic states in quantum dots from that by the single-band effective-mass approximation. In this picture, the linear polarization of intersubband transitions is a result of the symmetry of those minor components from the valence bands. While in the traditional single-band picture, the polarization of these transitions depends only on the symmetry of the dominant components from the conduction bands.

Incorporating the many-body effects, we further investigated linear polarization of the multiexciton emission from self-assembled quantum dots. The polarization of the primary interband transition is shown to have an almost linear dependence on the lateral aspect ratio of the structures, and more importantly, is insensitive to both the excitonic and random intermixing effects, which make it an appropriate tool for structure characterization. Our work is expected to help to establish a direct manifestation of geometrical anisotropy by optical spectroscopy.

ACKNOWLEDGMENT

This work is supported by the NSFC, the 973 projects of MOST of China, and the STCSM.

Session 1A6
Poster Session 1

Aspect on Vortices in Multicomponent Superconductors

Tao Xu and Yaqiong Han
Huazhong University of Science and Technology, Wuhan 430074, China

Abstract— To the present day the overwhelming majority of works on the theory of superconductivity have been devoted to single-gap superconductors. The vortices govern the electromagnetic response of type-II superconductors and have been extensively studied, both experimentally and theoretically. The possibility of superconductors with two superconducting order parameters was considered in the model of a superconductor with overlapping energy bands on the Fermi surface. Experimentally, two-gap superconductivity has been observed in the transition metals Nb, Ta, V, Nb-doped MgB_2. In an ordinary superconductor the Abrikosov vortices can carry only an integer number of magnetic flux quanta. But a two-gap superconductor allows several types of vortices, such as vortices carrying an arbitrary fraction of the magnetic flux quantum, which have no counterpart in ordinary one-gap superconductors. Here, we focus on the structure of vortices in multicomponent Ginzburg-Landau model.The topological structures of vortices are characterized by Brouwer degree and Hopf index. The London law in the two-gap superconductor is actually violated for the fractional vorticity of vortices. The vorticity is not a universal function of fundamental constants irrespective of microscopic details. Indeed, it depends on densities and the gradient of density. It is clearly that vortices are carrying an arbitrary fraction of magnetic flux quantum locally, which is different from the usually result of one-gap superconductor. The London law in two-gap superconductor is calculated for the case that each individual condensates is conserved or not conserved. Because the existence of background vorticity field, the vortices in nonconserved condensates is different from vortices in conserved condensates. The q term is originated from nonconserved wave function. We propose that a small angle neutron scattering measurement of the resulting magnetic field distribution may observe a lattice of fractional flux near to the critical field.

Discussion of Reverberation Chamber Uniformity Using Neural-network Method

Li Zhang[1], **Yong Qi**[2], **and Guizhen Lu**[1]

[1]Communication University of China, Beijing 100024, China
[2]China Radio International, Beijing 100040, China

Abstract— In this paper, a new method is applied to discuss the uniformity of a reverberation chamber. The calibration of reverberation chamber uniformity is a tedious task and the examination of field uniformity requires a great number of computing. Here a neural-network method is presented to analyze the uniformity. According to some of the evaluation data got by GEMS, the network is trained on both GRNN method and BP method, then the obtained neural network is used to predict the rest of data, which are used to analyze uniformity.

Power Frequency Magnetic Field Stimulates Ca^{2+} Related Reorganizations in Cytoskeleton Microfilaments of Human Smnion FL Cells

Ruohong Xia
East China Normal University, Shanghai, China

Abstract— To investigate how cytoskeleton-EGFR signal pathway responds to magnetic field exposure, our present research reveals the effects of that. After 0.2 mT power frequency magnetic field (PFMF, 50 Hz) exposure which has shown effects similar to that of EGF stimulation (1) new filopodias and lamellipodias grow at the cell periphery (2) we observed for the first time that the intracellular $[Ca^{2+}]_i$ evidently increased which was blocked by decreasing the $[Ca^{2+}]_o$ as well as by cell membrane Ca^{2+} channel inhibitor NIF (3) the microfilament reorganization was also greatly prevented by an associated treatment of the inhibitor of EGFR tyrosine kinase PD153035 and decreasing $[Ca^{2+}]_o$ prior exposing the cells to the field (4) a downgrading tendency of cytoskeleton F-actin population in the cell after exposure, similar to the effect of EGF was detected. These results suggest that the PFMF exposure may disrupt the cytoskeleton reorganization functions defined by the EGFR-cytoskeleton signal pathway, and the extracellular Ca^{2+} plays a significant role in the disruption.

Application of EH4 in the 102 Ore Belt in Shihu Gold Deposit of Western Hebei, China

Xiaoming Fu[1], **Tagen Dai**[1], **and Chaozhuang Xi**[2]

[1]School of Geosciences and Environmental Engineering, Central South University
Changsha, Hunan 410083, China
[2]Hunan Jinxin Gold Group Co., Ltd., Changsha, Hunan 410015, China

Abstract— Shihu gold deposit is under the administrative divisions of Chenzhuang town Lingshou Country Hebei Province. The authors have reached the conclusion that the gold ore bearing horizon is Tuanpokou Formation of Archean Fuping Goup, the Mapeng rock mass is I-type granite. EH4 is widely used in solid minerals, especially in finding concealed ore deposit. In this paper, the author adopted EH4 method to make a synthetic study on 102 ore belt in Shihu gold deposit in Hebei. The result showed that the geophysical method was quite useful in the exploration of concealed ore deposit.

Propogation of an Electromagnetic Beam at the Interface of Isotropic Medium and Gyroelectric Medium

Qi Liu, Hui Huang, and Yinde Zhang
School of Electrical Engineering, Beijing Jiaotong University, Beijing 100044, China

Abstract— A detailed study on the reflection and transmission characteristics of an electromagnetic beam propogating at the interface of an isotropic medium and a gyroelectric medium in Voigt configuration is presented, for both TM and TE waves. We derived the reflection coefficient and transmission coefficient, respectively. Using the stationary phase approach, analytic expressions for lateral displacements of the reflected and transmitted waves from a gyroelectric medium are obtained, and we also give examples for both cases. It is found that the lateral displacements for TM and TE waves have different characteristics. Only the TM mode is affected by the gyrotropy.

Surface Waves at the Interface between Isotropic Medium and Gyroelectric Medium

Bo Huang and Hui Huang
School of Electrical Engineering, Beijing Jiaotong University, Beijing 100044, China

Abstract— A detailed study on surface TM waves at the interface between an isotropic medium and a gyroelectric medium in Voigt configuration is presented. The conditions for the existence of surface modes are derived, showing that the existence of the surface waves is determined by the parameters of the media and the working frequency. The paper also gives the group velocity and the Poyting vector along the propagating direction.

On the Vision of Depth

S. L. Vesely[1] and A. A. Vesely[2]

[1]I.T.B. — C.N.R., Italy
[2]Via L. Anelli 13, Milano, Italy

Abstract— 2-D reconstruction algorithms have been developed for high resolution X-band imaging radars, which scan target scenes by means of encoded w-b pulses, and for tomographs. Now the trend is toward building 3-D systems. In order to render spatial scenes on a screen there are already 3-D computer graphics techniques, which adopt realistic illumination conditions to give the illusion of depth. However, as depth sensation is effectively elicited under natural lightning conditions, we are concerned on how depth information is normally obtained, and how it could be encoded so as to be rendered by 3-D imaging systems [1].

Often, to reproduce stereographic imagery of geomorphologic structures, a viewer uses two slightly different perspectives. Either two photographs of the same landscape, but taken with different angles, are viewed at the same time by looking into a stereoscope; or alternatively the images are projected on the same plane support and then separated by means of anaglyphic filters. Thus, although either image taken separately represents a flat perspective of the scenery, once both are taken with matched perspectives, the binocular vision conveys the illusion of an intervening empty space between raised areas and drop-offs. Here the word "illusion" means that there was plenty of clean air to stare at in the place where the photographs were taken, but that it could not have been rendered by single-picture photographic techniques. It is common knowledge that, because of the arrangement of the eyes, the parallax shown either by the true landscape or by the coupled perspective pictures, gets interpreted as third dimension. If parallax is taken as the basic attribute of the genuine as well as the fake depth, a flying bee should under natural lightening conditions often exhibit problems in evaluating distances, if its compound eyes dont even focus the stereoscopic pictures like we do [2, 3].

As an alternative to the assumptions above, the more recently discovered holographic techniques seem to point out that depth may be encoded in the signal and decoded by the eyes upon receiving it, quite independently of its interpretation. Correctly reconstructed holograms allow humans to interpret the sceneries and perceive their depth, because of the parallax effect, which comes about by looking at one holographic plate and moving the head sideways. The holographic methods to obtain depth encoding are highly sophisticated, and do not make use of natural lightening [4]. Therefore they could be interpreted differently by the bee in our example. However, there is depth encoding in natural light too, as the amount of blur in photographs of regions extended frontward or backward generally depends on the depth of field.

On the basis of the bees eyes structure and of human perception of the hidden image stereograms, we suggest that the repetition of quasi periodical patterns in the focal plane of a lens, or else the telescopic view of a scene through the hemispherically disposed ommatidia of a compound eye may form a space-extended image upon passing to the stigmatic picture. Quasi periodical patterns encode depth information also if they are too big to be seen through a converging lens.

REFERENCES

1. Lee, L. P. and R. Szema, "Inspirations from biological optics for advanced photonic systems," *Science*, Vol. 310, 1148–1150, 2005.
2. Altenburg, E., "A working model for demonstrating the mosaic theory of the compound eye," *J. Exp. Biol.*, Vol. 4, 38–45, 1926.
3. Tanida, J., "Artificial compound-eye camera and its application to visual information processing," *Conference on Lasers and Electro-Optics*, Baltimore, U.S., CtuR1, May 2007.
4. Lunazzi, J. J. and N. I. Rivera, "Pseudoscopic imaging in a double diffraction process with a slit," *Opt. Express*, Vol. 10, No. 23, 1368–1373, 2002.

Modeling of Electromagnetic Coupling in Finite Arrays Using Scale-changing Technique

Aamir Rashid[1, 2] **and Hervé Aubert**[1, 2]

[1]CNRS, LAAS, 7 avenue du colonel Roche, F-31077 Toulouse, France
[2]UPS, INSA, INP, ISAE, LAAS, University of Toulouse, F-31077 Toulouse, France

Abstract— Large planar structures containing complex geometric patterns are increasingly being used in radiating and scattering applications, e.g., FSS, phased-arrays and reflectarrays. Though of finite extent, these structures are often analyzed under infinite periodicity assumption to avoid prohibitive memory and processing requirements. An original technique called the *Scale Changing Technique* (SCT) has been proposed and applied for whole-scale modeling of complex planar structures comprised of cellular geometries. In this technique the planar geometry of the structure is partitioned into mutiple domains bounded by artifical bounday conditions and defined at multiple scale-levels. At a given scale-level only the electromagnetic coupling within the elements of a domain is considered and not between the sister domains. At a higher scale-level several of these sister-domains are grouped into a parent domain incarporating the mutual coupling between them [1]. This process continues until at the highest level we have only one parent domain that spans the complete array plane. Therefore in SCT this multi-scale structure is seen as the cascade of *Scale-Changing Networks*, each network modeling the electromagnetic coupling between two successive scale levels [2].

In this communication, the modeling of mutual coupling by SCT has been demonstrated. In the first step, the electromagnetic coupling between two half-wave dipole scattering strips is characterized as a function of the separation between them (Fig. 1(a)). The results are compared to that of simple superposition of radiation from each element in the absence of mutual coupling. In the second step the scattering from a square array of 16 dipole elements is considered under normal plane-wave incidence. Here again the results of costructed radiation pattern from array factor calculations is given as a comparison case of the absence of mutual coupling (Fig. 1(b)). In addition the results from the Method of Moments are plotted. The good agreement between the results of the two techniques validates the point that SCT characterizes the mutual coupling accurately.

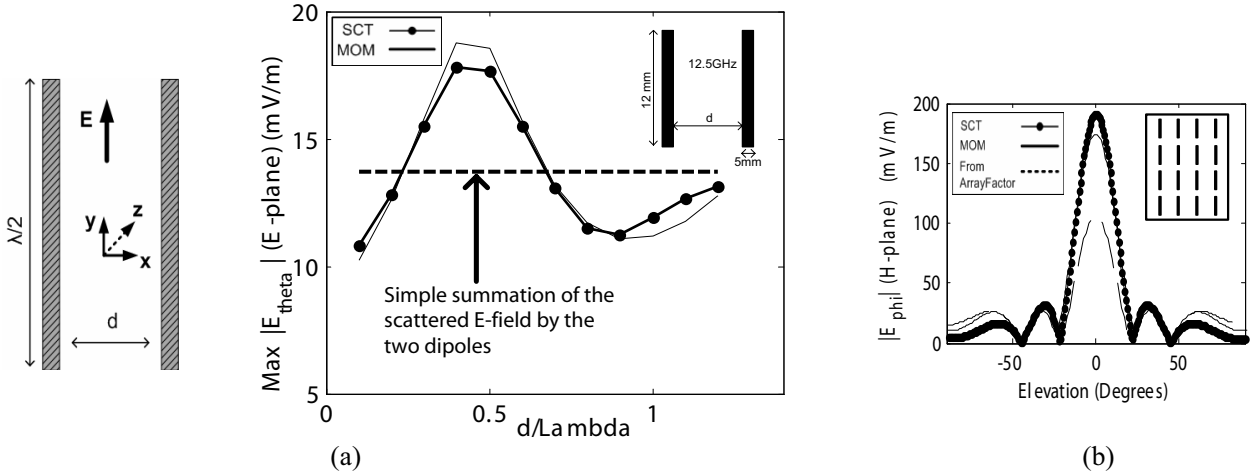

Figure 1: (a) Scattering from two half-wave dipoles separated by 'd' under normal incidence at 12.5 GHz. Maximum E-field magnitude is considered in the normal direction, i.e., theta = 0° in E-plane (phi = 90°). (b) H-plane radiation pattern of a 16-elements square array of the same dipole elements (as in (a)). Normal plane-wave incidence is considered at 12.5 GHz.

REFERENCES

1. Rashid, A., H. Aubert, and H. Legay, "Modeling of finite and non-uniform patch arrays using scale-changing technique," *IEEE International Symposium on Antennas and Propagation*, Charleston, South Carolina, USA, June 5–12, 2009.

2. Aubert, H., "The concept of scale-changing network in global electromagnetic simulation of complex structures," *Progress In Electromagnetics Research B*, Vol. 16, 127–154, 2009.

Analysis of Coupled Nonuniform Transmission Lines as an Initial Value Problem

Mohammad Khalaj-Amirhosseini
College of Electrical Engineering, Iran University of Science and Technology, Tehran, Iran

Abstract— Coupled Nonuniform Transmission Lines (CNTLs) are widely used in RF and microwave circuits. The differential equations describing CNTLs have non-constant matrices, so except for a few special cases no analytical solution exists for them. Some methods such as decoupling, cascading many short sections, finite difference, Taylor's series expansion, Fourier series expansion, the equivalent sources method and the method of moments have been introduced to analyze CNTLs. In some of these methods such as finite difference and Taylor's series expansion, it is necessary to use an optimization process to satisfy terminal conditions. This is due to the nature of terminal conditions in CNTLs, which are two-point type. In the other word, the analysis of CNTLs is a Boundary Value Problem (BVP) naturally. To overcome needing optimization process, we propose an approach to analyze CNTLs as several Initial Value Problems (IVPs), in this paper. First, the necessary IVPs are defined. Then the solution of the main BVP is obtained as the linear summation of the solutions obtained from IVPs. Finally, the validity of the introduced approach is studied using an example.

Figure 1 shows a typical CNTL consisting of N lines with length d and with arbitrary terminal loads of $Z_{S,n}(\omega)$ and $Z_{L,n}(\omega)$, in which $n = 1, 2, \ldots, N$. In this paper, the analysis of CNTLs are presented as an IVP. For this purpose, we define the following $2N$ boundary conditions instead of conventional boundary value conditions.

$$\begin{cases} \mathbf{I}(0) = 0 \\ \mathbf{V}(0) = [\ 0 \quad 0 \quad \cdots \quad V_n(0) = 1 \quad \cdots \quad 0\ ] \end{cases} \tag{1}$$

$$\begin{cases} \mathbf{V}(0) = 0 \\ \mathbf{I}(0) = [\ 0 \quad 0 \quad \cdots \quad I_n(0) = 1/Z_0 \quad \cdots \quad 0\ ] \end{cases} \tag{2}$$

where $n = 1, 2, \ldots, N$ and Z_0 is an arbitrary impedance value. The voltage and currents determined from the IVPs are denoted by $\left\{\mathbf{V}_V^{(n)}(z)\,,\,\mathbf{I}_V^{(n)}(z)\right\}$ and $\left\{\mathbf{V}_I^{(n)}(z)\,,\,\mathbf{I}_I^{(n)}(z)\right\}$, respectively. Because of the linearity of differential equations, we can use the superposition principal to write the voltage and current of CNTLs as follows

$$\begin{bmatrix} \mathbf{V}(z) \\ \mathbf{I}(z) \end{bmatrix} = \begin{bmatrix} \mathbf{T}_{VV}(z) & \mathbf{T}_{VI}(z) \\ \mathbf{T}_{IV}(z) & \mathbf{T}_{II}(z) \end{bmatrix} \begin{bmatrix} \boldsymbol{\alpha}_V \\ \boldsymbol{\alpha}_I \end{bmatrix} \tag{3}$$

where $\boldsymbol{\alpha}_V = [\ \alpha_V^{(1)} \quad \cdots \quad \alpha_V^{(N)}\ ]^T$ and $\boldsymbol{\alpha}_I = [\ \alpha_I^{(1)} \quad \cdots \quad \alpha_I^{(N)}\ ]^T$ are the vectors of coefficients and the dimension of four submatrices is $N \times N$. The vectors of coefficients can be obtained using (3) in the conventional boundary conditions as follows

$$\begin{bmatrix} \mathbf{T}_{VV}(0) + \mathbf{Z}_S\mathbf{T}_{IV}(0) & \mathbf{T}_{VI}(0) + \mathbf{Z}_S\mathbf{T}_{II}(0) \\ \mathbf{T}_{VV}(d) - \mathbf{Z}_L\mathbf{T}_{IV}(d) & \mathbf{T}_{VI}(d) - \mathbf{Z}_L\mathbf{T}_{II}(d) \end{bmatrix} \begin{bmatrix} \boldsymbol{\alpha}_V \\ \boldsymbol{\alpha}_I \end{bmatrix} = \begin{bmatrix} \mathbf{V}_S \\ \mathbf{0} \end{bmatrix} \tag{4}$$

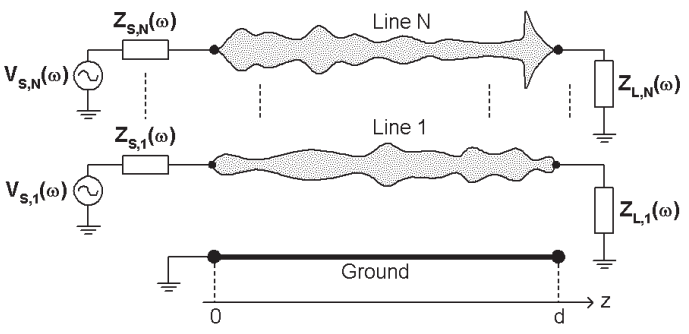

Figure 1: A typical coupled nonuniform transmission line.

The $ABCD$ matrix that relates the voltage and current vectors at $z = 0$ to those at $z = d$ can be obtained as follows

$$\begin{bmatrix} \mathbf{A} & \mathbf{B} \\ \mathbf{C} & \mathbf{D} \end{bmatrix} = \begin{bmatrix} \mathbf{T}_{VV}(0) & \mathbf{T}_{VI}(0) \\ \mathbf{T}_{IV}(0) & \mathbf{T}_{II}(0) \end{bmatrix} \begin{bmatrix} \mathbf{T}_{VV}(d) & \mathbf{T}_{VI}(d) \\ \mathbf{T}_{IV}(d) & \mathbf{T}_{II}(d) \end{bmatrix}^{-1} \tag{5}$$

Finally, some examples are presented to verify the validity of the introduced approach.

Synthesis about Analytical Approaches for Calculating the Magnetic Field Produced by Permanent Magnets of Various Topologies

R. Ravaud and G. Lemarquand
Laboratoire d'Acoustique de l'Universite du Maine, UMR CNRS 6613, Le Mans, France

Abstract— This paper discusses the way of choosing an analytical model for calculating the magnetic field produced by permanent magnets of various topologies.

Many studies have led authors to calculate the magnetic field produced by permanent magnets by using 1D, 2D or 3D analytical models, always based on the Maxwell's equations. Strictly speaking, authors generally use the coulombian model [1], the amperian current model [2, 3], the scalar potential, the vector potential, the Green's function or the Maxwell tensor [4] for calculating the magnetic field created by permanent magnets or currents in massive disks or in coils.

For parallelepipedic magnets with uniform polarizations, the magnetic field can be determined analytically by using the coulombian model, the amperian current model or the magnetic scalar and vector potentials. All these methods lead authors to determine the three magnetic field components in a fully analytical form. Indeed, the analytical expression of the magnetic field produced by parallelepipedic magnets does not use any special functions. For parallelepipedic coils, by using the analogy between the coulombian model and the amperian current model, the magnetic field can also be determined in a fully analytical form. However, the loops are replaced by fictitious current density layers.

For arc-shaped permanent magnets, it is more difficult to guess what model to use for calculating the three magnetic field components. For example, the amperian current model of a magnet is more suitable than the coulombian model for calculating the magnetic field created by radially magnetized arc-shaped permanent magnets. Conversely, the coulombian model is more suitable than the amperian current model for calculating the magnetic field produced by arc-shaped permanent magnets with orthoradial polarizations. The radial currents flowing in massive disks generate a magnetic field that is often modeled with the Biot-Savart Law. Such an approach allows us to use both elliptic integrals and a numerical term for calculating the three magnetic field components. However, by using the analogy between the Maxwell's equations, it is more interesting to use the coulombian model that gives fully analytical expressions of the magnetic field created by radial currents flowing in massive disks.

In short, all these studies lead us to conclude that some simple rules allow us to guess what model is the most appropriate for calculating the magnetic field produced either by permanent magnets or by currents. This paper makes a review of the main configurations studied in the literature and gives indications about how to use an analytical model for calculating the magnetic field created by charge or current distributions.

REFERENCES

1. Ravaud, R., G. Lemarquand, V. Lemarquand, and C. Depollier, "Discussion about the analytical calculation of the magnetic field created by permanent magnets," *Progress In Electromagnetics Research B*, Vol. 11, 281–297, 2009.
2. Akyel, C., S. I. Babic, and M. M. Mahmoudi, "Mutual inductance calculation for non-coaxial circular air coils with parallel axes," *Progress In Electromagnetics Research*, PIER 91, 287–301, 2009.
3. Ravaud, R. and G. Lemarquand, "Comparison of the coulombian and amperian current models for calculating the magnetic field produced by arc-shaped permanent magnets radially magnetized," *Progress In Electromagnetics Research*, PIER 95, 2009.
4. Varga, E. and A. Beyer, "Magnetic field of a uniformly magnetized hollow cylinder," *IEEE Trans. Magn.*, Vol. 34, No. 3, 613–618, 1998.

New CAD Method for Microwave Filter Design Based on Numerical Solution of Laplace Equation in the Structure

Ali Khoshniat and Bedri A. Cetiner
Electrical and Computer Engineering Department, Utah State University, USA

Abstract— Microstrip filters are one of the passive elements used in RF circuits. Utilizing tables, plots and formulas are the first steps in designing a filter. The structure should be simulated and optimized by full-wave analyses to get an accurate result. Full-wave simulations and iterative optimizations are time consuming. In this paper, we provide a new CAD method for filter design which yields an accurate design in a time effective manner. Our numerical method relies on solving the Laplace equation in the structure. The code is able to find the coupling as well as optimizing the geometry in order to get desired coupling which is needed to implement a filter. This method, in particular, is useful for band pass filters using coupled lines.

In this method, each section of the filter is considered as a coupler and the coupling is indicated by the frequency response of the design. The width of lines and the gap between them are two design parameters which determine the desired coupling. Coupling is calculated by even and odd excitations of the lines and solving the Laplace equation to find the electrical potential distribution in the cross section of a single coupler shown in Fig. 1. After converging the electric potential of each point to its final value, electric fields, capacitances, and impedances, respectively, are calculated. The optimization method used in this code is able to change those parameters for required coupling. Effective permittivity, which is a critical parameter in determining electrical length of each coupler, is found by the ratio of two calculations: by the total capacitance with a dielectric substrate and with an air substrate. To show the accuracy of this method, a sample of fifth order band pass Chebyshev filter is designed using our code with 10% bandwidth at 1 GHz microstrip hairpin structure composed of folded coupled lines. The result of the simulation by HFSS agrees with the desired frequency response displayed in Fig. 2.

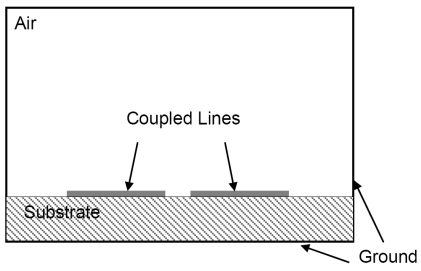

Figure 1: Cross section of two coupled lines.

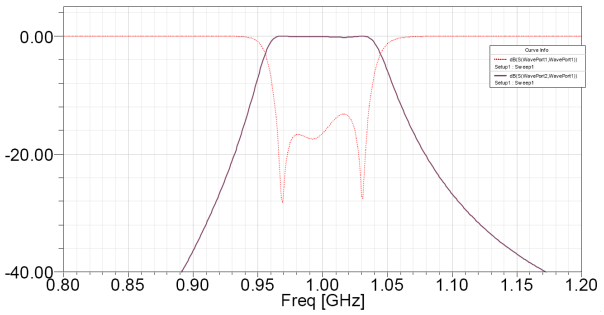

Figure 2: Frequency Response of simulated filter. (S_{11} (dB) - - - S_{21} (dB) ——).

Film's Forming Materials for THz Spectral Range Purposes

E. N. Kotlikov[1], **V. A. Ivanov**[2], **and A. N. Tropin**[2]

[1]St. Petersburg's State University of Aerospace Instrumentation, Russia
[2]Scientific Research Institute "Giricond", St. Petersburg, Russia

Abstract— At the presented work we inform about results of research of optical properties PbTe, ZnSe, ZnS, BaF_2 and PbF_2 thin films. These materials can be used for manufacturing thin film multilayer interference systems working in the middle and far infrared. Optical properties in our understanding are spectral dependences of refractive index and extinction coefficient of layers.

Films with thicknesses 3–7 microns were received by thermal vacuum deposition on single-crystalline silicon substrates. Initial substances were evaporated from molybdenum hull in vacuum value $3 \cdot 10^{-5}$ Pa. Refractive index and extinction coefficient dispersion in 1.5–150 microns spectral range (2–200 THz) were determined by method based on analysis of the transmission and reflection interference spectra. First of all for definition of substrate optical constants spectra of reflection and transmission of silicon wafer were analyzed. After that spectra of films on a substrate with known optical properties were investigated. Spectra of reflection and transmission were measured on Bruker FT-IR Spectrometer.

Films of PbTe under consideration do not possess appreciable absorption bands in the investigated spectral range. While, other investigated films have intensive absorption bands in the 25–100 microns region. Comparison with the results received for solid structures in some handbooks shows that usually for films take place decrease the refractive index and substantial growth of the extinction coefficient. As the reason for that the impurity presence in films caused by interaction of evaporated substance with a material of the evaporator and residual gases in the chamber. Also a deviation from stoichiometry at deposition and film's porosity are the cause of these side effects.

With using of the investigated materials the "solar blind" filter for 1.0–50 microns spectral range on the single-crystalline silicon substrate was designed and made. The received transmittance of the made filter is in accord with the calculation spectra.

Low Profile and Low Cost Efficient Linear Array Antenna Based Substrate Integrated Waveguide Technology for Millimeter-wave Sensing Applications

Wael M. Abdel Wahab, Safieddin Safavi-Naeini, and Dan Busuioc
Department of Electrical & Computer Engineering, University of Waterloo, Ontario, Canada

Abstract— Recently, developing the communication systems at frequencies in the millimeter-wave region (30–300 GHz) attracts a lot of interests. Such development allows for compact system components which are critical for mobile and portable systems. Antennas like other parts of wireless communication systems have to be devolved for high frequency applications. Dielectric Resonator Antennas (DRAs) have been shown to radiate efficiently at high frequency with wider bandwidth, which makes them more attractive for wireless applications operating at millimeter wave frequencies. They exhibit less conductor loss (high radiation efficiency), and larger bandwidth than microstrip patch antennas (MPAs) which suffer from power loss (conductors and dielectric), and fabrication difficulties when reduced to the sizes necessary to operate at this frequency band. Further DRAs have a lower profile than reflector and horn antennas, and they are compact and easy to fabricate.

Many different excitation methods have been used to couple energy to DRAs. This means that the DRAs are compatible with most of the feeding structures for different applications. Some of these feeding methods add large reactive components at high frequency, which degrades performance. As well, drilling holes in DRAs is sometimes difficult. Image guide lines and rectangular waveguides eliminates the conductor loss that caused by feeding structures, but they are bulky and not compatible with Monolithic Microwave Integrated Circuits (MMIC) technology and low profile applications. Other excitation compatible with MMIC, such as printed microstrip line, microstrip line coupled to a narrow slot or a narrow slot excited by coplanar waveguide, produce high losses undesirable back radiation. Moreover, the DRAs radiation pattern is affected by parasitic radiation of the feeding microstrip at high frequencies which degrades the antenna radiation efficiency. The SIW is a high Q-structure since it is a good compromise between an air-filled rectangular waveguide and a microstrip line. Accordingly, it can minimize the radiation loss and parasitic radiation and provides low cost, compactness, and low profile at this high frequency range.

In this paper, a low complexity, low cost, and low profile structure based on waveguide technology, Substrate Integrated Waveguide (SIW) is proposed as a novel feeding scheme to rectangular dielectric resonator antenna (RDRA) at millimeter wave frequency band in order to enhance the antenna radiation efficiency. Simulation results for both single RDRA element and linear array antenna fed by SIW at millimeter wave frequency have been presented. A 1×8 linear array antenna fed by SIW in a corporate feed layout is in planar form presented. The simulated results show an impedance bandwidth ($S_{11} \leq -10$ dB.) of 800 MHz around center frequency 35 GHz. The simulated result shows an efficiency of 84% within the operating bandwidth which ensure that the SIW is an effective feeding method for DRA at millimeter wave frequency band compared to other planar feeding methods. In addition, it is simple, low cost, and easy to fabricate using standard printed circuit board (PCB) and low profile. The array antenna aperture is almost 5×5 cm which is quite small and critical for portable systems. The developed planar antenna can be easily integrated with other RF circuits on the same substrate using a suitable transition and can be fabricated using printed circuit Board (PCB) technology at no cost.

Mutual Coupling Mitigation Using New Feeding Scheme Suitable for 2D Planar Antenna Array at Millimeter-wave Band

Wael M. Abdel Wahab, Safieddin Safavi-Naeini, and Dan Busuioc
Department of Electrical & Computer Engineering, University of Waterloo, Ontario, Canada

Abstract— Many applications such as satellite communication systems require multi-band, multi-beam antenna arrays to achieve optimal performance in terms of data transmission capacity. The choice of an optimal array layout is determined by many factors such as gain, bandwidth, efficient, and cost. Choosing the feeding scheme to form antenna array architecture is one of the most crucial aspects especially at millimeter-wave band. In the recent years, planar antennas such as microstrip patches become increasingly popular used as radiating elements for phased array. However, there is a problem that efficiency of the microstrip array antenna with a large aperture is degraded due to feeding lines losses. The common planar feeding schemes used in antenna arrays are microstrip lines and coplanar waveguide. Their losses are considerable, radiate, and form a source of coupling that affect the overall antenna radiation.

One major concern in designing wideband, wide scanning angle phased arrays is scan blindness caused by mutual coupling (MC) between radiating elements (or feeding lines). Recently substrate integrated waveguide (SIW), which is anticipated for future design and development of low cost millimeter wave RF circuits using conventional printed circuit board (PCB) technology, can provide a compact structure, and low profile feeding structure. Furthermore, it is low profile, compact structure, and a high Q-structure; it is a good compromise between air field rectangular waveguide and microstrip line. Accordingly, it can minimize radiation loss and parasitic radiation. Antennas based on SIWs with operation frequency range up to Ka-band have been realized using standard PCB processes. In this paper, the SIW concept is utilized as a new novel feeding mechanism to planar antennas to minimize the inter-elements mutual coupling (MC) for millimeter wave applications. In this paper, a new model is proposed to characterize mutual coupling and study the impact of changing the inter-element space between two antenna elements (dielectric resonator antenna DRA) fed by SIW structure at 35 GHz on both gain and bandwidth. The simulated results using HFSS for the proposed model show that the mutual coupling is less than -15 dB for minimum separation $\frac{\lambda_g}{2} \approx 3.20$ mm. This coupling is caused by space wave coupling rather than feed line coupling (substrate).

Wave Propagation in Corrugated Circular Grating

F. Emami
Optoelectronic Research Center
Electronic Department, Shiraz University of Technology, Shiraz, Iran

Abstract— We discuss the wave propagation in a hollow circular media, when the outer layer of the structure has a corrugated refractive index, as shown in Fig. 1. The grating period Λ is determined by medium wavelength and the order of Bragg diffraction [1]. Using the coupled mode theory (CMT) for this periodic structure [2], we can find the field distribution through the different layers of this structure, which is called *hollow circular dielectric waveguide* (HCDW), under the single mode condition. There is an energy interchange between the forward and backward electric fields with the aid of coupling coefficient. In general the coupling coefficient may be complex [3], (for example in gain guided lasers) but in our work it is considered as a real variable [4]. For this case, we have a stop band in the propagation of the waves (related to the coupling strength), and hence the medium can not support the propagating waves in this band. Using the CMT, we calculated the amount and dependencies of this parameter to the guide shapes and materials such as: Active region density (Fig. 2), waveguide and cladding layer indices (Fig. 3 and Fig. 4 respectively). In our model a five layers circular waveguide is considered. It is shown that there is a forward relation between coupling and the gratings height (Fig. 5), such as a slab corrugated waveguide [4]. The proposed structure is useful to design another group of distributed feedback (DFB) laser diodes [5]. We calculated the main mode field distribution through the different layers of the proposed structure (Fig. 6). In a HCDW there is an internal contact for $r = a$, and an external contact for $r = c > b$ (not shown in the Fig. 1). After the stimulated emission, we have the output light from the end facets of the diode. From the results of Fig. 2, we found that there is a small decrease in the amount of the coupling strength in the

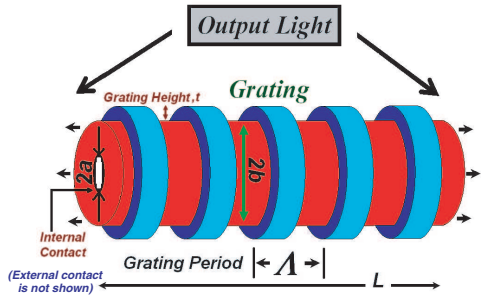

Figure 1: Schematic of a HCDW.

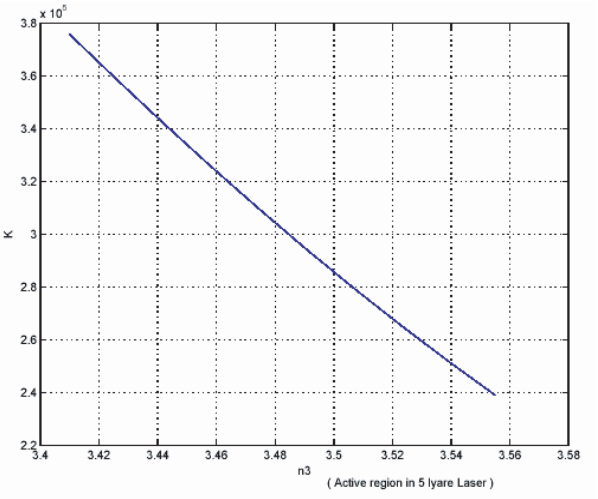

Figure 2: Coupling variations versus active region index.

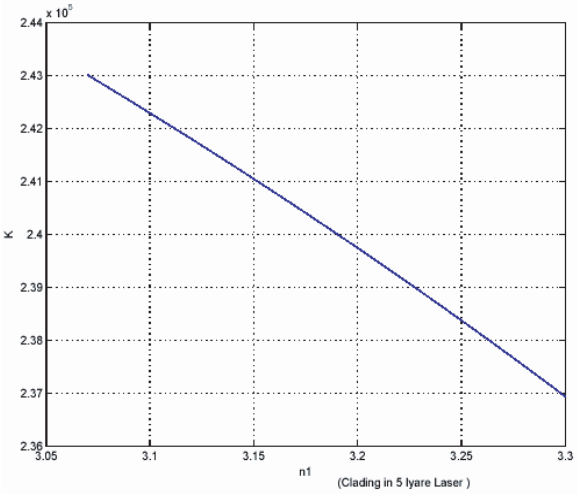

Figure 3: Coupling variations versus waveguide region index.

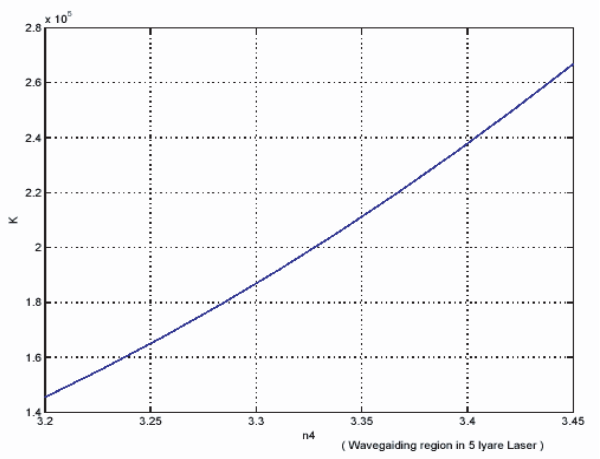

Figure 4: Coupling variations versus cladding region index.

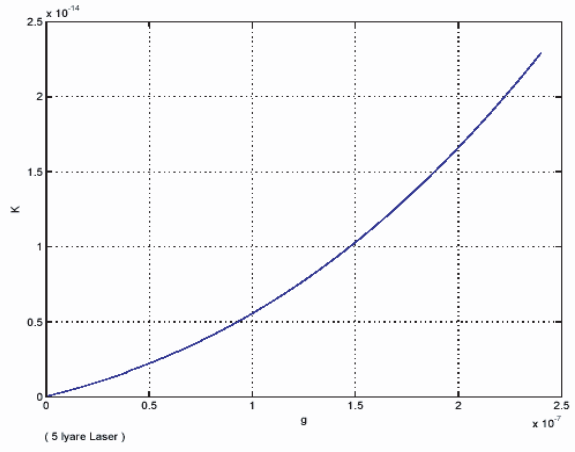

Figure 5: Coupling strength versus grating height.

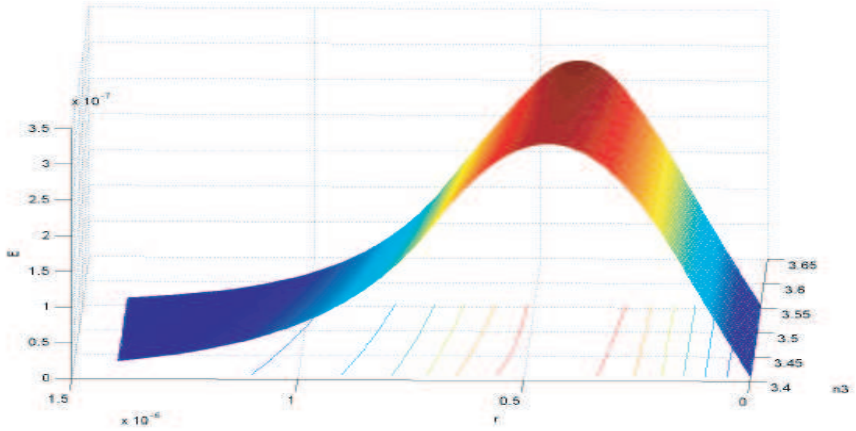

Figure 6: Main mode field distribution through the different layers of a HCDW, considering the active layer index variations (due to current injection).

active layer due to carrier injection, so we should consider this effect when we want to compute the threshold behavior of the laser. In fact, there is a small increase in the threshold current of the laser. Using a few HCDW, we can have an array with high laser power. Because of the circular nature of the proposed structure, data transforming to the optical fibers are easier.

REFERENCES

1. Agrawal, G. P. and N. K. Dutta, *Semiconductor Lasers*, 2nd Edition, Van Nostrand Reinhold, New York, 1993.
2. Morthier, G. and P. Vankvikelberge, *Handbook of Distributed Feedback Laser Diodes*, Artech House, Boston, 1997.
3. Wang, J. Y. and M. Cada, "Analysis and optimum design of distributed feedback lasers using coupled-power theory," *IEEE J. Quantum Electron.*, Vol. 36, 52–58, Jan. 2000.
4. Emami, F., "Effect of parameter variations of a corrugated periodic waveguide," *The Int. Multi-Conf. of Engineers and Computer Scientists*, 1696–1700, Hong-Kong, Mar. 2007.
5. Yang, C. S., Y. C. Chiang, and H. C. Chang, "Analysis of non-uniform non-linear distributed feedback structure using a simple numerical approach," *IEEE J. Quantum Electron.*, Vol. 40, 1337–1340, Sep. 2004.

Immunity of ICD Exposed to Low Frequency Magnetic Fields

Juliano Katrib[1], **Mustapha Nadi**[1], **Patrice Roth**[1], **Pierre Schmitt**[1], **Djilali Kourtiche**[1], **and Martine Souques**[2]

[1]L.I.E.N, Nancy University, Vandoeuvre les Nancy 54506, France
[2]EDF-R & D Site des Renardières, Ecuelles 77250 Moret sur Loing, France

Abstract— This paper presents an in-vitro approach for characterization of Implantable cardiovertor defibrillator (ICD) immunity. A test bench has been modeled based on a Helmholtz coil inside a Faraday cage, with an electric interface outside, capable of generating and controlling uniform magnetic fields. Two protocols are used in this study. A comparison was made between the parameters of disturbances emitted from our test bench at a given time and the time of the occurrence of each event recorded by the ICD. This has allowed us to deduce the signal level that caused false detections in the first case, or inhibition of the detection in the second case. We have plotted the curves representing the presence of false events, detected as a function of the disruptive level. Previously we have investigated the effect of fields up to 1000 µT and found no false detection or inhibition of detection. Here, the evidence demonstrates that at a frequency of 50 Hz, the number of false detections increases in the higher strength EMFs, above 1400 µT. We find both false detection and dysfunction of the implant. In addition, we have discovered that when we vary the angle of inclination of the ICD and the probe to the field, at higher angles, we can observe false detections in lower field strengths.

Materials and Methods: An experimental set-up, using a source for environmentally relevant interferences, has been developed. The experimental set-up included the instrumentation for data acquisition of the telemetric signals emitted from the ICD. The signal disturbance was applied to the implant placed within a phantom, a plexiglas tank filled with gelatine with appropriate electric properties. As the position of the probe and the coil were of primary importance, a plexiglas support for the ICD and the probe was specially designed to ensure the reproducibility of the spatial positions and to avoid any contact between the probe and the ICD case. The metallic electrodes and the device under test (DUT) were placed in a Faraday cage. The entire set-up was controlled by a PC with HP-VEE software. A telemetric system permitted us to check the records of the ICD.

Results and Discussion: Below 1000 µT, no relevant effect was noticed or recorded at any frequency (50 & 60 Hz). In this paper, magnetic fields of 1000 µT up to 4000 µT were applied to determine if either false detection or inhibition of detection could be observed in fields of higher strength. At a frequency of 50 Hz, perturbations were observed in the higher levels of EMFs, above 1500 µT. The position of the ICD and its probe were also investigated by varying their angular position. At a frequency of 50 Hz, when the angle of inclination of the field was 19 degrees, false detections were observed at the higher fields, especially above 3200 µT. When we increased the angle further we observed false detections at low fields, even as low as 2000 µT. It appears that increasing the angle of inclination from 75 degrees to 90 degrees does not have any additional effect on the probability of false detections observed at fields higher than 3000 µT.

At a frequency of 60 Hz, with no inclination, perturbations were observed in the higher strength EMFs, above 1500 µT. When we increased the angle of inclination above 19 degrees, we also observed false detections at magnetic fields strengths above 1900 µT. When the angle of inclination was 27 degrees, we could observe false detections above 2400 µT, whereas increasing the angle of inclination further, to between 56 and 75 degrees, resulted in false detections being observed in lower fields of 1800 µT. It appears again that increasing the angle of inclination from 75 degrees to 90 degrees does not have any additional effect on the probability of false detections, at a frequency of 60 Hz. In addition, we investigated different configurations, both in air and in the gelatine. These effects show the necessity of a well documented and reproducible experimental set-up (geometry, position of the device and the source, field levels) when in vitro results are reported.

Frequency Selective Surfaces with Thin Triangular Conducting Elements

A. Pekmezci and T. Ege
Faculty of Engineering, Department of Electrical and Electronics Engineering, University of Gaziantep
Gaziantep 27310, Turkey

Abstract— In this paper, the scattering characteristics of a planar Frequency Selective Surface (FSS) comprising of thin triangular-shaped conductors printed on a dielectric substrate are investigated for both TM and TE incidence. Although FSSs formed using arrays of strips, squares, rings, Jerusalem crosses etc., have been treated by many researchers there is no study related to triangular shaped elements in the literature [1]. Furthermore, this initial study will later be extended to analyze a metamaterial formed by cascading a triangular FSS to another FSS comprising of infinitely long thin conductors, as suggested in [2].

Since the conducting elements are etched periodically on the surface, all fields and currents must satisfy Floquet's condition and should be written as Floquet modes. Using Floquet's theorem and satisfying the required boundary conditions, an integral equation is obtained for the unknown induced current density on the surface of a triangular conducting element in a unit cell. This current is then expressed as a finite sum of piecewise triangular basis functions having unknown coefficients. The resulting integral equation is converted to a linear matrix equation by using the Moment Method. Inversion of the matrix equation yields the unknown current coefficients which are then used to obtain the reflection and transmission coefficients. The algorithm developed for the FSS having triangular shaped conductors is also used to obtain results for the FSSs employing strips or L-shaped conductors, simply by removing the sides of the triangle. Verification of the results has been carried out by comparing the results from this algorithm with the results of other researchers using strips or L-shaped conductors.

Figure 1 is a typical plot showing the variation of the reflection and transmission characteristics with frequency for a two dimensional periodic array of triangular elements printed on a 5 mm thick dielectric substrate having a dielectric constant of $\varepsilon_r = 2.3$. This result is obtained for an array of equilateral triangles of side 9.4 mm and width 0.47 mm, arranged in a square lattice of side 10 mm when the array is illuminated by a normally incident TM wave.

As seen from the figure the proposed FSS exhibits full transmission and reflection at $f_r = 10.1$ GHz. It has also been observed that, with proper design, the shifts of resonant frequency and changes in bandwidth for various incidence angles, which are normally encountered with such surfaces, can be reduced.

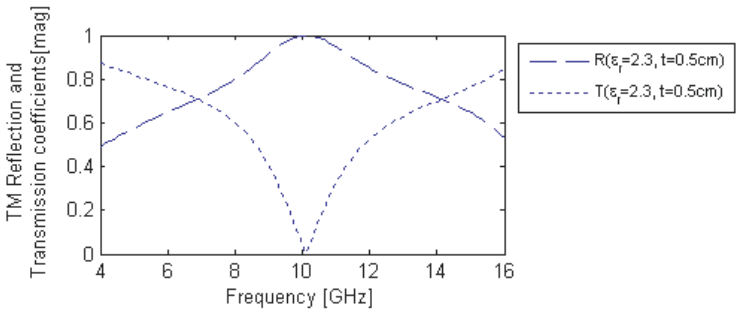

Figure 1.

REFERENCES

1. Munk, B. A., "Frequency selective surfaces: Theory and design," *Wiley Interscience*, United States of America, 2000.
2. Sabah, C., "Analysis, application and a novel design of double negative metamaterials," Ph.D. Dissertation, University of Gaziantep, Gaziantep, Turkey, 2008.

A New Phase Measurement Technique for RF Power Amplifier Only Measuring Magnitudes

A. H. Yuzer[1, 2] **and S. Demir**[1]

[1]Electrical and Electronics Engineering, Middle East Technical University, Ankara, Turkey
[2]Electrical and Electronics Engineering, Zonguldak Karaelmas University, Zonguldak, Turkey

Abstract— Amplifier characterization is an important issue especially in the design of amplifiers and systems involving amplifiers such as linearizers and wireless communication systems. Behavioral modeling is one of the characterization techniques where a mathematical relation between input and output is constructed. There are number of behavioral modeling technique. First step of modeling is measurement of the magnitudes and phases of signals to be wanted to construct model.

In this study, a new measurement technique is proposed to measure both the magnitudes and the phases of signals generated by the amplifier. When an amplifier is excited with a one-tone signal, AM/AM and AM/PM distortion appears at the output. When an amplifier is excited with a two-tone signal, inter-modulation distortion (IMD) components appear at the output. Magnitudes and phases of these signals must be measured to construct an accurate model. The measurement setup given below is prepared to measure AM/AM, AM/PM distortion, magnitudes and phases of IMD and Fundamental (Fund) components created by the amplifier.

Phase measurement setup is constructed based on complex number addition.

It is assumed that there are two complex numbers named the first complex number and the second complex number; in phasor domain representation $m_{SG1}\angle\phi_1$ and $m_{SG2}\angle\phi_2$. Another number, $m_{tot}\angle\phi_{tot}$ is defined as in (1). Phase difference between the first and the second complex number can be found mathematically as given in (2).

$$m_{SG1}\angle\phi_1 + m_{SG2}\angle\phi_2 = m_{tot}\angle\phi_{tot} \tag{1}$$

$$|\phi_1 - \phi_2| = \cos^{-1}\left(\frac{m_{tot}^2 - m_{SG1}^2 - m_{SG2}^2}{2 * m_{SG1} * m_{SG2}}\right) \tag{2}$$

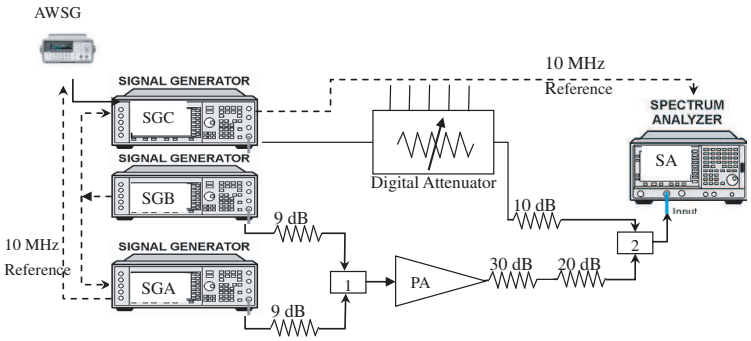

Figure 1: Measurement setup.

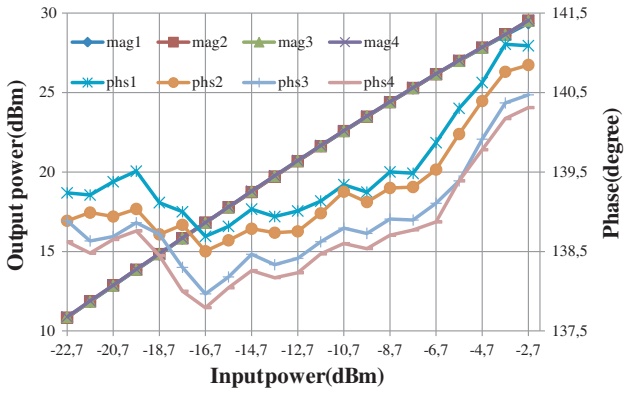

Figure 2: Repeated phase measurement.

Signal generators (SGA and SGB) as shown in Figure 1 are used to create two-tone signal. m_{SG1} represents the magnitude of the signal created at the output of the amplifier and ϕ_1 represents the phase of that signal. m_{SG2} represents the magnitude of the signal created at the output of the digital attenuator. m_{tot} represents the value read at the spectrum analyzer (SA). If we know/measure "m_{SG1}", "m_{SG2}" and "m_{tot}", we can find "$|\phi_1 - \phi_2|$" by using (2). Although only the phase difference can be found by using (2), absolute phase can be found by applying substitution method. Since absolute phase can be measured, phase difference between IMD and Fund can also be measured.

While measuring the phase, magnitude of the signal is measured at the same time. Magnitude/Phase vs. power measurement can be performed by sweeping the power level of signal generators SGA and SGB. Also frequency spacing between excitation tones can be swept.

Phase error between repeated measurements is maximum 1° and magnitude error between repeated measurements is less than 0.07 dB as seen in Figure 2. Dynamic range is very wide. Measurement setup is controlled with a program prepared on computer.

Analysis and Modelling of Arbitrarily Shaped Microstrip Discontinuities

Malika Ourabia
University of Sciences and Technologies Houari Boumediene, Algeria

Abstract— A new and efficient method is presented for the analysis of arbitrarily shaped discontinuities. The discontinuities is characterized using a hybrid spectral/numerical technique.

The structure presents an arbitrary number of ports, each one with different orientation and dimensions.

This article presents a hybrid method based on multimode contour integral and mode matching techniques. The process is based on segmentation and dividing the structure into key building blocks.

We use the multimode contour integral method to analyze the blocks including irregular shape discontinuities.

Finally, the multimode scattering matrix of the whole structure can be found by cascading the blocks. Therefore, the new method is suitable for analysis of a wide range of waveguide problems.

Therefore the present approach can be applied easily to the analysis of any multiport junctions and cascade blocks.

The accuracy of the method is validated comparing with results for several complex problems found in the literature. CPU times are also included to show the efficiency of the new method proposed.

Session 1A7
Poster Session 2

Characteristics of Water Soluble Ions in PM_{10} in the Vicinity of High Voltage Transmission Lines

S. C. Hong[1], **K. Y. Kim**[1], **M. D. Han**[1], **and J. M. Jeon**[2]

[1]Deptartment of Occupational Health & Safety Engineering, Inje University, Republic of Korea
[2]Green Environmental Complex Center, Suncheon first College, Republic of Korea

Abstract— Hypotheses are being proposed on the health effects of the secondary electromagnetic field (EMF) on the respiratory and circulatory systems, including the charged aerosol created by corona discharge near the high voltage transmission line (HVTL) and the resulting aerosol condensation and local concentration of harmful aerosol. In this study, fine particle (PM10) concentration in the air near the HVTL was measured by seasonal variation, the chemical composition was examined via ion analysis, and their correlations were studied to understand the distribution characteristics of water soluble ions near the HVTL.

In summer and winter, charged aerosol current, electromagnetic field, fine particles, temperature, humidity and airflow were continuously measured using Aerosol Electrometer 3068B (TSI, U.S.A), EMDEX E-probe (Enertech, U.S.A) and Cyclone sampler (U.R.G., U.S.A), and after measuring the mass concentration, ion analysis was performed using ion chromatography (Dionex, DX-120)

As a result of the ion analysis of the measured fine particles, the number of F ions was highest, and the detected ions were Cl^-, NO^{2-}, Br^-, NO^{3-}, PO_4^{3-}, SO_4^{2-}, Li^+, Na^+, NH_4^+, K^+, Mg^{2+} and Ca^{2+}. The detected ions differed according to the seasonal variation, and a specific ion (NH_4^+) showed a difference in concentration. The correlations between ions were 0.601 ($p < 0.05$), 0.845 ($p < 0.01$) and 0.764 ($p < 0.01$) between SO_4^{2-} and $NH_4^+/K^+/Ca^{2+}$, respectively, and 0.804 ($p < 0.01$) and 0.741 ($p < 0.01$) between NH_4^+ and NO^{3-}/Ca^{2+}, respectively, which were high positive correlations. Li^+ and Na^+ showed a negative correlation (-0.845, $P < 0.01$).

It was found that the water soluble ions near HVTL do not significantly differ from those in the normal ambient air. However, F^- ions, which do not usually appear in the ambient air, are known to irritate skin, eye and respiratory system. Further study will be needed to find out whether they exist due to the HVTL or not.

Structure Improvement for Suppressing High Mode of Folded Waveguide Traveling Wave Tube

Tianyu Fang, Jin Xu, Huarong Gong, Hairong Yin, Zhigang Lu, and Tao Tang
School of Physical Electronic, University of Electronic Science and Technology of China
Chengdu 610054, China

Abstract— The Folded Waveguide Traveling-Wave Tube (FWTWT) is known as a slow wave structure that has advantages of high power capability, high thermal capacity and robust structure comparing to the conventional Helix-TWT and Coupled-Cavity TWT. Though it has these advantages, the interaction between microwave and electron beam is usually disturbed by high modes. Thereby it affecting the performance of FWTWT. There are already a lot of studies about "loss button" on the Coupled-Cavity TWT since this additional part has great ability to restrain its upper band-edge. So, theoretically, by adding oscillators filled with loss medium to regular structure, high modes in FWTWT can be restrained distinctly as well.

The improvement is based on a regular folded wave guide traveling wave tube operating at 24–65 GHz. The main mode and slot mode of the FWTWT is working at 24–44 GHz and on the frequency higher than 45 GHz respectively. The loss oscillators are designed for operating at certain frequency and restraining high mode greatly. Based on oscillation conditions in this paper, main parameters of the oscillators such as the measurements and the loss medium are synthesized and optimized. Detailed theoretical analysis of this new structure will be presented in this paper.

Design of Flexible Bandpass Filter Using CRLH

Jin-Sup Kim, **Jae-Young Lee**, **and Kyu-Bok Lee**
Wireless Communication Research Center, Korea Electronics Technology Institute, R. O. Korea

Abstract— The 2.4 GHz filter is proposed and implemented using CRLH (Composite Right/Left handed), aiming at bending the substrate. In conventional filters, we just get changed characteristics of it because of flexible substrate. But if we use CRLH, we can get the better electrical characteristics than conventional one because of zeroth order resonator. It is composed of shot stub and interdigital capacitor. After optimization of this filter, a good bandpass behavior with transmission poles is theoretically realized and experimentally confirmed. Suppose the PCB substrate is flexible and it can be bent toward arbitrary angles. Two configurations of the same band-pass filter are shown in Figure 1. To validate the above design approach, the proposed filter was fabricated on a flexible substrate with relative dielectric of 2.17 and thickness of 5 mil. The frequency response is specified with a pass band of 2.4–2.5 GHz, and with less than 0.92 dB insertion loss and more than 10 dB return loss in bending structure.

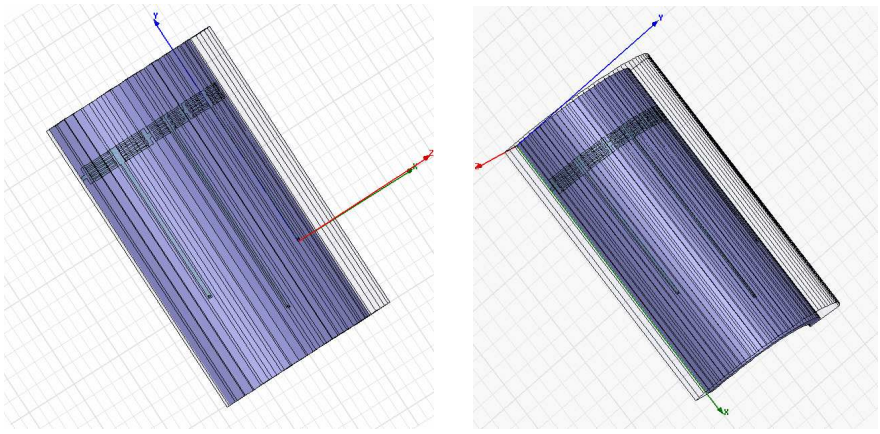

(a) 86 degrees (b) 143 degrees

Figure 1: Bandpass filter using CRLH.

A Study on Tunable Bandpass Filter Using Tapped Resonators Loaded with Varactors

Ryoichi Komagamine, Noritake Koura, Takanobu Ohno, and Kouichi Ishii
Kisarazu National College of Technology, Japan

Abstract— This paper presents a tunable coplanar waveguide (CPW) bandpass filter (BPF) consisting of tapped resonators with a variable capacitor (C_v). Firstly, basic characteristics of the whole element including C_v, a chip-capacitor (C_d), and a resistor (R) are examined experimentally. After that, tapped resonator loaded with the element above is measured and applied to a BPF.

Figure 1 shows a schematic circuit of the BPF using tapped $\lambda/2$ and $\lambda/4$ resonators loaded with the capacitors. The simulated result of the BPF is shown in Fig. 2. The results indicate the almost same bandwidth, and the center frequency (f_0) is shifted from 2.0 to 2.77 GHz (38.5% change). Moreover, lower and higher attenuation poles (f_L, f_{H1}, f_{H1}) are shifted from 1.50 to 1.93 GHz in f_L, from 2.45 to 3.48 GHz in f_{H1}, from 2.6 to 3.65 GHz in f_{H2}, respectively.

Figure 3 shows a photograph of the BPF using tapped resonators with C_v. The measured result of the BPF is shown in Fig. 4. In the experiment, the loaded elements including C_v are applied to 0–20 V to change their capacitance. The result indicate the almost same bandwidth, and f_0 can be shifted 29.8% (2.05–2.68 GHz). f_L and f_H are tuned to 23.0% (1.69–2.08 GHz), and 30.2% (2.85–3.71 GHz), respectively. As a result, a good tunable characteristic has been acquired by using variable capacitor.

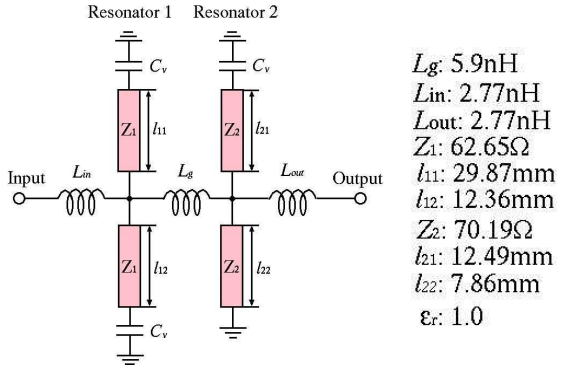

Figure 1: Schematic circuit of BPF using tapped resonators loaded with capacitors.

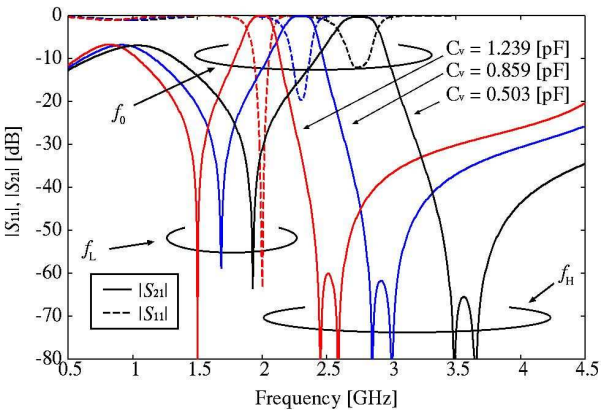

Figure 2: Simulated results of BPF shown in Fig. 1.

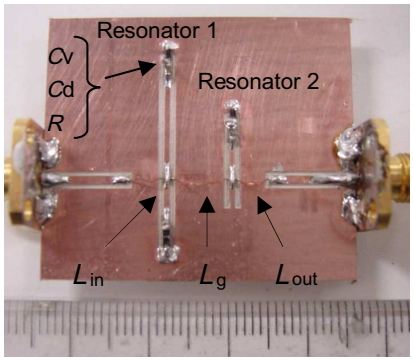

Figure 3: Photographs of BPF using tapped resonators with C_v, C_d and R.

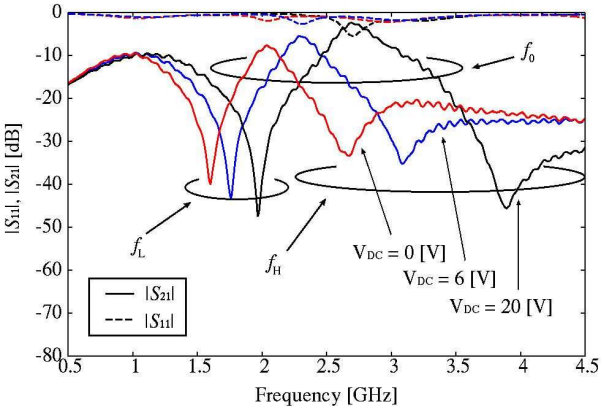

Figure 4: Measured results of the BPF shown in Fig. 3.

Size Reduction and Harmonic Suppression of Narrow Bandpass Waveguide Filters Using Nonuniform Waveguides

M. Yazdani, **M. Khalaj-Amirhosseini**, **and F. Hosseini**
Department of Electrical Engineering, Iran University of Science and Technology, Tehran, Iran

Abstract— Recent advancements in wireless communications in conjunction with the ever increasing demand for size reduction of various wireless systems and devices have led to numerous constraints on the size, weight, and power consumption of modern communication systems and devices. RF/Microwave filters, which are integral parts of any wireless communication system, are not exceptions to this rule. Besides size reduction, low insertion losses and large stopband without spurious response are other points which are important in microwave filters. Combining all these features with a good return loss (better than 10 dB in the passband region) constitutes a great challenge.

In this paper, a nonuniform rectangular narrow bandpass waveguide filter coupled by inductive irises is considered. We use Nonuniform Transmission Line (NTL) theory to compact the shunt inductive irises narrowband waveguide filter. The basic idea comes from replacing the hallow Uniform WaveGuides (UWGs) between shunt inductive irises with optimized Nonuniform WaveGuides (NWGs). By using NWG instead of UWG, the distance between shunt inductive irises is reduced. In addition to size reduction, spurious suppression and large stopband are the other advantages of the designed filter.

As an example a two order chebyshev shunt inductive irises waveguide BPF is considered. The specifications of the proposed filter are as follows: Center frequency ($f_0 = 4.135$ GHz), Fractional bandwidth (BW) = 0.5% and Ripple = 0.38 dB. Figure 1 depicts the conventional two order chebyshev waveguide BPF. As it is shown this filter is composed of two waveguides which their lengths are the same. We replaced two optimized NWG instead of two uniform waveguides. By doing this replacement, the whole size of nonuniform shunt inductive irises waveguide BPF is reduced about 68%. The important point which must be considered is substituting UWG instead of NWG cause the suppression of spurious response which exists in uniform shunt inductive iries waveguide BPF at 7 GHz. This advantage besides size reduction is attractive points of this paper. Figure 2 shows the schematic of nonuniform designed and simulated waveguide BPF.

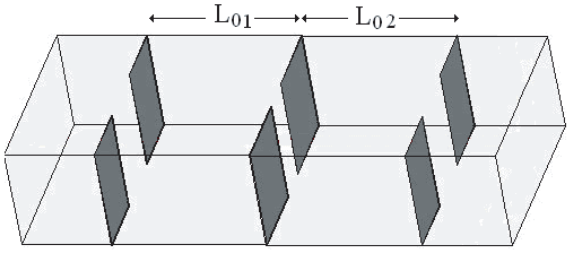

Figure 1: Two order chebyshev conventional waveguide BPF.

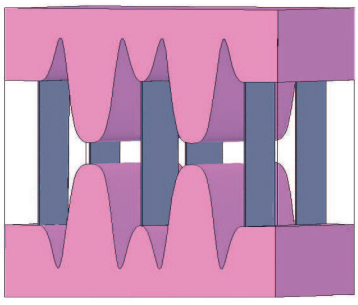

Figure 2: Two order chebyshev compacted nonuniform waveguide BPF.

An Asymmetric Dual-band HTS Band-pass Filter for American Mobile Phone System

A. M. Abu Hudrouss[1, 2], **A. B. Jayyousi**[1, 3], **and M. J. Lancaster**[4]

[1]Electrical Engineering Department, Birmingham University, UK
[2]Electrical Engineering Department, IUG-Gaza, P. O. Box 108, Gaza, Palestine
[3]Electrical Engineering Department, University of Amman, Jordan
[4]Electrical and Comp. Department, Birmingham University, Edgbaston, Birmingham, B15 2TT, UK

Abstract— Modern mobile communication systems require improved sensitivity and selectivity to support the growth in multimedia services, increased coverage, longer talk time and large number of subscribers. This in turn leads to demands for highly selective RF filters. This also forces the operators to seek more efficient sharing of the limited frequency spectrum.

The American Mobile Phone System (AMPS) uses the frequency band from 824 to 849 MHz for communication from the handset to their base stations (often called uplink) and 896.0 to 894.0 MHz for the communication from the base stations to the handset (the downlink). This frequency spectrum is shared between two operators (A and B).

The downlink and uplink pass- band filters must have a very rapid roll off (within each 30 kHz channel) and provide high adjacent channel attenuation at the operators' band edges. Limiting interference with the non-contiguous frequency allocations often requires highly selective filters that can easily be realized using High Temperature Superconductor (HTS) technology.

In this paper, a nine-pole planar passband HTS filter is presented. The filter can be used for reception on the masthead for B operator. The filter has dual-band characteristic which is realized by optimization. The asymmetry of the filter response is achieved by cascaded tri-sections.

A New Algorithm about Extrapolating Near Distance Field to Far-field of Large Size Antenna

Yongxin Zhao[1], **Jianjun Wei**[2], **Nan-Jing Li**[3], **and Chu Feng Hu**[3]

[1]The 46th Middle School of Xi'an, Shaanxi, China
[2]Shaanxi Qiangde Technology Co., Ltd., Shaanxi, China
[3]National Key Laboratory of UAV Specialty Technique, Northwestern Polytechnic University
Xi'an, China

Abstract— In order to meet the approximate plane-wave irradiation condition, adequate large field or compact range system is needed for antenna pattern measurement, especially for large size antenna, but an outside testing field site or a compact range system is very expensive. Near-field planar scanning system is another method, however it is time-consuming and only suited for directional antenna. In this paper, a new extrapolating technique by connecting near-distance field with far-field of large-size antenna is set up. If a large size antenna is short in vertical plane, its irradiating field in horizontal plane can be respected as cylinder wave distribution, an ideal aperture as a reference irradiating source is utilized; its width is the maximum size of the tested antenna. In term of the ideal aperture a phase-correction coefficient $g(x)$ connected with spherical and plane wave can be deduced, and used to calculate the far-field of the tested antenna. In fact the convolution calculation between $g(x)$ and near-field can be replaced by Fast Fourier Transform, thus the calculating procedure could be completed simply and quickly. By theoretical simulation for a simple long antenna, the pattern extrapolated can be obtained correctly. Experimental results of complex antenna show that this new technique makes experiment agree to theory precisely, moreover, it permits the measurement distance to be reduced by 15 percent of the minimum distance of far-field. Also, there is no serious limitation of measurement for antenna in dimension of aperture and depth.

Design of Multi-band Antenna Using Sperrtopf

Tsutomu Yokoyama[1], **T. Hoashi**[2], **and T. Nakamiya**[3]

[1]Department of General Education, Sojo University, 4-22-1 Ikeda, Kumamoto 860-0082, Japan
[2]Department of Electronics, Computer and Network, Sojo University
4-22-1 Ikeda, Kumamoto 860-0082, Japan
[3]Department of Electronics and Intelligent Systems Engineering, Tokai University
9-1-1 Toroku, Kumamoto 862-8652, Japan

Abstract— The development of mobile communication standards that can operate different type of communication leads to have a great demand on designing compact mobile terminals such as Global System for Mobile Communication and Digital Communication System.

We have investigated the characteristics of the multi-band antenna by measuring the current distribution of the antenna using a shield loop [1–3]. When a shielded loop is near a test antenna, the electromotive force (EMF) on the loop is induced by the whole current on the antenna. Therefore, as the shielded loop is moved along the antenna, the current distribution can be inferred the relative value of EMF on the loop. The measurement of current distribution is important to estimate the radiation pattern of the linear antenna.

In this paper, we have designed the multi-band antenna for mobile and digital communications using Superrtopf. This multi-band antenna is composed of wires with Superrtopf. The current distribution and VSWR of the multi-band antenna are measured using a shield loop. When the operation frequency was changed from 700 MHz to 2.5 GHz, the value of VSWR became 1.5 at 790 MHz and 1.5 at 2.02 GHz, respectively.

In addition, we have developed the simulation model of multi-band antenna. The simulation results of the current distribution and VSWR of the antenna are compared with the experimental results.

REFERENCES

1. Yokoyama, T., K. Koga, and S. Egashira, "Estimation of radiation pattern by near field measurement of linear antenna," *ICMMT*, 357–360, 2002.
2. Nakamura, T., S. Yamaguchi, T. Yokoyama, and S. Egashira, "Ladder antenna," *3rd International Conference on Microwave and Millimeter Wave Technology*, 369–372, Bejjing, Aug. 2002.
3. Yokoyama, T., T. Hoashi, K. Murata, S. Egashira, K. Egashira, and T. Nakamiya, "Design of multi-band antenna using different radius wires," *PIERS Proceedings*, 1273–1276, Beijing, China, March 23–27, 2009.

Radiation Patterns of Circumferential-spherical Arrays of Circular Patches

D. B. Ferreira, A. F. Tinoco S., and J. C. da S. Lacava
Instituto Tecnológico de Aeronáutica, Brazil

Abstract— Microstrip antennas are customary components in modern communication systems, since they are low-profile, low-weight, low-cost, and well suited for integration with microwave circuits. Antennas printed on planar surfaces or conformed onto cylindrical bodies have been discussed in many publications. However, such is not the case of spherical microstrip arrays, a canonical configuration of great practical interest because of their potential of 360° coverage in any radial direction. This paper presents an efficient approach for the calculation of the radiation patterns of circumferential-spherical arrays of thin circular microstrip antennas. Differently from planar and cylindrical geometries, where truncated grounds and diffraction at the edges of the conducting surfaces affect the radiation patterns, spherical arrays can be accurately analyzed with the electric surface current model. Using the global coordinate system technique and *Mathematica*®'s powerful algorithms for calculating spherical harmonics functions, a computationally-efficient CAD was implemented. The array geometry under consideration is shown in Fig. 1. It is conformed onto a dielectric layer (of relative permittivity ε_r, magnetic permeability μ_0 and thickness $h = b - a$) that covers a ground sphere of radius a. The n-th circular patch whose center is located at $(\alpha,\ \beta_n)$ is fed by a coaxial probe at $(\theta_{pn},\ \varphi_{pn})$. The array is embedded in free space of characteristics ε_0 and μ_0. After applying the vector-Legendre transformation and a circuit model to evaluate the spectral Green's functions, the surface current density on the n-th patch is properly estimated from the cavity model. However, for any of the patches shown in Fig. 1 that is not symmetric around the z-axis, the numerical computation becomes too complex because, in such cases, the associated Legendre functions of the first and the second kind are both required for the calculation of the surface current density. To overcome this limitation, use was made of the pattern rotation technique. Starting from the expressions for the far electric fields from a circular patch that is symmetrical around the z'-axis (in which case the associated Legendre function of the second kind is not part of the solution) the far electric field in the global coordinate system can then be determined. To illustrate the developed approach, Figs. 2 and 3 present the radiation patterns of a 4-element array, designed to operate at 3.1 GHz (TM_{11} mode, $h = 0.762\,\text{mm}$, $\varepsilon_r = 2.5$, $\tan\delta = 0.0022$ and $a = 100\,\text{mm}$), compared with those calculated in *HFSS* version 11.1. For this array, $\alpha = 35°$, $\beta_1 = 0°$, $\beta_2 = 90°$, $\beta_3 = 180°$, $\beta_4 = 270°$ and all elements are fed by identical currents.

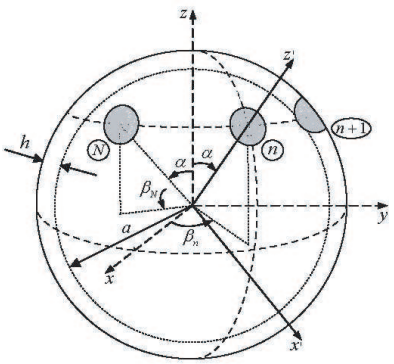

Figure 1: Circumferential-spherical array geometry.

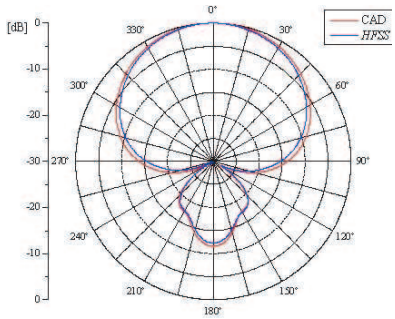

Figure 2: E_φ radiation pattern: xz plane.

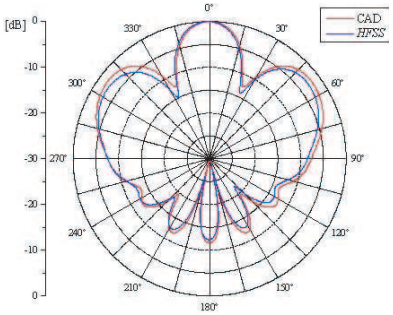

Figure 3: E_θ radiation pattern: yz plane.

Design of Low-cost Antennas for Globalstar Applications

Daniel C. Nascimento, R. Schildberg, and J. C. da S. Lacava
Laboratório de Antenas e Propagação, Instituto Tecnológico de Aeronáutica, Brazil

Abstract— The last generation of communication satellites supports mobile communication applications, enabling mobile phone operators like Globalstar, among others, to offer global coverage services. This system provides voice and data connections by means of satellite phones, as well as solutions for asset tracking, remote sensing, environmental and geographic monitoring and control of in-field operations by means of the integrated satellite modem. Subscribers have access to the system through LEO (Low Earth Orbit) satellites, operating in a Walter delta constellation. Manufacturing of the second-generation Globalstar satellites proceeds and the constellation deployment is expected to begin in the summer of 2010. Due to the wide application of this system and the recent expansion of its ground structure, the user's terminal antenna is an important development topic. Helical structures can be used as antennas on mobile terminals, particularly on cars or trucks, but they tend to be bulky. On the other hand, microstrip antennas are widely used in mobile communication systems, radar systems, and aerospace applications due to their low weight, low profile and easy manufacturing. Thus, this paper reports a microstrip antenna (Fig. 1) specifically designed for Globalstar applications printed on a low-cost FR4 substrate and convenient to series production. To improve the radiation efficiency over the uplink (T_x: 1.61073 to 1.62549 GHz) and the downlink (R_x: 2.48439 to 2.49915 GHz) bandwidths, electrically thick substrates (h = 6.2 mm) must be used. Consequently the antenna input impedance becomes strongly inductive if the standard design of probe-fed truncated-corner square microstrip patches is followed. To overcome this limitation, rectangular truncated corner patches are used instead of the square ones. Under this approach the antennas can then be closely matched to a 50-Ω SMA connector at the central frequencies of the operating bands. Results for the reflection coefficient magnitude and axial ratio (at the boresight region of the R_x antenna) simulated by the HFSS software and measured in anechoic chamber are shown in Fig. 2. As seen, the axial ratio is less than 3 dB and the reflection coefficient magnitude is better than −20 dB over the R_x bandwidth, showing the antenna proper operation. The angular axial ratio is another important parameter for satellite communication; Fig. 3 presents a HFSS-simulated rotating dipole radiation pattern at 2.4918 GHz, which is in good agreement with the measurement. Similar behavior is also observed for the T_x antenna.

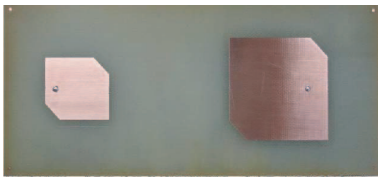

Figure 1: Reflection coefficient and axial ratio: R_x antenna.

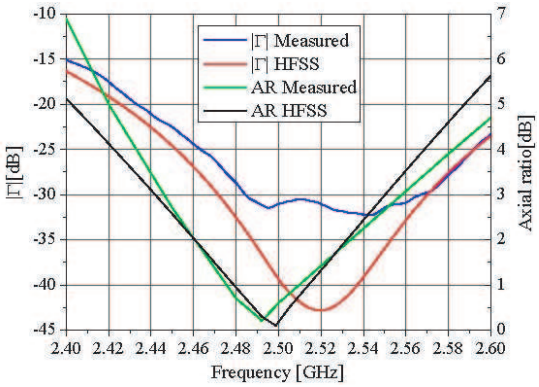

Figure 2: Reflection coefficient and axial ratio: R_x antenna.

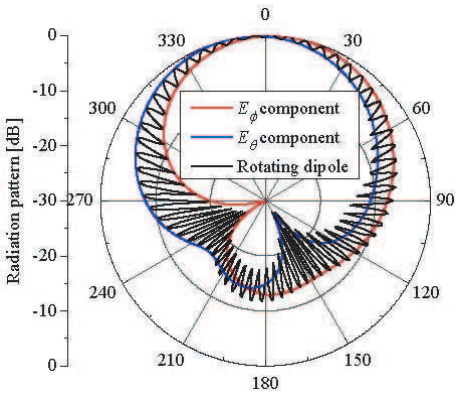

Figure 3: Radiation pattern (yz plane): R_x antenna.

A Waveguide Slot Array Antenna with Improved Radiation Pattern

Se-Hwan Choi, **Jin-Sup Kim**, **and Jae-Young Lee**
Korea Electronics Technology Institute, Republic of Korea

Abstract— In recent years, the wireless vehicular radar systems have been developing in the license-free 24 GHz industrial, scientific and medical (ISM) band. Millimeter-wave antennas are important for the radar system and low-cost communication because they decide the radiation gain and the spatial resolution of radar system. There are many kinds of the millimeter-wave antenna. Among millimeter-wave antennas, waveguide types are still used because they have merits such as low loss, high power capability and radiation gain.

In this paper, the 4 by 3 slot array antenna with improved radiation pattern using a waveguide feeding is proposed at 24 GHz. The antenna consists of a waveguide feed, waveguide power dividers waveguide slots and extra slots. Extra slots are located on both sides of radiation slot array. The leakage electric field on surface of the antenna is blocked by these slots. Because higher sidelobes and backlobes result from the leakage radiation, this structure can reduce the unwanted radiation. In the slot array antenna, feeding waveguide uses the WR-42 ($10.7 \times 4.3\,\mathrm{mm}^2$) standard waveguide. There are two types of waveguide power dividers. One is π type that power is divided unequally and the other is T type that power is divided equally. The π type is used to reduce the sidelobe level. Waveguide slots are located by the offset from the center of waveguide. These offsets play a role of power divider and impedance matching. Antennas are simulated by Ansoft HFSS and analyzed by a network analyzer HP8510c. Both antennas have the gain of 18 dBi and the half power beamwidth of 20 degree. The antenna without extra slots has the sidelobe level of 22.8 dB and the backlobe level of 24.6 dB. But the antenna with extra slots has the sidelobe level of 26 dB and the backlobe level of 26.2 dB. This antenna can be used for commercial millimeter-wave applications by reason of that this technique can reduce the unwanted radiation.

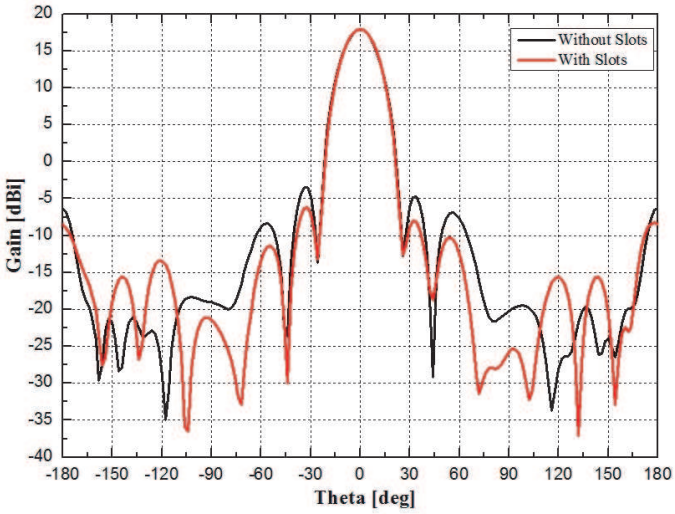

Figure 1: Radiation patterns.

Miniaturization of a Ultra Wide Band Antenna

Hyung Kuk Yoon, **Jin A. Park**, **Yohan Lim**, **Young Joong Yoon**, **and Cheon-Hee Lee**
Yonsei University, South Korea

Abstract— In this paper, a research on the miniaturization of UWB antenna is presented. The main concept is to secure current paths to support additional resonance mode over wide bandwidth using tapering, modified sleeve and truncated ground plain. It is designed in the frequency band of 2.9–9.1 GHz to support UWB services. The proposed antenna has a dimension of $10 \times 8 \times 0.652\,\mathrm{mm}^3$ and the ground size of $30 \times 30\,\mathrm{mm}^3$. Since the proposed antenna has printed structure and very compact size, it can be easily integrated with the other RF circuit.

Bandwidth Estimating Strategy for a 2-Layer Rectangular Suspended Microstrip Antenna

Laila F. Marzall[1] **and J. C. da S. Lacava**[2]

[1]TSM Antennas, Brazil
[2]Laboratório de Antenas e Propagação, Instituto Tecnológico de Aeronáutica, Brazil

Abstract— Suspended microstrip antennas are an effective option when features like wide impedance bandwidth (BW), high input power and low cost are required for the same structure. Such characteristics can be achieved by introducing between the ground and the suspended substrate an air-gap, whose thickness defines the antenna's impedance behavior and, as a consequence, improves its BW. Nowadays, although antenna designers may be aided by commercial software like the *HFSS*® package, the procedure for calculating the antenna's BW becomes a tedious iterative process, taking a long time to evaluate the antenna's current distribution and then, its input impedance and BW. Consequently, it is instrumental to create a simplified model to assist the designers in establishing the initial substrate and air-gap thickness, in order to accelerate the attainment of the desired BW. With this intent, a method to estimate the impedance bandwidth of a rectangular suspended microstrip patch, based on the cavity model and the conformal mapping for calculating the effective permittivity of a 2-layer microstrip line, is proposed. An algorithm was implemented in *Mathematica*® to estimate the 10-dB return loss bandwidth. For validation purposes, a set of rectangular patches ($h_r = 1.5\,\text{mm}$ and $w_r = 100\,\text{mm}$) printed on a thin substrate ($h_{s1} = 1.524\,\text{mm}$ and $\varepsilon_r = 2.5$) was designed in *HFSS*® to operate at 2.45 GHz. The thickness of the air-gap layer (h_{gap}) was swept between 1 and 9 mm. The dimensions (w_p, l_p, and, y_p) were established by designing the patches to operate at the zero input reactance $X_{in} = 0$ condition. The advantage in this case is the antenna 10-dB return loss bandwidth is symmetrical with respect to the operating frequency (2.45 GHz). Simulated and estimated results are compared in Fig. 2. As can be seen, they are in very good agreement.

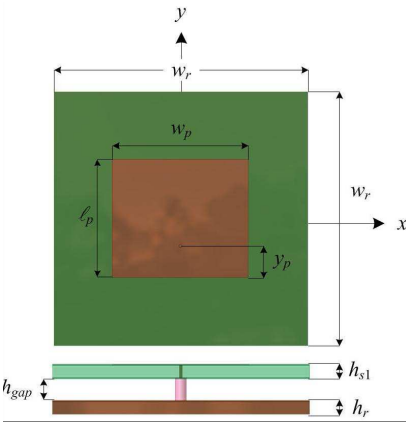

Figure 1: Suspended microstrip antenna geometry.

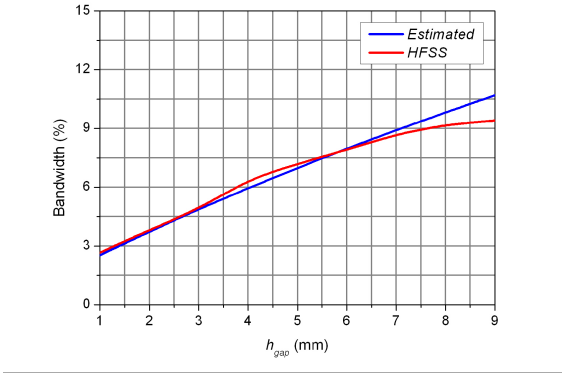

Figure 2: Return loss 10 dB bandwidth.

An Effective Strategy for Designing Probe-fed Linearly-polarized Thick Microstrip Arrays with Symmetrical Return Loss Bandwidth

Laila F. Marzall[1], **Daniel C. Nascimento**[2], **R. Schildberg**[2], **and J. C. da S. Lacava**[2]

[1]TSM Antennas, Brazil
[2]Laboratório de Antenas e Propagação, Instituto Tecnológico de Aeronáutica, Brazil

Abstract— When the standard design procedure is applied to probe-fed linearly-polarized (LP) microstrip radiator with a thick substrate, which is a practical way to increase bandwidth, the antenna exhibits an inductive input reactance that is difficult to match to the feeder network, affecting significantly its bandwidth symmetry. Many techniques are available to compensate for the probe inductance but their use depends largely on the expertise of the antenna designer. Series capacitors, which can be implemented in several ways, are a possibility. The modification of the probe geometry is another technique. However, if one of these modified elements is used for designing a linear array, the complexity of its feeder network increases correspondingly. To overcome this limitation, a new strategy for designing probe-fed LP thick microstrip antennas, resulting in arrays with symmetrical bandwidth and, as a consequence, simple feeder network, is presented. First, the new strategy is applied to the design of a single element. Simulated results for the reflection coefficient magnitude of a rectangular patch antenna consisting of a $h = 6$ mm thick, air ($\varepsilon_r = 1$) substrate, designed to operate at 2.45 GHz, are presented in Fig. 1, in comparison with the standard design. Clearly, the new procedure can perfectly match the antenna with a 50-Ω SMA connector, presenting in addition a symmetrical bandwidth. Subsequently, the proposed strategy is used for designing a WLAN array of suspended microstrip antennas to comply with the IEEE 802.11b (2.4–2.4835 GHz) protocol and the ETSI EN 301 525 V1.1.1 (2000-06) standards. According to the ETSI standard, linear arrays must have a minimum gain of 14 dBi. To guarantee this threshold, an eight-element array was implemented. To reduce the cross-polarization level the elements were divided in two-subgroups with 180° phase shift excitation. To control the side lobe level (SLL), the Dolph-Chebyshev method was used to determine the excitation coefficients for a −20 dB SLL. Experimental and simulated results for the reflection coefficient magnitude are shown in Fig. 2. A picture of the feeder network is shown in Fig. 3.

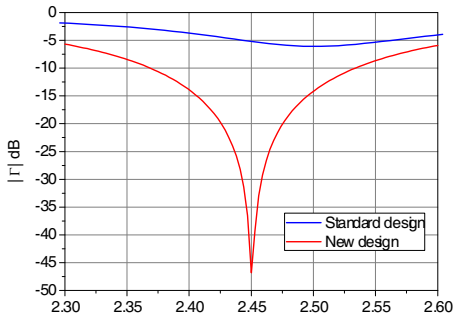

Figure 1: Single-element reflection coefficient magnitude.

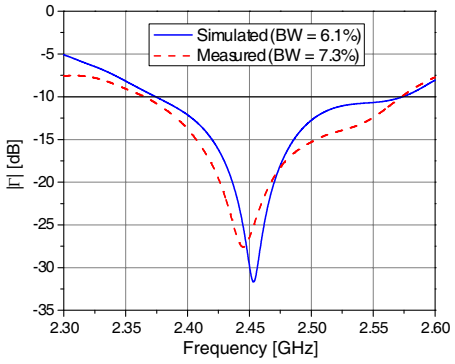

Figure 2: Array reflection coefficient magnitude.

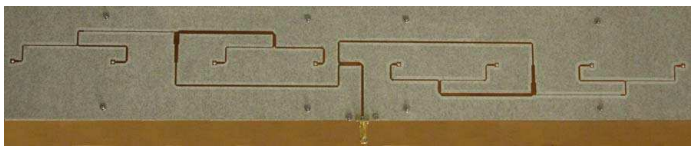

Figure 3: Actual picture of the prototype feeder network.

Structural Analysis of the Microstrip Sample Holder

M. R. F. Gontijo[1], **E. Y. S. Lutif**[1], **A. J. F. Orlando**[1], **and A. C. C. Migliano**[1, 2]

[1]Aerospace Technological Institute (ITA), CTA, Brazil
[2]Advanced Study Institute (IEAv), CTA, Brazil

Abstract— The innovation of the techniques in the characterization of thin films was motivated by the nanotechnology progress. The exact knowledge of material permittivity and permeability is essential in the study of physical phenomena which govern interactions between electromagnetic wave and matter. The different techniques have been developed for measuring the intrinsic properties of materials such as, microstrip, stripline and coplanar. The challenge in the characterization thin films is low sensibility of the holder sample and a mode of the observation of the sensibility of the sample holder is the study of the reflection parameters and transmission parameters of the electromagnetic wave. The reflection parameters and transmission parameters are dependents of the physical property and geometric parameters, this approach can be analyzed through computerized simulation XFDTD. XFDTD is a computer simulation technique with which an arbitrary space is meshed with small cells (Δx, Δy, $\Delta z : \Delta x$, Δy, $\Delta z < \lambda/10$) and the electromagnetic field and current are calculated in the space by solving Maxwell's equations in each cell at each time step of Δt ($< \lambda/10c$). In this study, is present an simulation using XFDTD of the holder sample microstrip structure modeled to investigate the electromagnetic sensibility, the largest work area, input impedance and output impedance, distribution of the magnitude of the electromagnetic vectors, density of electric current and average electric potency. The critical dimensions for the microstrip sample holder are as follows: the housing is perfect electrical metal with inside dimensions of $(12.00 \times 10.00 \times 0,64)$ mm, the permittivity relative of the air equal 1.0 and perfect dielectric with dimensions $(11.00 \times 7.00 \times 0.64)$ mm. For each simulation the width of the conductor perfect center varied of (2.60, 2.80, 3.00, 3.20, 3.40, 3.60, 3.80 and 4.00) mm and to validate the simulation use the Newton's Complex Iterative Method to determine the real permittivity and imaginary of the sample holder. The largest work area went to $w/h = 5$, in which possess a broad band between 0.326 GHz to 4.12 GHz.

Novel Application of CPW in Antenna Design for Dual-frequency Operation

Guo-Chao Wang and Jia-Dong Xu
School of Electronics and Information, Northwestern Polytechnical University
Xi'an 710072, China

Abstract— In this paper, we propose a novel application of coplanar waveguide (CPW) in antenna design: by appropriate adjusting its impedance, CPW can act as both a transmission line and radiator at the same time. That is, unlike the traditional way, an extra independent frequency can be obtained without adding new component or increasing the complexity. So the new design and the original one are almost the same in geometry however completely different in capability. Through this method, antenna design could be more simple and flexible. To do this, the impedance of CPW should be carefully designed and most of all, avoid of being 50 Ω, otherwise the CPW will turn out to be merely transmission line (the traditional and most common usage of CPW). Here, we choose a classical single frequency planar antenna as an example to prove that by incorporating the advanced CPW, the former single frequency antenna could resonates at two different frequencies independently — the original one and the one comes from CPW. In addition, two frequencies share a very similar pattern. Since each resonant point relates to one parameter exclusively, we only need to modify one parameter at one time to place the two frequencies at the anticipate points to meet different requirements. However, impedance of CPW should be changed correspondingly to ensure sufficient gain at each frequency. In order to determine the performance of CPW's impedance as well as other two geometry parameters on frequency, parametric study is carried out using simulation software HFSS and experimental results. At last, by careful adjustment of these three parameters, we merge the two frequencies so as to acquire a wide-band operation which covers 4 GHz and more than 50% relative band-width. Simulated and measured results show excellent agreement; hence proves the validity of the new capability of CPW.

Ground Slotted Landa Shape Single Feed UWB Circular Polarized Antenna for 2.4 GHz RFID Reader

E. A. F. Abdallah[1], **T. G. Abo-Elnaga**[1], **and H. El-Hennawy**[2]

[1]Electronics Research Institute, Egypt
[2]Faculty of Engineering, Ain Shams University, Egypt

Abstract— The first RFID application was the "Identification Friend or Foe" system (IFF) and it was used by the British in the Second World War. Transponders were placed into fighter planes and tanks, and reading units could query them to decide whether to attack. Successors of this technology are still used in armies around the world. The first commercial RFID application was the "Electronic Article Surveillance" (EAS). It was developed in the seventies as a theft prevention system. In the eighties RFID technology got a boost when Norway and several US states decided to use RFID for toll collection on roads. In recent years, RFID technology has been rapidly developed and applied to many service industries, distribution logistics, manufacturing companies, and goods flow systems. In RFID system, the role of antennas (for reader and tag) is very important. The reader antenna should have circular polarization (CP) characteristic since the tag antenna can be arbitrarily positioned on the target. Most RFID systems operate at ISM frequencies, such as 13.56 MHz, 2.45 GHz and 5.8 GHz, some work at UHF frequencies such as 840 $\sim$ 845 MHz, 920 $\sim$ 925 MHz (China), 952 $\sim$ 954 MHz (Japan), 868 $\sim$ 870 MHz (Europe) and 902 $\sim$ 928 MHz (USA), etc. In this paper, an Ultra Wide Band (UWB) circularly polarized antenna is proposed for the supper high frequency (SHF) 2.4 $\sim$ 2.483 GHz Radio Frequency Identification (RFID) applications. The antenna is composed of FR4 layer with dielectric constant of 4.65 and height of 1.5 mm. Microstrip patch antenna is placed on the top of the substrate and no ground plane beneath it. The patch antenna excited through microstrip line matched to the antenna through $\lambda/4$ microstrip line transformer with stub and their dimensions are optimized to enhance the matching between the antenna and the microstrip line. The ground plane lies beneath the feeding scheme. Landa shape slot is etched in the ground plane and its dimensions are optimized to enhance the circular polarization. The proposed antenna achieves measured -10 dB bandwidth of 1.77 GHz from 2.34–4.11 GHz which agrees with the computed results. The proposed antenna has 3 dB axial ratio bandwidth of 89.1089 MHz (2.39934 MHz–2.48845 MHz) which cover the required band (2.400 MHz–2.483 MHz). The antenna scheme occupies an area of $29 \times 32\,\text{mm}^2$. Finally, the proposed antenna is simple, cheap and offers an acceptable other antenna parameters on the 2.4 GHz RFID readers bandwidth.

Ground Slotted Phi Shape UWB Stacked Circular Polarized Antenna for 5.8 GHz RFID Reader

E. A. F. Abdallah[1], **T. G. Abo-Elnaga**[1], **and H. El-Hennawy**[2]

[1]Electronics Research Institute, Egypt
[2]Faculty of Engineering, Ain Shams University, Egypt

Abstract— Radio frequency identification (RFID) is a generic term that is used to describe a system that transmits the identity (in the form of a unique serial number) of an object or person wirelessly, using radio waves. The purpose of an RFID system is to enable data to be transmitted by a portable device, called a tag, which is read by an RFID reader and processed according to the needs of a particular application. The data transmitted by the tag may provide identification or location information, or specifics about the product tagged, such as price, color, date of purchase, etc. Recently, from security and control point of view, the radio frequency identification (RFID) systems have received much attention for use in efficiently tracking and identifying objects in the various supply chains such as logistics, automatic billing, access control and work tracking for factory automation, inventory management and bio-engineering applications. Most RFID systems operate at ISM frequencies, such as 13.56 MHz, 2.45 GHz and 5.8 GHz, some work at UHF frequencies such as 840 ∼ 845 MHz, 920 ∼ 925 MHz (China), 952 ∼ 954 MHz (Japan), 868 ∼ 870 MHz (Europe) and 902 ∼ 928 MHz (USA), etc. 125 kHz, 13.56, 869, 902–928 MHz, 2.45 and 5.8 GHz. The 5.8 GHz band (5.725 GHz–5.875 GHz) gains very high data rates and almost used by movement sensor systems such as those in shops or department stores. In this paper, an Ultra Wide Band (UWB) circularly polarized antenna is proposed for 5.8 GHz band (5.725 GHz–5.875 GHz) Radio Frequency Identification (RFID) applications. The antenna is composed of three layers, upper FR4 layer with two stacked Cross-slotted circular patch antennas separated by the thickness of this layer and well aligned with each other, middle foam layer, bottom FR4 layer with stepped L shape microstrip line on the top and almost phi shape slot etched in the ground plane beneath L shaped microstrip line. Feeding scheme dimensions optimized to guarantee the circular polarization operation of the proposed antenna. The proposed antenna achieves −10 dB measured bandwidth of 690 MHz (5.48 GHz–6.17 GHz) which agrees with the computed counterpart. The proposed antenna achieves 3 dB axial ratio bandwidth of 207.921 MHz (5.6732 GHz–5.88119 GHz) which cover the required band. The cross slotted circular patch occupies an area of radius 6.7 mm and square of 25 mm length for the ground plane. Finally, the proposed antenna is simple, cheap and offers an acceptable other antenna parameters on the 5.8 GHz RFID readers bandwidth.

A High Gain Wide Band Parasitic Dipole Antenna with Inverted L Parallel Feeding Line

Pui-Yi Lau, **Kenneth Kin-On Yung**, **and Edward Kai-Ning Yung**
City University of Hong Kong, USA

Abstract— A high gain and wide bandwidth parasitic dipole antenna is proposed and investigated, which a inverted L microstrip is fed by an SMA connector and parallel to a pair of shorting strips. Parametric studies are performed to optimize the antenna performance. Experimental results reveal that it can achieve an impedance bandwidth of 78% for SWR < 2 from 1.4 GHz to 3.2 GHz. With a parasitic dipole on the top, the gain is enhanced by 60% from 8 dBi to more than 12 dBi. It is more or less a 4 by 4 dipole array but the size is much smaller and without the complex feeding network.

To achieve a wide bandwidth antenna, an inverted L parallel feed is employed. This feed consists of three portions, which is made by folding a straight metallic strip of rectangular cross-section into an inverted L shape. The first portion which is vertically-oriented has one end connected to a SMA connector mounted below the grounded plane. This portion is parallel to one shorting strip of the shorted patch antenna acts as a microstrip line with 50 Ω characteristic impedance. It transmits the electrical signal from the SMA connector to the second portion of the feed. The second portion is located horizontally and connected to one of the shorting strip which is responsible to couple the electrical energy to the planar dipole and the shorted patch antenna.

Later on, we shall give the analysis on the parasitic elements' effect to the antenna gain, radiation patterns and impedance.

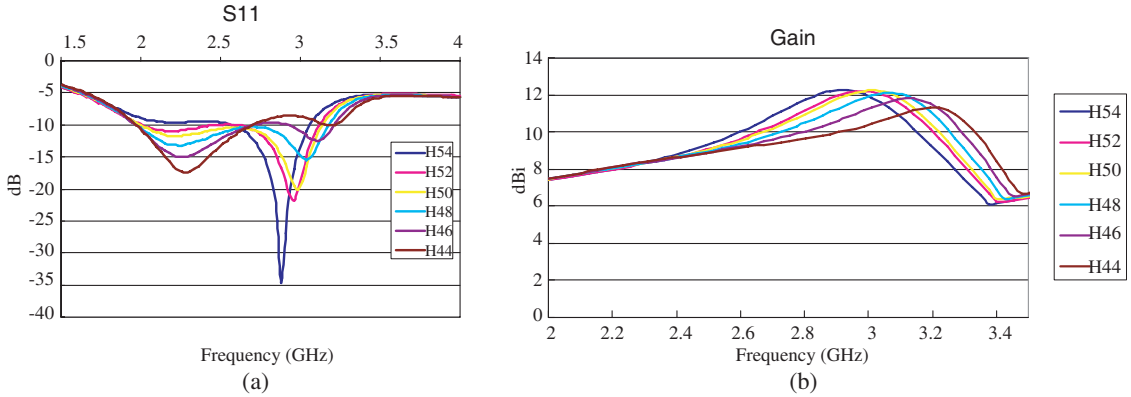

Figure 1: Theoretical return loss (a) and antenna gain (b) against frequency for the proposed antenna with various thickness of the parasitic patch.

Session 1P1
Electromagnetic Modeling, Inversion and Applications 2

Microwave Sensing of Maple Trees for Pest Detection

Kassi Stein and Carey Rappaport
Gordon-CenSSIS, Northeastern University, Boston, MA 02115, USA

Abstract— The Asian Longhorned Beetle is a pest that poses a current threat to hardwood tree species, particularly maples. They ultimately kill these trees by eating away at the wood, leaving large air holes that interrupt the flow of food and water through the trunk. A larger problem is that they tend to infect an entire area at once rather than just a single tree, since the beetles from one infected tree will move on to lay their eggs in others nearby. There is currently no reliable way of detecting these pests since they lay their eggs beneath the bark and seal up entrance holes, thus leaving no visible evidence, and tree symptoms themselves do not necessarily appear immediately following infestation, or even for years after, until it is too late to treat and heal the damage. Microwave sensing offers a potential means of detecting these beetles.

A computational electromagnetic scattering analysis was conducted to determine the feasibility of using microwave imaging radar to non-invasively sense pest damage in trees. Two sample cross sections of a maple tree were generated, one that had been infected and damaged and one that had not. Well-documented frequency-dependent dielectric constants were specifically assigned to the three major regions of the cross sections: bark, sapwood, and heartwood. Finite Difference Frequency Domain (FDFD) models were run at the 0.433, 0.915, and 2.45 GHz ISM frequencies.

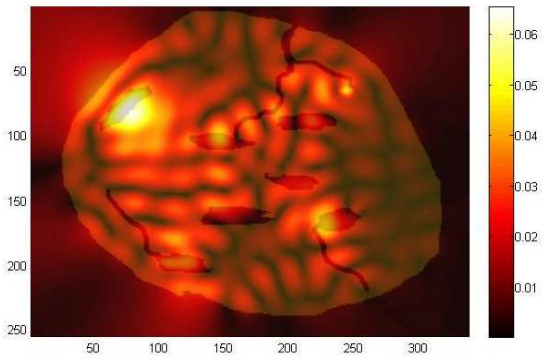

Using four point sources located at (50,50); (50,225); (300,50); and (300,225), images were generated for infected and healthy cross sections using the computed electromagnetic fields. The difference was taken between the two computations to generate the fields scattered by just the air spaces. The excitation at 2.45 GHz did not penetrate far enough into the relatively wet tree to produce significant scattering, while 433 MHz yielded indistinct and uncorrelated scattered field. The optimal frequency of 915 MHz penetrated the wood far enough and produced adequate resolution.

The original sample cross section of the infected tree was overlaid on the image of the electric field, as shown for 915 MHz in the figure. There is a measurable response outside the perimeter of the tree due to the damaged areas. In addition, almost all the high field values correspond to hole locations in the tree. For pest detection, it is not so much being able to find the specific geometry of features within the tree that is important, but rather being able to detect non-uniformity in the tree cross section that predicts damage. Therefore, it is not necessary to reconstruct the damage pattern, just unambiguously sense its effect.

An Electromagnetic Target Classification Method for the Target Sets with Alien Target: Application to Small-scale Aircraft Targets

M. Secmen[1] and G. Turhan-Sayan[2]

[1]Department of Electrical and Electronics Engineering, Izmir Institution of Technology, Izmir, Turkey
[2]Department of Electrical and Electronics Engineering, Middle East Technical University, Ankara, Turkey

Abstract— The electromagnetic target classification is a challenging problem since the scattered field from a target is highly dependent on operating frequency, polarization and aspect angle. In order to minimize adverse effects of these dependencies an intelligent classifier containing some distinguishable target features is needed. Besides, the criteria of the accuracy, satisfactory noise performance, high decision speed in real time, small memory requirements and simplicity should be satisfied. In addition, in order to be suitable for real target applications, the properties of operating with moderate frequency bandwidth and discriminating an alien target from a target set containing friend targets are important.

In this study, an electromagnetic target classification method for isolated targets using noisy data in the classifier design to obtain high accuracy performance in a wider SNR range and having the ability of discrimination of an alien target without any priori information is introduced. The proposed method is mainly based on a late-time resonance region target classification technique, which was reported recently to use the multiple signal classification (MUSIC) algorithm and natural-resonance mechanism modeled by singularity expansion method (SEM) for target feature extraction, and modified for target sets containing alien target(s). The method obtains fused MUSIC spectrum maps (FMSMs) of each friend targets as target features, which are extracted from optimal late-time interval of scattered signals of these targets, and stores these maps. In the decision phase, the scattered signal received from an unknown (test) target at an unknown aspect is processed to obtain the similar MUSIC spectrum map (MSM) belonging to same optimal late time interval. Then, the MSM of test target and FMSMs of friend targets are compared according to correlation coefficients obtained from these maps. If the highest correlation coefficient among these coefficients is sufficiently high, test target will be classified as one of friend targets in database giving highest correlation coefficient. On the other hand, test target will be identified as an alien target if the highest correlation coefficient between test MSM and friend targets' FMSMs is sufficiently low.

As being an application, the performance of the proposed classifier design method is demonstrated for a target set of five small-scale friend aircraft (Airbus, Boeing 747, Caravelle, P-7 and Tu 154) and an alien aircraft (DC 10). All six aircraft targets, whose dimensions are scaled by 1/100, are modeled by perfectly conducting, straight, thin wires. The backscattered responses of targets are numerically generated using Method of Moments (MOM) technique at the frequency bandwidth 0–1024 MHz with frequency resolution 4 MHz. The FMSM features of friend targets are obtained by using specific MUSIC parameters and noisy reference signals with SNR level 10 dB at some specific aspect angles. The classifier is tested with noisy test scattered signals having SNR levels 20, 15, 10, 5 and 0 dB. According to the test result, the proposed method gives almost 100 percent accuracy for SNR levels higher than 15 dB and this rate gradually drops to 89 percent for SNR level 0 dB. The more details about the construction of FMSMs, the classification algorithm of the proposed method and test results will be explained in full paper.

Unsupervised Electromagnetic Target Classification by Self-organizing Map Type Clustering

T. T. Katilmis, **E. Ekmekci**, **and G. Turhan-Sayan**
Department of Electrical and Electronics Engineering, Middle East Technical University, Ankara, Turkey

Abstract— In this paper, design of an unsupervised electromagnetic target classifier will be described by making use of the Wigner distribution (WD) based target feature extraction technique and the Self-Organizing Map (SOM) type clustering algorithm. Most of the target classifier design methods reported in literature use supervised design with a fixed size database composed of labeled reference signals. In the suggested classifier design method, however, designer does not need to have an a priori information about the number of library targets or about the origin (or target label) of reference scattered signals used in classifier design. He/she will be just given a set of transient response waveforms each of those has been scattered by one of the candidate targets at arbitrary aspect angles. Target features extracted from these response waveforms will be processed by a self-organizing map (SOM) type neural network which is based on an unsupervised learning algorithm. Separate cluster regions are expected to be formed for each library target at the end of the learning iterations due to the training of weight vectors of the neurons of the SOM output map.

The suggested classification technique will be demonstrated for a target library of dielectric spheres which have exactly the same size but slightly different permittivity values. These targets will be classified using their bi-static scattered electromagnetic data which are analytically computable for these spherical geometries. Data will be produced over an ultra-wide frequency band in resonance region. Electromagnetic target recognition from scattered data is a highly aspect and polarization dependent problem. In resonance region problems, late-time transient response of a target can be expressed as a weighted sum of damped sinusoidal components by using complex natural resonance frequencies (i.e., the system poles of the target) and their residues as described by the singularity expansion method. Not the poles themselves but their residues are strong functions of aspect and polarization. Therefore, instead of using scattered target response information directly, aspect and polarization invariant target features extracted from these response waveforms should be used for target recognition purposes. Use of time-frequency transformations such as the Wigner distribution (WD) has been recently demonstrated to be quite effective in extracting almost aspect invariant target features. The WD based feature extraction technique will be utilized in this classifier design study.

Developments in the Classification of TAOS Optical Scattering Patterns from Single, Heterogeneous Airborne Particles

Giovanni Franco Crosta[1], **Yongle Pan**[2], **Gustavo Eddino Fernandes**[3], **and Richard K. Chang**[4]

[1]Dipartimento di Scienze dell'Ambiente & Territorio, Univ. Milan-Bicocca, Milan, Italy
[2]US Army Research Laboratory, Adelphi, MD 20783, USA
[3]Division of Engineering, Brown University, Providence, RI 02912, USA
[4]Department of Applied Physics, Yale University, New Haven, CT 06520, USA

Abstract—

Experimental: *TAOS* (two-angle optical scattering) instruments record the intensity patterns of laser light scattered by single airborne particles over a wide range of the scattering angles $\{\theta, \varphi\}$ [1]. Large data sets are available, which consist of scattering patterns from a variety of known materials and from environmental sampling.

Data analysis: Due to the lack of methods which exactly solve the inverse obstacle scattering problem, artificial intelligence techniques can be used. A classifier has been developed that is based on the spectrum enhancement algorithm [2]. This classifier extracts vectors of morphological descriptors from *TAOS* patterns and submits them to principal components analysis. Supervised training of the classifier occurs by processing hundreds of patterns from known materials and maximizing a suitable figure of merit. The trained and validated classifier is applied to patterns from new materials for the purpose of recognition. A typical recent classification result is shown by Figure 1 below.

The purpose of ongoing work is to design classification experiments with patterns from new materials (NaCl crystals, soot, outdoor dust, ...) and apply the above outlined method to particle recognition and scoring.

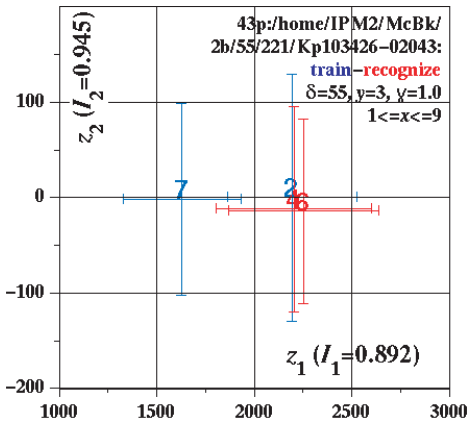

Figure 1: Classifier output on the plane of the first two principal components $\{z_1, z_2\}$. The centroids of pattern classes **2**, **4**, **6**, **7** are mapped on $\{z_1, z_2\}$. Training class **2** corresponds to single, 1.4 micrometer polystyrene latex (*PSL*) spheres, training class **7** to single *Bacillus subtilis* spores. Classes **4** and **6**, respectively coming from pairs and clusters of four *PSL* spheres and used as confounders, are assigned to class **2** with 80% success rate. I_1, I_2 are the fractions of sample variance explained by z_1 alone and by z_1 and z_2 together.

REFERENCES

1. Fernandes, G. E., Y. L. Pan, R. K. Chang, K. Aptowicz, and R. G. Pinnick, "Simultaneous forward- & backward-hemisphere elastic-light-scattering patterns of respirable-size aerosols," *Opt. Lett.*, Vol. 31, 3034–3036, 2006.
2. Crosta, G. F., "Image analysis and classification by spectrum enhancement: New developments," *Proceedings of SPIE*, Vol. 7532, 75320L01–75320L12, 2010, DOI: 10.1117/12.838694.

The Semi-analytic Mode Matching Algorithm for GPR Wave Scattering from Complex Objects Buried in a Dielectric Soil Half Space Illuminated by a Dipole Source

Ann W. Morgenthaler and Carey M. Rappaport
Northeastern University, Boston, MA 02115, USA

Abstract— The Semi-Analytic Mode Matching (SAMM) algorithm is an efficient computational method for modeling single frequency wave scattering from multiple complex-shaped objects in half spaces illuminated by plane wave or dipole sources. SAMM relies heavily on the appropriate choice of coordinate scattering centers (CSCs) to expeditiously expand scattering solutions as superpositions of cylindrical (2D) or spherical (3D) modes, these modes being matched at all dielectric boundaries spanned by discrete "fitting" points to arrive at numerical solutions for the mode coefficients from which the fields may be constructed. Because the CSC locations have been found to be essentially frequency independent and also do not depend strongly on the dielectric contrast between scatterer and background, it can be worthwhile to carefully analyze particular scattering object shapes and store the optimal CSC locations for future use. Scattering fields from multiple targets buried within half spaces can then be assembled from simpler SAMM simulations of the individual targets taken independently in uniform backgrounds, which requires only those CSCs relevant to the particular target to be used in the algorithm. Appropriate combination of the simpler simulations leads to an effective starting solution for a SAMM simulation of a more complex multiple-targets-in-half space geometry. Constructing complex scattering problems from simpler ones can greatly reduce overall computational time, decrease the number of CSCs required, and increase robustness in the full simulations without loss of accuracy in the final fields; this method is not perturbative. Simple configurations of approximate single-target SAMM solutions to initialize multi-target geometries have previously been described for plane wave sources, and this method is extended for dipole sources for which unperturbed analytic solutions are unavailable. Excellent results are obtained by comparing SAMM and Finite Difference Frequency Domain (FDFD) simulations for multiple 2D scattering objects 0.1–15 wavelengths in size buried within dielectric half spaces with either plane wave or dipole sources.

Computing Casimir Forces with LibRWG: An Open-source C++ Code Suite for Boundary-element Analysis of EM Scattering Problems

M. T. Homer Reid[1], **Jacob White**[2], **and Steven G. Johnson**[3]

[1]Department of Physics, Massachusetts Institute of Technology, Cambridge, MA 02139, USA
[2]Research Laboratory of Electronics, Massachusetts Institute of Technology, Cambridge, MA 02139, USA
[3]Department of Mathematics, Massachusetts Institute of Technology, Cambridge, MA 02139, USA

Abstract— Casimir forces are small but measurable interactions between objects that become significant at separation distances around 500 nm or less. Although first predicted in 1948 [1], Casimir forces have only become experimentally relevant in the past decade, with experimental observations in several nanoscale geometries and in commercial MEMS devices [2, 3].

Although the Casimir effect is an entirely quantum-mechanical phenomenon, theoretical work in the 1950s [4] established a connection to classical electromagnetism by showing that the Casimir force between two objects could be computed from knowledge of the *imaginary-frequency dyadic electromagnetic Green's function* $\mathcal{G}(\mathbf{x}, \mathbf{x}'; \beta)$, which describes the field amplitudes at $\mathbf{x}$ produced by a point source of radiation at $\mathbf{x}'$, including the effects of scattering from the material objects in the geometry, and with all quantities having time dependence $\sim e^{+\beta t}$.

The computation of Casimir forces between arbitary objects thus reduces to the problem of determining the electromagnetic scattering properties of the objects, including both geometric effects and the influence of material properties (conductivity, dielectric permittivity, and magnetic permeability). Although this is a well-studied problem in computational electromagnetics, the need to compute all quantities at *imaginary* frequencies introduces new complications and has inspired the development of new algorithms.

We have developed an open-source C++ code suite, libRWG, that uses boundary-element methods to analyze electromagnetic scattering from objects of arbitrary 2D and 3D geometries, with arbitrary material properties (including conductors, dielectrics, and magnetic materials), at both real and imaginary frequencies, using both direct ($O(N^3)$) and fast ($O(N \log N)$) algorithms. The libRWG suite provides both standalone applications and C++ libraries for use in developing higherlevel codes and will be useful to a wide range of researchers in electromagnetic phenomena.

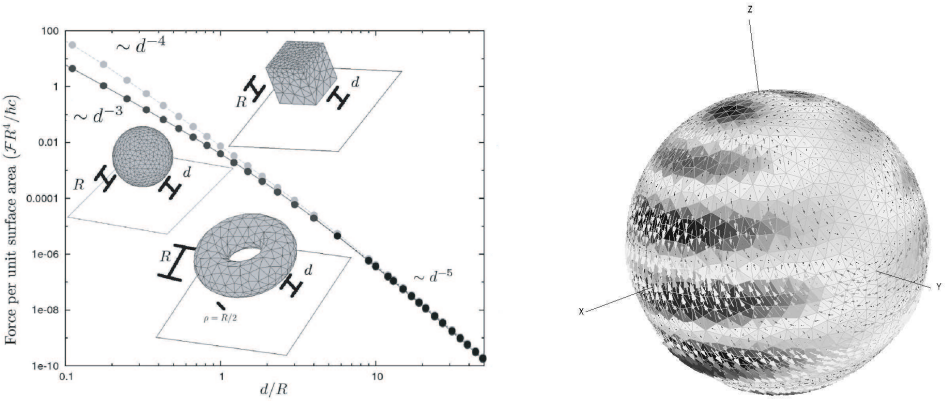

(a) (b)

Figure 1: (a): Casimir force on torus, sphere, and cube above conducting plane, as computed using libRWG. (b) Charge density and surface current induced on a metallic sphere by a (real-frequency) plane electromagnetic wave, as computed using libRWG.

REFERENCES

1. Casimir, H. B. G. and D. Polder, "The influence of retardation on the london-van der waals forces," *Phys. Rev.*, Vol. 73, 360, 1948.

2. Capasso, F., et al., "Casimir forces and quantum electrodynamical torques: Physics and NanoMechanics," *IEEE. J. Select. Topic Quantum Electron.*, Vol. 13, 400, 2007.
3. Ardito, R., et al., "An experimental assessment of casimir force effect in micro-electromechanical systems," *IEEE Sensors 2008 Conference*, 90, 2008.
4. Lifshitz, E. M. and L. P. Pitaevskii, *Statistical Physics*, Part 2, Pergamon, Oxford, 1980.

Computing the Magnetic Induction Field Due to a Radially-magnetized Finite Cylindrical Permanent Magnet by Employing Toroidal Harmonics

J. P. Selvaggi, **S. J. Salon**, **and M. V. K. Chari**
Rensselaer Polytechnic Institute, Troy, NY 12180-3590, USA

Abstract— The authors present a method for computing the external magnetic induction field from a radially-magnetized cylindrical permanent magnet. The method relies on the application of the cylindrical free-space Green's function. The cylindrical free-space Green's function can be expanded in terms of zeroth-order toroidal functions, and this leads to a toroidal harmonic expansion for the inverse distance function between a source point and an observation point. The toroidal harmonic representation allows the cylindrical azimuthal variable to be uncoupled from its axial and radial variables. The uncoupling of the cylindrical azimuthal variable leads to some useful simplifications in the analysis of cylindrical permanent magnets. We will compare this method to a number of other methods and give a few insightful examples of the application of toroidal harmonics.

High Order OcTree Discretization for Maxwell Equations

L. Horesh[1], **E. Haber**[2], **and A. R. Conn**[1]

[1]IBM TJ Watson Research Center, NY, USA
[2]University of British Colombia, BC, Canada

Abstract— OcTree emerges as an appealing discretization structure for modeling and inversion of large-scale problems. Similarly to structured grids, meshing and local mesh refinement are almost trivial, whereas in terms of parameter space representation, it offers great reduction, just like conventional unstructured grids. On the computational level, these structures are natively designed for hierarchical processing by means, offering natural means for application of multi-level pre-conditioners and solvers. All these virtues come with a price, as the construction of differential operators, and in particular the adjoint curl and the gradient operator, is non-trivial. In this study, we introduce for the first time a framework for construction of such operators for 2nd order accuracy. Our approach is based on a two stage process. First, the topology of the OcTree grid is classified, then interpolation conditions provide a set of local systems. The solutions for these small systems yield the desired operator entries. One of the interesting observations we underline is that in a heterogeneous grid, of multiple finite length sizes, there is an interplay between care for construction of differential operators leaning on compact support, and asymptotic error convergence. Lastly, we present results for solution of large-scale systems evolving from Maxwell's equations. In that context, we highlight the difficulties that arise from loss of mimicking properties and symmetry which are sacrificed for higher accuracy. We further show how low order solution for the Maxwell system can be used as a preconditioner for the high order one. The proposed approach seems particularly promising for modeling large-scale PDE problems and its extension to operators of higher order is straightforward.

Ultra Wide Band Communication through Plasma Generated by Corona Effect around High Voltage Line

M. Johnny and S. A. Hassani Gangaraj
Iran University of Science and Technology, Iran

Abstract— The transfer of information plays an important role in communications systems. There is an on going increase in the extension of the lines of information transfer and communications antenna. However, what is very important is this, to forward the greatest amount of information with the least waste of energy. Among these, the communication channel have noticeable share of transferring information. In earth communication applications transmission lines and wave guides act more efficiently than antennas, and with the less power have the best signal to noise ratio. In this paper, we explain the transmission lines created by ionization of gasses surrounding the lines and at the same time we explain the guides parameters this environment and it's taking effect in proportion to the foreign factors such as wind and existing electromagnetic waves of the air. And we'll see that it can be as a channel of transferring information with an ultra wide band.

Novel GLLH EM Cloak with Front Branching and without Exceed Light Speed Violation

Ganquan Xie, **Jianhua Li**, **Lee Xie**, **and Feng Xie**
GL Geophysical Laboratory, USA

Abstract— In this paper, we proposal a GL GravityLess Cloak device. The Gravity wave can not access into the GL gravityless device. The objects inside of the gravityless cloak avoids to be affected by gravity and presents weightless. The simulations of the gravityless cloak and visualization stereographic technology are presented in this paper. It has important applications in novel weightless material and new scientific digit movie visualization as in a new other AVATOR like movie. Its practice will perform myth light effort "Dodge".

Three Dimensional Imaging and Focusing of Ground Penetrating Radar Data

Said I. Elkhetali
The Higher Institute of Electronics Bani Walid, Libya

Abstract— This paper presents three dimensional modelling of electromagnetic wave propagation into the ground to obtain images as seen by ground penetrating radar and the focusing of these images. The proposed application is detection of groundwater in the desert. It takes into consideration the rough surface scattering by subterranean interfaces. Interfaces between earth layers may be rough, causing clutter to the radar receiver. The interfaces could have boulders, surface irregularities and grooves. Especially when the subsurface had been a river channel in the past. This type of channel is a potential aquifer called buried valley aquifer.

Two approaches for modelling scattering from rough surfaces have been tried, namely facet modelling and the continuous rough surface.

Measurements were performed to determine scattering patterns of facets that are smaller than the wavelength since no published data was found in the literature even after searching for scattering by single hydrometeors. The measured scattering patterns are fitted to cosine functions having different powers to compare them to the point scatterer model. The results of simulation by facets are compared to reflection by using geometrical optics. Spatial averaging to reduce the effect of rough surface scattering is investigated.

In addition to buried valleys, bowl and dome shapes are includes, these shapes could be the fundamental "building blocks" for constructing, perhaps, any geological model of a complex ground. Understanding how these appear on the radar image would help in interpretation.

The results of imaging are compared with ray tracing technique because it has been used extensively and proven to give adequate results.

Synthetic aperture radar technique is used for focusing the images.

Session 1P2a
Magnetic Based Composite Materials

A New Mixing Rule for Frequency Dependence of Permeability in Composites

Konstantin N. Rozanov[1], **Marina Y. Koledintseva**[2], **and James L. Drewniak**[2]

[1]Institute for Theoretical and Applied Electromagnetic of Russian Academy of Sciences
13 Izhorskaya ul., 125415 Moscow, Russia
[2]Center for Electromagnetic Compatibility, Missouri University of Science and Technology
4000 Enterprise Dr., HyPoint, Rolla Missouri 65401, USA

Abstract— To engineer microwave properties of composites, including nanocomposites, it is important to be able to adequately predict wideband frequency responses of effective material parameters of composites with various concentrations of inclusions. A number of mixing rules are proposed in the literature to solve this problem, see, e.g., [1]. Currently, for an important case of composites filled with ferromagnetic metal powders, there is no standard and unified experimentally validated mixing rule for calculating dependences both on frequency and concentration [2].

Alternatively to the mixing rules, properties of composites can be considered in terms of the Bergman-Milton theory (BMT), which is based on the concept of a spectral function, an unambiguous and universal characteristic of a composite [3]. All known mixing rules turn out to be particular cases of the BMT, differing by spectral functions. Particularly, the Ghosh-Fuchs theory (GFT) has been proposed recently based on the BMT [4], and it agrees well with measured permittivity and permeability of composites [5], in contrast to the existing mixing rules. However, the GFT as in [4] is not convenient for use, as it exploits an integral representation for the spectral function.

Herein, a simple analytic formulation of the GFT is proposed. The new mixing rule is based on the shape of the spectral function typical for the Bruggeman approximation with both averaged depolarization factor of inclusions and the percolation thresholds introduced as fitting parameters. As the permittivity and permeability of a composite are known to be governed by the same mixing rule [3], these fitting parameters are found from the concentration dependence of permittivity of the composite for further making use for analysis of the permeability. Also, the limiting case of inclusions of low contrast coincides with the Landau-Lifshits-Looyenga (LLL) mixing rule. These requirements lead to a unified equation for the effective material constant (either magnetic or dielectric susceptibility) as a function of inclusion concentration, percolation threshold, and dimension (2D or 3D) of the composite. The mixing law is valid for the case of nearly spherical shape of inclusions in the composite, e.g., stone-like inclusions.

The new presented mixing rules are compared with the measured microwave permittivity and permeability of composites, showing better agreement with the measurements than existing mixing laws. The results obtained, such as the percolation threshold and the intrinsic permeability of inclusions, are consistent with available reference data.

ACKNOWLEDGMENT

K. Rozanov acknowledges financial support of the study from the Russian Foundation for Basic Research (grant Nos. 07-08-92111 and 09-08-00158).

REFERENCES

1. Sihvola, A., *Electromagnetic Mixing Formulas and Applications,* IEE Publishing, 1999.
2. Lagarkov, A. N. and K. N. Rozanov, *J. Magn. Magn. Mater.*, Vol. 321, 2082, 2009.
3. Bergman, D. J. and D. Stroud, *Solid. State Phys.*, Vol. 46, 147, 1992.
4. Ghosh, K. and R. Fuchs, *Phys. Rev. B*, 38, 5222, 1988.
5. Rozanov, K. N., A. V. Osipov, D. A. Petrov, et al., *J. Magn. Magn. Mater.*, Vol. 321, 738, 2009.

Effective Electromagnetic Parameters of Composites Containing Magnetic Platelets

Marina Y. Koledintseva[1], **James L. Drewniak**[1], **and Konstantin N. Rozanov**[2]

[1]Center for Electromagnetic Compatibility, Missouri University of Science and Technology
4000 Enterprise Dr., HyPoint, Rolla Missouri 65401, USA
[2]Institute for Theoretical and Applied Electromagnetic of Russian Academy of Sciences
13 Izhorskaya ul., 125415 Moscow, Russia

Abstract— Design of non-conductive absorbing-type wideband electromagnetic shielding materials is important for EMC/EMI purposes. Absorbing materials are able to eliminate possible surface currents, which are culprits of undesirable emissions [1]. Application of ferrites for developing absorbing materials is attractive, since they possess a unique combination of high permittivity, spontaneous magnetization, and extremely low d.c. conductivity. However, neither hexagonal ferrites, nor isotropically (arbitrarily, randomly) shaped spinels can effectively absorb energy in the frequency range from 100 MHz to 2.5 GHz, which is currently the most interesting range for high-speed electronics applications [2]. But if crystallographically "isotropic" magnetic alloy or ferrite particles are shaped as platelets, they may exhibit high field of form anisotropy due to internal demagnetization. This will substantially help "overcoming" Snoek's limit [3] and increase frequency range of absorbing materials based on such platelets. An analytical model for a composite material containing randomly oriented magnetic platelets presented herein is based on the modified asymmetric Bruggeman's effective medium theory ("1/3-power rule") for permeability. The model takes into account crushing of bulk magnetic material and demagnetization factors of inclusions. Also, some results of analytical modelling of composites containing aligned magnetic platelets are presented.

REFERENCES

1. Koledintseva, M., J. Drewniak, R. DuBroff, K. Rozanov, and B. Archambeault, "Modeling of shielding composite materials and structures for microwave frequencies," *Progress In Electromagnetics Research B*, Vol. 15, 197–215, 2009.
2. Koledintseva, M., J. Drewniak, Y. Zhang, J. Lenn, and M. Thoms, "Engineering of ferrite-based composite materials for shielding enclosures," *Journal of Magnetism and Magnetic Materials*, Vol. 321, 730–733, March 2009.
3. Nakamura, T., "Snoek's limit in high-frequency permeability of polycrystalline Ni-Zn, Mg-Zn, and Ni-Zn-Cu spinel ferrites," *J. Appl. Phys.*, Vol. 88, No. 1, 348–353, 2000.

Electromagnetic Wave Absorption Properties of Metallic Magnet Based Nanocomposites

Jiurong Liu[1], **Jing Kong**[1], **Fenglong Wang**[1], **Masahiro Itoh**[2], **and Ken-ichi Machida**[2]

[1]School of Materials Science and Engineering, Shandong University, China
[2]Center for Advanced Science and Innovation, Osaka University, Japan

Abstract— The rapid development of wireless telecommunication systems and high-frequency circuit devices in GHz range calls for the study of microwave absorbing materials in anti-electromagnetic interference, self-concealing technology, microwave darkrooms and high-frequency circuit design. Comparing with ferrites, metallic magnetic materials have large saturation magnetization values and their Snoek's limit is at a high frequency level. Consequently, the values of complex permeability can remain still high in high frequency range. Therefore, it is possible to make thinner absorbers from metallic magnetic materials than those of ferrites in GHz range. Here, we present the electromagnetic wave absorption properties of metallic magnet based nanocomposites such as α-Fe/Y_2O_3, α-Fe/$Ba_3Co_{1.8}Fe_{23.6}Cr_{0.6}O_{41}$, Fe nanowires et al. in different frequency ranges. Comparing with ferrites as conventional microwave absorption materials, the thicknesses of these nanocomposites containing metallic magnetic nanoparticles decreased by 30–50% in the same frequency region.

High Frequency Magnetic Behaviour of Composites Based on Nanocrystalline Microwires

P. Marín and A. Aragón
Departamento de Física de Materiales, Instituto de Magnetismo Aplicado
Universidad Complutense de Madrid, Nacional VI Km 22,5, Las Rozas, Madrid 28230, Spain

Abstract— Magnetic composites have been prepared by means of amorphous magnetic powder obtained by cutting of FeSiBCuNb of amorphous magnetic microwires fabricated by Taylor's technique. Previously, the influence of annealing temperature on powder chacteristics, like particle size and shape distribution, has been analysed by means of SEM microscopy and XRD and low frequency hysteresis loops of the powders have obtained by means of Vibrating Sample Magnetometer. The influence of powder characteristics on electromagnetic waves absorption has been also characterized at frequencies between 5 and 20 GHz.

"Yin-Yang" Reflection from a Magnetic Photonic Crystal

Shiyang Liu[1], **Wanli Lu**[1], **Zhifang Lin**[1], **and S. T. Chui**[2]

[1]Surface Physics Laboratory, Department of Physics, Fudan University, Shanghai 200433, China
[2]Bartol Research Institute and Department of Physics and Astronomy
University of Delaware, Newark, DE 19716, USA

Abstract— Anyone who has looked at himself in a mirror expects a faithful image from a localized source. As is illustrated in Figs. 1(a)–(c), we find a very surprising result that when an oscillating line source is placed in front of a special mirror consisting of a uniformly spaced flat collection of ferrite rods (indicated by the black circles), the left half of the image disappeared near some particular frequency. We call this phenomenon "Yin-Yang" reflection (YYR), with "Yin" denoting the darkened region and "Yang" the brightened region. The physics behind this is related to the quantized Hall effect (QHE) and one-way magnetic surface plasmon band states.

Electric currents that circulate around the edge of the sample are believed to be responsible for the QHE. Because of the broken time reversal symmetry (TRS) caused by the external magnetic field, this current only goes in one direction. There has recently been much interest in exploring if related phenomena can occur with photons. Among others, a skew scattering effect involving electromagnetic (EM) waves was discussed by Rikken and coworkers, possible edge-like one-way waveguide from magnetic photonic crystal (MPC) bands with finite Chern numberswas discussed by Haldane and Raghu and Wang and coworkers.

We have also been searching for similar phenomena involving EM waves. All QHE experiments deal with transmission. Because of the continuity of the electric and magnetic fields at the boundary, photonic states with giant circulations can be probed using reflection. States with the largest one way circulation are derived from the magnetic surface-plasmon (MSP) bands.

Plasmonic materials are capturing increasing interest due to their different promising applications. Most attention until now has been focused on the electric surface plasmons originating from the collective resonance of electronic density wave and hosted by metallic building blocks. The symmetry of Maxwell's equations with respect to the magnetic and electric degrees of freedom enables a symmetric type of phenomenon in magnetic systems, which is known as a "magnetic surface plasmon". When a periodic array of such material is assembled together, the photonic states that hop from one MSP state to another form a MSP band. In contrast to the electric surface plasmon band, the MSP band states only go in one direction (clockwise, for example),

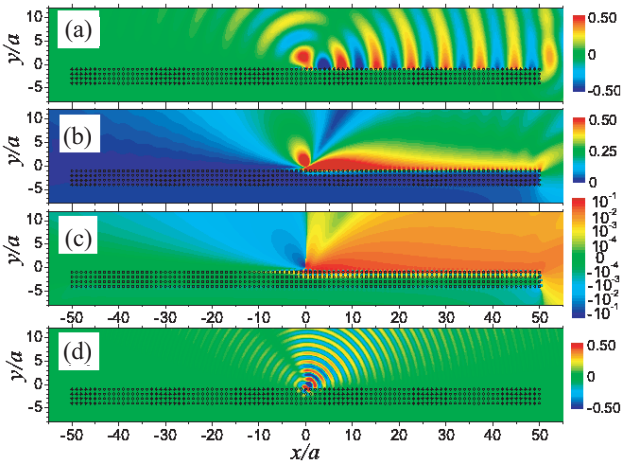

Figure 1: The profile of the electric field with the sinusodial spatial dependence included (a), the amplitude of the electric field (b), and the x-component of the Poynting vector (c) when a line source oscillating at a frequency close to the magnetic surface plasmon resonance is placed near the surface [(0,1.5a)] of a special mirror made of a slab composed of a square lattice of YIG ferrite rods, indicated by the black dots in the figure. Fig. 1(d) displays the electric field when the line source oscillates at a frequency corresponding to the one-way edge mode studied in.

resulting from the breakdown of time reversal invariance caused by the finite magnetic field. The YYR effect comes from the coupling to states derived from these bands.

The YYR effect has the potential to revolutionize microwave circuitry. The diffraction limit requires that the minimum size of waveguides be larger than half the wavelength of light. Surface plasmons have attracted much attention as a way of circumventing the diffraction limit. We show below that the YYR can be exploited to build tunable subwavelength waveguides, beam benders and beam splitters. Furthermore, in these circuits, the EM wave exhibit a "superflow" behavior; the magnitude of the Poynting vector does not decrease in the presence of different kinds of defects.

Session 1P2b
Scattering, Diffraction and Rough Surface Scattering

Relativistic Scattering Processes of Charged Particles in Presence of a Laser Field

Younes Attaourti
University of Cadi Ayyad, Morocco

Abstract— Relativistic Quantum Mechanics as well as Quantum Electrodynamics (QED) are both at the core of the formalism needed to describe the physics of laser-assisted relativistic scattering processes of charged particles. First, a seminal result concerning the important process of Mott scattering in presence of a laser field [1–3] namely the corresponding exact expression of the first order differential cross section (DCS) is presented in the first part of this talk using the relativistic Dirac-Volkov (DV) states [4].

The second part is devoted to specific applications of the DV formalism.

The first one concerns the effects of relativistic electronic dressing in laser-assisted electron-atom elastic collisions [5]. Two main results emerge: dressing effects reduce considerably the magnitude of the first order DCS while a simple formal analogy links the analytical expressions of the DCS in absence and in presence of a laser field.

The second one concerns the effects of this dressing in laser-assisted ionization of atomic hydrogen by electron impact [6].

The third part of this talk will be devoted to the influence of the laser polarization (linear, circular, elliptic) upon the DCS [7]. I will also address the technically difficult study of laser-assisted Mott scattering of polarized electrons [8, 9] where the helicity formalism [10] is of a paramount importance. Finally, I will briefly mention the theoretical breakthroughs needed to tackle the Dirac-Coulomb problem (i.e., the solution of the Dirac equation for atomic hydrogen in presence of a laser field) as well as the extension of the DV formalism to other laser-assisted QED processes.

REFERENCES

1. Szymanowski, C., et al., *Phys. Rev.*, Vol. A56, 3846, 1997.
2. Attaourti, Y. and B. Manaut, *Phys. Rev.*, Vol. A68, 067401, 2003.
3. Manaut, B., Y. Attaourti, S. Taj, and S. Elhandi, *Can. J. Phys.*, Vol. 87, No. 4, 299–310, 2009.
4. Greiner, W. and J. Reinhart, *Quantum Electrodynamics*, 3rd Edition, Springer-Verlag, 2003.
5. Attaourti, Y. and B. Manaut, *Phys. Rev. Phys. Rev.*, Vol. A69, 063411, 2004.
6. Attaourti, Y. and S. Taj, *Phys. Rev.*, Vol. A69, 063411, 2004.
7. Attaourti, Y., B. Manaut, and S. Taj, *Phys. Rev.*, Vol. A70, 023404, 2004.
8. Attaourti, Y., B. Manaut, and S. Taj, *Phys. Rev.*, Vol. A71, 043401, 2005.
9. Manaut, B., Y. Attaourti, S. Taj, and S. Elhandi, *Phys. Scr.*, Vol. 87, No. 4, 299–310, 2009.
10. Leader, E., *Spin in Particle Physics*, Cambridge University Press, 2001.

Enhancement of Radio-wave Diffraction by a Dielectric-column-edge for an Indoor High-frequency Ad Hoc Network: Experiments

Toyokatsu Miyashita, Toshitaka Kato, and Ayumu Kashihara
Dept. Electronics and Informatics, Ryukoku University, Otsu 520-2194, Japan

Abstract— Recently high-speed or high-capacity wireless communications or data transmissions in a small area like room and small building are required and developed for high-quality multimedia devices such as high-definition digital TVs. For such requirements wireless networks at high-frequency and with large frequency bandwidth like UWB are very promising and inevitable. Then we encounter a fundamental problem in the high-frequency radio-wave transmissions, namely sharp geometrical shadowing projected by all kind of metallic or high-absorptance furniture and bulletin boards in the room and walls in the building. Usual indoor reflections and classical knife-edge diffractions [1] prevent insufficiently the high-frequency geometrical shadowing of the radio-waves.

We have reported recently a novel and powerful way to increase the electric field deep in the geometric shadow (GS) by means of a wave-optics originated diffraction by a dielectric-column placed at an obstacle-edge [2, 3]. We have shown by numerical simulations by the FDTD method that (1) enhancements of the electromagnetic field deep in the geometric shadow amount to about 25 dB at 5 GHz, 30 dB at 10 GHz, and 35 dB at 20 GHz, respectively, compared with those by the knife-edge diffraction, and that (2) absolute values of the increased electric field strengths at those frequencies are approximately independent of frequency.

This paper reports an experimental verification of the above mentioned novel enhancement of the radio-wave diffraction into the deep geometric shadow by a dielectric-column-edge. We constructed a half-infinite obstacle of a metallic plate with a dielectric-column-edge and placed a pair of sleeve antennas for transmission and reception in an anechoic chamber, as illustrated in Fig. 1. The distances between each antenna and the obstacle were both 45 cm. The transmitter antenna was oriented toward the edge of the obstacle at grazing incidence, and the receiver antenna moved along Line B keeping a distance of 45 cm from the surface of the obstacle. Removing the dielectric column from the obstacle, we measured the so-called knife-edge diffraction fields at the receiver antenna, as shown in Figs. 2 and 3 by black lines. We use these electric field strengths as the reference values to evaluate the enhancement of the diffraction field.

A dielectric column with a diameter of 7 cm, 6 cm, or 5 cm, which is made of polymethyl methacrylate (PMMA), was attached to the edge of the obstacle, as illustrated in Fig. 1. The measured electric field strengths at 5.6 GHz are plotted in Fig. 2, being compared with those by the knife-edge diffraction of the obstacle itself. These experimental results agree well with the numerical simulations for the same alignments by the FDTD method, and they show a 20 dB enhancement of the electric field strength deep in the geometric shadow, namely at 130 cm from the diffraction edge of the obstacle almost independent of the diameter of the dielectric column, as shown in

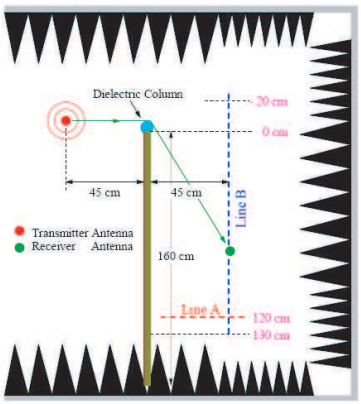

Figure 1: Experimental setup in an anechoic chamber.

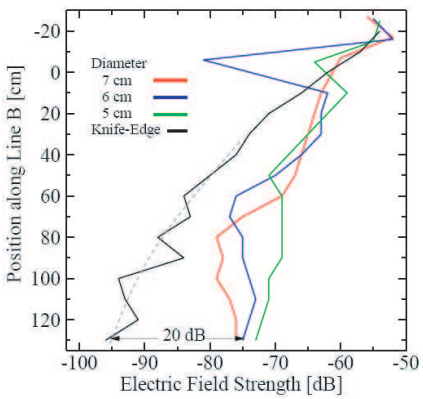

Figure 2: Measured electric field strength at 5.6 GHz.

Fig. 2 and Fig. 3(b). A wideband enhancement of about 10 dB was measured in the geometric shadow at 20 cm from the edge in a frequency range between 3.5 and 13 GHz, as shown in Fig. 3(a).

From these results we can expect that dielectric columns attached to the obstacle edges improve the circumstance of the radio-wave propagation required for high-speed data transmissions and communications in rooms and buildings.

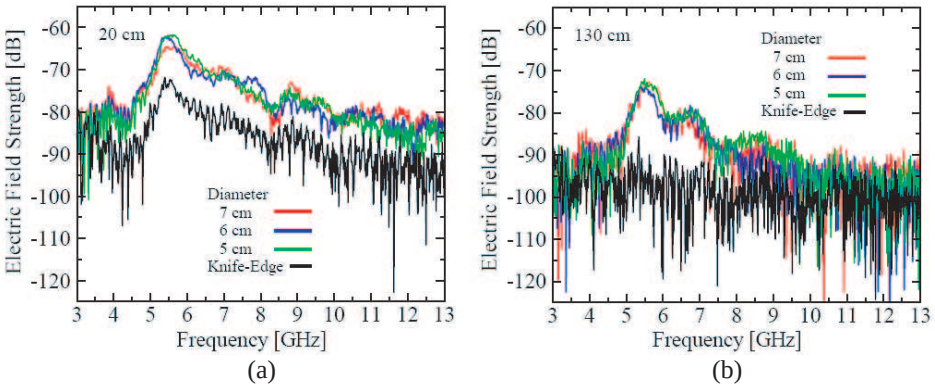

Figure 3: Measured electric field strength along line B. (a) 20 cm in GS, (b) 130 cm deep in GS.

REFERENCES

1. ITU Rec. P.526-10, "Propagation by diffraction," ITU, Geneva, 2007.
2. Vandamme, J., B. Baranowski, and P. Mariage, "High frequency diffraction by a dielectric wedge — Three-dimensional study," *Proc. IEEE Int. Symp. on Personal, Indoor and Mobile Radio Communications*, Vol. 1, 125–129, Sep. 1995.
3. Miyashita, T. and T. Nonaka, "Diffraction of radio waves for ad hoc network in a building by an elliptical dielectric column at the end of an obstacle," *Proc. 38th European Microwave Conference*, 1284–1287, Amsterdam, Oct. 2008.

Qualitative Scattering and Energy Conservation

R. Aramini[1], **G. Caviglia**[2], **A. Massa**[1], **and M. Piana**[3]

[1]Dipartimento di Matematica, Universita di Trento, Trento, Italy
[2]Dipartimento di Matematica, Universita di Genova, Genova, Italy
[3]Dipartimento di Informatica, Universita di Verona, Verona, Italy

Abstract— The linear sampling method is the prototype of qualitative inverse scattering, whereby the scatterer's boundary is highlighted by means of an indicator function related to an approximate solution of the far-field equation. However, some open issues related to the theoretical foundation of this method still hold and are concerned with the physical interpretation of the method. We show that the far-field equation at the basis of the linear sampling method can be interpreted as a constraint on the power fluxes carried out by the Poynting vector associated to the scattered field. Under appropriate assumptions, we prove that this constraint and energy conservation along the flow tubes of this Poynting vector are sufficient conditions for the linear sampling method to work. As an immediate practical consequence, we are also able to specify the role of Tikhonov regularization in the implementation of approximate solutions of the farfield equation.

A Predicting Methodology of Scattering by Clusters of Multi-Objects/Systems Based on Plane Wave Database

Xin-Qing Sheng, **Xiao-Min Pan**, **and Chu-Qiang Deng**
Center for Electromagnetic Simulation, School of Information Science and Technology
Beijing Institute of Technology, China

Abstract— A predicting methodology of scattering by a cluster of multi-objects/systems is proposed in this paper. In this predicting methodology, a representation of scattering by each object/system in the cluster is formulated with plane waves. Then an equation based on this plane wave representation is established for formulating interaction among objects/systems in the cluster. Finally, the equation is efficiently solved with iterative solvers, and the scattering by the cluster is computed. The accuracy and efficiency of this predicting methodology are well validated by various numerical experiments. The numerical performance of the equation for the interaction is also studied in detail. It is shown that the equation established in this paper converges much faster than those in the fast multipole method (FMM). Since the plane wave representation for each object/system can be determined by either measurement or simulation, this predicting methodology can well integrate the measured data and simulation results together for predicting scattering by very complex clusters. Furthermore, since the plane wave representation of each object/system can be established as a database and reused in other clusters, this predicting methodology has high efficiency.

ACKNOWLEDGMENT

This work was supported by the NSFC under Grant 10832002 and the 973 Program under Grant 2005CB321702.

Vectorial Extended Geometrical Optics for Scattering of a Spheroid

K. F. Ren[1], **F. Onofri**[2], **C. Rozé**[1], **and T. Girasole**[1]

[1]UMR 6614/CORIA, CNRS, Université & INSA de Rouen, Av. de l'Université BP 12, 76801, France
[2]IUSTI, UMR CNRS n°6595, Université de Provence, Polytech'Marseille-DME
Technopôle Château Gombert, 5 rue Enrico Fermi, 13453 Marseille cedex 13, France

Abstract— Geometrical optics is a very simple and intuitive method to treat the interaction of an object with light or high frequency electromagnetic waves. One of its main advantages over the others is that it can be applied to objects of complex shape, which are hard or even impossible to be dealt with by rigorous theories or most numerical techniques. The separation variable methods based on the solution of Maxwell equations (or its equivalents) are limited to the objects which can be described in a coordinate system of the same geometry, such as sphere, spheroid, ellipsoid, circular or elliptical cylinder. Even in these "simple" cases the numerical calculation remains still as another obstacle. Except for the sphere and the circular cylinder, the size of the scatterer can hardly exceed few tens of wavelengths. Other "rigorously" established numerical methods such as the T-Matrix, or the Discrete Multipole Approximation, etc. can be applied to non-spherical particles, but the size parameter of the scatter is also severely limited [1].

Many researchers have contributed to the improvement of geometrical optics. Some take into account the forward diffraction or other particular wave effects (Airy theory for the rainbow, and Marston for the critical scattering). Others combine directly geometrical optics with electromagnetic wave method [1, 2]. Really, by these improvements the geometrical optics can be applied to objects as small as about tens of wavelengths. But in these studies interference effects are rarely taken into account. We have shown that, by taking into account the interference of reflection and all refraction rays, as well as forward diffraction, we can predict correctly the scattering diagram in all direction, although the scattering diagram near the critical and rainbow angle is still to be improved [3]. This work confirms that by taking into account properly all the aforementioned effects, we call as "extended geometrical optics", can be precise enough to predict the scattering diagram.

But as soon as geometrical optics is extended to a 3D-object of irregular shape, three difficulties are encountered: 1) Determination of reflection and refraction angles; 2) Calculation of local divergence factors for smooth dielectric surfaces and 3) Phase shift due to focal lines and focal points. To surpass those obstacles, we are developing a so called "Vectorial EXtended Geometrical Optics method (VeXgO)" which consists of three points: rays is dealt with vectors, divergence and focal line phase shifts are calculated by differential geometrics [4] and the total scattered field is treated as the superposition of contributions of all complex fields. For the two special cases of sphere and circular cylinder, we have shown recently that the divergence factors deduced with the differential geometrics are identical to those given by the classical geometrical optics. But the former permits to calculate the divergence factor of single ray bundle and it is very easy to extend to irregularly shaped 3D-objects.

In this communication, we will present the formalism as well as numerical results obtained with VeXgO for the scattering of a Gaussian beam by a spheroid at oblique incidence.

REFERENCES

1. Mishchenko, M. I., J. W. Hovenier, and L. D. Travis, *Light Scattering by Nonspherical Particles: Theory, Measurements, and Applications*, Academic Press, 2000.
2. Yang, P. and K. N. Liou, "Geometrics-optics-integral-equation method for light scattering by nonspherical ice crystals," *Appl. Opt.*, Vol. 35, No. 33, 6568–6584, 1996.
3. Xu, F., K. F. Ren, X. Cai, and J. Shen, "Extension of geometrical-optics approximation to on-axis Gaussian beam scattering II. By a spheroidal particle with end-on incidence," *Appl. Opt.*, Vol. 45, No. 20, 5000–5009, 2006.
4. Deschamps, G. A., "Ray techniques in electromagnetic," *Proc. IEEE*, Vol. 60, No. 9, 1022–1035, 1972.

On the Scattering from Tilled Row Soils

Francesco Mattia
Consiglio Nazionale delle Ricerche (CNR)
Istituto di Studi sui Sistemi Intelligenti per l'Automazione (ISSIA), Via Amendola 122/D, Bari, Italy

Abstract— Recent experimental studies have documented the existence of strong differences (e.g., 3 dB–6 dB) between the C-band backscatter of agricultural fields observed, within 30 minutes of each other, by the ENVISAT ASAR and the ERS-2 AMI systems nominally under the same imaging geometry (a difference in the azimuthal look angle less than 1 deg. can be estimated). Such a very directional scattering pattern in the backscatter response of sparsely vegetated agricultural soils (denominated "flashing fields", see [1]) require a better understanding of the scattering from anisotropic rough surfaces (i.e., tilled soils) and, in particular, of the coherent contributions arising in the backscattering from agricultural surfaces. Previous studies [2] have modelled the tilled soils as quasi-periodic rough surfaces and shown that their scattering pattern is a convolution of the scattering of sinusoidal and isotropic rough surfaces. Shin and Kong (1984) have demonstrated that the total backscatter of quasi periodic surfaces consists of three terms, one due to the coherent field and the other two arising from the incoherent scattered field. However, all the simulations reported in Shin and Kong (1984) only concerned with one of the terms contributing to the incoherent scattering and could not predict highly directional backscattering patterns. The other two terms were disregarded because their expressions were found depending on the Dirac-δ function and therefore were not given in a finite form.

In this context, the objective of this work is to extend the Shin and Kong (1984) model in order to compute in a finite form all the coherent and incoherent terms contributing to the total backscatter of quasi-periodic rough surfaces and investigate the zenithal and azimuthal patterns of the derived backscatter. The aforementioned extension requires to take explicitly into account the sphericity of the incident wave and the antenna pattern characteristics and leads to new expressions of the radar backscatter. The latter not only depend on the surface parameters introduced by Shin and Kong (1984) but also on the radar spatial resolution (i.e., ρ_x & ρ_y). Furthermore, the new model can describe the case of quasi-periodic rough surfaces having quasi-parallel row directions as this is a more realistic condition for agricultural soils.

In the paper, the behaviour of the new backscattering coefficient, in the zenithal and azimuthal planes, as a function of SAR and roughness parameters is illustrated and discussed.

REFERENCES

1. Wegmüller, U., et al., "'Flashing fields' in nearly simultaneous ENVISAT and ERS-2 C-band SAR images," *IEEE Transactions on Geoscience and Remote Sensing*, Vol. 44, No. 4, April 2006.
2. Shin, R. T. and J. A. Kong, "Scattering of electromagnetic waves from a randomly perturbed quasi-periodic surface," *J. Appl. Phys.*, Vol. 56, No. 1, 1984.

Analysis of Electromagnetic Scattering from Rough Layered Interfaces by Means of the Curvilinear Coordinate Method

Kofi Edee[1, 2], Gérard Granet[1, 2], Richard Dusséaux[3], and Saddek Afifi[4]

[1]Clermont Universite, Universite Blaise Pascal, LASMEA, BP 10448, Clermont-Ferrand F-63000, France
[2]CNRS, UMR 6602, LASMEA, F-63177 Aubiere, France
[3]Universite de Versailles, LATMOS, UMR 8190, 10-12 Avenue de l'Europe, Velizy 78140, France
[4]Department of Electronics, University Badji Mokhtar, P. O. Box 12, Annaba 23000, Algeria

Abstract— We consider the problem of scattering from a layer with two faces separated by a mean distance d. Functions $a_1(x)$ and $a_1(x)$ describe the upper and lower interfaces respectively. We assume that the interfaces are Gaussian random processes, centered and stationary to the second order. For numerical applications, the random interfaces are uncorrelated and characterized by Gaussian correlation functions. We also study the case where the interfaces are identical and are thus perfectly correlated. The scattering properties relevant to the statistical surface are obtained by averaging the fields over N realizations of the random profile. These profiles are obtained by a Gaussian filter applied to random uncorrelated numbers characterized by a normalized Gaussian distribution. The structure is illuminated by a Gaussian beam.

The solution to the electromagnetic problem is obtained by using the Curvilinear Coordinate Method which is an exact modal method based on Maxwell's equations under covariant form written in a non-orthogonal coordinate system [1]. In our previous work [2–5], we have presented the implementation of this covariant formalism for analyzing 1D and 2-D random rough surfaces and we have checked Monte-Carlo simulation results by comparison with published numerical and experimental data. The present work deals with a new development of the Curvilinear Coordinate Method as applied to scattering from layers with rough faces. Indeed, since each face is associated to a coordinate system, it is necessary to match eigensolutions obtained in one coordinate system to those obtained in the other one. The above approach has already been used in the case of periodic structures. For the first time, it is implemented for layers with rough faces and successfully compared with results given by a surface integral method [6].

REFERENCES

1. Chandezon, J., D. Maystre, and G. Raoult, "A new theoretical method for diffraction gratings and its numerical application," *J. Opt. (Paris)*, Vol. 11, 235–241, 1980.
2. Dussèaux, R. and C. Baudier, "Scattering of a plane wave by 1-dimensional dielectric rough surfaces — Study of the field in a nonorthogonal coordinate system," *Progress In Electromagnetics Research*, PIER 37, 289–317, 2002.
3. Baudier, C., R. Dusseaux, K. S. Edee, and G. Granet, "Scattering of a plane wave by one-dimensional dielectric random surfaces — Study with the curvilinear coordinate method," *Waves in Random and Complex Media*, Vol. 14, 61–74, 2004.
4. Ait Braham, K., R. Dussèaux, and G. Granet, "Scattering of electromagnetic waves from twodimensional perfectly conducting random rough surfaces — Study with the curvilinear coordinate method," *Waves in Random and Complex Media*, Vol. 18, 255–274, 2008.
5. Dussèaux, R., K. Ait Braham, and G. Granet, "Implementation and validation of the curvilinear coordinate method for the scattering of electromagnetic waves from two-dimensional dielectric random rough surfaces," *Waves in Random and Complex Media*, Vol. 18, 551–570, 2008.
6. Saillard, M. and G. Toso, "Electromagnetic scattering from bounded or infinite subsurface bodies," *Radio Sci.*, Vol. 32, 1347–1359, 1997.

Session 1P3a
Static Magnetic Fields — Biological Effects

Biological Effect of Strong Static Magnetic Field on Mosquito Egg Hatching and Bacterium Shewanelle Oneidensis Gene Expression

Hongjun Pan
Department of Chemistry, The University of North Texas, Denton, Texas 76203, USA

Abstract— The biological effects of strong static magnetic field on mosquito egg hatching and bacterium Shewanelle oneidensis gene expression were studied. In the study of the effect of strong static magnetic field on mosquito egg hatching, fresh laid mosquito eggs were placed in the centers of 9.4 T and 14.1 T magnets, the bottom floor of the magnets and 8 m away from the 9.4 T magnet respectively; the room compressed air was blown around the samples boxes to keep the same temperature and moisture around the sample boxes. The hatching status of the eggs was monitored by counting the larvae hatched in various time periods. Apparent biological effects of strong magnetic fields were observed in the hatching behavior of fresh mosquito eggs. In the first experiment performed at $20 \pm 1^{\circ}$C, the hatching was delayed 32 h by a 9.4 T magnetic field and 71 h by a 14.1 T magnetic field. In the second experiment performed at $22 \pm 1^{\circ}$C, the hatching was delayed 14 h by a 9.4 T magnetic field and 27 h by a 14.1 T magnetic field. In the magnetic field range of this study, the hatching delay increases nonlinearly with the intensity of the magnetic field. The experimental results also suggest that the biological effects of magnetic fields could be reversible or partially reversible to some extent.

In the study of the effect of strong static magnetic field on bacterium Shewanelle oneidensis gene expression, the Shewanelle oneidensis cells in mid-log phase were inoculated at the ratio 1 : 100 and transferred to two sterilized glass vials containing 15 ml Luria Broth agar liquid medium, the glass vials were mounted on a mechanical shaking device and then were inserted into the 14.1 T magnet, one glass vial was at the center of the 14.1 T magnet and the other vial was at the bottom floor of the magnet. The effect of a 14.1 T magnetic field on log phase cells of bacterial strain Shewanella oneidensis MR-1 after 12 hours in the 14.1 T magnetic field was evaluated by using whole genome microarray of this bacterium. The result indicates that no differences were observed between the treatment and control by measuring the optical density (OD), colony forming unit (CFU), as well as post-exposure growth of cells; however, according to our microarray data, transcriptional expression levels of 65 genes were altered. Among these genes, 21 were upregulated while other 44 were downregulated, compared with control.

High Magnetic Fields Interact with the Vestibular System of Rodents

Thomas A. Houpt[1] **and James C. Smith**[2]

[1]Departments of Biological Science, Florida State University, Tallahassee, FL 32306, USA
[2]Departments of Psychology, Florida State University, Tallahassee, FL 32306, USA

Abstract— With increased magnetic field strength in MRI machines, there are also more reports of vestibular perturbation such as motion sensations, vertigo, and nausea while moving through the large gradients.

We have developed an animal model to explore the interactions of high magnetic fields with the vestibular systems. Rats or mice were exposed to magnetic fields of 7–14 T. We have observed 4 phenomena: 1) Immediately after exposure, rats and mice walked or swam in tight circles; the direction of circling was dependent on the orientation of the animal during exposure, 2) when magnet exposure was paired with consumption of a novel, sweet solution, animals acquired a conditioned taste aversion and subsequently avoid the sweet solution. 3) Magnet exposure activated vestibular nuclei within the brainstem, as measured by the induction of c-Fos. 4) When trained to climb a plastic mesh ladder to reach a food reward, rats refused to climb into the bore of a 14 T magnet, suggesting immediate detection of the magnetic field.

These phenomena are consistent with vestibular perturbation. To test this hypothesis, rats were chemically labyrinthectomized. In the absence of the inner ear, all of the effects of the magnetic field were abolished. To test a specific component of the inner ear, we tested mutant mice lacking otoconia. Both head-tilt and tilted-head mice were not responsive to the magnetic field. Thus, high magnetic fields appear to interact with the calcium carbonate otoconia that serve as inertial masses in the inner ear.

Phagocytosis of Dying Cells: Influence of Static Magnetic Fields

Luciana Dini
Dept. Biological and Environmental Science and Technology, University of the Salento, Lecce, Italy

Abstract— One of the paradoxes of the life is that cell death is crucially required for the survival and homeostasis of multicellular organisms. The mass of dead cells need to be promptly and selectively removed by phagocytosis for tissue homeostasis to be maintained. It is becoming evident that failure in the removal of dying cells causes and/or promotes the onset of chronic diseases. Impairment of phagocytosis of apoptotic cells can be due to many factors that are not only due to genetic or molecular malfunctioning but also to external/environmental factors. Static magnetic fields, one of these environmental factors, has been recently reported to modulate the clearance of apoptotic cells. Phagocytosis of apoptotic cells by sinusoidal liver cells is down-regulated when performed in presence of static magnetic fields (SMFs) of moderate intensity. However, the influence of SMFs on the phagocytic ability of macrophages is also related to the degree of differentiation of the cells. Monocyte/macrophage differentiation can be achieved by incubating THP-1, monocytic, and U937, promonocytic cells, with 12-O-tetradecanoylphorbol-13-acetate (TPA, 50 ng/mL), a phorbol ester, for 3 days. Progressively cells acquire the ability to internalize becoming active phagocytes. Fluid phase endocytosis and phagocytosis of latex particles and apoptotic cells in TPA-induced U937 and THP1 cells were studied in the presence of 6 mT SMF. Phagocytosis but not fluid phase endocytosis was affected by SMF exposure. During the phagocytosis assays (with latex particles) under SMF exposure, the phagocytosis index decreased while the number of particles bound to the plasma membrane increased. These SMF mediated effects were higher at the early stages of the macrophage differentiation (THP1 > U937 cells). Only differentiated THP1 cells could bind and internalize apoptotic cells. Non-differentiated THP1 cells could only bind apoptotic cells at very low rate (5–7%) but not engulf them. Exposure of differentiated THP-1 cells to SMF during phagocytosis promoted engulfment of apoptotic cells preventing their binding. Modulation of the phagocytosis of apoptotic cells by SMFs is likely dependent by a combination of factors: Alteration of the distribution and exposure of membrane proteins and glycoproteins, dearrangement of cytoskeleton and alteration of trans-membrane fluxes of $[Ca^{2+}]i$.

Mice Can Detect Very Low Frequency Magnetic Fields: The Threshold Amplitudes of These Nano Tesla Are Frequency Dependent

Frank S. Prato
Lawson Health Research Institute, Canada

Abstract— Previous experiments with mice have shown that a repeated 1 hour daily exposure to an ambient magnetic field-shielded environment induces analgesia (antinociception). This shielding reduces ambient static and extremely low frequency magnetic fields (ELFMF) by more than fifty times for frequencies below 120 Hz. To determine the threshold of ELFMF amplitude that would abolish this effect, 30 and 120 Hz magnetic fields were introduced into the shielded environment at amplitudes of 25, 50, 100 and 500 nT. As the frequency was increased from 30 to 120 Hz, the threshold decreased from approximately 500 nT to 50 nT. At 60 Hz the threshold was below 300 nT. Surprisingly, these results support a simple induced current mechanism rather than a radical pair mechanism. Further, these results suggest that mice may be able to detect the weak magnetic fields introduced into their environment by electrical power distribution and use.

Effects of Long Term Exposure of GH3 Cells to Static Magnetic Fields

Arthur D. Rosen and Erin E. Chastney
Department of Biological Sciences, Purdue University
Lilly Hall West Lafayette, IN 47907,USA

Abstract— There is considerable interest regarding the influence of static magnetic fields (SMFs) on biological systems. Moderate intensity fields (1 mT to 1 T) have been shown to affect the somatosensory evoked potential in rats, the visual evoked potential in cats, movement of *Paramecia*, the spontaneous discharge frequency of cells in the lateral geniculate body of cats, the frequency of miniature end plate potentials at the murine neuromuscular junction, the spontaneous discharge frequency of ganglia cells in *Helix aspersa*, and the evoked potential in the mouse hippocampus. All of the effects attributed to brief exposure to moderate intensity SMFs have been of relatively short duration, with return to baseline function within minutes following termination of exposure. It appears that the major factor involved in moderate intensity SMF influence on cellular function is related to changes in intracellular Ca^{2+} concentration. It has been suggested that the transient effects of exposure to these fields may be attributable to the collective diamagnetic properties of membrane phospholipids that realign sufficiently to distort the intramembraneous portion of ion channels. An alternative hypothesis suggests that their effect is by means of alterations in the release of Ca^{2+} from cellular stores. The present study was carried out to ascertain if a prolonged exposure to moderate intensity SMFs might have an effect on such basic cellular functions as growth and size.

In the present study GH3 cells were cultured during continuous exposure to a 0.5 T SMF, for periods of up to five weeks. Following a one week exposure, cell growth was found to decline by 22% with return to control levels in one week. Although this was not statistically significant it did represent a trend. A two week exposure was associated with a statistically significant decline of 37% with return to control levels in two weeks, and a four week exposure was associated with a statistically significant decline in growth of 51% with return to control levels delayed for up to four weeks. Cell diameter, on the other hand, was seen to significantly increase following three weeks of exposure with return to control levels after three weeks following termination of exposure.

Ca^{2+} dependent changes in the dynamic reorganization of the actin cytoskeleton are suggested as the probable explanation for these observations. This structure is involved in a continuous process of dynamic reorganization modulated, in large measure, by calcium. Cytoskeleton reorganization, although relatively slow, is cumulative. It would eventually be reflected not only in the structure of the plasma membrane but in cytokinesis, disruption of which would explain decreased rate of growth coupled with an increase in cell size. In addition, this process is expected to be reversible, since the genetic components of the cell remain unchanged.

Session 1P3b
Applicators for Medical and Industrial Applications of EM Field

A Variable Step Size Algorithm for Blind Equalization of QAM Signals

Wei Xue[1, 2], **Xiaoniu Yang**[1], **and Zhaoyang Zhang**[2]

[1]National Laboratory of Information Control Technology for Communication System
Jiaxing, Zhejiang 314033, China
[2]Department of Information Science and Electronic Engineering
Zhejiang Uinversity, Hangzhou, Zhejiang 310027, China

Abstract— The constant modulus algorithm (CMA) is one widely used algorithm for blind equalization of QAM signals. The algorithm exhibits slow convergence rate and large steady state mean square error and the phase-blind nature in comparison with the algorithms used in conventional data-aided equalization schemes. In this paper, a variable step size modified constant modulus algorithm is proposed. The proposed algorithm can speed up convergence rate and decrease steady state mean square error and correct phase error and frequency offset at the same time. The simulation results demonstrate the effectiveness of the proposed algorithm in improving convergence rate and reducing steady state mean square error.

Metamaterial Hat

Soheil Hashemi[1], **Ali Mohtadi**[1], **Ali Abdolali**[2], **and Homayoon Oraizi**[2]

[1]Department of Electrical and Computer Engineering, Tehran University
Tehran 14395515, Iran
[2]Department of Electrical Engineering, Iran University of Science and Technology
Tehran 1684613114, Iran

Abstract— Due to the fact that the electromagnetic fields have an effect on different body organs and their functions and that there should be a specific range for these fields, in this paper the attempt is to decrease the transmission of waves to the interior body organs by means of utilizing an appropriate covering on the body. So the main goal of this paper is acquiring the optimal characteristics of that covering and comparing the conventional materials with Metamaterial.

Validating the Four-zero Conductivity Model for Wave Propagation in Dispersive Media with FDTD

Sarah Brown, Sherrette Yeates, and Carey Rappaport
Gordon-CenSSIS, Northeastern University, Boston, MA 02115, USA

Abstract— For wave-based sensing applications, such as microwave cancer detection, it is essential to carefully model frequency dependent propagation and scattering of lossy dispersive biological tissue. In order to apply finite difference time domain (FDTD) techniques, a supplemental time domain equation can be used to model the conductivity function, with an assumption of constant average real permittivity. The Four-Zero Conductivity Model provides a single-pole, rational function of the Z-transform variable well suited for finite difference applications. The residual frequency-dependent imaginary part of the conductivity adds to the average dielectric constant, which in most cases, results in reasonable fit for the complex wave number. A major consideration is the equation for stability, which requires that its four zeros to lie within the unit circle in the complex Z-plane.

The powerful technique of time reversal imaging is currently limited to lossless media, both for frequency domain and time domain computations. This is due to the instability caused by inverting loss for the forward problem into gain for the reverse problem. FDTD has the potential to accurately model loss in time reversal, since the computation can be terminated before a growing signal becomes unbounded, but the usual von Neumann stability condition must be modified. For dispersive media, this is even more critical, since the models for dispersion produce multiple zeros, all of which must be in stable regions of the complex plane. Artificial loss can be added to stabilize time reversed dispersive models and drive all the zeros into the stable regions. As this artificial loss is applied in the time difference operator, a corresponding amount of gain can be reintroduced to the field everywhere after several time steps to compensate for the step-by-step attenuation. The artificial loss parameter is tested in the frequency domain model and shows promising increased stable solutions.

The unique tissue parameters generated by the data and stability analysis model are validated in a second model. This one dimensional FDTD model uses a modulated Gaussian wave to simulate the forward propagation of electromagnetic waves in each tissue. It was found that it is essential to launch the wave into a layer of dispersive medium from a free space half space. Absorbing Boundary Conditions are placed at the first and last space points to reduce reflections in the reverse direction of propagation. A table of stable and verified Four Zeros Conductivity parameters has been compiled. The models currently demonstrate stability in forward propagation for twelve tissues including breast fat, cancellous bone, liver and kidney tissues.

Microwave Heating of Acids in Chemical Industry

Jan Vrba[1], **Jan Vrba (Jr.)**[2], **and David Vrba**[1]

[1]Czech Technical University in Prague, Dept. of EM Field
Technicka 2, Prague 6, Czech Republic
[2]RWTH Aachen University, Chair of Electromagnetic Theory
Kopernikusstraße 1652074, Aachen, Germany

Abstract— In cooperation with Research Institute in Ustí n/L we developed applicator for microwave heating of acids, which is working at frequency 2.45 GHz. In this contribution we would like to describe our new analytic model of microwave applicator. The purpose of the present work is to investigate influence of distribution of the electric field strength on the dielectric properties of acids. We have numerical simulation and the analyses of the electric field strength in the acid volume.

Our new model is created by several cells. Every cell has own magnetron which is source of electromagnetic energy. Magnetron is situated in the waveguide which is ended with acid load.

Conclusions: New results in optimization of microwave heating of acids are described in this paper. These results will enable us to increase efficiency of industrial processes.

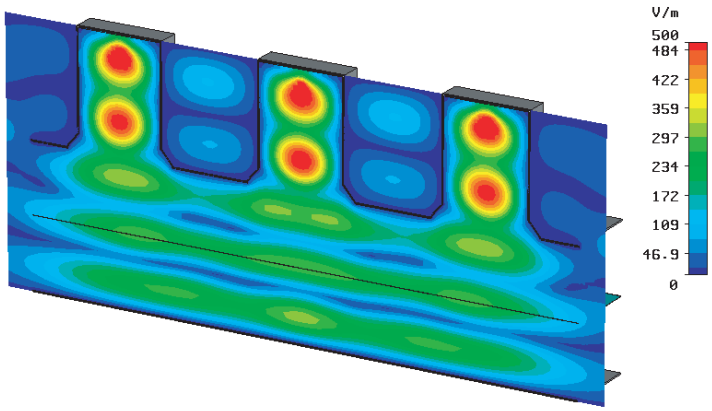

Figure 1: Distribution of electric field strength in applicator.

Resonances in Aperture of Waveguide Applicators for Microwave Thermotherapy

Jan Vrba[1], **Jan Vrba (Jr.)**[2], **and David Vrba**[1]

[1]Czech Technical University in Prague, Dept.of EM Field, Technicka 2, Prague 6, Czech Republic
[2]RWTH Aachen University, Chair of Electromagnetic Theory
Kopernikusstraße 1652074, Aachen, Germany

Abstract— In this contribution we would like to describe our new results dealing with waveguide hyperthermia applicators, typically used for cancer treatment. We have designed and evaluated a water filled lens applicator (aperture of a the rectangular waveguide applicator is divided into 3 or 5 sectors with shifted excitation).

We would like to present theoretical model of this applicator, results of numerical modelling and experimetal evaluation as well. Focusing principle of the lens applicator enables to increase the depth of efficient heating in comparison with waveguide applicators.

The basic schematics of the discussed type applicator is shown in the following figure. The aperture of lens applicator is divided into 3 or 5 sectors with shifted excitation (i.e., different amplitude and phase). To achieve deep local treatment by aid of this applicator we can thus use a focusing principle.

In our contribution we will discuss our results with the design of this type applicator and also some first experiments will be presented.

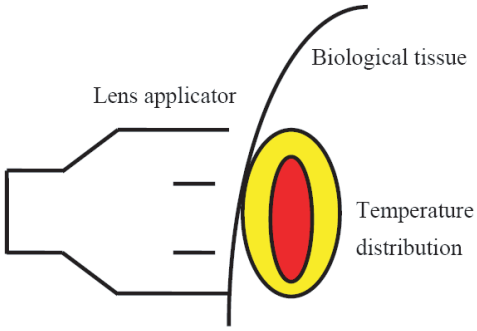

ACKNOWLEDGMENT

This research is supported by the Grant Agency of the Czech Republic and by the Ministery of Education, Youth and Sport of the Czech Republic.

Exposure Systems for Research of EM Field Biological Effects

Jan Vrba[1], **Lukas Visek**[1], **Ladislav Oppl**[1], **David Vrba**[1], **and Luca Vannucci**[2]

[1]Czech Technical University in Prague, Dept.of EM Field, Technicka 2, Prague 6, Czech Republic
[2]Institute of Microbiology, Czech Academy of Sciences, Prague, Czech Republic

Abstract— Microwave thermotherapy is being used in medicine for the cancer treatment and treatment of some other diseases just for many years. The goal of the proposed paper is to describe design and experimental evaluation of a new type applicator for microwave thermotherapy, which will be compatible with MR. The first applicator of this type is just being used for a hyperthermia treatment of the experimentally induced pedicle tumors of the rat.

Description of the Discussed Applicator: The main goal of the planned biological experiment is a hyperthermia treatment of the experimentally induced pedicle tumors of the rat to verify the feasibility of ultrasound diagnostics and magnetic resonance imaging respectively to map the temperature distribution in the target area of the treatment. That means to heat effective volume of approximately cylindrical shape (diameter approx. 2 cm, heigth approx. 3 cm). Temperature to be reached is 41°C or more (i.e., temperature increase of at least 4°C from starting point 37°C), time period of heating is 45 minutes.

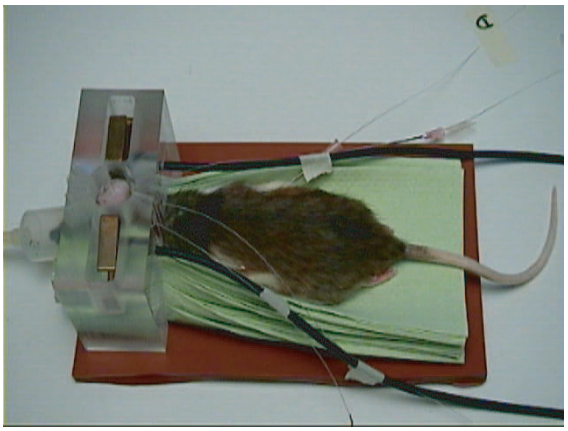

Figure 1: Photograph of the discussed applicator.

Considering the necessary effective heating depth for the planned experiments, we have found 915 MHz to be suitable frequency. As an excellent compatibility of the applicator with non-invasive temperature measurement system (ultrasound or MR) is a fundamental condition for our project, we should have to use non-magnetic metallic sheets of minimised dimensions to create the conductive elements of the applicator. Therefore, the applicator itself is created by two inductive loops tuned to resonancy by capacitive elements. The position of the loops is fixed by persplex holder. There is a special cylindrical space for experimental animal in lower part of this persplex holder. As the heated tissue has a high dielectric losses, both loops are very well separated and so no significant resonance in heated area can occur. From this follows, that either the position of the loops with respect to heated area or the distance between the loops is not very critical.

Evaluation of the Discussed Applicator: First measurements to evaluate the basic properties of the discussed applicator were done on agar phantom of muscle tissue:

- evaluation of basic microwave properties (transfer of EM energy to the tissue, reflections),
- evaluation of compatibility with US and MR,
- calculation and measurement of SAR and temperature distribution and its homogeneity.

ACKNOWLEDGMENT

This research is supported by Czech Research Programme: "Transdisciplinary Research in the Area of Biomedical Engineering" (J04/98: 210000012) and by Grant Agency of the Czech Republic, project: "Microwave Thermotherapy in Cancer Treatment" (102/02/0128).

Session 1P4
Microwaves and Magnonics: Metamaterials, Antennas, Near-field Structures

Arrays of Magnetic Nano-elements as Magnonic Meta-materials: Insights from Analytical and Numerical Modeling

M. O. Dvornik[1], **O. Dmytriiev**[1], **P. V. Bondarenko**[2], **B. A. Ivanov**[2], **and V. V. Kruglyak**[1]

[1]School of Physics, University of Exeter, Stocker Road, Exeter, EX4 4QL, UK
[2]Institute of Magnetism, NASU, Kiev 03127, Ukraine

Abstract— Magnonics (the study of spin waves at the nanoscale and their coupling to excitations of other nature) is rapidly gaining momentum as a new interdisciplinary field of research. In this paper, we report results of our numerical and analytical studies of arrays of magnetic nano-elements as magnonic meta-materials. The analytical modeling is based on the theory described in Ref. [1]. The micromagnetic simulations have been performed using the Object Oriented Micromagnetic Framework (OOMMF) [2], modified to take advantage of parallel calculations.

We show that, in closely packed magnetic arrays, the discrete spectrum of magnonic excitations in individual nano-elements splits into magnonic bands separated by magnonic band gaps, very much in the same way as discrete electronic levels of isolated atoms split into electronic band structure in natural materials. With respect to long wavelength spin waves and microwaves, the arrays behave like effective materials — magnonic meta-materials.

The coupling between elements responsible for the splitting is largely due to the dynamic magneto-dipole interaction. Also, the non-uniform average demagnetizing field within whole arrays leads to localization of magnonic modes in regions of low average internal field near the arrays' edges perpendicular to the applied magnetic field. Due to the absence of exchange coupling between elements within arrays, their ground configuration of the arrays is significantly non-uniform, leading to a remarkable complexity of the observed magnonic spectrum. When the value of magnetic damping is increased, the spectrum consists of fewer peaks of larger width, formed by many modes. We show however that, even in the case of realistic damping investigation of the spatial charter of individual modes might be possible. The theory is then applied to the experimental data acquired using time resolved scanning Kerr microscopy [3]. Finally, we compare the dynamical behavior of finite size arrays of nano-elements against continuous magnetic elements of the same size.

ACKNOWLEDGMENT

The research leading to these results has received funding from the European Community's Seventh Framework Programme (FP7/2007-2013) under Grant Agreement No. 233552, from the Engineering and Physical Research Council (EPSRC) of the UK, and from the Oversees Research Scholarship Academic Scheme (ORSAS).

REFERENCES

1. Galkin, A. Y., B. A. Ivanov, and C. E. Zaspel, *Phys. Rev. B*, Vol. 74, 144419, 2006.
2. Donahue, M. and D. G. Porter, "The Object oriented micromagnetic framework (OOMMF) project at ITL/NIST," URL: http://math.nist.gov/oommf.
3. Kruglyak, V. V., P. S. Keatley, A. Neudert, R. J. Hicken, J. R. Childress, and J. A. Katine, *Phys. Rev. Lett.*, Vol. 104, 027201, 2010.

Patch Antenna with Small Ferrite Particles

M. Sigalov[1], **R. Shavit**[2], **and R. Joffe**[2]

[1]Research Department, RF Dynamics LTD, Kfar Saba 44643, Israel
[2]Department of Electrical and Computer Engineering, Ben-Gurion University of the Negev
Beer-Sheva 84105, Israel

Abstract— The inherent anisotropy and nonreciprocal properties of ferrite materials make them very attractive for using in different types of antenna applications. A ferrite is a magnetic dielectric with low losses. This characteristic allows the electromagnetic waves to penetrate into the ferrite and results in an effective interaction between the electromagnetic waves and the ferrite magnetization. Several applications for frequency tuning, pattern beam steering and radar cross section control using an integration of ferrite materials into printed microstrip antennas have been published in the literature.

In this work, we will show that insertion of a small piece of a magnetized ferrite into a cavity region of the patch antenna (see Fig. 1) leads to very specific topological-phase characteristics. We will demonstrate that the power-flow lines of the microwave-cavity fields interacting with a ferrite sample, in the proximity of its ferromagnetic resonance (FMR), may form whirlpool-like electromagnetic vortices (see Fig. 2). This fact, arising from special boundary conditions for the tangential components of the fields on the dielectric-ferrite interface, causes the time-reversal symmetry breaking effect in microwave resonators with the inserted ferrite samples. When microwave resonators contain enclosed gyrotropic-medium samples, the electromagnetic-field eigenfunctions will be complex, it means that the fields of eigen oscillations are not the fields of standing waves in spite of the fact that the eigen frequencies of a cavity with gyrotropic-medium samples are real.

Our numerical and experimental investigations show that the structures of the near and far fields of the patch antenna are intimately related to the ferrite-induced topological singularities. We show that different types of the field polarizations can be obtained in different frequency bands by appropriate manipulations with the number of ferrite particles and their positions under the patch.

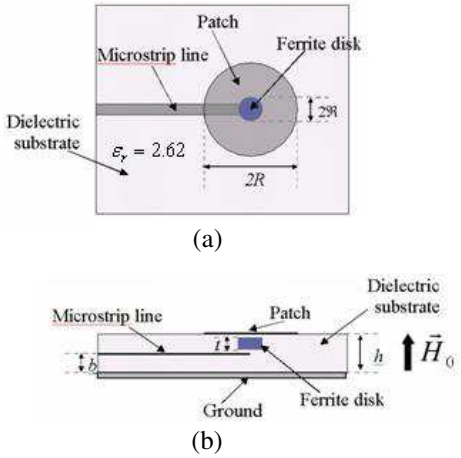

Figure 1: Circular patch antenna: (a) Top view, (b) side view.

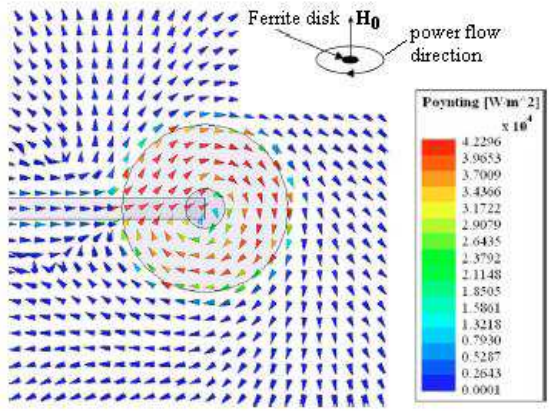

Figure 2: Power flow vortices in the cavity region of the patch.

Modeling Spin-wave Dispersion in One and Two-dimensional Magnonic Crystals by Structural Changes

M. Krawczyk, **S. Mamica**, **J. W. Kłos**, **M. Sokolovskyy**, **and J. Romero-Vivas**
Surface Physics Division, Faculty of Physics, Adam Mickiewicz University
Umultowska 85, Poznań 61-614, Poland

Abstract— The possibility of existence of complete energy gaps in the spectra of excitations propagating in periodic macrostructures has been considered already in a number of studies for different kind of waves: electromagnetic, elastic, plasmonic, water waves and also for spin waves. In this work, we continue to investigate the magnonic spectrum of two-dimensional periodic composites — magnonic crystals consisting of ferromagnetic rods periodically embedded in a homogeneous medium with properties differing from those which are characteristic for the rods. We use the plane wave method to determine spin-wave spectra of magnonic crystals composed of two and three different ferromagnetic or paramagnetic materials. We show the results of systematic studies of spin wave dispersion in dependence on structural changes, i.e., changes on the cross-sectional shape of the rods (from circular to rectangular) and on their arrangement. In this way, we cover a broad spectrum of structures, placed in between the two following cases: one-dimensional structures (superlattices composed of ferromagnetic materials for which some experimental results already exist and stacks of thin slabs composed of two kinds of infinitely long ferromagnetic stripes in a periodic arrangement along one direction and separated by distinguished material from stripes) and two-dimensional magnonic crystal slabs of finite and infinite thicknesses (see Fig. 1).

We show the range of applicability of the plane wave method for the calculation of the spin-wave spectrum in magnonic crystals, especially when a paramagnetic material is included. Numerical results were performed for magnonic crystals created from ferromagnetic metals: Co, Ni, Fe and their alloys. This allows for successful comparison our results with experimental one taken from literature and also provides predictive information necessary to create magnonic crystal with complete or partial energy gaps — see Fig. 2. As a last point, the optimal configurations for creation of magnonic gaps in the case of slabs composed of cobalt and permalloy stripes in periodic arrangement are defined.

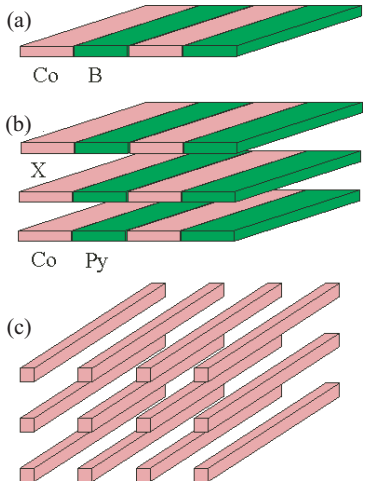

Figure 1: Magnonic structures studied in this paper. B and X mark the different materials.

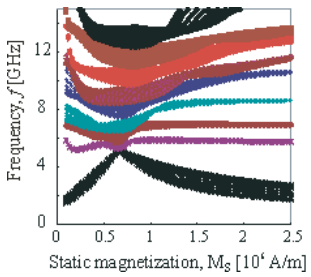

Figure 2: Magnonic bands as function of static magnetization of B stripes in a superlattice composed of Co stripes separated by material B.

ACKNOWLEDGMENT

The research leading to these results has received funding from the European Community's Seventh Framework Programme (FP7/2007-2013) under Grant Agreement No. 233552 and No. 228673.

Gyrotropic Mode Splitting in Pair of Magnetostatically Coupled Permalloy Disks in an Ordered Array

Anjan Barman[1, 2], **Saswati Barman**[1, 2], **T. Kimura**[2, 3], **Y. Fukuma**[2], **and Y. Otani**[2, 3]

[1]Department of Materials Science, S. N. Bose National Centre for Basic Sciences
Block JD, Sector III, Salt Lake, Kolkata 700 098, India
[2]RIKEN ASI, 2-1 Hirosawa, Wako, Saitama 351-0198, Japan
[3]Institute for Solid State Physics, University of Tokyo
5-1-5 Kashiwanoha, Kashiwa, Chiba 277-8581, Japan

Abstract— We present the experimental observation of gyrotropic mode splitting by time-resolved magneto-optical Kerr effect in magnetostatically coupled pairs of Ni81Fe19 (permalloy) disks of 1 μm diameter, 50 nm thickness and edge to edge separation varying between 150 nm to 270 nm. A clear splitting of the gyrotropic oscillation mode of the vortex core is observed when the edge to edge separation is 200 nm or less and the splitting can be controlled by a bias magnetic field. Micromagnetic simulations of the dynamics of pairs of disks reproduce the observation and show that the mode splitting depends strongly on the magnetic ground states of the disk pair, in particular, on the combination of vortex core polarization and chirality and the relative positions of the cores in the ground state. We have interpreted the observed mode splitting due to the appearance of normal modes of oscillations of the cores, which depends strongly on the strength of the magnetostatic coupling between the disks due to the magnetic side charges. Vortices with opposite core polarization and chirality give rise to the high interaction energy, which increases as the cores shift away from each other and hence the splitting can be controlled by the bias magnetic field. The influence of the magnetic ground states on the inter-disk separation and on the bias field and subsequently the mode splitting in the dynamics is significant for applications of such magnetic disk arrays in high frequency magnonic crystals.

Spin Waves in 2D Magnetic Vortices

Jean-Claude Serge Levy[1], **Philippe Depondt**[2], **Slawomir Mamica**[3], **and Maciej Krawczyk**[3]

[1]Lab. MPQ, UMR CNRS 7162, Univ. Paris 7, 10 r. A. Domon, Paris 75013, France
[2]INSP, UMR CNRS 7588, Univ. Paris 6, Paris Cedex 05 75252, France
[3]Surface Physics Div., UAM, Umultowska 85, Poznan 61-614, Poland

Abstract— 2D confined magnetic vortices are deduced from Langevin dynamics simulations for samples of different sizes and different dipolar versus exchange d ratios. When d is increased, at low d value, there is a progressive reduction of out-of-plane magnetic contributions before a vortex appears with an out-of-plane core. A further d increase leads to the appearance of more vortices with reduced out-of-plane cores up to obtain an XY vortex structure. In the intermediate structure shown the X and Y axes yield the positions of the spins, while the Sz axis gives the Z components of the spins and the color scheme represents the spin in-plane orientation angles.

Spin waves are deduced from Langevin dynamics and compared with a dynamical matrix analysis using for approximate ground state an in-plane vortex or a partly pyramidal out-of-plane vortex. Unusual localization properties are due to the long range character of dipolar interaction. These localization properties are not the same for in-plane, at left, and out of plane, at right, spin wave components as shown on bottom figures for the first mode with a moderate d value. A frequency gap which increases with d is also observed. A breathing mode of the vortex core, i.e., a modulation of the vortex core lateral size, is also directly observed as well as vortex motions.

So the dynamical matrix analysis enables us to classify the mass of dynamic observations.

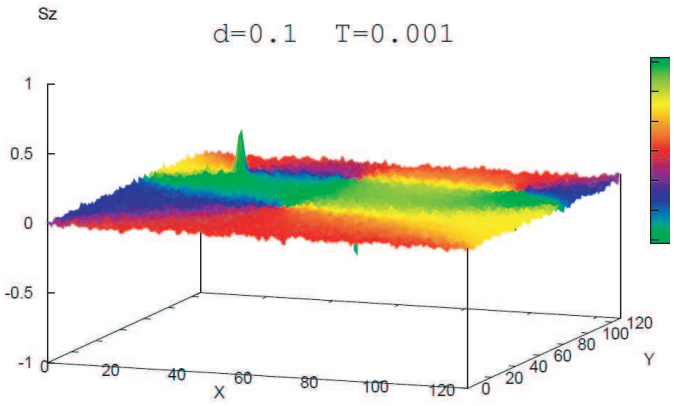

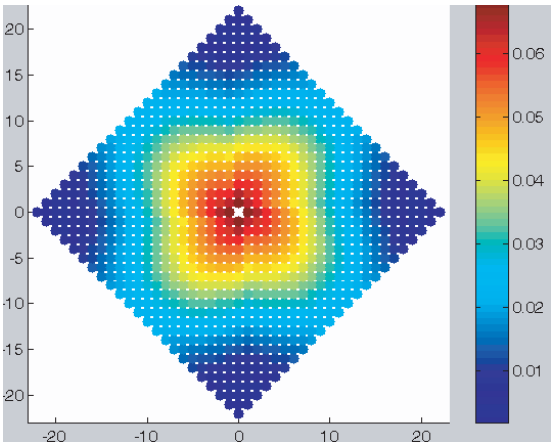

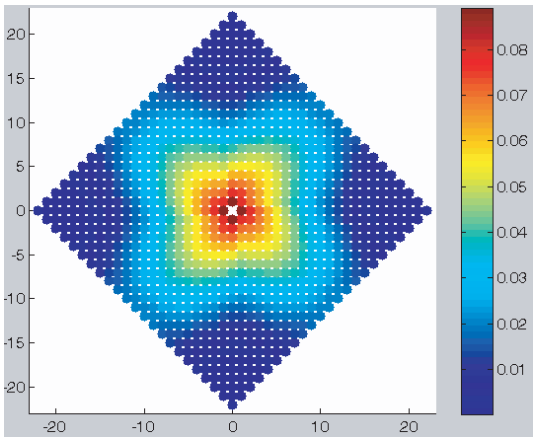

Arrays of Magnetic-dipolar-mode Particles

M. Sigalov[1], **E. O. Kamenetskii**[2], **and R. Shavit**[2]

[1]RF Dynamics LTD, Research Department, Kfar Saba 44643, Israel
[2]Electrical and Computer Engineering Department
Ben-Gurion University of the Negev, Beer-Sheva 84105, Israel

Abstract— In optics, the possibility of compressing electromagnetic (EM) fields in space to a degree much better than predictable by classical diffraction theory is realized due to resonant interactions of the EM fields with the quasielectrostatic (plasmon) oscillations. This allows creation of a number of new plasmonic devices [1, 2]. It appears that in microwaves, solution of the problem of the EM field compressing can be found based on resonant interactions of the EM fields with magnetic-dipolar-mode (MDM) [or magnetostatic (MS)] oscillations in small ferrite disks. Recently, it was found that a number of unusual effects are possible when microwave EM fields interact with MDM ferrite particles [3–5].

The MDMs take place in ferromagnetic bodies with sizes much smaller than the EM wavelength. Because of the essential temporal dispersion of permeability in ferrites and small sizes of magnetic samples, variation of the electric-field energy is negligibly small compared to variation of the magnetic-field energy. Solution of the MDM spectral problem is based on use of the notion of the MS-potential wave function ψ. The spectral problem shows the presence of the MDM vortices and eigen electric and magnetic moments of the ferrite particle [6, 7]. One has the resonant interactions between the eigen moments of MDM ferrite disks and the external EM fields. MDM oscillations in a ferrite disk are origins of topological singularities of the microwave near fields. The MDM vortices act as traps, providing purely subwavelength confinement of the EM fields. The fields outside a ferrite disk are evanescent fields in nature: they decay exponentially with distance from the ferrite surface.

We show that an array of evanescent-tail-coupling MDM disks is an effective waveguide structure with low losses. This is the demonstration of effective non-diffraction-limited microwave waveguides. Due to the heightened local fields surrounding MDM-disk guiding structures, such microwave devices have potential applications not only in microwave photonics. Symmetry breakings of near fields in such structures will allow localized sensing of chiral biological and chemical objects in microwaves.

REFERENCES

1. Barnes, W. L., A. Dereux, and T. W. Ebbesen, *Nature*, Vol. 424, 824, 2003.
2. Maier, S. A. and H. A. Atwater, *J. Appl. Phys.*, Vol. 98, 011101, 2005.
3. Sigalov, M., E. O. Kamenetskii, and R. Shavit, *J. Appl. Phys.*, Vol. 104, 053901, 2008.
4. Kamenetskii, E. O., M. Sigalov, and R. Shavit, *J. Appl. Phys.*, Vol. 105, 013537, 2008.
5. Kamenetskii, E. O., M. Sigalov, and R. Shavit, arXiv, http://arxiv.org/abs/0908.4383, 2009.
6. Kamenetskii, E. O., *J. Phys. A: Math. Theor.*, Vol. 40, 6539, 2007.
7. Kamenetskii, E. O., arXiv, http://arxiv.org/abs/0909.4920, 2009.

Simulation Studies of Propagation of Local Magnetic Excitation in One Dimensional Chains of Nanomagnets

Saswati Barman[1, 2], **Anjan Barman**[1, 2], **Y. Fukuma**[2], **and Y. Otani**[2, 3]

[1]Department of Material Sciences, S. N. Bose National Centre for Basic Sciences
Block JD, Sector III, Salt Lake, Kolkata, 700098, India
[2]RIKEN ASI, 2-1 Hirosawa, Wako, Saitama 351-0198, Japan
[3]Institute for Solid State Physics, University of Tokyo
5-1-5 Kashiwanoha, Kashiwa, Chiba 277-8581, Japan

Abstract— We report the efficient manipulation of propagation of gyrotropic excitation of magnetic vortex through one dimensional chains of physically separated but magnetostatically coupled nanomagnetic disks by using micromagnetic simulations. We have used a localized rotating magnetic field to resonantly excite the gyrotropic oscillation of a single disk at one end of the chain and simulated the time evolution of magnetization of every individual disks in that chain. The efficiency of the propagation, quantified as transmittance of the peak amplitude of the excitation, depends on the intrinsic and extrinsic properties of the vortex chain, including polarization, chirality and shape of the disks. The velocity of propagation is also affected by the above parameters and the optimum values of transmittance and velocity of propagation occur for a particular shape with some geometric asymmetry and magnetic configuration of the vortex chain. The efficient control of the transmittance and the velocity of propagation of localized magnetic excitation in physically separated magnetic nanodisks is particularly important for the design of high frequency spin logic systems and the so called magnonic crystals.

Long-range Magnetic-dipolar Interactions in Confined Magnetic Structures

E. O. Kamenetskii
Electrical and Computer Engineering Department
Ben-Gurion University of the Negev, Beer-Sheva 84105, Israel

Abstract— Classically, distant magnetic dipolar (MD) fields can be modeled as a sum of the fields produced by the magnetic dipoles. The possible numerical model of dipolar interactions involves a discrete lattice of classical spins and direct summation of their magnetic fields. The boundary conditions for the dipolar-mode fields are imposed on the phenomenological magnetization and it is supposed that there exist the long-range magnetization wave propagation [1]. Another classical approach in analyzing a long-range mechanism of the dipole-dipole interaction is based on consideration of a magnetic medium as a continuum. For calculation, the formulation based on the magnetostatic-Green-function integral problem for magnetization was suggested [2]. In this case one solves "pure static" MS equations for a dipolar field. The sources of such a field are both volume "magnetic charges", arising from $\nabla \cdot \vec{m}$, and surface "magnetic charges", arising from discontinuity of the normal component of $\vec{m}$ on the surface of a ferrite sample. For a confined magnetic structure with homogeneous material parameters, the spectral problem formulations [1, 2] for MD modes are applicable only if (a) exchange interaction is taken into account and/or (b) an internal DC magnetic field is non-homogeneous. At the same time, one has to note, however, that the dynamic magnetization at the boundary of a magnetic element is undefined from classical electrodynamics.

It is well known that magnetostatic ferromagnetism has a character essentially different from exchange ferromagnetism. Experimentally, it was shown that in "big" (when the exchange fluctuations are neglected) spherical ferrite samples, having homogeneous internal DC magnetic field, the MD modes occur [3]. For such samples, Walker [4] obtained spectral solutions based on the differential-operator equation for a "fictitious" MS-potential wave function $\psi(\vec{H} = -\nabla\psi)$. For a quasi-2D ferrite disk, the MD spectral properties were analyzed based on postulates about a physical meaning of MS-potential functions $\psi(\vec{r}, t)$ as complex scalar wave functions with energy-eigenstate orthogonality conditions. The spectral problem shows the presence of the MD vortices and eigen electric and magnetic moments of the ferrite-disk particle [5–7]. With the spectral properties of scalar wave functions $\psi(\vec{r}, t)$, one can explain experimentally observed discrete energy states and eigen electric moments of oscillating MD modes in a ferrite disk [8–10].

REFERENCES

1. Puszkarski, H., M. Krawczyk, and J.-C. S. Levy, *Phys. Rev. B*, Vol. 71, 014421, 2005.
2. Guslienko, K. Y., et al., *Rev. B*, Vol. 66, 132402, 2002.
3. White, R. L. and I. H. Solt, Jr., *Phys. Rev.*, Vol. 104, 56, 1956.
4. Walker, L. R., *Phys. Rev.*, Vol. 105, 390, 1957.
5. Kamenetskii, E. O., *J. Phys. A: Math. Theor.*, Vol. 40, 6539, 2007.
6. Kamenetskii, E. O., arXiv, http://arxiv.org/abs/0909.4920, 2009.
7. Kamenetskii, E. O., M. Sigalov, and R. Shavit, *J. Appl, Phys.*, Vol. 105, 013537, 2009.
8. Kamenetskii, E. O., A. K. Saha, and I. Awai, *Phys. Lett. A*, Vol. 332, 303, 2004.
9. Sigalov, M., E. O. Kamenetskii, and R. Shavit, *Appl. Phys. B*, Vol. 93, 339, 2008.
10. Sigalov, M., E. O. Kamenetskii, and R. Shavit, *J. Appl. Phys.*, Vol. 104, 053901, 2008.

The Influence of Electric Field on Magnetic Vortices in Confined Magnetic Structures

A. P. Pyatakov[1, 2] **and G. A. Meshkov**[1]

[1]Physics Department, M. V. Lomonosov Moscow State University, Russia
[2]A. M. Prokhorov General Physics Institute, Russian Academy of Science, Russia

Abstract— Nowadays the magnetic dots that stabilize the magnetic vortex state are considered as promising elements of recording media and microwave signal-processing devices [1, 2]. The control of vortexes characteristics such as chirality, polarity or winding number (the topological charge) remains a challenging problem. Several means of magnetic vortex state control such as remagnetizing with pulses of magnetic field [3–5] or spin currents [6] have been proposed. However all this techniques imply high current density and, as a consequence, the energy loses.

The alternative way of magnetic state switching based on the electric field induced micromagnetic structure transformation in magnetoelectric media was recently demonstrated in the series of work [7–11]. There is an additional interaction that should be taken into account when we consider micromagnetic structure under influence of electric field or the structures in magnetic ferroelectrics (multiferroics). It is proportional to spatial derivatives of magnetic order parameter vector $P_i M_j \nabla_k M_n$, where ∇ is differential operator, and P, M are electric and magnetic order parameters, respectively. This type of interaction is responsible for electric field driven magnetic domain wall motion in ferrimagnetic iron garnet films [11], local junction of electric and magnetic properties in the Tellegen particles of magnetoelectric metamaterial [12], and magnetically induced electric polarization in spiral multiferroics [13].

In this report, we will show that the gradient of electric field produced by point electrode (e.g., cantilever tip of atomic force microscope) might have strong influence on the micromagnetic structure of magnetic dielectric and can stabilize in magnetic dielectric nanoparticle either vortex or antivortex state depending on the electric polarity of the tip that besides fundamental interest can be considered as a prototype of electrically switchable magnetic system with two logic states.

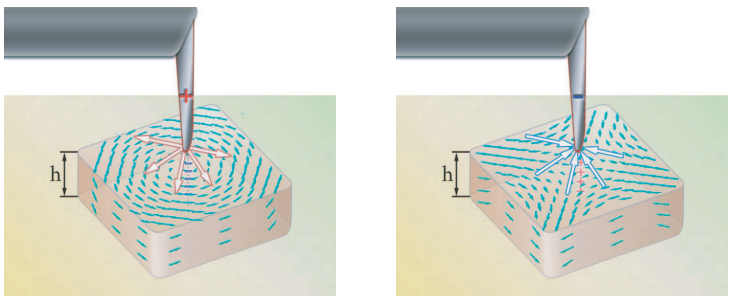

(a) (b)

Figure 1: Magnetic dielectric nanoparticle subjected to the electric field from the cantilever tip. (a) Electrically induced magnetic vortex state, (b) electrically induced magnetic antivortex state.

ACKNOWLEDGMENT

The support of RFBR grant No. 08-02-01068-a is acknowledged.

REFERENCES

1. Pribiag, V. S., I. N. Krivorotov, G. D. Fuchs, et al., *Nature Physics*, Vol. 3, 498–503, 2007.
2. Guslienko, K. Y. and J. Nanosc, *Nanotechn.*, Vol. 8, 2745–2760, 2008.
3. Van Waeyenberge, B., et al., *Nature*, London, Vol. 444, 461, 2006.
4. Tanase, M., A. K. Petford-Long, O. Heinonen, et al., *Phys. Rev. B*, Vol. 79, 014436, 2009.
5. Prosandeev, S., I. Ponomareva, I. Kornev, and L. Bellaiche, *Phys. Rev. Lett.*, Vol. 100, 047201, 2008.
6. Yamada, K., et al., *Nature Materials*, Vol. 6, 269, 2007.

7. Chu, Y.-H., L. W. Martin, M. B. Holcomb, et al., *Nature Materials*, Vol. 7, 478, 2008.
8. Zavaliche, F., H. Zheng, L. Mohaddes-Ardabili, et al., *Nano Lett.*, Vol. 5, 1793, 2005.
9. Chung, T. K., G. P. Carman, and K. P. Mohanchandra, *Appl. Phys. Lett.*, Vol. 92, 112509, 2008.
10. Palkar, V. R. and K. Prashanthi, *Appl. Phys. Lett.*, Vol. 93, 132906, 2008.
11. Logginov, A. S., G. A. Meshkov, A. V. Nikolaev, et al., *Appl. Phys. Lett.*, Vol. 93, 182510, 2008.
12. Kamenetskii, E. O., M. Sigalov, and R. Shavit, *J. Appl. Phys.*, Vol. 105, 013537, 2009.
13. Cheong, S.-W. and M. Mostovoy, *Nature Materials*, Vol. 6, 13, 2007.

Session 1P5
Optical Properties of Semiconductors and Nanostructures 2

GaAs Micro-nano Disks for Opto-mechanics Applications

L. Ding[1], **C. Baker**[1], **P. Senellart**[2], **S. Ducci**[1], **G. Leo**[1], **and I. Favero**[1]

[1]Laboratoire Matériaux et Phénomènes Quantiques, Université Paris Diderot
CNRS-UMR 7162, 75205 Paris Cedex 13, France
[2]Laboratoire de Photonique et Nanostructures, LPN/CNRS, Route de Nozay, 91460 Marcoussis, France

Abstract— The coupling between light and mechanical oscillators has seen a recent surge of interest: applications of opto-mechanical systems are rapidly evolving, from sensing to fundamental tests of quantum mechanics. Recent reviews see Refs. [1] and [2]. At the nano-scale, the opto-mechanical coupling increases thanks to a smaller opto-mechanical interaction volume and reduced mass of the mechanical oscillator [3, 4].

Here we present a semiconductor opto-mechanical resonator implemented directly on chip which combines all assets for nano-optomechanics experiments: sub-pg motional mass, nanoscale mode volume and high optical Q. It consists of a GaAs micro-nano disk evanescently coupled to a tapered nano-waveguide.

Using a microheater, we show fabrication of silica nanotapers with record low-loss level [5], which are used to perform near-field opto-mechanical characterization of the disks. Whispering gallery modes with optical Q factor up to a few 10^5 were observed. Thanks to these high-Q optical modes, we achieved interferometric displacement sensing of the disk vibrating motion with a shot-noise limited sensitivity of $10^{-17}\,\mathrm{m}/\sqrt{\mathrm{Hz}}$. High frequency disk mechanical modes between 0.1 and 1 GHz were observed, with Q factors up to 10^3 in ambient conditions. They were identified by monitoring their dispersion with the disk size. We observed that mechanical modes with highest azimuthal symmetry couple strongly to the gallery modes, with record opto-mechanical coupling over the GHz/nm [6]. In addition, mode splitting is observed when the motion of the disk couples to the disk pedestal. Experimental results show excellent agreement with numerical simulations.

Last, when in resonance with a gallery mode, we observe an optical force actuation of the nanotaper motion, with amplitude as large as a few microns. This is an example of an opto-mechanical phenomenon "visible to the naked eye", showing that optics and mechanics naturally tend to couple at the micro-nano scale.

REFERENCES

1. Favero, I. and K. Karrai, *Nature Photonics*, Vol. 3, 201, 2009.
2. Marquardt, F. and S. Girvin, *Physics*, Vol. 2, 40, 2009.
3. Favero, I. and K. Karrai, *New Journal of Physics*, Vol. 10, 095006, 2008.
4. Favero, I., S. Stapfner, D. Hunger, P. Paulitschke, J. Reichel, H. Lorenz, E. M. Weig, and K. Karrai, *Optics Express*, Vol. 15, 12813, 2009.
5. Ding, L., C. Belacel, S. Ducci, G. Leo, and I. Favero, *Appl. Opt.*, Vol. 49, 2441, 2010.
6. Eichenfield, M., J. Chan, R. M. Camacho, K. J. Vahala, and O. Painter, *Nature*, Vol. 462, 78, 2009.

Optical Spectroscopy of Single Quantum Dots in Advanced Photonic Structures

Megan Creasey[1, 2], **J. Bleuse**[2], **J. Claudon**[2], **N. S. Malik**[2], **M. Bazin**[2], **I. Maksymov**[3], **C. Sauvan**[3], **J.-P. Hugonin**[3], **P. Lalanne**[3], **J.-M. Gérard**[2], **Xiaoqin Li**[1], **J. H. Lee**[4], **Zh. M. Wang**[5], **and G. J. Salamo**[5]

[1]Physics Department, University of Texas, Austin, Texas, 78712, USA
[2]CEA-CNRS-UJF "NanoPhysics and SemiConductors" Joint team, CEA/INAC/SP2M
17 rue des Martyrs, 38054 Grenoble cedex 9, France
[3]Institut d'Optique/LCFIO, Campus Polytechnique, RD 128, 91127 Palaiseacedex, France
[4]Department of Electrical Engineering, Kwangwoon University, Seoul 139-701, South Korea
[5]Institute of Nanoscale Science and Engineering, University of Arkansas
Fayetteville, Arkansas, 72701, USA

Abstract— Epitaxially grown InAs quantum dots (QDs) have been extensively studied both as-grown and when coupled to resonant microcavities. Devices based on self-assembled QDs are potential candidates for a variety of applications ranging from conventional optoelectronics to single photon sources and entangled photon sources. Here, we present optical studies of two newly developed quantum dot structures, quantum dot clusters (QDCs) and QDs embedded in photonic wires.

The first of these studies was performed on InGaAs QDCs grown by a combination of droplet homoepitaxy and Stranski-Krastanov growth. This study focused on a particular structure comprising six QDs morphologically similar to a benzene ring. We performed microphotoluminescence characterization on this sample including temperature and excitation power dependence and time-resolved spectroscopy. Our results suggest that excitons are confined within individual quantum dots rather than in the entire cluster, therefore, promising for applications which require controllable coupling among QDs.

Time-resolved microphotoluminescence measurements were also made on InAs QDs inside photonic wires. The QDs in these samples were grown by molecular beam epitaxy, and the wires were processed using electron beam lithography and reactive ion etching. The wires were specifically designed to allow only a single electromagnetic mode. A systematic study of the radiative lifetimes of exitons in QDs inside wires of various diameters showed a large factor (~ 20) of inhibition in small diameter wires. This is a great improvement upon previous studies of QDs in 2D photonic crystals or microcavities where the best inhibition measured was a factor of 10.

Polaronics

H. C. Liu
Institute for Microstructural Sciences, National Research Council, Ottawa K1A 0R6, Canada

Abstract— The coupled mode excitation of electron and phonon in solids is referred to as a polaron. Equivalently the quasiparticle resulting from the mixture of electron and phonon excitations is defined as a polaron. In the past, polarons have been mostly a pure physics phenomenum. Here we investigate the active use of polarons for realizing new optoelectronics devices and propose a new research direction of "polaronics". We present an application of the concept to photodetection in the terahertz (THz) spectrum. The ability to design a polaron is the first step in making use of them. We show this by a model system employing the electron intersubband excitation in quantum wells coupled with phonon modes. This results in a photodetector with a high response at the selected wavelength. This work opens possibilities for making use of polarons in realizing new optoelectronic devices.

Tuning the Optical Properties of Semiconductor Nanowire Heterostructures

Leigh M. Smith[1], **Howard E. Jackson**[1], **Jan Yarrison-Rice**[1], **Chennupati Jagadish**[2], **and Jin Zou**[3]

[1]Department of Physics, University of Cincinnati, Cincinnati, OH 45221-0011, USA
[2]Department of Electronic Materials Engineering, Australian National University, Canberra, Australia
[3]Center for Microscopy and Analysis, University of Queensland, Brisbane, Australia

Abstract— Semiconductor nanowires are one dimensional structures that can be grown in axial and radial hetero- or homo-structures which can be engineered for particular physics or technological applications. In this talk, I will discuss how semiconductor nanowires can be designed to manipulate both the electromagnetic field as well as the electron or hole wavefunctions within semiconductor nanowires. We probe the interesting quantum phenomena with spatially- and temporally-resolved optical experiments.

Semiconductor nanowires are cylinders with tens of nanometers in diameter and 5 to 10 microns in length. While the electron and hole wavefunctions show little effect of quantum confinement, the electromagnetic field is strongly affected by the nanowire resulting in light strongly polarized parallel to the nanowire. This results in a dramatic increase in the radiative lifetime for excitons whose dipoles are aligned perpendicular to the nanowire so that light emission is polarized parallel to the nanowire. We have used both CW and time-resolved photoluminescence measurements in single GaAs/AlGaAs core-shell nanowires to study the spin relaxation dynamics of excitons which are photopumped into nonequilibrium populations. We find that the relaxation time is strongly decreased when excitons are excited non-resonantly at higher energies, or when the exciton density is increased. Under optimal conditions the relaxation time can be as long as 200 ps or as short as 5 ps [1].

Using axial and radial heterostructures, semiconductor nanowires can be grown which directly manipulate the electron and hole wavefunctions. We demonstrate that axial homostructures of zincblende and wurtzite layers can be used to strongly quantum confine both the electrons and holes and that the spatially-indirect alignment of the wavefunctions result in a dramatic increase in the radiative lifetime at lower energies [2]. Axial heterostructures of GaAs/AlGaAs nanowires can result in cylindrically symmetric quantum wells which exhibit a true one-dimensional density of states, and for which the orbital angular momentum is quantized. Preliminary efforts to grow and characterize such structures will be discussed.

Finally, we will show preliminary results on the use of strain in lattice mismatched core-shell nanowire heterostructures to tune the energy states. We have fabricated GaAs/GaP core shell structures where lattice mismatch is 3.6%. This results in significant compressive strain in the GaAs core, equivalent to 50 kbar of pressure, which shifts the direct band gap upwards in energy by nearly 300 meV. Using experimental results from Raman scattering and PL spectroscopy as well as theoretical calculations, we develop a consistent picture of this effect which opens up significant new abilities to tune the band structure and energies for new devices.

We acknowledge the support of the National Science Foundation through grants 0701703 and 0806700 and 0806572, the Australian Research Council and the Australian National Fabrication Facility.

REFERENCES

1. Hoang, T. B., L. V. Titova, J. M. Yarrison-Rice, H. E. Jackson, A. O. Govorov, Y. Kim, H. J. Joyce, H. H. Tan, C. Jagadish, and L. M. Smith, *Nano Letters*, Vol. 7, 588–595, 2007.
2. Pemasiri, K., M. Montazeri, R. Gass, L. M. Smith, H. E. Jackson, J. Yarrison-Rice, S. Paiman, Q. Gao, H. H. Tan, C. Jagadish, X. Zhang, and J. Zou, *Nano Letters*, Vol. 9, 648–654, 2009.

Near-field Optical Imaging of Enhanced Photon Fields and Plasmon Waves in Metal Nanostructures

Hiromi Okamoto[1] **and Kohei Imura**[2]

[1]Institute for Molecular Science and The Graduate University for Advanced Studies, Japan
[2]Waseda University, Japan

Abstract— In metal nanostructures, motion of conduction electron is restricted to confined spaces which causes peculiar electronic and optical properties very different from bulk metals. It is of fundamental importance to understand spectral and spatial characteristics of plasmon resonances (distribution of the enhanced photon fields, wavefunctions of the plasmon modes, etc.), for fundamental studies in physical sciences as well as chemical and biological applications of plasmons. For this purpose, we have made use of near-field transmission and two-photon excitation imaging methods with aperture-type probes, which achieve visualization of localized (1 optical fields with spatial resolution beyond the diffraction limit of light. In this presentation we report near-field imaging of localized photon fields and plasmonic waves in metal nanostructures.

As typical examples for observation of plasmonic waves in single metal nanoparticles, we measured near-field transmission images of gold nanorods and nanodisks. For nanorods, we observed spatially oscillating features along the long axes of the rods, whose wavenumber is dependent on the dimension of the rod and the wavelength of observation. For nanodisks, features of two-dimensional waves are observed, whose structures are dependent on the size of the disk and the wavelength of observation.

For assemblies of gold nanoparticles, we visualized spatial structures of enhanced photon fields by the near-field two-photon excitation imaging method. We observed clearly the enhanced optical fields at the gaps between the nanoparticles when the incident polarization is parallel to the interparticle axes. This finding is consistent with the theoretical prediction of "hot spot" in metal nanoparticle assemblies. We also found for arrays of circular nanoholes on a gold film with narrow gaps between the holes that enhanced optical fields are generated at the gaps.

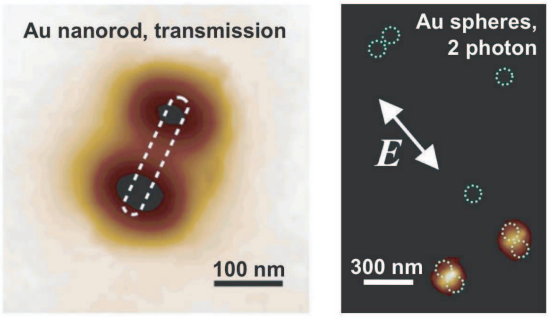

Hexagonal Boron Nitride as a New Ultraviolet Luminescent Material and Its Device Application

Kenji Watanabe[1], **Takashi Taniguchi**[1], **Kenta Miya**[2], **Yoshitaka Sato**[2], **Kazuhito Nakamura**[2], **Takahiro Niiyama**[2], **and Masateru Taniguchi**[2]

[1]National Institute for Materials Science, 1-1 Namiki, Tsukuba, Ibaraki 305-0044, Japan
[2]Futaba Corporation, 1080 Yabutsuka, Chosei-mura, Chosei-gun, Chiba 299-4395, Japan

Abstract— The potential of hexagonal boron nitride (hBN) as a new far ultraviolet (FUV) fluorescent material was studied. Specifically, taking advantage of the highly luminous properties of hBN [1, 2], an FUV plane-emission device was fabricated, and its stable operation was demonstrated. The fabricated device consists of an hBN fluorescent screen and a Spindt-type field emission array [3] as an excitation source. It achieved an output power of 0.2 mW at 225 nm with good stability. Low current consumption for exciting the hBN screen makes it possible to operate the device with dry batteries [4].

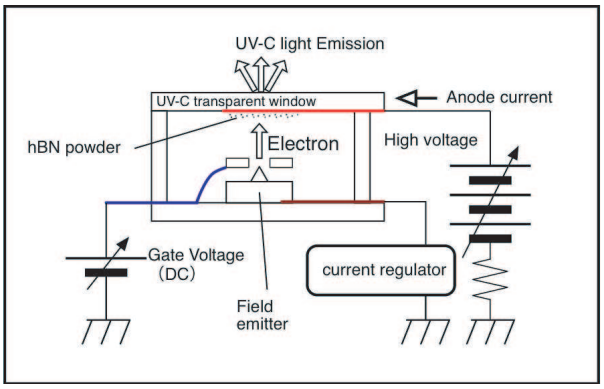

Figure 1: Cross-sectional drawing of FUV plane-emission device and connected electric circuits.

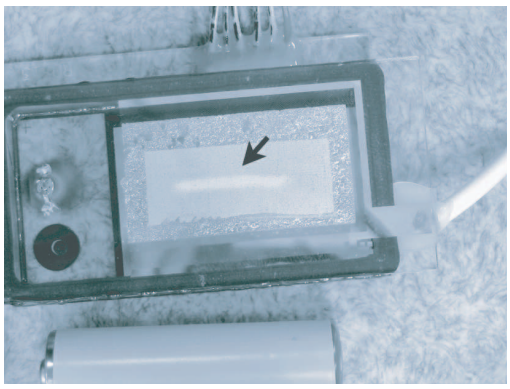

Figure 2: Photograph of prototype FUV plane-emission device in operation. Filament shape of white line indicated by arrow shows far-UV light emission of $1.7 \times 0.16\,\mathrm{cm}^2$. A size-AA dry battery is shown for size comparison.

REFERENCES

1. Watanabe, K., T. Taniguchi, and H. Kanda, *Nature Materials*, Vol. 3, 404, 2004,
2. Watanabe, K. and T. Tanguchi, *Phys. Rev. B*, Vol. 79, 193104, 2009.
3. Spindt, C. A., I. Brodie, L. Humphrey, and E. R. Westerberg, *J. Appl. Phys.*, Vol. 47, 5248, 1976.
4. Watanabe, K., T. Taniguchi, T. Niiyama, K. Miya, and M. Taniguchi, *Nat. Photonics*, Vol. 3, 591, 2009.

Luminescence Imaging and Blinking Behavior of Individual InGaN Nanoclusters Formed in GaN Matrix

S. J. Xu[1], **D. G. Zhao**[2], **and H. Yang**[3]

[1]HKU-CAS Joint Laboratory on New Materials, Department of Physics
The University of Hong Kong, Pokfulam Road, Hong Kong, China
[2]State Key Laboratory on Integrated Optoelectronics
Institute of Semiconductors, Chinese Academy of Sciences, Beijing 100083, China
[3]Suzhou Institute of Nano-tech and Nano-bionics, Chinese Academy of Sciences
Suzhou 215125, China

Abstract— In this talk, we report an observation of luminescence imaging and blinking behavior of single indium rich nanoclusters spontaneously formed inside GaN matrix. At room temperature, light emissions from individual nanoclusters have been spatially and spectrally detected using scanning confocal micro-Raman microscopy/spectroscopy system. Under the continuous excitation of continuous-wave laser, spectral jump and intensity intermittence of light emissions from these individual nanostructures inside solid state environment have been interestingly observed. The "on" and "off" events in the light emission of individual InGaN nanoclusters have been monitored as a function of time. In order to understand physical mechanism of the blinking behavior, statistical analysis of both "on" and "off" time durations has been performed.

Influence of Ion Implantation on Second Harmonic Generation in ZnO Single Crystals

C. C. Zheng[1], **S. J. Xu**[1], **J. Q. Ning**[1], **Y. N. Chen**[1], **and C. C. Ling**[2]

[1]HKU-CAS Joint Laboratory on New Materials, Department of Physics
The University of Hong Kong, Hong Kong SAR, China
[2]Department of Physics, The University of Hong Kong, Hong Kong SAR, China

Abstract— ZnO has recently re-attracted a considerable interest due to its potential applications in photonics. In this talk, influence of ion implantation on second harmonic generation (SHG) efficiency in ZnO single crystals at room temperature was investigated. SHG emissions from as-grown, nitrogen- and copper-implanted ZnO single crystals were measured by employing femtosecond laser as the excitation source. The results show that ion implantation has a distinct influence on the SHG efficiency. According to the relative intensity of the SHG signal to the band edge emission, the SHG efficiency of ZnO single crystals was improved by several times after the ion implantation. This enhancement was attributed to quasi-interface formation and disorder increment in implanted crystals. It was also interestingly found that the N-implanted sample has a higher SHG efficiency than the Cu-implanted one. Detailed results will be presented in the talk.

From Nanosphere Lithography to Self-assembled Photonic Crystals

W. Y. Fu, K. H. Li, and H. W. Choi
Semiconductor Lighting and Display Laboratory, Department of Electrical and Electronic Engineering
The University of Hong Kong, China

Abstract— Amongst nanolithography methods, electron-beam lithography (EBL) and nano-imprint lithography are most popular for fabrication of photonic crystal structures due to their high precision. However, cost of fabrication and yield are factored in for consideration, selfassembly methods have better potential towards commercialization; nanosphere lithography is one of the most feasible approach.

Employing nanosphere lithography, we are able to pattern hexagonally close-packed arrays, and hence fabricate different kinds of photonic crystal structures. The inherent high refractive index of Gallium Nitride (GaN), which limits the light extraction efficiency of light-emitting diode (LED), in fact provides an excellent platform for the integration of photonic crystals. The light extraction problem of GaN can be solved by suppressing the guiding modes within in the LED structure. Intuitively, photonic crystal has extensively been utilized for light manipulation in different areas, and has been demonstrated as a mean of spontaneous emission control [1]. Its periodic nature with dimensions close to the wavelength of light forbids the existence of certain optical modes, thereby achieving light confinement effects [2].

REFERENCES

1. Noda, S., M. Fujita, and T. Asano, "Spontaneous-emission control by photonic crystals and nanocavities," *Nature Photonics*, Vol. 1, 449–458, 2007.
2. Joannopoulos, J. D., *Photonic Crystals: Molding the Flow of Light*, 2nd Edition, Princeton University Press, Princeton, 2008.

Session 1P6
Poster Session 3

A Novel and Reliable Method for Bandwidth Expansion in Microstrip Array Antenna

Mohsen Fallah, **F. H. Kashani**, **and S. H. Mohseni**
Department of Electrical Engineering, Iran University of Science and Technology (IUST), Tehran, Iran

Abstract— In this paper, a new and simple method for increasing the bandwidth of microstrip array antenna is presented. In this method, which we call it low match method, all elements of array antenna are matched in a frequency very closed to the resonant frequency of each element of antenna. This method is implemented in an array of 8 by 8 elements array antenna and a increased of 4% in bandwidth in the frequency rang of 10.2–10.6 GHz, 23.42 dBi Gain, and 58% efficiency is obtained. The simulation results and the experimental results show good agreement between them.

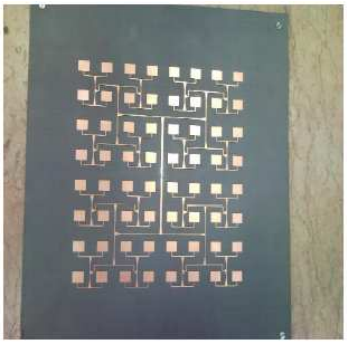

Figure 1: Fabricated antenna.

Unified Statistical Modeling of RF Multipath in Wireless Communications

Kung Yao
Electrical Engineering Department, UCLA, L.A., CA 90024-1594, USA

Abstract— RF multipath fading phenomena can significantly degrade the performances of many wireless communication systems. Extensive field measurements over many years have yielded fading envelope statistics modeled by Rayleigh, Rician, Weibull, Nakagami-m, K_v, etc. pdfs. Recent we have provided a unified spherically-invariant random process (SIRP) model for the fading channel that requires the non-negative valued fading envelope rv $X = V \bullet R$, where R is either the Rayleigh rv (in the Non-Line-of-Sight (NLOS) case) or the Rician rv (in the LOS case), V is a non-negative scalar rv independent of R, and $\bullet$ is the multiplication of the two rvs. For various known $f_X(.)$ fading envelope pdfs (such as those listed above), corresponding $f_V(.)$ pdfs having been found with some efforts using Mellin transform and Fox H-function methods. The associated $f_V(.)$ pdfs can be used for bit-error-probability (BER) evaluations of communication system performances much simpler than directly using the $f_X(.)$ pdfs. While the SIRP model may justify various known fading envelope pdfs from the statistical point of view, can these pdfs be justified from the physical RF propagation point of view? The Rayleigh fading envelope pdf follows from the effects of CLT on the sum of large number of small iid rvs associated with uniformly distributed phase. The Rician fading effect results from one large dominant term in the sum of the large number of small iid rvs. Nakagami, over thirty years of analytical and experimental work in fading radio channel research (1940–1960), has found various complicated fading envelope pdfs with non-uniform phases, based on physical modeling of the random phasors in the fading channels. However, from the work of A. Ichimaru (recent private communications) in optical and RF propagations through random media, it appears these fading phenomena with non-uniform phase distributions are associated with transmission intensity normalized variance D values near or greater than unity, which are due to complex wave-random media turbulence interactions. Turbulence effects are known to exhibit non-linear dynamical (chaotic) properties. R. J. Sasiela (1994 and 2007) has also used Mellin transform methods to study EM wave propagation in turbulence. In the SIRP fading model, we have obtained a "half-Cauchy-like" fat-tailed $f_X(.)$ pdf, that does not have a finite mean nor a finite second moment but does have an explicit associated $f_V(.)$ pdf. Asymptotic analysis shows such a pdf can have an arbitrarily large value of D as predicted by the Ichimaru conjecture. Infinite variance pdfs (such as the half-Cauchy pdf) can be used as the Frobenius-Perron (FP) invariant pdf in non-linear dynamical theory to generate chaotic waveforms (K. Umeno, 98). Recent result of T. Akimoto (DDAP, Sept. 08)) shows our "half-Cauchy-like" pdf can also be used as the invariant pdf in the FP method to generate chaotic waveforms. Yet, using the $f_V(.)$ pdf associated with the "half-Cauchy-like" $f_X(.)$ applied to a BPSK communication system, its BER has well behaved values not very different from those of Rayleigh fading statistic. Thus, the unified SIRP fading model encompasses not only the known fading envelope pdfs but may predict envelope pdfs associated with strong wave-random media interactions associated with chaotic properties. Technical discussions with Prof. A. Biglieri and Dr. F. Lorenzelli of UCLA are highly appreciated.

Detection Algorithm for MIMO Systems Based on Genetic Algorithms with Variable Population Size

A. M. Abu Hudrouss
Electrical Engineering Department, IUG-Gaza, P. O. Box 108, Gaza, Palestine

Abstract— Multiple-Input-Multiple-Output (MIMO) systems exploit the multi-path scattering characteristics of the wireless channel to increase the system capacity and spectral efficiency. Many detection schemes have been developed to detect the transmitted signals in a fading MIMO channel. The most efficient one in term of performance is the Maximum Likelihood detection which enables the full utilization the capacity and diversity potentials of MIMO channel. However, the complexity of this scheme is high and increases exponentially with the number of the transmitted/received antennas. On the other hand, low complexity schemes like zero-forcing or MMSE suffers significant power and diversity losses and therefore does not fully exploits the potential of MIMO systems.

Genetic algorithms (GAs) have also been used to for MIMO signal detection. The GAs have been previously proven to significantly outperform than ZF or MMSE detection algorithms. Genetic algorithms have been used to reduce the complexity of ML scheme in trade of with performance. An initial population of potential solutions is selected on random basis and tested using ML equations. Iteration after iteration, a new set of possible solutions is created by selecting individual based on fitness level and performing crossover and mutation. Bigger populations size give a better results but it takes much longer time in convergence. In this research, we will study the effect of population size on convergence. Variable population size has been used to reduce the convergence time and maintain performance.

A Highly Efficient Doherty Power Amplifier with Impedance Transform

Guorui Yang, Quanyuan Feng, and Wen Pan
Institute of Microelectronics, Southwest Jiaotong University, ChengDu 610031, China

Abstract— This paper analyses the efficiency influence factors for the Doherty amplifier output network with finite device output impedance. It presents an impedance transform method which changes the proportion of impedance to enhance efficiency, and reduces the load impedance of Doherty from 25 Ω to 12.5 Ω for decrease loss. So an enhanced Doherty amplifier is implemented at 2.14 GHz using freescale devices. It achieves a linear power gain of 14.4 dB with 1-dB output compression at 53.6 dBm while PAE is 58.4%, and the PAE is 39.5% at 46 dBm which is improved about 5.2% comparison with the classical structure.

Comparison of Bit Error Rate for Propagation Mechanisms of Millimeter Waves in a Practical Communication Systems Employing PSK and FSK

Preethi Kumar and M. Jayakumar
Applied Electromagnetics Research Group, Department of Electronics and Communication Engineering
Amrita Vishwa Vidyapeetham (Amrita University), Coimbatore, India

Abstract— Millimetre waves have opened a new door to next generation communication systems. These high-frequency signals are advantageous due to the high bandwidths, and hence, the high data rates they present. However, their main drawback is the presence of attenuation factors that adversely affect the quality of the received signal. The effect of these attenuation factors are illustrated by the Bit Error Rate (BER). The design of a communication system starts with the analysis of Bit Error Rate as a function of Signal to Noise ratio. The BER for communication systems employing different modulation schemes are evaluated and compared, for high data rate signals undergoing attenuation due to natural and man-made phenomena in the millimetre wave frequency band.

We have described the various propagation mechanisms that lead to the attenuation of radio waves in the frequency range of 40 GHz.This frequency band is finding many applications in modern wireless communication technologies like 4 G cellular communication. The attenuation due to each propagation mechanism is expressed mathematically and a final expression for received power in a NLOS communication system employing millimetre waves is described. The resulting Bit Error Rate of this communication is then derived. The BER of a BPSK, QPSK, 8-PSK and 16-PSK are compared. Similarly, the BER of a PSK system is compared to that of an FSK system.

The propagation mechanisms reviewed include free space path loss, attenuation due to atmosphere and water vapour, scattering and reflection due to buildings and loss due to vegetation. These analytical results will be useful for choosing the necessary power levels to optimise the link. The comparison shows that, as the number of signals needed to represent the digital information increases, the BER of the PSK system increases, while the BER of an FSK system decreases. We have concluded that BPSK, QPSK or 8FSK are the most advantageous modulation schemes in a practical communication system, under worst case climatic conditions.

Using Parallel Computing for Adaptive Beamforming Applications

Eman Ahmed[1], **K. R. Mahmoud**[2], **Safwat Hamad**[1], **and Z. T. Fayed**[1]

[1]Faculty of Computer and Information Sciences, Ain Shams University, Abbassia 11566, Cairo, Egypt
[2]Faculty of Engineering, Helwan University, Helwan, Egypt

Abstract— Recently, Smart antenna systems have been widely considered to provide interference reduction and improve the capacity, data rates, and performance of wireless mobile communication. Smart antenna arrays with adaptive beamforming capability are very effective in the suppression of interference and multipath signals. The techniques of placing nulls in the antenna patterns to suppress interference and maximizing their gain in the direction of desired signal have received considerable attention in the past and are still of great interest using evolutionary algorithms such as genetic algorithms (GA) and particle swarm optimization (PSO) algorithm. In this paper, for adaptive arrays using space division multiple access (SDMA), the optimal radiation pattern design of smart antennas is developed based on the particle swarm optimization (PSO) technique. The PSO is applied to a 24-element uniform circular array (UCA) to calculate the complex excitations, amplitudes and phases of the adaptive array elements. The antenna elements consist of vertical (z-directed) half-wave dipole elements equally spaced in the x-y plane along a circular ring, where the distance between adjacent elements is $d_c = 0.5\lambda$. It is found that the resulting beampattern optimized by the PSO required a large processing time which is not acceptable for an on line applications. Hence, the demand for a parallel solution that accelerates these computations is considered. Therefore, a parallel version of PSO is proposed and implemented using Compute Unified Device Architecture (CUDA) then applied on a graphics processing unit (GPU). The comparison is presented to show how the parallel version of the PSO outperforms the sequential one, thus an online procedure is available for time-critical applications of the adaptive beamforming.

Compact Wideband Antenna for Mobile Handsets

Ho-Jun Lee, Kyu-Bok Lee, and Jong-Kyu Kim
Convergence Communication Components Research Center
Korea Electronics Technology Institute, R. O. Korea

Abstract— In this paper, we proposed a novel design of 4 G antenna for mobile handsets. The proposed antenna configuration is shown in Figure 1. This antenna has a coplanar waveguide (CPW) fed that is optimized the 50 Ω impedance matching by positioning via and substrate height and radiator size. Antennas in this paper are simulated by using the Ansoft simulation software high-frequency structure simulator (HFSS). The measurements of electrical characteristics such as radiation patterns, VSWR, and return loss of the implemented antenna were conducted in an anechoic chamber equipped with a HP 8510C network analyzer and far field measurement system. Figure 2 shows VSWR characteristics. The measured impedance bandwidth of the antenna is from 2.3 to 3.8 GHz for VSWR < 1.5. Figure 3 shows a photograph of the fabricated antenna. This antenna is made by using low temperature co-fired ceramic (LTCC) process and the size of this antenna is $12 \times 2 \times 2\,\text{mm}^3$. We manufactured the antenna based on the results of optimized simulation results and measured characteristics of the suggested antenna in the anechoic chamber. Details of the proposed antenna designs are described, and typical experimental results are presented and discussed.

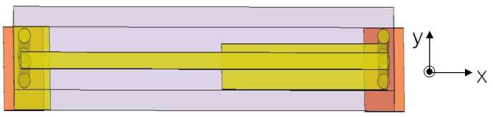

Figure 1: Proposed antenna.

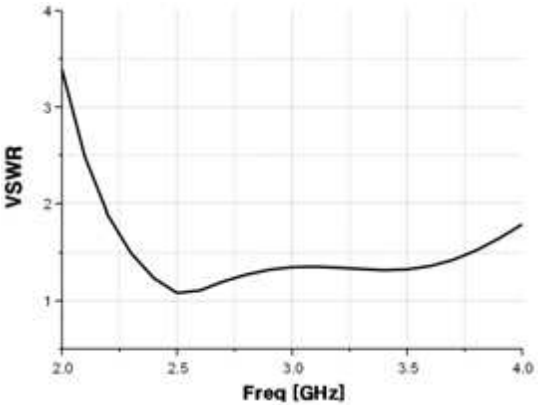

Figure 2: Measured VSWR.

Figure 3: Photograph of the fabricated antenna.

REFERENCES

1. Balanis, C. A., *Advanced Engineering Electromagnetics*, John Wiley & Sons, 1989.

GSM/DCS Dualband Antenna for Mobile Handsets

Ho-Jun Lee[1], **Seok-Ho Choi**[2], **and Byoung-Jun Yim**[2]

[1]Convergence Communication Components Research Center
Korea Electronics Technology Institute, R. O. Korea
[2]Partron Co., Ltd, R. O. Korea

Abstract— In this paper, we proposed a novel internal antenna design with a small size and low profile could be achieved. The proposed antenna obtained bandwidths cover the global system for mobile communication (GSM: 890–960 MHz), digital communication system (DCS: 1710–1880 MHz) bands within a VSWR of 4.0 : 1. The internal antenna has compact dimensions and is mounted on the printed circuit board (PCB, 40×100 mm) an FR4 substrate (thickness 1.0 mm and relative permittivity 4.7), which can be treated as the circuit board of a piratical mobile phone. Many configurations, having different dimensions and different numbers of elements have been tried experimentally in order to determine the most possible compact geometry. A considerable number of simulations, by modifying the parameters one by one, have been conducted to optimize the design that ensures satisfying the requirement of the frequency sweep for the dual-band mobile handset antenna. The proposed antenna is tested with the actual mobile phone. It is clearly seen that two wide operating bandwidths are obtained. The lower bandwidth, determined by 1 : 4 VSWR, reaches 80 MHz and covers the GSM band (890–960 MHz). On the other hand, the upper band has a bandwidth as large as 196 MHz and covers the DCS (1710–1880 MHz) bands. The measured antenna gain for the GSM and DCS bands. For the GSM band the antenna average gain is about 0.57–3.57 dBi; for the DCS band the antenna gain ranges from 0.57–2.89 dBi. Details of the proposed antenna designs are described, and typical experimental results are presented and discussed.

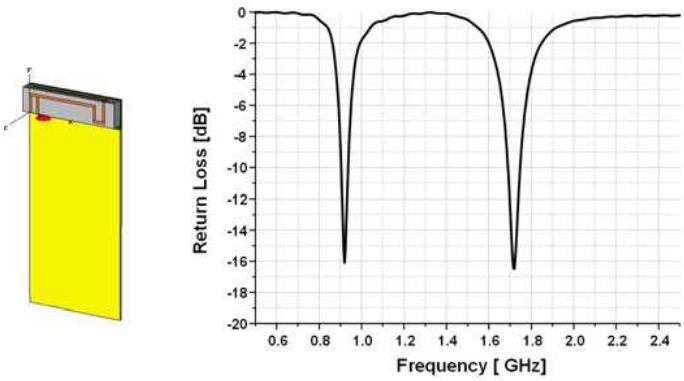

Figure 1: Proposed antenna & return loss.

REFERENCES

1. Balanis, C. A., *Advanced Engineering Electromagnetics*, John Wiley & Sons, 1989.

Permanent Magnet Synchronous Motor Decoupling Control Study Based on the Inverse System

Xiaoning Li[1], **Xumei Mao**[1], **and Weigan Lin**[2]

[1]School of Mechanical Engineering, University of Electronic Science and Technology of China
No. 4, Section 2, North Jianshe Road, Chengdu 610054, China
[2]School of Electronic Engineering, University of Electronic Science and Technology of China
No. 4, Section 2, North Jianshe Road, Chengdu 610054, China

Abstract— In this parer, multivariable, nonlinearity inverse system method is applied on the PMSM control system, which is complicated nonlinearity, strong coupled, and we have realized global linearization, at the same time, the motor rator speed and electromagnetic torque have been dynamic decoupled.The validity of this method can be proved by the simulation result.

Introduction: The PMSM is a multivariable, nonlinearity,strong, coupled controlled object. It is very hard to control its speed and electromagnetic torque by extra signal. Only can we precisely control it after the speed and torque have been dynamic decoupled. Vector control adopted the coordinate transform to realize decouple based on the motor electromagnetic field theory, but vector controlling just achieve the static decoupling not dynamic doing. Inverse system theory is a new strategy. Its essence is to realize multivariable,nonlinearity, strong coupled system decouple linearization by feedback linearization.

ACKNOWLEDGMENT

This work was supported by: 1. National Natural Science Foundation of China (60971037). 2. University of Electronic Science Technology of China youth fund accented term ((JX0792)

REFERENCES

1. Thomas, M. J., "Recent advances in power electronics technology for industrialand traction machine drivesitle," *Proceedings of the IEEE*, Vol. 89, No. 10, 1064–1076, 2001.
2. Wittenmark, B., R. Middlelon, and G. C. Goodwin, "Adaptive decouplina of mullivariable systems," *Controller*, Vol. 46, No. 6, 1993–2009, 1987.
3. Zhu, K., X. F. Qin, and T. Y. Chai, "A new decouplina design of selftuning multivariable generalized predictive control," *Adaptive Control and Signal Processing*, Vol. 13, No. 3, 183–196, 1999.

Modeling Buck Converter by Using Fourier Analysis

Mao Zhang[1], **Weiping Zhang**[2], **and Zheng Zhang**[2]

[1]School of Computing, Engineering and Physical Sciences, University of Central Lancashire, UK
[2]North China University of Technology, Shijingshang District, Beijing, China

Abstract— By employing theory of PAM (pulse-amplitude-modulation), Buck converter (DC/-DC) have been modeled in this paper. The main contributions are as the followings: (1) A DC transformer model has been proposed to analysis of the voltage gain, efficiency and some steady-state properties for DC/DC converter; (2) Two a.c. small signal models have been put forward in order to get the transfer functions of input to output and control to output. These a.c. small signal models play an important role on predicting the dynamic behaviors and designing its control system.

In this paper, we have utilized the signal processing theory and approaches to analyze and model Buck -DC/DC converter which is a power converter, and figured out that it (the signal processing theory and approaches) also is a powerful tool in power electronics field. For example, analysis and model of Buck converter is a problem in power electronics and PAM is a problem which belongs to signal processing. However, this paper has shown that both Buck converter and PAM have a same mathematic model. So, a mature theory and method about PAM has been successfully employed to predict the behaviors of Buck converter, extracting the following conclusions,

(1) A DC transformer model, describing the main function of a DC/DC converter, has been proposed to analysis of the voltage gain, average current gain, efficiency and some steady state properties as well as how to controlling the output energy;

(2) An a.c. small-signal model for input-output has been developed. According this model, one can easily get the transfer function of input to output and dynamic input resistance as well as output resistance;

(3) An a.c. small-signal model for control-output and its transform function have been investigated. This model and transform function are necessary for deigning its control system and for analyzing the stability of the closed loop control.

In one words, this paper has a new window opened for employing the mature theory and approaches in signal process to study DC/DC converter.

The Comparison of Direct and Indirect Matrix Converters

P. Chlebis, **P. Simonik**, **and M. Kabasta**
Department of Electronics, VSB — Technical University of Ostrava, Czech Republic

Abstract— The matrix converters are currently the center of attention of many research centers because the power conversion is important for many industrial applications as robotics, assembly line and etc. The matrix converter seems to be a universal converter and the reason for this statement is inherent bidirectional power flow and the possibility of combinations of input and output phases. The other advantage is no need of the energy storage elements.

At the Department of Electronics were assembled basic types of matrix converters and were developed various types of controls, e.g., vector control, for these types of converters. For these types of converters were performed numeric simulations and verification of the real characteristics. The comparison was realized for direct and un-direct DC/DC, DC/AC, AC/DC and AC/AC three-phase converters. On these types of converters was the theory of universal converter control confirmed. The Matlab/Simulink and the ORCAD PSpice were used for simulation and microcontroller Freescale 56F8013 with inputs of the A/D converter and outputs for PWM outputs was used for control.

In this paper are presented results of these types of converters and main output and input characteristics are compared. The criterions for our comparison were the quality of input energy, the quality of wave forms and the quality and form of output voltage. By the comparison was also evaluated complexity of the converter circuits and its commutation. This contribution summarizes results of some tests and measurements that refer to conclusion that the special types of matrix converters have characteristics fully comparable with the conventional un-direct frequency converters.

Design of a High Speed Universal Motor for Organic Agriculture Applications

Hanzhou Liu[1], **David Woodburn**[1], **Shaohua Lin**[1], **Thomas X. Wu**[1], **Jianjian Wei**[2], **and Keqiang Cao**[3]

[1]School of Electrical Engineering and Computer Science, University of Central Florida Orlando, FL 32816, USA
[2]Beijing TEPEC Technology Corporation, Beijing 100086, China
[3]Agriculture University of Hebei, Baoding, Hebei 071001, China

Abstract— We report on the design of a high speed and highly efficient universal motor for organic agriculture applications. Recently, we find that pests can be effectively controlled after spraying by a high voltage electrostatic sprayer. Instead of using pesticide, a natural product derived from lignite was used so that this novel pest control is environmental friendly. Key to the sprayer system is a university motor that pumps liquid out of container. Based on the sprayer system, the motor requires 1 kW for input power, 220 volts for input voltage, 20 krpm for rotating speed and 77% for efficiency. Following these specifications, we propose a systematic methodology for the design of a universal motor. Firstly, we propose a two pole structure with twenty two slots on the rotor. Secondly, we analyze the structure using magnetic circuit analysis and derive a set of design equations, from which we can obtain initial dimensions. Thirdly, we input our fundamental design into Ansys RMxprt and then optimize the dimensions to meet the design goals. Finally, we use Ansys Maxwell to check the design and do further optimization. Besides electrical design, we also choose suitable cooling methods in order to make maximum interior temperature under control.

Use of FACTS Devices in Power Systems for Power Quality Improvement

H. D. Sharma[1], **Malay Ranjan Tripathy**[2], **and S. K. Gupta**[3]

[1]Department of Electrical & Electronics Engineering, JIET, Jind, Haryana, India
[2]Department of Electronics & Communication Engineering, JIET, Jind, Haryana, India
[3]Department of Electrical Engineering, DCRUST, Murthal, Haryana, India

Abstract— An electrical power system [1] can be seen as interconnection of generators and electrical loads through a network of transmission lines, transformers and ancillary equipments. In the power system, power flows throughout the network are mainly distributed as a function of line impedance [2]. A transmission line with low impedance allows larger power flows through it than with high impedance. This is not always the most desirable outcome because it gives number of operational problems, such as loss of system stability, high transmission losses, voltage limit violation, an inability to utilize transmission line capability up-to their thermal limit.

A new solution to such operational problems will relay on upgrading of existing transmission corridors, by using latest methods and equipments of power electronics. FACTS (Flexible Alternating Current Transmission Systems) [1–4] are the latest technology which is capable to address all these problems like transient breaks, sag, harmonics and voltage flicker. In this paper we have described various types of FACT devices. Towards the end of the paper we have considered STATCOM (Static Synchronous Compensator) [5] as power quality improvement equipment to improve the voltage profile of a five bus electrical network. The simulation is done by using MATLAB. The results are obtained by connecting STATCOM at different bus bars of the network.

REFERENCES

1. Acha, E., C. R. Fuerte-Esquivel, H. Ambriz-Perez, and C. Angeles-Camacho, *FACTS: Modelling and Simulation in Power Network*, John Wiley & Sons Ltd., 2004.
2. Hingorani, N. G. and L. Gyugyi, *Understanding FACTS Concepts and Technology of Flexible AC Transmission Systems*, IEEE Press, New York, 2000.
3. Mathur, R. M. and R. K. Verma, *Thyristor — Based FACTS Controllers for Electrical Transmission Systems*, IEEE Press, New York, 2002.
4. Song, Y. H. and A. T. Johns, Eds., *Flexible AC Transmission Systems, (FACTS)*, IEE Press, London, 1999.
5. Mienski, R., R. Pawelek, and I. Wasiak, "Shunt compensation for power quality improvement using a STATCOM controller: Modelling and simulation," *IEE Proc. Genr. Transm. Distrib.*, Vol. 151, No. 2, 274–280, March 2004.

Study on the Interference Effect of ZigBee by Interference Signal Using GTEM Cell

Sangbong Jeon[1], **Chang-Han Jun**[1], **Youngho Kim**[2], **Yeon-Choon Chung**[3], **and Sangho Choi**[1]

[1]Korea Radio Promotion Association, Korea
[2]Electronics and Telecommunications Research Institute, Korea
[3]Seokyeong University, Korea

Abstract— Recently short range wireless communication services are being widely used. Especially in 2.4 GHz band, radio communication service such as Bluetooth and ZigBee is widely used. This frequency band is assigned by ISM (Industrial, Scientific, and Medical) band and a lot of industry apparatus are used. The ISM bands are many interference sources such as WLAN, Microwave Oven, and so on.

To evaluate the interference of communication, generally it is embodied by putting both EUT and the antenna in the in non-echo chamber extended by cable from communication AP (Access Point) outside of the non-echo chamber. However, this is difficulty in the realization as well as the expensive cost. According to the recent paper, it is introduced the interference test method using PW Cell (Parallel Wired Cell) to possibly communicate with each other between EUT and AP [1]. This is basically the same theory as TEM Cell. However, the effect for the noise from many other sources can't be totally excluded in yielding the measurement results because the side of PW Cell is opened. In this paper, we are embodied by GTEM Cell to the effect of the electromagnetic interference to ensure the reliability because the GTEM Cell is the closed structure unaffected by the interference from the other noise of the environment. Also the undesired waves are used as the interference signals which are CW (continuous wave), white noise, AM modulation signal (1 kHz and modulation depth 80%) and ASK (Amplitude Shift Keying) signal.

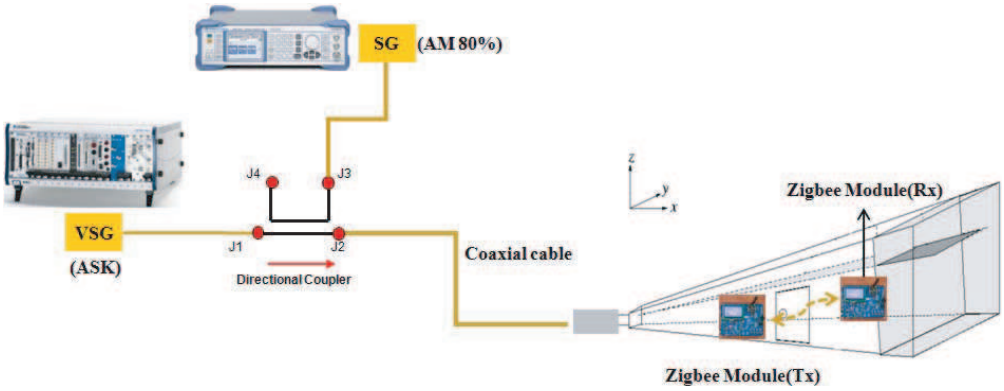

Figure 1: Setup for interference measurement.

ACKNOWLEDGMENT

This work was supported by IT R&D program of MKE/IITA. [2008-F-014-01, Study on Electromagnetic Compatibility for Protecting Electromagnetic Environment in Ubiquitous Society].

REFERENCES

1. Tokuda, M., K. Ichikawa, Y. Honma, and M. Kitora, "Radio wave interference test method for wireless communication system by opened parallel wired cell," *IEICE Trans. Commun.*, Vol. E88-B, No. B, 3242–3228, Aug. 2005.

Interference Test from Unintentional Noise to Terrestrial-DMB Using GTEM Cell

Sangbong Jeon[1], **Chang-Han Jun**[1], **Youngho Kim**[2], **Yeon-Choon Chung**[3], **and Sangho Choi**[1]

[1]Korea Radio Promotion Association, Korea
[2]Electronics and Telecommunications Research Institute, Korea
[3]Seokyeong University, Korea

Abstract— In Korea, T-DMB (Terrestrial Digital Multimedia Broadcasting) was serviced from December 2005. T-DMB services are being widely used in Korea and it is a digital radio transmission technology for sending multimedia such as TV, radio, and data broadcasting to mobile devices such as mobile phones.

It has a portable terminal with various functions such as DMB receiver, phone, and camera so on. The portable terminal is weak in Electromagnetic interference phenomenon. In this paper, we evaluated the interference effect of T-DMB by unintentional noise with GTEM Cell. And the used unintentional noise are interference signals which are CW(Continuous Wave), white noise, and AM modulation signal(1 kHz and modulation depth 80%). Also GTEM Cell was used to realize the environment for the evaluation of interference [1].

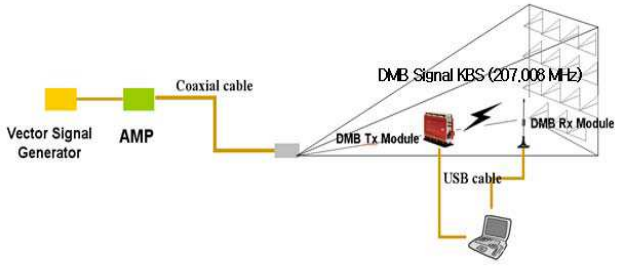

Figure 1: Setup for interference measurement.

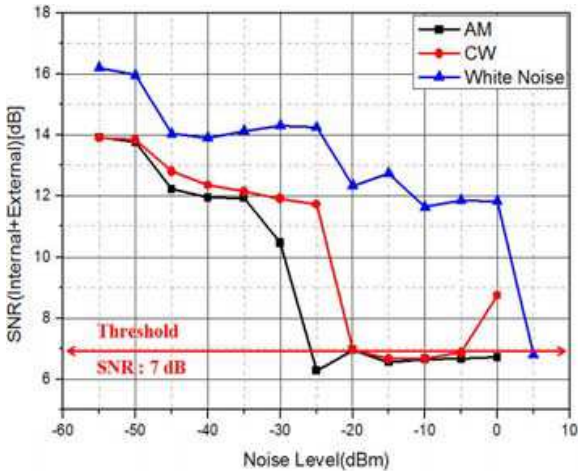

Figure 2: Results of measured interference effect.

ACKNOWLEDGMENT

This work was supported by IT R&D program of MKE/IITA. [2008-F-014-01, Study on Electromagnetic Compatibility for Protecting Electromagnetic Environment in Ubiquitous Society].

REFERENCES

1. Jeon, S. B., Y.-C. Chung, C.-H. Jun, S.-T. Kwun, J. H. Yun, and S. H. Choi, "Evaluation of interference between microwave oven noise and IEEE802.11b using a GTEM cell," *PIERS Online*, Vol. 5, No. 6, 571–575, 2009.

Shielded and Unshielded Three-conductor Transmission Lines: Modeling and Crosstalk Performance

Mnaouer Kachout, **Jamel Bel Hadj Tahar**, **and Fethi Choubani**
Research Unit Systems of Telecommunications (6'Tel) SUP'COM, Tunisia

Abstract— In this paper, we study the effect of shielding on the crosstalk between three-conductor transmission lines. The objective of this work is to show that shielded lines can be more compact with best performance in term of crosstalk than unshielded conductors. In other word, we will demonstrate that by using shielded line we can reduce crosstalk with minimum spacing between wires. We used ribbon cable with circular cylindrical section be immersed in a homogeneous medium. Ribbon cables are frequently being used to interconnect electronic systems, such as computers. First, we present Π-T hybrid electric equivalent model for three conductor transmission lines. At this stage, we are interested in calculating various per-unit-length parameters for shielded and unshielded conductors. This model allows us to calculate crosstalk between conductors. We calculate near-end crosstalk using S parameters. Secondly, we present theoretical foundation for shielded and unshielded conductors to calculate near-end crosstalk between wires. To validate the presented Π-T hybrid electric equivalent model, we will compare the theoretical results with simulation obtained results. Finally, one hand we calculate near-end crosstalk versus separation distance between unshielded lines. On the other hand, we calculate near-end crosstalk versus separation distance between shielded lines for different radii of shielding. Comparison between these two results shows that the shielded lines with a radius of shielding h gives a near-end crosstalk reduced compared to unshielded lines separated by $4h$. In conclusion, the use of shielded conductors allows us to reduce spacing between conductors with a ratio of 4 compared to unshielded conductors with best crosstalk performance.

Side Effect Characterization of EBG Structures in Microstrip Patch Antenna

M. Fallah, **F. H. Kashani**, **and S. H. Mohseni**
Iran University of Science and Technology (IUST), Tehran, Iran

Abstract— The unwanted side effect of EBG structures when integrated with microstrip antenna are investigated in this paper. The main goal of using EBG structures in microstrip antenna is to achieve better gain and efficiency, lower side-lobes and back-lobes levels, and better isolations among array elements, by suppressing surface wave modes. The two dominating side effects may be named as parasitic effect and cavity effects. The parasitic effect of EBG structure causes the multi resonance antenna resulting in larger bandwidth. Cavity effect on the other hand, is due to reflecting energy from EBG toward antenna and results in a larger Q value and so decreasing the bandwidth. These two side effects are characterized in this work and the EBG structure parameters and number of EBG rows is related to these effects. The design parameters of EBG structures can be managed such that the parasitic effect of EBG structure can be the dominating effect and consequently results in larger bandwidth. This theoretical model is implemented in to a two element microstrip array antenna integrated with conventional mushroom type EBG structure in E plane. According to our results, there is an optimal design for EBG unit cell parameters and number of rows so that in addition to surface wave reduction, a larger bandwidth is achieved.

The Eigenvalues of Quantized Spin Waves and the Uniaxial Anisotropy in a Biferromagnetic System

Xiao Juan Hou[1, 2], **Guo Hong Yun**[1, 3], **Yu Hao Bai**[1], **and Narsu Bai**[3]

[1]College of Physical Science and Technology, Inner Mongolia University, Hohhot 010021, China
[2]Department of Applied Physics, School of Mathematics, Physics and Biological Engineering
Inner Mongolia University of Science and Technology, Baotou 014030, China
[3]Inner Mongolia Key Laboratory of Physics and Chemistry of Functional Materials
College of Physics and Electronic Information, Inner Mongolia Normal University, Hohhot 010022, China

Abstract— Magnetic multilayers have been increasing interest in the areas of magnetism and spintronic devices [1], due to their potential applications to solid-state data-storage and data-processing devices. At the beginning of magnetic data storage it is important to understand spin waves to reduce their harmful influence or their assistance for the magnetization reversal [2]. More recent publications have shown that it is impossible to use spin waves for logic devices [3]. To make a first step towards future devices minimizing magnons' disturbing influence or using magnons, spin waves and their properties have to be understood [4]. The eigenproblems of quantized spin waves in a (100) ferromagnetic bilayer system have been investigated theoretically by using the interface rescaling approach. The energy-band structure of the system has been obtained and the effect of the uniaxial bulk anisotropy field of easy-axis type on the energy bands are exploreded thoroughly.

REFERENCES

1. Smith, D., E. Chunsheng, S. Khizroev, D. Litvinov, *J. Appl. Phys.*, Vol. 99, 014503, 2006.
2. Nembach, H. T., P. M. Pimentel, S. J. Hermsdoerfer, B. Leven, B. Hillebrands, and S. O. Demokritov, *Appl. Phys. Lett.*, Vol. 90, 062503, 2007.
3. Khitun, A., B. Mingqiang, and K. L. Wang, *IEEE Trans. Magn.*, Vol. 44, 2141, 2008.
4. Wieser, R., E. Y. Vedmedenko, and R. Wiesenganger, *Phys. Rev. B*, Vol. 79, 144412, 2009.

Session 1P7
Poster Session 4

Magnetostrictive Bending of a Cantilevered Ultura-thin Film-substrate System

Jiangang Li[1] and Guohong Yun[1, 2]

[1]College of Physical Science and Technology, Inner Mongolia University, Hohhot 010021, China
[2]Key Laboratory of Physics and Chemistry of Functional Materials
Inner Mongolia Normal University, Hohhot 010022, China

Abstract— Micro-nanometer thin film-substrate cantilever system is becoming more important in the modern physics and materials science. With the development of the microminimization in devices, the thickness dimension has reached several nanometers. The surface and interface effect of the cantilever has been more and more important for designing devices in nanometer scale. O'handley first report the difference between surface magneto-elastic coupling and the bulk [1]. E. du Tre'molet de Lacheisserie first defined the surface magneto-elastic coupling coefficients and calculated the bending characteristic of ultra-thin film-substrate cantilever system using three-parameter model [2]. But three-parameter is flawed for description of this problem [3, 4].

We calculated the nature of bending cantilevered ultura-thin film-substrate system using four-parameter model [3, 4, 7, 8]. Under the cylindrical symmetry, we reckon in the surface stress [5], surface elastic and magneto-elastic coupling coefficient [2], and the homogeneous strain caused by lattice mismatch [6]. Using the principle of minimal free energy, we derived the curvature of bending, deflection of the free end, homogeneous strain by the misfit and the system stress. We have considered a film where surface effect can be negligible, when film becomes isotropic. The results are identical with previous work, that certificate the correctness of our theory.

The results show that the isotropic surface stress and the homogeneous strain caused by mismatch have no contribution on the deflection of free end. The surface stress affects the curvature of the system, while the homogeneous strain by mismatch has impact on the stress of the cantilever system. For a certain thickness of the substrate, there is a maximum of the deflection as a function of the film-substrate ratio k. surface effects not only affect the maximum size, but also makes the maximum value shift. The thicker the substrate is, the smaller the importance of surface effect. The location of maximum does not shift when ignore the surface effect.

REFERENCES

1. Sun, S. W. and R. C. O'Handley, *Phys. Rev. Lett.*, Vol. 66, 2798–2801, 1991.
2. Du Tre'molet de Lacheisserie, E., *Phys. Rev. B*, Vol. 51, 15925–15932, 1995.
3. Narsu, B. and G. H. Yun, *Sci. China: Ser. E*, Vol. 50, 454–461, 2007.
4. Narsu, B. and G. H. Yun, *Sci. China: Ser. E*, Vol. 50, 683–693, 2007.
5. Zang, J. and F. Liu, *Appl. Phys. Lett.*, Vol. 92, 021905-1-3, 2008.
6. Marcus, P. M., *Phys. Rev. B*, Vol. 53, 7460–7465, 1996.
7. Narsu, B. and G. H. Yun, *J. Phys. D: Appl. Phys.*, Vol. 41, 095309-1-9, 2008.
8. Narsu, B. and G. H. Yun, *Sci China: Ser. G*, Vol. 51, 1357–1366, 2008.

Structure Optimization for Magnetic Equipment of Permanent Magnet Retarder Using ANSYS

B. F. Jiao, **D. S. Li**, **Y. K. Sui**, **and L. Z. Ye**
School of Mechanical Engineering and Applied Electronics Technology
Beijing University of Technology, China

Abstract— The main purpose of this research is to perform a magnetic analysis on magnetic equipment of permanent magnet retarder (PMR) and optimize the structure of magnetic equipment with ANSYS, finite element analysis software and its design optimization module. The physical model is built as axisymmetric model according to the characteristics of the structure in magnetic equipment. Using this model, the magnetic field distribution and magnetic force is calculated by ANSYS. Mathematical model of structure optimization is also built. The design variables are structural parameters including the dimensions of permanent magnets and magnetic yoke; the objective function is the magnetic force. The unconstrained optimization model takes the maximum value of magnetic force as the objective. First order optimization method is used to determine the optimum design of this problem. The optimization process works entirely with the ANSYS Parametric Design Language (APDL). The ANSYS optimization module offers several tools that attempt to address the mathematical model in different ways. The design tools are used to understand design space and the behavior of the dependent variables. It is showed that designing a structure with ANSYS optimization module and its design tools is an effective means to make improvements of structure.

Analysis of Drilling Parallel Horizontal Twin Wells Rotating Magnetic Beacons Magnetic Field Strength Size in SAGD

B. Tu, **D. S. Li**, **E. H. Lin**, **B. Luo**, **J. He**, **L. Z. Ye**, **J. L. Liu**, **and Y. Z. Wang**
School of Mechanical Engineering and Applied Electronics Technology
Beijing University of Technology, China

Abstract— Rotating magnetic beacons magnetic field strength size is very important to drilling parallel horizontal twin wells in Steam Assisted Gravity Drainage (SAGD). This paper analyzes a small magnet by made of diameter is 25.4 mm at both ends when a single length of 12.6 mm by permanent magnet and in the middle of the length is 78 mm magnetic materials. Analysis the magnetic material composition of 1J12, 1J50, 1J79 generated magnetic field strength size. Use ANSOFT software simulation the magnetic field strength to different magnetic materials and build experimental methods to a specific experimental test. According to the simulation results and experimental results compared and analyzed 1J12, 1J50, 1J79 three kinds of magnetic materials generated magnetic field strength size. Experimental results and simulation results are basically consistent and the results show that the magnetic material 1J50 that applied to the rotating magnetic beacon generated magnetic field strength that fluxgate can effective collect rotating magnetic beacon generated magnetic field strength in the horizontal distance of 55.5 m and it can to meet the specific requirements of engineering applications.

Full-wave Equivalent Circuit of Planar Multilayer Structures for Remote Sensing Applications

D. B. Ferreira[1], **S. J. S. Sant'Anna**[1, 2], **and J. C. da S. Lacava**[1]

[1]Laboratório de Antenas e Propagação, Instituto Tecnológico de Aeronáutica, Brazil
[2]Divisão de Processamento de Imagem, Instituto Nacional de Pesquisas Espaciais, Brazil

Abstract— The scattering matrix is considered the most important parameter within polarimetric SAR analysis, since it provides complete information about the scattering mechanism and from which all polarimetric features that describe the scattering target can be derived. The scattering matrix can be regarded as the mathematical signature of a scattering target, as it relates the scattered wave's electric field to the incident one. Recently a new electromagnetic methodology for the simulation of polarimetric SAR images had been proposed in [1]. It starts from Maxwell's equations, applies the spectral domain full-wave technique and the moment method to evaluate the electromagnetic fields scattered by a multilayer planar structure excited by plane waves. However, the calculations of spectral fields and the related Green's functions in multilayer structures are usually tedious and error-prone when done by hand. To overcome these limitations, a circuital model has been employed. Following [2, 3], but using a different approach, a new elegant and straightforward procedure for obtaining the full-wave equivalent circuit of planar multilayer structure based on auxiliary potential functions and transmission ($ABCD$) matrix is presented. The electromagnetic characteristics of each layer are incorporated into the transmission matrix and the circuital parameters are evaluated by using the symbolic capability of the *Mathematica* package. Asymptotic expressions for the far electromagnetic fields scattered by the structure into free space is obtained by applying the stationary phase method. From these expressions and the knowledge of the electric current densities on the interfaces, the scattering matrix elements can then be completely determined for any incidence and scattering direction. However, for simple target such as a dipole (described in [4]) the electric current densities became a multiplicative factor of the scattering matrix and its elements can be obtained directly from the Green's functions terms. Therefore, the use of circuital model to generate the Green's functions of a multilayer structure can be extremely helpful to the determination of simple target scattering matrix and consequently its related polarimetric features. In this work, the circuital model is used to describe a planar multilayer structure composed of $N + 2$ isotropic, linear and homogenous layers stacked up in z direction. The layers are assumed to be unbounded along the x and y directions. The lower layer, having complex permittivity ε_g and complex permeability μ_g, is denoted as ground layer and occupies the negative-z region. The next N layers are characterized by thickness ℓ_n, complex permittivity ε_n and complex permeability μ_n, where $1 \leq n \leq N$. The planar interface $z = d_N$ separates the N-th layer from free space (the upper layer). Metallic patches, which behave as scattering elements, are printed at arbitrary positions on each one of the $N + 1$ interfaces of the structure. Based on the circuital parameters the scattering matrix and the polarimetric response of a particular structure having only one electric dipole printed on interface $z = d_N$ are derived. The polarimetric response is a feature typically employed in remote sensing to characterize the scattering properties of a target. It is a graphical representation of the target scattering cross section as a function of the ellipticity and the orientation angles of the transmitted electromagnetic wave that can be directly computed from the target's scattering matrix.

REFERENCES

1. Sant'Anna, S. J. S., J. C. S. Lacava, and D. Fernandes, "From Maxwell's equations to polarimetric SAR images: A simulation approach," *Sensors*, Vol. 8, No. 11, 7380–7409, 2008.
2. Itoh, T., *Numerical Techniques for Microwave and Millimeter-wave Passive Structures*, John Wiley, New York, 1989.
3. Dreher, A., "A new approach to dyadic Green's function in spectral domain," *IEEE Trans. Antennas and Propag.*, Vol. 43, No. 11, 1297–1302, Nov. 1995.
4. Sant'Anna, S. J. S., J. C. S. Lacava, and D. Fernandes, "Closed form expressions for scattering matrix of simple targets in multilayer structures," *International Geoscience and Remote Sensing Symposium*, 714–717, Barcelona, 2007.

Tumor Classification Using Radar Target Signatures

R. C. Conceição, M. O'Halloran, D. Byrne, E. Jones, and M. Glavin
Electronic and Electrical Engineering, College of Engineering and Informatics
National University of Ireland Galway, Ireland

Abstract— The use of Ultra Wideband (UWB) radar to detect early-stage breast cancer has been extensively investigated. The basis for this imaging modality is the significant dielectric contrast between normal and cancerous breast tissue at microwave frequencies.

However, based on the recently-established dielectric similarities between malignant, benign and fibroglandular tissue within the breast, differentiating between these types of tissues in microwave images may be problematic. Therefore, it is important to investigate alternative methods to analyse and classify dielectric scatterers within the breast. One such approach is to classify scatterers based on their radar target signature, which carries information about scatterer size and shape.

Benign tumors tend to have smooth surfaces and are compact and oval in shape. Conversely, malignant tumors tend to have rough and complex surfaces with spicules or microlobules. These properties can significantly influence the radar target signature, potentially allowing for dielectric scatterer classification.

This paper presents a method to model the growth pattern of benign and malignant tumors, based on the use of Gaussian Random Spheres (ranging between smooth, macrolobulated, microlobulated and spiculated shapes), while classification algorithms that attempt to define the nature of tumors based on radar target signatures are also examined.

Optimizing Windows Security Features to Block Malware and Hack Tools on USB Storage Devices

Dung Vu Pham[1], **Malka N. Halgamuge**[2], **Ali Syed**[1], **and Priyan Mendis**[2]

[1]School of Computing and Mathematics, Charles Sturt University, Victoria 3000, Australia
[2]The Department of Civil and Environmental Engineering, The University of Melbourne Victoria 3010, Australia

Abstract— USB based malware including worms, virus, Trojan horses and other malicious codes such as data theft tools have been serious security issues for the last few years. The majority of these malicious codes exploit Windows Autoplay features to automatically launch attacks on host computer transparently to computer users. In this research, we propose a security-service architecture for Windows operating systems on Windows Vista, Windows 7, and Windows 2008 platform to address USB based malware. The deliverable of the research includes a new Windows security service architecture with the source code of a simulated Windows security feature which coordinates Windows security services and feature to better handle USB based malware written in Windows PowerShell language.

Introduction: Universal Serial Bus (USB) storage devices have been one of the most common means of malware and hack tools attacks on host computers for the last few years. This has been possible due to two factors involving the lack of a security mechanism for Windows Autoplay features as well as the popularity of USB storage devices. Malware that exploit Autoplay features to replicate and automatically launch attacks are known as Autorun malware, one of the most common types of malware in the last three years. Microsoft and security firms such as McAfee and Symantec have invested considerable effort in re-engineering their software to mitigate the impact of Autorun malware. Recently, Microsoft decided to disable the Autoplay feature for USB drives on Windows 7 which is their latest desktop operating system in an effort to reduce the impact of Autorun malware. However, such a solution do not directly address the issues of malware and hack tools stored in USB drives. In this paper, we will provide a new Windows security service architecture with simulation which helpsWindows better manage software attacks, especially Autorun malware, from USB drives.

Windows Security Service Architecture: Our proposed architecture involves the use of Microsofts latest security features available on some latest Windows operating systems including Vista, Windows 2008 and Windows 7, and the deployment of a new Windows service, which is called Parse Autorun. Although the solution can be implemented in Windows XP, the best results can only be achieved on Windows 2008 R2, and Windows 7 which fully supports our utilised security features including Windows Firewall, Windows Defender, Microsoft Security Essential, User Account Control, and AppLocker.

Conclusion: The implementation of Parse Autorun service helps maximise the effectiveness of the current Windows security services including User Account Control, Windows Defender, Microsoft Security Essentials, Windows Firewall, AppLocker, and Windows Update services in addressing software threats from USB storage devices, especially USB based malware. In addition, the simulated Windows security service architecture provides an efficient malware scanning scheme for USB storage devices which helps Windows self-defending services quickly locate and mitigate the threat at low system resource consumption. The efficiency of the solution also reflects in the level of maintenance requirements and the simplicity of the feature which do fit for all computer users in both office and home environment. Finally, the enforcement of signed applications and trust publishers in the Parse Autorun service is just another step towards a secure computing environment which is currently the common trend in the computing industry.

REFERENCES

1. McAfee Avert Labs, *McAfee Threats Report: Second Quarter 2009*, McAfee, Inc, 2009.

Evaluated the High Rang Resolution Profile Identifying Simulation by Laser Radar of the Rotation Targets

M.-J. Wang[1, 2], **Z.-S Wu**[3], **Y.-L. Li**[1], **and J.-D. Xu**[2]

[1]Institute of E.M. Wave Propagation & Scattering, Xianyang Normal College, Box 103, 712000, China
[2]The School of Electronic Information, Northwestern Polytechnical University
Xi'an, Shaanxi 710076, China
[3]Science School, Xidian University, Box 273, 710071, China

Abstract— Recently, we presented a study of pulse beam scattering from a rigid body on the estimation by used with laser high-range resolution profile (LHRRP) simulations. However, there has been an increased interest in study of the LHRRP of a moving object. The LHRRP of rigid bodies are tightly connected with their posture and sensitive to the angle of their rotation. This paper presents a line of sight (LOS) method for analyzed the influence of a rotation angle of the targets, and compare the difference between their LOS projection and LHRRP simulations.

ACKNOWLEDGMENT

This works is supported by the National Natural Science Foundation of China (Grant No. 60801047, 60771038, 60971079), China Postdoctoral Science Foundation funded project (Grant No. 200904613-08).

Problems of Statistical Decisions in Ocean Monitoring

F. A. Mkrtchyan
Department of Informatics, V. A. Kotelnikov's Institute of Radioengineering and Electronics
Russian Academy of Science, Fryazino 141190, Russia

Abstract— Application of means of geoinformation monitoring in many cases is connected to acceptance of the statistical decision on presence on a surveyed part Terrestrial surface of this or that phenomenon. One of features of a condition of gathering of the information for such decision is the impossibility of reception the big statistical samples.

Therefore development and research of optimum algorithms of distinction of the casual signals characterized by samples of limited volume, in conditions of parametrical aprioristic uncertainty are necessary.

At present time there are many methods of recognition which are caused appreciably by variety of statements of concrete tasks.

The feature of remote measurements is information acquisition, when the data of measurements, acquired during tracing of flying system along routes of survey, are directed to input of the processing system. As result the two dimensional image of investigated object is registered. Statistical model of spottiness for investigated space is one of models for this image.

In real conditions, the study of spots, the acquiring of their statistical characteristics and their using in a problem of detection is enough a complex problem. It is necessary to develop the criteria allowing the distinguishing the spots from other phenomena. For example, it is necessary to determine such threshold the exceeding of which is the spot indicator. Also it is necessary to develop model presentation of processes of spots detection.

Statistical characteristics "spottiness" microwave temperatures can be used at recognitions and classifications of the phenomena on a surface of the ocean, distinguished by a degree of excitement. The analysis of empirical histograms for "spottiness" shows, that in most cases ($l+$, $l-$) — characteristics will be coordinated with exponential distribution, and amplitude characteristics will be coordinated with normal distribution. Therefore for detection and classification of the phenomena on a surface of ocean it is necessary to apply optimal algorithms for the Computer training to taking statistical decisions for the aforesaid distributions.

In the present work the generalized adaptive algorithm of training to acceptance of statistical decisions for exponential classes of distributions is developed at aprioristic parametrical uncertainty of conditions small samples. Numerical examples are shown. Efficiency of the developed optimum procedure for small samples is shown.

An Adaptive Spectroellipsometric Identifier for Ecological Monitoring of the Aquatic Environment

F. A. Mkrtchyan, **V. F. Krapivin**, **V. I. Kovalev**, **and V. V. Klimov**
Institute of Radioengineering and Electronics, Russian Academy of Sciences
1 Vvedensky Square, Fryazino, Moscow Region 141190, Russia

Abstract— The creation of multichannel polarization optical instrumentation and use of spectroellipsometric technology are very important for the real-time ecological control of aquatic environment. It should be mentioned that efficient solution of this multiparametric problem greatly depends on the precision and simplicity of ellipsometric devices.

This report is aimed to describe

- A technology of combined use of spectroellipsometry and algorithms of identification and recognition that allowed the creation of a standard integral complex of instrumental, algorithmic, modular and software tools for the collection and processing of data on the aquatic environment quality with forecasting and decision — making functions.
- A compact measuring — information multichannel spectroellipsometric device for monitoring the quality of aquatic environment, that is based on the combined use of spectroellipsometry and training, classification, and identification algorithms.

This spectroellipsometric system will differ from modern foreign analogues by the use of a new and very promising method of ellipsometric measurements, an original element base of polarization optics and a complex mathematical approach to estimating the quality of a water object subjected to anthropogenic influence.

Unlike foreign analogues, the system has no rotating polarization elements. This allows one to increase the signal-to-noise ratio and the long-term stability of measurements, to simplify and reduce the price of multichannel spectroellipsometers.

The system will be trainable to the recognition of the pollutants of aquatic environment.

For the first time the combined use of real — time spectroellipsometry measurements and data processing methods has been realized in an **Adaptive Identifier.**

- The algorithmic support of the Adaptive Identifier is based on a complex application of recognition and classification algorithms on the basis of 128 spectra images registered during a fixed period of time.
- A time interval of 1 second is usually established and provides about 30 value of brightness for each of the 128 optical channels.
- The spectra obtained are sources of set of statistical parameters and different characteristics united into vector spaces for their comparison with the standard samples of famous pollutants stored on the computer.
- The technology of this comparison depends on the diversity of identification methods.

The system is trainable to the recognition of the pollutants of aquatic environment.

Excitation of Surface Plasmon and Its Sensing Application Based on a Metal Grating

Taikei Suyama[1], **Yaoju Zhang**[2], **and Yoichi Okuno**[1]

[1]Graduate School of Science and Technology, Kumamoto University, Japan
[2]College of Physics and Electronic Information, Wenzhou University, China

Abstract— We investigate excitation of plasmon on surface of a metal grating placed in planer or conical mounting. Yasuura's mode-matching method is employed in the investigation of plasmon excitation on a metal grating. Results of numerical computations are compared with experimental data. When a TM wave illuminates a metal grating, total or partial absorption of incident light occurs at angles of incidence at which the plasmon surface waves are excited. In planer mounting the absorption is generally strong and nearly total absorption is observed. While in conical mounting, it is not so strong as that in the planer mounting case and a considerable amount of incident power is reflected. This, however, is accompanied by enhanced TM-TE mode conversion and the greater part of the reflected wave is in the TE polarization. The reciprocal of the TM-wave efficiency, hence, is a practical measure in finding the angles of incidence at which the plasmons are excited. Because the angles are sensitive functions of the refractive index of a material over the grating surface, this phenomenon can be applied to an index sensor.

Introduction: A metal grating has an interesting property known as the resonance absorption in optics region [1]: partial or total absorption of incident light occurs at a specific angle of incidence, which is called a resonance angle. This is caused by excitation of plasmon surface waves and is accompanied by an abrupt change of diffraction efficiency known as a resonance anomaly [2, 3]. This can be seen in TM incidence alone for a grating placed in planer mounting (the plane of incidence is perpendicular to the grooves). While in conical mounting (the plane of incidence is not perpendicular to the grooves), the absorption occurs in both TM and TE incidence. For a TM-wave incidence the absorption in conical mounting, in general, is not so strong as that in planer mounting. The absorption in this mounting, however, is accompanied by enhanced TM-TE mode conversion [4]. Although the mode conversion can always be seen in conical diffraction, it is enhanced by the excitation of surface plasmon. In fact, when the resonance absorption occurs, the TM component of the reflected wave almost vanishes and the TE component is dominant. The reciprocal of the TM-wave efficiency can be a practical measure in finding the resonance angle. We know that the resonance absorption occurs when a phase-matching condition is satisfied: the phase constant of an evanescent order coincides with the real part of an eigenvalue of surface plasmon. This means that the resonance angle is determined by the grating parameters, the incident wave, and the refractive index of a material over the grating surface. Hence, if we measure the resonance angle by observing the TM-wave efficiency, we can find the index of the material over the grating by making comparison with results of computer simulation. On the other hand, if we can measure the phase of a diffracted wave on a metal grating by using an interferometer, we will be able to determine the index to a high accuracy.

REFERENCES

1. Raeter, H., "Surface plasmon and roughness," *Surface Polaritons*, V. M. Argranovich and D. L. Mills (Eds.), 331–403, North-Holland, New York, 1982.
2. Nevièr, M., "The homogenous problem," *Electromagnetic Theory of Gratings*, R. Petit (Ed.), 123–157, Springer-Verlag, Berlin, 1980.
3. Kong, F. M., K. Li, B.-I. Wu, H. Huang, H. Chen, and J. A. Kong, "Propagation properties of the spp modes in nanoscale narrow metallic gap, channel, and hole geometries," *Progress In Electromagnetics Research*, PIER 76, 449–466, 2007.
4. Bryan-Brown, G. P., J. R. Sambles, and M. C. Hutley, "Polarization conversion through the excitation of surface plasmons on a metallic grating," *J. Modern Optics*, Vol. 37, No. 7, 1227–1232, 1990.

A Uniform Asymptotic Solution for Diffraction by a Right-angled Dielectric Wedge

G. Gennarelli and G. Riccio
D.I.I.I.E., University of Salerno, Via Ponte Don Melillo, 84084 Fisciano (Salerno), Italy

Abstract— Diffraction by a wedge is a well-covered topic, but the results available in the scientific literature are mainly relative to impenetrable structures. This is due to the difficulty of the diffraction problem in the case of penetrable materials, where a complex coupling between the external and the internal problems arises, and the field inside the scatterer needs to be evaluated. In particular, it appears that no exact solutions have been found to date for the diffraction by dielectric wedges of arbitrary angle and dielectric constant. The existing approaches can be characterized by either trying to provide analytical or heuristic approximate solutions to the original problem under certain assumptions, or trying to solve the problem in an exact sense using combined analytical-numerical methods. Some contributions are given in [1–4].

The aim of this work is to provide a Uniform Asymptotic Physical Optics (UAPO) solution (see [5]) for the field diffracted by a lossless and right-angled dielectric wedge in the case of plane waves having normal incidence with respect to the edge. To this end, the original problem is subdivided into two parts relevant to the internal region of the wedge and the surrounding space. For what concerns the evaluation of the interior diffracted field, equivalent electric and magnetic surface currents are used as sources in the radiation integral. Such currents lie on the internal faces of the wedge and are expressed in terms of the field transmitted inside the wedge material. A useful approximation and a uniform asymptotic evaluation of the resulting radiation integral allow one to obtain the diffraction coefficients in terms of the reflection and transmission Fresnel's coefficients and the standard transition function of the Uniform Theory of Diffraction [6]. The exterior problem is tackled and solved by using equivalent surface currents on the external faces of the wedge. Their expressions change depending on the incidence direction. As a matter of fact, they involve the reflection and transmission Fresnel's coefficients when one external face is directly illuminated, and only the reflection Fresnel's coefficients if both the external faces are considered. Once the currents are determined, the exterior diffracted field is evaluated by using a method like that employed for the interior problem.

The here proposed UAPO solution for the diffracted field perfectly compensates the Geometrical Optics discontinuities in the interior and exterior regions. Furthermore, it is simple to handle and implement, and its accuracy is well assessed by comparisons with Finite-Difference Time-Domain results.

REFERENCES

1. Berntsen, S., "Diffraction of an electric polarized wave by a dielectric wedge," *SIAM J. Appl. Math.*, Vol. 43, 186–211, 1983.
2. Joo, C. S., J. W. Ra, and S. Y. Shin, "Scattering by a right angle dielectric wedge," *IEEE Trans. Antennas Propag.*, Vol. 32, 61–69, 1984.
3. Burge, R. E., et al., "Microwave scattering from dielectric wedges with planar surfaces: A diffraction coefficient based on a physical optics version of GTD," *IEEE Trans. Antennas Propag.*, Vol. 47, 1515–1527, 1999.
4. Rouviere, J. F., N. Douchin, and P. F. Combes, "Diffraction by lossy dielectric wedges using both heuristic UTD formulations and FDTD," *IEEE Trans. Antennas Propag.*, Vol. 47, 1702–1708, 1999.
5. Gennarelli, C., G. Pelosi, C. Pochini, and G. Riccio, "Uniform asymptotic PO diffraction coefficients for an anisotropic impedance half-plane," *Journal of Electromagnetic Waves and Applications*, Vol. 13, No. 7, 963–980, 1999.
6. Kouyoumjian, R. G. and P. H. Pathak, "A uniform geometrical theory of diffraction for an edge in a perfectly conducting surface," *Proc. of IEEE*, Vol. 62, 1448–1461, 1974.

Diffraction by a Double-negative Metamaterial Layer with PEC Backing

G. Gennarelli and G. Riccio
D.I.I.I.E., University of Salerno, Via Ponte Don Melillo, 84084 Fisciano (Salerno), Italy

Abstract— Double-Negative (DNG) metamaterials (MTMs) have negative permittivity and permeability simultaneously (or negative refractive index), so that waves propagate with antiparallel phase and group velocities unlike conventional Double-Positive (DPS) materials. They can be manufactured by embedding small inclusions in host media (volumetric DNG MTMs) or by connecting inhomogeneities to host surfaces (planar DNG MTMs) for obtaining electromagnetic properties not generally found in nature, and this justifies the interest on them [1–3].

This work deals with the diffraction problem originated by a plane wave normally impinging on the edge of a lossy, isotropic and homogeneous DNG MTM layer with a perfect electric conductor (PEC) backing. Its solution represents the key to very important applications involving DNG MTMs based structures and devices, such as modern antenna systems to be mounted on civil or military vehicles. Moreover, the MTMs coating of their otherwise metallic surfaces may be used for controlling their radar cross section.

A Uniform Asymptotic Physical Optics (UAPO) solution has been recently developed by the authors for determining the field diffracted by the edge of a lossless, isotropic and homogeneous DNG MTM layer [4]. It gives accurate results, and it is easy to handle and apply, so that it can be convenient to work in this context for solving the here tackled problem.

The starting point is that of considering the radiation integral with a PO approximation of the electric and magnetic surface currents assumed as sources of the scattered electric field. Such currents lie on the half-plane representing the structure and are expressed in terms of the incident field and the reflection coefficient, which is here evaluated by considering the equivalent transmission line circuit. A useful approximation and a uniform asymptotic evaluation of the resulting radiation integral allow one to derive the closed form UAPO solution for the field diffracted by the edge. Such a solution is given in terms of the Fresnel's reflection coefficient of the DNG MTM layer with PEC backing and the standard transition function of the Uniform Theory of Diffraction [5]. As demonstrated by numerical simulations, it fulfils expectations since it perfectly compensates the Geometrical Optics field discontinuities at the reflection and incident field shadow boundaries. Moreover, its accuracy is demonstrated by the good agreement obtained in comparisons with the RF module of Comsol Multiphysics, a commercial tool based on the Finite Element Method.

REFERENCES

1. Engheta, N. and R. W. Ziolkowski, "A positive future for double-negative metamaterials," *IEEE Trans. Microwave Theory Tech.*, Vol. 53, 1535–1556, 2005.
2. Engheta, N. and R. W. Ziolkowski, *Metamaterials: Physics and Engineering Explorations*, Wiley-Interscience, 2006.
3. Caloz, C. and T. Itoh, *Electromagnetic Metamaterials: Transmission Line Theory and Microwave Applications,* Wiley-Interscience, 2006.
4. Gennarelli, G. and G. Riccio, "A UAPO-based solution for the scattering by a lossless double-negative metamaterial slab," *Progress In Electromagnetics Research M*, Vol. 8, 207–220, 2009.
5. Kouyoumjian, R. G. and P. H. Pathak, "A uniform geometrical theory of diffraction for an edge in a perfectly conducting surface," *Proc. IEEE*, Vol. 62, 1448–1461, 1974.

Interaction of Metal Nanoparticles with Multilayered Substrates

Silvia M. del Río, P. Albella, F. González, J. M. Saiz, and F. Moreno
Facultad de Ciencias, Departamento de Física Aplicada, Universidad de Cantabira
Avda de los Castros SN, Santander 39005, Spain

Abstract— Optical phenomena on a scale smaller than the wavelength of light, are gaining importance in different fields, and more specifically in Nanotechnology [1]. During the last two decades, research involving metal nanoparticles (NPs) interacting with substrates has grown very fast in part because the need of different technological industries to inspect, monitor and characterize materials, looking for particulate contaminants, roughness, and other defects in the subwavelength limit. The work we present is part of a recent research where the main objective was to go deeper in the study of metal NPs interacting with substrates [2]. So far we have studied the influence that the presence of an inhomogeneous substrate has on the plasmon resonances excited on the metal NP [3]. In this contribution we extend the study to systems where the metal NP interacts with multilayered substrates. We will see that the use of this kind of substrates may be a good solution for tuning the optical response of the system.

When a NP is located on/or close to a substrate, the Localized Surface Plasmon Resonance (LSPR) excited on the NP not only depends on the geometrical properties of the system (mainly the distance to the substrate) but also on the dielectric properties of the substrate. Fig. 1 Shows as an advance how the presence of a multilayer substrate shifts the dipolar plasmon resonance either to the blue or to the red depending on the refractive index and/or the layers thickness.

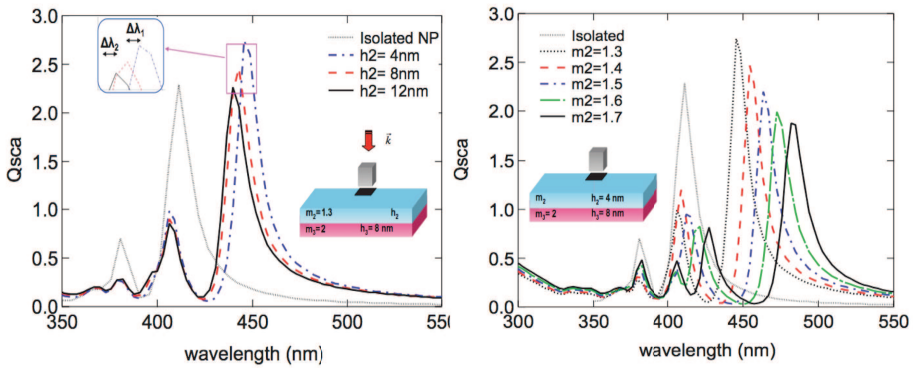

Figure 1: Scattering Efficiency of a 40 nm silver NP located at 2 nm of a 2-layer substrate for different layer thickness (left) and different layer optical properties (right).

ACKNOWLEDGMENT

This research has been supported by the Ministry of Education of Spain under project #FIS2007-60158 and USAITC-A through R&D 1275-PH-01. The authors thankfully acknowledge the computer resources provided by the RES node at University of Cantabria.

REFERENCES

1. Ozbay, E., "Plasmonics: Merging photonics and electronics at nanoscale dimensions," *Science*, Vol. 311, No. 5758, 189–193, 2006.
2. Moreno, F., F. González, and J. M. Saiz, "Plasmon spectroscopy of metallic nanoparticles above flat dielectric substrates," *Opt. Letters*, Vol. 31, No. 12, 1902, 2006.
3. Albella, P., F. Moreno, J. M. Saiz, and F. González, "Surface inspection by monitoring spectral shifts of localized plasmon resonances," *Opt. Express*, Vol. 16, No. 17, 12872–12879, 2008.

A Novel Four-port De-embedding Method and the Parametric Extraction of MOSFETs

C. I. Lee, **W. C. Lin**, **C. C. Chen**, **Y. T. Lin**, **and Y. T. Lee**
Department of Electrical Engineering, National Sun Yat-Sen University, Taiwan, R.O.C.

Abstract— A new four-port de-embedding procedure based on the transmission-line theory for on wafer S-parameter measurement is demonstrated in this paper for the first time. Although the traditional open and short test structures can characterize the resistive and inductive properties of the parasitic effects of the metal interconnect lines, the conductive and capacitive characteristics are hardly eliminated only with lumped equivalent circuit models in high substrate loss CMOS process. In this paper, we employed the transmission-line based technique to accurately remove not only the resistive and inductive parasitic effects but also the conductive and capacitive ones in the four-port measurement. We only used one simple open and one through test structures to remove the unwanted parasitic effects from pads and interconnects. In addition, the poly ground-shielded technology was adopted underneath the pads to reduce the parallel parasitic capacitance of shielded-based test structures without influencing the isolation between the signal ports in this work. First, extracting the propagation constants and characteristic impedances of the interconnect lines was carried out by the simple open and through test structures. Next, the four-port MOSFET characteristics can be determined directly after removing the pad parasitic effects and the interconnect line ones calculated from the extracted transmission line parameters. This de-embedding methodology for extracting the four-port MOSFET parameters including the substrate network can be realized up to 10 GHz operating frequency in this work. In addition, in comparison with the traditional four-port open-short de-embedding procedure, the greatest advantage of our proposed method is the significant chip area reduction, and we expect to construct equivalent circuit models for different dimensions and bias through our proposed de-embedding method for future rf circuit designers.

The RF I-V Curve for PHEMT through the Small Signal S-parameter Extraction Method

C. I. Lee, W. C. Lin, Y. T. Lee, and Y. T. Lin
Microwave Circuit and Device Lab, Department of Electrical Engineering, National Sun Yat-Sen University
Kaohsiung, Taiwan, R.O.C.

Abstract— In this paper, the rf (radio frequency) I-V (current-voltage) curve and its equivalent circuit for a 0.15 μm gate length GaAs pHEMT with four fingers up to 26.5 GHz is presented for the first time. For the application to high-frequency integrated circuit design, it is necessary to pay more attention to the high-frequency characteristics of the transistors. However, the traditional dc I-V curve obtained by dc measurement was unable to provide sufficient information. In this paper, the rf I-V curve was determined by high-frequency measurement and each component of the equivalent circuit was extracted directly using the measured S-parameters. Through the above measurement and mathematical calculation, the rf I-V curve has been established by integrating the extracted component gm and gds. It can be observed that the knee voltage of the transistor depends on the operation frequency, when the transistors operate in saturated regions. Due to the slow deep level traps and surface state effect, the rf I-V curve shows a higher transconductance. Furthermore, under high drain-source bias conditions, the hot carrier effect observed in the rf I-V curve is weak. The above phenomena explain the significant difference between the rf and dc I-V curve, and the rf I-V curve does reveal the high frequency characteristic of the transistor. For the front-end circuit of wireless communication systems, the selection of the bias point has a key influence on the performance of the power amplifier, and its operation mode also depends on the bias voltage. The information from the rf I-V will provide circuit designers a more accurate way to select the most appropriate bias point for the high-frequency operation and bias the transistor in the correct operation region.

A Novel H-shaped Slot-coupled Antenna for the Integration of Power Amplifier

C. I. Lee, W. C. Lin, Y. T. Lin, and Y. T. Lee
Microwave Circuit and Device Lab, Department of Electrical Engineering
National Sun Yat-Sen University, Kaohsiung, Taiwan, R.O.C.

Abstract— This paper presents a novel H-shape structure with the meander shaped feed slot to integrate the power amplifier. This compact structure is appropriate to apply in wireless communication system. The novel H-shaped antenna has many excellent advantages over the conventional rectangular microstrip antenna such as the harmonic mode suppression, bandwidth enhancement, and the increase of the whole transmitter efficiency. The proposed H-shaped antenna adopts slot-coupled microstrip patch structure to achieve the harmonic termination and good wideband matching. The return loss reveals that almost pure reactive impedance is achieved while operating at the second and third harmonic frequency. Due to the reduction of the surplus harmonic content from the nonlinear circuits, the improvement of the whole performance of the transmitter is achieved. To enhance the efficiency and bandwidth, the topology is electromagnetically coupled to H-shaped antenna spaced by a layer of foam from the ground plane etching in meander aperture. In addition, the T shape feed line, which mounted on another side, is designed to improve the matching. The novel structure, which is modified from conventional rectangular ground plane with the long slot across another side feed conductor, is used in this work. This proposed structure not only realizes the wide stop band property in the high order harmonic region, but also maintains the high antenna gain. The whole characteristic demonstrates that the cross-plane level below E-plane and H-plane at least 20 dB and the 3 dB bandwidth at 2.45 GHz center frequency is 20%. Furthermore, the patch antenna is modified to perform light weight and low profile for compact circuit design. The advantage of our proposed novel structure is effective to decrease the additional area for harmonic tuning network and suitable to match maximum output power. The output circuit of power stage is designed to match the antenna under large signal operation. The microstrip antenna is studied by the simulation and experiment to operate at 2.45 GHz for WLAN. This whole compact structure achieves good performance and is suitable for the WLAN standard application.

Session 2A1
EM Modeling and Inversion for Well Logging Applications

Review of 3D EM Modeling and Interpretation Methods for Triaxial Induction and Propagation Resistivity Well Logging Tools

S. Davydycheva[1] and M. A. Frenkel[2]

[1]3DEM Consulting, Texas, USA
[2]EMGS Americas, Texas, USA

Abstract— The 3D EM modeling and inversion techniques for the geological formation evaluation have been experiencing significant progress since the early 90s. There are three main 3D EM numerical techniques: finite-difference (FD), finite element (FE), and integral equation (IE). They have been used for simulating arbitrary 3D media as well as for development of 3D inversion-based interpretation of well log data acquired by the conventional and new generation of logging tools. We present a brief review of these three techniques as to their ability to simulate and interpret the new-generation of triaxial tensor wireline and LWD measurements.

The wireline and LWD electromagnetic tools of the new generation provide full triaxial tensor measurement, in addition to the conventional axial measurement, when the formation is excited by an axial z-directed magnetic dipole transmitter, and the response of axial receivers is analyzed. Due to full 3D sensitivities, the new tools allow significantly enhanced formation resistivity interpretation. Considering the FD modeling method, we demonstrate the error cancellation property of so-called Lebedev staggered grid on dipping medium interfaces. We show that it enables obtaining reliable results on relatively coarse grids, when the standard Yee grid provides a solution whose cross-measurements are distorted at dipping boundaries by strong oscillating errors.

We present 3D anisotropic synthetic logs for four different new-generation tools: two triaxial induction and two directional resistivity LWD tools. We also consider new features and differences in the new tool responses and discuss various post-acquisition processing techniques. These approaches allow to better visualize tool responses by separation of the anisotropy, dipping, and eccentricity effects and enable efficient application of fast stable inversion schemes for resistivity interpretation.

2.5D Finite-difference Modeling of Directional EM Propagation Tools in High-angle and Horizontal Wells

Yong-Hua Chen, **Dzevat Omeragic**, **Vladimir Druskin**, **Leonid Knizhnerman**, **Valery Polyakov**, **Tarek Habashy**, **and Aria Abubakar**
Schlumberger-Doll Research, USA

Abstract— We developed 2.5D finite-difference (FD) code for modeling EM tool response when the conductivity distribution can be defined in a plane and well trajectory is 3D. The tool could be at any azimuth with respect to the plane defining arbitrary 2D structure, with non-parallel layers, faults, general 2D bodies, contacts, and unconformities. The code is primarily used for well placement and 3D formation evaluation applications to analyze responses of new generation of deep directional EM tools in high angle and horizontal wells.

Frequency-domain Maxwell equations are solved using electric field formulation. The problem is discretized using a staggered optimal FD grid in the x-z plane, and a spatial Fourier transform in the y-direction, using Zoltarov discretization. Grid sizes are automatically calculated according to the shortest skin depth in the formation at each operating frequency. This allows us to control the simulation accuracy and thus the speed by specifying the number of grid points per skin depth. Material averaging is applied in conjunction with optimal grids, resulting in small problem size, allowing use of a direct solver. The code is parallelized to run on GPU. We review the algorithm performance on serial processors and on GPU for models of different complexities.

The forward modeling code is validated by comparing its results with those produced by a real axis integration method for various 1D layered media. Consistency tests are performed for different tool orientations and formation dip. We use the modeling code to analyze directional tool responses in 2D wedge structure, for different tool azimuth. We analyze in details dependence of equivalent boundary orientation and its dependence on tool azimuth for various tool positions. We also analyze the response to unconformity, when the internal layering closes variable angle with respect to main boundary. In addition to response dependence we also show how the results of 1D inversion, typically used for real-time interpretation, are affected in such 2D formations.

3D IE Modeling with a Linear Dependence on Model Size

Dmitry Avdeev and Sergei Knizhnik
Halliburton Energy Services, Exton Technology Center, 710 Stockton drive, Exton, PA 19341, USA

Abstract— We have improved the integral-equation method for modeling 3D electromagnetic fields by using the separability of its inherent 3×3 dyadic Green's tensors. Conventional integral-equation approaches exhibit a quadratic dependence on model size, for at least the vertical dimension, N_z. This dependence creates an obvious bottleneck and limits its applicability to some large-scale problems. This is particularly apparent for induction logging problems, where large values of N_z are commonly used for an adequate representation of formation and borehole, and for the eddy currents which are generated by multicoil, multicomponent sondes.

We propose a further development in the integral equation method that exhibits linear dependence on the horizontal dimensions N_x and N_y, as well as on the vertical dimension N_z. This approach yields a much better solution, in terms of computational loads, since it requires only a partial set of the Green's tensors to be calculated and stored. This is important in practice, because shrinking the Green's matrix widens the range of models that can be investigated by the integral equation method. Some models that were previously too large to be stored in RAM can now be processed there, providing much faster execution. Other models that were too large to fit on a hard drive can now be accommodated.

Although we use an example of induction logging to demonstrate how our method works, the method is applicable to other EM applications, including airborne and ground electromagnetics, and magnetotellurics.

Nitsche-type Mortaring for Maxwell's Equations

K. Hollaus[1], **D. Feldengut**[1], **J. Schöberl**[2], **M. Wabro**[3], **and D. Omeragic**[4]

[1]RWTH Aachen University, Germany
[2]Vienna University of Technology, Austria
[3]CST AG, Germany
[4]Schlumberger-Doll Research, USA

Abstract— We propose a new method for treating transmission conditions on non-matching meshes. The basic method is a hybrid version of Nitsche's method. By introducing a scalar potential on the interface we obtain a robust method for the low frequency limit. In order to simplify numerical integration, we use smooth B-spline basis functions on the interface. We present the formulation for scalar potential problems and for time-harmonic Maxwell's equations. A simple well logging example is used to benchmark the algorithm.

Correction for the Borehole Effect of Multi-component Array Induction Log Data

Junsheng Hou and Michael Bittar
Halliburton Energy Services, Inc.
3000 N Sam Houston Parkway E, Houston, TX 77302, USA

Abstract— Multicomponent array induction (MCAI) logging has been used in the oil/gas exploration and development for a few years. In addition to conventional induction logs, MCAI tools also provide the information on formation resistivity anisotropy, relative dip angle, and azimuthal angle for a wide range of borehole-formation environments. This additional information is very important for improving analysis of low-resistivity payzones, laminated/thin-bed reservoirs, and geological structure. However, the presence of a borehole significantly affects MCAI measurements in both water-based mud (WBM) and oil-based mud (OBM) borehole environments. Borehole effects on MCAI log data are greater than those in the conventional array induction logging. The raw MCAI log data must be corrected for these effects before they can be used for determining all the formation properties above. So far the borehole-effect correction (BHC) is still a big challenge for the MCAI log data processing and interpretation.

A forward model was built to develop BHC schemes for the MCAI measurements. This model consists of a circular borehole surrounded by a homogenous formation. The borehole may be vertical or deviated, and the logging tool can be centered or eccentered in the borehole. Formation resistivity can be isotropic or transversely isotropic (TI anisotropic). It is obvious that the numerical simulation of the MCAI response is a three-dimensional (3D) electromagnetic (EM) forward issue based on this BHC forward model. Extensive simulations of the MCAI response have been performed using this model. These simulations show that for a given subarray and operating frequency the borehole effect depends on eight model parameters: formation horizontal and vertical resistivities borehole diameter mud resistivity tool eccentric distance (or standoff), tool eccentricity azimuthal angle borehole relative dip and azimuthal angles.

We have developed a new real-time BHC system specifically for the MCAI log data processing. This new BHC system consists of the following basic steps: input of raw data and preprocessing, estimation of the tool eccentricity azimuthal angle, inversion of the unknown BHC forward model parameters, correction of the borehole effects, and output of the BHC-corrected results for other applications such as one-dimensional (1D) inversion. The inversion of the unknown model parameters is the key for the whole system. Due to the complication of the 3D BHC inversion, the new inversion algorithm is implemented by splitting the inversion problem of one high-dimension unknown vector into a few lower-dimension ones based on their sensitivity to different components of the measured conductivity tensor for different subarrays. This dimensionality reduction makes the BHC inversion overall easier, more reliable and robust. Because the 3D MCAI simulation is time-consuming, the forward modeling used in the inversion is based on the pre-calculated look-up tables. The inversion is fast and the BHC processing is applicable in real time or well site. To validate the new BHC scheme, some synthetic MCAI data are processed by using this new scheme. The obtained BHC-corrected results demonstrate its reliability and effectiveness.

Determination of Dip and Anisotropy from Multi-frequency Tri-axial Induction Measurements

Teruhiko Hagiwara
Aramco Service Company, Houston, Texas, USA

Abstract— The tri-axial (or multi-component) induction log is used to as an oil-base mud dip-meter. It has been noted that tri-axial induction measurements in an anisotropic formation can determine not only the anisotropy but also the relative dip of the tool with respect to the formation. The anisotropic resistivity and the relative dip of layered formations are also inverted from the tri-axial induction measurements at a depth in a homogeneous anisotropic formation or from multiple depths by assuming a layered earth model.

When the tri-axial induction log is run at multiple frequencies, multi-frequency focusing can be applied to the measurements. Then, the true dip can be algebraically calculated from the frequency-focused tri-axial induction data at a depth in an anisotropic formation. The apparent dip algebraically derived at a depth may be applied to layered formations. The apparent dip has been shown to estimate the true dip in many examples. However, it cannot give the accurate dip when the formation is not thinly bedded. It is important to assess how accurate the apparent dip is to the true dip.

I can show that the true anisotropy is algebraically calculated from the frequency-focused tri-axial induction data at a depth in an anisotropic formation. Similarly to the apparent dip, the apparent anisotropy algebraically derived at a depth may be applied also to layered formations. The apparent anisotropic resistivity (horizontal and vertical) can be similarly determined algebraically from the frequency-focused tri-axial data. Unlike the apparent dip that estimates the true dip in thinly bedded formations, the apparent anisotropy gives accurate anisotropy in thick formations.

By modeling the tri-axial induction responses in 3-layer dipping anisotropic formations at multiple frequencies, I found that the apparent dip gives a smaller dip than the true dip when the anisotropy is small (the anisotropy effect) in thick formations, while the apparent anisotropy is affected by the shoulder bed anisotropy when the formation is not thick (the shoulder bed effect).

The results from this study will be useful to accurately determine the formation dip and the formation anisotropy from the multi-frequency tri-axial induction log.

Application of the 2.5D Multiplicative-regularized Gauss-Newton Inversion for Single-well Triaxial Induction Data

Aria Abubakar, Tarek M. Habashy, Maokun Li, Jianguo Liu, and Guangdong Pan
Schlumberger-Doll Research, Cambridge, USA

Abstract— We present an application of the so-called multiplicative-regularized Gauss-Newton inversion method to the interpretation of the triaxial single-well induction measurements. The forward simulator is based on a finite-difference approach in which a multi-frontal LU decomposition algorithm simulates multi-source experiments at nearly the cost of simulating one single-source experiment for each frequency of operation. The inversion algorithm employs a regularized Gauss-Newton minimization approach with a multiplicative cost function. By using this multiplicative cost function, one does not need a priori information on how to determine the so-called regularization parameter in the optimization process, rendering the algorithm fully automated. The algorithm is equipped with two regularization cost functions that allow us to reconstruct either a smooth or a sharp conductivity image. The derivative (the Jacobian matrix) is calculated efficiently using the adjoint approach. To increase the robustness of the algorithm, we also constrain the minimization and use a line-search approach to guarantee the reduction of the cost function after each iteration. In this method there are two intensive computational parts: (1) the forward simulation; and (2) the solution of the linear system of equations associated with the inverse problem. These computationally expensive parts of the algorithm are parallelized efficiently using the MPI library. To demonstrate the pros and cons of the algorithm, we present synthetic data inversion results for both isotropic and TI-anisotropic media. We will also show that by employing the triaxial induction data we are able to robustly retrieve the conductivity spatial variation around the well-bore.

Inversion of Triaxial EM Measurements in Horizontal Wells

Hanming Wang
Chevron Energy Technology Company, 1500 Louisiana Street, Houston, TX 7002, USA

Abstract— The fully-triaxial electromagnetic measurement provides a complete tensor measurement offering three-dimensional sensitivity which can be used for detecting resistivity anisotropy, structure dip and bed boundary position in vertical wells as well as in deviated wells when the logging tool penetrates through the formation. The sensitivity of the full tensor measurement in homogeneous medium and layered medium with vertical/deviated wells has been studied and documented. The inversion algorithm has been developed and widely used in practical applications.

In the paper, we will explore the applications of the triaxial measurement in horizontal wells to facilitate formation evaluation and reservoir navigation. The sensitivity of the tensor measurement with respect to formation parameters is studied in several common scenarios such as cap shale approaching from above, oil-water contact approaching from below, thin reservoir sandwiched by two conductive shale beds. With the help of sensitivity function, the information content and the relative importance of individual component are summarized. The depth of investigation of directional measurements, z-related cross-couplings, will be presented.

Due to the complexity of the tool response, it is difficult to extract the physical parameters by visualizing the tensor measurement. The mathematical processing (inversion) is a common and popular way to accomplish the task. In the paper, we will present an efficient inversion algorithm to solve for resistivity anisotropy, formation dip and the distance to boundary simultaneously. A practical way to set constraints and initial guesses is implemented to further improve the efficiency. In addition, guided by the sensitivity function, the confidence level of inverted parameters, a piece of vital information for better geosteering decision, is proposed. The algorithm is validated by the synthetic data and field data.

Measuring the Soil Water Content of a Sandy Soil with a Frequency Cross-hole Radar: Antenna Design and Experiments

F. Rejiba[1], **F. Sagnard**[2], **C. Schamper**[1], **M. Froumentin**[3], **and Guérin**[1]

[1]Université Pierre et Marie Curie, Paris 6, UMR Sisyphe, Boite 105
4 place Jussieu, 75252 Paris cedex 05, France
[2]LRPC Rouen, ERA 23, 10 chemin de la Poudriére, 76120 Le Grand Quevilly, France
[3]CER Rouen, ERA 23, 10 chemin de la Poudrire, 76120 Le Grand Quevilly, France

Abstract— Road surface quality is very sensitive to mechanical properties of the underground structure, and particularly to its water content. Electromagnetic frequency cross-hole radar associated with a Zero Offset Profiling (ZOP) acquisition mode has been used as a non destructive technique to evaluate the vertical distribution of the water content inside a multi-layered clay sand embankment test site. In order to fit two borehole diameters (40 and 67 mm), that are used for civil engineering monitoring, two specific radar transmission links (with a distance less than 1 m) have been developed to work in the frequency band [0.5; 1.5] GHz. These borehole transmission links have led to the design of two types of ultra-wideband symmetric antennas: a 3D "folded dipole" made of thin wire elements, and a planar "blade dipole". Numerical electromagnetic modeling associated with both antenna geometries, and their integration in a transmission link have been performed using two complementary FDTD softwares: A commercial software EMPIRE® based on an adaptative grid, and a laboratory-made software which relies on parallel calculation and can consider a soil made of a random dielectric distribution. The comparison of measurement and simulation results with both folded and blade dipoles, has allowed to highlight contrasts of real permittivities induced by water content and soil compaction level.

Session 2A2
Microspheres and Waves

Electromagnetic Scattering by Charged Water Aerosols

A. Heifetz, **N. Gopalsami**, **H. T. Chien**, **E. R. Koehl**, **and A. C. Raptis**
Nuclear Engineering Division, Argonne National Laboratory, USA

Abstract— We present a phenomenological model of electromagnetic (1 GHz to 1000 GHz microwave to submillimeter wave band) scattering and absorption of charged water aerosols with radii from 5 nm to 500 nm. The approach is based on classical electrodynamics model of scattering from a dielectric sphere with diffusion-deposited mobile surface charge. In this model, scattering and absorption cross-sections are calculated for a charged Rayleigh particle with effective dielectric constant. The effective dielectric constant consists of the volume dielectric function of the neutral sphere and surface dielectric function due to the oscillation of the surface charge in the applied electric field. We use the double Debye model of frequency and temperature dependent permittivity of bulk water as a model of the neutral water sphere. The surface dielectric function is obtained from the damped harmonic motion model of an electron. The key parameters for the surface dielectric function are the number of charges on the sphere and the damping constant. We use the model that predicts that the number of charges on water aerosol is proportional to the radius of the aerosol. To calculate the temperature dependent damping constant, we use the model of linear viscous drag on a particle in water. Our computer simulations indicate that scattering efficiency is more sensitive to charging at higher frequencies for aerosols of smaller sizes, while absorption efficiency is more sensitive for larger-size aerosols at lower frequencies. The model needs to be extended to that of a charged mist with size distribution, where multiple scattering effects need to be accounted for. Possible application of this work is to indirect remote sensing of radioactive gases via their charging action on atmospheric mist.

ACKNOWLEDGMENT

Work supported by U.S. Department of Energy, under Contract DE-AC02-06CH11357.

A Mie Approach to Non-spherical Particles

B. Hourahine and F. Papoff
SUPA, Department of Physics, University of Strathclyde, Glasgow, UK

Abstract— Mie theory has proved over the years to be extremely fruitful and useful in understanding and predicting the optical properties of homogeneous spheres. The key ingredient behind the success of this theory is the existence of exact solutions to the Maxwell's equations — electric and magnetic multipoles — that form a complete and orthogonal basis on the surface of a sphere. For each external field, and for any homogeneous sphere, this means that internal and scattered fields can be expanded in a series with coefficients which can be found analytically by enforcing the boundary conditions. An important feature of Mie theory for spheres is that once a sufficient number of coefficients of the field expansions are determined, the fields can be propagated from the surface of the sphere to any point in space at a very low computational cost just by using the known analytical form of the electric and magnetic multipoles. In this paper and its companion we show how we have recently developed an approximate theory for non-spherical particles [1] that retains most of the nice features of the Mie theory described above, while also allowing us to study systematically the dependence of near and far field optical properties on particle shape and input field. At the core of our theory are expansions of internal and scattered fields in terms of exact multipolar solutions of Maxwell's equations, also called sources. For non-spherical particles, however, the multipolar sources are not all centered on the same points, but are distributed inside the particles according to its symmetry. Finite expansion of internal and scattered fields in terms of these sources can be used to approximate the boundary condition with a precision in principle arbitrary. In particular, by enforcing the boundary condition on an set of points on the surface, we can derive a linear system of equations that depends only of the geometry and the material of the particle and not on the external field. This system of equation can easily be solved for any given external field, allowing us to determine the internal and scattered fields with a precision that improves with the distance from the surface. As in Mie theory, the knowledge of the multipolar sources allows us to propagate the fields away from the particles surface at a very low computational cost. We extend the results of Ref. [1] for convex particles to concave metallic particles which can act as micro-mirrors.

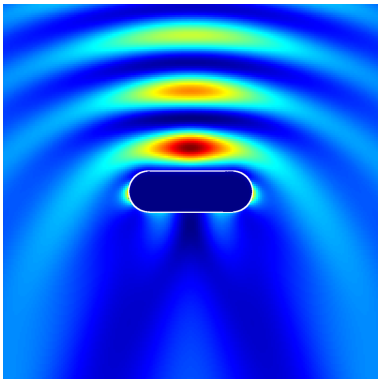

Figure 1: Optical near field around a disk-shaped gold particle of a few wavelengths diameter before the introduction of a parabolic mirror structure.

REFERENCES

1. Holms, K., B. Hourahine, and F. Papoff, "Calculation of internal and scattered fields of axisymmetric nanoparticles at any point in space," *J. Opt. A: Pure Appl. Opt.*, Vol. 11, 054009, 2009.

Hot Spots and Photonic Jets: From Spheres to Disks and Rods

B. Hourahine and F. Papoff
SUPA, Department of Physics, University of Strathclyde, Glasgow, UK

Abstract— Many experiments and most theoretical investigations of particles of similar size to the wavelength of incident radiation are performed using spheres, for which Mie theory provides solid foundations. Some of the most interesting properties discovered are that dielectric spheres have the highest quality factor identified to date and can focus light into sub-wavelength photonic jets. However, these interesting effects are not limited only to spheres: the optical response of nano- and micro-particles depend not only on the constituent material and particle size, but also on their shape. Experimentally a great variety of particle shapes have been used in a wide range of applied and fundamental research, including investigations of various types of surface enhanced nonlinear spectroscopies and single photon light-matter interaction.

In order to systematically study the dependence of near and far field optical properties on particle shape and input field, we need a theory that mirrors many of the important aspects of Mie theory, but can extend to non-spherical particles. We have recently derived an approximate theory in which combinations of electric and magnetic multipolar terms centered at different locations inside of particles play the role of the multipolar terms of Mie theory [1]. These combinations, or "singular vectors" in the language of linear algebra, are found by imposing boundary conditions which enforce solutions of Maxwell's equations. We have used this method to calculate scattered and internal fields at any point in space with a very modest numerical effort. Here we expand this theory to analyze how the extinction cross sections and internal and scattered fields change as we deform continuously a sphere into a rods and disks. This type of analysis requires minimization of the error with which the boundary conditions are fulfilled in order to improve the precision on the field. Furthermore, as this error depends on the incident field, we need to estimate *a priori* the error at any point in space and for any incident field. By using the structure of the singular modes we can fulfill these requirements and are able to study the position of points of surface field enhancement and the extinction cross sections for dielectric and metallic rods and disks, considering incident fields propagating at angles with respect to the symmetry axis of between 0° and 90° degrees.

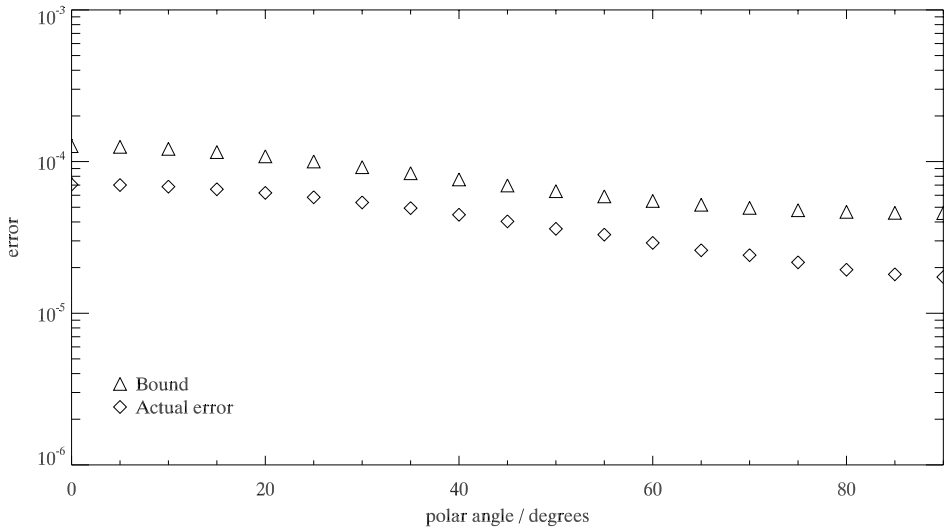

Figure 1: Calculated and *a priori* error estimates of the *maximal* fractional error in scattered light calculated for an elongated gold particle with a diameter of 0.8λ and length 2λ, as a function of angle of illumination.

REFERENCES

1. Holms, K., B. Hourahine, and F. Papoff, "Calculation of internal and scattered fields of axisymmetric nanoparticles at any point in space," *J. Opt. A: Pure Appl. Opt.*, Vol. 11, 054009, 2009.

Focusing Microprobes Based on Integrated Chains of Microspheres

Vasily N. Astratov, **Arash Darafsheh**, **Matthew D. Kerr**, **Kenneth W. Allen**, **and Nathaniel M. Fried**
Department of Physics and Optical Science, Center for Optoelectronics and Optical Communication
University of North Carolina at Charlotte, Charlotte, North Carolina 28223-0001, USA

Abstract— Focusing optical microprobes are used in a broad range of biomedical and photonics applications, including laser tissue surgery, optical endoscopy and spectroscopy, high-density optical data storage, and photo-induced patterning of thin films. It is well known that the spatial resolution of conventional lens-based devices is limited by the diffraction of light from the lens aperture. In recent years, it has been demonstrated [1] that a small, wavelength-scale microsphere with an index of around 1.6 can produce a narrow focused beam, termed "nanoscale photonic jet". The nanojet propagates with little divergence for several wavelengths into the surrounding medium while maintaining a subwavelength traverse beamwidth. More recently, our group studied [1, 2] the periodic focusing of light in chains of polystyrene microspheres assembled on substrates. In these chains, the focused beams are quasi-periodically reproduced along the chain with progressively smaller sizes, reaching wavelength-scale dimensions even for noncollimated input beams.

In this work, the chains of microspheres with different indices of refraction were assembled inside flexible microcapillaries and hollow waveguides to create a compact focusing tool for biomedical applications. The optical attenuation and focusing properties of such structures are studied using imaging techniques. The results are found to be in agreement with the ray tracing performed by ZEMAX-EE software. The results allow developing surgical laser scalpels capable of operation in tissue-contact conditions with the wavelength-scale resolution.

The advantages provided by the chains of microspheres over single lenses in light focusing applications are illustrated by numerical ray tracing in Figs. 1(a) and 1(b) for high (1.9) and medium (1.59) index spheres, respectively. It is seen that the paraxial incident beams have minimal propagation losses in such structures which results in the filtering of modes with the best focusing properties. This allows the use of multimodal sources of light with imperfect input beam properties in such applications.

On a fabrication side, a variety of microspheres obtained from different manufacturers with refractive indices from 1.47 to 1.9 were used to infiltrate plastic and glass microcapillaries as well as hollow waveguide structures. A gel-like medium was used to mimic the optical properties of a biological tissue. Such structures allow one to obtain focused beams with spot sizes of several wavelengths and with a depth of treatment of approximately 10–20 μm in tissue, as shown in Fig. 1(c). The light attenuation properties of the chains of microspheres inside capillary tubing were investigated by using local sources of light (dye-doped spheres) and imaging through the sidewall. The measured attenuation data was found to be in agreement with the results of modeling by ray tracing.

In conclusion, due to a simple integration with the fibers and hollow waveguides, sharp focusing of the beam, and the ability to operate in a tissue-contact mode, chains of microspheres can be used in a variety of biomedical and photonics applications as a compact focusing tool. The examples of such applications include ultra-precise intraocular and brain laser surgeries, photoporation of cells, and coupling of light in photonic nanostructures. The authors gratefully acknowledge

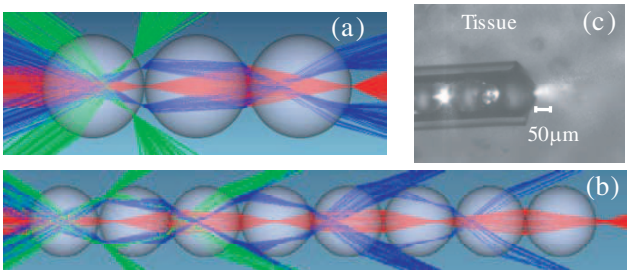

Figure 1: Ray tracing of paraxial (red) and skew (blue and green) beams for chains of spheres with (a) $n = 1.9$, and (b) $n = 1.59$. Focusing at $\lambda = 0.63\,\mu$m in tissue-contact conditions.

support from U.S. Army Research Office (ARO) under Contract No. W911NF-09- 1-0450 and from National Science Foundation (NSF) under grant ECCS-0824067.

REFERENCES

1. Chen, Z., A. Taflove, and V. Backman, "Photonic nanojet enhancement of backscattering of light by nanoparticles: A potential novel visible-light ultramicroscopy technique," *Opt. Express*, Vol. 12, 1214–1220, 2004.
2. Kapitonov, A. M. and V. N. Astratov, "Observation of nanojet-induced modes with small propagation losses in chains of coupled spherical cavities," *Opt. Lett.*, Vol. 32, 409–411, 2007.
3. Yang, S. and V. N. Astratov, "Photonic nanojet-induced modes in chains of size-disordered microspheres with an attenuation of only 0.08 dB per sphere," *Appl. Phys. Lett.*, Vol. 93, 261111, 2008.

Optical Detection of a Nanometer-thick Dielectric Layer via Cepstral Analysis of Photonic Backscattering

Jamesina J. Simpson
ECE Department, University of New Mexico, Albuquerque, NM 87131, USA

Abstract— A broad goal of the research reported here is a fundamental advance in inverse scattering. The present work tests the hypothesis that the backscattered spectrum resulting from visible-light illumination can be analyzed to characterize nanoscale-thin (i.e., ultra-subdiffraction thickness) localized dielectric inhomogeneities within a three-dimensional (3-D) structure. That is, can a 3-D inverse-scattering problem be effectively reduced to what amounts to be one dimensional (1-D)?

The motivation for the present work is a partial wave spectroscopy (PWS) technique pioneered by Prof. Backman of Northwestern University. He has provided experimental and clinical evidence that analyzing the spectrum of light backscattered from biological tissues that appear to be normal under conventional optical microscopy can reveal the presence of a nearby early-stage cancer. PWS is based upon the assumption that generation and detection of photons propagating in 1-D permit a reflected optical signal to be sensitive to length-scales of refractive index fluctuations much smaller than the classical diffraction limit. I interpret PWS as a technique that exploits the fact that in 1-D, the time-domain Green's function is simply a time-retarded Dirac delta function. Hence in 1-D, ultra-subwavelength-scale dielectric inhomogeneities locally generate high spatial frequency electromagnetic fields which propagate to the end of the universe without attenuation or spreading.

Recent literature shows a candidate for generating and detecting quasi 1-D electromagnetic waves is the photonic nanojet. I have found that the backscattered specrum is extremely sensitive to the presence of dielectric inhomogeneities within the nanojet. This is especially revealed by examining the DFT of the backscattered spectrum, which yields the backscattered cepstrum.

In my presentation, I will report computational results from 1-D and 3-D finite-difference time-domain (FDTD) simulations which indicate that the backscattered cepstra of a nm-thick dielectric layer embedded within a dielectric slab are nearly identical. The implication of this is that the nanojet yields a sufficiently 1-D electromagnetic excitation/backscattering geometry to allow detection of extraordinarily thin dielectric inhomogeneities.

What Can Be Learned from Light-microsphere Interaction for Tissue Imaging?

Zhengbin Xu, Jingjing Liu, and Young L. Kim
Weldon School of Biomedical Engineering, Purdue University, USA

Abstract— When dielectric microspheres have similar sizes compared with the wavelength of incident light (i.e., Mie scattering), a significant portion of the light is scattered in the same direction with respect to the incident direction. In other words, light scattered from relatively large size microspheres comparable to the wavelength is highly anisotropic. The overall directional tendency of the scattered light is represented by the anisotropy factor (also called the asymmetry parameter) and in Mie scattering the anisotropy factor is close to one. This further indicates that in the Mie scattering regime, directional gating can be used to select the forward scattering component. For example, let us consider a target embedded in a scattering medium consisting of polystyrene microspheres whose sizes are comparable to the wavelengths. In this configuration, the contrast and resolution of the target can be improved by simple back-directional gating. Interestingly, most biological tissue including major organs is highly anisotropic with the anisotropy factor $> 0.8 - 0.95$. Thus, in back-directional gating, the light scattered from biological tissue will slightly deviate from its original incident direction for moderate depths. This implies that in back-directional gating, the high anisotropic property of the surrounding medium can serve as a waveguide in a moderate depth. We experimentally demonstrate that back-directional gating in an imaging setup can improve the contrast and resolution of an embedded object in biological tissue. Our finding can be easily implemented into imaging platforms for tissue imaging.

Near-field Electromagnetic Effects in Thermal Radiative Transfer

Arvind Narayanaswamya[1], **Karthik Rao**[1], **Ning Gu**[2], **Sheng Shen**[3], **and Gang Chen**[3]

[1]Department of Mechanical Engineering, Columbia University, New York 10027, USA
[2]Department of Electrical Engineering, Columbia University, New York 10027, USA
[3]Department of Mechanical Engineering, Massachusetts Institute of Technology
Cambridge, MA 02139, USA

Abstract— Near-field radiative transfer is known to be significantly different from that of far-field radiative transfer based on Planck's theory of blackbody radiation. Theoretical predictions point to a significant enhancement of radiative transfer between closely spaced objects due to the tunneling of surface phonon polaritons. Despite extensive theoretical predictions of enhancement between parallel surfaces, experimental evidence of near-field radiative transfer in excess of Planck's limit has been elusive due to experimental difficulties. We have overcome these difficulties by investigating near-field effects on thermal radiative transfer between spherical surfaces.

In this talk, we will present results of our theoretical and experimental investigations into near-field radiative transfer between two microspheres or between a microsphere and a flat surface. We have developed a theoretical method based on the dyadic Green's function technique to model near-field thermal radiative transfer between two microspheres. The method relies on expanding the Green's function in a series of vector spherical waves centered at the centers of the two spheres. When the microspheres can support surface phonon polaritons (such as silica), the convergence criteria for the number of vector spherical waves required for convergence changes dramatically, mimicking the physics of the problem.

Concurrently, we have developed a sensitive technique of measuring near-field radiative transfer between a microsphere and a substrate using a bi-material atomic force microscope (AFM) cantilever, resulting in "heat transfer-distance" curves. Measurements of radiative transfer between a sphere and a flat substrate show the presence of strong near-field effects resulting in enhancement of heat transfer over the predictions of the Planck blackbody radiation theory.

Elastic Backscattering Spectroscopic Microscopy for Understanding Light Propagation at Microscopic Level

Yang Liu[1, 2] **and Pin Wang**[1]

[1]Division of Gastroenterology, Hepatology and Nutrition, Department of Medicine
University of Pittsburgh, 5117 Centre Ave, Pittsburgh, PA 15232, USA
[2]Department of Bioengineering, University of Pittsburgh
5117 Centre Ave, Pittsburgh, PA 15232, USA

Abstract— Light scattering has shown great potential in detecting subtle changes in refractive index heterogeneity of biological cells at different disease states, thus providing promising biomarkers for both clinical diagnosis and basic science research. There has been significant interest in understanding the origin of light scattering signals from biological cells and image formation in optical microscopy, spectroscopic optical coherence microscopy and optical phase microscopy. Conventional light microscopy does not provide sufficient quantitative information on light propagation with sub-cellular organelles of a biological cell. Here, we present Elastic Backscattering Spectroscopic Microscopy (EBSM) that simultaneously characterizes the spectral signatures and a microscopic image, which allows us to quantitatively analyze the spectral patterns at microscopic level. This instrument presents three technical advantages: (1) Due to the backscattering geometry, the phase-matching condition picks up the largest possible wave vectors in the Fourier-space representation of the refractive structure of the object, which carry information about its finest features. (2) White-light spectroscopic detection allows us to analyze multiple interference effect due to refractive index variations within the object. (3) Low spatial coherent illumination from the thermal light source provides a spatial coherence length of approximately 700 nm, which serves as virtual aperture to decompose a 3D complex scattering medium into many 1D channels.

We used a single microsphere as a model system to investigate the light propagation within a homogenous micron-size sphere. We have identified very distinct and highly localized scattering spectral features at different pixels ($\sim$ 200 nm apart) of a microscopic image of single homogeneous polystyrene micron-sized particle. The origin of spectral features is due to the interference between the light reflected from the sphere-medium interface and one traveling a round-trip optical path through the sphere. Through Fourier analysis, we have constructed the microscopic optical pathlength (OPL) map of a single microsphere. The center of the sphere corresponds to the wave traveling a round-trip optical path through the center of the particle (2^*n^*D, where n is the refractive index of the sphere and D is the diameter of the sphere). Interestingly, there is a gradual increase in OPL when moving away from the center toward the periphery of microsphere, indicating that the wave traveling a longer path length than that at the center (2^*n^*L, where L is the optical pathlength, $L > D$).

In conclusion, elastic backscattering spectroscopic microscopy enables the detection of the highly localized optical pathlength within a single scattering particle. This technique may be used for characterization of the internal structure of living or fixed cells as potential diagnostic biomarkers for clinical and basic research.

Numerical Investigation of Dielectric Properties of Metallic Microspheres in the Microwave Frequency Based on a Volume Integral Approach

Wendy Yip and Xu Li
Department of Electrical Engineering and Computer Science, Northwestern University
Evanston, IL 60208, USA

Abstract— Microwave technology for breast cancer detection and hyperthermia is an emerging research area with potential improvements towards better diagnostics and treatment methods. Introduction of metallic nano/micro particles into diseased tissue sites may enhance microwave imaging and selective heating at tumor sites. In order to optimize the design of the particles in these applications, a better understanding of the dielectric properties of metallic nano/micro particles in the microwave frequency must be established.

In this paper, we report a numerical study of dielectric properties of a variably of microspheres using a rigorous solution of Maxwell Equation to simulate the microwave interactions with these particles. First, we use the Generalized Multiparticle Mie-solution, which is a full-vector numerical solution of the Maxwell's equations to calculate the internal field and scattered field of different ensembles of spherical microparticles. The Generalized Multiparticle Mie-solution allows the scattered field of individual particles to be transformed into the incident fields of other particles in the ensembles, hence accounting for multiple scattering effects. Next, we can calculate the equivalent permittivity of these ensembles since the scattered field from an object is related to its internal field distribution and permittivity via an integral of the Green's function.

We generate realizations of particle ensembles with specified particle size and volume fraction in the simulations and calculate the corresponding permittivity and conductivity of the ensembles. By comparing the single-scattering and multiple scattering results, the relationship between the volume fraction of the particles and the equivalent dielectric properties of the volume is examined. The study allows us to determine if particle interactions contribute to the dielectric properties of the equivalent volume. If particle interactions do indeed produce nonlinear effects on the dielectric properties, we can determine at what volume fraction nonlinear effects become significant. By examining the results of the simulation, we can provide a better understanding of the dielectric properties of metallic particles in the microwave region and the characteristics of particles ensembles that would produce better contrast and heating effects for imaging and hyperthermia applications.

Session 2A3a
Power Electronics

Sensorless Control of Permanent Magnet Synchronous Motor Using Luenberger Observer

P. Brandstetter, P. Rech, and P. Simonik
Department of Electronics, VSB-Technical University of Ostrava, Czech Republic

Abstract— The paper describes sensorless control of the permanent magnet synchronous motor (SMPM). The control method uses a Luenberger state reduced observer for estimation the back electromagnetic force. The speed, direction and position of rotor are calculated from this estimated quantity. The SMPM is controlled by the vector control with estimated signals in the feedback. The simulation results, block schemes and mathematical description are contained in the paper.

Currently there are very promising controlled AC drives with the sensorless control. This control without speed sensor can be based on a many principles. Some of them are systems working with math model of the motor. The estimators and observers are two essential facilities for processing of them. The difference between them is that, the first mentioned doesnt contain the feedback loop. There are many problems at sensorless control of AC drives particularly at the low speed range. Because at this domain there are sluggish changes of signals and offsets, and inaccuracies of sensors are more evidently.

The main advantages of sensorless vector control are following. The sensorless vector control brings the cost saving. If the drive doesnt have the speed sensor there are smaller dimensions and weight. Next they achieve more reliability and noise immunity by elimination the number of sensors. The computing power of digital signal processor (DSP) allows the application with complicated math models and their processing in real-time.

The behavior of SMPM at dynamic or steady states is based on the equations which describe electric and mechanic dependencies of the SMPM quantities. The Luenberger state reduced observer (LSRO) uses similar principle.

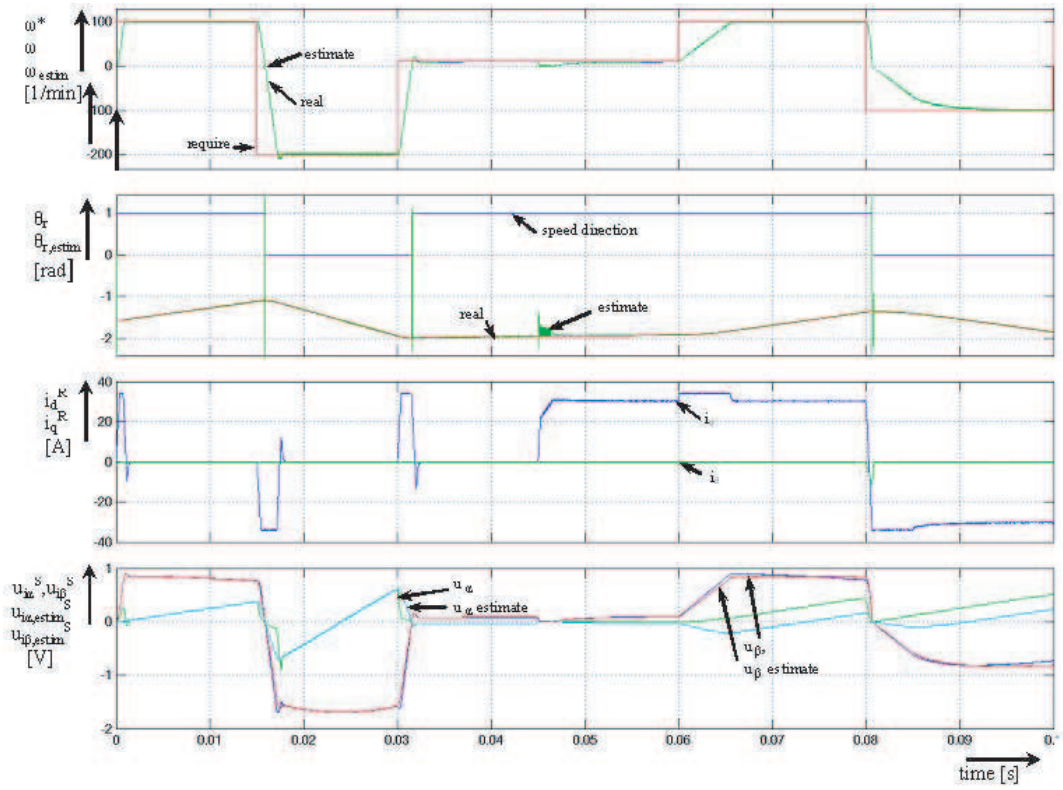

Figure 1: Time courses of the actual and estimated quantities.

The relations among stator voltages, stator currents and back electromagnetic force are the voltage equations. The generated voltage is proportional to the angular speed. There is a precondition of constant angular speed during computing cycle. Short time interval and high mechanical constant are the parameters, which help realize it. The LSRO can be applied for the estimation of the back electromagnetic force instead of a complex full order observer.

After connection stator currents and voltages at stator reference frame we obtain an induced voltage waveform. The speed calculation is based on similar principle.

The speed direction uses same signal as angle estimation. The benefit of this method is that the speed and angle calculation are independent. So the error in position estimation doesnt affect the magnitude of speed estimation if compare it with calculation from the change of position.

The speed is obtained from magnitudes of back electromagnetic force according to following equation.

$$\omega_{r,est(el)} = \frac{1}{\Psi_{PM}} \sqrt{\left(u^S_{i\alpha}(t)\right)^2 + \left(u^S_{i\alpha}(t)\right)^2} sign\left(\frac{d\theta_{r,est}}{dt}\right) \tag{1}$$

The simulation results are shown on the Figure 1 which shows waveforms with calculated speed and angle values in feedback. We can see from them, that the described method provides high-quality results. Only around zero speed there is an inaccuracy on load. Really it is not possible to obtain the true information from estimation process around zero crossing because the input measured voltage values are low and then back electromagnetic force is also near zero.

Figure 1 can be divided into four blocks. The first from top shows angular speed at revolution per minute. There is a required, real and estimated speed. The calculated speed track of real speed is without great errors. Next block represent real and estimated rotor electric angles and signal of speed direction. The value 1 represents the positive speed and the value 0 represents the negative speed. The third block shows real currents in rotor reference frame. The last part of waveforms represents real and calculated back electromagnetic force. It means that this estimation structure works and provides good results.

Control Algorithms of Active Power Filters

P. Brandstetter, **P. Chlebis**, **and P. Simonik**
Department of Electronics, VSB-Technical University of Ostrava, Czech Republic

Abstract— The paper presents some results of controlling of the voltage-source active filter for reduction of high harmonics in the supply current. The filter is suitable for symmetrical three phase loads such as rectifier or frequency inverter. Several ways of current flow controlling and regulation of the filter currents are described and experimentally proved. Simulation and practical results showing the dynamic state system's performance are presented.

The power semiconductor converters are becoming to typical load in the distribution mains. Input circuits of this converters are often designed as a control or non-control rectifier, which consists of power semiconductor devices. Converter is non-linear load in the mains and its current consumption it is not only sinusoidal, but there are higher current harmonics, which unfortunately influence feed system. For reduction of the higher harmonics influence the filters compounded by inductors and capacitors are used. However these devices have many basic disadvantages, for example they and inner line impedance are making resonance circuit with sharp tuned resonances. All these undesirable properties it is possible to remove by using active power filters. For this purpose a semiconductor converter with current or voltage source shows as suitable. That converter is able to add or to take the theoretically any course of current in mains. The active filters with current source have more complicated structure and their purchase price is higher then price of the filters with voltage source. That is why the voltage source filters are often used and we are interesting in them in our investigation.

The active filter consists of six a semiconductor switches (IGBT transistors), dc link capacitor as a voltage source and reactors for limitation of the current rate of rise. A fast microcomputer control system is needed of course. Principle of the filter is such, that a filter current is injected to mains by generation of output voltage out of converter. It can be achieved desired course of then current by suitable switching of converter's switches. A voltage of the dc link capacitor (voltage source) have to be kept with desired value. It is achieved by means of an active power flow through the converter. For correct work of the filter it is necessary exactly and fast to determine a magnitude of the filter currents, which have to be added to load currents so as to be removed higher harmonics. The filter currents are calculated from the measured load currents. There exist several ways how to solve the problem of determination of the filter currents and we describe three of them. It is effort to achieve as high rate of current rise as possible, because in this way the highest harmonics are filtered. At the same time the ripple of current increases if converter switching frequency is not high enough.

The real effect of the filtration depends on the performance of the filter and on the properties of the loads to be compensated as well. In the case of feed system with finally short circuit power the inner line impedance have to be taken into consideration.

For correct action of the filter, it is necessary to determine magnitude of the currents, which have to be added to load current so as to eliminate high harmonics. This problem will be made easy very much by establishing a rotation axis system and by transformation load currents into this system. Rotation system forms two axes d and q, axis d is in supply voltage space vector direction and axis q is vertical to d. By the vector rotation the two current components are

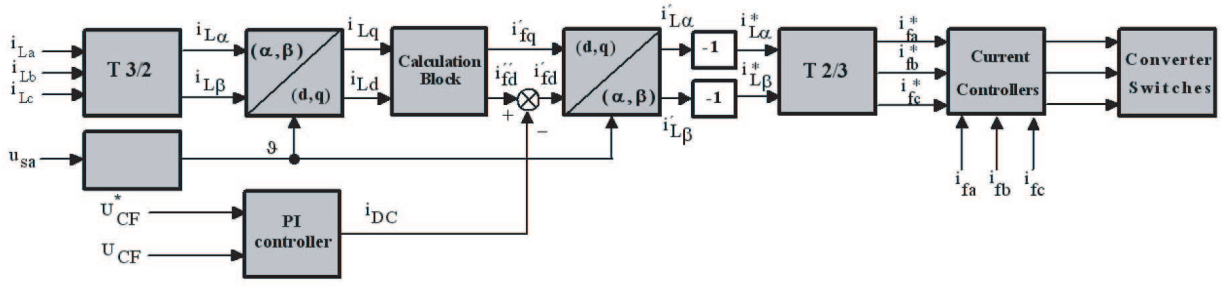

Figure 1: Control structure of active filter.

obtained, component in axis d, proportional to active power and component in axis q, proportional to reactive power. Course of orientated load currents is smooth for linear loads and course is rippled with frequency 300 Hz for rectifier loads.

The purpose of filtration is eliminating alternating component in both axis, or direct component in axis q for compensation of reactive power. There exists several methods of calculation reference filter currents. We are intended on three of them: determination of reference currents by means of high band pass filter, mean value method and PI-controller. Currents control is performed by two-level hysteresis controller, which is very simple and fast, or PI-controller with vector pulse width modulation (PWM). Control structure of active filter is shown in Fig. 1.

Compatibility of Different Types of Frequency Converters with Supply Network

J. Lettl and J. Bauer
Faculty of Electrical Engineering, Czech Technical University in Prague, Czech Republic

Abstract— The presented paper compares influence on the supply network of three different types of frequency converters. Two of them are commonly used indirect frequency converter topologies and the third one is a matrix converter.

The induction motors are used in most of recent electric drives. They have spread because of their robustness, durability, and low requirements on their maintenance. On the other hand their control is not simple task and it has high demands on the converter and control algorithm. The speed of the induction motor depends on the supply frequency and therefore frequency converters are mostly used as induction machine power supplies. In general there are two types of frequency converters — direct and indirect frequency converters.

Nowadays the indirect frequency converter is typically used for the induction motor feeding. This converter consists of the input rectifier, DC-link capacitor, and output inverter. The control algorithm of the output inverter has substantial influence on the induction machine behaviour. Many developed sophisticated control strategies for the inverter are able to ensure that this part of the converter is trouble-free. The weakness of the indirect frequency converter consists in its input part. As the input rectifier usually acts a three phase diode rectifier, or sometimes controlled thyristor rectifier that allows the DC-link voltage control. In case of the diode rectifier energy can flow through in one direction only, therefore energy recuperation is not possible. The rectifier also does not allow the power factor control and it consumes the non sinusoidal current due to the non linear characteristics of the diodes. As a result the supply network is loaded by high harmonics and reactive power. These disadvantages can not be ignored especially at high power converters such as in traction vehicles.

In recent years especially the traction converters are equipped by rectifiers that allow bidirectional power flow, so called "Compatible Rectifiers" or "Active Front End". Such rectifier uses semiconductor devices that can be both switched on and switched off, mostly IGBT's. The rectifier has an inductor on the input and it is controlled by a sophisticated control algorithm, for example some PWM strategy is employed. The rectifier controlled in this way consumes current of required waveform, which is mostly sinusoidal. It works with a given phase displacement between the consumed current and supply voltage, i.e., the power factor can be controlled. The energy recuperation is also possible and the converter has in such case minimal influence on the supply network.

The direct frequency converters are very popular today. They are not so widespread because their control requires more complex control algorithms that were not realizable till now without powerful microprocessors. The name "Direct Frequency Converter" comes out of the fact that they do not need DC-link. The output voltage is produced by direct switching of the input phases to the output phases. In consequence the maximal output voltage value is limited to 86% of the input voltage amplitude. The higher output voltage can be achieved only by overmodulation that causes the input current waveform distortion. "Matrix Converter" belongs to the direct frequency converters category, too. To the main advantages of this converter belong operation in all four quadrants, therefore the recuperation is possible. The converter has high dynamics, enables power factor control, and consumes nearly sinusoidal current from the supply network. It means that the matrix converter does not load supply network with higher harmonics and it can work with given power factor. As mentioned above, the converter has no DC-link, which is the great advantage of the converter, because the accumulation element in the DC-link is mostly very large, takes large room, and usually is very heavy.

The presented paper compares from point of view of compatibility with the supply network the above mentioned three frequency converter topologies that are being used for supplying of induction machines. The topic of the EMC of the converters becomes very important in these days, because some of the semiconductor converters can be ranked as the worse supply network polluters. These negative side effects of the converters were previously overlooked, but with the widespread of power electronics they can not be ignored more. That is why the test beds of these three frequency converter input parts were realized and experimental results obtained by the measurement were analyzed and discussed.

Magnetic Field Harmonics of Inductive Power Transmission Systems Fed by Square-wave Inverters

Daniel Kürschner and Christian Rathge
Institut f. Automation und Kommunikation e.V.
Wireless Power Transmission, Werner-Heisenberg-Straβe-1, Magdeburg 39106, Germany

Abstract— Inductive power transmission systems consist of the air gapped coil system and the power electronic devices on the primary and on the secondary side. Fig. 1 shows a minimum required configuration. To feed the primary coil, often a half-bridge or a full-bridge square-wave inverter is used. A high efficient energy transfer needs a leakage inductance compensation and a high field frequency. This make great demands on the power electronic devices. To analyse the switching behaviour, the simulation circuit shown in Fig. 2 (left) is used. The energy source and the D.C. link is modelled by a D.C. source (u_D) and the coil system is modelled by a series resonant circuit. Fig. 2 (right) shows a simulation of the used full-bridge inverter. The waveform of the coil current i_1 depends on the quality factor (Q) of the resonance circuit. At low Q there are current and field harmonics, which result in

- High power loss of the magnetic assembly and stricter limit values for the magnetic field,
- High power loss and high emitted interferences (EMC) because of hard switching operation and
- Restricted applicability of first harmonic approach and time harmonic field simulation.

To analyse the harmonics, the dynamic and the steady-state behaviour of the air gapped transformer can be described by the T-equivalent circuit and can be analysed by the Laplace transformation. The paper presents modelling methods and strategies to reduce the harmonics of the current and the magnetic field. Furthermore, it gives an overview of applications of inductive power transfer systems.

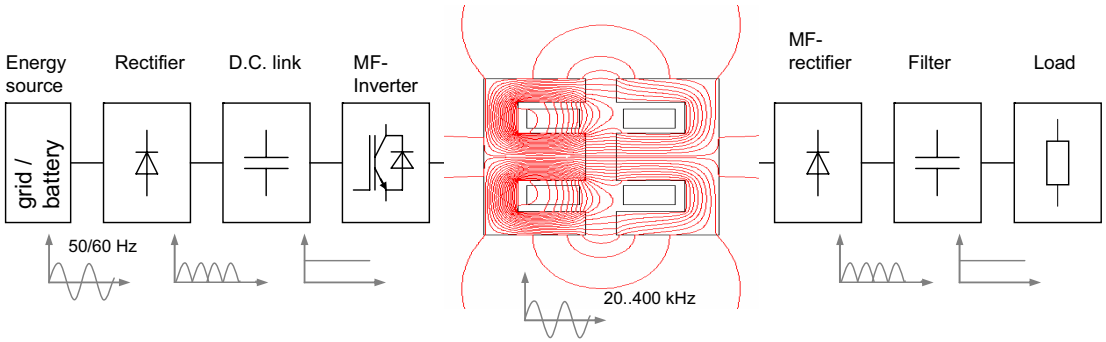

Figure 1: Minimum configuration of an inductive power transmission system (schematic).

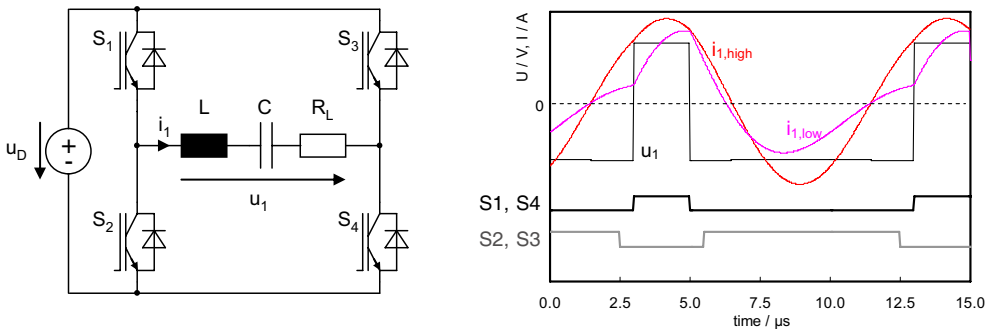

Figure 2: Left: Simulation circuit of the transmission system (incl. square-wave inverter stage); Right: Simulation result of the voltage (u_1) and the current at low resonance $Q(i_{1,\mathrm{low}})$ and at high $Q(i_{1,\mathrm{high}})$.

Leakage Inductance Determination for Transformers with Interleaving of Windings

R. Doebbelin and A. Lindemann
Institute of Electric Power Systems, Otto-von-Guericke-University Magdeburg, Germany

Abstract— Several aspects of the operation of power-electronic circuits with transformers are significantly influenced by the leakage inductance of the respective transformer. For instance, it concerns power transfer capability of the circuit and power semiconductor stress parameters. The tendency to higher switching frequencies of power-electronic apparatuses results in an increasing relevance of low transformer leakage inductance values. Mostly, the so-called interleaving of windings (i.e., the fragmentation of the primary and the secondary windings into a certain number of sub-windings and alternate interleaving of primary and secondary sub-windings) is used to meet this requirement.

Using an appropriate approximation method it is possible to determine the leakage inductance of a transformer already in the design phase on the basis of predicted geometry parameters. Thus, circuit simulation can be used to shorten the development process of power-electronic apparatuses. Formulas which are given in literature generally rely on an approximation method for leakage inductance determination which has been established by ROGOWSKI. It is based on the consideration of the energy of the leakage magnetic field and applies to a transformer design with windings arranged on the same leg. The basic formula of this method is

$$L_L = \mu_0 \cdot N^2 \cdot l_m \cdot \lambda \cdot k_\sigma \tag{1}$$

with L_L — leakage inductance, μ_0 — absolute permeability, N — number of turns of the winding to which the leakage inductance refers, l_m — mean length per turn for whole arrangement of windings, λ — relative leakage conductance (depending on geometry parameters and on the degree of interleaving of windings), k_σ — Rogowski factor.

The formulas which can be found in contemporary technical literature, mostly represent simplified variants of the mentioned basic formula. Usually the Rogowski factor is omitted and the formula describing the relative leakage conductance is included in the main formula. Often, constant factors like absolute permeability and numerical values are merged into one coefficient, so that the physical background of the formula is not recognizable anymore. In some cases different formulas are given for a transformer design without interleaving of windings and for transformer arrangements with interleaving of windings. The degree of interleaving is considered in literature by the number of the couples of sub-windings or by the number of interfaces (insulating interspaces) between the single sub-windings of an arrangement of windings. Furthermore, the aim to present a universal formula which is valid for transformer versions with concentric and also with pie windings arrangements often causes some confusion. It also results from the diversity of terms which are used for the dimensions of windings (e.g., breadth, width, traverse, build, height, length) comparing the formulas and their descriptions which are given in different books and papers.

To enable a correct application of a formula for leakage inductance calculation both for transformers with concentric and transformers with pie windings, the attribution of the chosen symbols for geometry parameters to the respective dimensions of the arrangement of windings has to be made quite clear. Therefore, based on variants which are valid for transformer versions without and with interleaving of windings, the following representation of the formula is proposed:

$$L_L = \mu_0 \cdot N^2 \cdot \frac{l_m}{n_{if}^2 \cdot X_{par\text{-}lf}} \cdot \left(\frac{\Sigma\, X_{perp\text{-}lf}}{3} + \Sigma\, \delta \right) \tag{2}$$

with $\Sigma X_{perp\text{-}lf}$ — sum of the dimensions of all sub-windings which are orientated perpendicular to the leakage flux, $X_{par\text{-}lf}$ — dimension of the sub-windings which is orientated parallel to the leakage flux, $\Sigma\delta$ — sum of the thicknesses of all insulating interspaces between the sub-windings, n_{if} — number of insulating interspaces between the sub-windings (no consideration of Rogowski factor).

Thus, in this formula the respective dimensions of the sub-windings are identified based on a comparison between their orientation and the orientation of leakage flux within the core window. The meaning of the geometry parameter symbols and the path of leakage flux Φ_l within the core

window are illustrated in principle in Fig. 1 assuming the leakage flux to be concentrated in the insulating interspaces between the windings or sub-windings.

The proposed representation and also the variants of the formula which are given in literature enable a relatively uncomplicated approximate calculation of the leakage inductance of a transformer even in the case of interleaving of windings. However, it has to be stated that the scope is limited to magnetically symmetric arrangements of windings, in which the outer sub-windings have a number of turns which is half of that of an inner sub-winding belonging to the same group of sub-windings (an inner primary sub-winding if the outer sub-windings belong to the primary winding; an inner secondary sub-winding if the outer sub-windings belong to the secondary winding). In connection with this, it can be assumed that the outer sub-windings show a dimension perpendicular to the leakage flux which is half of the same dimension of an inner sub-winding which belongs to the same group of sub-windings. Besides magnetically symmetric arrangements also magnetically asymmetric designs of windings are used in praxis. For instance in transformers for capacitor discharge welding machines a magnetically asymmetric design of windings is often used to enable a variation of the turns ratio by means of alteration between series and parallel connection of the primary sub-windings.

In the full-length paper an alternative method shall be explained which allows the leakage inductance calculation even in the case of magnetically asymmetric arrangements of windings. The obtainable accuracy shall be evaluated by means of comparison to leakage inductance values determined from measurements considering different transformer versions.

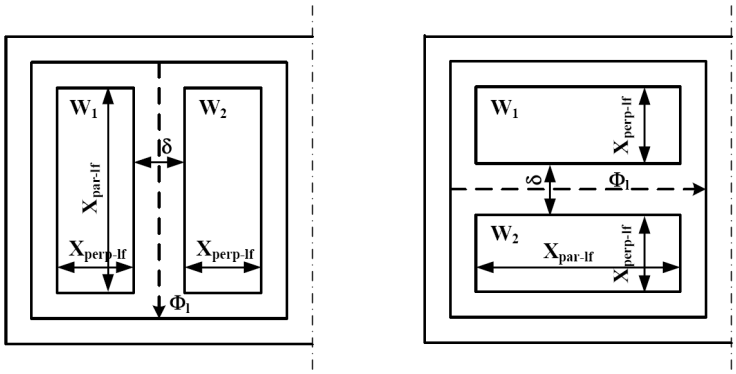

Figure 1: Illustration of attribution of the dimensions of the windings or sub-windings used in formula (2) and their orientation compared to the orientation of leakage flux Φ_l within the core window (left: concentric windings, right: pie windings, only left hemisphere of arrangement displayed).

Controlled Battery Charger for Electric Vehicles

M. Geske[1], **T. Winkler**[2], **P. Komarnicki**[2], **and G. Heideck**[1]

[1]Otto-von-Guericke-University Magdeburg, Magdeburg, Germany
[2]Fraunhofer Institute of Factory Operation and Automation IFF, Magdeburg, Germany

Abstract— Due to rising fuel consumption, the price of CO_2 emissions and growing urban air pollution, the global interest of the automobile industry, politics and scientists in electric mobility is increasing in the recent years worldwide. Thus, future challenges will be the integration of electric vehicles (EV) in distribution networks under the scope of balancing multiple charging processes while, at the same time, increasing dispersed generation. The development of a controlled battery charger for traction batteries aims to reduce the peak load and to shift energy demand.

During charging process, electrical energy is converted and stored in form of chemical energy. A conventional battery charger is supplied by mains voltage and feeds the battery with DC voltage and current. Therefore, the battery charger adapts voltage and charging current from the mains to the specified battery parameters. For electric mobility, battery chargers of EVs should fulfill additional future tasks. Controlling the charging current makes possible to keep load profiles inside defined ranges. Hence, a charging process can be adapted to the total power consumption of a household to reduce or shift power consumption. A charger for lithium iron phosphate batteries of a small-sized experimental vehicle has been developed and tested. A PI control algorithm has been implemented to enable the required constant current constant voltage (CCCV) charging characteristic of the battery. The results of the operation of the charger will be presented and discussed.

Modeling the Electromagnetic Behavior of Power Converters

S. Schulze, M. Al-Hamid, R. Vick, and R. Doebbelin
Otto-von-Guericke University of Magdeburg, Germany

Abstract— The density of electronic and power electronic devices is increasing in modern industrial surroundings. The electromagnetic compatibility must be considered in the development process with a high priority. Besides, the operating frequencies are increasing as well, so that the analysis of a complete system, such as a power converter combined with the motor is difficult. The compliance with the limit values for emission and immunity which are fixed for variable-speed drives in the product norm EN 61800 has to be guaranteed by evaluations, measurements or simulations.

The development of tools and methods to achieve the electromagnetic compatibility for variable-speed drive systems were the aim of the described investigations. The manufacturers of power drive systems should be enabled to qualify the EMC of their systems during development process by using these tools on the emission of the system.

At first, norm-compliant measurements of the radiated emission of a drive system consisting of a frequency converter, motor, mains filter, mains choke and wires were performed. Radiated disturbances were discovered in the frequency range from 80 MHz to 1 GHz which were mainly generated by the frequency converter. Furthermore, the common mode currents on the cables between motor and electronic were measured. i.e., the cable shield current.

It was examined if the radiated emission could be predicted by the use of a simple model for numerical field simulation. The software package CONCEPT [1] was used, which solves electromagnetic field integral equations (method of moments, MoM).

The simple model assuming an ideal conducting surface below the power drive system and the connecting wires is shown in Figure 1. One wire was fed by a common mode current near the converter, its input value was taken from the measurements. The comparison of simulated to measured electric field strength shows very good agreement.

At second, a network model for prediction of the common mode currents on the cable shields was investigated. Therefore knowledge about the parasitic capacitances inside the power converter, especially of the switching semiconductors, as well as the driving PWM signals is necessary. The network model is built up using a SPICE [2] simulator and are currently under investigation.

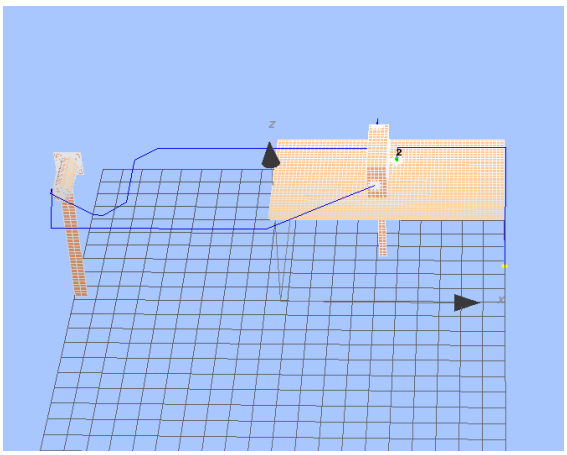

Figure 1: Model of the drive system consisting of frequency converter enclosure, motor housing, groundplane and earth straps.

REFERENCES

1. Brüns, H.-D., A. Freiberg, and H. Singer, "CONCEPT II User's Manual", http://www.tet.tu-harburg.de.
2. Linear Technology LTspice IV, http://www.linear.com.

Session 2A3b
Antennas and Array: Theory and Design 1

Frequency-adjustable Circularly-polarized Ceramic Dielectric Resonator Antenna

S.-S. Zhong[1], **L.-X. Li**[1], **S.-Q. Xu**[1, 2], **and M.-H. Chen**[1]

[1]School of Communication and Information Engineering, Shanghai University, Shanghai 200072, China
[2]Zhejiang Zhengyuan Electric Co. Ltd., Jiaxing, Zhejiang 314003, China

Abstract— The circularly-polarized (CP) ceramic dielectric resonator antenna (DRA) has received much attention in the last decade because of a number of advantages such as its small size, light weight, low cost, and because of its less sensitivity to the propagation environment of a CP system as compared with a LP (linearly-polarized) system. However, the resonant frequency of a DRA is determined as long as the dielectric resonator is chosen. In this article, a CP DRA with a large choice range of the resonant frequency is introduced, which is excited by a corner-cut square patch between the dielectric resonator and the substrate. The effects of patch size and cut size are investigated, showing that the resonant frequency of the antenna can be adjusted by simply changing the patch size, for example, the resonant frequency is 5.17, 5.23 and 5.31 GHz as the patch length a is 2.4, 2.5 and 2.6 mm, respectively. The reflection, axial ratio, and radiation characteristics of the antenna are found. Measurements were carried out to verify the design. The measured impedance bandwidth reaches 309 MHz, with good broadside radiation characteristics. And the axial-ratio bandwidth is 70 MHz, with a minimum axial ratio of 1 dB. The antenna is compact in structure, as it consists of only a cylindrical dielectric resonator with radius of 4.5 mm and a substrate of 40 mm × 40 mm. The compact CP DRA is attractive for the application as the terminal of satellite communication system.

Effects of Metallic Strips on the Radiation Characteristics of Dish Reflector Antennas

Ali H. Harmouch[2], **Walid A. Kamali**[1], **Ghaleb A. Sanjakdar**[1], **and Ahmad Y. El-Abed**[1]

[1]Al-Manar University of Tripoli, Lebanon
[2]American University of Science and Technology, Lebanon

Abstract— Reduction of side lobe level in reflector antennas is desirable in most applications. For antennas used as receivers, side lobes make the antenna much more exposed to noise from any other signal coming from any other source. For transmitting antennas side lobes represent security weakness, as an unintended receiver may pick up the classified communication. A simple way of achieving this reduction is to specifically add metallic strips over the main reflector surface, so they would diffract the incident waves and scatter the unwanted radiations thus reducing the biggest "first" side lobes in the antenna's radiation pattern. The position, shape and size of the scatters are also considered, and it has been proven experimentally that two flat symmetric strips may produce a side lobe reduction of about $-23\,\mathrm{dB}$.

The Gain Effects of Air Gap Quadratic Aperture-coupled Microstrip Antenna Array

M. F. Jamlos[1], T. A. Rahman[2], M. R. Kamarudin[2], M. T. Ali[2], M. N. Md Tan[2], and P. Saad[3]

[1]Faculty of Computer and Communication Engineering, University of Malaysia Perlis (Unimap), Malaysia
[2]Wireless Communication Center (WCC), University of Technology Malaysia (UTM), Malaysia
[3]Faculty of Computer Science and Information System (FSKSM)
University of Technology Malaysia (UTM), Malaysia

Abstract— This paper describes the concept of air gap structure to enhance the antenna's gain. The structure of the planar antenna array consisting rectangular16 elements is comprised based on corporate feed network. The advanced of this antenna design is the antenna's feeding network is etched on a different layer from the elements by certain of air gap distances. The air gap antenna was separated and measured from 0 mm to 20 mm, in 0.5 mm increments respectively. Quadratic slots enabled most of the induced current and power from source to the radiating patches. The magnetic characteristics of quadratic allowed absorbing the reflected electrical fields around the slots. The configuration of air gap is competent influencing a stronger fringing field at the edge of the patches. The fringing fields become stronger as the distance is getting increased. A strong fringing fields leads for the patches to radiate even further. The air gap increased the radiated power and reduced conductor loss. The gap coupling is more feasible to reduce surface wave excitation between elements which are separated by a ground plane. The combination of air gap structure with quadratic slots contrived the gain grooming 400% times larger than a quadratic aperture coupled microstrip array antenna without an air gap. The proposed antenna also has significant 50% of gain compared to the conventional transmission line antenna array. The air gap has successfully increased the level of isolation up to 1.5 times bigger than without air gap. The effects of the gap on parameters such as radiation patterns and gain are observed. Good agreement between simulations and measurements is also obtained. These results extend the validity of the analysis and will be useful for higher gain applications.

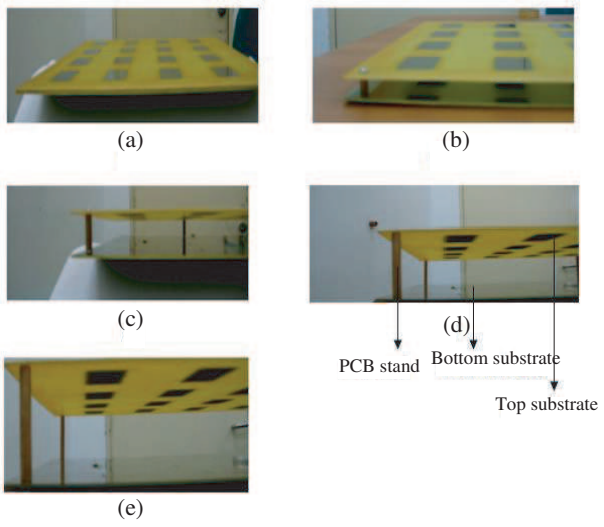

Figure 1: Layout view of Q-ACMAA with gap-coupling (a) $d = 0$ mm, (b) $d = 5$ mm, (c) $d = 10$ mm, (d) $d = 15$ mm, (e) $d = 20$ mm.

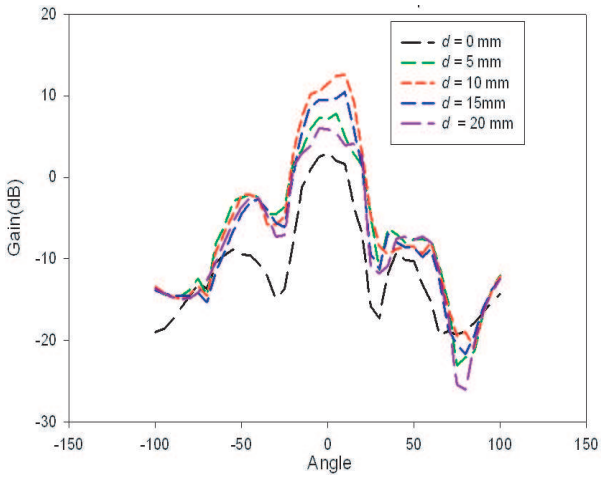

Figure 2: Measurements of radiation pattern at different distance of air gap, d.

Polarization Diversity Monopole Antenna

N. S. Awang Da, **M. R. Dzulkifli**, **and M. R. Kamarudin**
Wireless Communication Centre (WCC), Faculty of Electrical Engineering
Universiti Teknologi Malaysia, Malaysia

Abstract— The increasing number of user in ISM 2.4 GHz band has caused the spectrum to be crowded. The emerging technology of cognitive radio has paved the way of improving the spectrum utilization. Apart from that, antenna diversity is a well-known technique to enhance the performance of wireless communication systems by reducing the fading effects. In order to create an antenna diversity system on a wireless device, two or more antenna elements could be placed in positions that provide uncorrelated signals of the same power level. A printed polarization diversity monopole antenna for Cognitive Radio system application to improve the spectrum utilization in the 2.4 GHz ISM band is proposed in this paper. The proposed antenna is composed of two monopoles which are orthogonal to each other. Computer Simulation Technology (CST) Microwave Studio software was used to evaluate the antenna design. This antenna was fabricated on 50 mm × 50 mm FR4 board with thickness of 1.6 mm and dielectric permittivity 4.7. Even though the return at the two ports are different but the antennas have −15 dB and −12 dB return loss which were lower than −10 dB at 2.4 GHz. The radiation pattern for the antenna was different with single monopole antenna since the ground plane from antenna #2 reflected the signal radiated by antenna #1. This diversity antenna also offers wide bandwidth (∼ 17%) and low correlation since the antenna orthogonal to each other.

Session 2A4
Electromagnetic Theory

Complex Permittivity Estimation by Free Space Method Using Specular Reflected RCS

Masayuki Ishikawa and Hiroshi Shirai
Course of Electrical, Electronic, and Communication Engineering
Graduate School of Science and Engineering, Chuo University
1-13-27 Kasuga, Bunkyo, Tokyo 112-8551, Japan

Abstract— Electric permittivity of the materials is one of the important parameters for manufacturing high frequency electronic devices and circuits. Typical measurement methods may be co-axial probe, free space, transmission line, cavity methods, and so on. Nonetheless, these methods have their advantages and disadvantages for certain measurement ranges.

In this paper, rather simple calibration technique has been proposed to apply for a free space measurement method for relatively large and homogeneous sample objects. This method features non-contacting and non-destructive measurement without involved sample settings. The conventional free space measurement system measures the reflection (S_{11}) and the transmission (S_{21}) coefficients with a proper calibration which is critical for measurement accuracy.

Measurement method of the radar cross section (RCS), which shows an index that shows the amount of the electromagnetic scattering from the object, has already been established and its calibration method utilizes the monostatic setting, which is essentially obtaining the reflection (S_{11}) property from the material. For our proposed calibration, monostatic RCS at the only specular reflection direction is needed. Since the specular reflection gives us maximum return from the scattering object generally, this specular reflection direction is easy to find. Therefore, the calibration setting is rather easy and simple.

In order to isolate the only surface reflected contribution, time gating method is utilized. The frequency domain RCS is measured first at a certain frequency band, then the corresponding time domain RCS result is calculated via inverse Fourier Transformation. After identifying the surface reflection contribution and selecting it with a certain time width, Fourier transformation is used to obtain the desired surface response in the frequency domain. These RCS results are used to estimate the surface reflection coefficients from which the permittivities of the materials are calculated. The proposed method has been tested to evaluate the permittivities of some materials, and the results are compared with those obtained by the co-axial probe method. Good agreement has been found between them, and the validity of our measurement method has been confirmed.

Implications of an Inhomogeneous Lorenz Condition

I. M. Besieris[1] and A. M. Shaarawi[2]

[1]The Bradley Department of Electrical and Computer Engineering
VPI & SU, Blacksburg, Virginia 24061, USA
[2]The Physics Department, The American University in Cairo, P. O. Box 2511, Cairo 11511, Egypt

Abstract— The *inhomogeneous* Lorenz condition $\nabla \cdot \vec{A}(\vec{r},\tau) + (\partial/\partial\tau)\,\Phi(\vec{r},\tau) = g(\vec{r},\tau)$ is considered in conjunction with Maxwell's equations in free space. The wave equations for the vector magnetic potential $\vec{A}$ and the scalar electric potential Φ are inhomogeneous. On the other hand, the wave equations for the electric field $\vec{E}$ and the magnetic field $\vec{H}$ are homogeneous in a source free region provided that the function $g(\vec{r},\tau)$ obeys the homogeneous scalar wave equation. Such an approach to deriving free-space solutions to Maxwell's equations seems to be much more complicated than the one based on the ordinary homogeneous Lorenz gauge. It turns out, however, that when it is coupled to the Whittaker-Bateman potential theory, it yields classes of physically interesting solutions that are difficult to be obtained otherwise.

Within the framework of the Whittaker-Bateman potential theory, one starts with two "conjugate" functions $\alpha(\vec{r},\tau)$ and $\beta(\vec{r},\tau)$, any functionals of which obey the nonlinear characteristic (eikonal) equation associated with the scalar wave equation. The scalar and vector potentials are defined, then, as $\Phi = -\alpha\,(\partial/\partial\tau)\,\beta + \beta\,(\partial/\partial\tau)\,\alpha$, $\vec{A} = \alpha\nabla\beta - \beta\nabla\alpha$ and the electromagnetic fields are determined by the usual relations $\vec{E} = -\nabla\Phi - (\partial/\partial\tau)\,\vec{A}$, $\vec{H} = \nabla \times \vec{A}$.

Emphasis in this presentation is placed on appropriate choices of the conjugate functions $\alpha(\vec{r},\tau)$ and $\beta(\vec{r},\tau)$ that yield luminal finite-energy spatiotemporally localized *null* electromagnetic waves. Such wave packets, carrying angular momenta and characterized by vortex structures, are of physical importance and are being intensely studied in several areas, e.g., optical vortices, photon entanglement, etc. As a specific illustrative example, a linked and knotted electromagnetic solution is considered for which all electric and magnetic field lines are closed loops and any two electric (or magnetic) field lines are linked once with one another.

Effective Parameters of Artificial Material Composed of Dielectric Particles

Arun Kumar Saha and Matthew Hawthorn
Albany State University, USA

Abstract— Effective permittivity and permeability of artificial material composed of dielectric or metal slabs placed in 3 dimensional spaces in a regular fashion are calculated in terms of filling factor and verified with HFSS simulation and discrepancies are discussed.

The artificial material is considered to be composed of unit cells which contain unit particle which is dielectric slab or metal slab. A plane wave excitation is used in a parallel plate waveguide (PPWG) which is considered to be loaded with these unit cells. Each Unit particle contributes some lumped element impedance value to the distributed series impedance and shunt admittance value of the unit cell. The impedances resulted from dielectric or metal slab per unit cell is transformed into per unit length quantities of PPWG to calculate the effective parameters. This equivalent circuit approach of calculation provides a clear understanding as to why effective permittivity is enhanced more with a metal slab than a dielectric slab of same shape and size. This theoretical calculation also explains the anisotropic property of the material and calculation is verified with simulation. Some limiting circumstances have been explained with the developed theory and verified with simulation.

In case of dielectric slab, when the height of slab, in the direction of electric field is finite, a little discrepancy is observed due to the non uniform electric field distribution in the slab. When the slab height is infinite, in the direction of electric field, theatrical effective permittivity values are in very good agreement with the simulated values due to the reason that electric field lines are uniform inside the slab.

Franck-Hertz Experiment in Magnetic Field

Ying Weng[1] and Zi-Hua Weng[2]

[1]College of Chemistry & Chemical Engineering, Xiamen University, Xiamen 361005, China
[2]School of Physics and Mechanical & Electrical Engineering, Xiamen University, Xiamen 361005, China

Abstract— Franck-Hertz experiment is vital to the modern physics, for it confirmed first the existence of discrete energy levels in atoms. In a Franck-Hertz tube filled with argon, the inelastic collisions of electrons with argon atoms will alter the collided particles' velocity and direction. Along with the increasing of electric voltage continuously, the collected current will be oscillated periodically. This variation situation will be repeated again and again. The current variation is reported to be determined by the accelerating voltage, retarding voltage, and temperature etc. Besides those main factors, the magnetic field is also an important and more complicated factor.

The paper will study the applied magnetic field's impact on the inelastic collisions of electrons with argon atoms. The influence of applied magnetic field in Franck-Hertz experiment emerges complicated features. In the test, the impact of magnetic field variation is equal to that of temperature variety. In case the accelerating electric intensity becomes strong enough, enlarging magnetic flux density is equivalent to increasing of oven temperature. When the accelerating electric intensity is very weak, enhancing magnetic flux density is identical with oven temperature decreasing. Moreover, the same is true of non-uniform distribution of applied magnetic fields.

In the test a uniform magnetic field is applied in a direction perpendicular to the accelerating electric intensity. According to existing electromagnetic theory, the magnetic field has not an influence on the inelastic collisions or electrons' energy transferring. However the results contradict this usual assumption. Applying the magnetic field either steadily or instantaneously, the collected current of the collecting plate appears to fluctuate observably. But the classic electromagnetic theory does not explain why the phenomena will happen. The research assumes there may be one new kind of electromagnetic force component to transfer the electron energy.

The quaternion was invented by W. R. Hamilton, and was first used by J. C. Maxwell to represent electromagnetic theory. At present, the quaternion can be used to describe either electromagnetic field or gravitational field. The electromagnetic theory described by quaternions predicts that there exists one electromagnetic force component along the direction of magnetic field line. It will accelerate the electric charge along the direction of magnetic field line, and then vary the electric charge's energy. The results obtained indicate that the impact of magnetic field is different even contrary distinctly, when the accelerate electric field is situated on different intensity stage.

ACKNOWLEDGMENT

The author is grateful for the financial support from the National Natural Science Foundation of China under grant number 60677039.

Rough Space Travel

Karl Federico Kaspareck
CTE, Italy

Abstract— Travel interaction with non homogeneous, anisotropic space can induce Sun's systemic changes from virtual equilibrium position. This may induce inertial changes in electromagnetic star's emission power density and lower frequencies scattering. Mass deformation related to space travel and associated angular frequency changes can be described by Larmour equation. Group angular velocity dispersion would converge to near infrared, changing star's lower frequency net radiation emission.

This occurrence may be perceived as having an extraordinary low probability within our standard reference system, but it could be a normal probability of occurrence within a broad time reference/window.

The force involved in travel mass deformation can be described according to $(\Delta F_{t/}F)r^2/v \sin \Phi$ where v is the speed, r the radius and Φ the angle between trajectory and mass curvature. Φ can be assimilated to the angular hyperbolic eccentricity relative to system's travel trajectory, in first approximation the ratio between arccosine traverse radius and conjugate radius.

The resulting force range can be expressed in terms of Yukawa formula $h/2\pi c\mu$, with μ field quantum, c speed of light, h Plank's constant. The magnitude of change agrees with general space anisotropy (dT/T) as per Boltzmann relation.

Gravitational forces are independent on direction and equal to the module of the overall force involved. Near planetary convergence of forces cannot be excluded. The theoretical power change calculated through Yukawa formula is small, close to -140 dB from mean SHF power level at 6 GHz and it carries a contribution to earth's thermal intake/release. This value is three orders of magnitude less than space anisotropy, but the theoretical thermal differential contribution is within the order of magnitude of common greenhouse effect estimates.

Changes in solar emission spectral shape due to solar travel interaction with space perturbations are in principle of very small magnitude and relative high frequency. The integration of mean planet's temperature change calculated over a century from this hypothesis provides a value close to 1 Celsius. This value compares well with theoretical green housing hypotheses and the observed increase in temperature in the last two centuries. A shift of oceanic currents to shorter periods can also be linked to near field-space interaction intensity.

The energy level produced by human activities is near 10^{-3} incoming solar energy before re-radiation. Incoming energy disperses towards lower wave numbers along lower atmosphere differential greenhouse gases concentrations. Carbon dioxide, takes on complex molecular structures and is particularly compressible along atmospheric gradients. The resultant build ups cause lower atmospheric thermal and pressure anomalies and displace local gradients, generating sharp climatic variations over relatively short distances. Related atmospheric gaps result in pronounced cyclonic angular speeds and frequency changes. Similarly, seasonal variations take longer to stabilise. For instance, the gradient of seasonal pressure regime is not uniform and shows clear truncation effects with rapid variations at tail.

This paper outlines this theory and relates its outcomes to current green housing hypotheses, aiming also to provide a new and more balanced platform of discussion on global warming.

Potential Orbital Debris Protection Using a Gradient Magnetic Field

Adom Giffin, **Mikhail Shneider**, **and Richard B. Miles**
Applied Physics Group, Department of Mechanical and Aerospace Engineering
Princeton University, Princeton, NJ, USA

Abstract— In this paper, we examine the effects of a conducting sphere moving through a *gradient* magnetic field. Although the description is simple, the physics behind the solutions to these effects are not only understudied, but can be very complicated as well. Particularly when the conductor is moving very fast (non-relativistic) or better stated, when the magnetic Reynolds number is large. We attempt to discuss this problem by first examining a simple situation (low velocity) where we can describe the analytical solution, then move to a more complicated scenario (high velocity). Although there are numerical solutions to these cases, those solutions often fail to show the relationships between properties of the system.

For the low Reynolds number case, we conduct both an experiment as well as solve the problem by way of an analytical approximation. For the experiment, we have a superconducting magnet based on a Helmholtz coil. Various solid metallic spheres are dropped into the magnetic field and the fall time from release to the arrival at the center of the coil pair is recorded using laser beams. The interaction of the magnetic field with these spherical objects leads to the development of eddy currents that produce an induced magnetic field which then generates a force opposing the gravitational force, thus reducing the fall velocity and increasing the fall time. For the analytical model approximation, we use a piecewise linear approximation for the magnetic field. The most important feature of the field is the gradient and our linear approximation accurately captures that slope. The analytical approximation and the experimental results have very close agreement.

For the high velocity case, we use a commercial software package, MagNet by Infolytica Corporation. In this case, the Helmholtz coil configuration and spheres are modeled with the software. A low velocity simulation shows good agreement with both the analytical approximation and the actual experiment. Following this, the high velocity case is simulated. While the velocity decrease is only slight in this case, there are significant differential forces built up over the sphere. These forces seem to flatten and extrude the sphere into a prolate spheroid.

One possible application for this work would be for protection from space debris. The current configuration of the ISS shielding uses a "bumper" and "catcher" setup. The idea is that the debris will hit the bumper (aluminum), melt due to impact and spread out (due to design) across the catcher, thus distributing the force over a greater area. If this system also included a magnetic field, the forces on the mass could be further spread out and slowed. This would result in the need for less shielding.

Coordinate Transformations with Variable Speed of Light

Zi-Hua Weng
School of Physics and Mechanical & Electrical Engineering, Xiamen University, Xiamen 361005, China

Abstract— Making use of quaternion features, we can obtain Galilean transformation, Lorentz transformation, and some other feasible coordinate transformations, when the speed of light is invariable. But the viewpoint about invariable speed of light is being doubted and challenged for a long time. Consequently the people question the validity of these coordinate transformations with invariable speed of light as well. Up to now, this suspicion remains as puzzling as ever. The paper attempts to explain why the above coordinate transformations will be correct in most cases, in case the influence of field potential can be neglected.

The quaternion was invented by W. R. Hamilton in 1843, and was first used to demonstrate the electromagnetic field by J. C. Maxwell in 1861. At present, the gravitational field can be described by the algebra of quaternions as well. Though the gravitational field and electromagnetic field both can be demonstrated by quaternions, they are quite different from each other indeed. We add another quaternion space to one quaternion space to encompass the feature of gravitational field and electromagnetic field simultaneously. In terms of the algebra of quaternions, we can deduce the coordinate transformations with variable speed of light.

The idea for variable speed of light has been proposed long ago. This conception does not violate any physics principle. In the quaternion spaces, the radius vector can be mingled with the integral of field potential to become one compounding radius vector, while the velocity with the field potential to one compounding velocity. Accordingly the generalized Galilean transformation and generalized Lorentz transformation can be deduced from these compounding radius vector and compounding velocity. The research carries out the field potential and the velocity both have an impact on the coordinate transformations with variable speed of light.

ACKNOWLEDGMENT

The author is grateful for the financial support from the National Natural Science Foundation of China under grant number 60677039.

Radiometry, Wave Optics and Spatial Coherence

A. S. Marathay[1], **J. F. McCalmont**[2], **and D. B. Pollock**[3]

[1]College of Optical Sciences, University of Arizona, Tucson, AZ, USA
[2]Air Force Research Laboratory, Sensors Directorate, WPAFB, OH, USA
[3]Center for Applied Optics, University of Alabama, Huntsville, AL, USA

Abstract— Conventional radiometry concepts are based on geometry or ray optics. However, radiation is an electromagnetic wave. In this paper, radiometry is generalized to include the framework of wave theory. Key radiometric quantities and sources of conventional radiometry are redefined in the context of wave optics. The mutual coherence function and other statistical quantities are incorporated and play a central role in connecting the radiometric quantities of conventional radiometry to those of generalized radiometry. Stationary phase concepts are employed to determine the generalized radiometry of diffracting systems. Specific examples of generalized radiometry are examined such as black body radiation, partially coherent sources, and coherent sources.

Homogeneous Bianisotropic Medium, Dissipation and the Non-constancy of Speed of Light in Vacuum for Different Galilean Reference Systems

Namik Yener
Technology Faculty, Umuttepe Campus, Kocaeli University, Izmit, Kocaeli 41380, Turkey

Abstract— A procedure is developed which leads to a relation that can be used to argue the negation of the Special Relativity Theory when there exists a general homogeneous bianisotropic medium with dissipation. The unbounded general bianisotropic medium is interfaced with a perfectly conducting medium filling a half space so that the interface is an infinite plane. The perfectly conducting half space (medium (II)) is assumed to move uniformly and along the $O'z'$ axis of the Galilean reference system K' which is attached to medium (II), and the interface plane with medium (I), the bianisotropic medium which is at rest and to which is attached the Galilean reference system K, is assumed to be perpendicular to the $O'z'$ axis. The relation found is between constitutive parameters, the direction cosines with respect to $Oxyz$ axes of the incident plane wave impingent on the infinite plane interface, the incident wave parameters, v_1 the relative speed of K' with respect to K and c the speed of light in vacuum. This relation is shown to be interpretable to falsify the Special Relativity Theory. On the other hand it is demonstrated also that when the same homogeneous bianisotropic medium without loss is considered no such relation can be obtained and the Special Relativity Theory can not be contradicted.

Three examples are presented. One for a lossless electrically uniaxially anistropic medium, one for a dissipative simple medium and another for a dissipative electrically uniaxially anistropic medium. While the first one does not lead to any contradiction of Maxwell's equations with Special relativity Theory, the other two are shown to lead to such relations.

Enhanced Gain Planar Inverted-F Antenna with Metamaterial Superstrate for UMTS Applications

Hussein Attia, Mohammed M. Bait-Suwailam, and O. M. Ramahi
University of Waterloo, Waterloo, Canada

Abstract— Planar inverted-F (PIFA) antennas are widely used in wireless handheld devices due to their small-size, moderate bandwidth and radiation patterns. However, the radiation patterns of such antennas degrade when placed very close to a conductive finite ground plane. In this paper, an engineered magnetic superstrate is introduced to enhance the gain of PIFA antennas. The artificial magnetic superstrate is based on the broad-side coupled split ring resonator (SRR) inclusions which have high real permeability values at the resonance frequency of the antenna. Numerical full-wave simulations are carried out to analyze the entire radiating system (antenna with superstrate). By using the magnetic superstrate, a 3.2 dB improvement in the gain of the PIFA antenna working in the UMTS band was achieved. The total height of the proposed superstrate over the antenna is only $\lambda_0/14$ where λ_0 is the free-space wavelength at antenna's resonance frequency. Thus, the antenna structure remains low-profile, and is advantageous in many wireless handheld devices.

Session 2A5
Phase-Space Optics

Phase Space Analysis of Complex Optical Systems and Optics Challenges for Next Generation Synchrotron X-ray Sources

Detlef-M. Smilgies
Cornell High Energy Synchrotron Source (CHESS), Cornell University, Ithaca, NY 14853, USA

Abstract— Modern synchrotron radiation beamlines with multiple end stations require complex optical systems which need to be carefully modelled to optimize performance [1]. Within the paraxial approximation I have developed a compact 5D algorithm based on matrices and determinants, to characterize the relevant phase space quantities (beam size, divergence, and energy spread) with respect to their widths and correlations [2]. The optics modelling needs for next generation synchrotron light sources, just becoming operative and currently under design or planning, will be outlined.

REFERENCES

1. Ferrero, C., D.-M. Smilgies, C. Riekel, G. Gatta, and P. Daly, "New possibilities in phase space analysis of synchrotron radiation X-ray optics," *Applied Optics*, Vol. 47, E116–E124, 2008, (Special Issue on Phase Space Methods in Optics).
2. Smilgies, D.-M., "Compact matrix formalism for phase space analysis of complex optical systems," *Applied Optics*, Vol. 47, E106–E115, 2008, (Special Issue on Phase Space Methods in Optics).

Temporal Filtering in Phase-space

Cristina M. Gómez-Sarabia[1], **Pedro Andrés**[2], **and Jorge Ojeda-Castañeda**[1]

[1]University of Guanajuato, Salamanca, Guanajuato 36885, México
[2]Optics Department, Universitat de València, E46100 Burjassot, Valencia, Spain

Abstract— For visualizing the intensity-spectrum evolution through propagation, in a first-order dispersive medium, we use the formalism of phase-space representations. The formalism describes in a novel fashion the space-time duality between paraxial diffraction and linear dispersion of optical pulses. We explore new analogies between temporal filtering and space filtering.

Introduction: There is a useful analogy (duality) between the equations that describe paraxial, scalar diffraction and first-order temporal dispersion of optical short pulses. In a nutshell, the temporal frequency corresponds to the spatial frequency, in the lateral direction, time t corresponds to the z coordinate along the optical axis [1]. And consequently, there is also a correspondence between the temporal spectra and spatial frequency spectrum [2].

Novel Methods for Processing Temporal Signals: The spatial-temporal analogy helps to relate optical elements (prisms, lenses and zone plates) to temporal processing devices, which are useful for optical pulse compression, and for implementing temporal correlation and convolutions [3].

Here, we use the formalism of phase-space representations for visualizing the intensity-spectrum evolution through propagation, in a first-order dispersive medium. Based on this formalism, we explore new analogies between temporal filtering and space filtering.

REFERENCES

1. Lohmann, A. W. and D. Mendlovic, "Temporal filtering with time lenses," *Applied Optics*, Vol. 31, 6212–2746, 1992.
2. Flores-Arias, M. T., L. Chantada, C. Bao, M. V. Pérez, and C. Gómez-Reino, "Temporal zone plate," *J. Opt. Soc. Am. A*, Vol. 25, 3077–3082, 2008.
3. Dorrer, C. and I. Wamsley, "Phase space in ultrafast optics," *Phase-space Optics: Fundamentals and Applications*, Chapter 11, 337–383, Eds. M. Testorf, B. Hennelly, and J. Ojeda-Castaneda, McGraw-Hill, 2010.

Temporal Zone Plate by Linear Chirp Generator

Carlos Gomez-Reino, **Ana I. Gómez-Varela**, **Carmen Bao Varela**, **and M. Teresa Flores-Arias**
GRIN Optics Group, Optics and Optometry School and Faculty of Physics, Campus Sur,
Universidade de Santiago de Compostela, E15782 Santiago de Compostela, Spain

Abstract— By exploting the space-time duality between the paraxial diffraction of ligth confined in space and the linear dispersion of optical pulses in dielectrics it presents the time-domain analog of a spatial multiple image system, that is, of a spatial zone plate. The temporal system is created by a digital chirp signal generator with two dispersive lines. The linear chirp generator is used to design temporal generalized zone plates of phase or amplitude that compress in a multiple fashion optical pulses propagating in linear dispersive media. The temporal zone plates are represented by a sequence of rectangular pulses which takes two levels $+1$ and -1, for phase zone plates, or 1 and 0, for amplitude zone plates, arranged in such a way that the width of the zones (or pulses) is constant in time squared, and thus the width decreases in time with the square root of the zones of the natural numbers, just as does the width of the zones of the spatial zone plates. The temporal zone plate produces a quadratic-phase modulation of an optical pulse propagating through a dispersive delay line, and it acts as time multifocal lens. It was derived the condition which gives at the output multiple images of the input. Of particular interest is the case where the width of the unit cell of the temporal zone plate equals the semiperiod of a temporal zone. In this case, the rectangular form representing the binary modulation function of the temporal zone plate becomes the square form giving rise to the Fresnel zone plate in time. Main difference between such a temporal zone plate and a generalized zone plate in time is discussed. As an example to illustrate the behavior of a temporal multiple image system, it was considered an optical pulse propagating through a standard single-mode fiber. A digital chirp generator produces a train of rectangular pulses. The phase modulated signal was launched into a dispersion-shifted fiber and the multiple compression of the input signal was analyzed.

Second Order Moments of Superpositions of Hermite-Laguerre-Gauss Modes

A. Cámara and T. Alieva
Facultad de Ciencias Físicas, Universidad Complutense de Madrid
Avda. Complutense, s/n, Madrid E-28040, Spain

Abstract— The second order moments of the Wigner distribution of a beam are widely used for coherent and partially coherent beam characterization [1, 2]. Parameters such as the size in phase space, the orbital angular momentum, and the quality factor of the beam can be obtained from the second order moments. The analytical expression of these moments for a coherent beam expanded in series of Hermite-Gauss (HG) modes was developed in [3].

Besides the HG functions, there exist other families of orthonormal modes such as the Laguerre-Gauss (LG) modes and the Hermite-Laguerre-Gauss (HLG) modes. These modes are stable (they propagate without changing the form of their intensity distribution) and are used as a basis for the construction of rotating beams [4]. Moreover, the HLG modes as well as the LG modes can be obtained from the HG ones applying the gyrator transform [4].

In this contribution we generalize the formula developed by Bekshaev [3] to the case of partially coherent beams and derive the expression for the second order moments of the field expanded in series of HLG modes. Starting from the representation of the mutual intensity as series of HG modes and performing the Fourier transform we obtain the expression for the WD as series of LG modes. After proper integration, the WD moments of arbitrary order are obtained. In particular, for coherent fields, the expression for the second order moments is the same as in Ref. [3]. Using the transformation law for the second order moment matrix during the beam propagation through an ABCD-system, and in particular for the one described by the gyrator transform, the desired expression can be found.

Furthermore, the field expansion in LG modes is useful for the analysis of the second order moments of spiral beams [5, 6]. A spiral beam can be constructed as a superposition of LG modes whose indexes are restrained by a relation that defines its angular velocity. Note that its intensity distribution performs a rotation during free space propagation, maintaining the shape invariant. This property is attractive for many applications, including microparticle manipulation, microscopy depth estimation, etc. [5, 7].

REFERENCES

1. Siegman, A. E., "New developments in laser resonators," *Optical Resonators: Proc. SPIE*, Vol. 1224, No. 2, 1990.
2. Serna, J., R. Martnez-Herrero, and P. Mejas, "Parametric characterization of general partially coherent beams propagating through ABCD optical systems," *J. Opt. Soc. Am. A*, Vol. 8, 1094–1098, 1991.
3. Bekshaev, A. Y., "Intensity moments of a laser beam formed by superposition of Hermite-Gaussian modes," *Fotoelektronika*, Vol. 8, 22–25, 1999.
4. Rodrigo, J. A., T. Alieva, and M. L. Calvo, "Gyrator transform: Properties and applications," *Opt. Express*, Vol. 15, 2190–2203, 2007.
5. Abramochkin, E. and V. Volostnikov, "Spiral light beams," *Phys. Usp.*, Vol. 47, 1177–1203, 2004.
6. Asenjo García, A. and T. Alieva, "Alternative approach for rotating beam description," *Proceedings of the Topical Meeting on Optoinformatics*, 243–246, St. Petersburg, Russia, September 2008.
7. Greengard, A., Y. Y. Schechner, and R. Piestun, "Depth from diffracted rotation," *Opt. Lett.*, Vol. 31, 181–183, 2006.

The Phase-space Interpretation of Self-imaging and the Phase Retrieval Problem

Markus E. Testorf
Thayer School of Engineering at Dartmouth College, USA

Abstract— The Talbot effect [1] also known as self-imaging describes the propagation of a coherent optical wavefront, which is strictly periodic in lateral direction. In this case the complex amplitude distribution is automatically periodic in the direction of propagation. The longitudinal period is known as the Talbot distance. Fresnel diffraction at rational fractions of the Talbot distance is known as Fresnel imaging, or the fractional Talbot effect [2]. The fractional Talbot effect is remarkable in that it represents a discrete set of propagation distances for which the Fresnel diffraction integral can expressed analytically in simple form.

Self-imaging and related phenomena are particularly well suited to be investigated in terms of phase-space optics [3]. Using diagrams of the joint space-spatial frequency representation of the Wigner distribution function it is possible to derive all essential quantitative relationships from simple geometrical constructions and algebraic calculations.

Here, the phase-space analysis of self-imaging is used as a tool to address the phase retrieval problem. This is motivated by previous investigations aimed at designing periodic diffractive optical elements able to generate a predefined three-dimensional intensity distribution [4]. The use of the fractional Talbot effect as a conceptual framework has proved pivotal to determine the degrees of freedom for the design and the relation between the constraints of the optimization problem and the quality of the design.

The phase-retrieval problem constitutes a variant of the design problem. The three-dimensional intensity distribution which determines the complex amplitude in the input plane is given as a set of measurements, i.e., compared to the design problem it is ensured that the inverse problem has at least one solution. For a functional phase-retrieval method it is also important to retrieve the true complex phase, which is of less importance for the design problem, where any match of the desired intensity is regarded as a valid solution.

By considering deterministic phase retrieval methods, and namely phase-space tomography [5], the fractional Talbot effect can be identified as a special case, for which it is possible to identify uniquely the set of measurements necessary for recovering the complex amplitude of a single period of the wavefront with a given resolution. Each pixel of the unknown complex amplitude corresponds to a voxel in phase space which is recovered tomographically. As compared to the standard formulation of phase-space tomography, the discrete phase-space representation of periodic pixelated signals allows one to obtain unambiguous expression for the set of data required for successful retrieval of the phase information. In addition, relationships between the accuracy of the phase recovery and measurement errors estimated analytically, or semi-analytically.

REFERENCES

1. Talbot, H. F., "Facts relating to optical science. No. IV," *Philosophical Mag., J. Sci.*, Vol. 9, 401–407, 1836.
2. Winthrop, J. T. and C. R. Worthington, "Theory of Fresnel Images. I. Plane periodic objects in monochromatic light," *J. Opt. Soc. Am*, Vol. 55, 373–381, 1965.
3. Testorf, M. E., "Self-imaging in phase space," in M. Testorf, B. Hennelly, J. Ojeda-Castañeda, eds., *Phase-space Optics, Fundamentals and Applications*, 279–307, McGraw-Hill, New York, 2009.
4. Testorf, M., T. J. Suleski, and Y.-C. Chuang, "Design of Talbot array illuminators for three-dimensional intensity distributions," *Opt. Express*, Vol. 14, 7623–7629, 2006.
5. Semichaevsky, A. and M. Testorf, "Phase-space interpretation of deterministic phase retrieval," *J. Opt. Soc. Am. A*, Vol. 21, 2173–2179, 2004.

Digital Holography in the Light of Phase Space

B. M. Hennelly
Department of Computer Science, National University of Ireland, Maynooth, Co. Kildare, Ireland

Abstract— Digital Holography is an optoelectronic mode of imaging. The first half of digital holography is to record either one or multiple interferograms using a digital camera. These interferograms are recorded by intersecting a known reference beam with the light scattered by a reflecting or transmissive object. The second half of a digital holographc system is to numerically reconstruct the image using the recorded hologram as input to a numerical algorithm that simulates optical propagation of the wave field to the image plane. There are a host of different algorithms that can do this, each varying in accuracy and time taken and each providing a different point spread function for the overall record-reconstruction system. Microscopic digital holographic systems make use of a microscopic objective between the object and CCD and have become increasingly popular in recent years. This is firstly because because one can employ phase contrast techniques to the phase of the reconstructed image and secondly because it becomes possible to remove various types of aberrations digitally from these systems. In this paper we discuss both the recording and the reconstruction sides of digital holography from the phase space perspective. We show how phase space diagrams may be used to gain insight in the recording method and it provides a means of comparing different architectures in terms of resolution and information capacity. In addition we show how the numerical reconstruction algorithms may also be interpreted in phase space leading to optimisations as well as a framework for the invention of new algorithms.

Wigner Based Phase Space as a Tool to Analyze Super Resolved Imaging Configurations

Zeev Zalevsky
School of Engineering, Bar-Ilan University, Ramat-Gan 52900, Israel

Abstract— The resolution of conventional diffraction limited imaging systems is determined by the product between their F-number and the wavelength. This product determines the smallest spatial feature or degrees of freedom that can be transmitted through the system.

The process of super resolution involves conversion of the spatial degrees of freedom to other not fully occupied (with data) domains that are acceptable by the imaging system (e.g., code, time, field of view, wavelength or even the amount of light's coherence) such that those degrees of freedom will not be blocked by the system. Then, after their successful transmission through the system the spatial degrees of freedom are back converted into the space domain to reconstruct the requested high resolution image. This process is called adaptation of degrees of freedom. The multiplexing process itself is basically based upon encoding and decoding of spatial information. In order to do the adaptation properly one needs to have apriori knowledge that indeed those domains are not fully occupied by information and that there is sufficient "space" available there to accommodate the converted spatial degrees of freedom.

In this paper we provide a schematic description and an explanation for how the process of super resolved imaging may be understood by using Wigner based phase space. The advantage of using the Wigner space is related to the fact that it can mathematically be related to the spatial degrees of freedom of a signal and thus be used to understand how super resolving imaging system operates.

In this talk, we will focus on the diffraction related limitation of resolution where usage of Wigner phase space will be demonstrated for five types of multiplexing configurations: code, time, polarization, wavelength and gray levels. The operation principle of each type of super resolution concept will be illustrated and elaborated using the Wigner phase space.

Tomographic Reconstruction of the Wigner Distribution of Non-separable Beams

A. Cámara[1], **T. Alieva**[1], **J. A. Rodrigo**[2], **and M. L. Calvo**[1]

[1]Facultad de Ciencias Físicas, Universidad Complutense de Madrid
Avda. Complutense, s/n, Madrid E-28040, Spain
[2]Instituto de Óptica (CSIC), Imaging and Vision Department
Serrano 121, Madrid E-28006, Spain

Abstract— The determination of the phase of coherent beams or the mutual intensity of partially coherent beams is of great importance in many applications which require optical field characterization. Different interferometric and iterative methods have been developed to obtain this information, thought they present difficulties that make them unsuitable for a fast and precise determination of the mutual intensity of optical fields.

In 1994, a new method for the reconstruction of the Wigner distribution (WD) of a coherent or partially coherent beam from its projections was established [1]. The phase or the mutual intensity can be obtained applying the inverse Fourier transform to the WD. This reconstruction method is based on the rotation of the WD during the fractional Fourier transform (FRFT), and the fact that the intensity distribution at the output of a system performing the FRFT (fractional power spectrum) is associated to a WD projection. The lack of suitable optical systems to perform the FRFT of variable order has delayed the development of the method.

Recently, an experimental setup capable of performing the antisymmetric FRFT was proposed [2]. This system allowed the verification of the tomographic reconstruction of the WD for the case of separable beams [3]. The optical system consists of two generalized lenses separated a fixed distance. Each of them is formed by two convergent cylindrical lenses of the same power. The transformation parameter is changed by rotation of the cylindrical lenses.

In this contribution we extend the former work to beams which cannot be factorized in both orthogonal transversal directions (non-separable beams). For its implementation we use an optical system able to perform the FRFT without additional scales for any pair of transformation angles (α, β), where α,$\beta \in [\pi/2, 3\pi/2]$, which has been recently reported in Ref. [4]. This optical system is also constructed by two generalized lenses placed at a fixed distance, but they are implemented in spatial light modulators (SLMs) in order to achieve almost real-time performace in the fractional power spectra measurements.

We also propose a comprehensive way to display the WD of the non-separable beam. This is not a trivial task as the WD is a real-valued function that depends on four variables. By representing it as a 2D array of colored surface plots we gain the four variables (row and column of the array and two variables of the colored surface plot) to represent the value of the function (the color). Based on such graphics for the theoretical, the simulated and the experimental WD we demonstrate the feasibility of the proposed method for the case of the Laguerre-Gauss mode.

REFERENCES

1. Raymer, M. G., M. Beck, and D. F. McAlister, "Complex wave-field reconstruction using phase-space tomography," *Phys. Rev. Lett.*, Vol. 72, 1137–1140, 1994.
2. Rodrigo, J. A., T. Alieva, and M. L. Calvo, "Experimental implementation of the gyrator transform," *J. Opt. Soc. Am. A*, Vol. 24, 3135–3139, 2007.
3. Cámara, A., T. Alieva, J. A. Rodrigo, and M. L. Calvo, "Phase space tomography reconstruction of the Wigner distribution for optical beams separable in Cartesian coordinates," *J. Opt. Soc. Am. A*, Vol. 26, 1301–1306, 2009.
4. Rodrigo, J. A., T. Alieva, and M. L. Calvo, "Programmable two-dimensional optical fractional Fourier processor," *Opt. Express*, Vol. 17, 4976–4983, 2009.

Tunable Phase Masks for Extended Depth of Field

Jorge Ojeda-Castañeda, Myrna M. Rodríguez, and Rafael Naranjo
University of Guanajuato, Salamanca, Guanajuato 36885, México

Abstract— We apply the ambiguity function for designing a pair of phase masks that reduce the influence of focus errors, on the Modulation Transfer Function. We show that by using this pair of masks, in a tunable fashion one can extend the depth of field of an optical system.

Introduction: By using two suitable pair of phase masks, it is possible to implement a lens with variable optical power [1, 2]. On the other hand, it is known that some nonconventional phase masks are able to reduce the influence of focus error [3] on the Modulation Transfer Function (MTF) of an optical system. Here, we discuss the use of a pair of phase masks, which can extend the depth of field in a tunable fashion.

Ambiguity Function: The ambiguity function, of the pupil mask, is a powerful tool for analyzing the MTF of an optical system suffering from focus errors. Low sensitivity to focus errors is characterized by an ambiguity function with a "bow-tie" shape [3].

Here we indicate that the MTF of an optical system, suffering from focus errors, can suitably be shaped by employing a pair of conjugate phase elements. We show that in a tunable fashion, one can extend the depth of field of an optical system.

REFERENCES

1. Alvarez, L. W., "Two-element variable-power spherical lens," U.S. Patent 3, 305, 294, December 3, 1964.
2. Lohmann, A. W., "Lente focale variabile," Italian Patent 727,848, June 19, 1964.
3. Ojeda-Castañeda, J., J. E. A. Landgrave, and C. M. Gómez-Sarabia, "Conjugate phase plate use in analysis of the frequency response of optical systems designed for extended depth of field," *Applied Optics*, Vol. 47, No. 22, E1–E7, 2008.

Session 2A6
Photonic Crystals and Metamaterials 1

Equivalent Circuit Models for Split-ring Resonator Arrays

P. Yasar-Orten[1, 2], **E. Ekmekci**[1], **and G. Turhan-Sayan**[1]

[1]Department of Electrical and Electronics Engineering, Middle East Technical University, Ankara, Turkey
[2]ASELSAN Inc., Macunkoy, Ankara, Turkey

Abstract— Split Ring Resonator (SRR) is a well-known sub-wavelength metamaterial structure that exhibits negative values of permeability (μ) over a narrow frequency band when it resonates. Theory and applications of single ring, double ring or multiple ring SRR cells with circular or square/rectangular geometry have been investigated in microwave and optical frequencies in a large number of publications so far. Most of those studies have investigated the SRR behavior experimentally and/or numerically by using full-wave electromagnetic solvers such as the commercially available software packages HFSS and CST Microwave Studio. Number of publications concentrated on the investigation of SRR structures with equivalent circuit models has been relatively few. The experimental and numerical approaches have certainly been useful to conveniently analyze the already designed SRR structures. On the other hand, research studies for detailed modeling of SRR arrays by equivalent circuits are also needed for systematic design work. Such models will be invaluable to understand the coupling effects and loss effects in metamaterial arrays. Optimization of complicated array structures which are required to satisfy certain operational constraints will also be feasible if reliable and easily computable equivalent circuit models can be established.

In this study, a square-shaped single ring resonator with multiple-splits will be modeled first by using an admissible two-port equivalent circuit that also accounts for the conductor loss and dielectric loss effects. Next, the capacitive and inductive coupling effects as well as the additional coupling related dielectric loss effects between two and three unit cells will be modeled. Finally, a one-dimensional array composed of such SRR unit cells will be investigated. Analysis results of the equivalent circuit models will be compared to the numerical simulation results obtained by HFSS simulations for dependable validation.

Effects of Substrate Parameters on the Resonance Frequency of Double-sided SRR Structures under Two Different Excitations

E. Ekmekci[1, 2, 3], **R. D. Averitt**[3], **and G. Turhan-Sayan**[1]

[1]Department of Electrical and Electronics Engineering, Middle East Technical University, Ankara, Turkey
[2]Department of Electronics and Communication Engineering, Suleyman Demirel University Isparta, Turkey
[3]Department of Physics, Boston University, Boston, MA, USA

Abstract— The Split Ring Resonator (SRR) is a well-known and a special metamaterial structure, which finds itself so many applications in microwave and THz regions. Due to its special geometry, an applied time-varying magnetic field through the SRR axis induces a circulating current along the ring as it is shown in Figure 1(a). This induction mechanism results in a magnetic resonance, which leads to negative values of permeability (μ) over a relatively small frequency band. Herein, the value of the resonance frequency (f_0) is very important, because it is basically used to control the location of the μ-negative (MNG) region of frequency. In conventional THz transmission/reflection measurement setups, it is a real challenge to apply a time-varying magnetic field through the SRR axis, instead, the SRRs are electrically excited as shown in Figure 1(b) which leads to electrical resonances resulting in ε-negative (ENG) behavior.

The effects of substrate parameters (i.e., substrate thickness and permittivity) on resonance frequency for ordinary SRR structures have been reported in the literature. In this study, we investigate the effects of substrate parameters on double-sided SRR (DSRR) structures under two different excitations in a comparative manner. CST's Microwave Studio is used to obtain transmission spectra (i.e., magnitude of S_{21} spectra) in order to find the resonance frequencies. The results shows that, unlike the SRR structures, resonance frequencies of the DSRR structures are affected differently with respect to the changes in the substrate parameters under two different excitations.

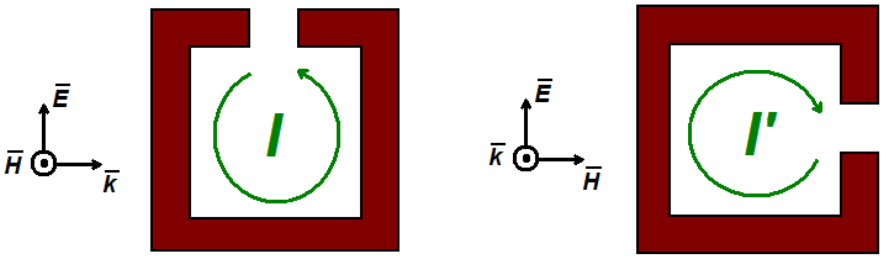

Figure 1: Two different SRR excitation techniques. (a) Magnetic excitation. (b) Electrical excitation.

Transmission through Kerr Media Waveguide Barriers: Dispersive Properties

A. R. McGurn
Western Michigan University, USA

Abstract— The transmission properties of guided waves in photonic crystal waveguides containing barriers formed from Kerr nonlinear media are studied theoretically using a difference equations approach. The photonic crystal waveguides are formed in a two-dimensional (square lattice) photonic crystal of linear dielectric cylinders by cylinder replacement, with replacement cylinders made of linear dielectric media. The channel of the waveguide is along the x-axis of the photonic crystal. Barriers formed of Kerr nonlinear media are introduced into the waveguide by cylinder replacement of waveguide cylinders in the barrier region with cylinders containing Kerr nonlinear media. The transmission of guided waves incident on the Kerr media barriers, from the linear media waveguides, is computed and studied as a function of two parameters characterizing the Kerr nonlinear barrier media and the wave number of the incident guided wave. A focus of the study is on the excitation of intrinsic localized modes within the barrier media and on the effects on these modes of additional in-channel and off-channel features that are introduced to or couple to the barrier of Kerr media. The off-channel and in-channel features may be formed of linear media and/or Kerr nonlinear media and are made by cylinder replacements within the barrier or within the photonic crystal sites adjacent to the barrier. In addition, the transmission properties of some basic photonic crystal circuits built from the earlier mentioned waveguide elements are discussed. A presentation and classification of the various types of modes excited by the resonant transmission of incident guided waves with different wave numbers are given in a two-parameter space characterizing the dielectric properties of the Kerr barrier media. Systems are found to exhibit a variety of single and multiple types of intrinsic localized modes and various kinds of Fabry-Perot excitations. Suggestions are presented for device applications involving amplification, switching, and rectification of modulated guided waves.

Light Transport in Disordered Metamaterials Made of Nanorods

Didier Felbacq[1], **Kevin Vynck**[2], **and Brahim Guizal**[1]

[1]Groupe d'Etude des Semiconducteurs UMR-CNRS 5650, Université de Montpellier 2, Montpellier, France
[2]European Laboratory for Non-linear Spectroscopy, Florence, Italy

Abstract— Light transport in two-dimensional disordered metamaterials made of high-permittivity rods is studied theoretically. Different regimes of transport are observed and explained in terms of coupled electric and magnetic dipolar resonances. Light propagation at frequencies close to the magnetic dipole resonance is shown to rely on hybrid, necklace-like, states.

Introduction: All-dielectric metamaterials have attracted much attention recently because of their potential ability to manipulate light without loss at optical frequencies [1]. Dielectric nano-rods in s-polarization have been shown to support overlapping electric and magnetic dipole resonances, yielding a left-handed behavior in periodic arrays of them [2, 3]. Interestingly, experiments by Peng and coworkers [2] revealed that this behavior was not particularly sensitive to structural disorder. Previous studies had also shown that photonic band gaps could resist a relatively high degree of disorder [4]. Actually, disorder is of critical importance for nanophotonics applications and is known to result in complex optical phenomena [5].

Light Transport: In this work, we study light transport in disordered arrays of high-permittivity nanorods by means of the scattering matrix method [6]. Such arrays are shown to exhibit three distinct regimes of transport, described by positive and/or negative effective permittivity ε_{eff} and permeability μ_{eff} (in s-polarisation). We find that disorder has only a weak effect on the "dielectric" optical features of the structure, i.e., right-handed bands ($\varepsilon_{eff} > 0$; $\mu_{eff} > 0$) and photonic band gaps ($\varepsilon_{eff} < 0$; $\mu_{eff} > 0$). The existence of an artificial magnetic activity at frequencies close to the magnetic dipolar resonance is evidenced by calculating the total magnetic moment. The structural disorder is found to play a critical role on light propagation in the double-negative ($\varepsilon_{eff} < 0$; $\mu_{eff} < 0$) frequency range. Microscopically, light transport is supported by hybrid modes assimilable to necklace states [7].

ACKNOWLEDGMENT

This work is partially supported by the french ANR project POEM-PNANO 06. Support from the Institut Universitaire de France is gratefully acknowledged.

REFERENCES

1. Ahmadi, A. and H. Mosallaei "Physical configuration and performance modeling of all-dielectric metamaterials," *Phys. Rev. B*, Vol. 77, No. 4, 045104, 2008.
2. Peng, L., et al., "Experimental observation of left-handed behavior in an array of standard dielectric resonators," *Phys. Rev. Lett.*, Vol. 98, No. 15, 157403, 2007.
3. Vynck, K., et al., "All-dielectric rod-type metamaterials at optical frequencies," *Phys. Rev. Lett.*, Vol. 102, No. 13, 133901, 2009.
4. Rockstuhl, C., U. Peschel, and F. Lederer, "Correlation between single-cylinder properties and bandgap formation in photonic structures," *Opt. Lett.*, Vol. 31, No. 11, 141–143, 2006.
5. Sheng, P., *Introduction to Wave Scattering, Localization and Mesoscopic Phenomena*, 2nd Edition, Springer, 2006.
6. Felbacq, D., G. Tayeb, and D. Maystre, "Scattering by a random set of parallel cylinders," *J. Opt. Soc. Am. A*, Vol. 11, No. 9, 2526–2538, 1994.
7. Pendry, J. B., "Quasi-extended electron states in strongly disordered systems," *J. Phys. C*, Vol. 20, No. 5, 733–742, 1987.

Photonic Crystal Fiber Analysis Using Cylindrical FDTD with Bloch Boundary Conditions

Adam Mock and Paul Trader
School of Engineering and Technology, Central Michigan University, Mt. Pleasant, MI, USA

Abstract— In this presentation an efficient approach to analyzing structures in cylindrical coordinates with periodic variation in the azimuthal direction is discussed. The specific structure of interest is photonic crystal fiber. Photonic crystal fiber is similar to conventional glass fiber, except that a microstructured periodic pattern is imparted to the cross section of the fiber. This periodic pattern can greatly modify the dispersion, loss and field properties of the propagating modes of the fiber [1]. In particular, if the photonic crystal supports photonic bandgap at the frequency of interest, the confinement of the fiber can be based on bandgap guiding instead of the conventional mechanism of total internal reflection. This has given rise to fibers with single mode behavior over wide bandwidth. Bandgap guiding has also made it possible to guide light in hollow core fibers where the majority of the field profile exists in silica free region. This has given rise to lower absorption loss and reduced unwanted nonlinearities associated with the fiber material. It has also proven useful for gas and liquid sensing. The hollow core fiber is infiltrated with gas or liquid. As the properties of the analyte change, so do its refractive index and absorption spectrum causing the electromagnetic properties of the fiber modes to change as well.

The modal properties of conventional fiber are well understood, and approximate closed form solutions exist [2]. The modal properties of photonic crystal fiber are still under investigation. The complicated hole pattern makes it difficult to write down solutions to Maxwell's equations in terms of known functions, and numerical analysis is typically required. Several techniques exist to perform the numerical analysis including the finite element method, finite difference frequency domain method and the finite difference time domain (FDTD) method [3]. In this work the FDTD method in cylindrical coordinates is used.

Because fiber geometries are uniform along the propagation direction, the computational burden can be reduced by assuming the field behavior along the propagation direction (z direction) is $\exp(j\beta z)$. Derivatives with respect to z do not need to be discretized and are represented simply as $\partial/\partial z = j\beta$. This allows for three dimensional fully vectorial analysis of the fiber using only two dimensional computer arrays for the cross section of the fiber. In conventional fiber in which the structure is uniform along the azimuthal direction as well, the azimuthal (ϕ) dependence can be represented as $\sin(m\phi)$ and $\cos(m\phi)$ where m is an integer. This represents further reduction in computational dimensionality. The only variation is in the radial direction, and only one dimensional arrays are needed [4]. In this scheme, individual simulation runs are carried out for each value of β and m.

In the case of photonic crystal fibers, the material is not uniform along the azimuthal direction. However, in many geometries it is periodic. For example, if triangular lattice is used with single missing hole defect for the core, the structure is periodic with six periods contained in the 2π azimuthal range. In this talk we will discuss using Bloch boundary conditions, so that only single period of the structure need be analyzed. This reduces the computational burden by factor of six in this example. The method will be discussed and applied to specific photonic crystal fiber geometries. Advantages and disadvantages will be discussed as well as future prospects and improvements.

REFERENCES

1. Russell, P. St. J., "Photonic-crystal fibers," *IEEE Journal of Lightwave Technology*, Vol. 24, No. 12, 4729–4749, 2006.
2. Marcuse, D., *Theory of Dielectric Optical Waveguides*, 2nd Edition, Academic Press, Inc., San Diego, CA, 1991.
3. Saitoh, K. and M. Koshiba, "Numerical modeling of photonic crystal fibers," *IEEE Journal of Lightwave Technology*, Vol. 23, No. 11, 3580–3590, 2005.
4. Yinchao, C. and R. Mittra, "A highly efficient finite-difference time-domain algorithm for analyzing axisymmetric waveguides," *Microwave and Optical Technology Letters*, Vol. 15, No. 4, 201–203, 1997.

Electro-inductive Waves for Geometrically-induced Plasmon-like Waves

M. Navarro-Cía[1], M. Beruete[1], S. Agrafiotis[2], F. Falcone[1], M. Sorolla[1], and S. A. Maier[2]

[1]Millimeter and Terahertz Waves Laboratory, Universidad Pública de Navarra, Spain
[2]Experimental Solid State Group, Physics Department, Imperial College London, UK

Abstract— Geometrically-induced surface waves [1] have recently attracted a lot of attention, because they can be a powerful tool to achieve tight bound modes at, for instance, THz, where common surface waves are loosely bound. This feature opens the path for efficient planar guiding in a regime where planar guiding is mainly limited to Goubau lines [2]. Nevertheless, classical geometrically-induced modes are based on simple periodic structures such as slit arrays or hole arrays, and, even though the confinement of the waves is enhanced with respect to Sommerfeld-Zenneck THz surface waves, it is still low for successful enrouting. Recently, more complex structures using the so-called Sievenpiper mushroom geometry [3] or complementary split-ring resonators [4] have reported as alternative candidates provided that their surface plasmon-like response is governed by several structural dimensions of the unit cell, giving more degree of freedom for design. In fact, true subwavelength confinement has been reported [3, 4].

From an engineering perspective based on equivalent circuit models and transmission lines, we give an explanation of both classical and Sievenpiper mushroom geometries by linking the surface plasmon frequency with the resonant frequency of the effective surface impedance. Moreover, stimulated by metamaterials and keeping this useful engineering perspective, we design another geometry based on complementary split ring resonators [4] in such a way that the supported electro-inductive fundamental mode exhibits tight confinement and resembles a TM-polarized surface plasmon polariton at the same time [5]. This qualitative analysis is supported by numerical results based on dispersion diagrams, field distribution, and electric energy density.

In conclusion, we review the classical geometrically-induced modes from equivalent circuit models and take advantage of this formalism to design a new structure that defeat in terms of energy confinement those presented up to day.

REFERENCES

1. Pendry, J. B., L. Martín-Moreno, and F. J. García-Vidal, "Mimicking surface plasmons with structured surfaces," *Science*, Vol. 305, 847–848, 2004.
2. Goubau, G, "Surface waves and their application to transmission line," *J. Appl. Phys.*, Vol. 21, 1119–1128, 1950.
3. Lockyear, M. J., A. P. Hibbins, and J. R. Sambles, "Microwave surface-plasmon-like modes on thin metamaterials," *Phys. Rev. Lett.*, Vol. 102, 1–4, 2009.
4. Falcone, F., et al., "Babinet principle applied to metasurface and metamaterial design," *Phys. Rev. Lett.*, Vol. 93, 1–4, 2004.
5. Navarro-Cía, M., M. Beruete, S. Agrafiotis, F. Falcone, M. Sorolla, and S. A. Maier, "Broadband spoof plasmons and subwavelength electromagnetic energy confinement on ultrathin metafilms," *Opt. Express*, Vol. 17, 18184–18195, 2009.

Simultaneous Negative and Positive Refraction Depending on the Incident Polarization to a Stacked Metasurfaces Prism

M. Navarro-Cía[1], **M. Beruete**[1], **F. Falcone**[1], **I. Campillo**[2], **and M. Sorolla**[1]

[1]Millimeter and Terahertz Waves Laboratory, Universidad Pública de Navarra, Spain
[2]CIC nanoGUNE Consolider, Tolosa Hiribidea 76, Donostia 20018, Spain

Abstract— Recently, it has been shown that extraordinary transmission and left-handed media can be merged in the same structure so as to overcome losses at millimeter-waves [1]. All this features were confirmed by interferometric techniques [1] and wedge experiment [2]. Moreover, this approach has been successfully replicated at near-infrared [3] which proofs the potential at any region of the spectrum of the close-stacking of subwavelength hole arrays to achieve a low-loss extraordinary transmission metamaterial.

On the other hand, we reported that by a simple modification of the holey pattern, the single-layer could become a self-complementary screen [4]. This gave as a result a linear polarizer in first term, and subsequently a linear polarizer with left-handed propagation when the layers were stacked. However, a by-product of the modification is that we have more degrees of freedom to play around with the fundamental modes of each orthogonal polarization: vertical (incident electric field parallel to the slits that connect consecutive holes) and horizontal. And thus, instead of choosing the parameters in such a way that left-handed propagation is achieved for vertical polarization while the orthogonal polarization is inhibited, we can have a stacked structure with left-handed propagation and right-handed propagation for the vertical and horizontal polarization at the same time. This let us design a polarization rotator [5].

In this communication, we report a prism to check in a straightforward pure geometrical and experimental demonstration the refractions associated to each component. The effective index of refraction is retrieved via the Snell's law and compared to those obtained through the dispersion diagram and the retrieval method from S-parameters computed with the commercial software CST Microwave Studio^{TM}.

REFERENCES

1. Beruete, M., M. Sorolla, and I. Campillo, "Left-handed extraordinary optical transmission through a photonic crystal of subwavelength hole arrays," *Opt. Express*, Vol. 14, 5445–5455, 2006.
2. Navarro-Cía, M., M. Beruete, M. Sorolla, and I. Campillo, "Negative refraction in a prism made of stacked subwavelength hole arrays," *Opt. Express*, Vol. 16, 560–566, 2008.
3. Valentine, J., S. Zhang, T. Zentgraf, E. Ulin-Avila, D. A. Genov, G. Bartal, and X. Zhang, "Three-dimensional optical metamaterial with a negative refractive index," *Nature*, Vol. 455, 376–379, 2008.
4. Beruete, M., M. Navarro-Cía, M. Sorolla, and I. Campillo, "Polarized left-handed extraordinary optical transmission of subterahertz waves," *Opt. Express*, Vol. 15, 8125–8134, 2007.
5. Beruete, M., M. Navarro-Cía, M. Sorolla, and I. Campillo, "Polarization selection with stacked hole array metamaterial," *J. Appl. Phys.*, Vol. 103, 053102-1-4, 2008.

Modelling Double-heterostructure Cavities Using Perturbation Theory

S. Mahmoodian[1], K. B. Dossou[2], C. G. Poulton[2], R. C. McPhedran[1], L. C. Botten[2], and C. M. de Sterke[1]

[1]IPOS, CUDOS, School of Physics, University of Sydney, Australia
[2]CUDOS, School of Mathematical Sciences, University of Technology, Sydney, Australia

Abstract— Optical cavities that spatially confine light over periods of many optical cycles are perhaps the ultimate device in photonics. Recently, much research has been undertaken to use photonic crystal (PC) bandgaps to create cavities with large quality factors [1]. The PC geometry most commonly employed is the double-heterostructure cavity (DHC). The DHC consists of a PC slab waveguide being weakly perturbed to increase the amount of dielectric in spatial region. This creates localized mode in the perturbed region which is bound to the waveguide due to bandgap effects but cannot propagate along the waveguide due to the edges of the perturbation acting like mirrors. The out of plane confinement is due to total internal reflection (TIR); the cavity's quality factor is limited by the number of Fourier components of the cavity mode that satisfy the TIR condition. This quantity is intimately related to the envelope function of the cavity mode [1, 2].

Recently, perturbation theory has been shown to be useful tool to calculate the modes of weakly perturbed photonic crystals [3]. Since the DHC involves weakly perturbing structure, which is periodic in one direction, it is promising candidate to be investigated using perturbation theory. We do this by expanding the cavity mode using the Bloch functions of the PC slab waveguide and obtain an equation in the frequency ω and envelope function $f(x)$ of the DHC

$$\left[\frac{d^2}{dx^2} - C_L\omega_L\right] f(x) = -\frac{\omega^2 C_L}{\omega_L}\left[1 + \frac{d}{\varepsilon}\int \delta\epsilon(\mathbf{r})\|\mathbf{E}_L(\mathbf{r})\|dydz\right] f(x), \tag{1}$$

where the subscript L indicates the band-edge field and frequency, while C_L is the band-edge curvature of the dispersion relation, d is the period of the PC slab waveguide and ε is normalisation parameter. Figure 1 compares the envelope function with the E_x field calculated using finite difference time domain method. Here, the DHC is constructed by creating photosensitive change in refractive index with Gaussian profile. The agreement between the two is excellent. The advantage of the perturbation method is that it is orders of magnitude less computationally intensive and typical computations take less than minute. It also enables the modelling of truly infinite structures rather than extrapolating their physics from finite computation domain.

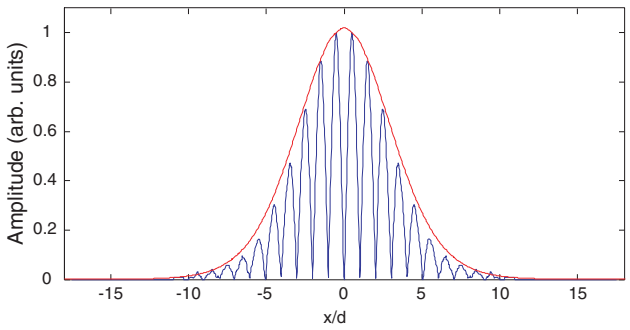

Figure 1: Comparison of envelope function (red) and FDTD calculations (blue) for DHC with period $= d$, slab height $= 0.7d$, hole radius $a = 0.29d$, background index $n_b = 2.7$, cylinder index $n_c = 1.0$. Gaussian photosensitive perturbation with width $\sigma = 6d$ and maximum index change $\Delta n = 0.02d$.

REFERENCES

1. Asano, T., et al., *IEEE Journal of Selected Topics in Quantum Electronics*, Vol. 12, No. 6, 1123, 2006.
2. Englund, D., et al., *Opt. Exp.*, Vol. 13, No. 16, 5961, 2005.
3. Mahmoodian, S., et al., *Opt. Exp.*, Vol. 17, No. 22, 19629, 2009.

Study of Resonance Effects in Dielectric Magneto-optical Structures through Analysis of Quasiguided Eigenmodes

D. A. Bykov[1, 2], **L. L. Doskolovich**[1, 2], **and N. L. Kazanskiy**[1, 2]

[1]Image Processing Systems Institute of RAS, Samara 443001, Russia
[2]Samara State Aerospace University, Samara 443086, Russia

Abstract— Magneto-optical (MO) properties of dielectric structure consisting of magnetized binary grating and magnetized homogeneous layer are investigated. The structure is magnetized in-plane perpendicularly to the grating slits (Figure 1, inset). Rigorous modeling revealed a resonance MO effects determined by the relative change in the intensity of the transmitted or reflected light when the sample is magnetized. Figures 1(a) and (b) show MO resonances in the transmission spectrum for both TE- and TM-polarizations of the incident wave. Magneto-optical effects are explained in terms of excitation of the structure eigenmodes. Eigenmodes' dispersion computed using the scattering matrix approach is presented in Figure 1(c). The freqences of resonances are exactly described by the dispersion curves. The variation of dispersion curves resulted from the structure magnetization is investigated.

A classification of magneto-optical resonances based on excited mode configurations is proposed. In case of non-magnetized symmetrical structure only even (symmetric) modes can be excited. In that case modes has the same polarization as the incident wave. In contrast to that, in case of magnetized structure the odd (antisymmetric) modes with polarization different from the incident wave polarization can also be excited.

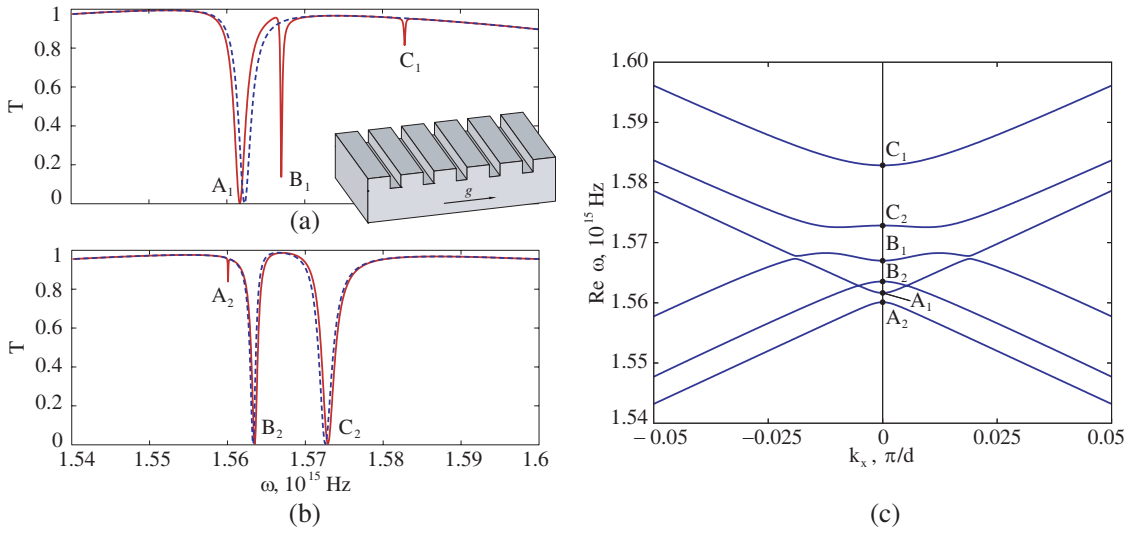

Figure 1: Transmission spectrum for (a) TE-polarization of incident wave, (b) TM-polarization. (Magnetized structure — solid red line; non-magnetized structure — dashed line). (c) Dispersion of structure's eigenmodes in the center of the first Brillouin zone.

ACKNOWLEDGMENT

The work is supported by RFBR (09-07-12147, 09-07-92421) and Leading Scientific Schools grant NSh.-3086.2008.9.

REFERENCES

1. Tikhodeev, S. G., A. L. Yablonskii, E. A. Muljarov, et al., "Quasiguided modes and optical properties of photonic crystal slabs," *Phys. Rev. B*, Vol. 66, No. 4, 045102, 2002.
2. Belotelov, V. I., D. A. Bykov, L. L. Doskolovich, et al., "Giant magneto-optical orientational effect in plasmonic heterostructures," *Optics Letters*, Vol. 34, No. 4, 398–400, 2009.

Stacking of Meta-foils

H. O. Moser[1, 2], L. K. Jian[1], M. Bahou[1], K. Banas[1], A. Banas[1], Wei Hua[1], H. S. Chen[3, 4], S. M. P. Kalaiselvi[1], S. Virasawmy[1], S. M. Maniam[1], S. P. Heussler[1], X. X. Cheng[1], and B. I. Wu[3, 4]

[1]Singapore Synchrotron Light Source (SSLS), National University of Singapore (NUS)
5 Research Link, Singapore 117603, Singapore
[2]Department of Physics, National University of Singapore
2 Science Drive 3, Singapore 117542, Singapore
[3]The Electromagnetics Academy at Zhejiang University, Zhejiang University
Hangzhou 310058, China
[4]Research Laboratory of Electronics, Massachusetts Institute of Technology
Cambridge, Massachusetts 02139, USA

Abstract— The THz meta-foil is a purely metallic space-grid that comprises parallel upright S-strings interconnected by metal lines running orthogonally to the S-strings and intersecting them in their nodes of oscillation such as to preserve the well-known S-string resonance. The importance of meta-foils rests on the fact that they consist of metal only and are no longer influenced by any supporting or embedding dielectrics. The meta-foil can be tailored and shaped according to the application and can be used at higher temperatures. Stacking of meta-foils is a way towards 3D metamaterials and advanced optical functions.

The coupling of an electromagnetic wave to the meta-foil is maximized for normal incidence with a broad useful angular range of about $\pm 30°$. The resonance spectra exhibit the typical magnetic left-handed and electric right-handed peaks. The amplitude of the left-handed peak grows with decreasing density of interconnecting lines. The spectra are insensitive to mechanical bending and to heating.

When stacking meta-foils, two main parameters are the relative orientation and the distance between foils. In the case of two foils at 25 µm gap with S-strings parallel, we find the same magnetic and electric resonances as for the single foil with a transmission and FWHM smaller than that of a single foil. However, the transmission is significantly larger than the product of the single transmissions which may indicate an interaction via evanescent fields. If we rotate foils by 90° such that the individual directions of S-strings are orthogonal, the magnetic peak is lost, while an electric peak is still maintained. This finding can be explained by the orthogonal structure of S-strings and interconnecting lines. Besides building 3D metamaterials, stacking of meta-foils may be used for polarization devices and the variable suppression of the magnetic peak as well as the control of the transmission.

Session 2A7
Poster Session 5

Design of Power Amplifier in 0.13 μm CMOS Technology at K-band

Se-Hwan Choi, **Jin-Sup Kim**, **Kyu-Ho Park**, **and Kyu-Bok Lee**
Korea Electronics Technology Institute, Republic of Korea

Abstract— FCC and ETSI have released a large bandwidth around the 22 GHz∼29 GHz ultra wideband(UWB) for vehicular radar applications. At K-band many research about components and modules progresses steadily. Most papers use GaAs HEMT and SiGe BiCMOS. However, one of the problems of these processes is the high cost. But the CMOS process that can be one chip with baseband part become an alternative process in the millimeter-wave band because it can reduce the cost of produce. Because CMOS technology has the characteristics of low power gain and lossy on-chip passive elements inherently, CMOS Power amplifier at K-band is the most challenging part to be implemented.

In this paper, at K-band Power amplifier in 0.13 μm CMOS technology is proposed. To consider the line inductance and increase the accuracy, Signal line and inductor are simulated by Ansoft HFSS. By using the two stage cascade structure, the amplifier has the maximum output power of 8 dBm and the output P1dB of 3.82 dBm. The supply voltage is 1.2 V and the current source is used for gate bias instead of voltage reference. The dissipated current is 48 mA totally. The proposed PA has the maximum power added efficiency (PAE) of 8%.

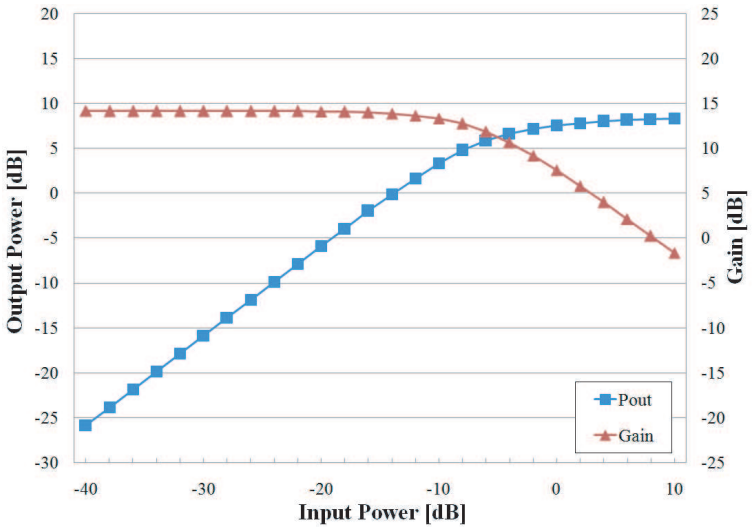

Figure 1: Output power and gain of the CMOS power amplifier.

A Ku-band CMOS VCO Using Colpitts Structure

Jin-Sup Kim, **Se-Hwan Choi**, **Jae-Young Lee**, **and Kyu-Ho Park**
Convergence Communication Components Research Center
Korea Electronics Technology Institute, R. O. Korea

Abstract— In this paper, a Ku-band voltage controlled oscillators (VCOs) is presented in a 0.13 µm CMOS technology. The fabricated output power compensated cable loss (5 dB) and the 2nd harmonic suppression are −10 dBm and −15 dBc from the carrier. The frequency tuning range is up to 250 MHz. The designed VCO consumes a dc power of 34 mA from a 1.2-V supply voltage.

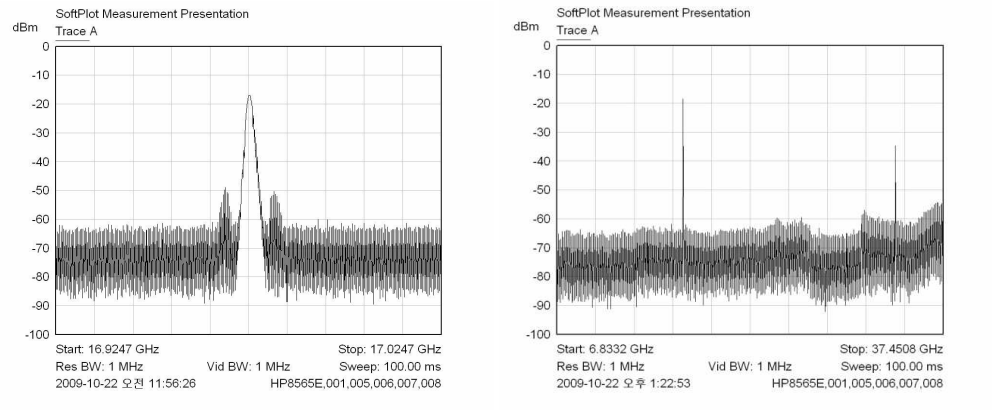

(a) Output characteristics (b) 2nd harmonic suppression

Figure 1: Output characteristics of Ku-Band VCO.

REFERENCES

1. Boon, C. C., M. A. Do, K. S. Yeo, J. G. Ma, and X. L. Zhang, "RF CMOS low-phase-noise LC oscillator through memory reduction tail transistor," *IEEE Transaction on Circuits and Systems*, Vol. 51, No. 2, Feb. 2004.
2. Li, X., S. Shekhar, and D. J. Allstot, "Gm-boosted common-gate LNA and differential Colpitts VCO/QVCO in 0.18-µm CMOS," *IEEE JSSC*, Vol. 40, No. 12, 2609–2619, Dec. 2005.

Cavity-backed Slot Array Antenna for Vechicular Radar Applications

Ho-Jun Lee[1], **Jae-Young Lee**[1], **Jong-Kyu Kim**[1], **and Hyoung-Seog Jin**[2]

[1]Convergence Communication Components Research Center
Korea Electronics Technology Institute, R. O. Korea
[2]ISR R&D Center, LIG Nex1 Co., Ltd, R. O. Korea

Abstract— In this paper, we proposed a novel design of cavity backed 4×2 slot antenna arrays with lower side lobe levels and higher front-to-back ratio are designed to improve isolation between receiving and transmitting antennas, which can be suitable the limited installation space. The proposed cavity backed 4×2 slot antenna array has an impedance bandwidth of 800 MHz (VSWR < 1.5) and gain of 17.70 dBi. Side lobe levels in E-plane and H-plane are under -8 dB and -12 dB respectively. Half power beam width in E-plane and H-plane are 22 degree and 34 degree respectively. Details of the proposed antenna designs are described, and typical experimental results are presented and discussed.

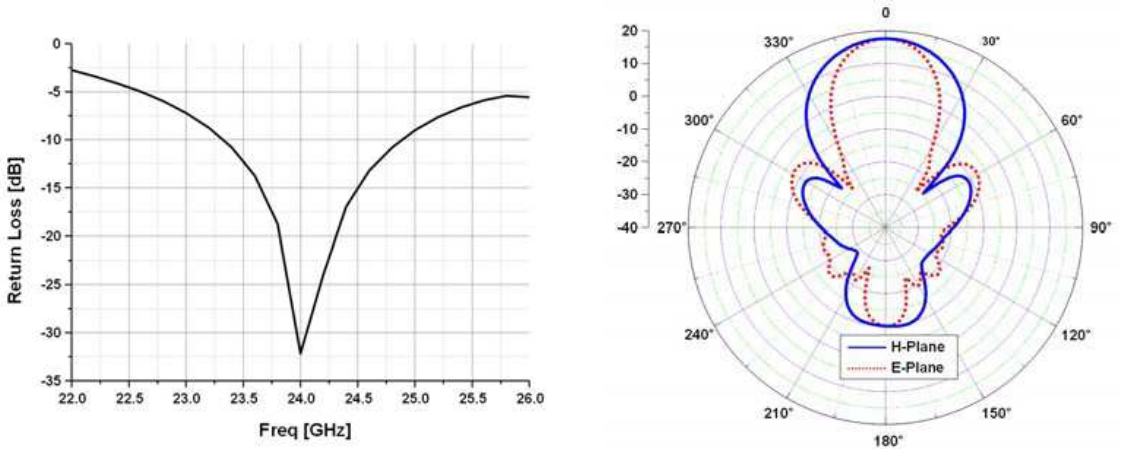

Figure 1: Proposed antenna and simulation result.

REFERENCES

1. Balanis, C. A., *Advanced Engineering Electromagnetics*, John Wiley & Sons, 1989.
2. Collin, R. E., *Foundations for Microwave Engineering*, 2nd Edition, McGraw-Hill, 1992.

Energy Band of Spin Waves in Ferromagnetic Bilayers with bcc Structures

Xiaoxia Wu[1, 2], **Guohong Yun**[2, 3], **Xiaojuan Hou**[1, 2], **and B. Narsu**[3]

[1]Department of Applied Physics, Inner Mongolia University of Science and Technology
Hohhot 014030, China
[2]College of Physical Science and Technology, Inner Mongolia University, Hohhot 010021, China
[3]Key Laboratory of Physics and Chemistry of Functional Materials
College of Physics and Electronic Information, Inner Mongolia Normal University, Hohhot 010022, China

Abstract— The mechanism of wave propagation in a ferromagnetic multilayered structure is one of the most interesting issues of recent research on material science. Because of the interface constructed from different materials, many new phenomenon and effect had appeared in heterogeneous multilayer systems. Spin waves in such a system exihibits different mode, bulk mode, interface mode and confined mode etc [1], such properties canbe applied for logical devices and valves [2].

Many authors have studied the Spin waves excitation and transmission properties of exchange coupled biferromagnetic system with simple cubic structures [3, 4]. As we know, however, most of the materials in cubic phase are not just simply with SC crystal structures. Therefore, the prevailing theories cannot applied to the practical systems.

To be more realistic, the eigen value problem of the spin wave excitation in a bilayered ferromagnets with body centered crystal structures have been investigated by using the full quantum interface rescaling approach. The energy band of the spin waves in the ferromagnetic A-A bilayers have been presented. The energy bands show that, bulk and interface modes have been excited in the bilayer system. For the antiferromagnetic interface coupling case, there apears a acoustic-acoustic interface mode. And for the ferromagntic interface coupling, both the optical-optical and the acoustic-acoustic interface mode appear in band structures. In addition, the evolution behavior of the interface modes are different for the spin waves with different parity.

REFERENCES

1. Yun, G. H. and J. H. Yan, "Spin-wave excitation in ferromagnetic multilayers," *Theories of the Electron-phonon Interaction and Spin-wavesin Layered Materials*, edited by X. X. Liang et al., Inner Mongolia University Press, 1994.
2. Livesey, K. L., D. C. Crew, and R. L. Stamps, Vol. 73, 184432, 2006.
3. Yaniv, A., *Phys. Rev. B*, Vol. 28, 402, 1983.
4. Zhou, W. P., G. H. Yun, and X. X. Liang, *Phys. Rev. B*, Vol. 77, 104403, 2008.

Design of the Index of Refraction in a Periodically Modulated Media to Minimize Radiative Loss

Braxton Osting and Michael I. Weinstein
Columbia University, NY 10027, USA

Abstract— We consider the propagation of light in a waveguide formed by a linear defect in a two-dimensional slab. The index of refraction is assumed to be periodically modulated in the direction of propagation and spatially varying in the transverse direction. Using the paraxial approximation, Maxwell's Equations for the TE-mode are transformed into the classical problem of a quantum particle confined by a potential V and subject to parametric forcing. The forcing is a consequence of the periodic modulation and the potential is determined by the index of refraction. Without forcing ($\epsilon = 0$), the governing Schroedinger equation has a spatially localized bound state ψ oscillating with frequency λ. For small forcing ($\epsilon \neq 0$), the solution with data given by the unperturbed bound state couples to radiation modes in a neighborhood of a wavenumber $k = k(\lambda)$, and diffractively spreads and tends to zero with advancing distance along the waveguide. The slowly decaying state is called a resonate state. The decay time, $\Gamma_\epsilon(V) = \mathcal{O}(\epsilon^2)$ is given by Fermi's Golden Rule and is a functional of the potential V. We pose the following question: What potential V_* maximizes the lifetime of the resonant state? We formulate this question as a constrained optimization problem over a set of admissible potentials. Locally optimal potentials are found which are periodic with a localized defect. The quality factor for an optimal potential is $\mathcal{O}(10^9)$ as compared to a generic potential with Q-factor $\mathcal{O}(10^2)$. By computing the transmission coefficient corresponding to the optimal potential V_*, we find that the coupling frequency k_* does not lie in the spectral gap formed by the periodicity of the potential. This work has implications for the design of photonic crystals which support maximal lifetime states.

Analysis Propagation Characteristics of the Surface Plasmon Polariton Trench Waveguides by Method of Lines

T. T. Minh[1, 2], **K. Tanaka**[2], **and M. Tanaka**[2]

[1]Researching Department of Furuno Electric Co., LTD, Japan
[2]Department of Electronics and Computer Engineering, Gifu University, Japan

Abstract— Construction of optical circuits on nanometric scales has attracted the attention of many researchers in the fields of nanophotonics and nanooptics. The diffraction limit of light makes it difficult to construct optical devices with dimensions that are much smaller than optical wavelengths and that have much higher integration densities than current optical integrated circuits. Theoretical and experimental studies have shown that optical circuits that use surface plasmon polaritons (SPPs) are promising candidates for future optical integrated circuits. Recently, various geometries have been proposed to achieve confinement of the plasmon-polariton in the plane transverse to the propagation direction. Among these proposals, the plasmon-polariton guided by a rectangular grooves (trenches) and triangular (V-shaped) in mental is particular interesting. The propagation characteristics of SPP trench have been investigated by the effective index method (EIM) and 3D-FDTD. However, the accuracy and the fundamental characteristics of SPP trench waveguide have been not been sufficiently revealed. In this paper, we present a numerical investigation of the SPP trench waveguide constructed of gold by the method of lines (MoL). We calculate the dependences of the complex propagation constants on the waveguide sizes and on the optical wavelength. The validity and limitations of the results are examined by comparing the present results with those calculated using the effective index method (EIM) and the finite-difference time-domain (FDTD). The fundamental, important, and interesting characteristics of the SPP waveguides have been investigated in detail. It is found that the possibility of decrease trench depth (cut-off) and strong field confinement inside trench depth can be obtained by filling dielectric inside the trench depth.

General Study on Coherent Beam Combining of Interferometric Fiber Laser Arrays

J. Cao, Q. Lu, J. Hou, and X. Xu
College of Opto-electronic Science and Engineering, National University of Defense Technology
Changsha, Hunan, China

Abstract— Coherent beam combining of fiber laser arrays is a promising way to achieve high-power lasers with good beam-quality. The interferometric fiber laser arrays (IFLA) is a sort of arrays for coherent beam combining. The IFLA is fabricated by adding ion-doped fiber (as the gain medium) in each arm of fiber interferometer. It was experimentally demonstrated that this array could make a small quantity of fiber lasers coherently combined (i.e., phase-locked) without any active control. This phenomenon is considered as self-organization, and thus, the IFLA is one category of self-organized laser arrays. In experiments, 50 W and 200 W laser beams were obtained from two-arm IFLAs with all-fiber [1] and free-space [2] configurations, respectively. The self-organization of the IFLAs was revealed as the result of longitudinal-mode competition in the compound cavity of the array [3–5]. However, presently, the theoretical understanding of this array is still limited: most of experimental results were interpreted with cold-cavity analysis which did not take the effect of gains into account; although the model presented in Refs. [3] and [4] took gains into account, only two and four-arm interferometric arrays were studied in these references. In this paper, a general study will be given on the IFLAs, which will be of great help to understand the scaling of the interferometric arrays.

In this paper, we focus our interests on the IFLA shown in Fig. 1. The array is fabricated with 2×2 couplers and single-mode fibers. With help of the model given in Ref. [3], we deduce the phase-locked states of the interferometric array. The phase-locking conditions needed to get high-efficiency beam combining of this array are given. It is found that the gains of the array do not only provide the mechanism of longitudinal-mode competition, but also affect the phase-locked state of the array because of the detuning between the laser frequency and atomic frequency. Nevertheless, the effect of gains on the phase-locked states can be neglected when the configuration of array is symmetric. The results also show that the phase-locked states are determined by the configuration of the compound cavity of the array when the effect of gains is neglected. That is the reason why the cold-cavity analysis can make effective interpretations of experimental observations [5]. The results also reveal that the dominant longitudinal mode in the mode competition should satisfy N conditions to realize high-efficiency beam combining. It means that the combining efficiency should be decrease with the increase of N (i.e., the number of the arms of the array). An example is also numerically studied to given an intuitional illumination of the scaling of this array (see Fig. 2).

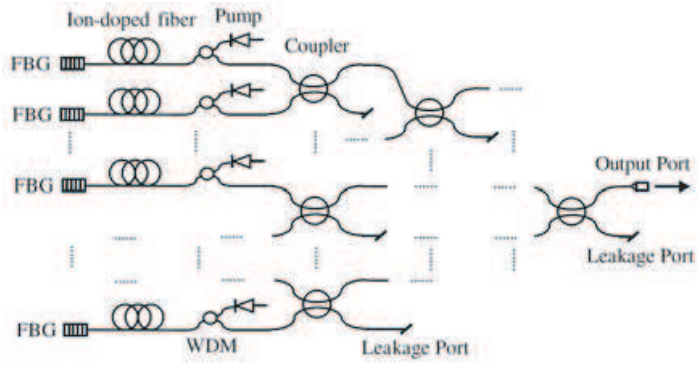

Figure 1: The configuration of N-arm interferometric fiber laser array.

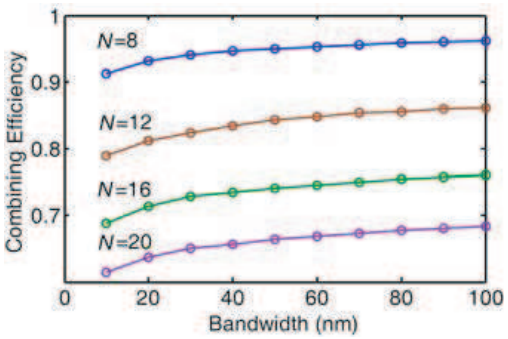

Figure 2: Plots of combining efficiency via the bandwidth of the compound cavity of array.

REFERENCES

1. Bruesselbach, H., et al., CLEO, 2005, paper CMDD4.
2. Wang, B., et al., *Opt. Lett.*, 863, 2009.

3. Cao, J., et al., *Opt. Express*, 5402, 2009.
4. Wu, T., et al., *Opt. Express*, 19509, 2009.
5. Cao, J., et al., *J. Opt. Soc. Am. B*, 1187, 2008.

The Effect of Temperature on the Soliton Propagation in Photorefractive SBN Crystal in One Dimension

Alireza Keshavarz[1], **Farzin Emami**[2], **Mohsen Hatami**[3], **and Parviz Elahi**[1]

[1]Department of Physics, Faculty of Science, Shiraz University of Technology
P. O. Box 313-71555, Shiraz, Iran
[2]Optoelectronic Research Center, Shiraz University of Technology
P. O. Box 313-71555, Shiraz, Iran
[3]Department of Atomic and Molecular Physics, Faculty of Physics, Yazd University
P. O. Box 741-89195, Yazd, Iran

Abstract— Spatial solitons that do not spread owing to diffraction when they propagate have been investigated by many researchers, because of their possible applications in photonic devices. Studying in this area shows that such solitons can be used to control of light by light. In especial case, photorefractive screening solitons, have been shown to exhibit very interesting behavior in one and two dimensions. These solitons results from the nonlinear and nonlocal characteristics of the photorefractive effect, which was first discovered in 1966 by Askin.

In this paper, the evolution of propagation of soliton simulated in photorefractive SBN crystal in one dimension by numerical solution of the wave equation. Our simulation shows the strong stability of the soliton under propagation. Also we investigated the temperature effects on the evolution of the soliton by Crank-Nicolson method. As a result the photorefractive soliton is stable, although it was bending towards the biased external electric field. This bending effect can be controlled by the amount of the temperature and the external field. The outcome can be used in fabrication of all optical switching elements.

REFERENCES

1. Kuroda, K., *Progress in Photorefractive Nonlinear Optics*, Taylor and Francis, 2002.
2. Stegeman, G., "Optical spatial solitons: Historical perspectives," *J. Select. Top. Quantum Electron. IEEE*, Vol. 6, 1419–1427, 2000.
3. Shi, T. and S. Chi, "Nonlinear photonic switching by using the spatial soliton collision," *Opt. Lett.*, Vol. 15, 1123–1125, 1990.
4. Evans, G., J. Blackledge, and P. Yardley, *Numerical Methods for Partial Differential Equations*, Springer Verlag, Berlin, 2000.
5. Zakery, A. and A. Keshavarz, "Simulation of the incoherent interaction between two bright spatial photorefractive screening solitins in one and two dimentions," *J. Phys. D: Appl. Phys.*, Vol. 37, 3409–3418, 2004.
6. Keshavarz, A., "Interaction between two photorefractive bright solitons in different dimensions," *PIERS Proceedings*, 1196–1198, Beijing, China, March 23–27, 2009.
7. Keshavarz, A., L. Sadralsadati, and M. Hatami, "Simulation of soliton propagation in photovoltaic photorefractive two-photon materials and study the switching behavior," *PIERS Proceedings*, 1823–1826, Moscow, Russia, August 18–21, 2009.

Calculating Complex Propagation Constants of Finite-size Two Dimensional Photonic Crystal Waveguides

Y.-P. Chiou[1, 2], **K.-H. Chi**[3], **and F.-C. Huang**[1]

[1]Graduate Institute of Photonics and Optoelectronics
National Taiwan University, Taipei 10617, Taiwan
[2]Department of Electrical Engineering, National Taiwan University, Taipei 10617, Taiwan
[3]Department of Electrical Engineering and Computer Science
University of California, Irvine, CA 92697, USA

Abstract— Finite-difference method is adopted to calculate the complex propagation constants of leaky guided modes in finite-size photonic crystal waveguides. The formulation is modified to solve complex wavevectors for a given frequency, instead of solving resonant frequencies for a given real wavevector. Periodic boundary conditions are imposed along the propagation direction, and perfectly matached layers are imposed on the transverse domain boundaries. Rectangular and hexagonal structures are investigated. Our results shows the logarithm of imaginary parts from the propagation constants are roughly proportional to the number of periods beside the waveguides, which is consistent to our semi-analytical derivation.

Frequency Characteristics of Specific Absorption Rates of Children for Whole-body Exposure from 10 MHz to 10 GHz

T. Nagaoka and S. Watanabe
National Institute of Information and Communications Technology, Japan

Abstract— The increasing use of radio-frequency (RF) applications has led to the growing presence of electromagnetic waves in various locations. According to the International Commission on Non-Ionizing Radiation Protection (ICNIRP) [1] guidelines, the safety of the RF electromagnetic fields (EMF) up to 10 GHz is evaluated on the basis of the specific absorption rate (SAR), which is the amount of RF energy absorbed per unit weight of the body and is used as a measure of the thermal effects in the body that are caused by the absorption of electromagnetic energy. A World Health Organization (WHO) report published in 2006 recommended that dosimetry studies on the effects of RF-EMF exposure on children must be conducted on a priority basis [2]. High-precision SAR dosimetry studies up to a few gigahertz have often been performed by using anatomically realistic human models [3]. Recent advances in computer technology have made it possible to estimate the studies using the anatomically realistic human models at higher frequencies. In this study, we present the frequency characteristics of the whole-body-averaged SARs of children exposed to vertically polarized plane waves in the frequency range of 10 MHz to 10 GHz propagating from the anterior to the posterior direction under isolated and grounded conditions. The whole-bodyaveraged SARs are calculated by using the finite-difference time-domain (FDTD) method. We used an NEC SX-8R supercomputer and a code written in-house to perform the calculations. We also present the incident electric field strength required to produce the exposure equivalent to the International Commission on Non-Ionizing Radiation Protection (ICNIRP) basic restriction for general public exposure, i.e., a whole-body-averaged SAR of 0.08 W/kg.

REFERENCES

1. ICNIRP, "Guidelines for limiting exposure to time-varying electric, magnetic, and electromagnetic fields (up to 300 GHz)," *Health Phys.*, Vol. 74, 494–522, 1998.
2. WHO, *Research Agenda for Radio Frequency Fields*, 2006.
3. Hand, J. W., "Modelling the interaction of electromagnetic fields (10 MHz–10 GHz) with the human body: Methods and applications," *Phys. Med. Biol.*, Vol. 53, R243–R286, 2009.

Level Set Method in EIT Image Reconstructions

J. Dědková, K. Ostanina, and Jan Mikulka
Department of Theoretical and Experimental Electrical Engineering, Brno University of Technology
Kolejní 2906/4, Brno 612 00, Czech Republic

Abstract— In present there are a lot of different numerical methods, ways and approaches to obtain the stable and effective image reconstruction process, which we can use for efficient applications in physical and biological sciences. Electrical impedance tomography belongs to the methods, which are very beneficial especially in a medical imaging. This method is noninvasive technique and can be used for the detection of conductivity tissue changes. Unfortunately the back image reconstruction based on electrical impedance tomography is highly ill-posed inverse problem and it is necessary to to find such techniques which offer stable, accurate and not too much time-consuming reconstruction process. This paper proposes new possibilities to improve the stability and the accuracy of today image reconstructions including the level set method. The level set method is very successfully used to identify regions with different image or material properties. The distribution of unknown conductivity (or resistivity) σ can be described in terms of level set function F depending on the position of the point r with respect to the boundary Γ between regions with different values of σ

$$\sigma(r) = \begin{cases} \sigma_{int}\{r : F(r) < 0\} \\ \sigma_{ext}\{r : F(r) > 0\} \end{cases}, \quad \Gamma = \{r : F(r) = 0\}$$

If the level set method is included smartly to the reconstruction algorithm we can obtain the very good tool for stable and accurate image reconstruction. There are compared different implementations of level set method to reconstruction process and their results.

REFERENCES

1. Cheney, M., D. Isaacson, and J. C. Newell, "Electrical impedance tomography," *SIAM Rev.*, Vol. 41, No. 1, 85–101, 1999.
2. Burger, M., "A level set method for inverse problems," *Inverse Problems*, Vol. 17, 1327–1356, 2001.
3. Sethiah, J., *A Level Set Methods and Fast Marching Methods*, Cambridge University Press, Cambridge, 1999.
4. Chan, T. and L. Vese, "Active contour without edges," *IEEE Trans. Imag. Proc.*, Vol. 10, 266–277, 2001.
5. Osher, S. and R. Fedkiw, *Level Set Methods and Dynamic Implicit Surfaces*, Springer-Verlag, New York, 2002.

An Effective Detection of Conductivity Changes in Biologic Tissue

T. Kříž, J. Dědková, and J. Mikulka
Department of Theoretical and Experimental Electrical Engineering, Brno University of Technology
Kolejní 2906/4, Brno 612 00, Czech Republic

Abstract— There are described positive and negative properties of weighty recent numerical techniques for a solution of electrical impedance tomography (EIT) inverse problem and their influences to the quality of image reconstruction. There are two different types of EIT image reconstructions, static and dynamic EIT. In static EIT, only the absolute conductivity in each element is computed and a picture of the internal organs of different conductivity is imaged. In dynamic EIT, temporal variations in conductivity are computed. Both types can be very useful especially in medical applications. The aim of this paper is to propose and realize a new algorithm for a successful detection of conductivity changes in biologic tissues. It is desirable to obtain high-quality reconstruction process because the medical imaging is a non-invasive and very helpful technique for a detection of pulmonary emboli, non-invasive monitoring of a heart function and a blood flow, or for the breast cancer detection. An image reconstruction of EIT is an inverse problem, which is usually presented as minimizing the suitable objective function $\Psi(\sigma)$ relative to conductivity σ. To minimize the objective function $\Psi(\sigma)$ we often use a deterministic approach based on the Least Squares method. To solve the inverse EIT problem the standard Tikhonov regularization method has to be used because of the ill-posed nature of the problem. So it is necessary to minimize the objective function $\Psi(\sigma)$

$$\Psi(\sigma) = \frac{1}{2}\Sigma \parallel U_M - U_{FEM}(\sigma) \parallel^2 + \parallel L\sigma \parallel^2 .$$

Here σ is the unknown conductivity distribution vector in the object, U_M is the vector of measured voltages on the object boundary, $U_{FEM}(\sigma)$ is the vector of computed peripheral voltages in respect to σ which can be obtained using the FEM, α is a regularization parameter and L is a regularization matrix connecting adjacent elements of the different conductivities. If we find the tissue conductivity changes in selected regions (lungs, heart) only, we can significantly reduce the number of unknown values during the reconstruction process. To separate the regions with different values of the conductivity we can use very effectively the level set method.

To obtain the stable reconstruction process for an effective detection of conductivity changes in biologic tissue we created a new algorithm based on Tikhonov regularization method and level set method. In the paper are described the obtained results.

REFERENCES

1. Cheney, M., D. Isaacson, and J. C. Newell, "Electrical impedance tomography," *SIAM Rev.*, Vol. 41, No. 1, 85–101, 1999.
2. Borsic, A., "Regularization methods for imaging from electrical measurement," PH.D. Thesis, Oxford Brookes University, 2002.
3. Burger, M. A., "Level set method for inverse problems," *Inverse Problems*, Vol. 17, 1327–1355, 2001.
4. Sethiah, J. A., *Level Set Methods and Fast Marching Methods*, Cambridge University Press, Cambridge, 1999.
5. Osher, S. and R. Fedkiw, *Level Set Methods and Dynamic Implicit Surfaces*, Springer-Verlag, New York, 2002.

Monitoring of Diseases Progression by MR

J. Mikulka
Department of Theoretical and Experimental Electrical Engineering
Brno University of Technology, Kolejni 2906/4, 612 00 Brno, Czech Republic

Abstract— This paper deals with methods for monitoring of development of diseases with using the nuclear magnetic resonance. The paper compares the methods for monitoring the qualitative and quantitative parameters in the NMR images. The main goal is usually comparing the observed images of the human tissues in the time. There are the surfaces, volumes and their changes in the time most often monitored. The typical examples of these objects are several tumors, tubers, polypus or discs of temporomandibular joint. The goal of these methods comparison will be selection of suitable method for monitoring of development of treatment of diseases in the human stomach with using the modern nuclear magnetic resonance tomograph and other approaches. The paper is made as research material for the future work.

The Comparative Study of Magnetized Physiological Solution-induced and Hydrogen Peroxide-induced Stimulation Effect on Heart Muscle Contractility

Erna Dadasyan and Sinerik Ayrapetyan
UNESCO Chair-Life Sciences International Postgraduate Educational Center
31 Acharyan St. 0040 Yerevan, Armenia

Abstract— At present the biological effect of magnetized physiological solution (MPS) on different cells and organisms can be considered as proven fact but the nature of the messenger transferring the signal of electromagnetic field (EMF)-induced water structural changes to the metabolic cascade is not clear yet. By previous our works have shown that MPS has dual effect on heart muscle contractility: on the one hand it leads to muscle relaxation, and on the other hand it stimulates the frequency of heart contractility. If the relaxing effect of MPS on heart muscle could be explained by the activation of cGMP-dependant Ca efflux bringing to the deflection of intracellular Ca ions and reactivation of Na^+-K^+ pump, the stimulatory mechanism of the MPS on heart beating is still unclear. It is known that the water molecule dissociation is the most variable water property, it is suggested that the magnetization of water could leads to the increase of dissociation products which are potential messengers through which could transfer biological effect of SMF (static magnetic field) and EMF from the aqua solution to the cells. Therefore, it is suggesting that the H_2O_2 could serve as one of the most reliable candidate for the messenger transferring EMF-induced water structure changes to cell metabolic cascades. For testing this hypothesis the comparative study of the effects of magnetized and H_2O_2 containing physiological solution (PS) on heart muscle contractility and ^{45}Ca uptake by muscle was performed. The isolated and intra cordially perfused snail heart muscles, which is able to contract *in vitro* state for more than 24 hours, was chosen as an experimental model for the present study.

Results: The data that the activation effects of H_2O_2 and MPS on Na^+-K^+ pump-induced muscle relaxation following the pre-incubation of the heart are present in both cases: in K-free medium or in case of heart re-incubation in K-containing solutions treated by EMF or H_2O_2 containing solution, i.e. when the pump was in active and inactive states, correspondingly, could serve as an evidence on the pump-independent stimulation effects of MPS and H_2O_2 on heart. It is shown that this effect does not depend on Ca metabolisms: in spite that the MPS and H_2O_2 in normal PS have activation and in K-free solution- inactivation effects on Ca uptake, in both cases MPS and H_2O_2 have stimulation effects on heart muscle contractility.

Conclusion: The main conclusion from the presented data is that H_2O_2 is one of the important messengers through which the biological effect of EMF on heart muscle contractility is realized.

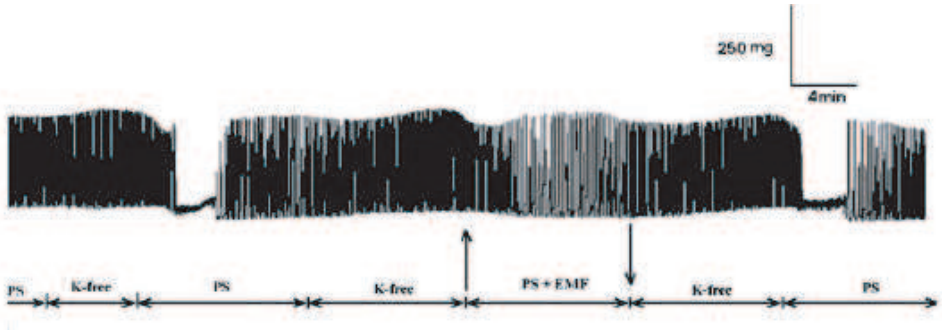

Figure 1: The effect of EMF-pretreated PS on Na^+-K^+ pump induced transient inhibition of heart muscle contractility.

Interaction of Doxorubicin with DNA Irradiated at Water Molecular Structure Oscillation Frequencies

Yu. Babayan, **A. Tadevosyan**, **and S. Harutyunyan**
Department of Medical Physics, Yerevan State Medical University, 2 Koryun Str. Yerevan, 0025, Armenia

Abstract— The interaction of calf thymus extracted DNA, which had been irradiated by non-thermal coherent millimeter (mm) electromagnetic waves, and antitumor compound doxorubicin has been investigated. For irradiation, microwave generators of Gi-142 and Gi-141 were used. The power density on the sample surface didn't exceed 50 mcW/sm^2.

The melting curves of the calf thymus extracted DNA, which were irradiated for 90 minutes at water molecular structure oscillation resonant (50.3 GHz and 64.5 GHz) and nonresonant (48.3 GHz) frequencies, and doxorubicin complexes have been investigated at different doxorubicin concentrations.

According to the experiments, the mechanisms of complex formation of doxorubicin with irradiated DNA qualitatively didn't differ from that of with nonradiated DNA, but with irradiated DNA, doxorubicin produces a more heat-resistant complex.

The values of changes in thermodynamical parameters of interaction of doxorubicin and irradiated DNA interaction have been calculated from titration spectra. Using the coupling coefficients obtained at different temperatures, the values of changes in Gibbs free energy, enthalpy and entropy have been determined. According to calculations, doxorubicin produces more stable complexes with DNA if the DNA solution was irradiated at the water molecular structure oscillation resonant (50.3 GHz and 64.5 GHz) frequencies. However, the thermodynamic parameters of interaction of DNA irradiated at 48.3 GHz frequency and doxorubicin, within the limits of the experimental error, didn't differ from those of interaction of nonradiated DNA and doxorubicin. Thus, from the obtained results it can be concluded that DNA, which had been irradiated at the water molecular structure oscillation resonant frequencies, produces more stable complex with the doxorubicin antitumor compound. The obtained result could be used in the process of working up of antitumor drug injection schemes.

Photodynamic Therapy in the Dermatological Field and Enhanced Cutaneous Absorption of Photosensitizer

Makio Akimoto[1], **Kazuhisa Maeda**[2], **Tokuya Omi**[3], **Tomonori Nishimura**[4], **and Michio Miyakawa**[5]

[1]Kanto Gakuin University, 1-50-1, Mutsuurahigashi, Kanazawa-ku, Yokohama 236-8501, Japan
[2]Tokyo University of Technology, 1404-1, Katakura, Hachioji, Tokyo 192-0982, Japan
[3]Queen's Square Medical Center, 2-3-5, Minatomirai, Yokohama 220-6208, Japan
[4]Atom Giken Co., Ltd., 92-2, Katase, Fujisawa, Kanagawa 251-0032, Japan
[5]Niigata University, 8050 Ikarashi-2, Niigata 950-2181, Japan

Abstract— Therapeutic and diagnostic techniques based on the interaction of visible and near infrared light with tissue are becoming increasingly important in medicine. The combination of light and chemicals to treat skin discases is widely practiced in dermatology. Within this broad use of light and drugs, in recent years the concept of photodynamic therapy (PDT) has emerged. Photodynamic therapy is a promising modality for the management of various tumors and nonmalignant diseases, based on the combination of a photosensitizer that is selectively localized in the target and illumination of the lesion with visible light, resulting in photodamage and subsequent cell death. Moreover, the fluorescence of photosensitizing compounds is also utilized as a helpful diagnostic tool for the detection of neoplastic tissue. The two most important interactions governing the transport of light through tissue are scattering and absorption. In photodynamic therapy for skin cancer, 5-aminolevulinic acid (ALA) is applied topically to the affected area to be absorbed percutaneously through passive diffusion, and typically requires 4–6 h before performing PDT. In this study, we attempted to reduce the absorption period in PDT by ionizing ALA using direct-current pulsed iontophoresis to treat disease.

Five patients who were diagnosed with actinic keratosis (two men and three women in ages ranging from 49 to 94 years, with an average of 79.6 years) and Bowen's disease at the outpatient clinic of the Department of Dermatology, Aichi Medical University, attended this study. Informed consent was obtained from all patients following a full written and oral explanation. Iontophoresis used in the present study was a direct-current pulsed type. When compared with conventional direct-current iontophoresis, pulsed iontophoresis was able to avoid electrode polarization, and drugs could be efficiently applied. For iontophoresis, 20% ALA was dissolved in distilled water, and then current was adjusted based on the area of the functional electrode between 0.25 and 0.50 mA/cm^2. In all subjects, the pulse wave was set at 50 kHz, and ALA was applied to lesion for 10 min. After application, the affected area was washed using distilled water and was shielded from light. One hour after ALA application, a fluorescent spectrometer was used to measure protoporphyrin IX (PpIX) photosensizatizer production. PDT was performed by excimer dye laser and emits 630 nm with pulsed light irradiation at 50 J/cm^2 per session. PDT was repeated three times, weekly (total dose: 150 J/cm^2). One week after the last PDT, a skin biopsy was performed in order to assess the therapeutic effects.

When compared with previous studies, our direct-current pulsed iontophoresis had a higher charge because the concentration of ALA was higher at 20% solution. With the equipment used in the present study, the pulse mode makes it possible to avoid the functional electrode depolarization associated with direct current iontophoresis, and ALA can be efficiently applied. In our study, there were no marked differences in the average PpIX production between 1 h after iontophoresis and $>$ 4 h after occlusive dressing technique. We think that ALA was apparently able to penetrate tumour cells faster with direct-current pulsed iontophoresis when compared with percutaneous absorption based on passive diffusion. Rapid ALA diffusion into cells also quickly depleted the rate-limiting enzyme, thus accumulating PpIX inside tumour cells.

In conclusion, our date suggested that when compared with conventional occlusive dressing technique, PDT could be performed much more rapidly with iontophoresis, resulting in lower a patient burden.

REFERENCES

1. Omi, T., M. Akimoto, M. Miyazaki, and S. Kawana, "Iontophoresis-enhanced cutaneous absorption of 5-aminolevulinic acid shortens the incubation period in photodynamic therapy," *Laser Therapy*, Vol. 18, No. 33, 143–149, 2009.

Developments of Transdermal Transport System during Skin Iontophoresis and Electroporation

Tomonori Nishimura[1], **Makio Akimoto**[2], **Michio Miyazaki**[2], **Mayumi Nomoto**[3], **and Michio Miyakawa**[4]

[1]Atom Giken Co., Ltd., 92-2, Katase, Fujisawa-city, Kanagawa 251-0032, Japan
[2]Kanto Gakuin University, 1-50-1, Mutsuurahigashi,,Kanazawa-ku, Yokohama 236-8501, Japan
[3]Nomoto Mayumi Skincare Clinic, 1-3-7, Bandai, Chuo-ku, Niigata 950-0088, Japan
[4]Niigata University, 8050 Ikarashi-2, Niigata 950-2181, Japan

Abstract— Oral and needle-based administration of drugs have long been accepted as a simple, convenient, and inexpensive mode of drug delivery. However, these methods are not suited for the delivery of new and highly complex drugs. And the barrier properties of the stratum corneum, the outermost layer of the skin, limit the rate, size, and type of molecules that can be delivered by patches. Several physical means have been demonstrated to increase the throughput of small and macromolecules across the skin. For example, iontophoresis employs low-level electrical current to deliver drugs through the skin. Patient compliance in transdermal drug delivery that utilizes physical means will greatly improve if the intervention is localized and minimally invasive. Here, we describe two approaches to spatially localized transdermal drug delivery: field-confined skin iontophoresis and electroporation. The first method employs low-level electrical current to deliver drugs through the skin. The second method employs field-confining electrodes to apply high voltage electrical pulses to create openings in the outer layers of skin.

Iontophoresis method involves enhancing the permeation of a topically applied therapeutic agent by the application of a low level electric current either directly to the skin or indirectly via the dosage form [1]. Increase in drug permeation as a result of this methodology can be attributed to either one or a combination of the following mechanisms; electrorepulsion (for charged solutes), electro osmosis (for uncharged solutes) and electropertubation (for both charged and uncharged). Parameters that affect design of an iontophoretic skin delivery system include; electrode type, current intensity, competitive ion effect and permeant type. Previous work has also reported that the combined use of iontophoresis and electroporation is much more effective than either technique used alone in the delivery of molecules across the skin. The limitations of ionotophoretic systems include the regulatory limits on the amount of current that can be used in humans (currently set at 0.5 $\mathrm{mA/cm^2}$) and the irreversible damage. In addition, iontophoresis has failed to significantly improve the transdermal delivery of macromolecules of $> 7\,\mathrm{kDa}$.

Electroporation involves the application of high voltage pulses to induce skin perturbation. High voltages ($\geq 50\,\mathrm{V}$) and short treatment durations (milliseconds) are most frequently employed. Other electrical parameters that affect delivery include pulse properties such as waveform, rate and number. The increase in skin permeability is suggested to be caused by the generation of transient pores during electroporation. The technology has been successfully used to enhance the skin permeability of molecules with differing lipophilicity and size including biopharmaceuticals with a molecular weight greater that 7 kDa, the current limit for iontophoresis. We have developed a prototype electroporation transdermal device, which has been tested with various compounds with a view to achieving delivery, improving drug delivery and aiding the application of cosmetics. More clinical information on the safety and efficacy of the technique is required to assess the future commercial prospects. Both field-confined skin iontophoresis and electroporation offer minimally invasive methods for delivering drugs across skin with minimal sensation. Both methods create high permeability pathways in a pain-free manner. These openings are similar in dimension to commonly experienced scratches and nicks on the skin. These localized openings provide pathways for sustained delivery of drugs either passively using a patch or actively using iontophoresis.

REFERENCES

1. Akimoto, M., M. Kawahara, M. Matsumoto, and H. Matsubayashi, "Development of the pulsed direct current iontophoresis and its clinical application," *PIERS Proceedings*, 157–162, Cambridge, Massachusetts, USA, 2006.

Comparing Effects of Extremely Low Frequency Electromagnetic Fields on the Biomass Weight of C3 and C4 Plants in Early Vegetative Growth

Azita Shabrangi[1], **Ahmad Majd**[2], **Masoud Sheidai**[3], **Mohammad Nabyouni**[1], **and Davoud Dorranian**[4]

[1]Department of Biological Science, Faculty of Science, Tarbiat Moalem University, Tehran, Iran
[2]Department of Biology, Faculty of Science, Islamic Azad University, Tehran North Branch, Tehran, Iran
[3]Biology Faculty, Shahid Beheshti University, Tehran, Iran
[4]Physic Plasma Research Centre, Science and Research Branch, Islamic Azad University, Tehran, Iran

Abstract— Low frequency electromagnetic fields (EMFs) are a ubiquitous factor in the Earth's environment. In this research two states of seeds (wet, dry) of *Brassica napus L* (canola) and *Zea mays L* (maize) were exposed to pulsed EMFs (15 min on, 15 min off) by magnitude of 1 to 7 mT in steps of 2 mT and the highest intensity was 10 mT for 1 to 4 hours in steps of 1 h. Exposure to EMFs was performed by a locally designed EMF generator (1). Tree replicates of ten 7 days seedlings were randomly taken in order to measure their fresh biomass weights. The same seedlings were placed in the oven with 60°C for 24 hours. Then dry biomass weights were measured. Total protein concentration was carried out by Bradford technique in 7 days seedlings.

Fresh biomass weight of maize seedlings grown from dry treated seeds showed increase in almost all treatments comparing to control. But we did not observe significant increase in dry biomass weight of the same seedlings except seedlings grown from 10 mT treatment. On the other hand fresh biomass weight of seedlings grown from wet treated seeds showed increase especially in 3 and 10 mT intensities for 4 hours exposure time. Dry biomass weight of the same seedlings showed an overall increase in almost all treatments. This increase in 1, 3 and 10 mT treatments were more significant. Also we observed that increase of fresh biomass weight was more than increase of dry biomass weight of the same seedlings, comparing to their corresponding control. The results were accorded to total protein amount of 7 days seedlings. We observed some different results in the other species. Fresh biomass weight of canola seedlings grown from dry treated seeds showed increase in most of treatments except 1 mT intensity. Dry biomass weight of the same seedlings showed an overall increase and the most increase was observed in 1 mT intensity for 3 hour exposure time. Therefore low intensity of EMFs treatment caused augmentation in dry biomass weight in canola. We observed significant decrease in fresh biomass weight of canola seedlings grown from wet treated seeds in 10 mT intensity for different exposure time. In contrary, other treatment including 1 to 7 mT intensities caused augmentation in fresh biomass weight. Dry biomass weight of the same seedlings decreased especially in 7 and 10 mT intensities and all exposure time.

All these results were similar to other developmental growth including root and shoot length. It is assumed that augmentation of dry biomass weight would be the result of more protein synthesis or more carbohydrate and lipid synthesis. We also believed that increase of fresh biomass weight would have the same reasons or it might be the result of more water absorption. In the present study all the results suggested that treated seeds of these two species react differently against EMFs as a biotic stress. EMF treatment by 10 mT intensity of wet treated seeds caused decrease in growth and dry biomass weight in canola. The same treatment cause increase in dry biomass weight in maize. In conclusion, canola (C3 plant) tends to damage more than maize (C4 plant) against EMFs.

REFERENCES

1. Shabrangi, A. and A. Majd, "Comparing effects of electromagnetic fields (60 Hz) on seed germination and seedling development in monocotyledons and dicotyledons," *PIERS Proceedings*, 704–709, Moscow, Russia, August 18–21, 2009.

Measurement of Complex Permittivity of Biological Tissues

J. Vorlíček, L. Oppl, and J. Vrba
Dept. of Electromagnetic Field, Czech Technical University, Czech Republic

Abstract— The goal of hyperthermia cancer treatment is to raise the temperature of the targeted tissue area. Thus, temperature can be maintained above 43°C for up to one hour. To evaluate the expositions of microwave radiation from thermo therapeutical microwave applicators, we need to know the dielectric properties of the tissues. This can be performed using measure of the complex permittivity of the tissues in the desired area of the treatment. For this purpose, we constructed a sensor based on the coaxial transmission line for measuring the complex permittivity. Measurement method on an open-ended coaxial line is based on the reality that the reflection coefficient of an open-ended coaxial line depends on dielectric parameters of material which is attached to the coaxial line. For calculation of biological tissue dielectric parameters from the measured reflection coefficient, it is necessary to use an equivalent circuit of an open-ended coaxial line. The values of elements in the equivalent circuit depend on the dielectric properties of the material attached to the end of coaxial line. To determine the values of elements in an equivalent circuit, we use calibration by means of material with known dielectric properties.

Open-ended coaxial probe has a capability of broadband measurements and simple sample preparation. Also, its nondestructive nature and capability for in-vivo measurements provide open-ended coaxial probes with a significant advantage over other techniques for biological applications. There have been many techniques to correlate the measured input admittance to the complex permittivity of the sample material, which resulted in significant improvement in the extraction process. Accurate measurements of the complex permittivity of biological tissues gain great importance in both basic and applied research.

The performance of this system was evaluated by measuring of the deionized water. The measured data were compared with the value calculated by Debye's model. The relative errors between the measurement and the calculation were less than ±4%. The reliability of this method was confirmed by the measurement of deionized water in wide frequency range.

ACKNOWLEDGMENT

This research is supported by Grant Agency of the Czech Republic, project: "Non-standard application of physical fields — analogy, modeling, verification and simulation" (102/08/H081).

Reduction of Four-Wave-Mixing in FDM Lightwave Transmission Systems by Asymmetric Repeated Unequally Spaced Frequency Allocations

Takuya Tamo and Takahiro Numai
Ritsumeikan University, Japan

Abstract— Transmission characteristics in frequency-division-multiplexing (FDM) optical fiber transmission systems with low-dispersion optical fibers such as dispersion-shifted fibers (DSFs) are limited by four-wave mixing (FWM). In recent years, several FWM suppression techniques such as optical multiplexers and demultiplexers with the combination of delay lines, modified return-to-zero (RZ) signals, hybrid wavelength-/time-division multiplexing (WDM/TDM) technique, arrangement of polarization allocations of channels, separation between signal frequencies and the zero-dispersion frequency, combination of frequency/polarization allocations and separation of signal frequencies from the zero-dispersion frequency, the hybrid amplitude-/frequency-shift keying (ASK/FSK) modulation with prechirped pulses, and unequal channel spacing have been reported.

Characteristics of FWM are also closely related to frequency allocations and modulation formats. From the viewpoint of frequency allocations, unequally-spaced (US) allocations, repeated US (RUS) allocations, and modified RUSs such as equally-spaced RUS (ERUS) and unequally-spaced RUS (URUS) allocations have been demonstrated to overcome the problems in equally-spaced (ES) allocation. It was found that RUS, ERUS, and URUS have lower FWM light intensities with channel frequencies than ES and narrower total bandwidths than US. From the viewpoint of modulation formats, FWM noises have been analyzed for non-return-to-zero (NRZ), random RZ, differential phase-shift keying (DPSK), and bit-phase arranged RZ (BARZ) in ES, RUS, ERUS, and URUS, and it has been revealed that FWM noises are lowest in URUS with BARZ.

In this paper, to reduce FWM noises further, asymmetric repeated unequally spaced (AS-RUS) frequency allocations, which are asymmetric with respect to the zero-dispersion frequency f_0, are proposed, and transmission characteristics are theoretically analyzed. It is found that crosstalk, bit error rate, and power penalty of AS-RUS are better than those of equally spaced frequency allocation, and an allowable input power of AS-RUS is expected to be as high as 4.58 dBm/ch. In our calculations, it is assumed that an oscillation wavelength for a light source is 1550 nm. A DSF is assumed to have the derivative dispersion coefficient $\mathrm{d}D_\mathrm{c}/\mathrm{d}\lambda$ of 0.07 ps/km/nm^2, the fiber length L of 80 km, and the decay rate α of 0.2 dB/km. The base unit and the channel spaces are common in all frequency allocations which are studied in this paper, and the frequency separations are the same as those in to make the pulse delay and pulse broadening as small as possible.

ACKNOWLEDGMENT

This research was partially supported by the Japan Society for Science, Grant-in-Aid for Scientific Research (C) 20560379, 2009.

Session 2P1
Modeling and Inversion for Geophysical EM Applications

A Feasibility Study of Land CSEM Reservoir Monitoring: The Effect of the Airwave

Marwan Wirianto[1], **Wim A. Mulder**[2], **and Evert C. Slob**[1]

[1]Delft University of Technology, Delft, The Netherlands
[2]Shell International Exploration and Production B.V., Rijswijk, The Netherlands

Abstract— A potential application of controlled-source EM is monitoring a hydrocarbon reservoir during the recovery process. Oil production with, for instance, water flooding or steam injection creates resistivity changes in the subsurface. These changes occur primarily in the reservoir. A central question in EM monitoring is whether or not these resistivity changes are detectable, and if so, if the value of that information is worth the effort compared to more established methods as time-lapse seismic measurements that provide far better resolution. With EM, the resistivity difference between rock containing hydrocarbons or saline water can be two or three orders of magnitude, making CSEM potentially more suitable if this difference can be detected in the presence of repeatability errors and noise. The diffusive character of EM, however, will always lead to poor spatial resolution at the low frequencies required to reach sufficient depth.

In the last two or three years, a number of papers have addressed the monitoring problem by numerical modelling. Several monitoring scenarios were used to investigate whether the method is able to detect the resistivity changes as would happen in the real case. The complexity of the geological background model varied from simply layered to fairly realistic. Those time-lapse EM feasibility studies was carried out by concentrating mainly on the time-lapse difference or ratio in the recorded EM data before and after production, when part of the oil has been replaced by saline water. In some studies, these data comparisons can provide a direct geometrical indication of the depleted area, while in others, more advance data processing was needed. However, the comparison of data recorded at the receivers offers little insight in how the EM fields interact with the depleted zone before and after production. Oil, for instance, may prevent the depleted zone from being "illuminated" by the source, then, the time-lapse difference in the EM signal may be too weak to be reliably measured at the receivers. Knowing how the fields interact with the depleted zone can help us to optimize an acquisition design.

The change in reservoir properties can be considered, to first order, as a scatterer that produces an additional signal. The behaviour of these additional signals are mostly determined by the size and the resistivity contrast of depleted bodies, and the background signals that are excited by a source. At the receivers, the sensors also record the background fields that can mask those additional signals. Consequently, there is a trade-off between background signals at the sensor and the signals at the depleted bodies. If the source is close to the receiver and the target, the signal will be dominated by the "direct field" and the time-lapse signal will be masked. If the distance is too large, the time-lapse signal will become too weak to be detected. In addition, a different orientation of the source leads to different geometrical behaviour of background fields, which is turn affecting the interaction with the depletion zone. In this paper, we investigate this interaction in more detail to obtain a better insight in the time-lapse response. We selected a simple half-space model. In that model, we conducted numerical experiments to study the sensitivity of EM data to changes in an oil-bearing reservoir after water injection. We considered a surface HED source as well as a VED source in a well. We investigated the optimal source-receiver pairs for a given reservoir location.

Our estimates show that land CSEM monitoring should be feasible, though not easily. The trade-off between signal strength and repeatability errors requires the source to be located at some distance from the reservoir. Our study also show that a HED source on the surface illuminates the depletion area quite well. However, the strong currents induced by the airwave energy also dominate the time-lapse signals. Therefore, a HED source would be useful if the airwave energy can be eliminated. If not, applying the source in a vertical well is the preferred option, although at higher cost.

Rigorous Interpolation of Tangential Fields Near the Seabed for 3D CSEM Modeling

Daniel Shantsev[1], **Frank Maaø**[2], **and Friedrich Roth**[1]

[1]EMGS, Trondheim, Norway
[2]Statoil, Trondheim, Norway

Abstract— We present a rigorous interpolation scheme for finite-difference modeling of controlled-source electromagnetic (CSEM) surveys. Nodes of the simulation grid do not necessarily coincide with exact positions of the modeled source and receivers, especially in a marine survey with complicated bathymetry. Even if they do, the staggered Yee grid conventionally used for CSEM modeling places different field components at different nodes, while a CSEM receiver measures all of them at the same location. In order to find all components at a desired recording position, one needs to interpolate the field values computed at the nearby nodes. For an accurate interpretation of the measured data one should take into account variations in the direction of the electric dipole antenna during the towing. Hence the source term in modeling must be represented by all three components, and a similar interpolation is needed again to properly distribute the source weight among adjacent grid nodes.

In marine CSEM surveys both the source and receivers are located close to the seabed. The water-formation interface is characterized by a strong conductivity contrast making the interpolation non-trivial. Here we focus on the *tangential* field components, E_x, E_y, H_x and H_y (the z-axis is assumed normal to the interface), which are most extensively used in CSEM data analysis. Even though the tangential fields are continuous across the interface, their *derivatives* along z experience an abrupt jump. In other words, the field profiles as a function of z exhibit a sharp bend when crossing the interface. Interpolation schemes that disregard this bend may lead to $\sim$10% errors for a cell size of 100 m and typical CSEM survey parameters (frequency of 1 Hz, seawater and formation conductivities of 3 and 1 S/m).

Existing approaches to this problem include: interpolation using only nodes above the seafloor [1], essentially non-oscillatory interpolation [2], and interpolation of only the secondary fields [3]. In the present work we propose a new interpolation recipe based on direct computation of the derivative jumps using Maxwell equations. We calculate the jumps in dE_x/dz, dE_y/dz, dH_x/dz and dH_y/dz from the behavior of other field components and the known conductivity contrast at the interface. The computed derivative jumps are then included into a non-linear interpolation scheme based on the Taylor expansion. For example, to find E_x at an arbitrary receiver location we use not only values of E_x computed at the surrounding nodes (at $4 \times 4 \times 4 = 64$ nodes for a cubic interpolation in 3 dimensions), but also values of E_z. Similarly, to model an electric dipole source in the x-direction, we place some source terms at the surrounding E_x nodes and some small "fictitious" source terms at E_z nodes.

Advantages of the new interpolation scheme are demonstrated on a custom finite-difference time-domain 3D modeling code solving the Maxwell equations in a modified wavedomain [4]. The accuracy of the computed fields as compared to the analytical 1D solution has shown to be almost independent of the relative position of source and receivers within the Yee cell. It implies that the interpolation error is essentially removed by the present scheme.

Use of the new interpolation scheme becomes especially important in the challenging case of very shallow water. For example, the interpolation using only nodes in the water [1] can hardly provide accurate results if the water column contains only one or two nodes. By contrast, the proposed scheme is likely to be more reliable since (i) it will also use nodes below the seabed, and (ii) it will make use of the known conductivity values at both sides of the interface.

REFERENCES

1. Abubakar, A., et al., *Geophysics*, Vol. 73, No. 4, F165–F177, 2008.
2. Wirianto, M., W. A. Mulder, and E. C. Slob, *EAGE*, 074, Extended Abstracts, Rome, 2008.
3. Streich, R., *Geophysics*, Vol. 74, No. 5, F95–F105, 2009.
4. Maaø, F. A., *Geophysics*, Vol. 72, No. 2, A19–A23, 2007.

3D Modeling of Novel Focused Source EM Survey versus the Standard CSEM

S. Davydycheva[1] and N. I. Ryhklinski[2]

[1]3DEM Consulting, USA
[2]Institute of Innovative Methods of Geophysics, Russia

Abstract— We present a novel Focused Source Electromagnetic (FSEM) method that exploits an idea of focusing the EM field in the vertical direction to provide deep-reading resistivity data. The focusing technique increases the spatial resolution and the depth of investigation of land and marine EM survey, as compared to the conventional Controlled Source EM (CSEM) method. We demonstrate the high efficiency of the focusing principle on challenging 3D models of the geological formation simulating seafloor bathymetry and other complicated shallow effects, which can mask the deeper reservoir response. The focusing reduces the distorting effect of shallow structures dramatically.

The idea of the vertical focusing of the EM field have been developed from Laterolog resistivity well logging principle. Laterolog is known to eliminate the axial borehole current at the receiver, reducing the effects of the conductive borehole and of the shoulder beds. However, Laterolog requires an automatic feedback loop to cancel the borehole axial current. It would be hardly feasible to apply such a feedback system on the earth's surface. We suggest a focusing procedure, which is rather based on software, than on hardware solution; still, it is an active focusing system giving results practically equivalent to the physical feedback-loop focusing.

Combining together the power of our focusing technique and the power of our 3D numerical modeling method, we handle exceptionally challenging test cases and show that FSEM allows simple visual interpretation of deep reservoir responses and automatic cancelling unwanted shallow effects in cases when the standard CSEM requires full 3D inversion for wide band of frequencies or measurement times. We show that FSEM has an advantage as compared to the standard CSEM in anisotropic formations as well.

Interpolation and Decomposition into Upgoing and Downgoing Wavefields for Undersampled CSEM Data

P. M. van den Berg[1], **Aria Abubakar**[2], **and Tarek M. Habashy**[2]

[1]Delft University of Technology, The Netherlands
[2]Schlumberger-Doll Research, Cambridge, USA

Abstract— For a controlled-source electromagnetic (CSEM) survey in a shallow water environment, the presence of the sea-surface hinders significantly the interpretation of the measured data. The electromagnetic (EM) wavefields are partly reflected and partly transmitted by the sea-surface. This means that the source and receiver signals are contaminated by the so-called source-ghost and receiver-ghost signals, respectively. Further the receiver-ghost signal can be considered as secondary-source signals that are transmitted in the earth. Hence, for shallow water environment, the removal of all these sea-surface ghost signals from the data is an important step in order to robustly interpret the collected data.

The first necessary step in the removal procedure is the decomposition of the signals into upgoing and downgoing electromagnetic wavefields. In the literature, it is proposed to carry out this decomposition in the spatial Fourier domain, but this procedure yields only acceptable numerical results if the acquisition area of receiver locations is very finely sampled, such that either numerical spatial differentiations or the equivalent multiplications in the wave vector domain can be carried out with sufficient accuracy. However, in the CSEM acquisition practice, the received signals are often very undersampled.

In the present paper, we use Huygens-type integral representation as the basis for the decomposition problem at hand. The integrals are spatial convolutions of the Green function and the tangential components of the electromagnetic field components. We propose an analytic continuation method for interpolating these components, in which the radiation characteristics of the electromagnetic dipole source are taken into account. After applying this interpolation step, we exploit the convolution structure of the Green function to finally perform the decomposition into upgoing and downgoing waves on a dense grid.

An Inversion Scheme for Anisotropic Resistivity

B. A. Hobbs
Petroleum Geo-Services, Birch House, 10 Bankhead Crossway South, Edinburgh EH11 4EP, UK

Abstract— Due to the work of Evert Slob, 2009 (personal communication) there now exists an analytic solution as a function of frequency for the in-line electric field response to an in-line source dipole for the case of a uniform, anisotropic halfspace (land case). The solution is particularly simple when both source and receiver lie on the surface of the halfspace. Frechét derivatives may be determined from this analytic solution and hence an iterative scheme may be devised to determine the properties of the halfspace (e.g., horizontal resistivity and anisotropy factor) from the frequency response measured at the surface.

Surface responses, either from synthetic data or from measured surveys, will be a function of source-receiver separation (offset) and frequency. Longer offsets and lower frequencies will penetrate deeper into a given subsurface. Thus, in the same way that a dc apparent resistivity sounding curve uses the response of a uniform halfspace to express apparent resistivity as a function of electrode separation (a proxy for depth), the above uniform anisotropic halfspace inversion can be used to express apparent anisotropy and resistivity as functions of frequency and offset (again being proxies for depth). Applying the inversion to a range of frequencies and offsets at a fixed surface location gives insights into the variation of resistivity and anisotropy with depth beneath that location. More generally, application to 2D and 3D data will determine cross-section and volumetric apparent resistivity and anisotropy variations which may be used as start models in more general 2D and 3D inversion schemes.

The uniform anisotropic halfspace inversion scheme will be described and its rapid convergence for a wide range of starting values will be demonstrated. Applications will be given to 2D synthetic data sets and to real survey data.

Inversion of 3D Marine CSEM Data Using Seed-type Initial Models

Michael A. Frenkel
EMGS, USA

Abstract— The marine Controlled-Source Electromagnetic (CSEM) method has been evolving into a subsurface resistivity imaging tool for increasingly complex geological settings. The measured EM field needs to be inverted to obtain accurate formation resistivity volumes. This information can be used to find reservoirs and determine hydrocarbon saturations. An important step in the resistivity interpretation process is the inclusion of constraints to guide inversion and reduce its non-uniqueness. In this paper, we use 2.5D and 3D synthetic models to investigate the accuracy of the subsurface resistivity reconstruction using additional information about the target body's position. We show that application of seed-type initial models leads to a significantly improved inversion-based CSEM resistivity interpretation.

Simultaneous Joint Inversion of Seismic and Magnetotelluric Data for Complex Sub-salt Depth Imaging in Gulf of Mexico

M. Viriglio, M. De Stefano, S. Re, F. Golfrè Andreasi, and F. F. C. Snyder
WesternGeco, Italy

Abstract— We present the first application of the 3D simultaneous joint inversion (SJI) between seismic and marine magnetotelluric data over the northern Gulf of Mexico; the numerous coalescing allochthonous salt canopies that cover potential reservoir structures are particular challenges to deepwater exploration in that region of the world. Properly interpreting the salt structures is a key to understanding and creating accurate tomographic velocity models, which in turn, are necessary to properly position and image the subsalt targets in the framework of the geophysical exploration.

The marine magnetotelluric method (MMT) is a geophysical exploration tool where natural electromagnetic fields are used to investigate the electrical conductivity structure of the subsurface. The natural sources of the MT field in a marine environment are the current systems in the magnetosphere set up by solar activity. Data are commonly acquired with an array of seabed receivers recording horizontal electric and magnetic fields. MMT is strongly sensitive to the conductive sediments just below the base of the salt, thus integrating MMT data provides to the seismic methods an enhanced capability and an independent way of detecting the deep boundary salt-sediments.

In this context, simultaneous joint inversion collects seismic and EM information into a single-objective function to be inverted, as opposed to the multiple functions inverted by both single-domain approaches (i.e., seismic tomography and MMT inversions algorithms). The ambition is to improve the existing velocity models for prestack depth migrations and the consistency of seismic and non-seismic representations of the subsurface in complex salt geometries.

The role of SJI is to combine the uncorrelated residuals, collate the constraints for single-domain models (regularization and preconditioning), and set the constraints between the models of different domains linking the unknowns belonging to different measurements. The algorithm inverts for all models providing updates for each of the different domains. The SJI workflow joins together only the inversion phases of the different marine measurements involved. As a general view, integration can take place at different levels of an exploration workflow; in Equation (1) the SJI is fully described by one single objective function used to integrate the problem at the inversion level.

$$\Phi(m, m_0) = r^T C_d^{-1} r + \alpha m^T L^T L m + \sum_{k=1}^{N_D} \lambda_k \left\| \Psi_k(m, m_0) \right\|^2 \tag{1}$$

m, m_0	Models	L	Regularizator
r	Residuals	N_D	Number of domains
C	Covariance matrix	Ψ_k	Links functions

Equation (1): The SJI cost function, collecting the residuals (data part, first addend) and the unknowns of different domains (models part, second addend). The third part of the equation describes the links between unknowns of different domains. α and λ are the weights for the addends in the summation.

We also demonstrate that SJI reduces inversion uncertainties, and defines a new strategy for subsalt interpretation, thereby enhancing the role of non-seismic methods as supporting complex seismic depth imaging. The well-known intrinsic non-uniqueness of the EM (MMT here) problems is reduced, improving the resolution, accuracy, and value of non-seismic data domains.

Integrating Well Log, Seismic and CSEM Data for Reservoir Characterization

Lucy MacGregor and David Andreis
OHM Ltd., UK

Abstract— Well logs provide a high resolution measurement of the properties of a reservoir and the surrounding strata, however properties can only be determined in a small area local to the well. However often measurements of reservoir properties across the extent of a field are desirable for reservoir management or production optimization. Remote geophysical measurements are therefore required. Seismic data are most commonly used for this purpose, however in recent years CSEM methods, which measure the resistivity structure of the seafloor have also been widely applied.

CSEM methods use a high powered source to transmit low frequency signals through the earth to an array of receivers. By interpreting the received signals using forward modelling and inversion approaches, the resistivity structure of the seafloor can be determined. In many situations electrical resistivity is driven by the properties and distribution of fluids in the earth. Resistivity well logs often show that commercial hydrocarbon deposits may be many times more resistive than surrounding lithologies. In principal such variations should be readily detected using CSEM tools. In contrast, seismic data are sensitive to boundaries between lithologic units but are less sensitive to fluid changes within these units. Given high quality seismic and well data and sophisticated seismic inversion and rock physics tools, we can sometimes relate these seismic changes to saturation effects. Nevertheless, the change in resistivity caused by variations in saturation should be much easier to detect.

However, despite the increased sensitivity of resistivity data over seismic for the determination of saturation, there are two inherent challenges to interpreting CSEM data. Firstly, the structural resolution of CSEM data is poor. Secondly, the cause of resistivity anomalies (particularly high resistivity features) cannot be uniquely linked to the presence of hydrocarbons in the subsurface when taken in isolation. In many situations these are equally likely to be caused by other high resistivity material (for example, tight carbonates, salt or volcanics). Both of these limitations must be addressed when considering the applicability of CSEM to answer a geophysical question, and as far as possible mitigated by the interpretation approach adopted.

CSEM data can, of course, be interpreted in isolation. However, with no constraints on this interpretation, the result will suffer from the non-uniqueness and ambiguity which blight unconstrained interpretation approaches. In the presence of seismic and well information, the question that we are trying to answer with the CSEM data becomes significantly better posed. The question is no longer one addressed at finding a reservoir, but rather one of determining the content of a defined structure. Using seismic information the reservoir structure is known (but potentially not its content or extent), and we have independent constraints on the surrounding strata within which it is embedded. This is therefore a constrained interpretation problem and one that the CSEM data are in a much better position to answer.

Joint Electromagnetic and Seismic Inversion Using Structural and Petrophysical Approach

Aria Abubakar, **Tarek M. Habashy**, **and Guozhong Gao**
Schlumberger-Doll Research, Cambridge, USA

Abstract— We present two algorithms for the inversion of joint electromagnetic and seismic for reservoir monitoring and exploration applications.

In the first algorithm, the electromagnetic and seismic data are jointly inverted using a cross-gradient constraint that enforces the structural similarity between the conductivity image and the compressional (P-wave) velocity image. From the extensive test results that we conducted, this joint inversion algorithm shows a significant improvement over the results obtained from the separate electromagnetic or seismic inversions.

In the second algorithm we directly estimate the reservoir petrophysical parameters such as porosity and fluid saturations by simultaneouly inverting the electromagnetic and seismic data. Electromagnetic data are connected to porosity and fluid saturations through Archie's equations, while seismic data are connected to porosity and fluid saturations through a rock physics model. This approach provides substantial advantage for an improved estimation of porosity and fluid saturation distribution over the one obtained from the separate inversion of electromagnetic and seismic data.

The inversion methodologies that we used in both algorithms are based on the Gauss-Newton minimization approach. Because of the ill-posed nature of the inverse problem, regularization is employed to narrow down the solution. In this work, the weighted L_2-norm regularization is used due to its excellent edge-preserving properties. We also employ the so-called multiplicative regularization technique to automatically select the regularization parameters, which improves the robustness of the algorithm.

We applied this joint inversion for integrating the marine controlled source electromagnetic (CSEM) data with surface seismic data for sub-sea reservoir exploration applications and also in integrating the cross-well electromagnetic and seismic data for reservoir monitoring and evaluation applications. We show that both joint inversion approaches implemented in this work may reduce the ambiguity on the data interpretaion, thus leading to improved reservoir characterization.

Crosswell Electromagnetic Inversion Constrained by the Fluid Flow Simulator

L. Liang, A. Abubakar, and T. M. Habashy
Schlumberger, USA

Abstract— Crosswell electromagnetic technology has been developed to obtain the resistivity distribution in the region between the wells. By looking at the resistivity changes over time, people can monitor the fluid front movements and saturation changes in the reservoir. Traditionally, the resistivity distribution is directly inverted from the crosswell electromagnetic data through a pixel-based inversion process. However, this inversion problem is highly non-unique and has limited spatial resolution. The quality of the inversion heavily depends on the accuracy of the background resistivity, the resistivity contrast, etc. There are different methods to improve the inversion of crosswell electromagnetic data. For example, resistivity logs can provide constraint to the nearwellbore region, joint inversion with crosswell seismic can also enhance the inversion since seismic can provide relatively accurate structural information. However, the improvements from these methods are still not satisfactory. Well logs only provide information in the vicinage of the wellbore, while seismic doesn't distinguish the oil-water interface very well.

In this study, we introduce several novel inversion approaches for improving the interpretation of the crosswell electromagnetic data. The inversion is constrained by using a multiphase fluid flow simulator that simulates the fluid flow in the reservoir and calculates the spatial distributions of the water saturation and the salt concentration, which are in turn transformed into the formation conductivity using a resistivity-saturation formula. Then, a 2.5D electromagnetic algorithm is employed to simulate the crosswell electromagnetic measurement. In these approaches, instead of directly inverting the resistivity distribution, we are inverting the formation petrophysical parameters such as permeability and porosity. A Gauss-Newton technique is employed to update these model parameters until a good match between the simulated and measured crosswell electromagnetic data. The Jacobian of electromagnetic data respect to the porosity is computed using an adjoint method. In this way, the reconstructed resistivity distribution is consistent with the fluid flow physics, and nonuniqueness of the interpretation is effectively reduced with an improved spatial resolution. Moreover, after the inversion, we naturally obtain a saturation distribution which is the direct indication of the fluid movement and saturation change. A synthetic case study has been carried out and the results show impressive improvement comparing to that acquired by a pixel-based inversion approach using only electromagnetic data.

Electromagnetic Imaging of Buried Objects Using a Decoupling-based Reconstruction Method

A. Lakhal
Faculty of Mathematics and Computer Sciences, Institute of Applied Mathematics
University of Saarland, Saarbrücken D-66041, Germany

Abstract— Inverse electromagnetic scattering is emerging as a prospecting method in many geophysical applications. We present here a decoupling-based imaging method to reconstruct the electromagnetic properties of some buried object from exterior measurements of scattered fields. Data are near-field measurements of scattered waves for multiple illuminations at a fixed frequency. The forward modeling is based on the full three-dimensional time-harmonic Maxwell equations in nonmagnetic inhomogenious media. They are reformulated as a system of integro-differential equations for the contrast functions between the unknown object and its background. In the inverse problem, we seek the unknown constitutive parameters of the object given by the electric permittivity and the electric conductivity. This problem is ill-posed since it is under-determined and ill-conditioned. Furthermore, it is nonlinear as the dependence of the fields on the medium properties is for many materials highly nonlinear. Besides, the mathematical complexity of the problem is enhanced as all components of the electromagnetic fields are coupled. A new approach using the concept of generalized induced source (GIS) was introduced in [1] for identifying current sources. The advantage there is that we recast the intertwined vector equations in the Maxwell's system into decoupled scalar problems. In [2], we applied this decoupling procedure to derive a fast reconstruction method for inverse medium electromagnetic scattering. The adaptation of this method to geophysical exploration is possible by considering the suitable geometrical setting. We obtain an efficient iterative method based on Kaczmarz'algorithm for recovering the electromagnetic refractive index of the unknown object. To validate the method we make numerical tests in 3D with simulated and experimental data.

REFERENCES

1. Lakhal, A. and A. K. Louis, "Locating radiating sources for Maxwell's equations using the approximate inverse," *Inverse Problems*, Vol. 24, 18, 045020, 2008.
2. Lakhal, A., "A decoupling-based imaging method for inverse medium scattering for Maxwell's equations," *Inverse Problems*, Vol. 26, 015007, 2010.

Session 2P2
Electromagnetic Remote Sensing for Defense and Homeland Security

Closed-form, Bistatic, 3D Scattering Solution for a Dihedral Corner Reflector

Julie Ann Jackson
Air Force Institute of Technology, USA

Abstract— Scattering prediction models may be used to extract features of interest in measured synthetic aperture radar (SAR) data. The electromagnetic community routinely uses computationally intensive numerical scattering prediction codes to obtain accurate scattering solutions for a given object or scenario. The signal processing community prefers closed-form scattering models that allow for computationally efficient generation of the scattering predictions as a function of relevant feature parameters, such as object location and size. Optimization techniques are then used to estimate the scattering feature parameters by matching the predicted response to the data. Often, signal processing models sacrifice accuracy in the scattering prediction in order to obtain an easily-invertible mathematical form (e.g., the isotropic point scatterer model). This work attempts to bring together the signal processing and electromagnetic modeling goals by deriving an accurate yet closed-form, bistatic solution for 3D scattering for a dihedral corner reflector.

There is much work in the open literature on electromagnetic scattering from dihedrals for monostatic radar. A variety of approaches, including geometric optics (GO), physical optics (PO), physical theory of diffraction (PTD), and uniform theory of diffraction (UTD), have been used to derive radar backscatter when the transmit/receive antenna is aligned with the plane of the dihedral corner mechanism. Backscatter is greatly reduced for angles away from the plane of the corner, so the two-dimensional scattering problem is of most interest. However, bistatic antenna configurations are able capture the specular returns for transmitters outside of the plane of the dihedral corner. Thus, three-dimensional (3D), bistatic scattering predictions are desired. In this paper, we extend the monostatic works to derive in closed-form the 3D bistatic scattering predictions for a right-angle, rectangular dihedral. We validate the resulting scattering model against numerical electromagnetic prediction codes.

We derive a closed-form scattering model using a hybrid GO-PO method. We use GO to trace ray reflections, and we evaluate the PO integral(s) for the field scattered by each plate of the dihedral. Multiple cases of reflection geometry are considered to account for effects of the dihedral plate size and antenna aspect angles. The complex-valued (amplitude and phase) scattering response is derived. The resulting parametric scattering model is presented in terms of the vertical and horizontal co-polarization and crosspolarization responses that correspond to the outputs of industry-standard numerical prediction codes. Thus, for feature extraction optimization routines, the aforementioned prediction codes may be replaced with an accurate, parameterized model that is more efficiently computed. Because the parameterized model does not depend on a surface mesh, the computational speed-up (minutes versus hours) is especially desirable for electrically large objects that would require a large number of mesh nodes for a Method of Moments (MoM) code. The proposed work provides a dihedral scattering model that supports development of optimal feature extraction methods. This model will aid future research in using dihedral features for target recognition, image registration, and scene visualization problems for bistatic (and monostatic) polarimetric SAR.

Experimental Demonstration of Photonic Band Gap Channel Drop Filters at Sub-Terahertz Frequencies

D. Yu. Shchegolkov[1], **L. M. Earley**[1], **C. E. Heath**[1], **E. I. Smirnova**[1], **and B. D. Schultz**[2]

[1]Los Alamos National Laboratory, Los Alamos, NM 87545, USA
[2]International Technology Center, Raleigh, NC 27617, USA

Abstract— We have successfully designed, fabricated and tested several Photonic Band Gap (PBG) Channel Drop Filters (CDFs) operating in a low THz frequency range. We demonstrated a metal PBG CDF operating at about 100 GHz and a dielectric (silicon) PBG CDF operating at about 240 GHz. The unique ultra-compact 240 GHz filter is finding important applications in remote chemical detection.

Introduction: A PBG CDF is a device that allows channeling of selected frequencies from the continuous spectra into separate waveguides through a PBG structure (Figs. 1(a)–1(d)). It is compact and configurable and, thus, can be employed for mm-wave spectrometry with applications in communications, radio astronomy, and radar receivers for remote sensing and nonproliferation.

Results: The metal PBG CDF was fabricated in two ways: via conventional machining and via electroforming. It was operated at higher order modes to mitigate ohmic loss. We have observed up to 35 dB frequency selectivity with the metal CDF at 107 GHz in the detector output channel.

For dielectric CDFs, we developed robust designs and a unique fabrication method through deep reactive ion etching applicable at frequencies of 200 GHz and above. This fabrication technique provided several very similar working CDF samples operating at 240 GHz. Measured in a millimeter wave laboratory the transmission characteristics were in excellent agreement with the results of computations. The frequency of 240 GHz was transmitted into channel #4 with the linewidth of less than 1 GHz and the background lower than −25 dB (Fig. 1(d)). Transmission into channel #3 and reflection into channel #1 were 10 dB below the transmission into channel #4. We observed ohmic losses inside of the filter of about 3 dB (50 percent), which proved the possibility of stacking multiple filters together to form a spectrometer for detecting molecular signatures.

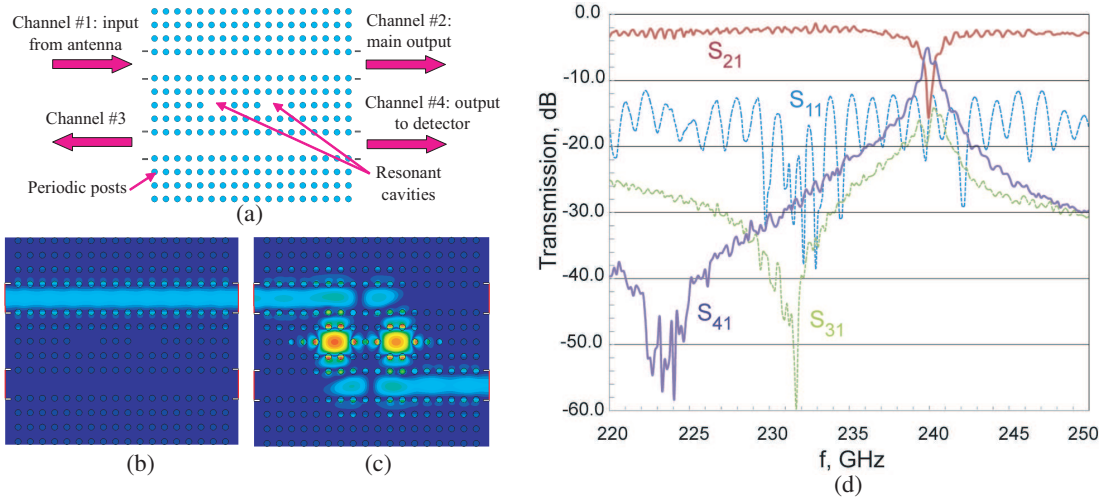

Figure 1: (a) Schematic of the channel-drop filter with silicon posts. (b) Electric field energy density for non-resonant frequency and (c) for the resonant frequency. (d) Power transmits straight into channel 2 for all frequencies, except for the resonant frequency, which is transmitted into channel 4 through the resonant cavities. Measured transmission characteristics.

ACKNOWLEDGMENT

The authors gratefully acknowledge the support of the U.S. Department of Energy through the LANL LDRD Program.

Sub-terahertz Radiometric Imaging System for Concealed Weapon Detection

Alexey Vertiy, Mustafa Tekbas, Ahmet Kizilhan, Sergey Panin, and Sunullah Ozbek
International Laboratory for High Technology, TUBITAK-MRC, MI
1 Dr. Zeki Acar Str., Gebze/Kocaeli 41470, Turkey

Abstract— At present, passive radiometric imaging technology is one of the most promising approaches to disclosure of dangerous objects (weapons, explosives, drugs, etc.) concealed under persons' clothing, without revealing itself. In light of the terroristic threat the high-resolution radiometric systems for fast imaging in short distances are essential for concealed weapon detection in public places. Such an imaging system of sub-terahertz range is currently developed in Marmara Research Center, TUBITAK.

In our passive imaging system of 3-mm wave range the reproducing of the radiometric image, corresponding to the brightness temperature of the target, in the plane of scanning was achieved by the long-focus teflon lens objective. The dielectric objective was designed by the matrix method in geometrical optics approximation. Also the single parabolic reflector and the double-reflector antenna based on the Cassegrain design were numerically modeled and optimized for radiometric imaging application. The current radiometric system exploits the one channel design for scanning in the focal plane of the dielectric lens. As radiometric receiver module was employed conical horn and direct detection receiver. The receiver amplifier stage involves three cascades of the low noise amplifiers. The output signal was converted for subsequent imaging processing by the high sensitive detector. The maximum amplification factor achieved is about 45 dB. Preliminary results obtained for outdoor measurements show high contrast resolution of the system in the sub-terahertz range. The radiometric imaging peculiarities of the different reflecting and absorbing targets were investigated against the brightness temperature of sky. The system was demonstrated to successfully detect and recognize the metallic weapon hidden under outer clothing (topcoat, sweater) in the distance about 8 meters.

MIMO Radar Concept for Detecting Human Beings through Walls in the Presence of Background Clutter

P. Millot, B. Boudamouze, T. Volpert, and C. Pichot
Radar and Electromagnetism Department, ONERA
2 avenue E. Belin, BP 4025, Toulouse 31055, France

Abstract— In the last years, a great consideration has been brought to the new concept of MIMO-radar [1]. This radar concept deals with a large number of antennas, both used as transceivers and receivers, the use of orthogonal waveforms and some diversity gain both in frequency and angular domain brought to improve detection. In this paper, we investigate the potentiality of MIMO radar at short range for the detection of human beings hidden inside rooms. Through-the-Wall radar (RTTW) detection as already been used with UWB waveforms to draw benefit from high space resolution capabilities to eliminate clutter [2].

For the purpose of studying MIMO radar performances in this configuration, we have developed a simulation tool with the help of a 3D FDTD code, which has been optimized for parallel computing. The frequency spectrum of the injected pulse is 500 MHz–2 GHz. 20 cm thick walls are modeled by their dielectric constant and electromagnetic conductivity. We simulate an array of 67 elements spaced of 7.5 cm (half a wavelength at 2 GHz) over 5 m, both used in transmit and received mode. For the moment, the problem of channel decoupling with orthogonal waveforms is not taken into account and we assume that the orthogonally conditions are fulfilled. The human beings are modeled by 1.7 m high cylinders of 50 cm diameter on the soil (with a given average dielectric constant). They can take various positions in a room of dimensions (4 m × 5 m × 2 m). First, we present the results of UWB-SAR processing (in near field) on the simulated data by using a given frequency bandwidth. UWB SAR processing with ultra large baseline is often seen as a performing processing tool that has the drawback of experimental complexity. Furthermore, effects of wall transmission mitigation and background clutter rejection are not usually considered with such a processing. By sparsing both the array and the frequency band, i.e., using other more simple antenna configurations in (Tx, Rx) mode, we can simulate new MIMO radar configurations, that could be more efficient in the multi-static mode at short range. These results are presented and some conclusions will be drawn on the estimated efficiency of MIMO-RTTW in terms of detection.

ACKNOWLEDGMENT

DGA is acknowledged for financial support of these researches.

REFERENCES

1. Fishler, E., A. Haimovich, R. Blum, D. Chizhik, L. Cimini, and R. Valenzuela, "MIMO radar: An idea who's time has come," *Proceedings of the IEEE Radar Conference*, 71–78, Toulouse, France, April 26–29, 2004.
2. Maaref, N., P. Millot, and C. Pichot, "A study of UWB FM-CW radar for the detection of human beings in motion inside a building," *IEEE Trans. on Geoscience and Remote Sensing*, Vol. 47, No. 5, 1297–1300, May 2009.

FMCW SAR Imaging of Body Worn Explosives from FDFD Modeled Scattered Field Data

Justin Fernandes, **Richard Obermeier**, **Jose Martinez**, **and Carey Rappaport**
Department of Electrical and Computer Engineering, Northeastern University
Suite 302 Stearns Building, 360 Huntington Avenue, Boston, MA 02115, USA

Abstract— In the increasingly important problem of identifying suicide bombers wearing explosives concealed under clothing, it is essential to detect suspicious individuals at a distance. Current systems employ multiple sensors to determine the presence of explosives on people, including observing and following individuals, identifying explosive residues or heat signatures on the outer surface of their clothing, or by characterizing explosives using penetrating X-rays or terahertz wave radar. At present, millimeter-wave (MMW) radar is the only modality that can penetrate and sense beneath clothing at a distance of 10 to 50 meters without causing physical harm. Recent advances in digitally controlled FMCW radar frequency sources are making ultra-wide band (UWB) imaging at MMW frequencies a more realizable and cost efficient solution for remote sensing applications.

In this paper, MMW frequency-modulated continuous wave (FMCW) synthetic aperture radar (SAR) imaging of humans wearing body worn explosives is simulated. Channel spectral responses as a function of range and look angle are obtained from two-dimensional transverse magnetic (TM) finite difference frequency domain (FDFD) full wave numerical analysis. The channel spectral responses are used to synthesize FMCW radar signals.

Two-dimensional SAR images (see example below) are created using a manual focusing technique based on the Rayleigh-Sommerfeld diffraction formula and compared to images generated via Fourier based imaging. Multistatic, monostatic, and multi-monostatic synthetic aperture configurations are simulated and evaluated. Results of the simulations are being used to design a portable and cost effective solution for standoff detection of suicide bombers.

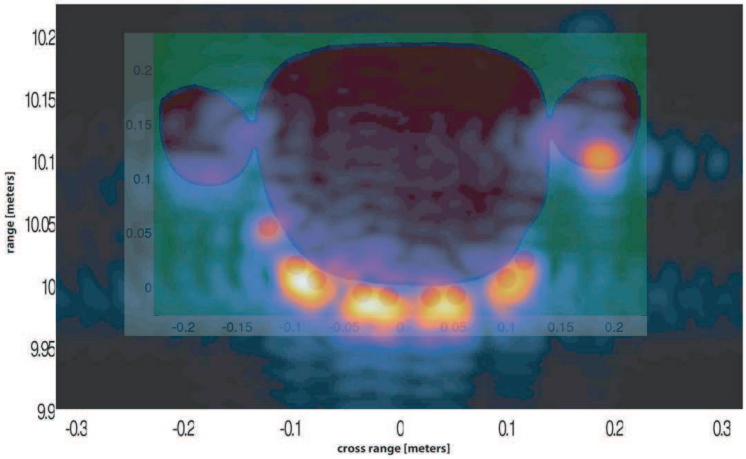

Figure 1: Example SAR image of male body with 9 PEC cylinders on chest. Original geometry overlaid. Image created using scattered fields from FDFD analysis. Target simulated at 10 meter range with 1 meter wide synthetic aperture.

Effect of Antennae Polarization Relative to Tunnel Orientation on Electromagnetic Wave Scattering Due to Underground Tunnels

Arvin Farid
Civil Engineering, Boise State University, USA

Abstract— Clandestine tunnels have been used by illegal immigrants and smugglers to avoid border security and checkpoints. In recent years, international terrorists have shown interest in using tunnel to cross borders, smuggle weapons, and infiltrate their target facilities. This has become a pertinent threat, which in turn, has made the effort to detect tunnels a national security priority. Versatile geophysical techniques are the most promising and least costly methods to detect tunnels. However, no single technology or sensing modality has proven successful at detecting tunnels in heterogeneous soil environments. The challenge of balancing the trade-off between image resolution and penetration depth is also a main challenge against these techniques, especially in case of deep small tunnels. Use of broadband antennas at different polarizations with respect to tunnel orientation, seems very promising to overcome this latter challenge.

The goal of this research is to study and evaluate the validity of this hypothesis via a 3D theoretical finite element simulation (using COMSOL software) validated by experimentation. Both theoretical and experimental simulations are 1/100 scaled. A versatile tunnel detection technology requires above surface transmitting and receiving antennas. However, to avoid the surface roughness at this stage, cross-borehole depth profiling approach is used. The soil used in the experiment is dry fine Ottawa sand. PVC-cased ferrite-bead-jacketed borehole monopole antennae are used as the source and receiver for the experiment.

New Scheme for Radar Target Identification via Target's Internal Modes

Haythem H. Abdullah[1], **Khalid F. A. Hussein**[1], **Mostafa El-Said**[2], **and Essam A. Hashish**[2]

[1]Electronics Research Institute, Egypt
[2]Faculty of Engineering, Cairo University, Egypt

Abstract— The extension of the abilities of human senses using synthetic devices or systems is of main concern for long time. So, the trend of developing remote sensing systems has attracted attention of electromagnetic researchers for its important applications such as Air-traffic control, Air defense, exploration geophysics, and several important applications in medicine. In this paper, the target identification of the conducting objects that have cavities with small apertures is considered.

The impulse response of the conducting targets always exhibit two distinct regions; the early time, forced component, representing the back scattered field excited by currents during the time when the impulse is traversing the target and the late time where the target can be discriminated. If the target is closed, then a free oscillating damped signal will appear as a sum of constant amplitude natural modes and exist for all time $t > 2\,\mathrm{T}$. These types of targets can be discriminated using techniques such as, the K pulse technique, the modified prony's method or the E pulse technique. But in other cases where the target has small apertures in its body, some internal modes will be excited. These apertures act as coupling windows. If the aperture couples waves to any cavity structure, the fuel tanks apertures, internal resonant fields will be excited. The internal resonant field appears as slowly damped sinusoidal signals in the late time. The internal modes are almost dominated over the target natural modes in the very late time.

In the very late time where the internal modes dominate over the natural modes, one can assign a sampling window for the analysis. The proposed scheme can be described in the following few words; the sampling window takes samples from the backscattered signal starting in the very late time and lasts for more than 10 cycles of the signal fundamental frequency. The sampled signal is normalized to its maximum value. The normalized signal is fed to a bank of band pass filters. The central frequencies of the filters are assigned according to a data base containing the resonant frequencies of each target. The outputs of the filters are summed. The normalized signal is correlated with the summed signal. There are two cases for the output of the correlator. If the filters central frequencies are in consistence with those resonant frequencies corresponding to the existing target then the maximum output of the correlator will be the greater one. In this case, the index of the target is taken from the data base and hence the target is detected. On the other case where the output of the correlator is not the maximum, then the index of the target in the data base is incremented. The process will be repeated till the correlator maximum output will be the greater one. At this time the index of the target will be known and the target is detected according to its internal modes. The bank of filters is designed using the bilinear transformation of the transfer function of a second order IIR filter. The back scattered signal and the radar cross section of the targets are calculated using our home made Moment method software. The Rao-Wilton-Glisson basis function in conjunction with the triangular patch model is used to model the targets in the Moment method. The identification scheme is applied to three conducting targets, a sphere with aperture, a slotted cylinder, and a slotted cube. It is noticed that the scheme is efficient even with targets that have close resonances and with minimum number of modes.

Time-Domain Wall Parameter Estimation and Mitigation for Through-the-Wall Radar Image Enhancement

Christopher Thajudeen, **Wenji Zhang**, **and Ahmad Hoorfar**
Center for Advanced Communications, Villanova University, Villanova, PA 19085, USA

Abstract— Recent advances in both algorithm and component technologies have made through-the-wall imaging an affordable sensor technology for applications in both civilian and military settings. The ability to employ through-the-wall imaging techniques in urban environments is of paramount interest. Specifically, the ability to detect and identify targets of interest within enclosed building structures when entry would be deemed dangerous or impossible would be of great benefit. In order to achieve proper target registration behind walls, knowledge of the wall effects on the radar returns from targets within a building structure must be understood and exploited. The strong returns from conventional exterior urban wall materials can shade or completely obscure the much weaker signals from targets within the building. This effect is intensified if the target is close enough to the wall for its return to be blended with that of the wall itself. Furthermore, the wall can add dispersion and range ambiguity which can only be compensated for through the use of refocusing algorithms which rely on apriori knowledge of the wall parameters such as the dielectric constant and thickness, ε_r and d, respectively [2].

In this paper, we present a method to extract the aforementioned wall parameters from the time-domain scattered field. In addition, the time-domain response of the wall is then analytically modeled [1] and removed from the measured wall response to mitigate the shadowing effect of the wall on targets of interest within a building structure. This method allows the acquisition of the necessary wall parameters to allow for wall mitigation as well as the implementation of techniques to refocus the resulting image to compensate for the dispersive effects of the wall. Imaging results after the application of this wall mitigation technique will be presented for numerically generated wall-target scenarios to demonstrate its effectiveness.

REFERENCES

1. Karousos, A., G. Koutitas, and C. Tzaras, "Transmission and reflection coefficients in time-domain for a dielectric slab for UWB signals," *2008 IEEE Vehicular Technology Conference, VTC2008-Spring*, 455–458, May 11–14, 2008.
2. Dehmollaian, M. and K. Sarabandi, "Refocusing through building walls using synthetic aperture radar," *IEEE Trans. Geoscience and Remote Sensing*, Vol. 46, 1589–1599, 2008.

Through Wall Imaging Using the DORT Method

M. Davy, T. Lepetit, J. de Rosny, C. Prada, and M. Fink
Laboratoire Ondes et Acoustique, Institut Langevin, ESPCI ParisTech, CNRS UMR 7587
Université Denis Diderot Paris 7, 10 rue Vauquelin, 75231 Paris Cedex 05, France

Abstract— Imaging of targets behind obstacles is an intensive research topic as it concerns domains like surveillance or reconnaissance in complicated environments. We propose here to use the DORT method with microwaves to detect and image experimentally a target behind a wall. The DORT method, French acronym for Decomposition of the Time Reversal Operator, consists in studying the eigen-vectors of the time reversal operator, which is built from the the inter-element responses between two antenna arrays. In our case, two arrays of seven Vivaldi antennas are used: one in transmission and one in reception. Microwaves measurements are performed between 2 and 8 GHz with a vector network analyzer. To decrease the weight of direct reflections off the wall, the response with and without the target are subtracted. Hence, even if echoes from the wall are not totally cancelled, the target response clearly appears. After applying a fast Fourier Transform to the subtracted signal, the time-dependent signals are divided into short time-windows and the eigen values are plotted for each time-window. Eigen values associated to our target clearly appear. To find the target location, we back-propagate the eigen vectors corresponding to the eigen values associated to the target. In other words, we compute the correlation between the eigen vectors to test Green's functions of our medium. These test Green functions are very sensitive to the wall permittivity and width. Those two parameters are experimentally determined. A 4.5 refractive index has been measured. This value shows that the waves are strongly refracted. The last part of this work concerns the detection of two scatterers behind the wall. We use the MUSIC estimator to accurately localize them. We discuss on the DORT-MUSIC method resolution limit. Finally, we apply this technique to follow a scatterer which is moving behind the wall.

Inverse Scattering Problems in Modern Homeland Protection Systems

M. D'Urso[1], **A. Buonanno**[1], **G. Prisco**[1], **and A. Farina**[2]

[1]Giugliano Research Center, SELEX Sistemi Integrati, Via Circumvallazione Esterna di Napoli Zona ASI, I-80014, Giugliano in Campania, Napoli, Itlay
[2]Integrated System Analysis, SELEX Sistemi Integrati, Via Tiburtina Km. 12400, I-80032, Roma, Itlay

Abstract— Through-the-wall imaging is an emerging technology, with increased interest in military and civil applications. Police and other law enforcement agencies are interested in developing systems able to detect and localize one or more persons on the other side of a door, behind a wall, above the ceiling, or below the floor. Such kind of systems are also useful in rescue missions, earthquake situations [1–3].

The general goal of using through-the-wall radar is to detect persons behind the wall and, if possible, trace his/her movement trajectory when located in a not accessible environments. These are very complex problems and several solutions have been introduced in last years.

We are working on these problems and simple systems and signal processing procedures have been developed and experimentally tested such to detect, in complex scenarios, the human presence. In particular, the developed systems and procedures allows:

- to detection the human presence behind a wall, or many walls by detecting two of the main life signs, i.e., the breathing and heartbeat activities.
- to detect, localize and track the person with his/her motion by means of a low computational cost algorithm, with "almost" real time imaging refresh.
- to estimate the internal building layout from the outside.

As the first application is concerned, note that the proposed system is mainly based on the Doppler Radar principle. In particular, it is possible to show that when a person is exposed under the incidence of a Continuous Wave source (in the microwave range), the reflected signal is phase-modulated due to the (periodic) chest movements due to respiration and heartbeat. Accordingly, as in radar applications, the frequency or phase of the incident wave can be changed according to the nature and characteristics of the chest movement. So, by adopting appropriate demodulation techniques, inspired by radar processing procedures, one can detect the vital signs from the phase distributions of the measured reflected waves. The de-modulated phase gives back a signal which is proportional to the chest-wall positions, and so to the heartbeat and respiration activities. An ad-hoc signal processing procedure has been developed in SELEX Sistemi Integrati. An X-Band Experimental set-up has been also adopted to experimentally validate the developed procedures. The achieved results shows that, by using a very low cost hardware and very simple procedures is possible to detect the presence of human body behind wall through his/her life signs. As the second and third activities is concerned, innovative procedures with very low computational complexity have been developed at SELEX Sistemi Integrati to detect moving targets behind walls, and to estimate the internal building layout, which is generally unknown.

This are not trivial problems. The solution of Maxwell equations in so complex scenarios, like furnished rooms is a very complex problems. The presence of walls, as well as the mutual interactions between the static targets located behind walls, make the problem not simple and many efforts have be done to develop a simple processing scheme able to solve the problem in real time.

REFERENCES

1. Aryanfar, F. and K. Sarabandi, "Through wall imaging at microwave frequencies using space-time focusing," *Antennas and Propagation Society International Symposium*, Vol. 3, 3063–3066, June 20–25, 2004.
2. Baranoski, E., "Visibuilding: Sensing through the walls," DARPA Special Projects Office, IEEE SAM Workshop, 2006.
3. Baranoski, E., "New sensor signal processor paradigms: When one pass isn't enough," *Argon ST-HPEC 2008*.

Multi-temporal Hyperspectral Images Unmixing and Classification Based on 3D Signature Model and Matching

I. R. Farah[1, 2], **S. Hmissi**[1, 2], **K. Saheb Ettabaa**[1, 2], **and B. Souleiman**[2]

[1]RIADI-GDL, ENSI, Tunis, Tunisia
[2]Télécom Bretagne, Dép. ITI, Technopôle Brest-Iroise-CS 83818, 29238 BREST CEDEX 3, France

Abstract— Land cover and land use types are challenged to access real-time and precise information of interest. The recent advent of sophisticated sensors enables to exploit independent observations of a phenomenon and to extract more detailed information and performs a decision level for scene classification. This allows the monitoring of spectral or spatial characteristic changes over time more precisely. Hence, multitemporal data may facilitate accurate image analysis in situations where data coming from a single sensor lack fidelity in the spectral or/and spatial domains [1].

In unmixing task, the measured mixed spectrum is decomposed into a set of endmembers and their corresponding fractional abundances within the pixel The problems of multi-temporal image classification and unmixing are highly relevant in most remote sensing study [2]. To address this problem, several strategies have been proposed. Such as in [3], Du et al. proposed an unsupervised linear unmixing approach for multi-temporal hyperspectral change detection In [4], Prasad et al. proposed a framework in which they incorporate a subspace identification procedure to partition the hyperspectral space into multiple contiguous subspaces, and then a decision fusion mechanism was employed to melt local classification resulted from each subspace. In [5] the authors proposed a new method to combine original spectral information with multitemporal texture extracted by the Pseudo Cross Variogram algorithm (PCV). Several other approaches using neural networks [6, 7] or SVM [8, 9] have been proposed.

However, several problems are identified in the presented approaches. First, classifiers are, in general, sensitive to the high dimension of pixels in hyperspectral images or to higher dimensional feature space generated by putting together multi-dates features. Next, the learning of most proposed classifiers is based on different temporal data sets, i.e., a pixel group for each date. Nevertheless, at different time instants each pixels sample present distinctive characteristics due to differences in atmospheric conditions, sensor drifts, etc. Hence, the learning paradigm, investigated on data coming from different distributions, is violated. It does not respect the independence of features over different temporal data sets and the non-linear cross information among pixels at different temporal dates [6]. So, an appropriate interpretation of temporal information calls for designing an appropriate spectral modeling and classification approaches.

In this paper, we propose a 3D model that characterizes all the pixels in a scene by considering their reflectance values as a function of time of imaging and spectral waveband. To achieve this goal, we propose a new approach for designing multi-temporal spectral signature as a three dimensional function (time, reflectance, and wavelength band). Hence for each pixel, we generated a surface which generalizes the usual signature by adding a time dimension. Despite classical bi-dimensional spectral representation, we call this new representation the multi-temporal spectral signature. The proposed method includes several steps: 1) The first one is an off-line step and consists on building a 3D hyperspectral library from field missions and in situ data collected using a spectroradiometer. Other steps are on-line and include: 2) An analytical 3D surface is generated for each pixel, Delaunay triangulation was used to generate and parameterize the surface. Then, the respective coefficients will be introduced to 3D spectral matching block; 3) The next step consists of finding the highest match score between pixels surface in the image and the surfaces stored in our 3D spectral library, a shape differentiation of freeform surfaces using a similarity measure was used; 4) Finally, we use the spectral distance calculated between surfaces to estimate and to generate abundances maps for each material from the scene. We can also use this distance for classification task to generate a thematic map. Fig. 1 depicts the proposed 3D model for multi-temporal hyperspectral classification and unmixing Logistic regression models were structured using the multi-temporal abundance maps for land cover prediction.

In this work, we showed the use of such modeling strategies in overcoming the dimensionality problem and improving both multi-temporal classification and unmixing problems associated with hyperspectral data.

The advantages of the proposed approach take into account the reflectance spectra at different time instants and multiple points in the growing process. The procedure can handle data from

different sensors such as Hyperion and AVIRIS since the wavebands need not be the same at each date. In addition, storing the analytical surfaces of multi-temporal pixel signature as 3D function coefficients reduces significantly the amount of data processing.

The experimental results show an application example of the proposed methodology using Hyperion images; a case study was conducted on multi-temporal Hyperion series located in southern Tunisia. The estimated abundance maps and spectrums of endmembers are comparable with that of the real ones. The obtained results show good classification accuracy.

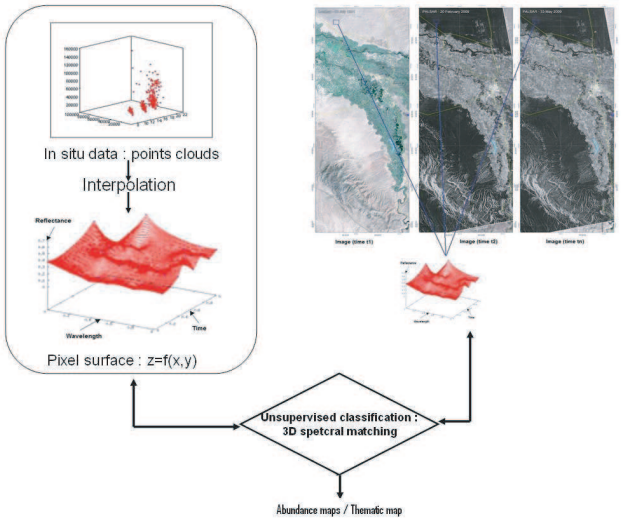

Figure 1: Proposed 3D approach for multi-temporal hyperspectral unmixing and classification.

REFERENCES

1. Jeon, B. and D. A. Landgrebe, "Decision fusion approach for multitemporal classification," *IEEE Transactions on Geoscience and Remote Sensing*, Vol. 37, No. 3, 1227–1233, May 1999.
2. Radke, R. J., S. Andra, O. Al-Kofahi, and B. Roysam, "Image change detection algorithms: A systematic survey," *IEEE Trans. Image Process.*, Vol. 14, No. 3, 294–307, March 2005.
3. Du, Q., L. L. Wasson, and R. King, "Unsupervised linear unmixing for change detection in multitemporal airborne hyperspectral imagery," *Proceedings of the 3rd International Workshop on the Analysis of Multi-Temporal Remote Sensing Images*, Biloxi, MS, 2005.
4. Prasad, S., L. M. Bruce, and H. Kalluri, "A robust multi-classifier decision fusion framwoek for hyperspectral, multi-temporal classification," *Geoscience and Remote Sensing Symposium, 2008, IGARSS*, Vol. 2, No. 3, 273–276, July 2008.
5. Trombetti, M.. D. Riaño, M. A. Rubio, Y. B. Cheng, and S. L. Ustin, "Multi-temporal vegetation canopy water content retrieval and interpretation using artificial neural networks for the continental USA," *Remote Sensing of Environmen*t, Vol. 112, No. 1, 203–215, January 15, 2008.
6. Plaza, J., A. Plaza, R. Perez, and P. Martinez, "On the use of small training sets for neural network-based characterization of mixed pixels in remotely sensed hyperspectral images," *Pattern Recognition*, Vol. 42, No. 11, 3032–3045, November 2009.
7. Ghoggali, N. and F. Melgani, "Genetic SVM approach to semisupervised multitemporal classification," *IEEE Geoscience and Remote Sensing Letters*, Vol. 5, No. 2, 212–216, 2008.
8. Pal, M. and P. M. Mather, "Assessment of the effectiveness of support vector machines for hyperspectral data," *Future Generation Computer Systems*, Vol. 20, No. 27, 1215–1225, October 1, 2004,
9. Camps-Valls, G., L. Gómez-Chova, J. Muñoz-Marí, J. L. Rojo-Álvarez, and M. Martínez-Ramón, "Kernel-based framework for multitemporal and multisource remote sensing data classification and change detection," *IEEE Transactions on Geoscience and Remote Sensing*, Vol. 46, No. 6, June 2008.

Session 2P3
Microstrip, Printed Antennas and Phase Array

Aperture Coupled Multilayer Microstrip Power Divider

Sulaiman Lanre Taiwo and S. I. Mitu Sheikh
Electrical Engineering Department
King Fahd University of Petroleum & Minerals (KFUPM), Dhahran 31261, Saudi Arabia

Abstract— Power dividers are essential components in active array antennas used in microwave communication [1]. Wilkinson, branch-line and Gysel are among the popular power dividers often implemented using microstrip circuits to achieve minimal insertion loss, high isolation between output ports and exceptional phase and amplitude balance [2]. But the disadvantages of the planar power dividers include unwanted oscillation due to mutual coupling with other circuit components, size and fabrication related limitations. Also to use them in recent multilayer devices, such as laminated multi-chip modules, vertical transitions are needed which considerably increase the insertion loss and limit the operational bandwidth [3]. This paper details the design of an aperture coupled microstrip power divider, shown in Figure 1(a), with low insertion loss (< 0.5 dB), high isolation between the output ports (< 20 dB), large impedance bandwidth (20%). Professional EM-simulator is used to optimize the S-parameter response of the power divider before fabrication and testing. The simulated and measured reflection and transmission response of the device are plotted in Figure 1(b). The simplicity and compactness of this design can make it attractive for antenna arrays or microwave integrated circuits.

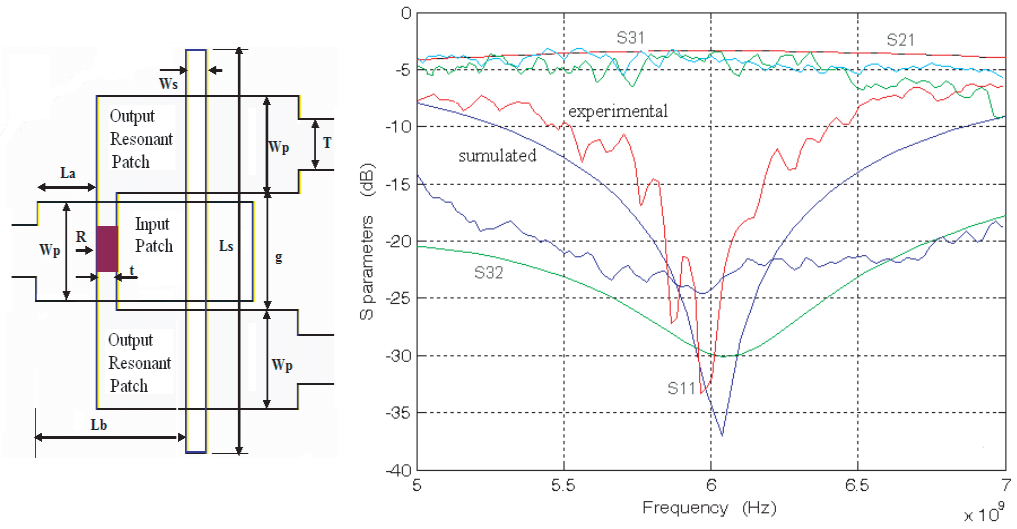

(a) (b)

Figure 1: (a) Schematic diagram. (b) Simulated & measured S-parameters of the power divider. $L_a = 4.5$ mm, $L_b = 9.2$ mm, $L_p = 16.2$ mm, $W_p = 4.5$ mm, $W_s = 1.2$ mm, $L_s = 17.7$ mm, $T = 3.04$ mm, $g = 4.9$ mm, $t = 1$ mm.

ACKNOWLEDGMENT

The authors are thankful for the support of King Fahd University of Petroleum & Minerals (KFUPM), Dhahran, Saudi Arabia.

REFERENCES

1. Hansen, R. C., *Phased Array Antennas*, John Wiley and Sons Inc, 1998.
2. Wilkinson, E. J., "An N-way power divider," *IEEE Trans. Micro. Theory Tech.*, Vol. 8, No. 960, 116–118, 1960,
3. Cai, X., T. Yu, and T. Ling, "Electromagnetic characterization analysis of the connecting structure of the via in multilayered microwave circuit," *Global Symposium on Millimeter Waves (GSMM)*, 275–278, April 2008.

A Telemetry Antenna System for Unmanned Air Vehicles

M. Dogan[1, 2] **and F. Ustuner**[1]

[1]TUBITAK, UEKAE, Kocaeli, Turkey
[2]Sabanci University, Istanbul, Turkey

Abstract— This paper presents a low VSWR high gain telemetry antenna system manufactured for UAVs that provides 360° coverage in the roll plane of the UAV. Proposed telemetry antenna system includes four telemetry antennas, one power divider that has one input and four output terminals which feeds the telemetry antennas with equal magnitude and phase. Proposed high gain telemetry antennas are based on the feeding of the microstrip patch antenna via aperture coupling. Full coverage in the roll plane of the UAV is obtained by using circular array configuration of telemetry antennas. RF power divider is designed by using couple of Wilkinson power dividers with equal line lengths and impedance sections from input terminal to the all four output terminals.

Introduction: Telemetry systems are used for remote data measurement and collection. Data transfer is usually done in wireless means. Telemetry systems have been used in several areas such as agriculture, defense, medicine ... etc. Airborne telemetry systems are used for remote monitoring the temperature, pressure, vibration and acceleration variations of the UAV during the flight time. The complete structure of a telemetry system includes sensors and transducers, signal conditioners, RF circuits and the transmitter.

Antennas and a power divider to feed the antennas with equal magnitude and phase are the main part of the transmitter. In this paper designed antennas and power divider are presented with the simulation and measurement results in the desired frequency range.

Telemetry System: Proposed telemetry system has four antennas and one RF power divider. Aperture coupled microstrip patch antennas are designed and printed on Roger 4003C substrate. Manufactured antennas have measured VSWR values lower than 1.5 and gain of 8.5 dBi in 2.2–2.4 GHz frequency band. Each individual antenna has 60° HPBW in the H-plane and more than 25 dB cross polarization ratio. In order to have full coverage in the roll plane, circular array configuration of all four antennas is used. Each antenna is placed on the four orthogonal side walls of the UAV and thus full coverage in the roll plane is obtained.

RF power divider has one input and four output terminals. All four output terminals are connected to the each telemetry antenna via extremely low loss coaxial cables. Wilkinson power dividers are used to manufacture RF power divider. In order to have equal magnitude and phase at each output terminal, individual paths from input port to the all four output port should have same length with the same line impedance variations. Return loss, insertion loss, phase delay and port isolation measurements are performed at TUBITAK — UEKAE EMC Laboratory facilies. Proposed power divider has a VSWR value lower than 1.25, maximum 0.5 dB insertion loss, maximum of 2°–3° phase variation between each path at 2.3 GHz and a minimum port isolation of 25 dB in the desired frequency range which is well below 30 dB at the center frequency. VSWR measurements are also performed on complete telemetry antenna system in anechoic chamber.

Defected Ground Structure for Coupling Reduction between Probe Fed Microstrip Antenna Elements

C. Vázquez, G. Hotopan, S. Ver Hoeye, M. Fernández, L. F. Herrán, and F. Las-Heras
Area of Signal Theory and Communications, Universidad de Oviedo
Edificio Polivalente de Viesques, Módulo 8, planta 1, Campus de Viesques, E-33203, Gijón, Spain

Abstract— In recent years, microstrip antennas have become a widespread choice for a great variety of applications, due to their well-known attractive features, such as low profile, light weight and low production cost. These properties, together with the capability to integrate the feeding networks, tuning devices or other kind of auxiliary circuitry on the same substrate, make this technology an interesting option for antenna array implementations. However, for two dimensional arrays where the feeding signals of the radiating elements must be separately controlled, the design of the feeding network can become a challenging task. Probe fed designs can be appropriate for these cases, as each radiating element can be directly fed from underneath the ground plane [1].

The mutual coupling between elements of antenna arrays is a critical aspect that must be conveniently taken into account in the design process, as it can lead to severe degradations in the overall performance. The mutual coupling between two probe fed microstrip antennas based on stacked patches, like those presented in [1], working around 10 GHz and aligned collinearly along their E-plane is analysed, both versus frequency and versus element separation.

In order to mitigate the detrimental mutual coupling between elements, a simple Defected Ground Structure (DGS) based on narrow, closely spaced, rectangular slots (Fig. 1(a)), is presented. Two designs with 3 and 5 slots have been optimised and studied through electromagnetic simulations. For the experimental validation of the simulated results, prototypes of two element antenna arrays with both DGS designs have been manufactured and measured, obtaining reductions in the value of the $|S_{12}|$ parameter of around 6 and 8 dB respectively (Fig. 1(b)).

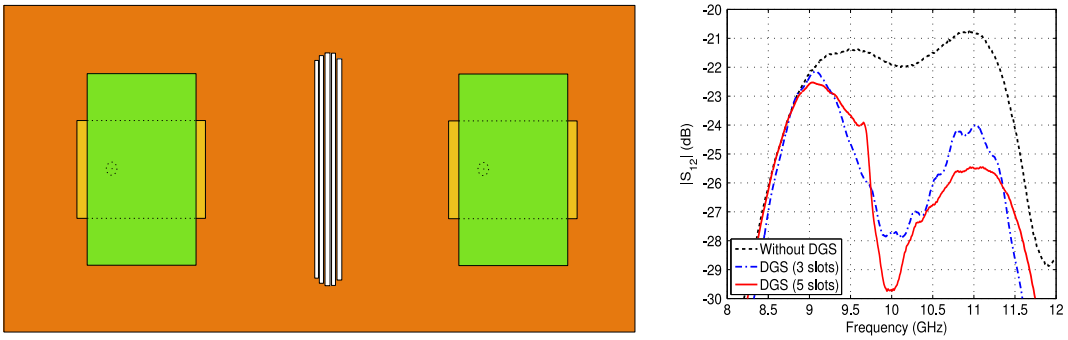

(a) (b)

Figure 1: (a) Outline of the proposed Defected Ground Structure design with 5 slots. (b) Measured $|S_{12}|$ versus frequency without DGS, with the 3 slot design and with the 5 slot design.

ACKNOWLEDGMENT

This work was supported by the "Ministerio de Ciencia e Innovación" of Spain and "FEDER", under projects TEC2006-12254-C02-01/TCM, TEC2008-01638/TEC (INVEMTA) and CONSOLIDER-INGENIO CSD2008-00068 (TERASENSE), by the "Gobierno del Principado de Asturias" under the "Plan de Ciencia y Tecnología (PCTI)"/"FEDER-FSE" by the grant BP08-082, the projects EQP06-015, FC-08-EQUIP-06, PEST08-02 and IB09081, and by the "Cátedra Telefónica" Universidad de Oviedo and "Fundación CTIC".

REFERENCES

1. Vázquez Antuña, C., G. Hotopan, S. Ver Hoeye, M. Fernández García, L. F. Herrán Ontañón, and F. Las-Heras, "Microstrip antenna design based on stacked patches for reconfigurable two dimensional planar array topologies," *Progress In Electromagnetics Research*, PIER 97, 95–104, 2009.

A Modified Antipodal Vivaldi Antenna with Improved Bandwidth and Radiation Pattern

Jian Bai, **Shouyuan Shi**, **and Dennis W. Prather**
Department of Electrical and Computer Engineering, University of Delaware, DE 19716, USA

Abstract— Vivaldi antenna has been widely used in ultra-wideband (UWB) technologies, e.g., UWB communication, imaging system, penetrating radar, due to its ultra-wide bandwidth, low profile, easy fabrication and low cost. Recently, Vivaldi antenna operating at the range of 1–20 GHz, i.e., 20 : 1 bandwidth, has been reported. When antenna is operated at high frequency, the surface mode is easily excited reducing the gain and deteriorating the radiation pattern. As a result, the substrate has to be very thin ($t(\sqrt{\varepsilon_r}-1) \leq 0.03\lambda_0$) or has very low dielectric constant. This restriction leads many difficulties, e.g., fabrication of very thin substrate, mechanical instability of antenna, particularly in millimeter-wave regime. There have been different ways to solve this problem, such as membrane-supported antennas backed by thick foam substrate, and selectively machining holes into the dielectric substrate to reduce the effective dielectric constant.

In this paper, a modified antipodal Vivaldi antenna is present. Compared with the traditional antenna, the bandwidth of the proposed antenna is extended approximately by 20 GHz based on the same substrate, i.e., RT/Duroid 5880 with dielectric constant of 2.2 and thickness of 10 mil, and the radiation pattern and the gain of antenna are also improved. The effective dielectric constant accordingly is equivalently reduced or thickness of substrate increased for a given frequency regime. The modifications are implemented in the following way. A number of slots are cut along the edge of the antenna. The configuration of these slots, i.e., depth, position, width and orientation, needs be optimized to create new current distribution we expect. It is observed, particularly at high frequency range, the current otherwise existing everywhere on the antenna tends to be mainly along the fingers left after slots are applied. Such slight fingers behave similarly as monopoles, allowing us to better control their effect on radiation pattern. In addition, the current distribution can be further controlled in another way at mean time. A lot of resonant rings are applied along the tapered slot of the antenna. They behave as in defected ground structure (DGS) to prevent current from passing through when their resonance happens. It is shown that the surface wave excited from current along tapered slot is effectively suppressed. At last, the proposed modified antenna is analyzed using HFSS commercial software and proven to be well worked at the range of 4–50 GHz.

Optimization of Aperture Coupled Microstrip Patch Antennas

M. Dogan[1, 2], G. K. Sendur[2], and F. Ustuner[1]

[1]TUBITAK-UEKAE, Kocaeli, Turkey
[2]Sabanci University, Istanbul, Turkey

Abstract— This paper presents the optimization of an aperture coupled microstrip patch antenna (ACMPA) that is manufactured for use on unmanned air vehicles. ACMPAs overcome the drawbacks of microstrip antennas such as low gain and narrow impedance bandwidth. ACMPA is a multilayer stacked type of an antenna and has several factors that affect the antenna performance. This paper explains the optimization of these factors to get the highest antenna gain, lowest VSWR in the desired impedance bandwidth with MATLAB Optimization Toolbox. The comparison between the optimization with MATLAB and optometric tool of HFSS is going to be investigated.

Introduction: Microstrip antenna (MSA) in its simplest form consists of a radiating patch on one side of a dielectric substrate and a ground plane on the other side. Even though MSAs have so many advantages in practice, they are suffered from the narrow impedance bandwidth, lower antenna gain and low power handling capability. Pozar first proposed ACMPAs to overcome these disadvantages. ACMPA is simply based on the coupling of the field on the microstrip feed line placed on the one side of the ground plane to the radiating patch through an electrically small aperture in the ground plane. It demonstrates significant improvement on impedance bandwidth and antenna gain.

Antenna Optimization: ACMPA is composed of 50 Ohm microstrip feed line below the ground plane, an electrically small aperture on the antenna ground plane and a patch over the antenna ground. The ground plane that the aperture lies on is a common ground for the microstrip feed line and the patch antenna. There are several factors that affect the performance of ACMPA such as length of tuning stub, relative location of the aperture w.r.t to the patch, antenna substrate properties, shape of coupling aperture, geometric parameters of the patch, height of each stacked layers from the ground plane. In addition, proposed antenna is buried in a metallic cavity which is opened on the sidewall of unmanned air vehicle; therefore the effect of the cavity to the antenna should be investigated.

Antenna designers usually use EM design tools such as HFSS, CST-MWS. These types of tools are very powerful on antenna design and also optimization with their own optometric analyzers where the antenna designer enters the desired criteria's to the optometric tool and then waits until the program stops. Unfortunately, designer has no idea what is going on and no control during optimization.

In this paper, we perform the antenna optimization with MATLAB optimization toolbox instead of using HFSS optometric. MATLAB runs the HFSS via scripts, takes the output data (VSWR, Gain) from the HFSS, processes them and finishes the optimization after couple of iterations and function evaluations. During optimization time designer will able to see and control the optimization process.

In this paper, the efficiency of antenna optimization with MATLAB Optimization Toolbox will also be demonstrated by comparing it with HFSS optometric with the optimized results and the time that the optimization takes.

A Compact and Low Cost Elementary Radiating Cell for Satellite Broadcasting Automotive Receiving Arrays

R. Torres-Sánchez[1], **J. R. Mosig**[1], **S. Vaccaro**[1, 2], **and D. Llorens del Río**[1, 2]

[1]Laboratory of Electromagnetics and Acoustics (LEMA)
Ecole Polytechnique Fédérale de Lausanne (EPFL), Switzerland
[2]JAST SA, PSE-EPFL Bat. C, CH-1015, Lausanne, Switzerland

Abstract— In this communication, the printed circuit board implementation of a complete elementary radiating cell for a low profile Ku-band array antenna with full electronic beam steering and polarization control capabilities is presented. The implementation effectively strikes a balance between cost, electromagnetic performance and aesthetics, as required by automotive consumer applications providing satellite broadcasting reception capabilities [1].

At the expense of a high level of integration of the required functionalities into a complex multilayered structure, such compromise has already been tackled at basic radiating element level, which allowed for both concept proofing [2] and mature design prototyping [3]. This compromise led to a miniaturized aperture coupled microstrip patch antenna type radiating element, with stripline feeding and dual linear polarization. The goal of this communication is, therefore, to illustrate the way this mature radiating element is integrated within the final multilayer buildup to become a programmable array cell and to demonstrate its standalone performance.

As shown in Figure 1(a), the elementary cell comprises, within the real state imposed by the actual array grid, the linearly polarized element, a stripline branch-line hybrid, a couple of long signal vias connecting the hybrid terminals to the microstrip layer where the active components are to be mounted and, finally, a power combiner joining the stripline feeding network to the outputs of the active components. The electromagnetic performances of the cell, although constrained by the aforementioned technological and dimensional factors (see Figure 1(b)), are very promising. Moreover, an overall performance improvement is expected to take place at array level once the benefits of the foreseen sequential rotation are effectively exploited.

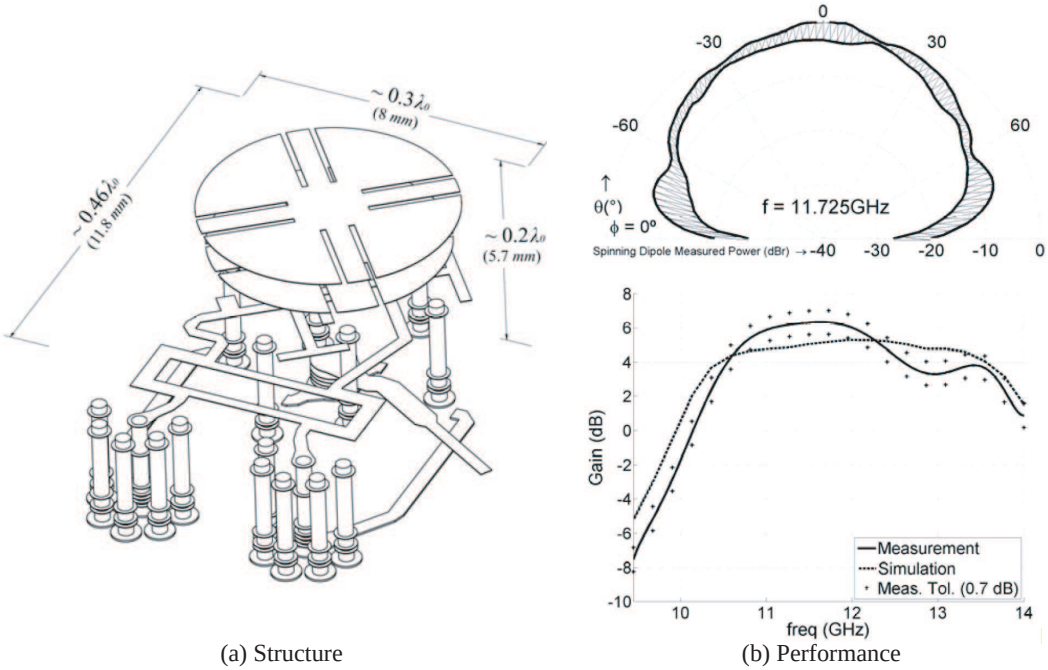

(a) Structure (b) Performance

Figure 1: Elementary radiating cell.

REFERENCES

1. Baggen, R., S. Vaccaro, and D. Llorens del Río, "Design considerations for compact mobile Ku-band satellite terminals," *Proceedings of the 2nd European Conference on Antennas and Propagation*, Edinburgh, UK, November 2007.
2. Torres-Sánchez, R., S. Vaccaro, and J. R. Mosig, "A compact and low cost radiating element for automotive satellite broadcasting reception arrays," *Proceedings of the 30th European Space Agency Antenna Workshop for Earth Observation, Science, Telecommunication and Navigation Space Missions*, ESA/ESTEC, Noordwijk, The Netherlands, May 2008.
3. Torres-Sánchez, R., J. R. Mosig, S. Vaccaro, and D. Llorens del Río, "On the design of a compact and low cost radiating element for satellite broadcasting automotive receiving arrays," *Proceedings of the 33rd Annual Antenna Applications Symposium*, Monticello (IL), USA, September 2009.

Analysis and Simulation of Different Bent Dipole Circularly Polarized Antenna Array Situated Close to Ground Plane

Saeed M. Khan
Kansas State University, USA

Abstract— Bent dipole antennas are being studied for the purpose of creating circularly polarized arrays with wide beamwidth. The analysis will begin with the analytical study of a bent dipole element in the proximity of a ground plane. The analytical results will be verified through experimental and simulation data. The impact of bend angle on impedance characteristics will be investigated using simulation and analytical modeling. Next, an array of four bent dipole elements with their feeds resting equidistant from adjacent elements on the perimeter of a circle is studied through simulation. The array is made to generate right circular polarization by feeding adjacent elements with equal amplitudes and a phase progression of 90°. The axial ratio, S-parameters, and beamwidth characteristics will be provided for this model. Two other arrays of 8 and 16 elements being fed with equal amplitudes with phase progressions of 45° and 22.5° be simulated and studied as above. It is noticed that the symmetry of the patterns and axial ratios in the three cases seemed to improve with increased elements. This concept will then be extended to a continuous structure which can seen as an infinite array of bent dipoles, however, only four feeds with equal magnitudes and a 90° phase progression will be used in this case. Measured and simulated characteristics of this antenna, which includes beamwidths, axial ratios, and impedances, will be presented. Comments will be made on the design and its characteristics.

Tapered-line Power Divider

B. K. Chung[1] and C. T. Chiang[2]

[1]Universiti Tunku Abdul Rahman, Malaysia
[2]Computer Simulation Technology (CST), Malaysia

Abstract— Ultra-wideband (UWB) power divider is required in UWB microwave systems. In addition to insertion loss, the other important parameters to achieve include low return loss, low amplitude ripple, high isolation, amplitude and phase balance between output ports, power-handling capability, and compact size. There are many works on obtaining wideband response. Multistage and dual-frequency approaches have been used to widen the bandwidth of Wilkinson power divider. The conventional Wilkinson power divider uses quarterwave transformer to provide the desired impedance transformation. Since the line length is exactly quarter wavelength only at the center frequency, the operating bandwidth of the power divider is limited in terms of return loss and isolation. Multiple quarterwave transformer connected in cascade improves the bandwidth but it increases the size of the device. Many methods have been proposed to reduce the size but they come with some degradation of the electrical performances. In this paper, the design of a tapered-line Wilkinson power divider with UWB performance is presented. The quarterwave transformer in the conventional Wilkinson power divider is replaced by an exponentially tapered line. Since the tapered line provide a consistent impedance transformation over all frequencies above the lower limit, the amplitude ripple and the input return loss is reduced. Two additional resistors are added along the tapered line to improve the output return loss and isolation. Simulation was performed using CST Microwave Studio CAD software. The simulated and measured results confirm the good performance of the proposed circuit. The return loss at its three ports and the isolation between the output ports are better than 15 dB across the band 2–10.3 GHz.

A Novel Feeding Scheme for Microstrip Patch Antenna (MPA) Array for Millimeter-wave Band Applications

Wael M. Abdel Wahab, **Safieddin Safavi-Naeini**, **and Dan Busuioc**
Department of Electrical & Computer Engineering, University of Waterloo, Ontario, Canada

Abstract— The rapid development of wireless communications systems operating at millimeter-wave (mmW) frequency range between 60 GHz–90 GHz, such as IEEE 802.15 wireless network, automotive radar, imaging sensors, and biomedical devices, requires low cost technology suitable for mass production. One of the key elements is a highly efficient antenna arrays and RF circuits to be integrated on the same substrate. Microstrip patch antenna (MPA) arrays are good candidate for low cost mmW applications. They are known for their low profile and low cost and ease of manufacturing. However, their radiation efficiency degrades as the frequency and number of elements in the array increase due to their feeding structure. Currently, the proposed substrate integrated waveguide (SIW) technique maintain the advantages of dielectric filledrectangular waveguide (RWG) as well as additional merits such as ease of integration with planar circuits, low fabrication cost, and compact size.

In this paper, we propose a microstrip patch antenna (MPA) array with high radiation efficiency for emerging 60 GHz wireless applications. A configuration of the proposed SIW-fed MPA array is presented. As an example 2D 2×2 MPA fed SIW array @ 60 GHz is described. The proposed array antenna consists of SIW 1×2 power splitter (two ways) and rectangular MPA radiating elements. Each MPA (formed on the top of dielectric substrate layer1) is excited by a narrow coupling slot cut on the SIW (formed in dielectric substrate layer2) top metal plane. The slot is excited by the TE_{10} waveguide fundamental model. The overall radiation efficiency of the proposed antenna is investigated by finite elements method (HFSS). It is shown that the simulated radiation efficiency is better than 90% and this due to the fact that the antenna excitation fields are mostly confined within the guiding structure and lower feed loss. The simulated antenna gain is 11.71 dB @ the design frequency of 59.95 GHz within an operating bandwidth of 500 MHz. The efficiency of the developed antenna is higher than that of conventional millimeter-wave microstrip array antennas. Furthermore, the developed planar MPA fed SIW antenna can be easily integrated with other RF circuits on the same substrate using a suitable transition and can be fabricated using printed circuit Board (PCB) technology at no cost.

Use of Attachment Functions in the Moment Method for Analysis of Planar Microstrip Structures

O. Nejla and T. Aguili
SysCom Laboratory, Electrical Engineering Department, Engineer School of Tunis, Tunisia

Abstract— In our work, we propose a solution to deal with the problem of the errors introduced by the presence of discontinuities in planar microstrip circuits in computing some physical quantities, like the distribution of the current, by the moment method.

In this approach, we combine the Moment Method with the generalized equivalent circuit method to analyze a planar circuit. The interest of the method resides on the use of the attachment functions in the base of sinusoidal trial functions in the moment method, generally one or two functions by interface.

This solution allows us to correct the mistake of our results at the discontinuities of the structure.

In the first part of the work, we study a rectangular microstrip antenna excited on the plane of the circuit by a localized voltage source. This structure is shielded in a rectangular metallic box with electric walls and which the top cover is placed endlessly.

We calculate the current traveling on the feed line toward the patch edge. The results are compared with those already published and they verify the limit conditions of the structure.

In the second part, we place a second patch antenna identical to the first in H plane configuration to study the mutual coupling phenomena.

We study the convergence of the mutual coupling coefficient $|S_{12}|$ with the number of basis functions and trial functions and we represent its frequency response.

We compare the convergence of TE and TM modes and we illustrate the comportment of $|S_{12}|$ with the distance between the two patches and the dielectric permittivity of the substrate. The results are compared with those of commercial software.

Microstrip Antenna for Wideband Applications with Sandwitch Substrate

Malay Ranjan Tripathy[1], **Pawan Kumar**[2, 3], **H. P. Sinha**[3], **and Rachid Talhi**[4]

[1]Department of ECE, JIET, Jind, Haryana, India
[2]Department of ECE, SDITM, ISRANA, Panipat, Haryana, India
[3]Department of ECE, M. M. University, Mulana, Haryana, India
[4]University of Tours and CNRS, UMR 6115, Orleans 45071, France

Abstract— Microstrip antennas are considered for wide applications due to its light weight, low profile, planar configuration, compactness and inexpensive fabrication process [1, 2]. The limitation of microstrip antenna technology is the narrow bandwidth of the basic element. The bandwidth of a basic patch element is usually 1%–3% [3]. The modern trends in wireless communication systems require wide bandwidth antennas, by which the voice, data, and video information can be transmitted. The bandwidth of the microstrip antenna can be increased by reducing the substrate permittivity (ε_r), increasing its thickness (h), adding an impedance matching network, stack patches, edge-coupled parasitic patches, lossy materials etc. [4, 5].

The proposed wideband microstrip antenna consists of multilayer dielectric substrate. The optimization of this antenna is carried out considering different thickness and dielectric parameters of sandwiched substrate. The microstrip antenna with multilayer dielectric substrate is seen to achieve impedance bandwidth more than 40% with return losses below −10 dB at resonant frequency (i.e., 3–5 GHz). Over the impedance bandwidth, the maximum directive gain and VSWR are seen to be more than 3 dBi and less than or equal to 2 respectively.

REFERENCES

1. Balani, C. A., *Antenna Theory: Analysis and Design*, John Wiley & Sons, Inc., USA, 2005.
2. Wong, K. L., *Compact and Broadband Microstrip Antennas*, John Wiley & Sons Inc., New York, NY, 2002.
3. Garg, R., P. Bhartia, and A. Ittipiboon, *Microstrip Antenna Design Handbook*, Artech House, Boston, London, 2001.
4. Liu, Z. F., P. S. Kooi, L. W. Li, M. S. Liong, and T. S. Yeo, "A method for designing broadband microstrip antenna in multi layered planar structures," *IEEE Trans. Antenna Prop.*, Vol. 47, No. 9, 1416–1420, 1999.
5. James J. R. and P. S. Hall, *Handbook of Microstrip Antnnas*, Peter Peregrinus, UK, 1989.

Effect of Distance between Feeding Point and Ground Point of PIFA Antenna on Its Resonant Frequency and S Parameter

J. Jamali[1], **R. A. Sadeghzadeh**[2], **and M. N. Moghaddasi**[3]

[1]Science and Research Branch, Islamic Azad University, Tehran, Iran
[2]Department of Electrical Engineering, K. N. Toosi University of Technology, Tehran, Iran
[3]Faculty of Engineering, Science and Research Campus, Islamic Azad University, Tehran, Iran

Abstract— The planar inverted F antennas (PIFA) are commonly used in mobile terminals. Because of compact size and low profile it is popular for portable wireless devices [1, 2]. The planar inverted-F antenna (PIFA) is an extension of the wire inverted-F antenna (IFA) in which the wire is replaced with a plate in order to increase the bandwidth. Conventional PIFA comprise of a top patch, a shorting pin and a feeding pin. The top patch is mounted above a ground plane; the ground pin and feed pin, connected at proper positions to the top patch, have the same length as the distance between the top patch and the ground plane [3]. Figure 1 shows the illustration of PIFA antenna. Placing L-shaped, U-shaped slits or other shaped slits (normally meandering techniques) in the main resonating patch produces dual frequency operation. Upper bound of the frequency is controlled by the length and width of the slit, and the lower resonant frequency is controlled by the length and width of the main patch.

The PIFA antenna is designed as receiver antenna for the UMTS I Band (R_x 2112.4 MHz–2167.6 MHz) [4]. In order to study the characteristic of PIFA antennas, effect of mainly parameter of PIFA distance between the feed point and the ground point on the resonant frequency and S parameters was investigated using full wave EM SIMULATOR tools like CST Microwave Studio [5]. The dimension of the ground plane is $100 \times 50\,\text{mm}^2$, which is the same as the standard stick type phone models, the length of top patch, L, is equal to 33.5 mm, and the height of shorting plate, h, is equal to 5.8 mm [4]. The distance between the feed point and the ground point was changed to observe different performances of the return loss of the designed PIFA antenna. The main purpose is to find a better performance at a certain resonant frequency.

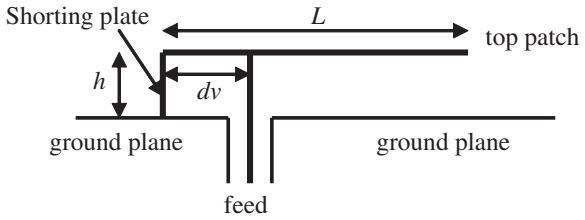

Figure 1: Structure of PIFA antenna.

REFERENCES

1. Chattha, H. T., Y. Huang, and Y. Lu, "PIFA bandwidth enhancement by changing the widths of feed and shorting plates," *IEEE Antennas and Wireless Propagation Letters*, Vol. 8, 637–640, July 2009.
2. Huynh, M.-C. and W. Stutzman, "Ground plane effects on planar inverted-F antenna (PIFA) performance," *IEE Proc. Microw. Antennas Propag.*, Vol. 150, No. 4, 209–213, August 2003.
3. Chattha, H. T., Y. Huang, X. Zhu, and Y. Lu, "An empirical equation for predicting the resonant frequency of planar inverted-F antennas," *IEEE Antennas and Wireless Propagation Letters*, Vol. 8, 856–860, August 2009.
4. Kildal, P.-S. and K. Rosengren, "Electromagnetic analysis of effective and apparent diversity gain of two parallel dipoles," *IEEE Antennas and Wireless Propagation Letters*, Vol. 2, No. 1, 9–13, 2003.
5. http://www.cst.com.

GA Optimization for Compact Broadband PIFA Application

Wen Pan and Quanyuan Feng
Institute of Microelectronics, Southwest Jiaotong University, Chengdu 610031, China

Abstract— In this paper, a Planar Inverted-F antenna (PIFA) applicable to the digital broadcasting service such as DMB and DVB-H is presented. Between the top plate and ground one part of the substrate is ferrite and the remaining is air-filled. This combined substrate structure as well as the utilization of T-shaped ground plane remarkably broadens the bandwidth and minimizes the antenna size. The optimizer by Genetic Algorithms (GA) cooperated with High Frequency Structure Simulator (HFSS) is adopted to obtain the optimal volume and shape of the PIFA. The mixed optimization program gives the scheme to cut out irregularly shaped slot windows on the patch which makes the Return Loss of the antenna proposed achieve −51.25 dB at the operation frequency. Finally, the antenna is fixed on 23 mm length, 5 mm width, 1 mm thick, over 72% reduction in the size compared with the conventional PIFA, relative bandwidth is 70% at 0.7 GHz, and VSWR is 1.05.

Session 2P4
Computational Electromagnetics

Numerical Computation of Capacitance of Oblate Spheroidal Conducting Shells

Omonowo D. Momoh, Matthew N. O. Sadiku, and Cajetan M. Akujuobi
Department of Electrical and Computer Engineering, Prairie View A&M University
Prairie View, TX 77446, USA

Abstract— A spheroid is obtained by rotating an ellipse about one of its principal axes. If the ellipse is rotated about its major axis, a prolate spheroid is formed, while an oblate spheroid is formed if the ellipse is rotated about its minor axis. However, if the generating ellipse is a circle, a sphere is formed. Spheroidal coordinates eliminate the cumbersome mathematical expressions obtained with rectangular coordinates and allow the simple determination of areas and volume. They offer an obvious generalization of physical processes described in spherical coordinate systems and in addition yield the extremely interesting limiting cases of the infinitely thin, finite "wire" and the infinitely thin circular disk. For instance, spheroidal antennas can be used to model a variety of different antenna shapes, from wire antennas, through cylindrical antennas, to disk antennas. Subsequently, for antennas that are long and thin, prolate spheroidal coordinates fit the geometry more closely while oblate spheroids should represent antennas in the shape of a disk.

In this research work, we implement the numerical computation of the capacitance in a conducting oblate spheroidal shell. The computation of the shell capacitance would help in future research efforts at finding the characteristic impedance and phase velocity in spheroidal shell conductors just like it has already been done for microstrip lines.

Explicit finite difference method was employed to numerically compute the potential distribution inside the conducting oblate spheroidal shell. The total charge (Q) enclosed by the oblate spheroidal shell was then calculated from the potential distribution. This was achieved by applying Gauss's law to a closed surface S enclosing the total electric fluxes. The capacitance values obtained matched with those obtained using exact solution method.

Guided and Leaky Modes of Planar Waveguides: Computation via High Order Finite Elements and Iterative Methods

D. Stowell and J. Tausch
Southern Methodist University, USA

Abstract— Guided and leaky modes of planar dielectric waveguides are eigen-solutions of a singular Sturm-Liouville problem. These modes are also the roots of a characteristic function which can be found using several methods that have been introduced in the past. However, the evaluation of the characteristic function suffers from numerical instability, and hence it is often difficult to find all modes in a given range. Here, a new variational technique is introduced. After discretization the variational formulation leads to a nonlinear eigenvalue problem in the propagation constant. Typically, this type of problem must be solved with a Newton-like procedure. Thus the modes that can be found depend on a judicious choice of the initial guess, which is normally not available. We show that after a change of variables the nonlinear problem can be transformed to either a quadratic or a quartic eigenvalue problem, depending on the waveguide structure. Using the companion matrix, such a problem can in turn be converted into a linear eigenvalue problem. The advantage is that now one can use standard numerical algorithms, such as the QR iteration or Arnoldi methods, which guarantee that all important modes are found. Because the resulting matrices are sparse, we use an Arnoldi method to compute the eigenvalues. Using the physical properties of the modes, we demonstrate how to compute the shifts that enable us to accelerate the convergence of the iterations to the desired portions of the spectrum. In addition, by using high-order finite elements, the resulting solutions can be made extremely accurate. Numerical examples demonstrate the speed and accuracy as well as the stability of the method.

A Closed Form Solution for Longitudinally Inhomogeneous Waveguides

Mohammad Khalaj-Amirhosseini
College of Electrical Engineering, Iran University of Science and Technology, Tehran, Iran

Abstract— Longitudinally Inhomogeneous Waveguides (LIWs) can be used in microwaves as phase changers, matching transformers and filters, especially for high power applications. The differential equations describing LIWs have non-constant coefficients and so except for a few special cases no analytical solution exists for them. There are some methods to analyze the LIWs such as cascading many thin layers, finite difference, Taylor's series expansion, Fourier series expansion, the method of Moments, the equivalent sources and equivalent circuit method. All of these methods are numerical and do not yield a closed form analytic solutions. However, in this paper, a closed-form analytic solution is introduced for arbitrary LIWs. First, the differential equations of LIWs are written as a suitable matrix differential equation. Then, the matrix differential equation is solved to obtain the chain parameter matrix of LIWs.

Figure 1 shows a typical LIW with dimensions a and b, filled by an inhomogeneous lossy dielectric with complex electric permittivity distribution $\varepsilon_r(z)$ and length d. The following closed form solution is obtained for the LIWs.

$$\mathbf{X}(z) = \exp\left(-\int_0^z \mathbf{A}(z')dz'\right)\mathbf{X}(0) = \mathbf{\Phi}(z)\mathbf{X}(0) \tag{1}$$

where

$$\mathbf{X}(z) = \begin{bmatrix} \bar{E}_y(z) & \bar{E}_y(z) \\ -H_x(z) & -H_x(z) \end{bmatrix} \tag{2}$$

and

$$\mathbf{A}(z) = \begin{bmatrix} \frac{1}{Z_g(z)}\frac{dZ_g(z)}{dz} & \gamma(z) \\ \gamma(z) & 0 \end{bmatrix} \tag{3}$$

in which

$$\bar{E}_y(z) = \frac{1}{Z_g(z)}E_y(z) \tag{4}$$

$$Z_g(z) = \frac{\eta_0}{\sqrt{\varepsilon_r(z) - (f_c/f)^2}} \tag{5}$$

$$\gamma(z) = j\frac{\omega}{c}\sqrt{\varepsilon_r(z) - (f_c/f)^2} \tag{6}$$

$$\begin{aligned} \mathbf{\Phi}(z) &= \begin{bmatrix} Z_g(z) & 0 \\ 0 & 1 \end{bmatrix} \exp\left(-\int_0^z \mathbf{A}(z')dz'\right) \begin{bmatrix} 1/Z_g(0) & 0 \\ 0 & 1 \end{bmatrix} \\ &= \begin{bmatrix} Z_g(z) & 0 \\ 0 & 1 \end{bmatrix} \exp\left(-\begin{bmatrix} \ln\left(Z_g(z)/Z_g(0)\right) & \int_0^z \gamma(z')dz' \\ \int_0^z \gamma(z')dz' & 0 \end{bmatrix}\right) \begin{bmatrix} 1/Z_g(0) & 0 \\ 0 & 1 \end{bmatrix} \end{aligned} \tag{7}$$

The obtained solution is applicable to arbitrary lossy and lossless LIWs. The validation of the introduced solution is studied using two comprehensive examples.

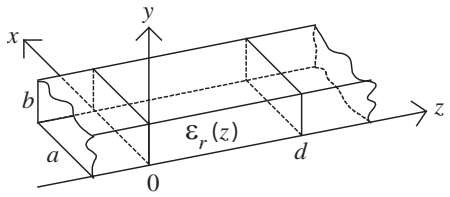

Figure 1: A typical LIW.

Modal Analysis of Lamellar Gratings: A New Formulation Based on the Moment Method with Subsectional Basis and Adaptive Spatial Resolution

Gérard Granet[1, 2], **Ana Maria Armeanu**[2, 3], **Kofi Edee**[1, 2], **Lala Bakonirina Andriamanapisoa**[2, 4], **and Karyl Raniriharinosy**[4]

[1]Clermont Uninversités, Université Blaise Pascal, Lasmea, BP10448, F-63000 Clermont-Ferrand, France
[2]CNRS UMR 6602, F-63177 Aubiéere, France
[3]CNRS LTM UMR 5129, 17 Avenue des Martyrs, 38054 Grenoble Cedex 09, France
[4]LAPAUF, BP 1264 CP 301, Faculté des Sciences, Université de Fianarantsoa, Madagascar

Abstract— Among the many existing rigorous methods for analyzing diffraction by periodic or aperiodic structures, Fourier based methods like the differential method, the Fourier Modal method, and the C method, are certainly the most popular. For that reason, they have been intensively researched and they can now handle most problems in optics and photonics. The above three methods share a common feature: they are based on an expansion of the field in terms of periodic functions. The intrinsic drawback of such a representation is that it requires a large number of terms to describe efficiently electromagnetic fields with sharp variations as is the case with highly conducting-gratings. We are thus lead to seek alternative expansions. Within the framework of numerical modal methods, polynomial expansions have already been used. Similarly, the method of lines [1] and the finite difference method in the frequency domain [2] may be considered as modal methods in which the field is expanded on pulse basis. The above formulations of the modal method compared favorably with the Fourier modal method for metallic gratings. Following the pioneering work of Edee et al. [3], this presentation is devoted to the modal method in which adaptive spatial resolution and a piecewise linear representation of the field are introduced.

It is organized as follows: first, we present the grating problem and its solution in terms of eigenmodes; then, the matrix from which eigenmodes are obtained is derived by using the method of moments [4] and subsectional basis. Lastly, we compare the convergence rate of the present method with that of the finite difference modal method and of the Fourier Modal Method.

REFERENCES

1. Pregla, R. and W. Pasher, *The Method of Lines Techniques for Microwaves and Millimeter-Wave Passive Structures*, Wiley interscience, 1989.
2. Lalanne, P. and J. P. Hugonin, "Numerical performance of finite-difference Modal Method for the electromagnetic analysis of one-dimensional grating," *J. Opt. Soc. Am.*, Vol. 17, No. 6, June 2000.
3. Edee, K., P. Schiavone, and G. Granet, "Analysis of defect in extreme UV lithography mask using a modal method based on nodal B-spline expansion," *J. J. A. P.*, Vol. 44, 6458–6462, 2005.
4. Harrington, R., *Field Computation by Moment Methods*, The Macmillan, New York, 1968.

A Green's Function Monte Carlo Algorithm for the Estimation of Derivatives of the Solutions of Partial Differential Equations

Kausik Chatterjee, Christopher Alesandro, and Christopher Mitchell
The Cooper Union for the Advancement of Science and Art, USA

Abstract— In this paper, we develop a Green's function Monte Carlo [1] algorithm for the estimation of the derivative of the solutions of partial differential equations. A unique advantage of the Monte Carlo method is that it requires no discretization of either the volume or the surface of the problem domains. As a result, the memory requirements are less than discretization-based numerical methods. Furthermore, the Monte Carlo method is inherently parallelizable and an almost linear rate of parallelization is obtained with a large number of processors. This work demonstrates a lesser known characteristic of the Monte Carlo method, i.e. the ability to estimate quantities related to the solution of a partial differential equation such as a derivative or an integral over the entire problem domain or any sub-domain without the need to estimate the solution at any point within the problem domain. This feature of the Monte Carlo method makes it uniquely advantageous in certain scenarios. For example in electrostatic problems, the electrostatic potential is given by the solution of the Laplace's equation. But often, one actually needs to obtain the electrostatic field (which is related to the spatial derivatives of the electrostatic potential) at certain points within the problem domain. The Monte Carlo method does just that. One can actually obtain the electrostatic field at any given point within the problem domain, without the need to obtain the electrostatic potential at any point within the problem domain. In this paper, we obtain the estimates of the derivatives of the solution of the two-dimensional Laplace's equation. We have chosen two benchmark problems, one with a finite problem domain and the other with an infinite problem domain. The problem in the infinite domain emphasizes the previously-mentioned advantage of the Monte Carlo method in the fact that discretization is not required. The algorithm has been parallelized and an almost linear rate of parallelization is obtained with as many as thirty-two processors.

ACKNOWLEDGMENT

This research has been supported by the Air Force Office of Scientific Research through a grant (FA9550-06-1-0439) monitored by Dr. F. Fahroo. Additional support has been provided in the form of summer fellowships for Prof. K. Chatterjee at Air Force Research Laboratory, Wright Patterson Air Force Base (AFRL/WPAFB). We would also like to acknowledge valuable discussions with Dr. D. Gaitonde at AFRL/WPAFB.

REFERENCES

1. Kalos, M. H. and P. A. Whitlock, *Monte Carlo Methods*, 2nd Edition, 161–169, Wiley-Vch, 2008.

Comparison between the Classical Integral Equations and a Well Conditioned Integral Equation

D. Levadoux[1], **F. Millot**[2], **and S. Pernet**[2]

[1]ONERA, France
[2]CERFACS, France

Abstract— The boundary integral methods (BIM) are commonly used for solving the scattering of arbitrarily shaped three-dimensional obstacles but also for the antennas design. Their popularity is due to a combination of factors. Firstly, the solutions of BIM fulfill causality and radiations conditions automatically. Secondly, it is only necessary to discretize the boundaries of the simulation domain and the simulation requires a smaller amount of unknowns than in the case when the finite element method or a finite difference method is used. One of the main drawback of using the BIM is that after discretization they result in dense systems of linear equations. If a large number of unknowns is involved, the only possibility is to use iterative solvers coupled with a fast matrixvector multiplication.

The basic principle of Boundary Integral Methods (BIM) in the frequency domain is to express the total electromagnetic fields in terms of the equivalent electric and magnetic currents flowing on the surface of the scatterer. These currents are determined via the boundary condition. But for a same scattering problem one can write various kinds of boundary integral equations depending for example on the choice of the boundary condition. It is well known that for example, if we consider the metallic scattering, the EFIE or MFIE or CFIE integral equation could be used. The main difficulty of the integral method is to choose the best boundary equation in sense that this equation gives rise to a well-conditioned linear system upon discretization and in sense that obtained solutions must be accurate. It is well known that the construction of integral equations is not an easy task for different reasons. For instance, the efficiency of the iterative solver is directly linked to the number of iterations needed to reach the solution. This is linked to the condition number, which depends on the spectral properties of the integral operator. For example, for the EFIE equation, the condition number of the matrix obtained after discretization will tend to infinity and the number of iterations will drastically increase. Moreover, the performance of the iterative solver is limited by the time of one matrix-vector multiplication. This limitation is weakened by the use of fast multipole methods [2, 3]. But the time of one matrix-vector multiplication must be cheaper as possible. And consequently, this induces a constraint on the choice of the integral formulation. Recently, new integral equations are constructed [1, 4, 5] in order to give rise to well-conditioned linear systems. This new-class of equations can be decomposed under the identity plus an operator C where C is compact operator.

Our purpose is to compare the classical BIM formulations commonly used with this new approach. More precisely, accuracy of solutions will be analysed. We focus also on the CPU time needed to obtain the solution and on the memory storage. In this paper, we mainly investigate the iterative solutions of problems involving in the case of perfectly conducting or impedant obstacles where a Leontovich condition is imposed at the boundary. Numerical results in the academic and non academic cases will be presented.

REFERENCES

1. Alouges, F., S. Borel, and D. Levadoux, "A stable well conditioned integral equation for electromagnetism scattering," *JCAM*, Vol. 204, No. 2, 2007.
2. Cheng, H., L. Greengard, and V. Rokhlin, "A fast adaptive multipole algorithm in three dimensions," *J. Comput. Phys.*, Vol. 155, No. 2, 468–498, 1999.
3. Chew, W. C., J. M. Jin, E. Michielssen, and J. M. Song, *Fast and Efficient Algorithms in Computational Electromagnetics*, Artech House, 2001.
4. Darbas, M., "Generalized cfie for the iterative solution of 3-D maxwell equations," *Applied Mathematics Letters*, Vol. 19, No. 8, 2006.
5. Pernet, S., "A well-conditioned integral equation for iterative solution of scattering problems with a variable leontovitch boundary condition," submitted.

Analysis of Scattering from Semi-infinitely Layered Periodic Array Using Equivalence Principle and Connection Scheme

Jiming Song and Fu-Gang Hu
Department of Electrical and Computer Engineering, Iowa State University, Ames, Iowa 50011, USA

Abstract— In this paper, an approach combining the equivalence principle algorithm (EPA) and connection scheme (EPACS) is presented to analyze the two-dimensional (2-D) scattering from semi-infinitely layered periodic array. In the semi-infinitely layered array, one unit consisting of several layers is repeated infinitely along one direction. Each layer may be filled with different media. Due to the periodicity of the array, the computational domain first is restricted to one period of the periodic array. In one period, each layer is treated as an individual cell. Then, the equivalence principle is applied separately to each individual cell to obtain the integral equations for equivalent currents on the outside boundary of the cell and the perfect electric conductor (PEC) surface. By combining the periodic boundary condition (PBC) with the connection scheme, the relationship is established between the currents or fields on the topmost and bottommost surfaces of one unit. The relationship is represented by the impedance matrix.

From the viewpoint of network, each unit is regarded as a two-port network. For this semi-infinitely layered array, the impedance matrix should be identical because the network is infinitely extended when one looks into it from the top surface of any unit. Based on this fact, the equation for this impedance matrix is established by EPACS and solved using a proper iterative method. After obtaining the impedance matrix, the integral equation on the topmost surface is required to construct the complete system of equations for solving the fields or currents on the top surfaces. Then the reflection coefficients of Floquet's harmonics is found. It should be mentioned that the direct IE approach definitely cannot handle the case of semi-infinitely layered array since the number of unknowns for the direct integral equation (IE) approach will be infinite. As an example, Figure 1 shows the reflection coefficient of the half-space medium. Excellent agreement between the numerical and analytical results can be observed. More numerical results and discussion will be presented in the conference.

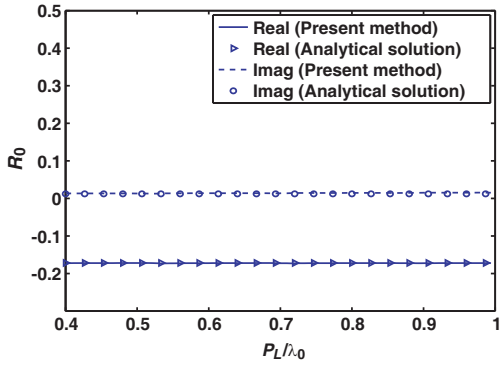

Figure 1: Reflection coefficient R_0 of semi-infinitely layered array without PEC object. $\varepsilon_r = 4 - j0.2$ and $\mu_r = 2$. One unit consists of one layer. Each cell is set to be square with periodicity P_L.

Analysis of Homogenization Techniques for Improving Electromagnetic Scattering Computation by Rough Surfaces

S. Tournier[1], **J.-R. Poirier**[2], **and P. Borderies**[1]

[1]ONERA, 2 avenue Edouard Belin, 31 055 Toulouse Cedex 5, France
[2]LAPLACE-ENSEEIHT-INPT, 2 rue Charles Camichel, 31071 Toulouse cedex, France

Abstract— Scattering of electromagnetic waves by randomly rough surfaces is a subject of great interest in electromagnetism, including Radar and microwaves applications. Although analytical simulation techniques are now well-established for an efficient analysis of scattering by rough surfaces, it remains interesting to deal with them through the use of numerical approaches, with the goal of assessing the validity domain of the analytical ones or to substitute them in some cases.

Whatever the numerical method under consideration (e.g., [1]), major challenge is the numerical efficiency to cope with representative patches both in terms of size and details: therefore, it is to get rid of the necessity of sampling the surface under consideration in very fine details with respect to wavelength and substitute them with effective boundary conditions, while maintaining the performances of the numerical method.

Formerly, in this objective, a homogenization technique has been proposed in the case of bidimensional geometry, Dirichlet case (TM polarization) [2], and it proved to be efficient. This technique has been extended to the Neumann case (TE polarization), which will be shown in this presentation. Then it will be analyzed how these approaches may be extended to the dielectric case considering also similar developments published in the literature ([3] for instance).

Numerical examples are presented to discuss the benefits of these approaches.

REFERENCES

1. Tournier, S., J.-R. Poirier, and P. Borderies, "Analysis of performances of a Floquet mode preconditioner for electromagnetic scattering computation by rough surfaces," *Progress In Electromagnetics Research Symposium Abstracts*, 397, Beijing, China, March 23–27, 2009.
2. Poirier, J.-R., A. Bendali, and P. Borderies, "Impedance boundary conditions for the scattering of time-harmonic waves by rapidly varying surfaces," *IEEE Transactions on Antennas and Propagation*, Vol. 54, No. 3, 995–1005, March 2006.
3. Holloway, C. L. and E. F. Kuester, "Impedance-type boundary conditions for a periodic interface between a dielectric and a highly conducting medium," *IEEE Transactions on Antennas and Propagation*, Vol. 48, No. 10, 1660–1672, October 2000.

Simulating Dispersive Left-handed Media with the TLM Method

Cédric Blanchard[1], **Didier Felbacq**[1], **Brahim Guizal**[1], **Jorge Andrés Porti**[2], **and Rachid Talhi**[3]

[1]Groupe d'Etude des Semi-Conducteurs, Université de Montpellier II, Montpellier, France
[2]Departamento de Física Aplicada, Universidad de Granada, Granada, Spain
[3]CNRS-UMR 6115, Université de Tours, Orléans, France

Abstract— The Transmission Line Modeling (TLM) method is a numerical time domain technique that was introduced by Johns in 1971 [1]. Since then, it has been successfully employed to solve many problems involving the propagation of waves in acoustic, diffusion and, especially, electromagnetic problems.

So et al. showed how to simulate left-handed materials with TLM [2]. Because of the special characteristics of TLM, modeling such metamaterials with this method is more than a simple extension to account for the negative values of the permittivity, ε, and permeability, μ: it is also a conceptual procedure that can be viewed as the numerical counterpart of what happens in a real left-handed transmission line network. This makes TLM an elegant approach to model metamaterials. The aim of this communication is to clarify the procedure to simulate a metamaterial with TLM and to point out the restrictions that can lead to difficulties.

TLM exploits the analogy between Maxwells equations and the equations of the transmission line theory. The electromagnetic medium to be simulated is discretized by an analogous mesh of interconnected transmission lines, while the electromagnetic wave is modeled by voltage and current pulses that propagate into such a network. A unitary cell of the mesh, called node, is defined as the intersection of constitutive transmission lines. At low frequency, a node can be understood in terms of lumped capacitors and inductors, i.e., a usual distributed L-C circuit. It is well known that a network of left-handed transmission lines (with the position of L and C interchanged, i.e., series capacitances and shunt inductances) can support backward electromagnetic waves [3]. A TLM node capable of modeling metamaterials naturally arises from these dual structures [2, 4].

Traditionally, in the modeling of usual materials, the optic constants are supposed to be non-dispersive if the wavelength is wide enough compared to the size of the nodes. On the contrary, the TLM numerical approach to simulate metamaterials includes the assumption of a working frequency at which the required permittivity and permeability are adjusted; both are altered at any other value. As a result, the TLM node for metamaterials is a dispersive system, which means that there is no need to add artificial dispersion, as it is the case for other comparable methods (FDTD for instance). Controlling the behavior of the simulated metamaterial in a given frequency range is fundamental; in this sense, it has been recently shown that the inherent dispersion is of Drude type [5].

Furthermore, in the usual TLM procedure, there is a certain degree of freedom in the selection of the TLM numerical parameters, such as the impedance of the constitutive transmission lines of the nodes or the time step, Δt. However, causality conditions may alter this statement if metamaterials are involved. In this communication, a particular emphasis will be placed on the restrictions imposed by these conditions.

REFERENCES

1. Johns, P. B. and R. L. Beurle, "Numerical solution of 2-dimensional scattering problems using a transmission-line matrix," *Proc. Inst. Elec. Eng.*, Vol. 118, No. 9, 1203–1208, 1971.
2. So, P. P. M., H. Du, and W. J. R. Hoefer, "Modeling of metamaterials with negative refractive index using 2-D shunt and 3-D SCN TLM networks," *IEEE Trans. Microwave Theory Tech.*, Vol. 53, No. 4, 1496–1505, 2005.
3. Ramo, S., J. R. Whinnery, and T. Van Duzer, *Fields and Waves in Communication Electronics*, 3rd edition, John Wiley and Sons, 263, 1994.
4. Blanchard, C., J. A. Portí, B.-I. Wu, J. A. Morente, A. Salinas, and J. A. Kong, "Time domain simulation of electromagnetic cloaking structures with TLM method," *Opt. Express*, Vol. 16, No. 9, 6461–6470, 2008.
5. Blanchard, C., J. A. Portí, J. A. Morente, and A. Salinas, "Dispersion inherent to TLM nodes for modelling of metamaterials," *Electron. Lett.*, Vol. 46, No. 2, 110–112, 2010.

Characterising THz Shielding Effectiveness Using the Engineering Approach

Stepan Lucyszyn and Yun Zhou
Optical and Semiconductor Devices Group, Department of Electrical and Electronic Engineering
Imperial College London, Exhibition Road, London SW7 2AZ, United Kingdom

Abstract— Shielding metal walls are found in many applications; ranging from the construction of high isolation subsystem partitions, screening individual components and integrating low cross-talk signal lines. Ideally, metal shielding walls should be made as thin as possible, while meeting the minimum level of shielding effectiveness at the lowest frequency of operation, in order to reduce weight and cost. For structural integrity, thin shielding metal can be deposited onto a plastic/ceramic wall. Moreover, thin shielding metal embedded between dielectric layers can avoid issues of poor topography when integrating signal lines within multi-layered architectures.

Shielding effectiveness is one figure of merit commonly quoted. However, there are different mathematical definitions and standards to quantify the ability to screen electromagnetic radiation. This paper will compare and contrast these definitions and standards. Moreover, room temperature simulations will be undertaken using the textbook approaches of "non-complex variables" and "classical skin-effect model". In addition, to characterize the intrinsic frequency dispersion in metals for terahertz shielding applications, the "classical relaxation-effect model" will be included [1–3]. Differences between classical skin-effect and relaxation-effect models have been quantified for metal-pipe rectangular waveguide structures at terahertz frequencies [1].

It has been recently shown that an engineering approach, which can include synthesizing equivalent transmission line models, can accurately solve electromagnetic problems [2, 3]. This new engineering approach will be applied to terahertz shielding applications, through detailed analysis. When compared to that calculated using the classical relaxation-effect model, the classical skin-effect model predicts a larger normal skin depth below $\omega\tau \approx 1.587$. This means that if a shielding metal wall is designed using the classical skin-effect model then the measured isolation will actually be higher than expected; above $\omega\tau \approx 1.587$, the converse is true.

REFERENCES

1. Zhou, Y. and S. Lucyszyn, "HFSS^{TM} modelling anomalies with THz metal-pipe rectangular waveguide structures at room temperature," *PIERS Online*, Vol. 5, No. 3, 201–211, 2009.
2. Lucyszyn, S. and Y. Zhou, "Engineering approach to modelling frequency dispersion within normal metals at room temperature for THz applications," *Progress In Electromagnetics Research*, PIER 101, 257–275, 2010.
3. Lucyszyn, S. and Y. Zhou, "THz applications for the engineering approach to modelling frequency dispersion within normal metals at room temperature," *PIERS Proceedings*, 1378–1384, Xi'an, China, March 22–26, 2010.

Scattering of Electromagnetic Waves by Inhomogeneous Metallic Gratings with Perfectly Conducting Strips

Tsuneki Yamasaki, Ryosuke Ozaki, and Takashi Hinata
Department of Electrical Engineering, College of Science and Technology, Nihon University
1-8-14, Surugadai Kanda, Chiyoda-ku, Tokyo 101-8308, Japan

Abstract— Recently, the inhomogeneous dielectric gratings have been proposed such as optical fiber gratings, photonic bandgap crystals, frequency selective devices, and other applications by the development of manufacturing technology of optical devices. However, many of the theoretical and numerical studies have considered the homogeneous structures in which the material forming grating was either metallic or dielectric.

In this paper, we proposed a new method for the scattering of electromagnetic waves by Inhomogeneous metallic gratings with perfectly conducting strips using the combination of improved Fourier series expansion method (IFEM) and point matching method (PMM) for TE and TM waves.

In the Inhomogeneous dielectric grating S_2 $(0 < x < D)$, the permittivity profile $\varepsilon(x, z)$ is generally not separable with respect to the x and z variables. So main process of our methods are as follows: (1) The inhomogeneous region is approximated by a modulated index profile with respect z. (2) Taking the electromagnetic fields are expanded appropriately by a finite Fourier series. (3) In the metallic regions with radius δ consists the thin perfectly conducting strip. (4) The electromagnetic fields in each layers are matched using an orthogonality relation which makes the matrix relation on both sides using PMM. (5) Finally, all layers include the metallic regions with perfectly conducting strips are matched using appropriate boundary conditions to get the inhomogeneous metallic gratings.

Numerical results are given for the transmitted scattered characteristics for the case of incident angle and frequency with δ for TE and TM waves.

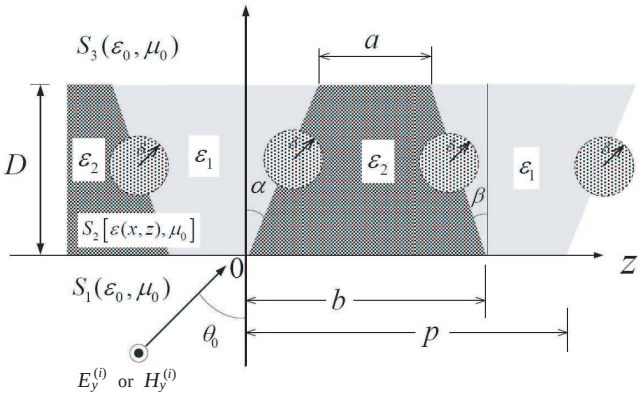

Figure 1: Structure of inhomogeneous metallic gratings with perfectly conducting strips.

Session 2P5
Theory and Modelling of Active Photonic Materials

Gain and Surface Plasmons to Improve Metal-Dielectric Multilayered Lenses

M. Kadic, J. Zhang, H. Jiang, B. Gralak, G. Tayeb, and S. Enoch
Institut Fresnel, CNRS, Université Aix-Marseille, Marseille, France

Abstract— Following a seminal work published By Sir J. Pendry in 2000 [1]; many works have been devoted to the so-called superlens that would potentially overcome the Rayleigh's diffraction limit.

We propose a theoretical study of optimization of metal-dielectric multilayer in order to approach -1 effective refractive index for transverse magnetic waves and a wavelength in the visible. The absorption losses of metal appear to be a crucial factor that affects the effective properties of the multilayer. Taking advantage of the dispersion relation of Bloch modes, we show that the losses not only decrease the transmission of the stack, but also change the negatively refracted angle. Then, we propose that using gain may allow compensating for the losses in metal layers. In theory, the performances of the structure can be improved greatly when gain is involved. When considering finite thickness structures, and with appropriate thickness for the terminating layers, it is possible to obtain a high transmission of the structure. A near -1 effective index metal-dielectric stack with high transmission may pave the way to the realization of negative quasi-isotropic refraction in the visible or ultraviolet.

In addition, in this communication we will show that we can design a one dimension (1D) structure (metallic dielectric layers stacks) that has a negative effective refractive index. However, this effective index tells us about the behaviour of the propagative part of the incident field but going beyond the diffraction limit would require enhancing the evanescent waves. We show that the exaltation of surface Plasmon modes in the multilayered structure can improve the resolution and can partially answer this problem.

REFERENCES

1. Pendry, J. B., *Phys. Rev. Lett.*, Vol. 85, 3966, 2000.
2. Zhang, J., H. Jiang, B. Gralak, S. Enoch, G. Tayeb, and M. Lequime, "Towards -1 effective index with one-dimensional metal-dielectric metamaterial: A quantitative analysis of the role of absorption losses," *Optics Express*, Vol. 15, 7720–7729, 2007.
3. Zhang, J., H. Jiang, B. Gralak, S. Enoch, G. Tayeb, and M. Lequime, "Compensation of loss to approach -1 effective index by gain in metal-dielectric stacks," *The European Physical Journal C– Applied Physics*, Vol. 46, 32603, 2009.

Theory and Modeling of Surface Plasmon Gain in Planar Metallic Structures

Israel De Leon[1] **and Pierre Berini**[1, 2, 3]

[1]School of Information Technology and Engineering, University of Ottawa
161 Louis Pasteur, Ottawa, ON, K1N 6N5, Canada
[2]Department of Physics, University of Ottawa, Canada
[3]Spectalis Corporation, P. O. Box 72029, Kanata North RPO, Ottawa, Ontario, Canada

Abstract— This paper discusses the amplification of surface plasmons via propagation through an optically pumped dipolar gain medium (e.g., a dye) incorporated into a cladding adjacent to a metal surface [1, 2]. Physically realisable structures based on the single metal-dielectric interface and on the thin metal slab bounded by dielectrics are described. The gain of the medium is non-uniform close to the metal surface due to position dependence in the dipole lifetime, and to the non-uniform distribution of the pump irradiance. Models of these effects are presented and merged with the transfer matrix method to compute the modal properties of the propagating surface plasmons. It is found that the non-uniformity of the gain medium limits the mode power gain available from the system. Nonetheless, net amplification of the long-range surface plasmon in the metal slab is possible at visible and infrared wavelengths using a reasonable pump power and dipole concentration; for example, assuming Rhodamine 6G, lossless propagation at $\lambda_0 = 560\,\text{nm}$ is obtained for pump irradiances of $175\,\text{kW/cm}^2$ and $430\,\text{kW/cm}^2$ for 5 mM and 40 mM concentrations, respectively. By comparison, in the case of the single-interface SPP, lossless propagation is obtained with 40 mM R6G concentration and a comparatively larger pump irradiance of $3.45\,\text{MW/cm}^2$.

REFERENCES

1. De Leon, I. and P. Berini, "Modeling surface plasmon-polariton gain in planar metallic structures," *Optics Express*, Vol. 17, 20191–20202, 2009.
2. De Leon, I. and P. Berini, "Theory of surface plasmon-polariton amplification in planar structures incorporating dipolar gain media," *Physical Review B (Rapids)*, Vol. 78, 161401(R), 2008.

Tremendous Enhancement of Active Photonic Phenomena via High-order Dispersionless Bands in Layered Plasmonic-dielectric Systems

Aristeidis Karalis, J. D. Joannopoulos, and Marin Soljačić
Center for Materials Science and Engineering, Research Laboratory of Electronics
Massachusetts Institute of Technology, Cambridge, MA 02139, USA

Abstract— The performance of active photonic devices depends on the presence of a large local density of photonic states at the location of the active materials. Therefore, nonlinear operations on traveling photonic pulses are, for example, enhanced when the speed (group velocity) of these pulses is small. However, slow group velocity comes usually at the expense of small frequency bandwidth of the pulse due to dispersion. Similarly, fluorescent and thermal emission processes are boosted by the presence of flat photonic bands, but the flatness of the bands is also limited by dispersion.

In recent years, plasmonic systems have become a popular candidate for improving performance of active photonic mechanisms, as they can support slow light close to their Surface Plasmon Polariton frequency, with very intense fields localized close to the surface of their confinement, where active materials can be placed. One of their limiting factors though has so far still been strong dispersion.

We present a class of multilayered axially uniform hybrid Surface PlasmonoDielectric Polaritonic systems, which can be tailored to support subwavelength light, simultaneously free of group-velocity and attenuation dispersion up to unusually high orders, for positive, negative or zero values of the group velocity. The physical mechanism underlying this tailoring capability is a fine balance of the plasmonic material dispersion with the geometric dispersion of the multilayered film stack.

This remarkable freedom from dispersion allows these systems to support extremely flat bands. In the case of zero group velocity, the density of states of these bands is extremely large and of a type not classified by van Hove. The associated enhancement of interactions in active processes can be orders of magnitude larger than previous experienced. In the case of small group velocity, the ability to design very linear bands allows for distortionless propagation of very slow and very short pulses. This may open the possibility of applying nonlinear actions on such short pulses without pulse reshaping. It furthermore enables the efficient storing of a huge number of such pulses on very compact plasmonic buffers.

Plasmonic systems may suffer from absorptive attenuation loss, but they do allow for photonic designs which may accomplish a significant reduction in size and power requirements for active photonic operations.

Dispersion and Diffraction Management in Active Subwavelength Waveguides

Viktor A. Podolskiy[1, 2] **and Alexander A. Govyadinov**[1, 3]

[1]Physics Department, Oregon State University, 301 Weniger Hall, Corvallis OR 97331, USA
[2]Department of Physics and Applied Physics, University of Massachusetts Lowell
One University Avenue, Olney Hall 136, Lowell, MA 01854, USA
[3]Department of Bioengineering, School of Engineering and Applied Science, University of Pennsylvania
210 S. 33rd Street, Room 240 Skirkanich Hall, Philadelphia, PA 19104, USA

Abstract— We consider the propagation of wavepackets in active nanoguides-optical waveguides that support propagating modes with sub-wavelength energy confinement. The behavior of two types of nanoguides is analyzed: that of plasmonic nanorods supporting highly confined surface waves, and that of waveguides with strongly anisotropic cores, enabling sub-diffraction confinement of volume modes.

In the plasmonic nanorods, Poynting flux is always co-aligned with the phase velocity. On the other hand, optics of waveguide modes in non-magnetic but anisotropic nanoguides can be mapped on the optics of plane waves in isotropic metamaterials that exhibit optical magnetism, presenting a unique platform for realization of negative refraction, inverse Doppler shift, and other phenomena commonly associated with magnetic negative index metamaterials.

Despite the fundamental difference in the structure of the surface — and the volume waves, the phase velocity of modes in nanoguides obeys the universal law: in the regime of subwavelength light confinement, phase velocity is proportional to the waveguide size. Thus, the effective modal wavelength self-adjusts to the confinement size, virtually eliminating the diffraction limit.

The drastic slow-down of the optical phase is accompanied by non-trivial modulation of the group velocity. In "conventional" waveguides with isotropic nondispersive dielectric cores, the product of the two velocities is constant; in passive plasmonic nanoguides both group and phase velocities are proportional to the waveguide size. In contrast to these behaviors, in active nanoguides group velocity is governed by the interplay between two main factors: material dispersion that is determined by optical resonances of components of waveguides and geometry dispersion that is determined by the size and shape of the waveguide. As result, geometry dispersion dramatically amplifies the effect of material dispersion, enabling strong modulation of the group velocity from ultra-small to superluminal values with minute modulation of material parameters of active nanoguides.

Compensation of Loss and Stimulated Emission of Surface Plasmons

G. Zhu and M. A. Noginov
Norfolk State University, USA

Abstract— Surface plasmons (SPs) and surface plasmon polaritons (SPPs) have become in recent years an important research topic because of their interesting physics and exciting potential applications ranging from sensing and biomedicine to nanoscopic imaging and information technology. However, many applications of surface plasmon polaritons are hindered by one common cause — Absorption loss in metal.

Over the years, numerous proposals have been made on how to conquer the plasmon loss. In this presentation, (1) the known solutions to the loss problem by adding optical gain have been reviewed; (2) conquering surface plasmon loss in aggregated silver nanoparticles has been demonstrated; (3) the propagation of surface plasmon polaritons without gain has been studied experimentally, and it is demonstrated that an addition of highly concentrated rhodamine 6 G chloride dye to the PMMA film adjacent to a silver film can cause 30% elongation of the propagation length of surface plasmon polaritons; (4) the propagation of SPPs with optical gain has been studied experimentally and compared to the theoretical predictions: the level of gain achieved in our experiments ($\approx 420\,\mathrm{cm}^{-1}$ at $\lambda = 594\,\mathrm{nm}$) was, in principle, sufficient to compensate the propagation loss of surface plasmon polaritons in high-quality silver films; (5) the stimulated emission of surface plasmon polaritons characterized by a distinct threshold in the input-output dependence and narrowing of the emission spectrum has been demonstrated; (6) the nano-laser based on surface plasmons has been demonstrated in nanoparticle of gold core coated with silica shell containing the rhodamine 6 G dye.

The realized compensation of the metallic absorption loss by gain and the observed stimulated emission of surface plasmon polaritons pave the road to a broad range of applications of metamaterials and nanoplasmonic devices. The authors cordially thank M. Mayy, A. M. Belgrave, R. A. Ritzo, K. Reynolds, N. Noginova, R. Bakker, E. E. Narimanov, V. M. Shalaev, S. Stout, E. Herz, T. Suteewong, and U. Wiesner, and V. A. Podolskiy for their contributions to this work. The work was supported by the NSF PREM grant # DMR 0611430, NSF NCN grant # EEC-0228390, AFOSR grant # FA9550-09-1-0456.

REFERENCES

1. Noginov, M. A. and G. Zhu, et al., *Nature*, 2009.
2. Noginov, M. A. and G. Zhu, et al., *Phys. Rev. Lett.*, 2008.
3. Noginov, M. A. and Podolskiy, et al., *Opt. Express*, 2008.
4. Zhu, G. and Mayy, et al., *Opt. Express*, 2008.
5. Noginov, M. A. and G. Zhu, et al., *Opt. Lett.*, 2006.

Computational Modeling of Linear and Nonlinear Optical Properties of Plasmonic Nanostructures

Nicolae C. Panoiu[1], **Lina Cao**[2], **Claudiu C. Biris**[1], **Fangwei Ye**[3], **Ryan M. Roth**[2], **and Richard M. Osgood, Jr.**[2]

[1]Department of Electronic and Electrical Engineering, University College London
Torrington Place, London WC1E 7JE, UK
[2]Department of Applied Physics and Applied Mathematics, Columbia University
New York, New York 10027, USA
[3]Department of Physics, Centre for Nonlinear Studies
The Beijing-Hong Kong-Singapore Joint Centre for Nonlinear and Complex Systems (Hong Kong)
Hong Kong Baptist University, Kowloon Tong, Hong Kong, China

Abstract— In the last decade the advances in integrated optics and photonic nanodevices have been greatly accelerated by the availability of high performance computing platforms and powerful numerical methods for device simulation and computer-aided design. Thus, high fabrication costs of complex photonic nanodevices make it imperative to have access to high-performance computational tools, which can greatly accelerate the device design process and reduce the design-fabrication-testing cycle. In this connection, in this talk we will briefly review and compare several numerical methods that are commonly used to model the optical properties of plasmonic nanostructures, namely the finite-difference time-domain algorithm (a key technique in our work), the multiple scattering matrix method, and the rigorous coupled-wave analysis, and subsequently, by using specific examples we will illustrate how these methods can be employed to characterize and design plasmonic nanostructures with unique linear and nonlinear optical properties Specifically, we demonstrate that by properly tailoring the material and geometric parameters of plasmonic nanostructures one can selectively excite localized or propagating surface-plasmon polariton (SPP) modes, and show that this effect can be used to achieve more than a tenfold enhancement of the efficiency of photovoltaic devices, such as solar cells or plasmon-based detectors.

We also show that the strong optical nonlinearities induced by the SPP-enhanced electromagnetic field can change dramatically the physical characteristics of the nonlinear interaction between electromagnetic waves and plasmonic nanostructures. As an example of such SPP-induced nonlinear optical effect, we show that one- and two-dimensional arrays of parallel metallic nanowires embedded in an optical medium with cubic (Kerr) optical nonlinearity support subwavelength plasmonic solitons and subwavelength plasmonic vortex cells. Finally, we demonstrate that the resonant excitation of localized SPP can strongly enhance the nonlinear scattering of plasmon or electromagnetic waves upon their interaction with surface nanodefects located at metal/dielectric interfaces or arrays of metallic nanowires, leading to an increased efficiency of nonlinear optical processes such as the second harmonic generation. A series of applications pertaining to plasmonic nanodevices are also discussed.

Nanoscale Nonlinear Photonics

C. Sibilia, **M. Centini**, **and A. Benedetti**
Dipartimento di Energetica, Universita' di Roma La Sapienza, Via Scarpa 16, 00161 Roma, Italy

Abstract— An overview of different nonlinear optical phenomena occurring in nanopatterned materials is presented. In particular a discussion about second order nonlinear effects is reported, including also some nonclassical properties of the interaction with non homogeneous materials.

Electromagnetic Wave Propagation in Transition Metamaterials

Natalia M. Litchinitser, **Irene Mozjerin**, **and Tolanya Gibson**
Department of Electrical Engineering, University at Buffalo, The State University of New York
309 Bonner Hall, Buffalo, NY 14260-1920, USA

Abstract— Photonic metamaterials enable a number of unique physical phenomena and functionalities, including negative refraction, anti-parallel directionality of the phase velocity and the Poynting vector, backward phase matching and negative phase shift facilitating new regimes of secondharmonic generation, parametric processes and bistability, unusual surface waves, and ultracompact cavities. While the optical properties and potential applications of metamaterials with constant values of material parameters (dielectric permittivity ε and magnetic permeability μ) have been studied in detail, light propagation in graded-index metamaterials — artificial nanostructures with refractive indices gradually varying in space from positive to zero to negative values — has become a topic of intense research only a few years ago. The enormous potential of graded-index metamaterial structures was recently exemplified by the first experimental demonstration of cloaking devices.

Recently, we studied a novel class of graded-index metamaterials-transition metamaterials-with ε and μ gradually changing from positive to negative values. We predicted resonant field enhancement occurring near the zero-refractive-index point under oblique incidence of both TE and TM polarized electromagnetic wave on such transition layer. Also, we found that transition through the point where ε and μ change sign is accompanied by a finite loss of incident wave energy even if the imaginary parts of ε and μ are infinitesimally small. In this talk, we discuss our recent studies on linear and nonlinear phenomena taking place in transition metamaterial structures, effects of realistic material losses, and Gaussian beam propagation in such structures. We will also discuss the optimization of the profile of the transition layer for various potential applications.

Carbon Nanotubes as Novel Photonic Materials

K. Kempa
Boston College, USA

Abstract— Carbon nanotubes are interesting nanomaterials, which show many unusual photonic and plasmonic effects. The single wall carbon nanotubes, due to singular nature of their density of states, have very rich dielectric response, characterized by a large number of resonant terms in the frequency expansion of its dielectric function. Numerous plasmon resonances follow, having cross-dimensional behavior. The multi-wall carbon nanotubes can be considered in most cases as metallic nanowires. As such, they can be used as polarizable components of the dielectric composites, with engineered dielectric response. In another application, they can be used as antennas for light, or nanocoaxial transmission lines. The nanocoaxial metamedium based on arrays of nanowires will also be discussed. This novel concept provides exceptional control over light propagation, and allows for optical nanomicroscopy and nanolitogrphy. Finally, a solar cell application of nanowires will be introduced and discussed.

Electromagnetic Metamaterials Mimic Celestial Phenomenon in the Lab

Dentcho A. Genov
The LONI Institute, Louisiana Tech. University, Ruston, LA 92720, USA

Abstract— Einstein's general theory of relativity establishes equality between matter-energy density and curvature of space-time. As a result, light and matter follow natural paths in the inherent space-time and may experience bending and trapping in a specific region of space. So far, the interaction of light and matter with curved space-time has been predominantly studied theoretically and through astronomical observations. This talk proposes to link the newly emerged field of artificial optical materials to that of celestial mechanics, thus opening the way to investigate light phenomena reminiscent of orbital motion, strange attractors and chaos, in controlled laboratory environment. Realistic metamaterial designs will be presented that provide laboratory environments for studies of light in close proximity to massive objects including gravitational singularities (black holes). Revision of the Bertrand theorem for the stability and closeness of orbital motion for photons will be presented with important ramifications for development of highly stable photonic traps and cavity lasers.

Thermal Radiation in Finite Photonic Crystals

Marian Florescu[1], **Christian Schuler**[2], **Christian Wolff**[2], **and Kurt Busch**[2]

[1]Department of Physics, Princeton University, Princeton, NJ 08544, USA
[2]Institut für Theoretische Festkörperphysik and DFG-Center for Functional Nanostructures (CFN)
Karlsruhe Institute of Technology, 76128 Karlsruhe, Germany

Abstract— The ability of microstructured photonic systems to significantly alter thermal radiation processes has recently received considerable attention [1–3] as it holds a tremendous potential for applications that range from thermophotovoltaic energy conversion devices [1, 4] to tunable infrared emitters [5].

We present a microscopic theory of thermal emission from truncated photonic crystals and show that the relevant physical parameters such as the directional spectral emissivity can be obtained from standard photonic bandstructure computations without any approximation [6]. We then analyze the origin of thermal radiation enhancement and suppression inside photonic crystals and demonstrate that the central quantity that determines the thermal radiation characteristics such as intensity and emissive power is the area of the iso-frequency surfaces and not the density of states as is generally assumed [1, 2, 7, 8]. We also identify the physical mechanisms through which interfaces modify the potentially super-Planckian radiation flow inside infinite photonic crystals, such that thermal emission from finite-sized samples is consistent with the fundamental limits set by Planck's law. As an application, we further demonstrate that a judicious choice of a photonic crystal's surface termination facilitates considerable control over both the spectral and angular thermal emission properties.

Finally, we outline design principles that allow the maximization of the radiation flux, including effects associated with the isotropy of the effective Brillouin zone, photonic band gap size and flatness of the band structure in the spectral range of interest.

REFERENCES

1. Fleming, J. G., S. Y. Lin, I. El-Kady, R. Biswas, and K. M. Ho, *Nature*, Vol. 417, 52, 2002.
2. Luo, C., A. Narayanaswamy, G. Chen, and J. D. Joannopoulos, *Phys. Rev. Lett.*, Vol. 93, 213905, 2004.
3. Florescu, M., K. Busch, and J. Dowling, *Phys. Rev. B*, Vol. 75, 201101, 2007.
4. Florescu, M., H. Lee, I. Puscasu, M. Pralle, L. Florescu, D. Z. Ting, and J. P. Dowling, *Solar Energy Materials and Solar Cells*, Vol. 91, 1599, 2007.
5. Pralle, M. U., N. Moelders, M. P. McNeal, I. Puscasu, A. C. Greenwald, J. T. Daly, E. A. Johnson, T. George, D. S. Choi, I. El-Kady, and R. Biswas, *Appl. Phys. Lett.*, Vol. 81, 4685, 2002.
6. Schuler, C. J., C. Wolff, K. Busch, and M. Florescu, *Appl. Phys. Lett.*, Vol. 95, 241103, 2009.
7. Florescu, M., H. Lee, A. J. Stimpson, and J. Dowling, *Phys. Rev. A*, Vol. 72, 033821, 2005.
8. Kee, C. S., S. S. Oh, K. J. Chang, J. E. Kim, H. Y. Park, and K. H. Lee, *Phys. Rev. B*, Vol. 60, 10573, 1999.

Modeling Photonic Crystal Microcavity Lasers

John O'Brien[1], **Adam Mock**[2], **and Ling Lu**[1]

[1]University of Southern California, USA
[2]Central Michigan University, USA

Abstract— The presentation will discuss the electromagnetic properties of photonic crystal lasers as they are related to optical loss, output beam quality, and output coupling. We use 3D parallelized Cartesian FDTD for analyzing the electromagnetic fields in these photonic crystal lasers. The basic algorithm uses split-field PMLs to truncate the boundaries. A resolution of 20 points per lattice constant is typical. 3D domains on the order of $1000 \times 350 \times 200$ are typical and parallelized on the order of 100 processors running for 10–20 hours. MPICH is used for parallelization.

The presentation will focus on microcavity lasers and resonant cavities. The calculated and experimental resonant spectra of high Q microcavities will be presented. The calculations use Pade interpolation for spectroscopic analysis of FDTD data. The temporal field evolution in response to an impulse initial condition is monitored at discrete points in the computational domain. A DFT is taken of the resulting time sequence. Resonance frequencies and Q factors are extracted via Pade interpolation. The resulting quality factors will be compared to experimental data. We have analyzed linear gain effects in microcavities numerically by including a dispersive gain model via an auxiliary differential equation. A particular analytical formulation of Pade interpolation allows us to characterize field decay and growth.

Lasing results along with efforts to reduce the absorption loss and improve the output coupling will also be discussed. Here the primary cavities of interest are photonic crystal heterostructure and L3 cavities in which three holes are removed from a triangular lattice. We have employed 3D FDTD to analyze photonic crystal double heterostructures with Q factors in excess of 1 million. Experimentally, we have obtained peak output powers in excess of 100 W from these devices by loading these cavities with an output coupling loss.

We are also investigating ways to improve the actual device performance by improving the heat dissipation capabilities of these lasers. Most of this strategy relies on placing these cavities on low index substrates. The presence of a substrate, in general, increases the optical radiation loss of the cavity. To reduce this loss, we have investigated heterostructure cavities employing a glide plane. In addition, to the FDTD analysis of these cavities, we have done a detailed space group analysis of these resonant cavities. The regular single-line defect (type A) waveguide belongs to a symmorphic group, while the half-lattice shifted geometry (type B) belongs to a nonsymmorphic group.

Session 2P6
Photonic Crystals and Metamaterials 2

Analysis of Linear and Non-linear Modes in Lithium Niobate Ferroelectrics

K. Choudhary[1], **A. K. Bandyopadhyay**[1], **P. C. Ray**[2], **and A. R. McGurn**[3]

[1]Govt. College of Engineering & Ceramic Technology, W. B. University of Technology
73, A. C. Banerjee Lane, Calcutta 700010, India
[2]Department of Mathematics, Govt. College of Engineering & Leather Technology
LB Block, Sector III, Salt Lake, Calcutta 700098, India
[3]Department of Physics, Western Michigan University, Kalamazoo, Michigan 49008-5252, USA

Abstract— Ferroelectricity is a well-studied property of solids, arising in crystals undergoing structural changes below a critical temperature, leading to the development of a spontaneous polarization. The transition that can be either first or second order is generally described by an appropriate Landau-Ginzburg (L-G) free energy functional. Ferroelectrics occur as collections of domains where the domains, as in ferromagnetic domains, are created and oriented by a need to minimize the free energy of the crystal and fields. The bulk properties and domain structure of these materials have been extensively studied. Recently, however, they have gained renewed interest for potential applications in nano science and in the design of nano devices, where the focus is on properties exhibited at small length scales, in the non-linear photonic materials. Hence, it is important to study these materials at nano scale lengths to reveal different interesting behaviour concerning different oscillations of both the linear and non-linear modes.

A model of a ferroelectric crystal in terms of a one-dimensional array of ferroelectric slab domains is treated for the dynamics of the 'array of domains'. Two approaches can be considered. The first consists of the system being treated within a continuum limit in which the space and time evolution of the polarization of the crystal are described by a non-linear Klein-Gordon equation involving L-G potential in the Hamiltonian formulation. Here, a multiple time-scale analysis (MTSA) is used to determine the linear and non-linear parts of the frequencies of the extended modes of oscillation of such domain arrays. These modes are also studied in the presence of impurities in inhomogeneous ferroelectric materials such as lithium niobate.

In a second approach, the discrete equations for the coupling of neighboring ferroelectric slab domains are used to study intrinsic localized modes (ILM) of the ferroelectric crystal. These are highly localized modes that arise from their self-consistent interactions with the non-linearity of the system. These current interests need a more detailed look at the dynamical properties of domain arrays which may become significant features at some of the length scales of interest and this aspect is definitely very important.

First of all, for the extended (i.e., plane wave like) modes of the array, the continuum model is treated to determine the renormalization of the mode frequencies with mode amplitude due to the system non-linearity. The time-dependence of the domain array is obtained using multiple time-scale analysis (MTSA) methods. The MTSA allows for a determination of the frequency and amplitude of the modes as an expansion in a series of relevant increasing time scales. It overcomes problems with singularities that arise in the traditional perturbation expansion in the non-linearity of the system as a small parameter. The plane wave like modes of the non-linear system are found to evolve from those of the linear limit of the system such that the non-linear component of the interactions adds a complicated renormalization of their properties. The effects of impurities in the system on this renormalization are considered using recent data on lithum niobate. These effects are of interest as they occur in many ferroelectircs and may have applications in non-linear optical communications.

Secondly, a study was made on a set of intrinsic localized modes (ILM) of the domain array that are highly localized pulses in space and are found in the discrete nonlinear model formulation. Unlike the plane wave like modes, ILM have no counterparts in the linear system, but exist only because of the system non-linearity in a periodic lattice. They are formed as a self-consistent interaction between the mode and the system non-linearity so that an ILM modifies the local properties of the system at the ILM peak, and the modified local properties of the system provide the environment for the ILM to exist. The existence of ILM have been proposed theoretically in a wide variety of discrete many-body systems, and they have been observed experimentally in a number of different types of such systems. Detailed discussions of ILM have been reviewed extensively in the works of Sievers group and Segev et al.. For our discussions we use a simple and general formulation given originally by Sievers et al. for the treatment of ILM in non-linear

vibrational systems. The formulation is appropriate to highly localized pulses having widths that are not large compared to the domain widths so that the continuum limit formulation cannot be applied to their study.

Ultimate Fast Optical Switching of Photonic Microcavities

Georgios Ctistis[1, 2], **Alex Hartsuiker**[2], **Maela Bazin**[3], **Julien Claudon**[3], **Jean-Michel Gérard**[3], **and Willem L. Vos**[1, 2]

[1]Complex Photonic Systems (COPS), MESA+ Institute for Nanotechnology
University of Twente, AE Enschede 7500, The Netherlands
[2]Center for Nanophotonics, FOM Institute for Atomic and Molecular Physics (AMOLF)
Science Park 113, XG Amsterdam 1098, The Netherlands
[3]CEA-CNRS-UJF "Nanophysique et Semiconducteurs" Joint Laboratory, CEA/INAC/SP2M
17 rue des Martyrs, Grenoble Cedex 38054, France

Abstract— Exciting prospects arise when the optical properties of photonic structures are switched on ultrashort timescales, by quickly changing the refractive index of the constituent materials. Of particular interest is the ultrafast switching of the resonance of a microcavity, wherein photons are stored in a tiny volume. Switching cavities allows the capture and release on demand of photons [1], as well as the quantum electrodynamical manipulation of the stored photons or of emitters in the cavity [2].

Ultrafast switching mechanisms, such as free-carrier switching, are mostly limited by the radiative and non-radiative recombination dynamics of free carriers involved, and are therefore at least of the order of picoseconds [3].

In contrast, instantaneous switching, where both on- and off-switching times are only limited by the used pulse durations, is only achievable by use of the electronic Kerr effect.

Here, we demonstrate the ultimate fast switching of a GaAs microcavity in the telecom band by exploiting the instantaneous electronic Kerr effect.

In order to get rid of two photon absorption and access the electronic Kerr switching regime, we designed our experiment to operate with low energy pump photons. We used an ultrafast setup with broadly and independently tunable pump and probe beams to measure the reflectivity of our samples. The samples with the ultrafast cavity ($\tau_{\mathrm{cav}} = 0.9\,\mathrm{ps}$) were designed to have the cavity in the original telecom band and were fabricated by means of molecular beam epitaxy.

Figure 1 shows the reflectivity of the cavity resonance versus the pump-probe delay time. In the region of pump-probe coincidence a red-shift of the resonance is observed, indicating an increase in refractive index, which is the fingerprint of the electronic Kerr effect. Furthermore, the reflectivity at the resonance decreases from 70% to 60% (Fig. 2). Our results show that the switching rate is limited by the cavity storage time. Since our cavity has a fast decay it paves the way to ultimate fast quantum electrodynamics and supra-THz data modulation.

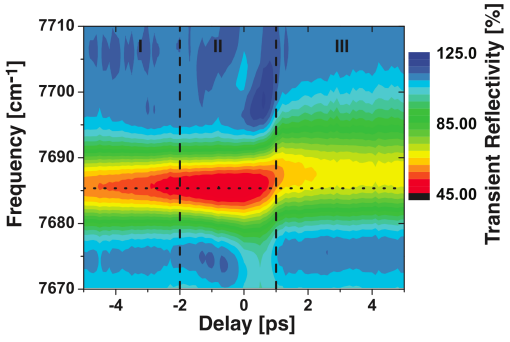

Figure 1: Reflectivity as a function of frequency and pump-probe delay. At pump-probe coincidence a red shift of the cavity resonance is observed.

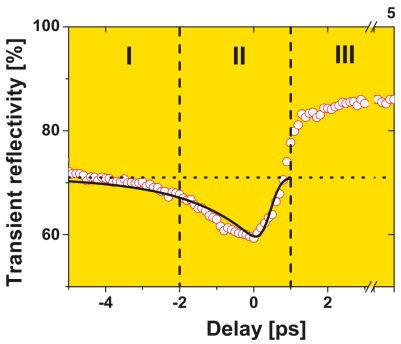

Figure 2: Transient reflectivity at the unswitched cavity resonance frequency as function of delay. A decrease in reflectivity is observed at pump-probe coincidence.

REFERENCES

1. Johnson, P. M., A. F. Koenderink, and W. L. Vos, *Phys. Rev. B*, Vol. 66, 081102, 2002.

2. Gérard, J.-M., B. Sermage, B. Gayral, B. Legrand, E. Constard, and V. Thierry-Mieg, *Phys. Rev. Lett.*, Vol. 81, 1110, 1998.
3. Euser, T. G. and W. L. Vos, *J. Appl. Phys.*, Vol. 97, 043102, 2005.

Ab Initio Description of Spatiotemporal Dynamics of Multi-level Atoms Resonantly Coupled to Plasmonic Materials

Maxim Sukharev
Department of Applied Sciences and Mathematics, Arizona State University, Mesa, AZ 85212, USA

Abstract— The research in plasmonics has been centered at linear optics of plasmonic structures with several attempts to go beyond linear regime and consider nonlinear properties of materials including noble metal nanoparticles aiming for a wide variety of nonlinear phenomena to appear. A newly emerging research field of nonlinear plasmonics takes two obvious routes, namely, combining linear plasmonic systems with highly nonlinear media or taking into account strongly inhomogeneous electromagnetic fields associated with surface plasmons that lead to spatial dependence of conductive electron density in metals and hence result in nonlinear phenomena such as second harmonic generation. The first route deals with nonlinear media at the macroscopic level while even a single atom or molecule located near plasmonic structure at resonant conditions may be considered as a nonlinear optical system due to high electromagnetic near-fields. For example, it is well known that a two-level atom exposed to strong resonant EM radiation has an average dipole moment that may be written as a sum over odd powers of the electric field amplitude. Such dipole coupled to plasmon fields via polarization currents in Maxwell equations results in a nonlinear optical system and obviously is able to lead to new venues of research now including nonlinear optics. It thus important to develop approach capable of capturing both size effects at the nanoscale and the time dynamics of electromagnetic fields. Generally speaking, such approach has to take into account Maxwell equations capturing electromagnetic waves and quantum dynamics of atoms or molecules in the vicinity of plasmonic materials. The latter can be accomplished by employing Bloch formalism. The resulting system of coupled Maxwell-Bloch equations contains the most accurate description of nonlinear phenomena driven by surface plasmon waves. I will discuss new concepts of atom-plasmon interactions at the nanoscale based on rigorous numerical solutions of self-consistent full-wave vector Maxwell-Bloch equations in two and three dimensions. Various nonlinear phenomena such as self-induced transparency will be considered. I will also discuss the Brumer-Shapiro scheme of coherent control implemented at the nanoscale.

Combined Direct Write Multiphoton Lithography and Proximity Nanopatterning for High throughput Writing of Non-periodic Structures with Periodic Sub-elements

Jonathan P. Singer[1], **Jae-Hwang Lee**[1], **Steven E. Kooi**[2], **and Edwin L. Thomas**[1]

[1]Department of Materials Science and Engineering, Massachusetts Institute of Technology
Cambridge 02139, USA
[2]Institute for Soldier Nanotechnologies, Massachusetts Institute of Technology
Cambridge 02139, USA

Abstract— For the next generation of photonic, opto-mechanical and microfluidic devices, the capability to create 3D structures is highly desirable. Fabrication of such structures by conventional top-down techniques generally requires many layer by layer steps. Two recent techniques that have shown potential for high degrees of control in producing 3D structures are interference lithography (IL), by multi-beam [1] or phase mask [2], and direct write multiphoton lithography (MPL) [3]. IL is able to pattern highly-uniform and periodic 3D structures over a wide area, but lacks arbitrary control over what regions are patterned, whereas MPL has the capability to draw nearly arbitrary structures but is an inherently slow serial writing process. One technique that has been used for enhanced contrast and writeable depth of IL is multiphoton proximity nanopatterning (PnP) [4], in which 3D features printed into the surface of a photoresist act as a phase mask for multiphoton IL.

We present here a method that combines multiphoton PnP with MPL to increase the speed and capability of both techniques. By exposing a thick photoresist layer (e.g., SU-8) having a phase mask pattern on its surface with a tightly focused MPL laser beam, it is possible to write locally either the periodic structure specified by the mask (focal point far above or below the sample) or unique complex structures that would be difficult to create with either technique alone (focal point at or just below the surface. These patterns may be written rapidly either in a single shot mode or by more arbitrary paths defined by the direct write, thus exploiting the control of MPL with an the enhanced speed of phase mask IL. Further, because the top relief pattern can be rewritable at a temperature over the flow temperature of SU-8 using thermoplastic behavior of uncrosslinked SU-8, multiple patterning steps are possible. Here we will present rigorous numerical simulations predicting possible 3D structures as well as experimentally fabricated structures of this novel method.

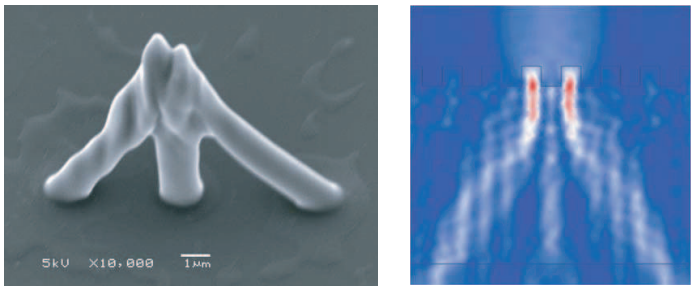

Figure 1: Tilted electron micrograph of a complex structure fabricated by focusing a MPL laser below an imprinted 1D phase mask in a 5 μm thick resist in a single shot (left) along with finite element simulation of the intensity distribution in the resist (right).

REFERENCES

1. Campbell, M., D. N. Sharp, M. T. Harrison, R. G. Denning, and A. J. Turberfield, "Fabrication of photonic crystals for the visible spectrum by holographic lithography," *Nature*, Vol. 404, No. 6773, 53–56, 2000.
2. Jeon, S., J.-U. Park, R. Cirelli, S. Yang, C. E. Heitzman, P. V. Braun, P. J. A. Kenis, and J. A. Rogers, "Fabricating complex three-dimensional nanostructures with high-resolution conformable phase masks," *Proc. Nat. Acad. Sci. U.S.A.*, Vol. 101, No. 34, 12428–12433, 2004.

3. Witzgall, G., R. Vrijen, E. Yablonovitch, V. Doan, and B. J. Schwartz, "Single-shot two-photon exposure of commercial photoresist for the production of three-dimensional structures," *Opt. Lett.*, Vol. 23, No. 22, 1745–1747, 1998.
4. Jeon, S., D. J. Shir, Y. S. Nam, R. Nidetz, M. Highland, D. G. Cahill, J. A. Rogers, M. F. Su, I. F. El-Kady, C. G. Christodoulou, and G. R. Bogart, "Molded transparent photopolymers and phase shift optics for fabricating three dimensional nanostructures," *Opt. Express*, Vol. 15, No. 10, 6358–6366, 2007.

Geometric Resonance-induced Gap in the Transmission Spectrum of a Periodic Waveguide

Victor A. Pogrebnyak and James J. Whalen
Department of Electrical Engineering, School of Engineering and Applied Sciences
University at Buffalo, State University of New York, 332 Bonner Hall, NY 14260-1920, USA

Abstract— We investigated theoretically and experimentally the microwave transmission spectrum of a rectangular metallic waveguide, having lower and upper walls with the identical sinusoidal profile and two smooth side walls. Amplitude and period of the corrugations equal correspondingly to 0.415 cm and $a = 3.15$ cm. The upper plate was made movable. It could easily move with respect to the stationary lower plate forming the phase shift between the periodic walls and varying the distance between them. This structure allows for controlling location and width of gaps in the transmission spectrum.

There are two important configurations of the waveguide: 1) when the upper and lower sinusoidal profiles are in phase, 2) when the upper and lower profiles are out of phase making a phase shift of $a/2$. In the first case, the distance between plates d is not changing along the waveguide; therefore Bragg gaps do not appear in the spectrum. However, because of the periodicity, the dispersion curves are folded but without gaps. As result the dispersion curves of different modes are intersecting at some frequencies. Interaction between the modes at these frequencies causes non-Bragg resonances and opening gaps. For some specific relation between d and a, the frequency of the lowest intersection can be equal to the cutoff frequency of the second mode. Transmission spectrum for such geometric configuration was theoretically investigated earlier [1]. In this communication, we report on observation of the transmission spectrum gap induced by the geometric resonance.

A standard microwave setup with the HP8510 network analyzer and two horn microwave antennas was used for measuring the transmission characteristics of the periodic waveguide at a frequency range between 5 and 18 GHz. We investigated propagation of the TE_{01} wave with the polarization vector parallel to grooves of the corrugation and perpendicular to the side walls. We observed the geometric resonance-induced gap between 9.2 and 12.5 GHz that is in good agreement with the theoretical result.

REFERENCES

1. Pogrebnyak, V. A., "Geometric resonance in a periodic waveguide," *J. Appl. Phys.*, Vol. 94, 6979, 2003.

New Classes of Non-crystalline Photonic Band Gap Materials

Marian Florescu[1], **Salvatore Torquato**[2, 3], **and Paul J. Steinhardt**[1, 2]

[1]Department of Physics, Princeton University, Princeton, New Jersey 08544, USA
[2]Department of Chemistry, Princeton University, Princeton, New Jersey 08544, USA
[3]Princeton Center for Theoretical Sciences, Princeton University, Princeton, New Jersey 08544, USA

Abstract— Due to their ability to control the most fundamental properties of light, photonic band gap (PBG) materials open a new frontier in both basic science and technology [1, 2]. Until now, the only materials known to have complete photonic band gaps were photonic crystals, periodic structures. We show that there exists a more general class of systems, called hyperuniform photonic structures, which exhibit large and complete photonic band gaps [3, 4]. The common feature of hyperuniform photonic structures considered here is that they are derived from hyperuniform point patterns [5]. Hyperuniform point patterns are those whose number variance within a spherical sampling window of radius R (in d dimensions) grows more slowly than the window volume for large R, i.e., $< N_R^2 > - < N_R >^2 < R^p$, where $p < d$. This classification includes all crystals and quasicrystals [6], as well as a special subset of disordered structures. We construct translationally-disordered photonic structures with complete PBGs using a special subclass of hyperuniform point patterns, called stealthy, whose structure factor $S(\mathbf{k})$ is isotropic, continuous and, precisely equal to zero for all $|k| < k_C$ for some positive k_C. Starting from a point pattern with the desired rotational symmetry and translational order, our design protocol determines the arrangement of dielectric materials around the point pattern that produces the largest complete PBG. The patterns are parameterized by χ, essentially equal to the fraction of wavenumbers k within the first Brillouin zone that are set to zero. Structures built around hyperuniform patterns with $\chi = 0.5$ are found to exhibit remarkably large TM (of 36.5%) and TE (of 29.6%) PBGs, making them competitive with many of their periodic and quasiperiodic counterparts [3, 4]. More importantly, there are complete PBGs of appreciable magnitude reaching values of about 10%, independent of system size over the range we tested, and our results strongly suggest that, for any finite size, the disordered stealthy hyperuniform configurations lead to complete PBGs of comparable size.

The existence of substantial PBGs in disordered structures is particularly surprising; we conjecture that stealthy materials could have novel electronic, elastic and phononic properties, as well. Although we restricted our analysis to 2D cases with large dielectric contrast, all currently known heterostructures with complete PBGs are hyperuniform independent of the dimensionality and dielectric contrast. The disordered hyperuniform PBG materials may offer advantages for certain applications, including highly-efficient thermal radiation sources [7] and waveguides with arbitrary bending angle. Due to their compatibility with general boundary constraints, photonic band gap structures based on disordered hyperuniform patterns can provide a flexible optical insulator platform for planar optical circuits.

REFERENCES

1. John, S., "Strong localization of photons in certain disordered dielectric superlattices," *Physical Review Letters*, Vol. 58, 2486, 1987.
2. Yablonovitch, E., "Inhibited spontaneous emission in solid-state physics and electronics," *Physical Review Letters*, Vol. 58, 2059, 1987.
3. Florescu, M., S. Torquato, and P. J. Steinhardt, "Complete band gaps in two-dimensional photonic quasicrystals," *Physical Review B*, Vol. 80, 155112, 2009.
4. Florescu, M., S. Torquato, and P. J. Steinhardt, "Designer disordered materials with large, complete photonic band gaps," *Proceedings of the National Academy of Sciences*, Vol. 106, 20658, 2009.
5. Torquato, S. and F. Stillinger, "Local density fluctuations, hyperuniform systems and order metrics," *Physical Review E*, Vol. 68, 041113, 2003.
6. Levine, D. and P. J. Steinhardt, "Quasicrystals: A new class of ordered structures," *Physical Review Letters*, Vol. 53, 2477, 1984.
7. Florescu, M., K. Busch, and J. Dowling, "Thermal radiation in photonic crystals," *Physical Review B*, Vol. 75, 201101, 2007.

Dielectric Resonators for Negative Index Dielectric Metamaterials

T. Lepetit[1], **E. Akmansoy**[2], **and Jean-Pierre Ganne**[3]

[1]Laboratoire Ondes et Acoustique, Institut Langevin, ESPCI ParisTech, CNRS UMR 7587
Université Denis Diderot Paris 7, 10 rue Vauquelin, 75231 Paris Cedex 05, France
[2]Institut d'Electronique Fondamentale, CNRS UMR 8622
Université Paris-Sud Paris 11, Bat 220, 91405 Orsay Cedex, France
[3]Thales Research and Technology, Route Départementale 128, 91767 Palaiseau Cedex, France

Abstract— Interest in dielectric metamaterials lies in their potential for low losses as well as isotropy. Dielectric metamaterials usually rely on Mie resonances in high-permittivity resonators. In the microwave domain ferroelectrics, whose permittivity can range from a few hundred to a few thousand, are the choice materials. Recently, experimental proof of negative index dielectric metamaterials has been given at 10 GHz.

Most negative index metamaterials to date rely on two distinct resonators, each resonating in a different mode in the same frequency band. Here, we show that with careful resonance engineering it is possible to use a single resonator with two almost degenerate resonances. Constraints on the fabrication of bulk metamaterials are therefore relaxed. This negative index scheme can be applied to either metallic or dielectric metamaterials. We propose to demonstrate it with dielectric metamaterials. Moreover, we show that this approach can be used with many different dielectric resonators, such as cylinders, rings and cubes. Consequently, a suitable choice can be made according to the targeted application.

However, for some resonators such as the sphere, degenerate resonances can be somewhat hard to obtain. To make up for this we demonstrate another means of resonance engineering via lattice radiative coupling. Indeed, we show that resonance frequencies as well as quality factor can be tailored in a wide frequency band by modifying lattice constants. A spheres array is chosen as example. Electric and magnetic dipoles coupling as well as transverse and longitudinal coupling is shown. Besides, their respective dependence on distance is also discussed.

We propose to show that a single resonator is enough to realize a negative index metamaterial. Indeed, even if straightforward resonance engineering is not enough, combined with lattice engineering any resonator can be made into a negative index metamaterial.

Integrated Magnetophotonic Circulators Operating in Uniform External Magnetic Field

W. Śmigaj[1], **J. Romero-Vivas**[1], **S. Guenneau**[1], **B. Gralak**[1], **L. Magdenko**[2], **B. Dagens**[2], **and M. Vanwolleghem**[2]

[1] Institut Fresnel, CNRS, Aix-Marseille Université, Ecole Centrale Marseille
Campus de St Jérôme, 13397 Marseille Cedex 20, France
[2] Institut d'Electronique Fondamentale, CNRS, Université Paris-Sud
Centre Scientifique d'Orsay, F-91405 Orsay, France

Abstract— Nonreciprocal isolators and circulators remain the last fundamental optical components that have not yet been successfully miniaturized. In 2005, Z. Wang and S. Fan [1] proposed a novel magnetooptical circulator with a footprint of the order of a squared wavelength, composed of three photonic crystal (PC) waveguides coupled to a cavity containing magnetooptical (MO) material and supporting a pair of degenerate eigenmodes. A static external magnetic field (SEMF) lifts this degeneracy, thus making the cavity act as a circulator by transferring energy preferentially in the clockwise or counterclockwise direction. The device bandwidth is proportional to the *coupling strength* V of the two eigenmodes, given by the integral of the cross product of their electric fields times the gyrotropic coefficient g of the MO material. For a typical cavity placed in a uniform SEMF, V is very small due to rapid sign changes of the cross product throughout the cavity volume. A possible remedy [1] consists in using a spatially nonuniform SEMF to partition the cavity into minuscule domains magnetized in opposite directions, thus inverting locally the sign of g. However, for devices working at telecommunications frequencies, this presents serious experimental difficulties, since it demands precise magnetic field control on the scale of $\sim$100 nm.

Our aim here is to overcome this technological obstacle by demonstrating that by proper cavity design one can achieve satisfactory coupling strengths also in uniform SEMF [2]. We start by showing that in the simple case of circularly-symmetric cavities built of concentric MO and non-MO rings, the coupling strength in uniform SEMF is maximized when each layer is made a quarter-wavelength thick in the sense of Bessel-function quasi-periodicity. This rule is identical with the design principle of circular Bragg mirrors. Applying it to the specific case of systems composed of air and bismuth iron garnet (BIG), we achieve a tenfold increase of coupling strength with respect to the values obtained previously [1] in uniform SEMF. We also study the integration of such cavities in PC lattices.

Subsequently, we present results of numerical simulations of circulators employing the proposed cavities and operating in uniform SEMF at infrared frequencies. We show that structures with traditional rib waveguides and no PC lattice (Fig. 1, left) can be a viable alternative to more complex PC-based structures (Fig. 1, right). For the operation wavelength $\lambda = 1.3\,\mu$m and $g = 0.1$, we obtain a 20-dB isolation bandwidth of 81 GHz. Finally, we report on the progress in fabrication of the proposed systems in BIG-GGG (gadolinium gallium garnet) heterostructures (Fig. 2).

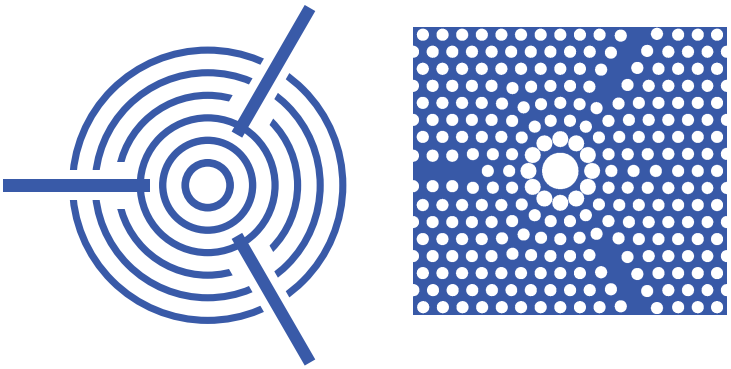

Figure 1: A rib-type and a PC-type circulator.

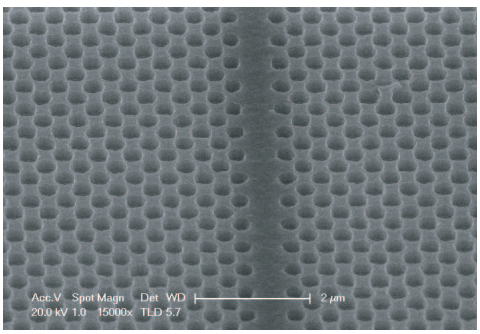

Figure 2: A PC waveguide etched in BIG-GGG.

REFERENCES

1. Wang, Z. and S. Fan, "Magneto-optical defects in two-dimensional photonic crystals," *Appl. Phys. B*, Vol. 81, 369–375, 2005.
2. Śmigaj, W., J. Romero-Vivas, B. Gralak, L. Magdenko, B. Dagens, and M. Vanwolleghem, "Magnetooptical circulator designed for operation in uniform external magnetic field," submitted to *Opt. Letters*, 2009.

Novel Design of 3D Metamaterial

Isaac Ehrenberg and B. I. Wu
Research Laboratory of Electronics, Massachusetts Institute of Technology
Cambridge, MA 02139, USA

Abstract— Recent studies have investigated the design of low profile antennas that rely on materials engineered to have specific electromagnetic properties, specifically artificial magnetic conductors (AMC). An AMC has the unnatural property of zero degree phase deflection of a reflected plane wave, which would enable antennas to achieve a higher gain without the quarter wave conducting backplane that would normally be required. Towards the goal of constructing an AMC, several designs have been studied including mushroom structures, Hilbert-Peano curves, Jerusalem Crosses and dipole or slot arrays. In this paper, we report on the investigation of an AMC that was constructed with a novel fabrication process, and utilized a new design based on the C ring structures normally used in the design of metamaterials. This design can be used to achieve AMCs of relatively low frequency, and can be assembly with relative ease over a very large area making it ideal for application with low profile low frequency antennae.

Subwavelength Imaging with a Dielectric Magnifier

Baile Zhang[1] **and George Barbastathis**[2]

[1]Singapore-MIT Alliance for Research and Technology (SMART) Centre, Singapore 117543, Singapore
[2]Department of Mechanical Engineering, Massachusetts Institute of Technology
Cambridge, MA 02139, USA

Abstract— Biological imaging at the molecular and cellular scale requires resolving of features in the order of 10's of nanometers. However, the fundamental diffraction limit discovered by Abbe in 1873 restricts the resolution of a conventional optical microscope to about half a wavelength (200 nm in air) due to the loss of high spatial frequency information carried in the evanescent waves. To break this diffraction limit, near field scanning imaging has been developed, but a generally slow scanning procedure in principle prevents users from observing dynamical processes which are of fundamental importance in many biological and medical studies. It is strongly desirable, therefore, to develop a real time imaging technique beyond the diffraction limit.

Aiming toward this goal, the recent metamaterial-based superlens and hyperlens have attracted a lot of interest. However, the original superlens did not provide any magnification. For the hyperlens with a cylindrical structure, the object to be imaged was required to have a curved surface or to be flexible so that it may conform to a curved surface. Moreover, the space-bandwidth product of the hyperlens is limited by the small curvature of the structure, meaning that the field of view is still not significantly enhanced over scanning techniques. Both the superlens and the hyperlens have three common practical limitations: material absorption, sensitivity to surface roughness, and narrowband operation.

We propose an approach for far-field sub-diffraction-limited optical imaging by using a dielectric magnifier with gradient refractive index. Different from previous superlens and hyperlens that form a real image with subwavelength features in front of the object, this magnifier creates a virtual subwavelength image that can be captured directly by a conventional microscope in the far field. Because the magnifier is made of isotropic dielectric materials, its fabrication will be greatly simplified. More importantly, this magnifier possesses a flat input plane and can provide broadband imaging with little influence from loss. We anticipate this will bring out more applications in future nanoscale imaging and lithography.

Session 2P7
Poster Session 6

Sensitivity Analysis of Pulse Broadening in Optical Fibres; A Stochastic Approach

F. Emami
Optoelectronic Research Centre
Electronic Department, Shiraz University of Technology, Shiraz, Iran

Abstract— The propagated pulses into the optical fibers are broadened and the amount of this broadening depends on the width and the shape of input pulses [1, 2]. Using a combination of the wave equations analysis and a stochastic treatment, the pulse broadening sensitivities are studied. The Gaussian shape pulses including dispersive effects up to the third order are considered. A measure of pulse width is considered as RMS width of the pulse in the form of: $\sigma^2 = \langle t^2 \rangle - \langle t \rangle^2$. Defining the *slowly varying amplitude* $A(z,t)$ of the pulse envelop, we can solve the nonlinear Schrodinger equation in Fourier domain, and find these first and second moments. Assuming the nonlinear effects is negligible, so the spectra of chirped pulses have some frequency dependent phase. The propagation constant of β depends on the frequency and the fiber length due to dispersion effects; this can be introduced a group delay in the pulse propagated through the fiber and therefore the pulse will be broadened. This is true for arbitrary pulse shape, width and chirp. Assume that the optical-pulse source generates nearly monochromatic pulses under CW operation and a stochastic treatment for input optical field. With the above conditions an expression for dispersion-induced broadening of Gaussian pulses can be derived in general case. This factor has some dependencies and sensitivities to the chirp, dispersion amount, dispersion slope, fiber length, wavelength, RMS width of input Gaussian pulse and the spectral width of

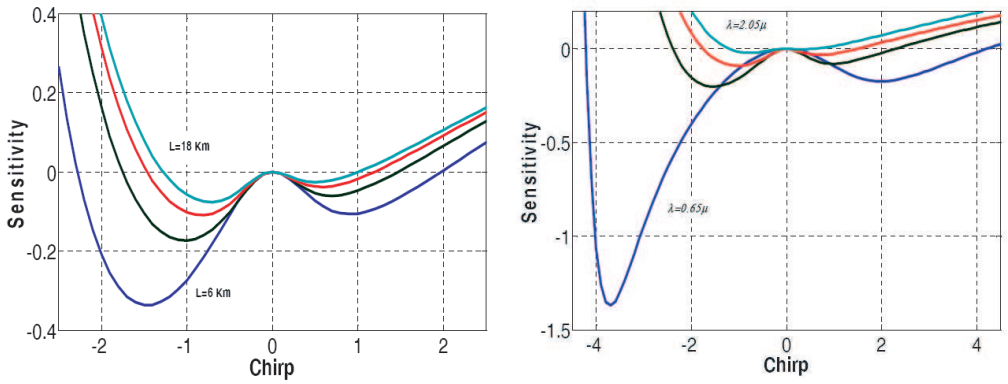

Figure 1: Broadening sensitivity versus the chirp factor for: (a) various fiber lengths and (b) different wavelengths.

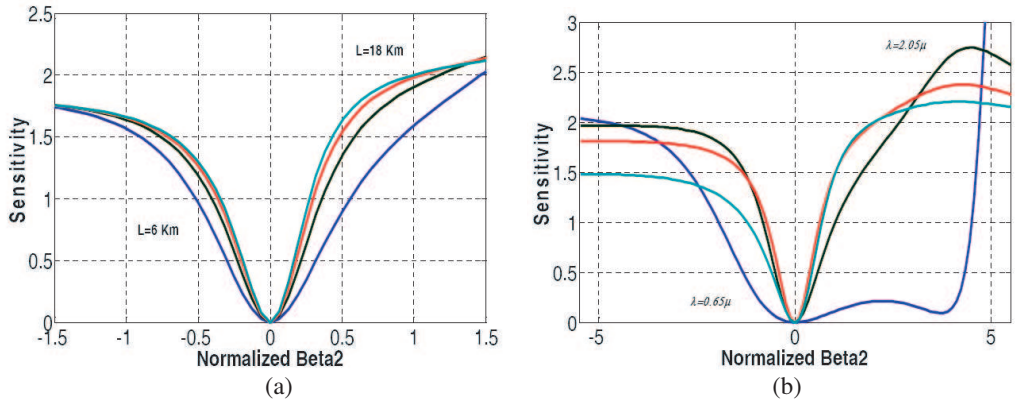

Figure 2: Broadening sensitivity versus the normalized β_2 factor for: (a) various fiber lengths and (b) different wavelengths.

the Gaussian source spectrum. For chirp-less pulses (zero chirp factor, $C = 0$) this sensitivity is zero and it is found that there is a negative chirp factor ($C < 0$) with such a specification (Fig. 1). Higher sensitivities are seen for longer fiber lengths and optical wavelengths with stronger dispersion (when the operating wavelengths are far from λ_{ZD}, see Fig. 2). In dominant dispersion slope regime ($\lambda \approx \lambda_{ZD}$), the broadening sensitivities increases for longer fiber lengths whereas increases for pulses up to 1550 nm and then decreases for higher wavelengths (Fig. 3). It is shown that for pulses with wider spectral widths (for example LEDs), there is a minimum for sensitivity which depends to the fiber length, used wavelength and RMS width of input Gaussian pulse. This minimum is equal to zero for short wavelengths ($\approx 0.65\,\mu$m) and is raised for longer fiber length.

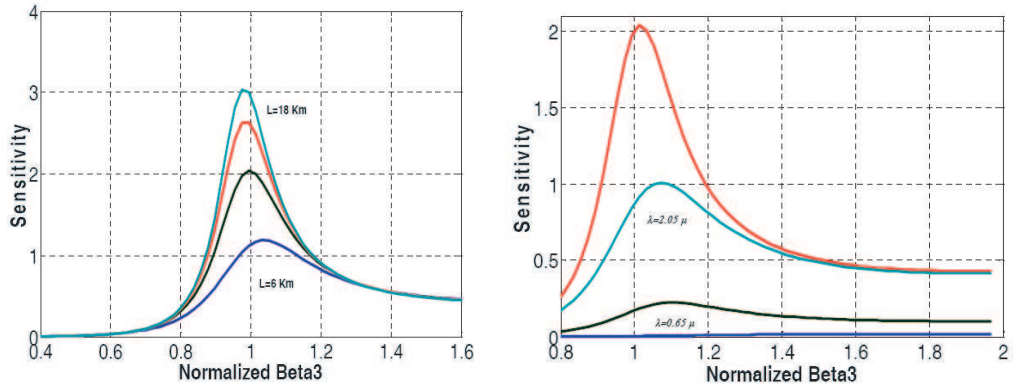

Figure 3: Broadening sensitivity versus the normalized β_3 factor for: (a) various fiber lengths and (b) different wavelengths.

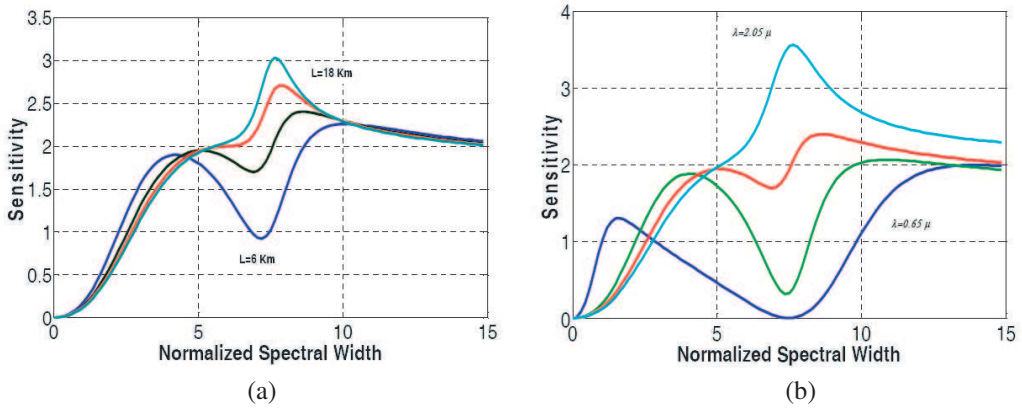

Figure 4: Broadening sensitivity versus the normalized spectral width for: (a) various fiber lengths and (b) different wavelengths.

Stress and Strain Sensing with Multimode POF Bragg Gratings

Yanhua Luo[1, 2], **Binbin Yan**[1], **Mo Li**[1], **Xiaolei Zhang**[1], **Qijin Zhang**[2], **and Gang-Ding Peng**[1]

[1]School of Electrical Engineering and Telecommunications, University of New South Wales
Sydney 2052, NSW, Australia
[2]CAS Key Laboratory of Soft Matter Chemistry, Key Laboratory of Optoelectronic Science and Technology
Department of Polymer Science and Engineering, University of Science and Technology of China
Hefei, Anhui 230026, China

Abstract— A longitudinal stress and strain sensor based on the multimode POF Bragg gratings was analyzed. Several fiber modes were propagating in this multimode fiber, but two fiber modes were chosen for the stress and strain sensing. Variations of the peak wavelengths for both modes were approximately linear, but eventual discrepancies may be attributed to a certain viscoelasticity of the fiber and measurement errors. The stress and strain coefficient was estimated to be about 5.3 nm/N and 11.8 nm/%, respectively. Furthermore, the effective strain-optic constant and the Young's modulus of POF were calculated to be about 0.248 and 3.367 GPa. All the results based on such multimode POF gratings sensor for the measurement of refractive index, strain, temperature, etc.

Novel Composite Non Reciprocal Right/Left-handed Line Made from Ferrite Material

F. Boukchiche[1], **T. Zhou**[2], **M. L. Berre**[2], **D. Vincent**[1], **B. Payet-Gervy**[1], **and F. Calmon**[2]

[1]Laboratoire DIOM, Saint-Etienne University, France
[2]INL-UMR5270, CNRS, INSA de Lyon, France

Abstract— Non reciprocal segments of line are using to connect series capacitors and shunt inductors in order to perform a right/left-handed planar medium. The artificial medium behavior is fixed by the value of L-C components and the transmission line characteristics. The effect of non reciprocal segments of line are studied. From the derivation of the dispersion relation, new behaviors may be expected and are observed for several applied magnetic D.C. values. The concept can be extended to active non reciprocal network.

A New Profile for Metal Post Circular Waveguide Polarizer

S. H. Mohseni Armaki, F. H. Kashani, and M. Fallah
Department of Electrical Engineering, Iran University of Science and Technology (IUST), Iran

Abstract— This paper presents a new profile for depth of metal posts in circular wave guide polarizer. Simple designs of metal posts depth arrangement are predefined by tangential profile. Finally exact depths of metal posts are tuned by HFSS. Measurement and simulation result have a good agreement in 18% bandwidth.

In circularly polarized antenna feed systems, polarizer are used to convert linearly polarized signals provided at the first interface port (circular waveguide) into circularly polarized signals supplied to the second interface port (antenna). Typical examples of polarizer are a circular waveguide polarizer with metallic posts, a corrugated waveguide polarizer and a dielectric slab waveguide polarizer [1–3].

A circularly polarized wave is represented by the superposition of two orthogonal linearly polarized weaves that posses identical magnitude and a phase difference of $\pm\pi/2$. In conventional polarizer such as metal post (pin) polarizes apart from good matching properties at each port, there are two basic demands on the design of these polarizer type. Firstly, the signals of the linearly polarized modes must be exactly divided (combined) into orthogonal components with identical magnitude. Secondly a differential phase shift of $\pm\pi/2$ between these semi signals has to be accomplished.

Thus, the complete polarizer can be regarded a combination of a power divider and two independent phase shifter. Both tasks must be realized simultaneously by differential phase shifting region that exhibit a physical alignment of 45 deg with regard to the incident linearly polarized mode supplied to import (TE11).

For designing this type of polarizer, we can use equivalent circuit, and then it is reached to desired result by empirical tuning depth of posts [4]. The depth of posts gradually increased from the beginning to the middle of circular waveguide. So far there isn't presented equation for optimum profile of posts depth. In this paper while presenting optimum profile, performance of polarizer is simulated and tested.

REFERENCES

1. Kitsuregawa, T., *Advanced Technology in Satellite Communication Antenna: Electrical and Mechanical Design*, Artech House, 1990.
2. Uher, J., J. Bornemann, and U. Rosenberg, *Waveguide Components for Antenna Feed Systems: Theory and CAD*, Artech House, 1993.
3. Unger, H. J., "Polarization wandler in hohlleitern," Frequentz, Band 16, 117–120, April 1962.
4. Marcuvitz, N., *Waveguide Handbook*, McGraw Hill, New York, 1951.
5. Arndt, F., W. Tucholke, and T. Wriedt, "Design of a wideband compact square waveguide polarizer," *Elecronics Letters*, Vol. 21, No. 12, 74–75, June 1985.

A Parallel Adaptively Modified Characteristic Basis Function Method for Analyzing Electromagnetic Scattering Problems

Fei Dai, **Zichang Liang**, **and Hui Yue**
The State Key-Lab for Electromagnetic Characters of Environment
The 802 Research Institute of Shanghai Academy of Spaceflight Technology, Shanghai 200438, China

Abstract— ElectroMagnetic (EM) scattering analysis, particularly the Radar Cross Section (RCS) evaluations, is a tremendous computational task. For engineering applications, there are a lot of problems with very large number of unknowns to be solved. However, the present computer technology can not provide sufficient memory size to store all of the data in the process of the computation. What is worse, the computational speed is not acceptable. It is not rare to spend several days to gain a solution of a complex target. In order to increase the computational efficiency and overcome the limitation of the computer capacity at the same precision, parallel algorithm has been introduced by many researchers. Characteristic Basis Function Method (CBFM) is a novel approach for analyzing the ElectroMagnetic (EM) scattering from electrically large objects. Based on dividing the studied object into small blocks, the CBFM is suitable for parallel computing. In this paper, a static load balance parallel method is presented by combining Message Passing Interface(MPI) with Adaptively Modified CBFM(AMCBFM). In this method, the object geometry is partitioned into distinct blocks, and the serial number of blocks is sent to related nodes according to a certain rule. Every node only needs to calculate the information on local blocks. A series of numerical results and computing performance are discussed, which show that the combination of parallel computing technology and AMCBFM is a promising solution for analyzing large-scale problems in electromagnetic field, and confirm the accuracy and efficiency of the proposed method in speeding up solving large electrical scale problems.

Unwanted Modes Caused by Asymmetrical Structures in BIT Line Resonator at Millimeter-wave Frequencies

Futoshi Kuroki, Hiroyuki Kawagashira, and Ryo-Ji Tamaru
Department of Electrical Engineering, Kure National College of Technology
2-2-11 Aga-Minami, Kure, Hiroshima 737-8506, Japan

Abstract— It was exhibited that low loss and cost-effective medium at millimeter-wave frequencies is the bi-laterally metal-loaded tri-plate transmission line (BIT line), which consists of two center conductors etched on both surfaces of a dielectric substrate inserted in the horizontal mid-plane of a below cutoff parallel metal plate waveguide. By biasing an equi-voltage to both center conductors, that is, by exciting an even TEM mode, the electric field distribution between two center conductors is reduced. The current on the under surface of the center conductor results in decreasing, and thus the transmission loss can be relatively unaffected by the roughness of the copper foils and by loss tangent of the dielectric substrate.

It may however face difficulties such as generation of unwanted modes due to happening to make asymmetrical structures in manufacturing process. For example, the dielectric-supported center conductors may be displaced for the horizontal mid-plane, the dielectric substrate being fixed by spacers with slightly-different dimensions, or a width of one of two center conductors may be unintentionally trimmed by actual etching. To evaluate increasing dissipation loss due to such asymmetrical structures, degradation of Q factors was calculated and measured using a BIT line resonator.

At first, the dielectric substrate was selected as a glass-fiber PTFE having a relative dielectric constant of 3, a loss tangent of 0.0028, and a thickness of 0.164 mm. The length of the resonator was set at 3.6 mm. In this structure, the resonant frequency and the unloaded Q factor were calculated by a commercially available simulator (HFSS). From these results, it can be seen that a radiating TEM wave generates together with the non-radiating TEM wave as an operating resonance when displacing the dielectric substrate. The unloaded Q factor was calculated at 390 for the non-radiating TEM wave. The degradation rate of the non-radiating TEM wave was less than 20% even if the displacement was set at 0.4 mm. Actually the displacement is usually less than 0.1 mm in manufacture process of the spacer to support the dielectric substrate, and thus there is no influence of such asymmetry.

Next consideration is concerned with generation of unwanted radiating TEM wave because the unwanted radiating TEM wave as well as degradation of unloaded Q factors is a severe problem. To evaluate this issue, scattering parameters of a BIT line bandpass filter, the dielectric substrate being displaced by 0.1 mm, were calculated. It was seen that a spurious response occurred due to causing a resonance of the radiating TEM wave in the housing. To suppress such influence, via-holes were installed at both edges of the resonators. As the result, good suppression of such unwanted spurious was performed.

Connection between Microstrip Circuits in Transmitter and Receiver of VSAT System

Futoshi Kuroki and Kosei Nishimura
Department of Electrical Engineering, Kure National College of Technology
2-2-11 Aga-Minami, Kure, Hiroshima 737-8506, Japan

Abstract— The VSAT (Very Small Aperture Terminal) system is one of the satellite-ground communication links and is applied to disaster prevention in public administration in Japan. The circuit configuration consists of heavy-sized transmitter and receiver because of high power handling.

To employ such VSAT system to commercially-available applications, downsizing and feeding power saving are indispensable technologies, and a new circuit structure of microstrip circuits, which were installed so as to be faced each other on inner surfaces in a parallel metal plate housing, was proposed where amplifier chips were bonded in one side of the microstrip circuit while phase shifters feeding a microstrip array antenna were embedded in another side.

To miniaturize the circuit configuration, a technique to connect such microstrip circuits was devised in this paper. This connector consists of a coaxial cable vertically-connected between micro-strip lines. At first, small windows on the ground conductor of the coaxial cable were installed not to short-circuit between the microstrip lines and the ground conductor. And moreover, a circular stub circuit with a sectorial slot was installed in the ground conductor to prevent unwanted radiation. Based on the numerical calculation, the performance of the connector was optimized as functions of the radius and opening angle of the sectorial slot in a bandwidth from 12 GHz to 15 GHz for the up and down links of the VSAT system.

Applying a simple matching element, small transmission loss of less than 1 dB as well as high return loss of larger than 20 dB was obtained in a bandwidth from 12 GHz to 15 GHz. The performance calculated in this paper can be satisfactory for the VSAT use, and thus the validity of the proposed connector is successfully confirmed.

Numerical Analysis of Q-factors in Millimeter-wave Oscillators

Futoshi Kuroki[1], **Shimpei Takeda**[1], **and Takashi Ohira**[2]

[1]Department of Electrical Engineering, Kure National College of Technology
2-2-11 Aga-Minami Kure 737-8506, Hiroshima, Japan
[2]Department of Information and Computer Sciences, Toyohashi University of Technology
1-1 Hibarigaoka, Tempaku, Toyohashi 441-8580, Aichi, Japan

Abstract— It is well known that Q-factors in oscillator circuits were given by the input impedances of the oscillator circuits and their frequency-derivations as

$$Q = \frac{\omega_0}{2}\left|\frac{Z_{in}(\omega_0)'}{Z_{in}(\omega_0)}\right|, \tag{1}$$

where ω_0, Z_{in} and the prime correspond to an oscillation angular frequency, an input impedance of the oscillation circuit and an angular frequency-derivation.

Actually this theory was applied to calculation of Q-factors of the NRD guide Gunn oscillators and its usefulness was confirmed. The numerical calculation accuracy may be however degraded when the impedance locus for frequencies drastically shifted. For the purpose of improving the numerical calculation accuracy of the Q-factor, the reflection coefficient having values from -1 to 1 was focus on in calculation procedure in this paper.

First, the Q-factor formulae based on the admittance; Y_{in} and the reflection coefficient; Γ were derived as

$$Q = \frac{\omega_0}{2}\left|\frac{Y_{in}(\omega_0)'}{Y_{in}(\omega_0)}\right|, \tag{2}$$

$$Q = \omega_0\left|\frac{\Gamma(\omega_0)'}{1-\Gamma(\omega_0)}\right|. \tag{3}$$

And their advantages were evaluated from the viewpoint of the convergence of the Q factor versus increment of the frequency in frequency-derivation by using examples of series and shunt resonant circuits. As the results, it was confirmed that the Q-factor formula based on the reflection coefficient had a good convergence performance for the increment in numerically-frequency derivation procedure.

As an actual example, this consideration was applied to the band-stop type of self-injection locked NRD guide Gunn oscillation, consisting of a free-running NRD guide Gunn oscillator coupled with a disk type ceramic resonator with an unloaded Q-factor of 4000 at 60 GHz. Because a part of the oscillation power returns back to the Gunn diode by the ceramic resonator, the oscillation frequency can be fixed by the resonant frequency of the ceramic resonator. From the numerical result, it was obvious that the Q-factor calculated by the reflection coefficient formula had good convergence in this oscillation configuration.

Generation of Ultrashort Pulses at 850 nm in a Newly Designed Photonic Crystal Fiber

K. Senthilnathan[1], **R. Vasantha Jayakantha Raja**[2], **K. Porsezian**[2], **Samuel Olupitan**[3], **and K. Nakkeeran**[3]

[1]Department of Physics, National Institute of Technology, Rourkela 769 008, India
[2]Department of Physics, Pondicherry University, Kalapet, Pondicherry 605 014, India
[3]School of Engineering, Fraser Noble Building, University of Aberdeen, Aberdeen AB24 3UE, UK

Abstract— We consider the pulse propagation in a photonic crystal fiber (PCF), whose central core is filled with chloroform, wherein the pulse propagation is governed by the dispersion and nonlinearity varying nonlinear Schrödinger (NLS) equation. By using appropriate self-similar scaling analysis, we delineate the generation of linearly chirped soliton like pulse in PCF. The analytical results demand that the effective dispersion must decrease while the nonlinearity must increase exponentially in the PCF. Thus, based on the analytical results, we propose the new designing of PCF to achieve the chirp and pedestal free ultrashort pulses at 850 nm though the pulse compression technique. To clearly explain the different stages of pulse compression process in the newly designed PCF structure, we adopt the projection operator method to derive the pulse parameter equations which indeed very clearly describe the self-similar pulse compression process at different parts of the PCF structures. In addition, we also compare the pulse parameters of chloroform filled PCF with that of standard silica PCF using projection operator method. The analytical results exactly match with the results obtained by the projection operator method. Further, we also adopt the split-step Fourier algorithm to investigate the pulse compression process in PCF and we find that the results obtained from direct numerical experiments also exactly match with those of analytical and semi-analytical results. The main advantages of the proposed chloroform filled PCF pulse compressor based on self-similar analysis are that the compression factor can be enhanced enormously and the resulting the compressed pulse is almost free from chirp and pedestal. Also, this newly proposed chloroform filled PCF exhibits low dispersion length for efficient pulse compression with low input pulse energy and low loss over small distances.

Photonic Band Gaps in Quasiperiodic Nanostructures

U. L. Fulco[1] **and E. L. Albuquerque**[1, 2]

[1]Departamento de Biofísica, UFRN, 59072-970, Natal-RN, Brazil
[2]Departamento de Fisíca, UFRN, 59072-970, Natal-RN, Brazil

Abstract— We intend in this work to show the polaritonic band gap spectra [1], which arises from the propagation of a plasmon-polariton excitation in quasiperiodic multilayer structures, forming a photonic crystal [2]. These multilayer structures are made from alternating layers of both positive (medium A: SiO_2-silica) and negative refractive index materials (medium B: metamaterials) following a Fibonacci pattern, using a theoretical model based on a transfer matrix treatment.

The plasmon-polariton dispersion relation is obtained by solving the electromagnetic wave equation for p-polarized electromagnetic mode, within the layers A and B of its nth unit cell, yielding $\cos(QL) = (1/2)Tr(T)$, where $Tr(T)$ means the trace of the transfer matrix T, which relates the electromagnetic field amplitudes of a layer in cell n to the equivalent one in cell $n-1$ [2]. The pass bands are then obtained when the absolute value of the right-hand side of the above equation is less than one, which means a real z-component k_z of the wavevector. On the other hand, when it is bigger than one, we have a stop band. However, some complex value of k_z can still make the left-hand side of the above equation smaller than one, and these complex solutions may have physical significance. This can be seen considering the dispersion curves corresponding to a fixed common dimensionless in-plane wavevector $k_xL/2\pi$, and a ratio d_B/d_A, where k_x is the in-plane wavevector, $L = d_A + d_B$ is the size of the unit cell of this structure, and $d_A(d_B)$ is the thickness of layer A (B). These dispersion curves are defined in the region where the average index of refraction of the superlattice vanishes, the so-called zero-$<\eta>$ photonic region [3], where $<\eta>=(\eta_A d_A+\eta B d_B)/L = 0$, with $\eta_A = -3.53$ being the refraction index for the metamaterial, and $\eta_B = 2.19$ the refraction index for SiO_2, respectively. Here the edges of the bulk bands are not characterized by the Floquet-Bloch condition, $QL = 0$ and $QL = \pi$. Also, for small values of k_xd_A the transmission through the superlattice is zero, except in certain transmission bands and for some values of $QL < \pi$. The discrete frequencies are then determinate by the Fabry-Perot resonance condition $k_{zA} = m\pi$ ($m = \pm1, \pm2, \pm3, \ldots$), where the waves reflected at consecutive interfaces arrive out of phase at the input facet of the superlattice.

The continuous bulk bands are characterized by the reduced Brillouin zone, $0 < QL < \Xi$, with Ξ being the values where the slope goes to minus infinity. The $<\eta>= 0$ band structure can be better seen in the projected band profile, where the consecutive pass bands are united to constitute a very large fragmented band, where we can observe discrete and continuous bulk modes.

The most important experimental techniques to probe these spectra are the Raman light scattering and attenuated total reflection (ATR). In the case of Raman scattering, one uses a grating spectrometer to detect and analyze the scattered light. The typical shift of the frequency of the scattered light is in the range 0.6–500 meV, which makes this technique very appropriate for probing the plasmon-polariton spectra.

REFERENCES

1. Albuquerque, E. L. and M. G. Cottam, *Polaritons in Periodic and Quasiperiodic Structures*, Elsevier, Amsterdam, 2004.
2. Johnson, S. and J. D. Joannopoulos, *Photonic Crystals: The Road from Theory to Practice*, Kluwer, Boston, 2002.
3. De Medeiros, F. F., E. L. Albuquerque, and M. S. Vasconcelos, *J. Phys.: Condens. Matter*, Vol. 18, 8737, 2006.

Transmission Spectra in a Multilayer Photonic Structure

P. W. Mauriz[1] and E. L. Albuquerque[2]

[1]Departamento de Física, IFMA, São Luís-MA 65.025-001, Brazil
[2]Departamento de Física, UFRN, Natal-RN 59072-970, Brazil

Abstract— Materials simultaneously possessing negative magnetic permeability and electric permittivity are physically permissible and would exhibit a negative refractive index [1]. They were coined as left-handed materials (LHM) because they support backward waves, for which the electric field **E**, the magnetic field **H**, and the Poynting vector **S** form a left-handed triplet. Besides, the group velocity of wave propagation in such media is opposite to its phase velocity, making the perfect lens possible.

Periodic multilayered structures containing negative refractive index materials can be considered as a sequence of perfect lenses with unique transmittance or reflectance properties in the Bragg regime [2]. More recently, it has been shown that a one-dimensional periodic stack of layers with alternating dielectric and negative refractive index material, with zero averaged refractive index, displays a narrow spectral gap in the transmission, which is quite different from a Bragg reflection gap [2]. On the other hand, the discovery of quasiperiodic structures has fired up a new field of condensed-matter physics, giving rise to many practical applications [3].

It is the aim of this work to investigate the transmission spectra of a light beam normally incident from a transparent medium into a multilayer photonic structure composed of SiO_2/metamaterial layers arranged in a quasiperiodical fashion, which follows the Fibonacci (FB) substitutional sequences. Although several theoretical techniques have been used to study the transmission spectra in these structures, in the present work we make use of the transfer matrix approach

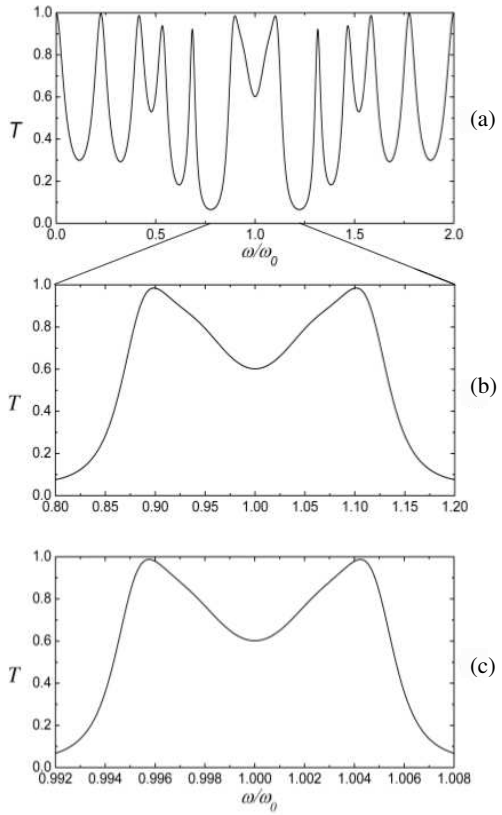

Figure 1: Normal-incidence transmission spectra of light beam into a quasiperiodic FB multilayered photonic structure: (a) the transmittance T as a function of the reduced frequency $\Omega = \omega/\omega_0$ for the 9th generation of the FB sequence; (b) same as in (a), but for the reduced range of frequency $0.8 < \Omega < 1.2$; (c) same as in (b), but for the 15th generation of the FB sequence.

to analyze them, simplifying the algebra which would otherwise be quite involved (for a review, see [3]).

The optical transmission spectrum for the 9th-generation (55-layer) quasiperiodic FB sequence, as a function of the reduced frequency $\Omega = \omega/\omega_0$, ω_0 being the midgap frequency, is depicted in Fig. 1(a). The transmission spectrum presents a unique mirror symmetrical profile around the midgap frequency $\Omega = 1$ (which is the midgap frequency of a periodic quarter-wavelength multilayer). Besides the structure is transparent at the reduced frequencies $\Omega = 0.898$ and $\Omega = 1.101$, as we can see in Fig. 1(b), forming two broad peaks, also distributed symmetrically around $\Omega = 1$.

Furthermore, the transmission spectrum has a scaling property with respect to the generation number of the FB sequence, within a symmetrical interval around $\Omega = 1$. To understand this scaling property, consider Fig. 1(b), which shows the optical transmission spectrum of Fig. 1(a) for the range $0.80 < \Omega < 1.20$. This spectrum is the same, as shown in Fig. 1(c), to the one representing the 15th-generation quasiperiodic FB sequence (i.e., it has been recovered after six Fibonacci generations), for the range of frequency reduced by a scale factor approximately equal to 25.

ACKNOWLEDGMENT

The authors want to acknowledge the Brazilian Research Agencies CNPq and FAPERN.

REFERENCES

1. Veselago, V. G., *Sov. Phys. Usp.*, Vol. 10, 509, 1968.
2. Ramakrishna, S. A., *Rep. Prog. Phys.*, Vol. 68, 449, 2005.
3. Albuquerque, E. L. and M. G. Cottam, *Phys. Rep.*, Vol. 376, 225, 2003.

Wireless Mass Sensor System with Four Mixers Structure Based on FBAR

Wei-Wei Cheng[1], **Shi-Sheng Jin**[2], **Shu-Rong Dong**[1], **and Yan Han**[1]

[1]Institute of Microelectronics and Optoelectronics, Zhejiang University, Hangzhou, Zhejiang 310027, China
[2]Guizhou Meteorological Information Center, Guiyang, Guizhou 550002, China

Abstract— A new-type wireless mass sensor system with four mixers structure based on FBAR is designed, fabricated and tested, which includes dual-path and a receiver to test the sensor circuit. The mixing-mode makes the result of measurement more accurate than the one which is based on dividing-mode. The result of measurement of mixing-mode depends on the accuracy and stability of the oscillators in mixers. In fact, this measured frequency is the real oscillating frequency which represents the practical change of mass on the FBAR sensor. And this wireless mass sensor system with four mixers structure is programmable of two working modes which are automatic frequency tracking and customizing frequency tracking for application.

Design and Simulation of Low Noise Amplifier for Radio Frequency Front End of Wireless Communication

Shi-Sheng Jin[1], **Wei-Wei Cheng**[2], **Shu Rong Dong**[2], **Yan Han**[2], **Shun Yuan**[1], **Jun-Yong Wang**[1], **and Jue Li**[1]

[1]Guizhou Meteorological Information Center, Guiyang, Guizhou 550002, China
[2]Institute of Microelectronics and Optoelectronics, Zhejiang University, Hangzhou, Zhejiang 310027, China

Abstract— This paper presents the design of 2 GHz front end low noise amplifier application. The progress of the 3G wireless communication has the demand for the development of low cost, low power and small size transceiver by using microstrip technology. Design and simulation of low noise amplifier circuits are presented. It is focusing on development of low noise amplifier operating at 2000 MHz for the third generation wireless communication application. The amplifier design comprised AT-41411 and lumped elements to implement the matching networks. Hewlett-Packard's AT-41411 is a general purpose NPN bipolar transistor that offers excellent high frequency performance. The target simulation are gain (S-21) > 10 dB, noise figure as low as possible (given the bias conditions) with < 10 dB, and input and output return loss < -10 dB at 2000 MHz.

Session 3A1
Stochastic versus Deterministic Geophysical Inversions

Large-scale 3D Iterative Migration of Marine Controlled-source Electromagnetic Data with Focusing Regularization

Michael S. Zhdanov, Martin Čuma, and Glenn Wilson
TechnoImaging and University of Utah, Salt Lake City, Utah, USA

Abstract— Given the limitations of 1D and 2.5D inversion methods for defining 3D structures related to direct hydrocarbon indication, the 3D interpretation of marine controlled-source electromagnetic (MCSEM) data still poses a very challenging problem. Such quantitative interpretations are complicated by the fact that the EM response of a hydrocarbon-bearing reservoir is very small in comparison to the total EM fields. Hence, it becomes important to constrain interpretations with a suite of a priori models constructed from all available seismic and resistivity log data, and geological prejudice. This is especially critical if the target consists of potentially stacked reservoir units. One must use efficient numerical methods to run multiple scenarios based on the suite of a priori models, different data combinations, and various other parameters so as to build confidence in the robustness of features in the model and to discriminate any artifacts that may arise from the interpretation of a single deterministic result. To that end, we present our implementation of rigorous inversion using an iterative migration algorithm based on the 3D integral equation method with inhomogeneous background conductivity, and focusing regularization with a priori terms. The use of focusing stabilizers makes it possible to recover subsurface models with sharper geoelectric contrasts than can be obtained using traditional smooth stabilizers. The method is implemented in a fully parallelized code which makes it practical to run large-scale 3D iterative migration within a day on multi-line MCSEM surveys for models with millions of cells. We demonstrate our workflow with the interpretation of a synthetic MCSEM survey computed from a very detailed model of the stacked anticlinal structures and reservoir units of the Shtokman gas field in the Russian Barents Sea.

Efficient Nonlinear Inverse Solution Uncertainty Estimation via Covariance-free Model Reduction and Sparse Posterior Sampling

Michael J. Tompkins[1] **and Juan Fernandez-Martinez**[2]

[1]Schlumberger-EMI Technology Center, 1301 South 46th Street, Bldg. 300, Richmond, CA 94804, USA
[2]Department of Civil and Environmental Engineering, University of California Berkeley
Berkeley, CA 94804, USA

Abstract— Among the most important aspects of geophysical data interpretation is the estimation and computation of inverse solution uncertainties. We present a general uncertainty estimation method that allows for the comprehensive search of model posterior space while maintaining computational efficiencies similar to deterministic inverse solutions. Integral to this method is the combination of an efficient parameter reduction technique, like Principal Component Analysis, a parameter bounds mapping routine, a sparse geometric sampling scheme, and a forward solver. Parameter reduction, based on either prior model covariances or training images, is required to produce both a reduced and orthogonal model space. Parameter constraints can then mapped to this reduced space, using a linear programming scheme, defining a bounded posterior polytope. Sparse deterministic grids are employed to sample this feasible model region, while forward evaluations determine which model samples are equi-probable. The resulting ensemble represents the equivalent model space, consistent with Principal Components, which can be used to estimate inverse solution uncertainty. Importantly, the number of forward evaluations is determined adaptively and minimized by finding the sparsest sampling set required to produce convergent uncertainty measures. We demonstrate, with surface electromagnetic examples, that this method has the potential to reduce the nonlinear inverse uncertainty problem to a deterministic sampling problem in only a few dimensions, requiring limited forward solves, and resulting in an optimally sparse representation of the posterior model space. Depending on the choice of parameter constraints, the method can be exploitative, searching around a given solution, or explorative, when a global search is desired.

Geophysical Inversion for Non-smooth Models

Randall Mackie[1] **and William Rodi**[2]

[1]Western Geco, USA
[2]Massachusetts Institute of Technology, USA

Abstract— The standard approach to geophysical inverse problems is to find nonlinear least squares solutions subject to smoothness constraints (regularized solutions). For example, it is common to minimize the L_2 norm of model roughness as defined by the integral of the squared laplacian (or squared gradient) of the model over the model volume. This results in a quadratic regularization function that fits easily into the framework of gradient-based minimization methods such as Gauss-Newton iteration. Smooth model inversion has found widespread use in geophysics because it is easily implemented, robust, and produces useful results. However, there are situations where it is desirable to find less smooth models. It is well known that L_1 norms are less sensitive to outliers and therefore minimizing an L_1 norm of model roughness would result in more sharply defined features, such as interfaces. However, L_1 norm minimization does not easily fit within the framework of gradient based methods. Therefore, it is common to use weighted L_2 norms that approximate an L_1 norm.

In this talk, we will establish a common framework that will allow us to study the properties of various non quadratic regularization functions. Furthermore, we will explore techniques for solving the minimization problem using weighted norms in an iterative regularized least squares solution (IRLS) and directly minimizing a nonlinear and non-quadratic function using the method of nonlinear conjugate gradients. We will demonstrate the effectiveness of various regularizers and minimization methods in electromagnetic inversion.

Geophysical Inversion with Geostatistical Regularization

W. Rodi[1] and R. Mackie[2]

[1]Massachusetts Institute of Technology, USA
[2]Western Geco, USA

Abstract— Stochastic inversion theory provides a rigorous framework for finding optimal models of Earth structure from geophysical data together with a measure of model uncertainty in the form of a posterior covariance operator on the model space. Longstanding problems for geophysicists have been (1) to find a plausible rationale for choosing the prior covariance operator required to apply stochastic inversion theory, and (2) to physically interpret the posterior covariance in high dimensional inverse problems, such as ones involving 2-D and 3-D Earth models.

Geostatistical concepts, which play a prominent role in the kriging method for data interpolation, help address these problems by relating the prior model covariance operator to physical quantities: the model variance as each point in the Earth, and correlation lengths that determine how the covariance of the model between two points depends on their separation distance and orientation. These parameters, which can vary with position, capture the Backus-Gilbert notion of expressing model uncertainty in terms of variance and spatial resolution. In the kriging method, variogram analysis is used to fit the prior model variance and correlation lengths to second-order statistics of the observed data, providing a principled means of choosing these parameters. The estimation and nunerical techniques used in kriging, however, are not particularly well-suited to geoelectromagnetic and other Earth structure inverse problems.

In this talk, we show how a geostatistical approach can be implemented as a standard regularized inversion involving the joint minimization of data misfit and a stabilizing function. The latter is defined by a differential operator whose Green's function is a prior covariance operator parameterized with given geostatistical parameters. We then consider the problem of fitting the geostatistical parameters to data, which is considerably more difficult in Earth structure inversion than in interpolation. The problem of interpreting posterior covariances in geostatistical terms is another difficult problem we discuss. Examples from seismic travel-time tomography will be used to illustrate the geostatistical approach to regularization and uncertainty, and we will show our progress to date in implementing the approach in 2-D and 3-D magnetotelluric inversion.

Using Sequential Inversion Schemes with Increasing Complexity to Tackle the Controlled-source Electromagnetic Imaging Challenge

Juergen J. Zach
EMGS ASA, Norway

Abstract— The Marine Controlled-Source Electromagnetic (CSEM) method has evolved into a standard geophysical tool to map complex 3D-resistivity distributions for hydrocarbon exploration. This has been enabled through advances in operations, acquisition hardware and inversion techniques.

The numerical complexity of the 3D-EM inverse problem is determined by the physical resolution as a function of the source spectrum, and is on the order of 10^6 grid cells or greater. Industrially applied 3D EM-inversions at present employ an iterative gradient-based deterministic algorithm. To avoid non-uniqueness, these rely on finding a geological background model sufficiently close to most of the real geology apart of the anomalies which are the exploration targets.

From hundreds of commercial surveys, it has been our experience that building a reliable background model should be aided by numerically less complex, more robust inversions of CSEM data before using 3D-inversion. This is particularly true if well control is not given in the immediate area. The toolkit employed to build starting models includes both deterministic and stochastic approaches, including Gauss-Newton based 2.5D-inversion and stitched 1D-inversions based on simulated annealing.

Using a recent 3D-data example from the Gulf of Mexico, we demonstrate a workflow to build various alternative starting models, followed by a full pixel-based 3D-inversion based on an inversion methodology with approximate Hessian-based optimization and a fast finite-difference time-domain forward operator. While stand-alone interpretation of CSEM inversion results without seismic data or wells is rarely possible, results are remarkably stable with respect to different starting models.

Stochastic Joint Inversion of 2D Seismic and Seismoelectric Signals

André Revil
Colorado School of Mines, Golden CO 80401, USA

Abstract— The interpretation of seimoelectrical signals is a difficult task because both co-seismic and seismoelectric converted signals are simultaneously recorded and the seismoelectric conversions are typically several orders of magnitude smaller than the co-seismic electrical signals. The seimic and seismoelectric signals are modeled using a finite element code with perfect matched layer boundary conditions assuming a linear poroelastic body. We present a stochastic joint inversion of the seismic and seismoelectrical data based on the adaptive Metropolis algorithm, in order to obtain the posterior probability density functions of the material properties of each geological unit. This includes the permeability, the porosity, the electrical conductivity, the bulk modulus of the dry porous frame, the bulk modulus of the fluid, the bulk modulus of the solid phase, and the shear modulus of the formations. A test of this approach is performed with a synthetic model comprising two horizontal layers and a reservoir partially saturated with oil, which is embedded in the second layer. The result of the joint inversion shows that we can invert the permeability of the reservoir and its mechanical properties.

Frequentist and Bayesian Experimental Design

E. Haber[1] and L. Horesh[2]

[1]UBC, Canada
[2]IBM TJ Watson Research Center, USA

Abstract— In this talk, we discuss experimental design issues in electromagnetic inverse problems. Design is typically optimized to reduce the overall risk in the recovered inverse problem. We discuss both frequentist and Bayesian approaches to risk minimization. We show that the different formulation lead to different designs. We give interpretation to each of the designs and discuss the pros and cons of each approach.

A Hybrid Stochastic-deterministic Approach for Producing Statistically Accurate Inverse Solutions and Corresponding Uncertainty

Timothy C. Johnson and Roelof J. Versteeg
Idaho National Laboratory, USA

Abstract— Optimization strategies within the geosciences often follow either the deterministic or the stochastic inversion philosophy. Deterministic approaches typically seek to estimate a single distribution of subsurface properties with minimum structure, subject to minimizing the misfit between simulated and observed data. In comparison to stochastic approaches, deterministic approaches are relatively efficient, but are not well suited for estimating the uncertainty associated with the solution, and generally do not reproduce the spatial variability expected in reality. Stochastic methods are well-suited for both reproducing spatial variability and estimating model uncertainty, but posterior sampling methods are computationally expensive and inefficient in terms sampling models which honor the observed data within the limits of data noise. We present a hybrid inversion approach which addresses the limitations of deterministic and stochastic inversion stated above. We use a gradient-based inversion algorithm to generate models which 1) honor the observed data to the appropriate degree given the data noise, and 2) honor the estimated subsurface spatial covariance structure. Therefore, the solution space is non-unique and contains models which both fit the data and honor the spatial covariance structure within the limits of data noise and semivariogram uncertainty. By sampling from this space we generate a suite of solutions which may be used to estimate measures of uncertainty through ensemble statistical analysis. We present synthetic and field applications to demonstrate the approach using electrical resistivity tomography, but the approach is generally applicable to any subsurface with spatial statistics that can be described by one or more semivariograms.

Session 3A2
Radar Target Detection

Analytical and Numerical Studies of Sea Surface Doppler

Guangdong Pan[1] and Joel T. Johnson[2]

[1]Schlumberger-Doll Research, Cambridge, MA 02139, USA
[2]ElectroScience Laboratory, The Ohio State University, Columbus, OH 43212, USA

Abstract— The ocean Doppler spectrum measured by a radar system is an important ocean surface observed parameter. It is well known that the Doppler shift is related to the radar range cell mean horizontal velocity (or mean drift), and the Doppler spectrum bandwidth is related to the horizontal velocity spread within the radar cell. Therefore, the Doppler information (shift and bandwidth) can provide surface wave information.

Many Doppler measurements are conducted at low-grazing-angles where the horizontal orbital velocity is an important effect. Numerical studies of Doppler spectra from theoretical electromagnetic scattering models have been performed successfully, for example, based on the two-scale model [1], or based on exact integral equation methods [2–4]. The nonlinear hydrodynamic models are applied in some studies. These studies show that the nonlinearity further broadens the Doppler bandwidth. In addition, modulation mechanisms have been considered in the Doppler spectrum analysis, and the intermediate scale wave in uence on the Doppler spectrum has also been accounted for. Our previous study [5] also demonstrated the intermediate wave impact on the short Bragg waves. Although the intermediate waves perturb the Doppler spectrum, their in uence will not be analyzed here.

As mentioned earlier, such Doppler information is related to hydrodynamics. To further explore the hydrodynamic in uence on the ocean Doppler, we perform an analytical Doppler derivation based on hydrodynamics using the "Watson-West" (WW) equations [6]. After some transformations and truncations, we obtain an analytical modulated short wave representation. This analytical formulation can help us to simplify the ocean Doppler analysis without further electromagnetic simulations. In order to further validate our analytical derivation and also apply this formula to electromagnetic analysis, we develop analytical range-resolved polarized scattering fields based on the derived analytical short wave surfaces by use of the step frequency radar technique. Then, range-resolved Doppler spectra are obtained from the autocorrelation function of the range-resolved scattering fields. Finally, some validations for the analytical short waves are performed with the original WW equations, and the numerical radar Doppler from the simplified WW surfaces is shown as well. We also show sea surface wave profile retrievals using the Doppler information. Results demonstrate that the simplified method works well under small long wave steepness.

REFERENCES

1. Komen, G. J. and W. A. Oost, *Radar Scattering from Modulated Wind Waves*, 2740, 1989.
2. Rino, C. L., T. L. Crystal, A. K. Koide, H. D. Ngo, and H. Guthard, "Numerical simulation of backscatter from linear and nonlinear ocean surface realizations," *Radio Sci.*, Vol. 26, No. 1, 51–71, 1991.
3. Toporkov, J. V. and G. S. Brown, "Numerical simulations of scattering from time varying, randomly rough surfaces," *IEEE Transactions on Geoscience and Remote Sensing*, Vol. 38, No. 4, 1616–1625, 2000.
4. Johnson, J. T., J. V. Toporkov, and G. S. Brown, "A numerical study of backscattering from time evolving sea surfaces: Comparisons of hydrodynamic models," *IEEE Transactions on Geoscience and Remote Sensing*, Vol. 39, No. 11, 2411–2420, November 2001.
5. Pan, G. and J. T. Johnson, "A numerical method for studying modulation effects in radar observations of the sea surface," *IEEE Transactions on Geoscience and Remote Sensing*, Vol. 46, No. 11, 3632–3636, 2008.
6. West, B. J., K. A. Brueckner, and R. S. Janda, "A new numerical method for surface hydrodynamics," *J. Geophys. Res.*, Vol. 92, 11803–11824, 1987.

A Chaos Based Waveform Approach to Radar Target Identification

F. J. Rachford and T. L. Carroll
Naval Research Laboratory, Washington, D.C. 6362, USA

Abstract— Much effort has been devoted to the task of identifying targets observed in radar. Two approaches have been employed with mixed success, high resolution radar and resonance excitation and detection. High resolution techniques use radar signals with sufficient bandwidth to resolve individual scatters on a complex target. The downrange distribution of scatters is used to identify specific classes of targets. Targets of interest usually have cavities or other resonant features that are specific to a particular platform. So detection of the ring down of these resonators in the late portions of the radar return also can be used for identification. Our low resolution method employs optimized waveforms in cross correlation with the return from a low frequency (e.g., VHF) chirp to distinguish between candidate targets. Target signature waveforms were generated every degree in azimuth for four similar generic wing-body-tail targets using FDTD simulation. The targets were four to five meters in length with approximately two meter wing spans. The transmitted linear chirp had a 20% band width 250 MHz center frequency. We generated candidate waveforms using a simple chaotic map to cross correlate with the target returns. The waveforms were generated by passing chaotic time series through a bandpass filter. Alternately the waveforms were constructed by concatenating constant amplitude sinusoids whose periods were specified by the amplitudes of the chaotic time series. In both cases the waveforms were constructed with the same bandwidth and center frequency as the transmitted chirp. Random variation of the generating chaotic map parameters was followed optimization where the cross correlation of one target (A) was maximized with respect to the cross correlation of the return of another target (B) and vice versa. Optimization was done over target azimuthal various azimuthal windows up to 10 degrees. Using this method pairwise discrimination between candidate targets could be achieved over most aspects where the signature of the respective targets are not varying too rapidly with angle.

Influence of Noise on Subwavelength Imaging of Two Close Scatterers Using Time Reversal Method: Theory and Experiments

M. Davy[1], **J.-G. Minonzio**[2], **Julien de Rosny**[1], **Claire Prada**[1], **and Mathias Fink**[1]

[1]Institut Langevin, ESPCI ParisTech, CNRS UMR 7587, Laboratoire Ondes et Acoustique
Université Denis Diderot Paris 7, 10 Rue Vauquelin 75231 Paris Cedex 05, France
[2]Laboratoire Imagerie Paramétrique, UPMC Univ. Paris 06, UMR 7623
15 Rue de l'Ecole de Médecine, 75006 Paris, France

Abstract— Although classical imaging is limited by the Rayleigh criterion, it has been demonstrated that subwavelength imaging of two point-like scatterers can be achieved with probing sensors arrays, even if the scatterers are located in the far field of the sensors. However, the role of noise is crucial to determine the resolution limit. We propose a quantitative study of the influence of noise on the subwavelength resolution obtained with the DORT-MUSIC method.

The DORT method, French acronym for decomposition of the time reversal operator, consists in studying the invariants of the time reversal operator. The DORT method is combined here with the estimator MUSIC (MUltiple SIgnal Classification) to detect and image two close metallic wires. We use two horn antennas moving along an axis to create two virtual arrays of 10 antennas. Our targets consists of two wires of $\lambda/100$ diameters set up in front of the arrays. The microwaves measurements are performed between 2.6 GHz and 4 GHz with a spectral analyser. We show that we manage to image experimentally wires separated by $\lambda/6$.

To interpret our results in terms of noise level, the sensitivity of the DORT-MUSIC method to noise will be quantitatively discussed for subwavelength resolution. Theoretically, without noise, the MUSIC estimator diverges on the two wires locations, whatever the distance between them. However, for any small perturbation, the MUSIC estimator remains finite and the resolution is therefore not systematically achieved. To quantify this effect, the analytical expression of the eigenvectors of the time reversal operator perturbed by the noise is established. We then deduce the noise level above which the subwavelength resolution fails. The numerical simulations and experimental results validate the theoretical developments.

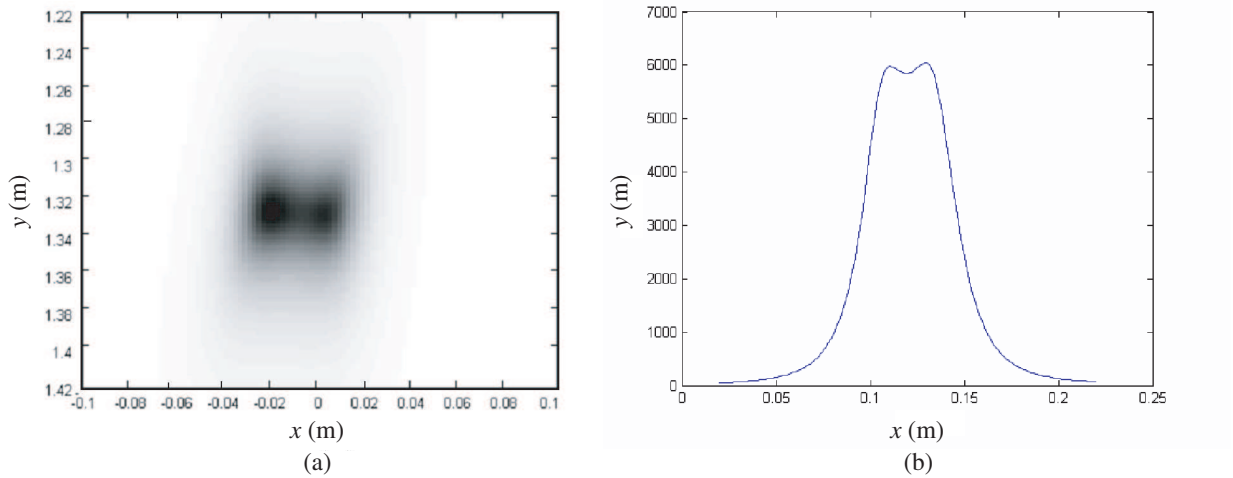

Figure 1: Imaged obtained with the DORT-MUSIC method of two wires separated by d with, (a) $d = \lambda/5$, (b) $d = \lambda/6$, ($\lambda = 11.5$ cm here).

A Quantitative Physics-based Study of Variability in Target Detection Due to Seasonal and Temporal Variation in Clutter Effects — Selected Case Studies

Jonathan Bredow
The University of Texas at Arlington, USA

Abstract— This paper considers the clutter-limited target detection case for simple ground- and aircraft-based surveillance radars, looking in particular at the seasonal and temporal variations in clutter strength and its impact on target detection. Both concealed and nonconcealed target cases are considered, with emphasis on the latter. Selected cases include monostatic and bistatic airborne and ground-based radars operating over gentle vegetated terrain, with a brief look at MIMO possibilities. The study includes variation in system parameters such as polarization, frequency, bandwidth, antenna type (adaptive versus nonadaptive), and bistatic angle. Evaluations are done to assess differences in detectability for targets with RCS as low as a few square meters. Simple detection criteria are used, e.g., based on scattering strength and Doppler shift effects. This is a comparative study that attempts to bring together several facets involving surveillance radar and the impact of clutter for simple signal processing scenarios.

Since the 1960's a number of scattering models have been developed to predict scattering coefficient for bare and snow covered soil, croplands and forested areas, as a function of frequency, incidence angle (and bistatic angle in some cases) and scene parameters such as soil dielectric constant, snow cover wetness, crop heights and biomass, and tree heights and branch and leaf distributions. Several of these models are used in this study to help map clutter over range and Doppler shift. Antenna effects, including adaptive and nonadaptive, and other system parameters are then included to produce a system-specific clutter map. Analysis is then done to observe how the system-specific clutter map varies over scene parameters. As this is done for multiple types of scene conditions, dry and wet and over seasons, it is expected to illustrate possible temporal and seasonal variations in clutter behavior, as "viewed" by a particular system.

As the quantitative impact of clutter on target detection is dependent on the detection criteria and type of signal processing used, i.e., to filter or otherwise reduce the impact of clutter, this study includes as the detection criteria scattering strength and Doppler shift, and employs simple time and frequency processing to make detection decisions. The monostatic and bistatic cases are contrasted, with and without a simple, but practical, MIMO configuration. Note that the clutter effects are provided in a sufficiently general way that a variety of detection and classification schemes can later be evaluated.

Using Chaos to Detect IIR and FIR Filters

T. L. Carroll
US Naval Research Lab, Code 6362, Washington, DC 20375, USA

Abstract— In many signal processing applications, IIR and FIR filters may be used interchangeably, as in the long delay limit, an FIR filter looks like an IIR filter. It is know in nonlinear dynamics that a properly tuned IIR filter can change the dimension of a chaotic signal. This occurs because the feedback in an IIR filter makes it a dynamical system, so it may be characterized in terms of dynamical quantities such as Lyapunov exponents. An FIR filter, on the other hand, is not a dynamical system, and should not change the dimension of a chaotic signal. In practice, however, an FIR filter with a long tail mixes parts of the chaotic signal that are uncorrelated in time, so that a finite length chaotic signal filtered with an FIR filter will appear to have a larger dimension.

I will show in this talk that it is possible to use a recently developed dimension estimation method to distinguish an IIR filtered chaotic signal from an unfiltered signal, or a signal filtered by an IIR filter. I can also distinguish different IIR filters from each other. I can even detect the presence of an IIR filter when I use a chaotic signal whose bandwidth is much smaller than the filter bandwidth.

Possible applications of this filter ID method could be in identifying radar or sonar targets based on resonant structures, or remotely identifying chemical compounds based on their resonance properties. The chaotic signal that I use may be modulated onto a higher frequency carrier, creating a signal that is suitable for radar applications. By adjusting modulation parameters, the bandwidth and Lyapunov exponent of the chaotic signal may be adjusted independently, which can allow the identification of a broad resonance with a narrow band signal.

Development of Polarimetric Ground Based-SAR System with Compact VNA and Vivaldi Antenna Array

M. Matsumoto and M. Sato
Tohoku University, Japan

Abstract— A polarimetric Ground Based-SAR system can be used not only to examine a scattering property of any target, but also to monitor vegetation or a landslide. Our laboratory has developed the system for several years. The system is a SF-CW (Step Frequency-Continuous Wave) radar system with a VNA (Vector Network Analyzer) and a dual ridged horn antenna. Our system could detect seasonal changes of trees by using polarimetric analysis [1]. While we carry out a measurement, we need to move the VNA with the antenna scanning due to limit of coaxial cables which connect the VNA and the antenna. Therefore antenna scanning was step-by-step scanning, not continuously scanning. Besides, the VNA and the dual ridged horn antenna in this system is excellent quality, but the equipments are relatively large.

In order to solve such problems, we developed a compact VNA and a box type Vivaldi antenna array shown in Fig. 1. The compact VNA which was developed by Anritsu and our laboratory achieves high speed measurement because it is specialized for S_{21} measurement. Therefore it can be attached to antenna positionner, and we can adopt continuously scanning. The box type Vivaldi antenna array consists of 4 Vivaldi antennas in order to achieve a full polarimetric measurement. By using the compact VNA and the antenna array, we could develop a more compact Ground Based-SAR system. A Block diagram of the compact polarimetric Ground Based-SAR system is shown in Fig. 2.

In this presentation, I'd like to evaluate effects of continuously measurement in SF-CW system. First, we measured SAR data with both of step-by-step scanning and continuously scanning. After that, we evaluated the difference of both scanning methods.

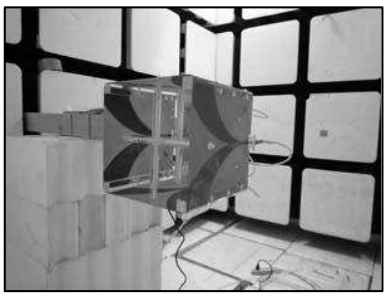

Figure 1: Antenna array composed by 4 Vivaldi antennas.

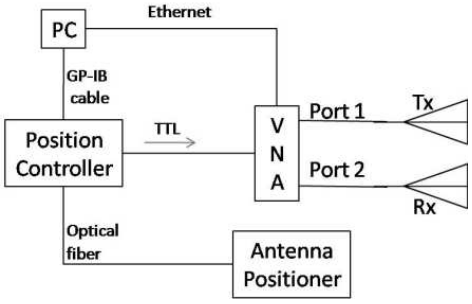

Figure 2: Block diagram of the polarimetric Ground Based-SAR system.

REFERENCES

1. Zhou, Z.-S., W.-M. Boerner, and M. Sato, "Development of a ground-based polarimetric broadband SAR system for non-invasive ground-truth validation in vegetation monitoring," *IEEE Transactions on Geoscience and Remote Sensing*, Vol. 42, No. 9. 1803–1810, 2004.

Full Polarimetric Calibration of Ground Based-SAR System with Thin Wire

M. Matsumoto and M. Sato
Tohoku University, Japan

Abstract— Our laboratory has developed a polarimetric Ground Based-SAR system with a compact VNA (Vector Network Analyzer) and a box type Vivaldi antenna array, shown in Fig. 1. This system can be used not only to examine a scattering property of any target, but also to monitor vegetation or a landslide. In a full polarimetric measurement, systematic errors caused by a transmitter and a receiver antenna results in distortion of a scattering matrix. Therefore we need a full polarimetric calibration in order to acquire the correct scattering matrix.

The full polarimetric calibration requires three different targets. One of solutions is to use a metallic sphere, 0 degree and 45 degree oriented dihedral corner reflector. Although the dihedral corner reflector has relatively large RCS (Radar Cross Section), it has a strong dependency as for incident angle of electromagnetic wave. Therefore we have to be very careful when we deploy the target. This is one of difficulties of using the dihedral corner reflector for the full polarimetric calibration. On the other hand, a thin wire can be put more easily than the dihedral corner reflector because one of rotation axes can be neglected. That is a reason why we used the thin wire for calibration. Analytic solution of the thin wire case is given by [1].

Firstly, we measured 0 degree, 45 degree and 90 degree inclined thin wire in order to derive calibration parameters. Fig. 2 shows signal amplitude of a co-polarization component in a frequency domain. After that, we calibrated the system using the estimated parameters. Evaluation of this calibration method will be presented.

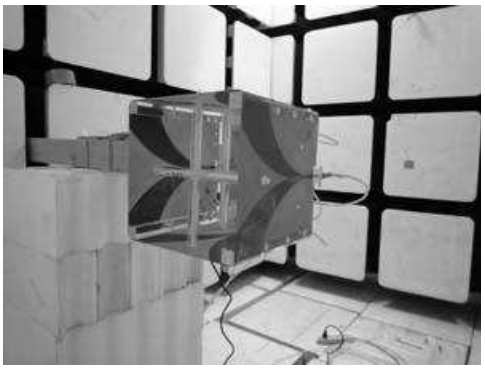

Figure 1: Antenna array composed by 4 Vivaldi antennas.

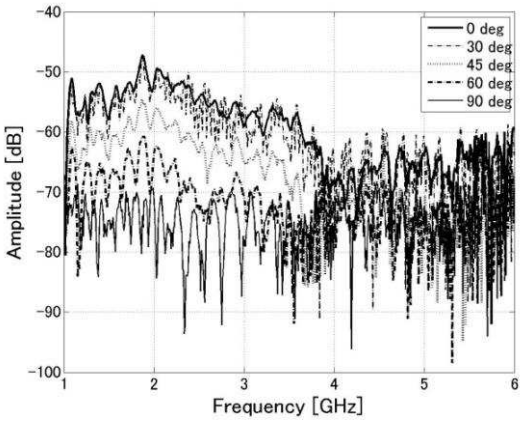

Figure 2: Signal amplitude of a co-polarization component in frequency domain from inclined thin wire.

REFERENCES

1. Yueh, S. H., J. A. Kong, R. M. Barnes, and R. T. Shin, "Calibration of polarimetric radars using in-scene reflectors," *Journal of Electromagneitc Waves and Applications*, Vol. 4, No. 1, 27–48, 1990.

A New UAV C-SAR for Environmental Monitoring

V. C. Koo[1], **Y. K. Chan**[1], **T. S. Lim**[1], **M. Y. Chua**[1], **C. C. Thum**[1], **Harita Jamil**[2], **Zahid Ahmad**[2], **Safiah Yusof**[2], **Khairul Annuar**[2], **and Mohamad Jamil**[2]

[1]Multimedia University, Malaysia
[2]Malaysian Remote Sensing Agency, Malaysia

Abstract— An Unmanned Aerial Vehicle (UAV) is an aircraft that is capable of operating without the presence of pilot or crew in the aircraft's cabin. It can be found extensively in the area of reconnaissance and surveillance as well as military purposes. In recent years, the usage of UAV in research area is rapidly growth and it has become an alternative platform for Synthetic Aperture Radar (SAR). As compared to conventional airborne or space-borne SAR systems, UAV-based SAR system has lower operation cost, lower risk, and suitable for *in-situ* measurement where frequent revisit is required.

A new C-band (5.3 GHz) UAV SAR has been designed and developed by Multimedia University, in collaboration with Malaysian Remote Sensing Agency (ARSM). The sensor operates in stripmap mode with 30 degrees incidence angle. It is capable of producing SAR imagery for all classes of terrain with scattering coefficient σ° above -30 dB. The spatial resolution is $5\,\mathrm{m} \times 5\,\mathrm{m}$.

Due to the limited working space and payload capacity of the UAV, the SAR sensor must be very compact and small in size. In this paper, the design and development of a miniature RF/IF subsystem, high-performance FPGA-based chirp generator, and on-board SAR processor will be discussed.

Session 3A3
Antennas and Array: Theory and Design 2

Input Characteristics of Coated Thin Wire Helix Antenna

S. A. Adekola[1], **A. I. Mowete**[1], **A. Ogunsola**[1, 2], **and A. Ayorinde**[1]

[1]Department of Electrical and Electronics Engineering, Faculty of Engineering
University of Lagos, Lagos, Nigeria
[2]Parsons Group International, Rail Transit Division, London, United Kingdom

Abstract— In this paper, we investigate the effects of the dielectric insulation on the input impedance and admittance characteristics of coated thin-wire helical antennas, using the quasi-static moment-method approach described elsewhere by Adekola et al. [1]. For the dielectric insulation modeled by a Schelkunuff's volume polarization current, the unknown quantity is the electric field in the dielectric region due to the distribution of current along the axis of the un-insulated wire, which is also an unknown quantity. By assuming that both unknowns are related in the manner specified by Richmond and Newman [2], and Lee and Balmain [3] we first evaluate the quasi-static magnetic field in the dielectric region, due to the current carried by the finite thin-wire antenna [4], and then using Maxwell's equations, obtain the corresponding electric field; the problem therefore becomes completely solved, when using the method of moments, the unknown current distribution is obtained. One interesting feature of this contribution, is the demonstration that the circuit-geometric character of the moment-methods enables the formulation for the coated elliptical cylindrical helical antenna to serve as a general case for certain regular thin-wire geometries.

Numerical results obtained for the representative examples of a coated monofilar helix (backed by a large ground plane) and a quadrifilar helix (backed by a finite ground plane) describe effects of coating these antenna types as consistent with those reported by Desplanches et al. [5].

REFERENCES

1. Adekola, S. A., A. Ike Mowete, and A. Ogunsola, "On the problem of dielectric coated thin wire antenna," *PIERS Proceedings*, 431–437, Moscow, Russia, August 18–21, 2009.
2. Richard, J. H. and E. H. Newman, "Dielectric coated wire antenna," *Radio Science*, Vol. 11, No. 1, 13–20, 1976.
3. Lee, J. P. Y. and K. G. Balmain, "Wire antennas coated with magnetically and electrically lossy material," *Radio Science*, Vol. 14, No. 1, 437–445, 1979.
4. Charitat, T. and F. Graner, "About the magnetic field of a finite wire," *European Journal of Physics*, Vol. 24. 267–279, 2003.
5. Desplanches, B., A. Sharaiha, and C. Terret, "Numerical analysis of helical antennas backed by finite ground planes," *Microwave and Optical Technology Letters*, Vol. 15, No. 6, 352–355, 1997.

Time Domain Analysis of Vivaldi TSA Using a Cubic Spline Taper Profile

Khabat Ebnabbasi and Carey Rappaport
Electrical Engineering Department, Northeastern University, Boston, 02115, USA

Abstract— Nowadays, time domain analysis, study and measurements are growing since; the UWB systems are well received for their specific features among them like high data transmission, using short duration pulse and large channel capacity. In high frequency, the electrical properties of antenna such as input impedance, radiation pattern, directivity and polarization are much more dependant frequency than narrow band applications and these parameters are not sufficient to analyze the transient radiation behavior of antenna.

In this paper, a Vivaldi TSA (Tapered Slot Antenna) is presented and its wide range of Gain in time domain in polar plot is given. The antenna's taper is cubic spline and it is a new and an alternative type in comparison with conventional exponential taper type. In previous work it was shown that in frequency domain it gives less reflection with improved gain and impedance band width. This taper was designed based on a Chebyshev transformer for the least reflection and better result was observed in comparison with mostly used exponential taper.

Here, we intend to analyze the time domain performance of a Vivaldi antenna which for smoothing the designed steps a cubic spline taper was exploited. In this design, the top points of modeled steps were selected to connect the points and curve fitting which in this paper is called Cubic spline-top points. The analysis is done by experimental measurements results for the designed antenna in frequency range 1–3 GHz which fabricated on a RT-Duroid board with dielectric constant equal to 6.15.

In the experimental results, in frequency domain, with a good precision a symmetric radiation pattern is observed with a high gain (< 12 dB) value. The time domain measurement of gain in polar plot shows that it provides a wide range of angle of gain bandwidth. Fig. 1 shows the polar plot of antenna's radiation pattern.

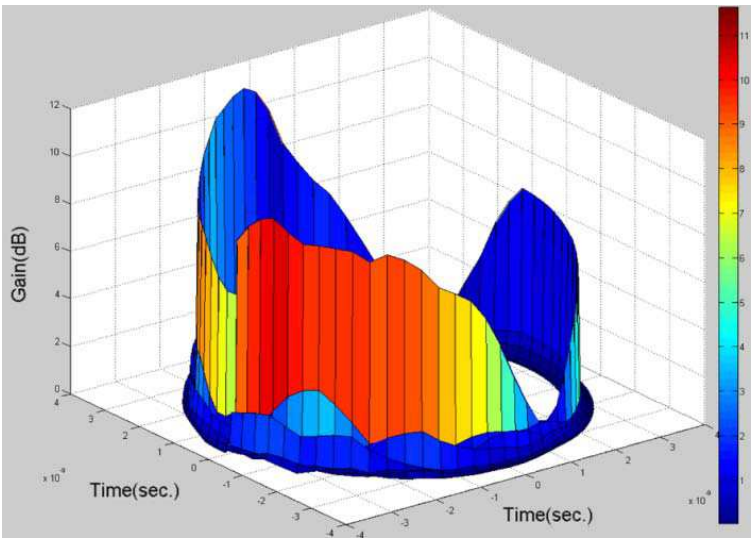

Figure 1: Time domain, radiation pattern of antenna in polar plot.

Design of Small Monopole Antennas Using Non-Foster Matching

Soon-Cheol Kong, **Ramakanth Munipalli**, **and Vijaya Shankar**
HyPerComp, CA, USA

Abstract— We apply active non-Foster matching circuits as means to improve the performance of electrically small antennas [1] over a wide bandwidth. We address small monopole antenna design by employing non-Foster negative impedance converter (NIC) circuit [2]. The input reactance of a small monopole antenna is modeled as a series connection of a capacitor and an inductor. In this approach, an active circuit is built such that we try to match and cancel out the lumped elements by generating negative capacitance and negative inductance from the NIC circuit. This comes from 180 phase shift, which flips the sign of the storage device's reactance, thus when it is added in series with the antenna we would like to match, we get a complete cancellation of the antenna's reactance.

Full-wave time-domain numerical simulations combined with SPICE simulations were conducted in a self-consistent way. An NIC circuit was employed to cancel out the input reactance component. It includes two transistors, which were modeled by a voltage controlled current source in the SPICE. Transconductance for transistors and parasitic circuit components were addressed in the simulation to consider the practical devices. From our numerical simulations as shown in Fig. 1, we obtained a very large bandwidth from 46 to 93 MHz (VSWR < 2) for a small monopole antenna with 60-cm length with an NIC matching circuit embedded, and furthermore our final result broke the Chu limit [3] by achieving Q factor less than 1/13th the Chu limit boundary value.

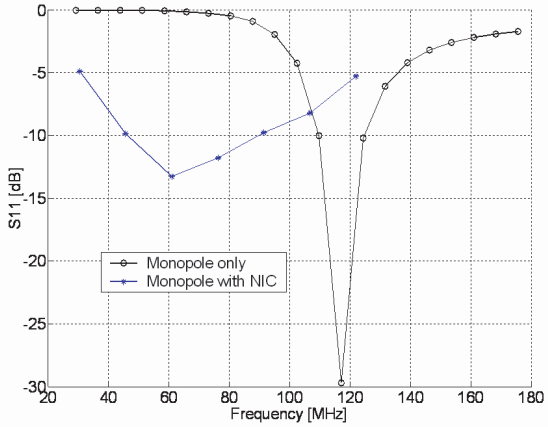

Figure 1: Computed S_{11} for a monopole antenna with and without NIC matching circuit.

REFERENCES

1. Wheeler, H. A., "Small antennas," *IEEE Trans. Antennas Propagat.*, Vol. 23, No. 4, 462–469, July 1975.
2. Horowitz, I. M., "Negative-impedance converters," *IRE Transactions on Component Parts*, 33–38, March 1962.
3. Chu, L., "Physical limitations of omni-directional antennas," *Journal of Applied Physics*, Vol. 19, 1163–1175, December 1948.

Aperture Coupled Phased Array with Novel Phase Shifter

Sharif Iqbal Mitu Sheikh, **S. M. Al-Shahrani**, **U. Johar**, **and S. Taiwo**
EE Department, King Fahd University of Petroleum & Minerals, Dhahran, KSA

Abstract— Phased array antennas are widely used in satellite and mobile communication, where antenna beams or nulls are electronically steered in desired direction [1]. However, due to the requirement of large number of phase shifters, the related cost, size and integration process plays an important role in the design process. Popular planar phase shifters used in this classes of array antenna includes digital switched-line phase shifters, where high resolution beam scan often requires complicated external control circuit [2]. Alternately, analogue microstrip ferrite phase shifters require bulky biasing magnetic for continuously controlling the insertion phase [3]. In this work, a novel analogue-digital techniques is employed to generate the phase function of the designed 4element active linear phased antenna. The discrete beam squints of 90° and 100° are achieved by 2-bit switched-line phase shifters and the superimposed 10° beam scan (from 90° to 100° and from 100° to 110°) is realized using microstrip ferrite phase shifters. Array feeder is implemented using corporate feed network and the rectangular patches are excited using aperture coupling technique avoid unwanted oscillations. To offset the losses associated with the array components (feeder, phase shifters) a GaAs-FET amplifier is introduced in the input-end of the circuit. The simulated reflection and transmission response of the antenna components are optimized to ensure impedance matching. The reflection response (15 dB), overall gain (10 dB) and beam scanning (20°) properties are plotted to satisfy the design requirements. This class array can be employed in the front-end of a 24-GHz microwave sensors. Since the accuracy of the simulated (HFSS) result depends on the experience of the simulator, the investigators will reference some of their previous work, where HFSS simulations are verified with experiments.

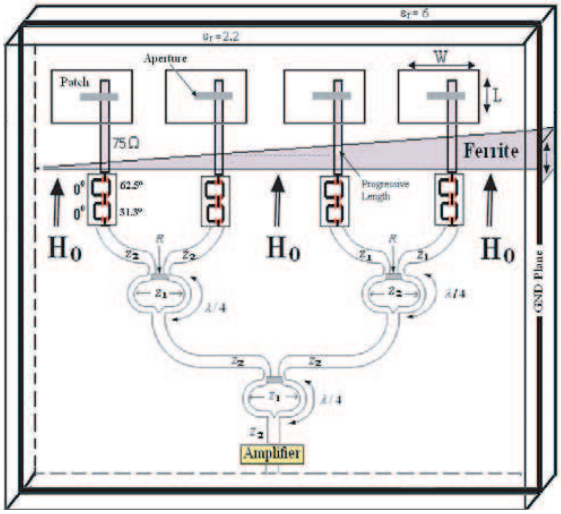

Figure 1: Schematic diagram of designed microstrip array.

ACKNOWLEDGMENT

Authors are thankful for the support of KFUPM, KSA (Project No. IN070345).

REFERENCES

1. Hansen, R. C., *Phased Array Antennas*, John Wiley and Sons Inc, 1998.
2. Batchelor, J. C., et al., "Scanned microstrip arrays using simple integrated ferrite phase shifters," *IEE Proc. Microwave Antennas Propagation*, Vol. 147, No. 3, 237–241, June 2000.
3. Gresham, I. and A. Jenkins, "A fast switching high isolation absorptive SPST SiGe switch for 24 GHz automotive applications," *33rd European Microwave Conf.*, 903–906, Munich 2003.

Antenna Design for a Portable RFID Reader

Manoel Vitório Barbin[1] and Silvio Ernesto Barbin[2]

[1]Flextronics Institute of Technology, Brazil
[2]Department of Telecommunication and Control Engineering, Polytechnic School
University of São Paulo, Brazil

Abstract— This paper presents the design of a circular polarized antenna for a portable RFID reader operating in the 900 MHz frequency band. For this type of application, an important challenge is the size reduction of the antenna which should be small enough to be used in restricted spaces. In general, this constraint results in degradation of some antenna parameters. The degradation is minimized printing the radiating structure on a high dielectric constant substrate, accordingly. The feeding structure is implemented on a different substrate and both circuits are stacked to constitute an electromagnetically coupled antenna.

Fractal Antenna Analysis in Frequency and Time Domain

Baso Maruddani[1, 2], Joko Suryana[2], and Tommi Hariyadi[3]

[1]Electrical Engineering Department, State University of Jakarta, Indonesia
[2]School of Electrical Engineering and Informatics, Bandung Institute of Technology, Indonesia
[3]Electrical Engineering Department, Indonesia University of Education, Indonesia

Abstract— A fractal structure is constructed to obtain ultra wideband (UWB) performance because of its self-similarity property and space filling property. This paper presents A crown circular fractal antenna (CCFA) fed by coplanar waveguide (CPW). The parameters and characteristics of the antenna and the simulation results show that the 8 GHz or more bandwidth is achieved with the second order iterative antenna structure. The simulated frequency domain analysis such as return losses, VSWR, and radiation patterns as well as time domain analysis-namely impulse response demonstrate that the CPW-fed UWB CCFA provides good UWB performance and the dimension of the antenna is small. Therefore, the antenna can be used in UWB systems.

From the simulated return loss parameter, we found that resonant frequency occur at 4.2 GHz and 7.5 GHz. The value of return loss of less than −10 dB and VSWR < 2 is ranging from 3.1 to 10.6 GHz as we expected for UWB frequency band specification. We also observed that VSWR of less than 2 is obtained for the same frequency band which is met the UWB specification of more than 7.5 GHz. The VSWR can achieve the required bandwidth of the UWB band at 3.1 GHz up to 10.6 GHz using the maximum value of VSWR of 2.

Three-dimension radiation pattern for the frequency at 3 GHz (the lower UWB frequency band) shows an omnidirectional pattern. This omnidirectional pattern is suitable for lower data rate UWB application such as sensor network for mobile computing. The simulated result of radiation pattern at 10 GHz band shows that the pattern is become directional as the frequency band is increased. We also observe from the figures the antenna gain. The higher the frequency is the higher the gain. The lowest gain is found to be 3.312 dBi occurring at around 5 GHz and the highest gain of 6.746 dBi appear at 10 GHz.

Finally, the simulated impulse response of the proposed antenna shows that duration of impulse response is less than 2 ns which means the simulated antenna has a very wide frequency band. This achievement of such impulse response of the antenna meets the specification for UWB application.

Characterization of Microwave Thin Radar Absorber Composed of Hexagonal Patch Array

L. Olivia, F. Kurniasih, and A. Munir
School of Electrical Engineering and Informatics, Institut Teknologi Bandung, Indonesia

Abstract— Recently the focus of intense research in the design of absorbing material is how to reduce the reflected electromagnetic energy scattered from some object. One of the effective methods is by use of texture surface technology comprised of a high impedance surface (HIS) as a perfect magnetic conductor. The method can remove the need of HIS for a quarter-wavelength-spacing between resistive sheet and a perfectly conducting metal ground plane; as a result the thickness of absorber can be reduced drastically.

In this work the characterization of microwave thin radar absorber based on textured surface technology is numerically investigated. The construction of absorber is comprised of a doubly periodic hexagonal patch with surface-mounted-resistive elements incorporated onto the array of surface to control its surface impedance. To investigate the characteristic of the absorber, we numerically analyzed a hexagonal patch as a unit cell that can operate whereby at the resonance frequency of resistively texture surface. The surface behaves like a perfect magnetic conductor (PMC); therefore the electric field is in tangential to the surface, i.e., x-axis direction.

The patch as shown in Fig. 1 consists of hexagonal shape of metallic copper with the edge length is 6.87 mm and the gap between patches in x-axis direction is 2.0 mm placed on a single-sided thick Taconic CER10 substrate. Permittivity and $\tan\delta$ of the substrate are 10 and 0.0035 respectively, whilst the thickness of metallic copper top patch as well as the ground plane of the substrate is 0.035 mm. Substrate and copper conductive losses are also accounted for. Surface-mounted-resistive elements are incorporated midway connecting between the adjacent patches in y-axis direction to reduce the amount of backscatter from the surface. Fig. 2 plots the simulated reflection magnitude of structure with 470 Ω of resistive elements whereupon the incident electromagnetic energy should be absorbed up to −30 dB.

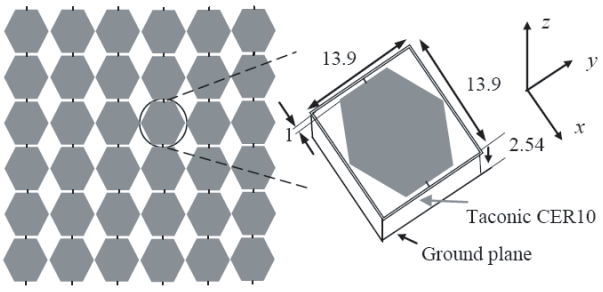

Figure 1: Doubly periodic hexagonal patch array.

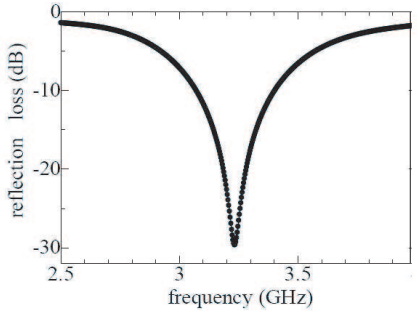

Figure 2: Simulated result of hexagonal patch with 470 Ω resistor.

Microstrip Array Antenna with New 2D-Electromagnetic Band Gap Structure Shapes to Reduce Harmonics and Mutual Coupling

Dalia N. Elsheakh[1], **Magdy F. Iskander**[1], **Esmat A. Abdallah**[2], **Hala A. Elsadek**[2], **and Hadia Elhenawy**[3]

[1]Hawaii Center for Advanced Communication, Hawaii, Honolulu, USA
[2]Electronics Research Institute, Cairo, Egypt
[3]Faculty of Engineering, Ain Shams University, Cairo, Egypt

Abstract— Microstrip patch antennas are widely used in various applications because of low profile, low cost, light-weight and conveniently integration with RF devices. However, microstrip antennas have many disadvantages. One of these disadvantages is the excitation of surface waves that occur in the substrate layer. Surface waves are undesired because when a patch antenna radiates, a portion of total available radiated power becomes trapped along the surface of the substrate. It reduces total available power for radiation to space wave as well as there is harmonic frequency created [1]. For arrays, surface waves have a significant impact on the mutual coupling between array elements [2]. One solution to reduce surface waves is using electromagnetic band-gap (EBG) or photonic band-gap structure (PBG). Recently, there has been an increasing interest in studying the microstrip patch antenna with various periodic structures including electromagnetic band-gap (EBG) [2]. For example, a microstrip patch antenna with 2D-EBG used to control harmonic is reported in [3]. Many shapes of EBG slots have been studied for single element microstrip antenna such as circles, dumb-bells and squares. However, not many have realized in antenna arrays [4]. In this paper presents microstrip array antenna integrated with novel shapes of 2D electromagnetic band-gap structure (2D-EBG). Three different shapes of 2D-EBG are used for harmonic suppression, optimizing the current distribution on the patches and decreasing the mutual coupling between array elements. As a result the performance of the antenna array is improved. The three novel shapes of 2D-EBG presented are star, H and I shaped slots. Simulated and measured results verify the improved performance of the array antenna compared to the antenna without EBG as well as antenna array with conventional EBG shapes. The harmonic suppression and the reflection coefficients are improved by about 18 dB and the antenna size is reduced by 15% compared to the original size.

REFERENCES

1. Gonzalo, R., P. De Maagt, and M. Sorolla, "Enhanced patch-antenna performance by suppressing surface waves using photonic-band-gap substrates," *IEEE Trans. Microwave Theory Tech.*, Vol. 47, 2131–2138, Nov. 1999.
2. Yu, A. and X. Zhang, "A novel method to improve the performance of microstrip antenna arrays using dumbbell EBG structure," *IEEE Antennas and Wireless Propagat. Lett.*, Vol. 2, 170–172, 2003.
3. Liu, H., Z. Li, X. Sun, and J. Mao, "Harmonic suppression with photonic bandgap and defected ground structure for a microstrip patch antenna," *IEEE Microw. and Wireless Compenents Lett.*, Vol. 15, No. 2, 55–56, Feb. 2005.
4. Yu, A. and X. X. Zhang, "A novel 2D electromagnetic band-gap structure and its application in microstrip antenna arrays," *Proc. 3rd Int. Conf. Microwave and Millimeter Wave Tech. ICMMT*, 580–583, 2002.

Integrated Design of Multiple Antennas for WiFi/Bluetooth/GPS Mobile Communication

Dong Wang and Qinjiang Rao
Research in Motion Limited, Canada

Abstract— A novel dual-feed, integrated antenna for WiFi, Bluetooth and GPS applications in portable device is described. The single antenna which has compact size and high efficiency can be used for wireless handset applications instead of the three individual antennas in mobile handsets. The specific dual feed design allows the WiFi and Bluetooth antennas to work simultaneously. This design created lower coupling which results in higher radiation efficiency and MIMO antenna application.

Increasing Integration in Composite Patch Antenna Arrays for Dual-band and Dual-polarized Uses

Monika Hornik and Pawel Kabacik
Institute of Telecommunications, Teleinformatics and Acoustics, Wroclaw University of Technology
Wybrzeze Wyspianskiego 27, Wroclaw 50-370, Poland

Abstract— Weight significant lowering objective and dualpolarized operation, possible in more than two bands, have driven our studies on composite antennas in last three years. With ready-at-hand technology making use of several dielectric layers, we have focused research on antenna element shaping and on element dense packaging. Accomplishing high quality of polarization and enabling inter-element spacing up to a half wavelength, were other two main objectives in our studies. The results of these research are presented for antenna clusters operating with dual linear polarization at both 2.45 and 5.3 GHz.

Novel MEMS Dipole/Monopole Antenna for Wireless Systems Operating at 77 GHz

E. A. Soliman, S. Sedky, M. O. Sallam, S. Hassan, O. El Katteb, A. K. S. Abdel Aziz, and M. Refaat
The American University in Cairo, AUC Avenue, P. O. Box 74, New Cairo 11835, Egypt

Abstract— This work presents a novel miniaturized MEMS antenna operating at 77 GHz that can be fabricated on a single silicon wafer without any need for wafer bonding or hybrid integration. The proposed antenna provides high radiation efficiency, high gain, and it can work as either dipole or monopole depending on the selection of the port of excitation. A schematic diagram of the proposed MEMS antenna is displayed in Fig. 1. It has two vertical silicon walls that are defined by deep reactive ion etching of high resistivity ($\sim 2,000\,\Omega$·cm) silicon wafer of thickness 0.675 mm. The width, length, and depth of each wall are 70 µm, 973 µm ($\lambda_g/2$), and 475 µm ($\lambda_g/4$), respectively. The remaining silicon volume, whose thickness is 0.2 mm, represents the substrate of the structure. Two horizontal metal arms are covering the top surfaces of the walls, while two vertical pillars with square cross-section are drilled through the entire wafer, as shown in Fig. 1. The surfaces of these pillars are covered with metal. It can be seen in Fig. 1. that there are gaps between the vertical pillars and the horizontal arms. The top surface of the substrate is covered with slotted ground metal plate, through which the silicon walls are going up. This plane serves as a reflector that increases the directivity of the antenna. Moreover, it isolates between the antenna and the bulk silicon substrate, which reduces the surface wave losses and increases the radiation efficiency. From the bottom side of the substrate, the pillars are connected to the two output ports of a ring coupler made of microstrip lines and fed with two 50 Ω lines. The proposed antenna has been fabricated using new process flow, which uses single wafer to realize the entire structure. A photograph of the fabricated walls is shown in Fig. 2.

If the excitation signal is applied to port 1 of the ring coupler, see Fig. 1, the antenna arms will be excited with the same amount of power, but with 180° phase shift. The currents on the vertical pillars will be opposite to each other, while on the horizontal arms the currents will be in the same direction. The horizontal arms are located a distance $\lambda_g/4$ on top of the slotted ground plane. By applying the image method, it is possible to replace this metal plane with another two horizontal dipoles out-of-phase with the original ones and located $\lambda_g/2$ away from them. Hence, the originals and their images add to each other constructively in the broadside direction and destructively in the end-fire direction. The presence of the gaps between the vertical pillars and the horizontal arms imposes current nulls around these gaps. This defines standing waves on the horizontal arms, where each wave is limited by two nulls separated by a distance of $\lambda_g/2$. As shown in Fig. 3, the impedance bandwidth of the dipole mode, along which $S_{11} < -10$ dB, is 3.8%. The 3D radiation pattern of this mode is shown in Fig. 4, in which it can be seen that the antenna is radiating mainly from the top side with maximum at broadside. The calculated gain and radiation efficiency of this mode are 8.6 dBi and 92%, respectively. Such high radiation efficiency at 77 GHz can't be achieved using the conventional planar antennas.

The excitation of the monopole mode is via port 2. In this case, the ring coupler delivers half of the input power to each antenna side with the same phase. Consequently, the horizontal currents

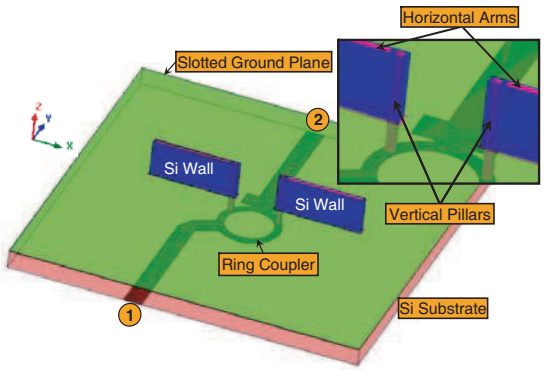

Figure 1: Structure of the proposed antenna.

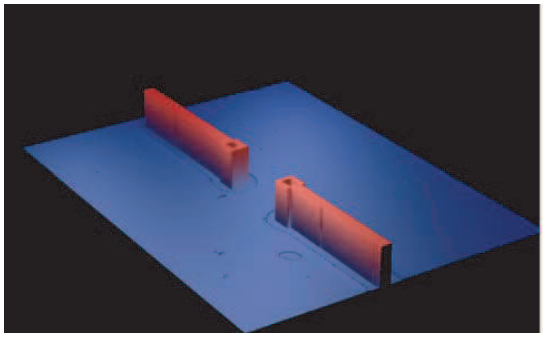

Figure 2: Photograph of the fabricated antenna walls.

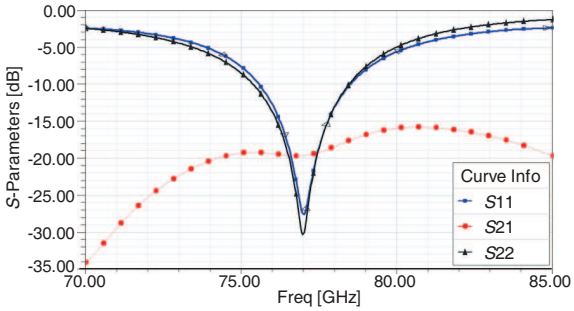

Figure 3: S-parameters of the proposed antenna.

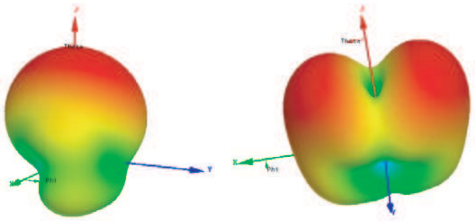

Figure 4: 3D radiation patterns: (left) dipole, (right) monopole mode.

are opposite to each other, while the vertical currents are in the same direction. If the image method is applied, the ground plane can be replaced by two $\lambda_g/4$ vertical currents in-phase with the original ones. The original and image currents, represent two $\lambda_g/2$ vertical dipoles radiating from the top side of the substrate. As in the dipole mode, the disconnection of the vertical pillars and horizontal arms imposes current nulls at the points of disconnection. The impedance bandwidth of this mode is 3.9%, and the coupling between ports is less than -15 dB, as shown in Fig. 3. The 3D radiation pattern of the antenna in the monopole mode is shown in Fig. 4. The calculated gain and radiation efficiency of this mode are 5.4 dBi and 93%, respectively. Unlike the dipole mode pattern, this pattern shows null at broadside and significant radiation close to end-fire. Switching between the two modes of operation allows better coverage of the half-space.

Session 3A4
Microelectronic Packaging

Fast Electromagnetic Modeling of 3D Interconnects on Chip-package-board

Boping Wu[1], **Xin Chang**[1], **Leung Tsang**[1], **and Tingting Mo**[2]

[1]Department of Electrical Engineering, University of Washington in Seattle, United States
[2]School of Microelectronics, Shanghai Jiao Tong University, China

Abstract— High speed vertical interconnects are among the key components for up-to-date 3D design and integration on chip-package-board. With the ever-increasing clock rate and operating frequency, massively-coupled multiple vias, such as BGA, LGA, PTH, microvia and TSV, behave like efficient radiators, thereby introducing significant electromagnetic interference, crosstalk, attenuation and other signal integrity issues. The segmented via analysis with local parametric optimization is important before going into further integration. However, simple approximations, such as physical and lumped models, are usually inaccurate due to their incapability of including all the couplings among multiple vias. On the other hand, the network analyzer has certain difficulties on hardware characterization of the complete network with many ports. In this paper, an efficient and mostly-analytic method, based on the Foldy-Lax equations for multiple scattering technique, will be presented for full-wave electromagnetic modeling of high density randomly-positioned vias. Various via structures in different kinds of multilayered substrates will be simulated and demonstrated using our recently-developed 3D interconnect simulator. In this paper, we will review previously computed cases as well as new cases including arbitrary shape of pad and antipad, substrates of layered dielectrics, differential via-pair in shared antipad and coated through silicon vias. Comparisons are made with commercial software and hardware measurements. The simulation results using our simulator are within 5% difference of accuracy compared with HFSS. The CPU consumption of our simulator is at least three orders of magnitude faster than that of the HFSS. The results are further validated by good correlations with experimental measurements.

An $\mathcal{H}$-LU Based Direct Finite Element Solver Accelerated by Nested Dissection for Large-scale Modeling of ICs and Packages

Haixin Liu and Dan Jiao
School of Electrical and Computer Engineering, Purdue University
465 Northwestern Avenue, West Lafayette, IN 47907, USA

Abstract— A finite element method (FEM) based analysis of a large-scale IC and package problem generally results in a large-scale system matrix. Although the matrix is sparse, solving it can be a computational challenge when the problem size is large. There exists a general mathematical framework called the "Hierarchical ($\mathcal{H}$) Matrix" framework [1–4], which enables a highly compact representation and efficient numerical computation of the dense matrices. It has been shown that the storage requirements and matrix-vector multiplications using $\mathcal{H}$ matrices are of complexity $O(N \log N)$, and the inverse of an $\mathcal{H}$ matrix can be obtained in $O(N \log^2 N)$ complexity. In [5, 6], we developed an $\mathcal{H}$-matrix based solver to efficiently compute and store the inverse of a finite element matrix. In this work, we develop an LU-factorization based fast finite-element solver. The $\mathcal{H}$-based LU is further accelerated by Nested Dissection [7].

The main contribution of this work is four-fold. First, we theoretically prove the existence of an $\mathcal{H}$-matrix-based representation of the FEM matrix and its inverse for electrodynamic problems. The existence of an $\mathcal{H}$-matrix approximation so far was only proved for elliptic partial differential equations (PDE) [8], whereas the Maxwell's equations are hyperbolic in nature. Second, we develop an $\mathcal{H}$-matrixbased LU solver of $O(kN \log N)$ memory complexity and $O(k^2 N \log^2 N)$ time complexity for solving vector wave equations, where k is a small constant that is adaptively determined based on the accuracy requirement. The $\mathcal{H}$-based LU is further accelerated by Nested Dissection [7]. Third, we develop a theoretical analysis of the complexity and accuracy for the proposed fast direct solver. In addition, we compare the proposed direct solver with the state-of-the-art direct sparse solver such as UMFPACK 5.0 [9]. UMFPACK has incorporated almost all the advanced sparse matrix techniques such as the multifrontal method and the AMD ordering for solving large-scale sparse matrices. The proposed solver is shown to outperform the UMFPACK 5.0 in both matrix decomposition and matrix solution time without sacrificing accuracy.

REFERENCES

1. Hackbusch, W. and B. Khoromaskij, "A sparse matrix arithmetic based on matrices. Part I: Introduction to matrices," *Computing*, Vol. 62, 89–108, 1999.
2. Hackbusch, W. and B. N. Khoromskij, "A sparse-matrix arithmetic. Part II: Application to multi-dimensional problems," *Computing*, Vol. 64, 21–47, 2000.
3. Borm, S., L. Grasedyck, and W. Hackbusch, "Hierarchical matrices," Lecture Note 21 of the Max Planck Institute for Mathematics in the Sciences, 2003.
4. Grasedyck, L. and W. Hackbusch, "Construction and arithmetics of matrices," *Computing*, Vol. 70, No. 4, 295–344, August 2003.
5. Liu, H. and D. Jiao, "A direct finite-element-based solver of significantly reduced complexity for solving large-scale electromagnetic problems," *International Microwave Symposium (IMS)*, 4, June 2009.
6. Liu, H. and D. Jiao, "Performance analysis of the H-matrix-based fast direct solver for finite-element-based analysis of electromagnetic problems," *IEEE International Symposium on Antennas and Propagation*, 4, June 2009.
7. George, A., "Nested dissection of a regular finite element mesh," *SIAM J. on Numerical Analysis*, Vol. 10, No. 2, 345–363, April 1973.
8. Bebendorf, M. and W. Hackbusch, "Existence of $\mathcal{H}$-matrix approximants to the inverse FE-matrix of elliptic operators with L^∞-coefficients," *Numerische Mathematik*, Vol. 95, 1–28, 2003.
9. UMFPACK5.0, http://www.cise.ufl.edu/research/sparse/umfpack/.

Application of Two Mixed Potential Integral Equations to Electromagnetic-circuit Simulation of Three-dimensional Interconnects in Layered Media

N. Kurt-Karsilayan[1] and K. A. Michalski[2]

[1]Texas A&M University and Mentor Graphics Corporation, USA
[2]Texas A&M University, USA

Abstract— A new full-wave, surface impedance equation method is proposed based on two mixed potential integral equation (MPIE) forms for electromagnetic-circuit simulation of three-dimensional arbitrary-shaped conducting objects over conducting substrate layers. Equivalence principle is used to model the electromagnetic-circuit interactions of interconnects in layered media. Arbitrary-shaped interconnects are considered as homogeneous conducting objects embedded in layered media. Interconnect surfaces are composed of non-contact and contact surfaces where electromagnetic and electromagnetic-circuit surface integral formulations are applied, respectively. The electromagnetic-circuit surface integral formulations are described for two MPIE forms of the Electric Field Integral Equation (EFIE) which are based on the Michalski-Mosig formulation where different sets of layered kernels are involved. The use of the two MPIE forms is discussed in detail. Unlike most of the existing approaches, no assumptions are made for the layered Green functions since the Sommerfeld integrals are computed directly for controllable accuracy. The layer information is independent of the interconnect geometries, therefore Sommerfeld integrals can be computed one time and used later during the geometry processing. Various new ways of applying external voltage and current sources are discussed in detail in the proposed electromagnetic-circuit simulation approach. The advantage of the proposed method is that the port admittance or impedance is computed directly, therefore no model order reduction techniques are required, unlike in Partial Element Equivalent Circuit methods. The Method of Moments (MOM) is used to discretize the surface integral equations with the Rao-Wilton-Glisson (RWG) basis and testing functions. The proposed method for electromagnetic-circuit simulation in layered media is addressed such that it can be incorporated into existing RWG-based MOM codes easily. Numerical results are presented for the validation of the proposed methods.

Discontinuous Galerkin Time Domain Method for Multiscale Microelectronic Packaging

Qing Huo Liu[1], **Jiefu Chen**[1], **Tian Xiao**[2], **Joon-Ho Lee**[2], **and Mengqing Yuan**[1]

[1]Department of Electrical and Computer Engineering, Duke University, Durham, NC, USA
[2]Wave Computation Technologies, Inc., Durham, NC, USA

Abstract— Multiscale microelectronic packaging problems pose significant challenges in computational electromagnetics because any single methodology (such as the finitedifference time-domain method or finite-element method) will be inadequate to simultaneously deal with both fine structures and large uniform spaces. For example, in time-domain design simulation of microelectronic packaging problems, if the FDTD method with a uniform grid is utilized to capture the complex fine geometrical details in the chip level, the number of grid points needed in a large domain with relatively uniform spaces typical in electromagnetic compatibility studies will be overwhelming.

To address this challenge in multiscale modeling, we have developed an efficient discontinuous Galerkin time domain (DGTD) method to combine several different methodologies. In this DGTD method, the fine geometrical details are modeled by the finite-element time-domain (FETD) method [1] and Crank-Nicolson enlarged cell technique (ECT), an improved version of the conformal finite-difference time-domain method [2, 3]. For the intermediate scale, the explicit enlarged cell technique is applied. For the coarse scale, a spectral element time-domain (SETD) method [4] is used. These three different scales and solvers are combined together by using a Riemman solver in the discontinuous Galerkin method. It is found that to avoid spurious modes, it is critical to use non-spurious elements in both the FETD and SETD methods.

This presentation will report the progress of this DGTD method. We will demonstrate the efficacy of this simulator by solving large-scale package level EMI/EMC problems.

REFERENCES

1. Chen, J., Q. H. Liu, M. Chai, and J. A. Mix, "A non-spurious 3-D vector discontinuous Galerkin finite-element time-domain method," *IEEE Microwave Wireless Compon. Lett.*, in Press.
2. Xiao, T. and Q. H. Liu, "Enlarged cells for the conformal FDTD method to avoid the time step reduction," *IEEE Microwave Wireless Compon. Lett.*, Vol. 14, 551–553, 2004.
3. Xiao, T. and Q. H. Liu, "A 3-D enlarged cell technique (ECT) for the conformal FDTD method," *IEEE Trans. Antennas Propagat.*, Vol. 56, No. 3, 765–773, March 2008.
4. Chen, J. and Q. H. Liu, "A non-spurious vector spectral element method for Maxwell's equations," *Progress In Electromagnetics Research*, PIER 96, 205–215, 2009.

A Novel Technique for Approximation of Summation with Corrected Integral (ASCI) to Accelerate the Spectral Domain Approach for Shielded Microstrip Lines

Jiming Song and Sidharath Jain
Iowa State University, Ames, IA-50011, USA

Abstract— A novel and simple technique for approximation of summation with corrected integral (ASCI) has been developed and applied to the acceleration of the shielded microstrip problem using the spectral domain approach (SDA). The SDA results in accurate results for propagation constants for shielded microstrip lines using a few basis functions. However, as the required accuracy increases the computation time increases because of the slow convergence of spectral series summation.

The longitudinal and transverse current are expanded in terms of even and odd Chebyshev basis, respectively, because their Fourier transform is a Bessel function. Further, by using Galerkin method in the Fourier domain, followed by the Parseval's theorem and the boundary conditions we can obtain the elements of the Galerkin matrix or K matrix. Finally, the propagation constant β is obtained by solving $\det[K] = 0$. The time intensive part in the SDA is the calculation of the matrix elements which are in the form of an infinite series summation.

In order to accelerate the formation of K matrix we truncate the infinite summation at a suitable $N_{\max}$. For the rest of the summation each term is approximated using the asymptotic expansion for the Greens function and the Bessel function and their summation from $N_{\max}+1$ to ∞ is approximated using ASCI.

$$K_{ij}^{pq} \approx \sum_{n=1}^{N_{\max}} F_{ij}^{pq} + \sum_{n=N_{\max}+1}^{\infty} \tilde{F}_{ij}^{pq} \tag{1}$$

where $F_{ij}^{pq} = \tilde{J}_{pi}(\alpha_n) G_{pq}(\alpha_n, \beta) \tilde{J}_{qj}(\alpha_n)$ and $\tilde{F}_{ij}^{pq}$ is the asymptotic approximation of F_{ij}^{pq} which has terms of the form $1/n^k$ or $g(n)/n^k$ where $g(n)$ is a sinusoidal function.

A general expression for $\Sigma_n f(n)$ is derived with ASCI which uses one term less than the Euler Maclaurin summation formula. We have also derived an expression with corrected coefficients for the special case $\Sigma_{n=N}^{\infty} g(n)h(n)$ when the mth derivative of $h(n) = h^{(m)}(n) \to 0$ for $m = 0, 1, 2, \ldots$ as $n \to \infty$ and $g(n)$ is a sinusoidal function.

The convergence of the elements of K matrix and the ϵ_{reff} increases drastically depending on the number of leading terms used. Using four leading terms and four basis functions for the longitudinal current and three for the transverse current i.e. (4, 3) basis, we get 12 significant digits of ϵ_{reff} by truncating the summation at $N_{\max} = 255$ using ASCI.

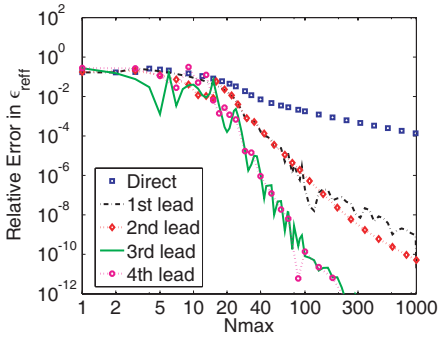

Figure 1: Convergence of ϵ_{reff} using different number of leading terms and (4, 3) basis.

Low Noise and High Current ASIC Package Power Delivery System Design and Validation

Antonio Ciccomancini Scogna[1], **Jianmin Zhang**[2], **Qinghua Bill Chen**[2], **and Kelvin Qiu**[2]

[1]CST of America, 492 Old Connecticut Path, #505, Framingham 02101, MA, USA
[2]Cisco Systems, USA

Abstract— Low noise level and high currents are key points to be addressed during the design process and validation of ASIC Package Power Delivery System. This paper investigates a flip chip 12 layer package and presents a simulation methodology to efficiently evaluate the self/transfer impedance and the ground bounce noise associated to the PWR/GND layers. Correlation with measurements is provided and sensitivity analysis with respect to location and values of decoupling capacitors is also investigated. Frequency domain results are numerically calculated by means of 3D field solver, used because of the presence of three dimensional geometries such as BGA and long vias, and an equivalent SPICE model is finally generated for time domain simulation.

Introduction: As microprocessor and ASIC power supply voltages are headed to 2.0V and below, and clock frequencies go up, the power distribution system of IC packages is becoming an increasingly important design challenge. In high-end flip-chip and ball-grid array (BGA) packages, multiple power and ground planes are often used to keep power supply noise low. An important design issue is, for a given power supply noise margin, how to determine the number of power and ground planes, and the number and the locations of power and ground vias. Electrical performances of power supply systems have often been characterized by the effective inductor model, which can be used to estimate power supply noise at low frequencies.

However for high-end packages, the frequency range of interest is from DC to a few GHz therefore there can be several package resonant frequencies and this model may become totally invalid. Accurate characterization of power supply system necessitates electromagnetic field simulations to take into account various electromagnetic interactions in packages. The present paper investigates the power supply noise in multilayered IC package and presents a simulation methodology to efficiently determine the self/transfer impedance and the ground bounce noise (GBN) associated to the power/ground (PWR/GND) layers. A simplified model of the package which does not include the signals layers is used and the reliability of such model is also validated by compared the results with those due to the full stack up. Numerical statistics regarding CPU and simulation time will be provided along with possible tradeoffs related to the proposed methodology.

The importance of using a 3D field simulator, because of the multilayer stack-up, the presence of three dimensional geometries such as ball grid array (BGA) as well as long vias, will be demonstrated and comparison with the results coming from a more standard two dimensional (2D) transmission line (TL) solver will be also discussed. Correlation with measurements is investigated and sensitivity analysis with respect to location and values of decoupling capacitors is also analyzed. The intent of the paper is to provide useful insights for design engineers in the field of Signal and Power Integrity (SI and PI) by providing a reliable workflow and analyzing a real world package model.

Design of an In-line CPW-stripline Transition without the Use of Signal Vias

Lionelle F. Wells and Kathleen L. Melde
Department of Electrical and Computer Engineering, University of Arizona
Tucson, AZ 85721-0104, USA

Abstract— The development of a coplanar waveguide (CPW) to stripline transition that will work over a broad frequency band is challenging because of the use of signal vias. The multiline TRL method assumes perfectly fabricated calibration standards containing uniform signal vias that do not actually exist in practice. In a typical transition design, the CPW is fabricated on an exposed surface of the board, while the center conductor of the stripline is fabricated on an internal layer. The fabrication requirement for the CPW comes about because it must interface to external probes, while the requirement for the stripline arises from the fact that the center conductor must have ground planes on the layers above and below it. The need for signal vias can be eliminated, however, if the CPW is fabricated on the same internal layer of the board as the center stripline conductor. To interface with the probes, the board material above the CPW structure is removed with machine tools, leaving a portion of the internal layer exposed. This method has been used to design and simulate a back-to-back CPW-to-stripline transition. Major design considerations include the board material used, the placement of ground vias to couple the CPW ground planes to the stripline ground layers, and the tapering geometry used to allow the two structures to physically interface with one another. Simulation results of the transition in the back-to-back configuration show that the transition as designed has a return loss below $-10\,\mathrm{dB}$ and an insertion loss above $-3\,\mathrm{dB}$ over a frequency range of $0.5\,\mathrm{GHz}$ to $40\,\mathrm{GHz}$. The paper will discuss the results of full-wave field analyses, fabrication and measurements.

Statistical Analysis of the Return Loss Performance of a Microprocessor Package Vertical Interconnect

Arun V. Sathanur[1], **Vikram Jandhyala**[1], **and Henning Braunisch**[2]

[1]Department of Electrical Engineering, University of Washington, Seattle, WA, USA
[2]Components Research, Intel Corporation, Chandler, AZ, USA

Abstract— Design of package- and board-level interconnects utilizing full-wave electromagnetic solvers is becoming increasingly important owing to increased frequencies of operation. With increasing density of components, subsequent miniaturization and design at the edge, manufacturing tolerances significantly affect the performance of interconnect based structures. Thus, it is important to compute the spread of the objective function around the optimized design. Our previous work [1–3] deals with methodologies for optimization of the return loss performance in microprocessor vertical interconnects. The same framework is extended to account for the manufacturing tolerances that produce a spread in the performance measure around the optimum value.

In this work, a total of 60 independent variables, representing geometry and electrical features of a differential microprocessor package vertical interconnect line, have been used in the statistical analysis. All these variables are assumed to be independent Gaussian random variables. Correlation information if available can be handled using appropriate linear transformations. The non-Gaussian input probability density functions (PDFs) can be handled through explicit Monte-Carlo runs using the closed-form expression developed.

In the absence of any analytical relationships between the objective functions and the geometry variables, there is a need to develop approximated closed-form expressions relating them, to facilitate PDF extraction. A two-level linear regression [4] needs 2^n simulations for n variables and such an approach becomes impracticable in this case. Alternatively, a multivariate Taylor series approach that retains only the linear terms in the relationship between the objective function and the geometry parameters is utilized. Using this approach accurate linear models can be developed by utilizing $(2n+1)$ simulations. For a vector of n input geometry variables, this results in the linear relationship

$$y(\omega) = y_0(\omega) + \nabla y(\omega) \cdot \Delta x = y_0(\omega) + \sum\nolimits_{i=1}^{N} a_i(\omega)\Delta x_i \tag{1}$$

where $a_i(\omega) = \partial y(\omega)/\partial x_i$ and ω is the angular frequency. Over small ranges of the variables, such a linear model can be adequate for modeling the differential return loss of a package line. The a_i are determined through accurate finite-difference computation and (1) is used to derive the PDFs of the performance objective functions, compute yield measures and also predict the spread in the performance objective function over a range of frequencies.

REFERENCES

1. Sathanur, A. V., V. Jandhyala, K. Aygun, H. Braunisch, and Z. Zhang, "Optimization of vertical interconnect of a microprocessor package using a fast full-wave electromagnetic analysis tool," *Progress In Electromagnetics Research Symposium Abstracts*, 388, Cambridge, MA, July 2–6, 2008.
2. Sathanur, A. V., V. Jandhyala, K. Aygun, H. Braunisch, and Z. Zhang, "Return loss optimization of the microprocessor package vertical interconnect," *Proc. IEEE Electronic Components Technol. Conf. (ECTC)*, 1636–1642, San Diego, CA, May 26–29, 2009.
3. Sathanur, A. V., V. Jandhyala, and H. Braunisch, "A two-level optimization scheme for bandwidth optimization of a microprocessor vertical interconnect," *Proc. IEEE Electrical Performance of Electronic Packaging and Systems (EPEPS)*, 133–136, Portland, OR, October 18–21, 2009.
4. Gu, X., A. Ruehli, and M. Ritter, "Impedance design for multi-layered vias," *Proc. IEEE Electrical Performance of Electronic Packaging and Systems (EPEPS)*, 317–320, San Jose, CA, October 27–29, 2008.

Modeling of Electromagnetic Wave Propagation in Printed Circuit Board Transmission Lines with Rough Conductors

M. Y. Koledintseva[1], A. Koul[1], J. L. Drewniak[1], M. Wang[2], R. Qiang[2], and J. Chen[2]

[1]Missouri University of Science and Technology, Rolla, MO, USA
[2]University of Houston, Houston, TX, USA

Abstract— EMC and SI engineers need accurate characterization of commercially available printed circuit boards, since they must provide proper technical characteristics of their designs and reduce cost-to-quality ratio. Adequate methods of PCB parameters characterization are also important for manufacturers of PCBs to improve their technological processes and products. Typically, PCB substrate dielectrics are described in terms of their dielectric constant (Dk), which is the same as its real relative permittivity ε'_r, and the dissipation factor (Df), equal to its loss tangent $\tan\delta = \varepsilon''_r/\varepsilon'_r$ [1].

The present-day multilayer PCBs for applications in the frequency range up to ~ 40 GHz typically employ fiber-glass filled epoxy resin composites as substrates. Copper foils used for PCB conductors are intentionally rough (at least on one of the foil's sides roughness is on the order of 1–10 μm) for better adhesion with a dielectric substrate [2]. Hence copper foil roughness is comparable or greater than the skin-depth. Surface roughness significantly contributes to conductor loss as a part of total attenuation α on a line. Due to surface roughness, conductor loss behavior deviates from the behavior as $\sim \sqrt{\omega}$ typical for smooth conductors [3]. This is a consequence of deviation from TEM mode propagation: conductor roughness may cause local excitation of surface waves and higher-order modes, which would contribute to total attenuation and affect the propagation constant of the main TEM mode. All these factors make it difficult to separate conductor loss from dielectric loss, and affect accuracy of dielectric substrate characterization using travelling-wave methods.

Another problem arises due to the fact that any PCB dielectric is not homogeneous, though it is characterized by an effective (averaged) value of complex permittivity $\varepsilon = \varepsilon' - j\varepsilon''$. Indeed, signal trace is typically surrounded by epoxy resin layer, and the space between conductors is filled by the woven structure of fiber glass bundles within a polymer (resin) host. This inhomogeneity is another source of deviation from the TEM mode propagation. Due to layered structure, substrate dielectrics are not isotropic either. Their reference or measured effective Dk and Df data are typically given only for one direction (in-plane or out-of-plane), depending on the main E-field orientation in a measurement technique.

The full-wave numerical model using the array-scanning-method (ASM) FDTD codes developed in the University of Houston for a realistic stripline structure is presented. The roughness of the surface is modeled as infinite periodic repetition in the propagation direction. Using periodic modeling technique, only single periodic element needs to be modeled. The particular stripline modeled here contains a signal trace made of a periodically rough conductor and surrounded by an epoxy resin coat. Outside the epoxy resin layer there is a composite fiber-glass epoxy resin dielectric with effective permittivity. The numerical model provides attenuation and propagation constants for a section of this line. The results are compared with an analytical electromagnetic model which treats rough metal surface and epoxy resin coat through complex surface impedance additional to conventional skin-effect surface resistance.

REFERENCES

1. Koul, A., P. K. R. Anmula, M. Y. Koledintseva, J. L. Drewniak, and S. Hinaga, "Improved technique for extracting parameters of low-loss dielectrics on printed circuit boards," *Proc. IEEE EMC Symp.*, 191–196, Austin, TX, 2009.
2. Hinaga, S., M. Koledintseva, P. Anmula, and J. Drewniak, "Effect of conductor surface roughness upon measured loss and extracted values of PCB laminate material dissipation factor," *Proceedings of the Technical Conference*, S20–2, IPC Expo/APEX 2009, Las Vegas, USA, Mar. 31–Apr. 2, 2009.
3. Koledintseva, M. Y., A. Koul, P. K. R. Anmula, J. L. Drewniak, S. Hinaga, E. Montgomery, and K. N. Rozanov, "Separating dielectric and conductor loss for rough striplines in printed circuit boards," *Progress In Electromagnetics Research Symposium Abstracts*, 213–214, Moscow, Russia, Aug. 18–21, 2009.

Metallic Rough Surface Effect on Signal Integrity of High-speed Interconnect by Small Perturbation Method in 3D Waveguide Structure

Ruihua Ding[1], **Leung Tsang**[1], **and Henning Braunisch**[2]

[1]Box 352500, Department of Electrical Engineering
University of Washington, Seattle, WA 98195, USA
[2]Components Research, Intel Corporation, Chandler, AZ 85226, USA

Abstract— A three-dimensional (3D) parallel-plate waveguide model excited by a line source is developed to study the rough surface effect on signal integrity in high speed interconnects. The root mean square (RMS) height of the rough surface between traces and substrate layers can be as large as 1 micron. At multi-gigahertz frequencies, the rough surface causes signal integrity problems such as acerbated attenuation, increased surface resistivity and reduced effective conductivity, since the skin depth is comparable to the RMS height.

The current work is in extension of our previous work that dealt with a two-dimensional (2D) parallel-plate waveguide model with one-dimensional rough surface [1, 2]. In this paper, a 3D parallel-plate waveguide model is built to study the rough surface effect in a waveguide structure environment for signal traces. The top plate of the waveguide is a smooth perfect electric conductor (PEC). The bottom plate is a finite-conductivity plate with 2D rough surface characterized by a stationary random process. The random rough surface profile is characterized by its 2D power spectral density (PSD) function with RMS height and correlation length included. Typical analytical PSD functions are Gaussian, Exponential and Generalized PSDs, with the latter covering PSDs ranging between Gaussian and Exponential. The problem is formulated based on the 3D extinction theorem. The unknowns are the tangential electric and magnetic fields along the rough interface. The Green's functions are Dyadic Green's functions. Small perturbation method (SPM) to the 2nd order is applied to solve the resulting vector equations. The 0th order SPM solution is shown to agree with the solution for a smooth parallel-plate waveguide structure. The 2nd order SPM solution obtained is a multiple Sommerfeld integral. The special case of isotropic surface roughness is considered and approximation of the Sommerfeld integral is studied to give a solution that can be calculated expediently. The enhancement factor, defined as the rough surface power loss over the smooth surface power loss and directly related to metrics of practical interest, is used to quantify the rough surface effect. At the end of this paper, the enhancement factors obtained by waveguide model and plane-wave model [3] are compared with each other.

REFERENCES

1. Ding, R., L. Tsang, and H. Braunisch, "Wave propagation in a randomly rough parallel-plate waveguide," *IEEE Trans. Microwave Theory and Tech.*, Vol. 57, No. 5, 1216–1223, May 2009.
2. Ding, R., L. Tsang, and H. Braunisch, "Rough surface effects in parallel plate waveguide at gigahertz frequencies," *Proc. IEEE Electronic Components Technol. Conf. (ECTC)*, 1132–1138, San Diego, CA, May 26–29, 2009.
3. Gu, X., L. Tsang, and H. Braunisch, "Modeling effects of random rough interface on power absorption between dielectric and conductive medium in 3-D problem," *IEEE Trans. Microwave Theory and Tech.*, Vol. 55, 511–517, Mar. 2007.

Session 3A5
Generation, Propagation and Applications for Special Laser Beams

Spectral Shift of an Electromagnetic Gaussian Schell-model Beam

Shijun Zhu and Yangjian Cai
School of Physical Science and Technology, Soochow University, Suzhou 215006, China

Abstract— Spectral changes of an electromagnetic Gaussian Schell-model beam focused by a thin lens are investigated by using a tensor method. It is shown that the spectral shift is mainly determined by the degree of polarization, twist phase and correlation coefficients of the initial beam. Generically the blue shift occurs at on-axis points, while the red shift can occur at off-axis points.

Generation of Hollow Beam and Vortex Beams by Multimode Fibers

Xuanhui Lu, Kaikai Huang, and Yunfeng Jiang
Department of Physics, Institute of Optics, Zhejiang University, Hangzhou 310027, China

Abstract— A novel method to generate hollow beam and vortex beams in experiment is demonstrated in this paper. The laser is used to enter a misaligned multimode fiber, at the output end of the fiber; hollow beams can be obtained. When relatively big misaligned coupling multimode fiber the vortex beam with helical wave front can be generated. By changing the misaligned angle or position, vortex beams with different topological charges can be obtained. The properties of the hollow beam and vortex beam depend on not only the tilt angle and location of the input beam on the front surface of the fiber, but also the length and core diameter of the fiber.

A Fiber Optic Evanescent Wave Sensor for Measuring Refractive Index Change of Liquids

Chenghua Sui, **Pinghui Wu**, **and Gaoyao Wei**
Institute of Laser and Optoelectronic Technology
Zhejiang University of Technology, Hangzhou 310023, China

Abstract— In the past few years, evanescent-field-based optical sensors have been under intensive investigation for deployment as biological and/or chemical sensors. For these applications, small size, high sensitivity, high selectivity, and low detection limits are the dominant requirements. Optical microfiber sensors meet all these criteria due to they have excellent properties such as low cost, low loss, and very large evanescent fields. Among the various sensing schemes, refractive index sensing is widely employed since many biological or chemical specimens can be indentified by measuring their refractive indices. However, in free space the fabrication of these microfibers with high reliability is challenging due to problems of stability, degradation, coupling, and cleanness. In this paper we demonstrate a robust evanescent wave sensor capable of detecting small refractive index change of liquids using single microfiber. Compared with the multiple-microfiber scheme that relies on the average response of many microfibers, single microfiber detection presents special advantages of high sensitivity and fast response. Here the sensor is based on the principle of superheterodyne frequency modulation technique and is used to measure the variation of refractive index with concentration of glucose in distilled water. The schematic diagram of the sensor is shown in Fig. 1. The experimental data were obtained with the sensor and calculated is plotted in Fig. 2. It is clear that the measured and theoretical values are in quite close agreement. In particular, the device has a higher sensitivity than common sensor and can measure an index variation of $\sim 10^{-5}$ with high repeatability. In addition, to study the sensor characteristics of the sensor, the important parameters, including sensitivity and detection limit, are also estimated. The sensor reported here is featured with high sensitivity, easy fabrication, compact size, and easy integration with optoelectronic devices, which make it suitable for bio/chemical analyses, pharmaceutical and process control.

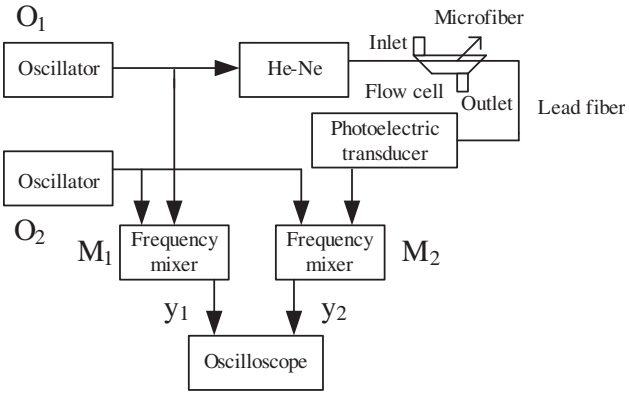

Figure 1: Schematic of the sensor.

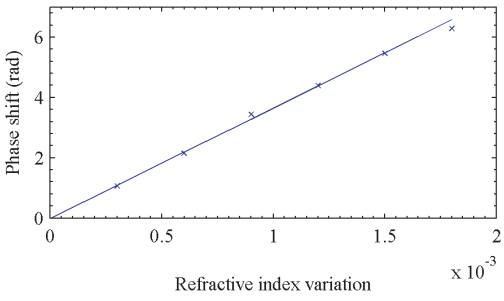

Figure 2: Comparison of experimental (×) and theoretical (solid line) phase shifts as a function the refractive index variation.

Lorentz and Lorentz-gauss Beams in Uniaxial Crystals

Chengliang Zhao and Yangjian Cai
School of Physical Science and Technology, Soochow University, Suzhou 215006, China

Abstract— Paraxial propagation of Lorentz and Lorentz-Gauss beams in uniaxial crystals orthogonal to the optical axis is investigated based on the beam propagation equations. Analytical propagation formulae for Lorentz and Lorentz-Gauss beams in uniaxial crystals are derived. The derived propagation formulae reduce to the propagation formulae for Lorentz and Lorentz-Gauss beams in free space under certain condition. The propagation properties of Lorentz and Lorentz-Gauss beams in uniaxial crystals and in free space are studied numerically and comparatively. It is found that the propagation properties of Lorentz and Lorentz-Gauss beams in uniaxial crystals behave much different from those in free space, and are closely determined by the parameters of the uniaxial crystals. The uniaxial crystals provide an effective way for generating astigmatic beams.

Wireless Fiber Laser Sensor Combining Photonic Generation Beat Frequency Demodulation Technology

Shengchun Liu[1, 2], **Zuowei Yin**[1], **Liang Gao**[1], **Liang Zhang**[1], **and Xiangfei Chen**[1]

[1]Nanjing National Laboratory of Microstructures, Nanjing University, Nanjing 210093, China
[2]Institute of Fiber Optics, Heilongjiang University, Harbin 150080, China

Abstract— Recent advances of radio frequency (RF) wireless communication and micro-electro-mechanical systems (MEMS) technology make wireless sensor net achieve great development for low-cost, large-scale, multifunctional sensor system. Therefore the wireless sensors have attracted tremendous interest for many important applications [1]. However, the wireless sensor seems helpless in some strong electro-magnetic interferency (EMI) fields and mass data transmission and process fields, because it is susceptible to EMI and the bandwidth of the wireless communication is very limited. However, the fiber sensor is immune to the EMI and its bandwidth is large. In Ref. [2], Liu et al. has proposed wireless fiber sensor system for strain and pressure measurement. But the system needs complicated phase demodulation for sending and receiving wireless data.

In this paper, a wireless fiber laser sensor (WFLS) system based on multi-longitudinal mode fiber laser is designed and fabricated. Fig. 1 shows the schematic setup of the proposed WFLS system. The laser resonator is formed by a piece of erbium doped fiber (EDF) and two wavelength-matched fiber Bragg gratings (FBGs). When the 980 nm pump power is strong enough, there are many longitudinal modes established with resonant frequency spacing of ν in the laser cavity. A beat frequency signal can be generated between any two modes of the laser by optic interference and it is used as sensing signal. The light containing beat sensing information is converted into electrical beat signals on the photodetector (PD). The electrical beat signals constitute with many beat signals that the frequencies are from tens of MHz to over 3 GHz. A RF band filter with the center frequency of 2.4 G is added after the PD so that only the beat signal of 2.4 GHz can pass nearly losslessly and then the amplified beat signal is sent by the transmission antenna. The receiving antenna receive this signal which is detected by the FSA after the RF band filter and RF amplifier. The beat frequency shift with the strain can be expressed as follows:

$$f_b = -n\frac{c}{2nL}\left(\frac{\delta n}{n} + \frac{\delta L}{L}\right) = -n\nu\left(\frac{\delta n}{n} + \frac{\delta L}{L}\right) = -n\nu(1 - P_e)\varepsilon \tag{1}$$

where P_e is the photoelastic constant, ε is the applied strain, and n is the number of resonant frequency spacing between two modes. Thus the strain can be monitored by measuring the beat frequency using the WFLS system.

Using this WFLS system, the strain sensing performance is tested. The results obtained from the WFLS system and the comparison with the wire fiber sensor system are shown in the full-length paper. The experimental strain sensitivities of wireless and wire sensor are 1.9 kHz/$\mu\varepsilon$ and 1.95 kHz/$\mu\varepsilon$, respectively. These are in good agreement with the theoretical prediction. The strain accuracies of the wire and wireless sensor are 2.1 $\mu\varepsilon$ and 3.9 $\mu\varepsilon$, respectively. The result indicates that the wireless sensor system has little signal distortion. We can also make use of existing 2 G/3 G mobile communications network composed of more powerful wireless sensor

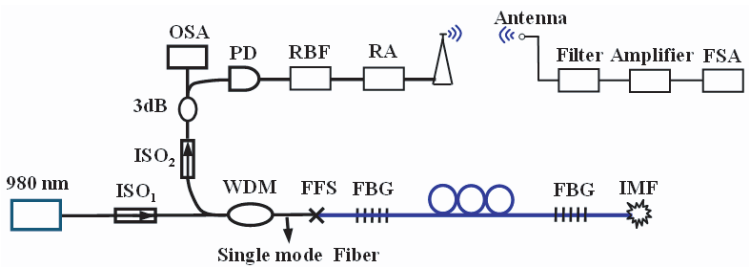

Figure 1: Experimental setup of the wireless fiber laser sensor. WDM: wavelength division multiplexer; ISO: isolator; 3 dB: 3 dB fiber coupler; OSA: optical spectrum analyzer; FFS: fiber fusion splicer; IMF: index-matching fluid; RBF: RF band filter; RA: RF amplifier.

network in 2 G/3 G standard band. Future work is needed to decrease the noise which comes from the perturbation of the wireless.

REFERENCES

1. Pottie, G. J. and W. J. Kaiser, *Communications of the ACM*, Vol. 43, No. 5, 551–558, 2000.
2. Liu, Y., et al., "Fiber optic sensors and applications V," *Proc. of SPIE*, Vol. 6770, 67700Y, 2007.

Ultrasonic Wave Detection in Atmospheric Pressure Plasma Using Fraunhofer Diffraction Effect

Toshiyuki Nakamiya[1], **Fumiaki Mitsugi**[2], **Shota Suyama**[2], **Tomoaki Ikegami**[2], **Yoshito Sonoda**[1], **Yoichiro Iwasaki**[1], **and Ryoichi Tsuda**[1]

[1]Graduate School of Industrial Engineering, Tokai University
Toroku 9-1-1, Kumamoto 862-8652, Japan
[2]Graduate School of Science and Technology, Kumamoto University
Kurokami 2-39-1, Kumamoto 860-0082, Japan

Abstract— Most of electric discharges emit acoustic ($20 \sim 20,000$ Hz) and ultrasonic (over 20 kHz) waves. Continuous and pulsed voltages initiate the electric breakdown which generates pressure deviation from equilibrium pressure. The sound waves are generated by the pressure change causing local compression and rarefaction. In our study, we measured applied voltage, current and electrical discharge sound, and examine the fundamental relationship between the discharge states and acoustic properties. The sound and ultrasonic waves include the information about discharge and the atmospheric condition around discharge. We have previously used a conventional condenser microphone to detect the discharge sound. However, the condenser microphone was not enough to detect the discharge sound because it could not detect the ultrasonic wave especially more than 100 kHz which may be generated by the pulsed discharge. In addition, it was not suitable to set the condenser microphone between or near the electrodes of the discharge device because it affects the electric field between the electrodes. Therefore, we have applied a new diagnostic method of an optical wave microphone [1]. The optical wave microphone is based on Fraunhofer diffraction between the sound wave and the laser beam. We expect that the understanding of acoustic and ultrasonic properties gives more details of electric discharge and also develops new applications in medical diagnostics, environments systems and so on.

REFERENCES

1. Nakamiya, T., Y. Sonoda, T. Ikegami, F. Mitsugi, K. Ebihara, and R. Tsuda, "Measurement of electric discharge sound by Fraunhofer diffraction and analysis," *PRZEGLAD ELEKTROTECHNICZNY (Electrical Review)*, Vol. 5, 143–146, 2009.

Partially Coherent Standard and Elegant High-order Beams in Turbulent Atmosphere

Fei Wang and Yangjian Cai
School of Physical Science and Technology, Soochow University, Suzhou 215006, China

Abstract— Propagation properties of partially coherent standard and elegant higher-order beams in turbulent atmosphere are investigated based on the extended Huygens-Fresnel integral. Explicit and analytical formulae are derived for the cross-spectral densities of partially coherent standard and elegant higher-order beams propagating in turbulent atmosphere. The average intensity and spreading properties of partially coherent standard and elegant higher-order beams in turbulent atmosphere are studied numerically. We find that partially coherent standard and elegant higher-order beams are less affected by the atmospheric turbulence than coherent standard and elegant higher-order beams, which has potential application in free-space optical communications.

The Study of the Radiation Force Caused by Different Laser Beams

Xuanhui Lu, **Kaikai Huang**, **Yuna Liu**, **and Yunfeng Jiang**
Department of Physics, Zhejiang University, Hangzhou 310027, China

Abstract— Optical tweezers, also known as a single beam gradient force optical trap, which a three-dimensional potential caused by high focused laser beam to trap and manipulate micro particles, including dielectric particles, metallic particles, biological cells and viruses etc. Different types of laser beams have been generated with the development of laser technology. These beams all have their properties. Therefore, the particles trapped by these beams would show different phenomena. So we should choose the different light beams to manipulate and trap the particles for different applications when we design devices of the optical tweezers. In this report, we reviewed the trapping, manipulating and guiding of the applications with different beams. Theoretical analysis of radiation force of different beams has been introduced. Finally, the outlook and the applications of the optical tweezers have been also introduced.

Session 3A6a
Photonic Crystals and Metamaterials 3

Dielectric-dielectric Composite Photonic Crystals for Negative Refraction of Unpolarized Electromagnetic Waves

N. Yogesh and V. Subramanian
Microwave Laboratory, Department of Physics
Indian Institute of Technology Madras, Chennai-600 036, India

Abstract— The investigations on negative refraction of unpolarized microwaves in dielectric-dielectric composite photonic crystals are presented. Similar to the metal-dielectric photonic crystals, common negative refraction regime for both polarization modes (transverse electric and transverse magnetic) are also found in these dielectric composites. This paper further investigates the beam steering ability of an unpolarized microwave in these composites by analysing the angular dispersion characteristics of both polarization modes. One can utilize this beam steering aspect in the fields of far-field imaging and microwave devices.

Magnetoplasmonics: Fundamentals and Applications

A. García-Martín, **G. Armelles**, **A. Cebollada**, **J. M. García-Martín**, **M. U. González**, **J. B. González-Díaz**, **J. F. Torrado**, **E. Ferreiro-Vila**, **and D. Martín-Becerra**
Instituto de Microelectrónica de Madrid (IMM-CNM-CSIC)
Isaac newton 8, Tres Cantos, 28770 Madrid, Spain

Abstract— Subwavelength composite materials constitute an interesting path towards the development of materials with "on demand" optical properties. We will present our latest results on systems composed of both noble and ferromagnetic metals, which we denote as magnetoplasmonic systems. While noble metals have intense and narrow plasmon resonances they lack magneto-optical (MO) activity at reasonable magnetic field intensities. On the other hand, ferromagnetic metals are MO active but their plasmon resonances are weak and broad. By combining both kinds of materials we intend to obtain systems which simultaneously exhibit plasmon resonances and MO activity. We will show that thus it is possible both to enhance the magneto-optical activity of the system via surface plasmon excitation, and to modulate the plasmon properties via application of a magnetic field [1].

First we will analyze concentrate the MO response of Au/Co/Au nanodiscs [2], where we will show how the excitation of a localized surface plasmon (LSP) produces an enhancement of the electromagnetic field within the MO active layer, leading to an enhancement of the MO activity. The same influence of the LSP on the MO properties can be observed when the constituents responsible for plasmon excitation and MO activity are spatially separated (structures formed by Au nanodiscs and Au/Co/Au continuous trilayers separated by layers of SiO_2 [3]).

The same system will allow the analysis of the effect of the MO activity on the plasmon properties. We will show that the wavevector of the surface plasmon polariton is the physical magnitude which is modified upon application of a magnetic field in the transverse configuration [4]. That modification can be used in a wide variety of scenarios. Here we will discuss its application in active microinterferometry and biosensing.

REFERENCES

1. Armelles, G., et al., *J. Opt. A: Pure Appl. Opt.*, Vol. 11, 114023, 2009.
2. González-Díaz, J. B., et al., *Small*, Vol. 4, 202, 2008.
3. Armelles, G., et al., *Opt. Express*, Vol. 16, 16104, 2008.
4. González-Díaz, J. B., et al., *Phys. Rev. B*, Vol. 76, 153402, 2007.
5. Ferreiro-Vila, E., et al., *Phys. Rev. B*, Vol. 80, 125132, 2009.

Plasmonic Crystals for Reproducible SERS Detection

S. Foteinopoulou[1, 2] and J. P. Vigneron[2]

[1]School of Physics, University of Exeter, Stocker Road, Exeter EX4 4QL, United Kingdom
[2]Laboratoire de Physique du Solide (LPS), Facultes Universitaires Notre-Dame de la Paix (FUNDP)
61 rue de Bruxelles, B-5000 Namur, Belgium

Abstract— The intensity of the electromagnetic field can experience enhancement by several orders of magnitude in the vicinity of metal nanostructures. Such enhancement can offer substantial magnification to Raman signals which are typically very weak. Therefore different types of metallic nanostructure based substrates are routinely employed in SERS detection platforms. Nevertheless, Raman signals of the same analytes are often irreproducible and have depolarization ratios that depend on the intensity of the illuminating laser beam [1]. The results in [1] suggest that an important factor in SERS detection which has been thus far overlooked is the polarization of the enhanced field.

In this talk, we analyze how the polarization of the enhanced near-field influences the reproducibility of the SERS spectra. We have employed the Finite Difference Time Domain (FDTD) technique for this investigation, with the Auxiliary Differential Equation (ADE) to model the plasmonic response of the metal at visible frequencies [2]. To evaluate the validity of the numerical results we have compared them with analytical Mie calculations for the single scatterer cases and have found excellent agreement [3]. Our studies indicate that in general the polarization of the enhancement around single metal spheres is very different from the polarization of the excitation source and in addition it is location dependent. On the other hand, nanoparticle dimers fix the polarization of the enhanced field along the dimer axis regardless the polarization of the excitation source [3]. We discuss how to employ such building blocks for the design of optimum SERS substrates.

REFERENCES

1. Etchegoin, P. G., C. Galloway, and E. C. Le Ru, "Polarization-dependent effects in surface-enhanced Raman scattering (SERS)," *Phys. Chem. Chem. Phys.*, Vol. 8, No. 22, 2624–2628, 2006.
2. Taflove, A. and S. C. Hagness, *Computational Electrodynamics: The Finite-difference Time-domain Method*, 3rd Edition, Artech House, 2005.
3. Foteinopoulou, S., J. P. Vigneron, and C. Vandenbem, "Optical near-field excitations on plasmonic nanoparticle-based structures," *Opt. Express*, Vol. 15, No. 7, 4253–4267, 2007.

FDTD Analysis of the Stealth Property of Metamaterials Based on Drude Model

Shi-Quan Zhang[1, 2], **Jian-Ping Liu**[1, 2], **Cong Chen**[1], **and Bing Wei**[2]

[1]Engineering College of CAPF, Xi'an, Shaanxi Province 710086, China
[2]Department of Physics, Xidian University, Xi'an, Shaanxi Province 710071, China

Abstract— In recent years, there has been a growing interest for the study of target stealth technique, while the special properties of left-handed metamaterials with negative values of permittivity and permeability exhibit brilliant prospect for applications in target stealth. In this paper, the electromagnetic scattering properties of the object such as metamaterial-coated metallic circular cylinder are analyzed and discussed by using finite-difference time-domain method (FDTD) based on Drude model.

The constitutive parameters of metamaterials are the function of frequency, hence, metamaterials are surely dispersive media. Their effective permittivity and permeability can be expressed in terms of lossy Drude model as follows:

$$\varepsilon(\omega) = \varepsilon_0\varepsilon_r(\omega) = \varepsilon_0\left(1 - \frac{\omega_{pe}^2}{\omega(\omega + \mathrm{j}\Gamma_e)}\right),$$
$$\mu(\omega) = \mu_0\mu_r(\omega) = \mu_0\left(1 - \frac{\omega_{pm}^2}{\omega(\omega + \mathrm{j}\Gamma_m)}\right).$$

The following electromagnetic field equations are derived and obtained by applying Maxwell's vortex equations and time-frequency relation:

$$\nabla \times H = \varepsilon_0\frac{\partial E}{\partial t} + J_e,$$
$$\nabla \times E = -\mu_0\frac{\partial H}{\partial t} - J_m,$$
$$\frac{\partial J_e}{\partial t} + \Gamma_e J_e = \varepsilon_0\omega_{pe}^2 E,$$
$$\frac{\partial J_m}{\partial t} + \Gamma_m J_m = \mu_0\omega_{pm}^2 H.$$

The above equations are discretized, two-dimensional recursive formulas are derived, and FDTD programs for both the metallic and metamaterial-covered targets are compiled. The radar cross sections (RCS) for metallic and metamaterial-coated metallic circular cylinders are computed. It is demonstrated that the backward scattering is reduced within a wide range of frequency band and the the RCS resonance region in the vicinity of the backward field is greatly expanded, in the mean time, the forward scattering is promoted significantly, when the target is coated with metamaterials. Therfore, it is obvious that the metamaterials take an active role in stealth applications.

Anomalous Infrared Transmission through Superconducting Structures

Oleg L. Berman[1], **Vladimir S. Boyko**[1], **Roman Ya. Kezerashvili**[1, 2], **and Yurii E. Lozovik**[3]

[1]Physics Department, New York City College of Technology
The City University of New York, Brooklyn, NY 11201, USA
[2]The Graduate School and University Center
The City University of New York, New York, NY 10016, USA
[3]Institute of Spectroscopy, Russian Academy of Sciences
142190 Troitsk, Moscow Region, Russia

Abstract— Anomalous far infrared monochromatic transmission across a lattice of Abrikosov vortices in a type-II superconducting film is predicted [1]. The transmitted frequency corresponds to the photonic mode localized by the defects of the Abrokosov lattice. These defects are formed by extra vortices placed out of the nodes of the ideal Abrokosov lattice shown on Fig. 1. The extra vortices can be pinned by crystal lattice defects of a superconductor. The corresponding frequency is studied as a function of magnetic field and temperature. The corresponding problem is reduced to the Dirac-type two-band model. While our approach is valid for all type-II superconductors, the specific calculations have been performed for the $YBa_2Cu_3O_{7-\delta}$ (YBCO). The control of the transmitted frequency by varying magnetic field and/or temperature is analyzed. It is suggested that found anomalously transmitted localized mode can be utilized in the far infrared monochromatic filters. Besides, anomalous infrared monochromatic transmission through a superconducting multiple conductor system consisting of parallel superconducting cylinders is found [2]. The transmitted frequency corresponds to the localized photonic mode in the forbidden photonic band, when one superconducting cylinder is removed from the node of the ideal two-dimensional lattice of superconducting cylinders. The corresponding frequency was calculated for the $YBa_2Cu_3O_{7-\delta}$ superconducting cylinders.

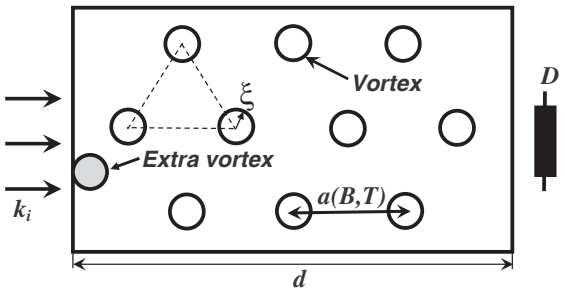

Figure 1: Anomalous far infrared monochromatic transmission across a film of type-II superconductor in the magnetic field (the vortices are aligned along the field). $a(B,T)$ is the equilateral triangular Abrikosov lattice spacing. ξ is the coherence length and the radius of the vortex. d denotes the length of the film. The shaded extra vortex placed near the boundary of the film and situated outside of the node of the lattice denotes the defect of the Abrikosov lattice.

REFERENCES

1. Berman, O. L., V. S. Boyko, R. Y. Kezerashvili, and Y. E. Lozovik, *Phys. Rev. B*, Vol. 78, 094506, 2008.
2. Berman, O. L., V. S. Boyko, R. Y. Kezerashvili, and Y. E. Lozovik, *Laser Phys.*, Vol. 19, 2035, 2009.

Optical Transmission through a Vortex Lattice in a Film of Type-II Superconductor

Oleg L. Berman[1], **Yurii E. Lozovik**[2], **Maria V. Bogdanova**[2], **Anton A. Kolesnikov**[2], **and Rob D. Coalson**[3]

[1]Physics Department, New York City College of Technology
The City University of New York, Brooklyn, NY 11201, USA
[2]Institute of Spectroscopy, Russian Academy of Sciences
142190 Troitsk, Moscow Region, Russia
[3]Department of Chemistry, University of Pittsburgh
Pittsburgh, PA 15260, USA

Abstract— We study the effect of anomalous optical transmission through (along) an array of vortices in a type-II superconducting film in a strong magnetic field. The photonic crystals formed by superconductors have been analyzed [1–3]. The mechanism responsible for this effect is resonance transmission between two surface plasmon polaritons (SPP) on the opposite surfaces of the film [4]. The SPP band gap in the system is studied as a function of magnetic field and temperature (Fig. 1). Control of transmission by varying magnetic field and/or temperature is analyzed. The conditions which are necessary for the anomalous transmission of an electromagnetic wave through an array of vortices in a film of type-II superconductor have been analyzed. Under double-resonance conditions, resonant tunneling between surface plasmon polariton states at the two interfaces leads to enhancement of the transmission efficiency. The light-transmission through the single finite length Abrikosov vortex cylinder embedded in a film of metallic phase has been calculated using the Finite-Difference Time-Domain (FDTD) method. By changing the external magnetic field and temperature one can control the period of the Abrikosov lattice, and hence the SPP band gap, the transmittance and the resonance frequency for the enhancement of the optical transmission in a film on a substrate.

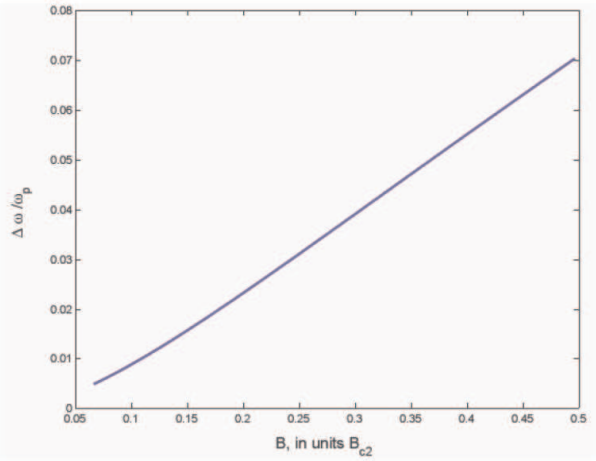

Figure 1: Upper and lower frequencies of the first SPP band gap at $(T_C - T)/T_C = 0.022$. Solid curve corresponds to ω_0; dotted curve to ω_a; dashed curve to ω_b.

REFERENCES

1. Berman, O. L., Y. E. Lozovik, S. L. Eiderman, and R. D. Coalson, *Phys. Rev. B*, Vol. 74, 092505, 2006.
2. Berman, O. L., V. S. Boyko, R. Y. Kezerashvili, and Y. E. Lozovik, *Phys. Rev. B*, Vol. 78, 094506, 2008.
3. Berman, O. L., V. S. Boyko, R. Y. Kezerashvili, and Y. E. Lozovik, *Laser Phys.*, Vol. 19, 2035, 2009.
4. Berman, O. L., Y. E. Lozovik, M. V. Bogdanova, and R. D. Coalson, submitted to *Phys. Rev. B*.

Session 3A6b
Electromagnetic Science and Design on The Optical Dispersive Metamaterials, Invisible Cloak and Photonic Crystals

Light Scattering from 3-D Nanoscale Disordered Media

G. Berginc[1] and C. Bourrely[2]

[1]THALES, 2 Avenue Gay Lussac, 78995 Elancourt Cedex, France
[2]Center for Theoretical Physics, CNRS-Luminy Case 90, 13288 Marseille Cedex 9, France

Abstract— Understanding how light interacts with random structures at the nano/micrometer scale is a fundamental issue in optoelectronics and photonics and has huge consequences for applications in communications, life sciences, imaging and sensing. Designing these disordered slabs can produce new optical components, which can transmit or scatter optical field with specified angular, spatial or spectral properties. The complete evaluation and definition of potential novel applications of such devices will require intensive theoretical modeling of light scattering by such random media.

In this paper, we consider a three-dimensional disordered medium with randomly rough interfaces. This structure describes a device based on metallic nanoparticles embedded in insulators or dielectric media. We gave in an explicit way [1–2] the theoretical formulas, which describe the light scattering from a disordered medium with rough surfaces. In this paper, we present a theory of transport based on the Bethe-Salpeter equation. The calculation of the intensities scattered by the considered structure for the ladder and most-crossed contributions is given by a Green tensor, which satisfies a Bethe-Salpeter equation. Diagrammatic expansions proved to be very useful for investigation of mesoscopic effects. Since we are unable to obtain an exact expression of the Green tensor for practical calculations, we rely on a perturbative method. In a previous approach [1], we considered the first-order perturbative expansion. Most of the study presented here is centered on the formulations of the second-order expansion of the Green tensor [3–4] to calculate the incoherent cross-section for a disordered slab with randomly rough interfaces. This order corresponds to a third-order approximation for the scattering cross-section. In this paper, we consider different objectives. We study the backscattering enhancement and the different phenomena due to the random medium and the randomly rough surfaces. Therefore, we calculated the incoherent cross-sections in the case of metallic or dielectric scatterers. These calculations were performed with the Mueller matrices taking into account the different polarization components. For these computations, we explored the effects of the different parameters which characterize the random medium and the rough surfaces. We observed interference effects, backscattering enhancement peaks for different examples in the case of the most-crossed contributions. Due to the large differences in the orders of magnitude of the computed quantities, a special attention must be paid to the precision in the calculation of multiple integrals. We also give numerical examples in the case of metallic particles with a large volume fraction, and media with two types of metallic particles. Scattering phenomena related to the presence of nano-components in biological tissues will be examined.

REFERENCES

1. Soubret, A. and G. Berginc, "Electromagnetic wave scattering from a random layer with rough interfaces II: Diffusive intensity," arXiv:physics/0312136, 2003.
2. Berginc, G. and C. Bourrely, "Electromagnetic wave scattering from a random layer with randomly rough interfaces," *Progress In Electromagnetics Research Symposium Abstracts*, 88, Prague, Czech Repulic, August 27–30, 2007.
3. Berginc, G. and C. Bourrely, "Electromagnetic wave scattering from a random layer with rough interfaces I: Multiple scattering theory," *Progress In Electromagnetics Research Symposium Abstracts*, 197, Cambridge, USA, July 2–6, 2008.
4. Berginc, G. and C. Bourrely, "Electromagnetic wave scattering from a random layer with rough interfaces II: Numerical experiments," *Progress In Electromagnetics Research Symposium Abstracts*, 198, Cambridge, USA, July 2–6, 2008.

Designer PhoXonic ($X = t, n$) Crystals

Cheong Yang Koh[1, 2] **and Edwin L. Thomas**[1, 2]

[1]Department of Materials Science and Engineering, Massachusetts Institute of Technology
77 Massachusetts Ave, Cambridge, MA 02139, USA
[2]Institute for Soldier Nanotechnologies, Massachusetts Institute of Technology
77 Massachusetts Ave, Cambridge, MA 02139, USA

Abstract— Periodic phoXonic ($X = t, n$) structures provide a novel route for controlling the propagation of light and sound. However, determining the optimal structural design for a particular application, such as ultra-compact optoelectronic components, remains an open problem despite the wealth of information contained within the dispersion relation of a periodic structure. The problem arises primarily due to the lack of a framework with which to interpret it completely and extract a particular design for a target application. The potential is huge-periodicity and combination of periodic hetero-structures offer the ability to tailor novel behavior such as negative refraction, complete band gaps as well as one-way states, among others.

By considering the design of periodic phoXonic structures in terms of a general symmetry network, we unify the design of a particular periodic structure for a target application by selecting the appropriate symmetry space (3D) (plane-2D) groups, and specific symmetry elements that may be optimized for it. In particular, we demonstrate, by using non-symmorphic space (plane) groups for our candidate structures, the ability to create "sticking bands" — These are pairs of bands that intersect with non-zero group velocities at a brillouin zone (BZ) boundary and remain degenerate across the **entire** face of the adjacent BZ boundary. Such a feature results purely from the choice of the space (plane) group and is distinct from normal point degeneracies present in conventional band structures of symmorphic space (plane) groups. Such sticking bands are attractive for effective negative refraction in periodic systems because they create close to linear dispersion relations with negative effective group velocities along all directions. We also demonstrate that by considering the various invariances of a particular structure as we selectively break certain symmetries, we can induce certain band gaps to form as a result of selective anti-crossing. Furthermore, we generalize all various forms of gap-opening mechanisms as "like-symmetry" anti-crossings. This is demonstrated for 1) Resonance-Induced Gap Opening 2) Generic Symmetric-Anti-crossing as a result of symmetry breaking. By generating two wide classes of periodic structures that can be loosely considered as 1) Coupled lattice of resonators to 2) extended lattice with periodic perturbations we can tailor/design the dispersion relation. Through these examples, we demonstrate that the symmetry framework illuminates an approach offering control over the dispersion relations of phoXons propagating through the medium and hence, provides a unifying design toolset for fabricating these structures for the manipulation of light and sound.

Analysis of Dispersion Properties of Waveguide Based on Metamaterials

S. Bouali and T. Aguili
Syscom, National Engineering School of Tunis, Tunisia

Abstract— This paper presents an analysis of dispersion properties of rectangular waveguide using the transmission line theory of metamaterials. The rectangular waveguide discussed in this paper is composed of an infinite repetition of unit cell in one dimension. By defining the matrix chain of the unit cell and using Floquet's theorem we obtain the equation of dispersion of the structure which is plotted and discussed, the results of this analysis are presented.

Results and Conclusion: The unit cell consists of a transmission line, the line's length is L, we place at the center of this line a symmetrical window formed by ultra-thin thickness of obstacles with edges parallel to the electric field (H_{10}) mode in rectangular guide, X depend on the frequency [1], we consider a unit cell as a three part network: one half ($L/2$) of the transmission line, the loading element JX, and another half ($L/2$) of the transmission line. Therefore, the matrix of the unit cell is given by: $C_T = C_{L/2} * C_e * C_{L/2}$, with $C_{L/2}$ is the matrix of the half TL, C_e is the obstacle matrix. Using Floquet's theorem we obtain two equations of dispersion of the structure. There are two equations of dispersion with condition, the first equation with varying attenuation constant α_p and fixed phase constant β_p. The second equation without attenuation constant $\alpha_p = 0$ and the phase constant is varying. We have analyzed the dispersion properties of our structure. The general dispersion relation for rectangular waveguide that considered as transmission line with lumped element (JX) (witch X depend on the frequency) has been formulated using the TL approach and solved using Floquet's theorem; we obtained tow equations which depend of the attenuation and phase constant. We simulated these equations using MATLAB. The results revel the presence of stop band and pass band. The attenuation and phase constant was calculated by using the two equations of dispersion and plotted, which agrees well with the stop and pass bands, a comparison with the static case (X is independent on the frequency) [2] is given, the result agrees well with our references.

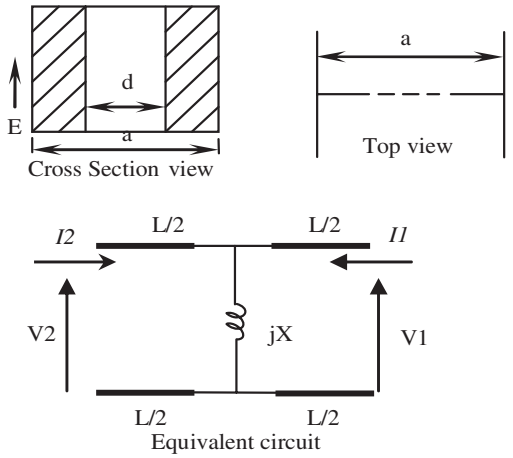

Figure 1: Schema of the cross section view, the top view of the rectangular waveguide and the equivalent circuit represented as a three part network: one half ($L/2$) of the transmission line, the loading element jX and another half ($L/2$) of the transmission line.

REFERENCES

1. Marcuvitz, N., *Waveguide Handbook*, Peter Peregrinus Ltd on behalf of the Institution of Electrical Engineers.
2. Bouali, S. and T. Aguili, "The study of electromagnetic dispersion in the periodic structures," *MMS*, 2008.

Session 3P1
Optics and Photonics

Three-dimensional Woodpile Photonic Crystal Materials and Microcavities

Tomoyuki Yoshie and Lingling Tang
Duke University, USA

Abstract— Yablonovitch [1] and John [2] originally proposed to use 3D dielectric superlattice structures for studying suppression of spontaneous emission and amorphous 3D photonic crystal for strong localization in disordered dielectric superlattices, respectively. The study of such 3D optical states has been hindered due to the lack of largevolume 3D photonic crystal materials with a complete band gap, which provides true optical counterparts of electronic band gap in bulk semiconductor. Although 2D photonic crystal slab system has advanced low-loss microcavity and waveguide technology due to simple fabrication, the system does not provide a complete band gap. We developed a simple two-directional etching method of fabricating large volume woodpile photonic crystal materials and microcavities in GaAs. Our fabrication methods use two precision electron beam lithography and two deep, anisotropic etching processes only. In addition, our microcavity design providing certain 3D optical states do not require wafer bonding. From an engineering viewpoint, the study of light localization in sub-wavelengthdimensions would not only advance miniaturization of optical devices, but also foster the performance and functionality of many optical devices, including low-threshold nanolasers, optical switches, surface-enhanced Raman spectroscopy devices, optical trapping devices, quantum entanglement devices, and single photon sources. Realizing light localization in a compact volume is a challenging task. For the past decade, microcavities based on 2D photonic crystal have advanced the performance of light localization technology. However, there are fundamental or technological limits in 2D photonic crystal slab system, and our microcavity technology is strongly limited by these boundaries. On the other hand, the most significant thing in 3D photonic crystal is that they can have a complete photonic band gap. This unique feature enables three-dimensional light localization in an extremely small space as a resonance state. Another unique character of 3D photonic crystals is that we can place miroresonators and waveguides in 3D space so that this is a good test bed for studying 3D optical integrated optics. Although it is a challenge to build 3D photonic crystal and introduce intentional disorders, we have developed highquality microcavity and waveguide designs suitable for woodpile photonic crystal fabrication method based on twodirectional etching.

REFERENCES

1. Yablonovitch, E., "Inhibited spontaneous emission in solid-state physics and electronics," *Phys. Rev. Lett.*, Vol. 58, 2059, 1987.
2. John, S., "Strong localization of photons in certain disordered dielectric superlattices," *Phys. Rev. Lett.*, Vol. 58, 2486, 1987.

Design of LED Optics to Generate Required Irradiance Distribution with Wide Angular Dimension

L. L. Doskolovich[1, 2], **N. L. Kazansky**[1, 2], **and M. A. Moiseev**[1, 2]

[1]Image Processing Systems Institute of RAS, Russia
[2]Samara State Aerospace University, Russia

Abstract— Optical design for illumination of a preset region is a very important problem arising in the process of designing automobile lighting devices, LCD-monitor illumination systems, etc. Nowadays the use of light emitting diodes (LEDs) is the most cost-effective way to produce compact light sources for lighting systems. Problem of LED optics design consists in calculation of refracting surface shape suitable for producing prescribed irradiance distribution in a certain plane. For a point light source, the problem reduces to solving nonlinear differential equations in partial derivatives, similar to the Monge-Ampere equations. Solving these equations is a challenging problem. Analytical solutions are known only for particular cases of radially or cylindrically symmetric surfaces. Complex freeform surfaces are calculated with the use of different iterative optimization procedures that require great computational efforts [1, 2]. The efficiency of the iterative procedures [1, 2] is not sufficient. Thus, the problem of designing a refractive optical surface intended for production uniform irradiance distribution in a wideangle rectangular region remains highly relevant.

We propose a new method for designing optical elements suitable for optical systems with point or extended light sources. It allows producing complex, nonradially symmetric irradiance distributions. The radius-vector of refractive surface is represented as a bicubic spline function in spherical coordinate system. The parameters of bicubic spline are the parameters of gradient optimization. As a residual function the relative root-mean-square error of produced irradiance distribution from required irradiance distribution is used. Optical element generating uniform irradiance distribution in the elliptic (with 50 mm and 25 mm semi-axes) region located at 15 mm distance from the light source have been computed (Figure 1(a)). The energy efficiency of element exceeds 75%; RRMSE of generated irradiance distribution (Figure 1(b)) is less than 12.5%. The method is suitable for designing backlight modules intended to produce uniformly illuminated regions of large angular size (140°–150°).

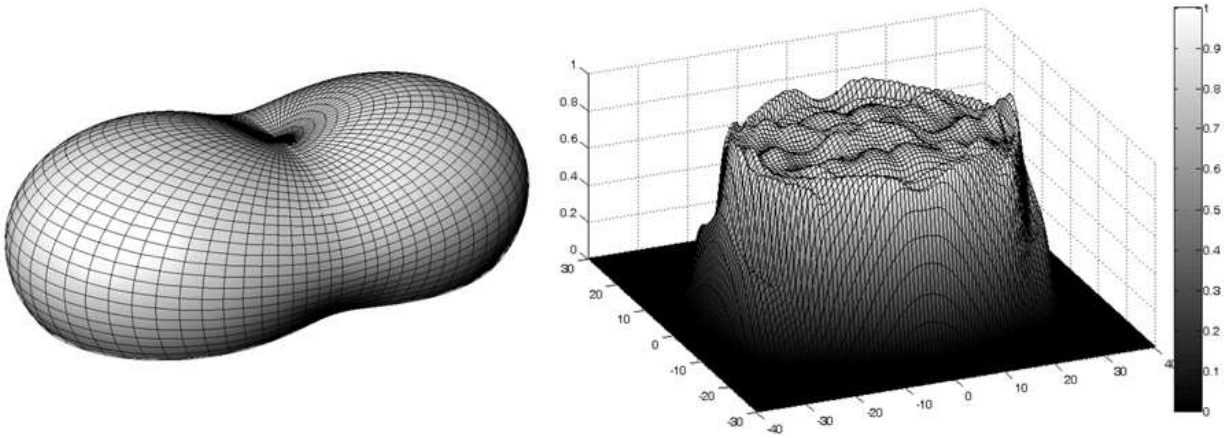

(a) (b)

Figure 1: (a) Optical element producing the uniform irradiance distribution in elliptic region. (b) Simulated irradiance distribution.

REFERENCES

1. Muschaweck, J. and H. Ries, "Tailored freeform optical surfaces," *J. Opt. Soc. A*, Vol. 19, No. 3, 590–595, 2002.
2. Ding, Y., X. Liu, Z.-R. Zheng, and P.-F. Gu, "Freeform LED lens for uniform illumination," *Optics Express*, Vol. 16, No. 17, 12958–12966, 2008.

Surface Plasmon Resonance Modes of Metal Nanostructures Embedded in Layered Media: A Full Analytical Method

Ergun Simsek, Tolga Aydogan, and Gokhan Barlak
Bahcesehir University, Istanbul, Turkey

Abstract— It has been shown that optical waveguides with sub-wavelength lateral mode confinement can be built using periodically located metal nanoparticle (NP) chains, where dispersion relation becomes a crucial parameter of the design. In this direction, many researchers have studied dispersion relation of surface plasmon resonance (SPR) modes of metal NP chains experimentally in the last decade. In the mean time novel theoretical models have been developed to analyze such systems. A very commonly used theoretical model is the discrete dipole approximation (DDA). DDA is a simple yet effective method but requires a homogeneous background that is not the case most of the time for real metal NP structures, e.g., metal NPs fabricated on top of indium tin-oxide coated-glass slides creating a three-layer media [1].

In [2], a simple effective refractive index (ERI) approximation is adopted to obtain the SPR modes of metal NP chains and arrays in embedded multilayered structures. This approximation represents the inhomogeneous background by an effective homogeneous medium, whose refractive index depends on the wavelength, refractive index and width of each layer. This approach can provide a good estimate of SPR modes but cannot explain the exact effect of an interface (such as air/glass interface) on the dispersion and extinction of surface plasmons.

Different from [2], Yang and Crozier propose a semi-analytical model for the NPs on top of a glass slide and show the good agreement between their model and experimental results for the first transverse mode [1]. Up to our knowledge, this is the first DDA based model, which can describe the effect of the air/glass interface. The main advantage of their model is that it only involves real valued frequencies. The drawback, however, is the requirement of a full wave solver in order to calculate the polarizability of the NP.

In this work, we overcome this requirement by appropriately modifying the polarizability factor using layered medium Green's functions (LMGFs). We also implement DDA with LMGFs and hence obtain a full analytical model that can accurately calculate SP resonance modes of metal NP structures embedded in a multilayered medium. This fully retarded theoretical model includes the effects of retardation, radiative damping, and dynamic depolarization due to the finite size of the NPs based on the Modified Long Wavelength Approximation. Numerical results show that discrete dipole implemented with layered medium Green's functions can provide a good estimate of the complete set of surface plasmon resonance modes in a multilayered medium, which might be very useful at the pre-experimental stage. Furthermore, it is numerically shown for the first time that constructive reflections from the multilayered structure can enhance the surface plasmon propagation length.

ACKNOWLEDGMENT

This research was supported by a Marie Curie International Reintegration Grant within the 7th European Community Framework Programme. Contract No. PIRG05-GA-2009-247876.

REFERENCES

1. Yang, T. and K. B. Crozier, *Optics Express*, Vol. 16, 13070, 2008.
2. Simsek, E., "Effective refractive index approximation and surface plasmon resonance modes of metal nanoparticle chains and arrays," *PIERS Online*, Vol. 5, No. 7, 629–632, 2009.

Stability of Bragg Grating Solitons in a Cubic-quintic Nonlinear Medium with Dispersive Reflectivity

Sahan Dasanayaka and Javid Atai
School of Electrical and Information Engineering, The University of Sydney, NSW, 2006, Australia

Abstract— Periodic variation of the refractive index along an optical fiber produces a fiber Bragg grating (FBG). The cross-coupling between counter-propagating waves in an FBG results in a strong effective dispersion that is approximately 6 orders of magnitude greater than the underlying chromatic dispersion of the fiber [1, 2]. At sufficiently high intensities the FBG-induced dispersion may be counterbalanced by nonlinearity resulting in the formation of a Bragg grating soliton.

Bragg grating solitons have been the subject of intense theoretical and experimental research over the past two decades (see for example Refs. [2–5]). In a uniform Bragg grating, the governing equations for nonlinear pulse propagation have been derived using coupled mode theory (CMT) [2]. In this case, BG solitons form a two-parameter family of solutions. One of these parameters is related to soliton's velocity, which can range between zero and the speed of light in the medium, and the other is dependent on the detuning frequency, peak power and soliton width. Due to their potential application in optical buffers and storage devices, significant efforts have been directed toward the generation of zero-velocity (quiescent) solitons.

The existence and stability of solitons have also been investigated in more sophisticated systems. For example, in Ref. [6], it was reported that in a medium with a cubic-quintic nonlinearity two disjoint families of BG solitons exist. In Refs. [7, 8], the existence and stability of solitons in a *non-uniform* Bragg grating was considered. A key result in these works is that reflectivity dispersion leads to the expansion of the stability region of the standard model.

In this paper we investigate the effect of reflectivity dispersion on the existence and stability of solitons in a cubic-quintic medium. The model is as follows:

$$iu_t + iu_x + \left[\frac{1}{2}|u|^2 + |v|^2\right] u - \nu \left[\frac{1}{4}|u|^4 + \frac{3}{2}|u|^2|v|^2 + \frac{3}{4}|v|^4\right] u + v + mv_{xx} = 0$$

$$iv_t - iv_x + \left[\frac{1}{2}|v|^2 + |u|^2\right] u - \nu \left[\frac{1}{4}|v|^4 + \frac{3}{2}|v|^2|u|^2 + \frac{3}{4}|u|^4\right] v + u + mu_{xx} = 0$$

where u and v are the forward and backward propagating components, m accounts for the strength of the dispersive reflectivity and $\nu > 0$ is a parameter to control the strength of quintic nonlinearity.

Using the relaxation technique, two disjoint families of solitons have been found in this model. The stability regions are dependent on the values of dispersive reflectivity parameter and the strength of quintic nonlinearity.

REFERENCES

1. Russell, P. St. J., *J. Mod. Opt.*, Vol. 38, 1599, 1991.
2. De Sterke, C. M. and J. E. Sipe, *Prog. Opt.*, Vol. 33, 203, 1994.
3. Aceves, A. B. and S. Wabnitz, *Phys. Lett. A*, Vol. 141, 37, 1989.
4. Eggleton, B. J., C. M. de Sterke, and R. E. Slusher, *J. Opt. Soc. Am. B*, Vol. 14, 2980, 1997.
5. Taverner, D., N. G. R. Broderick, D. T. Richardson, R. I. Laming, and M. Ibsen, *Opt. Lett.*, Vol. 23, 328, 1998.
6. Atai, J. and B. A. Malomed, *Phys. Lett. A*, Vol. 284, 247, 2001.
7. Atai, J. and B. A. Malomed, *Phys. Lett. A*, Vol. 342, 404, 2005.
8. Neill, D. R., J. Atai, and B. A. Malomed, *J. Opt. A: Pure Appl. Opt.*, Vol. 10, 085105, 2008.

Performance Assessment of the Logarithmic-hybrid Optical Neural Network Filter for Multiple Objects Recognition

Ioannis Kypraios
School of Engineering & Design, University of Sussex, Falmer, Brighton BN1 9QT, UK

Abstract— Previously, we have described the complex logarithmic r-theta mapping for hybrid optical neural network (L-HONN) filter for object recognition within cluttered scenes. The design of the filter is based on a space-variant imaging sensor combined with the hybrid optical neural network filter. The created L-HONN filter exhibits simultaneously and with a single pass over the input data in-plane rotation, out-of-plane rotation, scale and projection, and shift invariance. The window unit in the design of the L-HONN filter allows multiple objects of the same class to be detected and classified within the input image. Additionally, the architecture of the neural network unit of the filter allows the recognition of multiple objects of different classes within the input image by augmenting the output layer of the unit. We have presented results for multiple objects recognition within cluttered scenes. We have tested the filter with both still images and video sequences. L-HONN filter is able to successfully suppress the unknown background clutter and recognise the different classes of the objects in the input scene of a still image or a video frame. As for all the HONN-type filters, it is found that by altering the target classification levels for each of the object classes, the L-HONN filter's behaviour can be varied to suit different application requirements from more like a high-pass biased filter to more like a minimum variance synthetic discriminant function (MVSDF) filter. Here, for first time, we present, in detail, the full-series of tests for examining the performance of the L-HONN filter for its detectability and peak sharpness, performance with in-class distortion of the input objects, its discrimination ability between in-class and out-of-class objects and we record the results for the filter's tolerance-to-clutter in recognising the objects of different classes. From the performance analysis, L-HONN filter is shown to exhibit good peak correlation energy (PCE) values, good distortion tolerance by recognising the true-class object out-of-plane rotated for a range of 5° to 45° degrees, and it is able to discriminate between the different classes objects. Finally, it is shown to exhibit high tolerance-to-clutter ratio (TCR) values and is able to successfully recognise the area where the true-class object is located.

Optical Forces and Optical Torques on Particles Arising from Optical Lattices in the Lorentz-Mie Regime

Lin Jia and Edwin L. Thomas
Department of Materials Science and Engineering, Institute for Soldier Nanotechnologies
Massachusetts Institute of Technology, Cambridge, Massachusetts 02139, USA

Abstract— By combining the Maxwell stress tensor with the finite-difference time-domain method, we calculate the optical force and optical torque on particles from optical lattices. Energy analysis, the two component method and the electrostatic approximation are used to explain the optical forces arising from various optical lattices. We discuss how particle refractive index, shape, size and morphology of the optical lattice influence optical force and the condition to form stable optical trapping wells. In addition to optical forces, optical torque from the 1D optical lattice is discussed for particles having anisotropic shapes; metastable and stable equilibrium orientation states are found. A detailed understanding of the optical force and torque from optical lattices has significant implications for optical trapping, micromanipulation and sorting of particles.

The Investigation of Angular Dispersion Effect Based on Hetero Metal-dielectric-metal Plasmoic Waveguide

Chao-Yi Tai[1], **Wen-Hsiang Yu**[1], **and Sheng Hsiung Chang**[2]

[1]Department of Optics and Photonics, National Central University, Taiwan
[2]Institute of Atomic and Molecular Sciences, Academia Sinica, Taipei 106, Taiwan

Abstract— We report on the giant angular dispersion effect based on hetero metal-dielectric-metal waveguide structure. In contrast to the conventional analysis where the characteristic equation of a three-layer asymmetric waveguide was solved, we performed coupled mode analysis with phase velocity difference between two surface waves propagating alongside metal-dielectric interfaces. Under appropriate structural parameters, wavefront tilt mediated angular dispersion at the output of the waveguide as large as 2.1 degree/nm at the spectral range of 675 nm–695 nm can be achieved. The interplay between the electromagnetic fields, the induced polarization charges, and the spatial-spectral energy distributions are calculated in this study. The resulting angular dispersion can be explained by the competitive energy vortex which corresponds to the strong topological charge dispersion in close proximity to the output corners of the waveguide.

The "Missing Mass" in the Universe May Be Represented by the Dynamic-mass of the Photons

Antonio Puccini
Department of Neurophysiology of Order of Malta, Naples, Italy

Abstract— As we know the *missing mass* in the universe represents more than 90% of the universe mass. The adronic matter, in fact, corresponds only to a very small part of the total (about 4%). It is not known what the *missing mass* is represented of. It is thought that it is made of weakly interactive massive particles (WIMPS), massive particles (100 times heavier than a proton) which interact very little with the matter, even less than neutrinos. It may also be a supersimmetric particle, or something else.

We calculated that the momentum of a photon of the optic band, with a normal wave length, along with the formula $p = h/\lambda$, will be $6{,}625{\cdot}10^{-27}$[g·s]/$5{,}7{\cdot}10^{-5}$ [cm], which corresponds to $1{,}1623{\cdot}10^{-22}$[g· cm/s]. Thus we have that the photon has really a significant *dynamic mass*, about 100 times bigger than the mass of the proton. It is curious to notice that it corresponds just to the hypothetic mass given to the WIMPS.

Moreover, if we consider, along with what Weinberg tells us in "The First Three Minutes", that for each nuclear particle (proton or neutron) there a billion of photons, we may think that the photons can contribute to fill the vacuum of the missing mass in the universe.

The Inflationist Expansion of the Universe Was Conducted by Very High Energy Photons

Antonio Puccini
Department of Neurophysiology, Order of Malta, Naples, Italy

Abstract— The inflationist expansion of the universe was probably conducted by very energetic photons (Ps) since the Big Bang represents a source of very high electromagnetic emission. We think that the Ps emitted had an energy bigger than gamma Ps (10^{27} Hz). The fact that these Ps induced the inflationist event coincides with the extremely homogeneous and isotropic presence of the bottom cosmic radiation, which is just the phantom of the electromagnetic radiation initially emitted with the Big Bang.

There is no satisfactory physical explanation to justify expansion sped of the inflationist phase, much bigger than the speed of light. However, if we consider that the inflation was basically conducted by these extremely energetic Ps, we may be able to explain the high speed expansion. It may be explained with the Quantum Mechanics, through the Uncertainty Principle: $\Delta_E \cdot \Delta_T \geq h/2\pi$. Indeed, if we apply this principle to the electromagnetic radiation, we have that the bigger the Energy of the P, the bigger its speed.

Vertical Pillar Array Plasmon Nanocavities

Mihail Bora, B. Fasenfest, E. Behymer, A. S. Chang, H. T. Nguyen, J. A. Britten, C. Larson, and T. Bond
Lawrence Livermore National Laboratory, USA

Abstract— We investigate large area fabrication of plasmon resonant cavity arrays based on two nanowire waveguides. Resonances are observed when the length of the waveguide is an odd multiple of quarter plasmon wavelengths, consistent with the boundary conditions of node and antinode at the cavity ends. Nanocavity optical spectrum is tuned by adjusting the height and separation between pillars. Further, we show that the two nanowire waveguide satisfies a planar metal-dielectric-metal waveguide dispersion relation for which the effective width is calculated as an energy density weighted average of the gap. Large confinement factors of 10^4, calculated for the nanocavities discussed in this work are possible due to a plasmon self-focusing mechanism in the inter-pillar space.

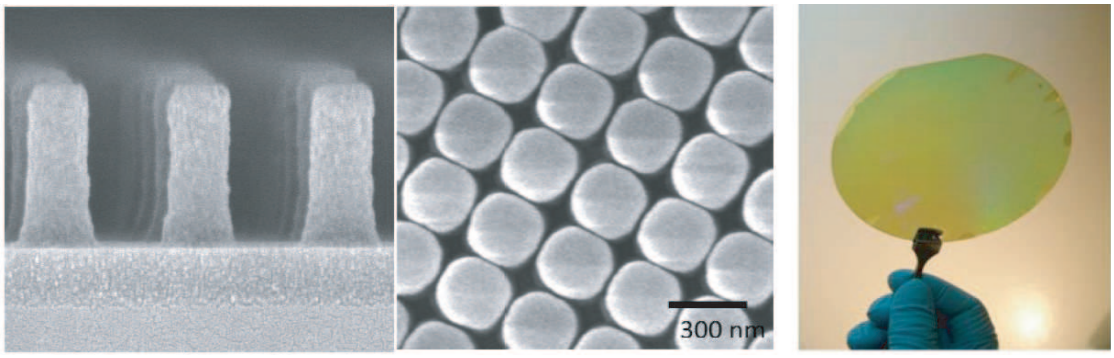

(a) (b) (c)

Figure 1: Vertical pillar array substrate. (a) Side view of resist pillars fabricated by laser interference lithography. (b) Top view of metallic nanowire cavity array coated with gold. The pillar center to center distance is 350 nm, and the edge to edge gap is 35 nm. The pillar height is controlled by the etch time during the RIE step. (c) Large area fabrication of the plasmon nano-cavities on a four inch diameter substrate.

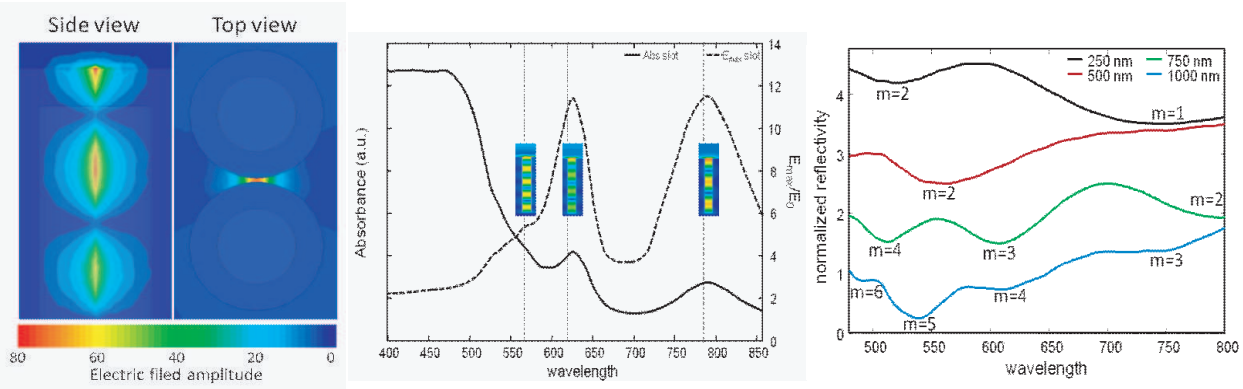

(a) (b) (c)

Figure 2: (a) Simulation of the electric field amplitude for the two wire resonator. A plasmonic standing wave is formed in the inter-pillar space. (b) Numerical simulations of absorbance and electric field. The maxima correspond to excitation of resonant plasmon modes in the cavity. (c) Normalized reflectivity plots for pillar array of height 250, 500, 750 and 100 nm. The reflectivity minima correspond to excitation of plasmon resonances labeled by their order m.

Silicon Quantum Dots in Microkylix and Microdisk Resonators: From Stress-induced Q-factor Tuning to Purcell Enhancement of Emission Rates

Mher Ghulinyan[1], **Alessandro Pitanti**[2], **Daniel Navarro-Urrios**[3], **Georg Pucker**[1], **and Lorenzo Pavesi**[2]

[1]Advanced Photonics & Photovoltaics, Fondazione Bruno Kessler, Trento, Italy
[2]Nanoscience Laboratory, Department Physics, University of Trento, Trento, Italy
[3]University of Barcelona, Barcelona, Spain

Abstract— We report on visible light emission from Si quantum dot (QD) based optically active planar micro-resonators [1]. The room temperature photoluminescence from single devices shows the characteristic modal structure of whispering-gallery modes (WGM). Highest quality factors of up to 7000 at visible wavelengths, where Si QD absorb strongly, have been measured for the first time.

Apart from conventional flat and circular resonators, we demonstrate for the first time a new class of active microdisk resonators with out-of-plane bending, which we refer to as *micro-kylixes* [2]. In these devices, composed of silicon nitride, Si_3N_4 and Si QD-rich silicon oxide, SiO_x, materials, the engineered stress at the interfaces results in concave (cup-like) and convex (umbrella-like) resonators, depending on which material is used as a top layer. Both type of bent devices support perfectly WGMs and, quite unexpectedly, offer a rich and interesting physics.

In particular, we demonstrate the possibility of blue-tuning and enhancing the highest Q-factors of WGM modes in bent disks with respect to similar-sized flat ones. Generally, the wavelength dispersion of two main different loss-channels, the material absorption and radiative losses, result in a limited bandwidth where the highest Q-factors can be observed. We show here, that in a bent resonator, with respect to a flat one (same diameter, thickness and amount of Si_3N_4 and SiO_x materials in both), the set of highest Q-modes blue-shifts by more than 70 nm (from 832 nm to 760 nm). To shift the Q-band by this amount towards short wavelengths in flat micro-disks a 50% diameter reduction is required, which causes severe radiative losses, suppressing Q's. With a micro-kylix, we achieve similar tuning by two orders of magnitude smaller diameter modification (0.4%). The phenomenon relies on geometry-induced smart interplay between modified dispersions of material absorption and radiative loss-related Q-factors (simultaneous increase of Q_{mat} and decrease of Q_{rad}).

Importantly, this tuning scheme does not require larger device sizes, but rather utilizes self-adjustment properties of originally stressed resonator core. Remarkably, the micro-kylixes benefit from unmodified free-spectral range and cleaner WGM spectra due to the absence of higher order mode families.

Moreover, we report on direct measurements of spontaneous emission rate enhancement of Si-ncs form these resonators at room temperature [3]. We demonstrate experimentally important life-time reductions (up to 70%) for nanocrystalline emitters coupled to WGM cavity resonances with respect to uncoupled ones. Comparing our experimental results with the theoretical prediction of Purcell enhancement in a "bad emitter regime", we estimate effective linewidths of ∼10 meV through which Si-ncs are coupled to the WGM cavity. Our study provides an alternative method for the estimation of sub-natural linewidths of quantum dots at room temperature.

REFERENCES

1. Ghulinyan, M., D. Navarro-Urrios, A. Pitanti, A. Lui, G. Pucker, and L. Pavesi, *Opt. Express*, Vol. 16, 13218, 2008.
2. Ghulinyan, M., A. Pitanti, G. Pucker, and L. Pavesi, *Opt. Express*, Vol. 17, 9434, 2009.
3. Pitanti, A., M. Ghulinyan, D. Navarro-Urrios, G. Pucker, and L. Pavesi, submitted, 2009.

Self-field Theory — A Possible Gravitational Structure for Galaxies

A. H. J. Fleming
Biophotonics Research Institute, Melbourne, Australia

Abstract— This report brings two seemingly unrelated phenomena together: the EPR paradox, a thought exercise Einstein used to infer quantum mechanics was incomplete, and the orbital rotation of solar systems in galaxies, mainly invariant with radial distance from the galactic centre that has been hypothetically explained via dark matter, a halo of matter invisible to Earth thought to surround galaxies. Self-Field Theory (SFT) is a new bispinorial description of electromagnetic (EM) interactions applying across physics. SFT utilizes exact closed-form solutions of the Maxwell-Lorentz (ML) equations containing two curl and two divergence equations. The eigenvalue equations indicate a photonic level physics sitting underneath the atomic level physics via two new quantum numbers relating to the phase length of photons and the discretization of the motions of atomic particles. Hence electrons and protons are in dynamic balance via photons acting as binding energy within atoms at the EM level while photons and other bosons again act as binding energy at the gravitational level between planets and suns. Strong nuclear (SN) regions of atoms can be described via trispinorial forms involving a modified system of ML equations incorporating three curl and three divergence equations instead of the two curl and two divergence equations of EM interactions. There is correspondence between the internal boson structure and the form of the gravitational structure: the photon corresponds to bi-rotational motion while the gluon corresponds to tri-rotational motion. There is an acoustic (A-) field in addition to the electrical and magnetic fields that binds the galactic constituents together within a 3-D system of forces that stiffens the galaxy into one viscous mass. The dynamics of solar systems orbiting within galaxies can be described using such trispinorial motions.

REFERENCES

1. Williams, H. S., *The Story of Nineteenth Century Science*, Harper and Brothers, 1900.
2. Rohde, R. A. and R. A. Muller, "Cycles in fossil diversity," *Nature*, Vol. 434, 208–210, 2004.
3. Medvedev, M. V. and A. L. Melott, "Do extragalactic cosmic rays induce cycles in fossil diversity?" *Astrophys. J.*, Vol. 664, 879–889, 2007.
4. Jenny, H., *Cymatics: A Study of Wave Phenomena and Vibration*, 3rd Edition, Macromedia Press, July 2001.
5. Lo, M. W. and M. J. Chung, "Lunar sample return via the interplanetary superhighway," *JPL, TRS*, 1992.
6. Binney, J. and S. Tremaine, *Galactic Dynamics*, Princeton University Press, 1987.
7. Klacka, J., "Galactic tide," arXiv-0912.3112v1 [astro-ph.GA], December 16, 2009.
8. Fleming, A. H. J., "Electromagnetic self-field theory and its application to the hydrogen atom," *Physics Essays*, Vol. 18, No. 3, 265–285, 2005.
9. Fleming, A. H. J., "Self-field theory, analytic spectroscopy of the ordinary photon," *Proc. 2nd Electromagnetics Health and Environment Intl Conf.*, Wroclaw, Poland, 18–23, 2007.
10. Fleming, A. H. J., *Self-field Theory — A New Mathematical Description of Physics*, Pan Stanford Publishing, to be published, 2010.

Self-field Theory-biodiversity May Be a Resonance Process

A. H. J. Fleming
Biophotonics Research Institute, Melbourne, Australia

Abstract— Self-Field Theory (SFT) is a new description of electromagnetic (EM) interactions that utilizes closed-form solutions of the Maxwell-Lorentz (ML) equations. Bispinorial motions apply to the motions of EM field-particles and interacting particles including electrons and protons. The strong nuclear region of atoms is described via trispinors involving modified ML equations incorporating three curl and three divergence equations. The complicated dynamics of suns can be described via a system of galactic gravitational fields. The bispinorial motions that apply to EM interactions are extended to trispinorial motions corresponding to tri-rotational galactic dynamics. In other words galactic dynamics can be described via three rotations enabling SFT be applied to the dynamics of suns and their planets. Recently a cycle of around 62 MY corresponding to the last 500 MY history of Earth's fossil diversity was found. This cycle corresponds to the motion of the Solar System as it bobs up and down around the Galactic Centre. It has been suggested that at these points in its orbit the Earth are relatively unprotected from nearby gamma-ray bursts. However it is also known that DNA is sensitive to certain frequencies which correspond to the cell-cycle. In fact the piecewise linear double helix of DNA is imitative of the bispinorial motions predicted by the atomic particles including electrons and protons within SFT. This paper examines these galactic, gravitational, and biological interactions and suggests alternatively that biodiversity on Earth may be a resonance process corresponding to the energy density and spectral fingerprint within our Milky Way Galaxy.

REFERENCES

1. Fleming, A. H. J., "Electromagnetic self-field theory and its application to the hydrogen atom," *Physics Essays*, Vol. 18, No. 3, 265–285, 2005.
2. Fleming, A. H. J., "Self-field theory, analytic spectroscopy of the ordinary photon," *Proc. 2nd Electromagnetics Health and Environment Intl Conf.*, 18–23, Wroclaw, Poland, 2007.
3. Fleming, A. H. J., *Self-field Theory — A New Mathematical Description of Physics*, Pan Stanford Publishing, to be published, 2010.

Self-field Theory-biophotons and EPR

A. H. J. Fleming
Biophotonics Research Institute, Melbourne, Australia

Abstract— The EPR paradox lies at the heart of the way Self-Field Theory (SFT) sees physics and biophysics. Einstein coauthored a paper on the paradox that challenged quantum theory as incomplete. Quantum entanglement is now understood as the way in which parts of a quantum mechanical system are connected. The quantum states of the constituent parts are linked; one part cannot be properly described without mention of all other parts within the system. Einstein referred to this as 'spooky action at a distance'. SFT too sees quantum theory as incomplete. SFT suggests a missing coordinate within the photon that is the underlying reason for Heisenberg's uncertainty principle and its lack of knowledge concerning photons. Like entanglement SFT suggests that photons link all atoms together as in a crystal lattice. In solid crystals according to SFT the atoms rotate in synchronized fashion. Photon interactions apply between many if not all atoms within the Universe in which dipole-dipole EM inter atomic forces exist sometimes as streams of photons between masses. DNA is an example of a liquid crystal that is capable of 'stiffening' as the biophotonic states change within the cell cycle. Biophotons link to objects around a biological system. This includes the biological ability of optical sight but can include other biophotons within the complete body-field. Biophotons are found in specialized physiological tissues including elasmobranch fish that use jelly-filled canals called the ampullae of Lorenzini on the lower peripheries of their fins for predation. As well as being absorbed, biophotons are emitted by biological systems.

REFERENCES

1. Fleming, A. H. J., "Electromagnetic self-field theory and its application to the hydrogen atom," *Physics Essays*, Vol. 18, No. 3, 265–285, 2005.
2. Fleming, A. H. J., "Self-field theory, analytic spectroscopy of the ordinary photon," *Proc. 2nd Electromagnetics Health and Environment Intl Conf.*, 18–23, Wroclaw, Poland, 2007.
3. Fleming, A. H. J., *Self-field Theory — A New Mathematical Description of Physics*, Pan Stanford Publishing, to be published, 2010.
4. Nakamura, J. and M. Hiramatsu, "Ultra-weak photon emission from human hand: Influence of temperature and oxygen concentration on emission," *Journal of Photochemistry and Photobiology B: Biology*, Vol. 80, 156–160, 2005.

Session 3P2a
Microwave Non-destructive Evaluation

Subsurface Sub-terahertz and Terahertz Tomography

A. A. Vertiy, H. Cetinkaya, and M. Tekbas
International Laboratory for High Technology, Material Institute, TUBITAK-MRC
Gebze/Kocaeli, Turkey

Abstract— Development of sub-terahertz and terahertz technologies is of great interest lately, especially for application in so called terahertz imaging. One of the hot and prospective topic for practical usage is application for imaging of internal materials structure, deformations, inhomogeneities etc.

In our paper we consider a tomography approach for obtaining 3-D imaging in frequency range between 100 GHz up to 325 GHz. Sub-surface tomography method which we developed earlier for lower frequency we applied the for extremely high frequencies. This method relates Fourier transform of backscattered field data at each excitation frequency to the sought object function defining normalized polarization currents (equivalent currents) induced in the target. With respect to this consideration, the inverse problem is solved. In this paper measurement set up is also described. It includes Vector Network Analyzer (Agilent E 8361 A PNA network analyzer), Probe Station (Cascade Microtech) and their control devices, antennas, and near field probes. Collected data processed by algorithm based on developed method. At final part of paper, obtained results are demonstrated for surface and sub-surface applications. So in the paper we present theoretical method, experimental set up and measurement results for selected samples. Results of nondestructive evaluation of composite materials, semiconductor wafers control etc at 100 GHz and 325 GHz have been presented.

The considered method and tomography setup may be used for 3D imaging in medicine, biology, microelectronics, non-destructive testing and security.

Advanced Studies of the Differential Phase Shift in the Azimuthally Magnetized Circular Ferrite Waveguide

Mariana Nikolova Georgieva-Grosse[1] and Georgi Nikolov Georgiev[2]

[1]Meterstrasse 4, D-70839 Gerlingen, Germany
[2]Faculty of Mathematics and Informatics, University of Veliko Tirnovo "St. St. Cyril and Methodius"
BG-5000 Veliko Tirnovo, Bulgaria

Abstract— Recently, iterative methods have been proposed for computation of the phase and differential phase shift characteristics of the circular waveguides with azimuthally magnetized ferrite, propagating normal TE_{01} mode, suitable for nonreciprocal phase shifters designs [1–5]. It turned out that the problems stated are much more complicated than expected and even in the simplest cases the workers in the field are still far from their complete solution [4, 5].

Two iterative techniques are developed and harnessed here to trace the limits of the domain in which the circular waveguide, uniformly filled with azimuthally magnetized ferrite produces differential phase shift for the aforesaid wave. Both of them use the expressions $\bar{r}_0 = (k\zeta_{k,n}^{(c)}/\alpha)\times \{[1+(\alpha/(2k))^2]/(1-\alpha^2)\}^{1/2}$ and $\bar{\beta} = \{(1-\alpha^2)/[1+(\alpha/(2k))^2]\}^{1/2}$ [1, 4] with $\bar{r}_0 = \beta_0 r_0\sqrt{\varepsilon_r}$, $k = \alpha\bar{\beta}/(2\bar{\beta}_2)$, $\bar{\beta} = \beta/(\beta_0\sqrt{\varepsilon_r})$, $\bar{\beta}_2 = \beta_2/(\beta_0\sqrt{\varepsilon_r})$, $\beta_0 = \omega\sqrt{\varepsilon_0\mu_0}$, α — off-diagonal ferrite permeability tensor element, β — phase constant, $\beta_2 = [\omega^2\varepsilon_0\mu_0\varepsilon_r(1-\alpha^2)-\beta^2]^{1/2}$ — radial wavenumber, r_0 — guide radius, ω — angular frequency of the wave, ε_r — ferrite relative permittivity, $\zeta_{k,n}^{(c)}$ — roots in x_0 of the characteristics equation of geometry $\Phi(a,c;x_0)=0$ [1, 4], written by the complex Kummer confluent hypergeometric function [6] in that $a = c/2 - jk$, $c = 3$, $x_0 = jz_0$, $z_0 = 2\bar{\beta}_2\bar{r}_0$, ($\bar{\beta}_2 = \zeta_{k,n}^{(c)}/(2\bar{r}_0)$) and $n = 1$. The first approach is connected with the normalized critical guide radii $\bar{r}_{0cr} = \zeta_{0,n}^{(c)}/[2(1-\alpha_{cr}^2)^{1/2}]$, (with the cut-off frequencies) and the second one — with the envelope curve in the phase diagram of configuration of equation $\bar{r}_{0en-} = L(c,n)/[|\alpha_{en-}|(1-\alpha_{en-}^2)^{1/2}]$, $\bar{\beta}_{en-} = (1-\alpha_{en-}^2)^{1/2}$ in which $L(c,n)$ are certain positive real numbers [1]. (The subscripts "cr" and "$en-$" mark the quantities, related to the cut-off and to the envelopes, resp. and the ones "+" and "–" — to positive ($\alpha_+ > 0$) and negative ($\alpha_- < 0$) magnetization.) For a fixed value of α ($|\alpha| < 1$) an arbitrary negative (positive) one of the parameter k is chosen in the first (second) case and the roots $\zeta_{k,n}^{(c)}$ of characteristic equation which have a bearing on it, are figured. Then, the numerical equivalents of α, k and $\zeta_{k,n}^{(c)}$ are put in the expressions for $\bar{r}_0$ and $\bar{\beta}$. The parameter k is varied, until the counted value of $\bar{r}_0$ coincides with the one of $\bar{r}_{0cr}$, resp. of $\bar{r}_{0en-}$ for the singled out $|\alpha| \equiv |\alpha_{cr}|$, resp. $|\alpha| \equiv |\alpha_{en-}|$ with the prescribed accuracy. The relevant computed value of phase constant $\bar{\beta}_{c-}$ (of the difference $\Delta\bar{\beta}_{en-} = \bar{\beta}_{en-} - \bar{\beta}_+$) yields the differential phase shift at cut-off (at the corresponding point from the envelope). Afterwards α is changed and the procedure is repeated.

REFERENCES

1. Georgiev, G. N. and M. N. Georgieva-Grosse, "A new property of the complex Kummer function and its application to waveguide propagation," *IEEE Antennas Wireless Propagat. Lett.*, Vol. 2, 306–309, December 2003.
2. Georgiev, G. N. and M. N. Georgieva-Grosse, "An application of the complex Tricomi function," *Proc. Eleventh Int. Conf. Electromagn. Adv. Applicat. ICEAA'09*, 819–822, in CDROM, Turin, Italy, September 14–18, 2009.
3. Georgiev, G. N. and M. N. Georgieva-Grosse, "Effect of the dielectric filling on the phase behaviour of the circular waveguide with azimuthally magnetized ferrite toroid and dielectric cylinder," *Proc. Asia-Pacific Microwave Conf. APMC-2009*, WE4B-4(1680), in CDROM, Singapore, December 7–10, 2009.
4. Georgiev, G. N. and M. N. Georgieva-Grosse, "Iterative method for differential phase shift computation in the azimuthally magnetized circular ferrite waveguide," *PIERS Online*, Vol. 6, No. 4, 365–369, 2010.
5. Georgieva-Grosse, M. N. and G. N. Georgiev, "Differential phase shift characteristics of normal TE_{0n} modes in an azimuthally magnetized coaxial ferrite waveguide," *Proc. 4rd Europ. Conf. Antennas Propagat. EuCAP 2010*, P4-53, Barcelona, Spain, April 12–14, 2010.
6. Tricomi, F. G., *Funzioni Ipergeometriche Confluenti*, Edizioni Cremonese, Rome, Italy, 1954.

Detection of Materials Structure via 3D Imaging

George G. Cheng, **Yong Zhu**, **and Jan Grzesik**
Allwave Corporation, 3860 Del Amo Blvd., #404, Torrance, CA 90503, USA

Abstract— We introduce a new imaging technique which determines the quality of materials by detecting only the received signals with no knowledge of the transmitting sources. The received signals are collected via planar, spherical, or cylindrical near-field measurements. The imaging of the material under test is achieved by processing the near-field data in accordance with the Field Mapping algorithm, which determines the electric and magnetic fields in any given region of interest. The image of the target materials is then ascertained from the field polarization attributes which indicate medium anomalies due to the defect.

The Field Mapping algorithm, as we called it, is one which transforms electromagnetic fields from one surface to another in an exact sense. This algorithm determines the entire electric and magnetic field everywhere based on two tangential field components, either electric or magnetic, on a surface, say a plane, a sphere, or a cylinder. In particular, the medium associated with the field distribution can thus be revealed as to its structure and electrical properties by way of the field polarization attributes. The Field Mapping is applicable in any region, either interior or exterior to the data surface, or in between. Moreover, the Field Mapping algorithm is a direct, closed-form solution which is numerically straightforward and efficient.

The procedure of imaging consists of two steps. First, one obtains the electric field in the vicinity of the region of interest. Normally the data is collected on a planar, spherical, or cylindrical surface. Regardless of the source, the required field can be of either a transmitted or reflected kind. Second, one provides this near-field data as input to the imaging algorithm, whose output reveals the medium structure across the area under investigation.

Five test cases, including two analytic examples, two FDTD simulation runs, and a hardware measurement, are given so as to verify the imaging technique. Excellent results are obtained.

Session 3P2b
Remote Sensing of the Earth, Ocean, and Atmosphere

A Study of Interferometric Phase Statistics for Sea Surface Height Retrieval Using Numerically Simulated Low Grazing Angle Backscatter Data

C. S. Chae and J. T. Johnson
ElectroScience Laboratory, Department of Electrical and Computer Engineering
The Ohio State University, 1320 Kinnear Road, Columbus, OH 43212, USA

Abstract— The retrieval of sea surface height profiles from low grazing angle radar data is a topic that has received recent research interest. Radar systems with two vertically separated receiving antennas and a capability of phase measurements can be used to estimate surface height information versus range; this is an interferometrybased sea height retrieval. The method uses phase difference between fields received at the two antennas in order to estimate surface height. It is also possible to estimate height information from other measured radar quantities such as the received power versus range and/or the Doppler frequency versus range. A recent study using numerically simulated scattering data for one-dimensional sea surfaces included interferometric simulations. The study showed that interferometric retrievals could provide reasonable accuracy retrieving surface height in visible, but not shadowed, portions of the surface.

An extension of this work to study the statistical properties of interferometric phases using numerically simulated scattered fields from ocean-like surfaces is presented in the talk. Numerical datasets generated using the one dimensional method of moments (MOM) simulator are analyzed to produce statistics of the interferometric phase difference for the low grazing angle observation geometry. Surfaces comprised of "short" sea waves only or a fixed "long wave" profile with stochastic shorter sea waves are considered. Phase difference histograms from the numerical simulations are compared with predictions from a previously reported theory of this process. The influence of the number of pulses integrated is also considered, along with the effects of changing geometrical and radar parameters such as the baseline distance. Result of error analysis in both visible and shadowed region which shows bias due to shadowing and multipath effect will be discussed. Also, several applications of the study will be presented, and implications of the results for practical sea surface height retrieval systems will be discussed.

Research of a Solid Object Impacting on the Water Surface

Ching-Jer Huang and Tsung-Mo Tien
National Cheng-Kung University, Taiwan

Abstract— The high-speed camera and an underwater hydrophone were applied to measure the trajectory and the underwater sounds of a solid object impacting on the water surface. The analysis methods include Fast Fourier Transform (FFT) and Gabor Transform, not only reveal sounds in frequency domain but also in tine — frequency domain. It is found that the frequency spectrum for the solid object impacting the water surface less than 10 kHz. Through this analysis, a better understanding of the mechanism of a solid object impacting on the water surface will be helpful to ocean remote sensing.

A Rectangular Patch Antenna Technique for the Determination of Moisture Content in Soil

K. Y. You[1], **J. Salleh**[1], **Z. Abbas**[2], **and L. L. You**[3]

[1]Radio Communication Engineering Department, University Teknologi Malaysia
UTM Skudai 81310, Malaysia
[2]Department of Physics, University Putra Malaysia, UPM Serdang 43400, Malaysia
[3]Department of Human Biology, School of Medicine and Health Sciences
International Medical University, Kuala Lumpur 57000, Malaysia

Abstract— This paper presents a compact and low cost rectangular patch antenna that was used as a sensor for real time agriculture measurements. There were two types of rectangular patch sensor have been fabricated using FR4 printed circuit board and tested on soil (peat and loam). Both sensors were designed based on resonant and reflection principle which were operated at frequency range from 1.5 GHz to 3 GHz. The peat and loam soil were measured in a range of moisture content, m.c from 0% to 30% and the fraction bond water in these soil samples were also analyzed.

Monitored Solar Cycle in Relation to an Approximated Model

Shigehisa Nakamura
Kyoto University, Kyoto, Japan

Abstract— This is a note to help a significant trend of the 11 year cycle in the solar activity. The monitored solar cycle for about 100 years is studied by an approximated model in order to understand a specific property of solar activity in a scope of dynamical electromagnetism. This solar cycle model could be a key to an answer at considering any one of the geophysical processes on the earth.

The solar cycle could be solved referring essentially to the Maxwell equations for the magnetic field B, the electric field E, and the electric current density j [I]. Then, an induction equation is reduced. Electric conductivity of the sun could be determined as that of the ionized gas (or plasma) following to Spitzer (1962). For the case of the dynamo problem in terms of a mean magnetic field, $B = {}^*B + b$, where ${}^*B$ may be understood as an average over longitude or, more generally, as an ensemble average. Then, ${}^*b = 0$. In a same way, $v = {}^*v + u$. Substituting these two into the induction equation, fluctuating part is obtained after separating the mean part.

Feature of the mean-field induction equation is the term involving a (called as "α effect"). Following to Knause (1967), $\alpha = +I\Omega$ (or $-1\,\Omega$) is the mean angular velocity of the Sun. The sign of α depends on helicity of the flow in the solar convection.

Stix (1976) has shown the meridional cross sections for contours of constant toroidal field strength and poloidal lines of force. The arrows are indicating strength and sign of polar field. An illustration is given in an adjusted time scale for 11 years for each half-cycle.

Theoretical butterfly diagram (contours of constant toroidal field) in an oscillatory kinematic $\alpha\Omega$ dynamo is shown by Steenbeck and Krause in 1969.

The numerical results noted above is obtained under several assumption with some conditions, so that specific patterns could be demonstrated on the bases of the dynamical theory in an approximated forms as introduced by Stix [I].

The author here has to notice that the scientists should have their understanding of the specific pattern in the solar activity at considering the geophysical processes on the planet earth.

Satellite Monitoring of Lunar Shadow on the Earth at Solar Eclipse

S. Nakamura
Kyoto University, Japan

Abstract— A problem is introduced for satellite thermal monitoring of the earth surface, i.e., on the ocean and on the land surfaces. This problem should be considered in relation to a satellite monitoring of the earth surface in the visible band. Some concerning note is given with a specific case of the recent events to have our physical understanding to a satellite monitoring of solar eclipse shadow 2009 on the earth surface. For several years of the minimum solar activity by 2008, the scientists had tending to doubt of the solar 11 year cycle. It was on 2009 July 22 an event of solar eclipse shadow was monitored by the satellite monitoring in the visible band, though the author has had worked for satellite thermal monitoring. On that day, the shadow was monitored by the satellite GMS-2 to show a supporting pattern in every 15 minutes. This monitoring in the visible band has given the data as distributed by Japan Meteorological Agency to demonstrate an agreeable prediction issued by the National Astronomical Observatory in a form of annual publication. The author here notices that the man-made satellite is effective to operate for monitoring the solar eclipse shadow on the earth surface which is seen at the lunar passage between the sun and the earth. This monitoring might be a key to evaluate the thermal effect of the solar eclipse shadow on the earth surface in an infrared band to see the actual radiation out of the earth, though the radiation out of the earth has been evaluated by a theoretical model under an assumption of that the planet earth is taken as a black body in the solar system.

Monitored Solar Cycle in Relation to Sea Surface Temperature at Azores in the Northeast Atlantic Ocean

S. Nakamura
Kyoto University, Japan

Abstract— This is a brief note to the monitored solar cycle in relation to the sea surface temperature at a station in the ocean. First of all, a short note on the monitored solar cycle as a part of "Astronomy". One of the most classic interests for the scientists is "global magnetism" of the sun just like the main magnetic field of the earth.

A convenient index of the solar cycle is the sun spot relative number. As for the two types of "sun spot models", the first one is an empirical one. The second one is the magnetohydrostatic model. A part of solar cycle variation of sun sopts is introduced in a diagram. This cycle was found first by Schwabe (l844). Hale had the first scientist of the magnetic field in sun spots in 1908. Hale (by 1923) had observed them and formulated his polarity rules. That is to say, that (1) the magnetic orientation of leader and follower spots in bipolar groups remains the same in each hemisphere over each 11-year cycle, (2) the bipolar groups in the two hemispheres have opposite magnetic orientation, and (3) the magnetic orientation of bipolar groups reverses from one cycle to the next. Another important result is known as butterfly diagram (Maunder, 1922) at present. The systematic behaviour of bipolar sun spot groups is readily understood in terms of a subsurface mean toroidal magnetic field, which is a field where lines of force are circles around the solar axis. In addition to the mean toroidal field there is a mean poloidal magnetic field. Cowling (1934) stated first the line-of-sight component of the magnetic field B. The mean field electrodynamics has been developed since 1955 by Parker (1955131, and the followers.

In 2007, the Azores Scientific Group showed that the observed sea surface temperature during the time period of 1960 to 2007 has shown a significant trend to fit the solar cycle variation of sun spots. Nevertheless, it is hard to accept what has introduced by the Azores Group for helping to understand any global trend of the sea surface temperature on the planet earth. The scientists for dynamics of the ocean and atmosphere have found already any dynamical processes of the geophysical fluid motions are not so simple to see on a basis of a limited data observed on the earth surface. The Azores Group had a lucky position of their station for obtaining their interesting finding.

The author here has to note whether the Azores Scientific Group could show a same trend for their extensive observation of the sea surface temperature in relation to solar spots for about several ten years trends of the two physical factors.

Session 3P3
Antenna Array Synthesis — Theory, Algorithms, and Applications

A Pattern Synthesis Technique for Multiplicative Arrays

Herbert M. Aumann
MIT Lincoln Laboratory, Lexington, Massachusetts, USA

Abstract— A two-dimensional multiplicative phased array, such as a Mills Cross array [1], is well known in radio astronomy for providing high angular resolution at low cost. When compared to an $N \times M$ element planar phased array, a multiplicative array provides the same null-to-null beamwidth with only $N + M$ elements. Typically a multiplicative array consists of two orthogonal linear arrays with coincident phase centers. A conventional fan beam is formed by each linear array. The two beams are then cross-correlated to generate a multiplicative array pattern. Multiplicative arrays with uniform excitation have sidelobes that are 6 dB higher than those of a planar array with uniform illumination. MacPhie [2] showed that the power pattern of a multiplicative array pattern can be made to match the power pattern of a planar array with uniform excitation.

In this presentation we generalize the power pattern technique. We will prove that an excitation function for the multiplicative array can be synthesized so that its power pattern is identical in every respect to a planar array pattern with an arbitrary excitation, provided that the planar array excitation is separable. It is shown that the excitation of each linear array of the multiplicative array has to be the auto-correlation of the excitation along the corresponding major axis of the planar array. The latter excitation can be obtained from any conventional pattern synthesis technique. Thus, a multiplicative array can match with $2(N + M - 1)$ elements the beamwidth and sidelobes of the $N \times M$ element planar array. The result is illustrated by the excitation function required to implement a two-dimensional 30 dB Chebyshev taper with a multiplicative array.

REFERENCES

1. Mills, B. Y. and A. G. Little, "A high resolution aerial system of a new type," *Australian J. of Phys.*, Vol. 6, 272–278, 1953.
2. MacPhie, R. H., "A mill cross multiplicative array with the power pattern of a conventional planar array," *Proceedings of the IEEE Antennas and Propagation Society Int. Symposium*, 1064–1076, Charleston, North Carolina, USA, July 2008.

Rectangular Thinned Array Design by McFarland Difference Sets

G. Oliveri, **F. Caramanica**, **P. Rocca**, **and A. Massa**
ELEDIA Research Group at DISI, University of Trento, via Sommarive 14, I-38123, Trento, Italy

Abstract— The problem of reducing the number of elements of large arrays is of great importance in satellite, remote sensing, radar and biomedical imaging applications in which the cost, weight, power consumption, mutual coupling effects, HW and SW complexity have to be as low as possible. Thinned arrays, however, are known to exhibit high peak sidelobe levels (*PSL*) if not suitably designed [1]. As a consequence, design techniques able to control and reduce the PSL of non-regular arrays have been subject of research since their introduction [1–5].

Random designs were among the first methodologies to be applied, due to their simplicity and their good performances [1]. Such approaches have been overcome only by the introduction of stochastic optimization techniques [1], which, however, can be computationally unfeasible for very large arrays, and do not allow a-priori estimate of their performances [1]. More recently, an innovative deterministic technique able to provide good and predictable performances with very low computational efforts has been proposed for the thinning of large arrays [1]. Such technique, which exploits the two-level autocorrelation function of binary sequences derived by *difference sets* (DSs), has been shown to provide predictable advantages in terms of PSL with respect to the corresponding random designs, both for linear and for square and almost-square designs [1]. Moreover, an extension of such an approach, based on Almost Difference Sets, has allowed its application in a significantly wider set of configurations [2, 3]. However, no rectangular DS (or ADS) designs with very different resolutions in the two angular directions have been investigated at present, despite the practical importance of such arrays in radar and remote sensing applications.

In this paper, the performances of a new class of DS-based thinned arrays will be investigated. The thinned geometries will be deduced by McFarland DSs [4], which are a class of non-cyclic DSs defined over a $p \times p(p+2)$ lattice (with p a prime number). The accuracy of the available PSL estimators will be assessed by means of an extensive numerical validation, and comparisons with state-of-the-art thinning techniques will be provided as well.

REFERENCES

1. Leeper, D. G., "Isophoric arrays-massively thinned phased arrays with well-controlled sidelobes," *IEEE Trans. Antennas Propagat.*, Vol. 47, No. 12, 1825–1835, Dec. 1999.
2. Oliveri, G., M. Donelli, and A. Massa, "Linear array thinning exploiting almost difference sets," *IEEE Trans. Antennas Propagat.*, Vol. 57, No. 12, 3800–3812, Dec. 2009.
3. Oliveri, G., L. Manica, and A. Massa, "ADS-based guidelines for thinned planar arrays," *IEEE Trans. Antennas Propagat.*, in press.
4. McFarland, R. L., "A family of difference sets in non-cyclic groups," *Journal of Combinatorial Theory, Series A*, Vol. 15, No. 1, 1–10, Jul. 1973.

Interleaved Array Antennas Design — (Almost) Deterministic Strategies

Massimiliano Simeoni[1], **Ioan E. Lager**[1], **Cristian I. Coman**[2], **and Christian Trampuz**[1]

[1]International Research Centre for Telecommunications and Radar (IRCTR)
Faculty of Electrical Engineering, Mathematics and Computer Science
Delft University of Technology, CD Delft, The Netherlands
[2]NATO Consultation, Command and Control Agency (NC3A), 2597 AK the Hague, The Netherlands

Abstract— The concept of interleaving sparse (sub)arrays for optimizing the aperture efficiency of an antenna system, advocated in [1], and based on the principle of accommodating various types of radiators on a common aperture, was detailed and discussed in [2]. The approach was referred to as the 'shared aperture concept'. The initial expectations were focused on reusing the empty space available in non-periodic arrays for deploying individual elements or sub-arrays supporting alternative services. Successively, array interleaving became a topic of investigation in itself, demonstrating the versatility of this technique with clear ramifications in implementing multi-functionality. Shared aperture array antennas were designed to operate concurrently on multiple bands [2], multiple polarizations [3] and to implement the different functions (i.e., transmitting and receiving) of a continuous-wave (CW) radar system [4].

Naturally, a number of issues need to be addressed in designing a shared aperture antenna. Firstly, the constituent sub-arrays need to be designed to satisfy their relevant requirements. Secondly, a strategy for collocating them on the common aperture needs being identified. At this stage, it is crucial avoiding any physical overlapping between the elements of the individual sub-arrays. Finally, optimal use of the available aperture surface has to be ensured. The statistical properties of the so-called Cyclic Difference Sets (CDSs), sets of numbers previously used in the realm of communication technology and cryptography, can be exploited to design naturally interleaved sub-arrays with well controlled radiation properties. The CDS-based technique is completely deterministic, enabling a fast design yielding well predictable radiation performance [2, 3]. The CDS-based technique, complemented by a trimming of the array elements, was adopted in [5] for reducing the side-lobe radiation of a CW radar antenna system. Another way of addressing the issues related to the design of a shared aperture antenna is resorting to statistical methods, an example of this approach being reported in [6].

The present contribution will briefly recall the benefits brought by the shared aperture concept in terms of implementing concurrent functionalities in the same array aperture. However, the focus will be on the synthesis strategies to be used for designing shared aperture antennas; ranging from the fully deterministic approaches to semi-deterministic ones up to purely statistical design techniques. The pros and cons of each technique will be discussed and compared. Finally, some practical implementations of the shared aperture concept will exemplify the advocated design techniques.

REFERENCES

1. Haupt, R. L., "Interleaved thinned linear arrays," *IEEE Transactions on Antennas and Propagation*, Vol. 53, No. 9, 2858–2864, Sep. 2005.
2. Coman, C. I., "Shared aperture array antennas composed of differently sized elements arranged in sparse sub-arrays," Ph.D. Dissertation, Delft University of Technology, Jan. 2006.
3. Simeoni, M., I. E. Lager, C. I. Coman, and A. G. Roederer, "Implementation of polarization agility in planar phased-array antennas by means of interleaved subarrays," *Radio Science*, Vol. 44, RS5013, Oct. 2009.
4. Trampuz, C., M. Simeoni, I. E. Lager, and L. P. Ligthart, "Complementarity based design of antenna systems for FMCW radar," *Proc. 5th European Radar Conference — EuRAD*, 216–219, Amsterdam, The Netherlands, Oct. 2008.
5. Lager, I. E., C. Trampuz, M. Simeoni, and L. P. Ligthart, "Interleaved array antennas for FMCW radar applications," *IEEE Trans. Antennas Propagat.*, Vol. 57, No. 8, 2486–2490, Aug. 2009.
6. Trampuz, C., M. Simeoni, I. E. Lager, and L. P. Ligthart, "Low sidelobe interleaved transmit-receive antennas for FMCW radar applications," *IEEE Antennas Propagat. Symp. Dig.*, Charleston, USA, Jun. 2009.

Antenna Array Synthesis through Time Modulation

L. Poli, **P. Rocca**, **G. Oliveri**, **L. Lizzi**, **and A. Massa**
ELEDIA Research Group at DISI, University of Trento, Via Sommarive 14, I-38123 Trento, Italy

Abstract— In the last years, there has been a renewed interest towards the use of time-modulated arrays (TMAs) thanks to the simplicity in reconfiguring the average pattern of the antenna just modifying the on-off sequence controlling a set of radio-frequency (RF) switches. TMAs have been originally introduced for the generation of low and ultra-low sidelobe patterns for radar arrays [1] thus avoiding the implementation of impracticable excitation tapering with high dynamic range ratios. However, they haven't received a large diffusion because of the power losses due to the generation of harmonic radiation at multiples of the time-modulation frequency. As a matter of fact, the periodic modulation of the static excitations causes a shift of the radiated power in the sideband radiation (SR) [2] with a consequent reduction of the directivity of the pattern at the carrier frequency.

Recently, thanks to the significant development of stochastic optimization algorithms boosted by the growing computational resources available with modern personal computers, several approaches have been proposed to deal with the synthesis of time-modulated arrays while keeping low the power losses in the SR. Both single-agent techniques (e.g., Simulated Annealing [3]) and evolutionary-based optimization methods (e.g., Differential Evolution [4] and Particle Swarm Optimization [5]) have been effectively applied. In such a framework, TMAs have been used for the generation of shaped beams as well as of sum and difference patterns for search-and-track antenna systems [6]. Moreover, they have demonstrated being suitable for the synthesis of pulse Doppler radars [7] and phase switch screens [8].

This contribution is aimed at reviewing the last advances in the synthesis of TMAs also showing that the introduction of additional degrees of freedom available in the time domain and suitable for the definition of the pulse sequence enables the synthesis of TMAs with improved performance. More specifically, besides the control of the durations of the time pulses controlling the RF switches for the definition of a desired pattern at the carrier frequency, also the optimization of the switch-on instants has been taken into account. Such a strategy allows to spread the energy lost in the SR on the whole visible range thus lowering the interferences, to generate and shape the harmonic patterns, and to avoid the instantaneous reduction of some pattern features [9].

REFERENCES

1. Kummer, W. H., A. T. Villeneuve, T. S. Fong, and F. G. Terrio, "Ultra-low sidelobes from time-modulated arrays," *IEEE Trans. Antennas Propag.*, Vol. 11, No. 6, 633–639, Nov. 1963.
2. Brégains, J. C., J. Fondevila, G. Franceschetti, and F. Ares, "Signal radiation and power losses of time-modulated arrays," *IEEE Trans. Antennas Propag.*, Vol. 56, No. 6, 1799–1804, Jun. 2008.
3. Fondevila, J., J. C. Brégains, F. Ares, and E. Moreno, "Optimizing uniformly excited linear arrays through time modulation," *IEEE Antennas Wireless Propag. Lett.*, Vol. 3, 298–301, 2004.
4. Yang, S., Y. B. Gan, and A. Qing, "Sideband suppression in time-modulated linear arrays by the differential evolution algorithm," *IEEE Antennas Wireless Propag. Lett.*, Vol. 1, 173–175, 2002.
5. Poli, L., L. Manica, P. Rocca, and A. Massa, "Handling sideband radiations in time-modulated arrays through particle swarm optimization," *IEEE Trans. Antennas Propag.*, in press.
6. Rocca, P., L. Manica, L. Poli, and A. Massa, "Synthesis of compromise sum-difference arrays through time-modulation," *IET Radar, Sonar & Navigation*, Vol. 3, No. 6, 630–637, Dec. 2009.
7. Li, G., S. Yang, and Z. Nie, "A study on the application of time modulated antenna arrays to airborne pulsed doppler radar," *IEEE Trans. Antennas Propag.*, Vol. 57, No. 5, 1578–1582, May 2009.
8. Tennant, A. and B. Chambers, "Time-switched array of phase-switched screens," *IEEE Trans. Antennas Propag.*, Vol. 57, No. 3, 808–812, Mar. 2009.
9. Manica, L., P. Rocca, L. Poli, and A. Massa, "Almost time-independent performance in time-modulated linear arrays," *IEEE Antennas Wireless Propag. Lett.*, Vol. 8, 843–846, Aug. 2009.

A Complete MIMO System Built on a Single RF Communication Ends

Vlasis Barousis, Athanasios G. Kanatas, and George Efthymoglou
University of Piraeus, Greece

Abstract— It is well known that Multiple Input — Multiple Output (MIMO) architectures improve significantly the performance of wireless communication systems. Depending on the system design, the effect of multiple antennas might be twofold; in spatial multiplexing mode, the objective is the data rate maximization, by exploiting appropriately the structure of the channel matrix to obtain independent signaling paths that can be used to support independent data streams. Alternatively, in diversity mode the multiple antennas are jointly used in order to effectively mitigate the negative effects of fading, thus improving the overall system reliability. Although the promising performance of MIMO systems necessitates their implementation to modern wireless communications, the corresponding hardware complexity hinders the wide application of such systems.

Recently, remarkable research work is drawn in order to investigate alternative MIMO architectures with reduced hardware complexity, while maintaining the total performance in the same levels as in conventional MIMO approach. The effort mainly is focused on the reduction of the required radio-frequency (RF) chains, which in classical approach equal the number of antenna elements utilized. Indeed, antenna selection, RF pre-processing, antenna subarray' formation and beamspace MIMO reflect significant research work towards this aim. In this paper, we propose a new MIMO architecture built on Electronically Steerable Parasitic Antenna Radiators (ESPAR). Such antennas consist of a single active element which is surrounded by several parasitic (or passive) elements in linear or planar arrangement. Beamforming abilities are achieved by tuning the varactors loaded directly to the parasitic elements. Since a single active element is present, a single driving port is required, thus reducing dramatically the implementation cost. However, well known MIMO transmission and reception techniques applied to antenna space cannot be used.

Therefore, we consider the whole design and operation at beamspace (i.e., wavevector) domain. In particular, we show a novel technique in which an appropriate radiation pattern is formed at each time slot, depending on the transmit symbol vector. In other words, in the proposed technique the information of the transmit symbol vector is encoded to the transmit radiation pattern. On the other hand, at the receiver we exploit ESPAR antennas to sample the impinging field during one symbol period with different orthogonal radiation patterns to detect and decode the received symbols. Moreover, the resulting bit error rate performance is compared with corresponding traditional MIMO systems to show that it is possible to maintain high performance levels using significantly reduced hardware MIMO transceivers.

Critical Wavenumbers in the Classification of Fractal Radiation Patterns

Giovanni F. Crosta
Inverse Problems & Mathematical Morphology Unit
Department of Environmental Sciences, University of Milan-Bicocca
1, piazza della Scienza, Milan, IT 20126, Italy

Abstract—

Motivation: Fractal models apply to radiation patterns from the so-called fractal antennas and to the description of wave propagation through a complicated environment. In antenna *design* the prototype antenna array factor has been provided by Weierstraß functions and their band-limited approximations. In antenna *characterization* one may want to assign a given (synthesized or measured) radiation pattern to a fractal class.

Fractal Pattern Synthesis: Array antenna factors are synthesized by means of Weierstraß functions [1]. In one spatial dimension (x_1) one has

$$f[x_1] := \sum_{m=0}^{\infty} b^{(D-2)m} \cos[2\pi b^m x_1]$$

where $1 < D < 2$, and b is the wavenumber such that $b > 1$. It can be shown that the box-counting (B) fractal dimension ($\dim_B$) of the graph of $f[.]$ (graph$[f]$) satisfies $\dim_B[\text{graph}[f]] = D$. Two-dimensional fractal radiation patterns can be synthesized by separation of variables.

Classification of Synthesized Fractal Patterns: The spectrum enhancement ($\sigma\eta$) algorithm, introduced a few years ago [2 and references quoted therein] operates on the Fourier transform of a function of two variables. It evaluates derivatives of integer [3] or of fractional order [4], followed by some non-linear operations. By applying $\sigma\eta$ to a synthesized fractal pattern one obtains a vector of morphological descriptors, which are submitted to a trainable classifier. A typical classification result is displayed by Figure 1 where the center panel shows the fractal pattern class centroids on the plane of the first two principal components z_1 and z_2. Each of the five classes (labelled $1, 3, 5, 6, 9$) is composed of patterns such that $b = 14$ and 16. Moreover, in class 1, $D = 1.1$; in class 3, $D = 1.3$ (sample pattern on the right panel); in class 5, $D = 1.5$; in class 6, $D = 1.6$ and in class 9, $D = 1.9$ (sample on the left panel).

Problem to be Addressed: There are critical values of the wavenumber [5] at which the numerical estimation of $\dim_B[\text{graph}[f]]$ is affected by relevant errors. The goal of this investigation is to determine whether or not the same wavenumber values are critical for the $\sigma\eta$ algorithm as well and, in case they are, provide an explanation.

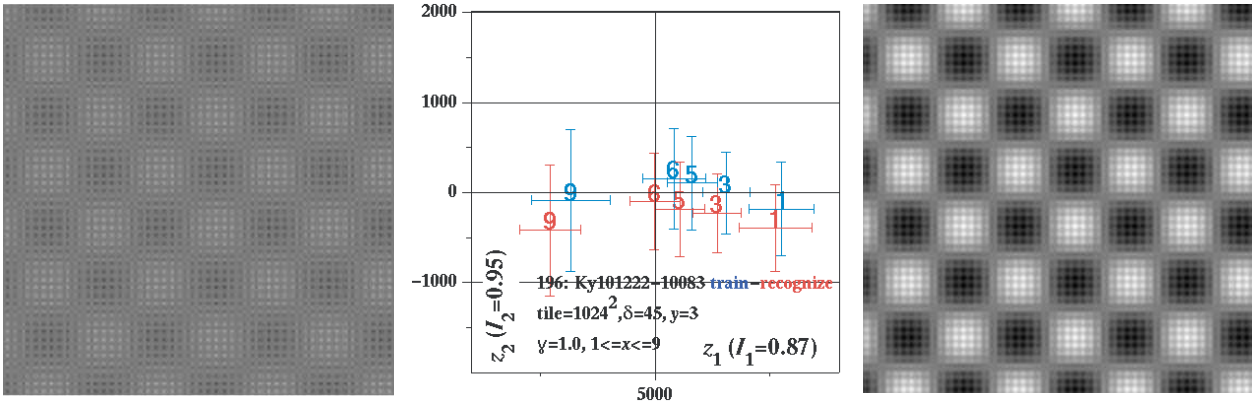

Figure 1.

REFERENCES

1. Werner, D. H. and P. L. Werner, *Radio Science*, Vol. 30, No. 1, 29–45, 1995.
2. Crosta, G. F., "Image analysis and classification by spectrum enhancement: new developments," *Proceedings of the SPIE*, Vol. 7532, 75320L01–75320L12, 2010, Doi: 10.1117/12.838694.
3. Crosta, G. F., "Feature extraction by differentiation of fractional order," *Progress In Electromagnetics Research Symposium Abstracts*, 425, Electromagnetics Academy, Cambridge, MA, 2006.
4. Crosta, G. F., "Morphological characterization of two-dimensional random media and patterns by fractional differentiation," *Progress In Electromagnetics Research Symposium Abstracts*, 627, Electromagnetics Academy, Cambridge, MA, 2008.
5. Jaggard, D. and X. Sun, "Scattering from bandlimited fractal fibers," *IEEE Trans. Ant. Propag.*, Vol. 37, 1591–1597, 1989.

Artificial Magneto-superstrates for Gain and Efficiency Improvement of Microstrip Antenna Arrays

H. Attia, O. Siddiqui, and O. M. Ramahi
University of Waterloo, Canada

Abstract— This paper presents an engineered magneto-dielectric superstrates designed to enhance the gain and efficiency of a microstrip antenna array without any substantial increase in the antenna profile. The broadside coupled split ring resonator (SRR) inclusions are used in the design of the superstrate. Numerical full-wave simulations of a 4×1 linear microstrip antenna array working at the resonance frequency of 2.18 GHz and covered by the superstrate show a gain enhancement of about 3.0 dB and an efficiency improvement of 10%. The total height of the proposed structure, is $\lambda_0/7$ where λ_0 is the free-space operating wavelength.

Analytical Model to Compute the Far-field Radiation of Patch Antennas Arrays Loaded with Metamaterial-superstrates

H. Attia, O. Siddiqui, and O. M. Ramahi
University of Waterloo, Canada

Abstract— The reciprocity theorem and the transmission line analogy are used to compute the far-field radiation of a linear microstrip antenna array covered with an engineered magnetic superstrate to increase the antenna gain. The single radiating element will be replaced by two magnetic line sources using the cavity model. The evaluation of the far-field is transformed into the evaluation of the field at the two magnetic line sources locations by applying the reciprocity theorem. The broadside coupled split ring resonator (SRR) inclusions acting as building blocks for the artificial magnetic superstrate are characterized analytically to obtain the effective permeability and permittivity to be used in the analytical model of the whole radiating system. Numerical full-wave simulations are provided to verify the analytical results for the far-field radiation.

Rectangular Ring Antenna for On-body Communication System

N. Zainudin and M. R. Kamarudin
Wireless Communication Centre (WCC), Faculty of Electrical Engineering
Universiti Teknologi Malaysia, Skudai Johor, Malaysia

Abstract— The demand of smaller and compact antennas in modern mobile and wireless communication system has been increasing [1]. Because of low cost and process simplicity, printed monopole antennas are popular candidates for these applications and applicable in body centric communications [2].

A simple and compact microstrip-fed printed monopole antenna is proposed in this design. The antenna is composed of a rectangular ring for operating frequency at 2.45 GHz. The fabricated printed rectangular ring antenna is shown in Figure 1. The configuration has rectangular base with rectangular slot cut inside the patch resulting the rectangular ring [3]. The dimension of the patch is 12 mm × 26 mm with ring width size of 1 mm along the patch. The size of partial ground plane is 20 mm × 9 mm while the dimension of substrate used is 20 mm × 40 mm. The antenna are designed on FR4 substrate with thickness of 1.6 mm, dielectric permittivity, ε_r is 4.7 and tangent loss is 0.019.

The designed antenna had been successfully simulated using CST Microwave Studio Suite. It was found that the antenna operate well at 2.45 GHz. Return Loss measurement had been done using spectrum analyzer and the simulated and measured results are in good agreement. The antenna covers bandwidth from 2.35 GHz to 2.8 GHz which is 17.54%.

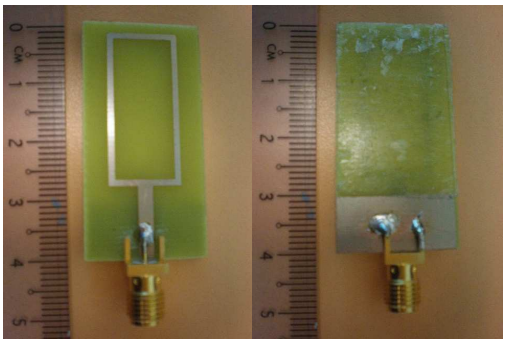

Figure 1: Antenna prototype front view and back view.

REFERENCES

1. Hall, P. S. and Y. Hao, (eds.), *Antennas and Propogation for Body Centric Wireless Communications*, Artech House, Boston/London, 2006.
2. Kamarudin, M. R., Y. I. Nechayev, and P. S. Hall, "Antennas for on-body communication systems," *IEEE International Workshop on Antenna Technology: Small Antennas and Novel Metamaterials, IWAT 2005*, 17–20, March 7–9, 2005.
3. Deng, H., X. He, B. Yao, and Y. Zhou, "A compact square-ring printed monopole ultra wideband antenna," *Microwave and Millimeter Wave Technology, ICMMT 2008*, 1644–1646, April 21–24, 2008.

A New Fractal Antenna for Super Wideband Applications

Abolfazl Azari
Young Researchers Club, Isalmic Azad University, Gonabad Branch, Iran

Abstract— Modern communication systems require small size and wideband antennas. Fractal geometries have been used to fabricate multi-band and broad-band antennas. In addition, fractal geometries can be miniaturized the size of antennas.

In this work, I have investigated a new fractal antenna with multi-band and broad-band properties. The proposed design is a loaded the 2nd iteration of a new fractal geometry to a square loop antenna. The simulation is performed via SuperNEC electromagnetic simulator software. The simulation results show that the proposed antenna is applicable in 1–30 GHz frequency range. Radiation patterns are also studied.

Koch Fractal Antenna for UWB Applications

Javad Rohani[1] and Abolfazl Azari[2]

[1]Islamic Azad University, Gonabad Branch, Iran
[2]Young Researchers Club, Islamic Azad University, Gonabad Branch, Iran

Abstract— Fractals have very unique properties, Therefore in recent years, antenna designers use fractal geometry in ultra wideband antennas designing.

In this paper, we have achieved an ultra wideband antenna by applying a Koch fractal geometry to a wire square loop antenna. Modelling and simulation is performed via SuperNEC electromagnetic simulator. Also, optimization is performed via GAO (genetic algorithm optimiser). This antenna is easy to be fabricated and has successfully demonstrated multi-band and broad-band characteristics. Results of simulations show that the proposed antenna has very good performance in bandwidth and Radiation pattern.

Session 3P4a
Approaches to Electromagnetic Simulation and Modeling for 2D and 3D Chips in the Nanometer Domain

Electromagnetic Simulation for Variation-aware Interconnect Parasitic Extraction

Tarek El-Moselhy and Luca Daniel
Massachusetts Institute of Technology, USA

Abstract— Advanced integrated circuit manufacturing steps such as etching, chemical mechanical polishing (CMP), electrodeposition, and photolithography produce large variabilities in the geometries of the manufactured interconnect structures. Such geometrical variabilities are not deterministic and are beginning to play a major role in determining the electrical characteristics of the interconnect structures. The development of efficient variation aware electromagnetic simulators is a critical step to promptly and accurately account for the effects of such variabilities.

Mathematically, variation aware simulators compute the solution of linear systems of equations, in which the coefficients of the system matrix are dependent on a set of random variables. Such solvers can be divided in general into two different categories, namely, those based on sampling algorithms (sometimes identified as non-intrusive) and those based on a stochastic formulation (sometimes identified as intrusive). In this talk we present two different variation-aware algorithms, namely, a non-intrusive stochastic model order reduction algorithm and an intrusive stochastic dominant singular vectors algorithm. Our algorithms have an unprecedented low complexity, which is asymptotically equivalent to the complexity of the standard deterministic solvers. We validate our algorithms on a variety of on-chip and off-chip capacitance and inductance extraction problems, ranging from moderate to very large size, not feasible using any of the available state of the art techniques.

A System for Electromagnetic Characterization of Inductors in the Presence of Other Nearby Inductors and Interconnect

Rafael Escovar, **Jean Christophe Tempesta**, **Navin Srivastava**, **and Roberto Suaya**
Mentor Graphics, Montbonnot, France

Abstract— Systems containing multiple inductors are common in wireless applications. Accuracy in the characterization of the frequency behaviour of impedance of these systems is a major design constraint. Design validation is typically done against test chips or Electromagnetic Field Solvers followed by SPICE simulations. The first technique is too constraining on design styles while the second one runs into capacity problems. The presence of nearby interconnect that could measurably affect the quality factors of the inductors exacerbates the capacity problem.

In this talk, we discuss a system level approach to the characterization and extraction of multiple inductors in the presence of interconnect. The accuracy of the extracted parameters for frequencies ranging from near DC up to hundreds of Gigahertz is better than 3%. Computational time for the extraction matrix as function of frequency is better than an order of magnitude faster than Finite element methods. The extraction algorithms incorporate the physics of proximity effects, skin effects and substrate Eddy currents. To address the downstream simulation problems we represent a system of n intentional inductors and or interconnect, with a $2n$-port model. It replaces the much larger PEEC representation. This compact representation is faithful to a complete RLC description. The parameters of the model (Z, Y or S parameter matrices) are obtained by solving a linear system resulting from the joint solutions to the magneto quasi-static and electro quasi-static problems of the intentional inductor and interconnect systems. For stability preservation this linear system is solved for significantly broader interval than that required for the design goal. The Padé approximates in the Laplace "s" plane for the S matrix are verified for stability.

The combination of system level extraction with the described reduction method, permits orders of magnitude faster Extraction/SPICE simulation of the circuit. We have tested the combined scheme on circuits containing tens of Inductors and local interconnect.

FastCaplet: A Template-based Capacitance Field Solver for 3D VLSI Interconnect

Yu-Chung Hsiao, **Tarek El-Moselhy**, **and Luca Daniel**
Massachusetts Institute of Technology, USA

Abstract— State-of-the-art capacitance extraction methods for Integrated Circuits (IC) involve scanning 2D cross-sections, and interpolating 2D capacitance values using a table lookup approach. This approach is fast and accurate for a large percentage of IC wires. It is however quite inaccurate for full 3D structures, such as crossing wires in adjacent metal layers. For such cases electrostatic field solvers are required. Unfortunately standard field solvers are inherently very time-consuming, making them completely impractical in typical IC design flows. Even fast matrix-vector product approaches (e.g., fastmultipole or precorrected FFT) are inefficient for these structures since they have a significant computational overhead and scale linearly with the number of conductors only for much larger structures with more than several hundreds of wires. In this talk we present therefore a new 3D extraction field solver that is extremely efficient in particular for the smaller scale extraction problem involving the ten to one hundred conductors in the 3D structures that cannot be handled by the 2D scanning and table look up approach.

Because of highly restrictive design rules of the recent sub-micro to nano-scale IC technologies, smooth and regular charge distributions extracted from simple model structures can be stored beforehand as "templates" and instantiated and stretched to fit practical complicated cases as basis function building blocks. This "template-instantiated" strategy largely reduces the number of unknowns and computational time without additional overhead. Given that all basis functions are obtained by the same very few stretched templates, Galerkin coefficients can be readily computed from a mixture of analytical, numerical and table lookup approaches. Furthermore, given the low accuracy (i.e., 3%–5%) required by IC extraction and the specific aspect ratios and separations of wires on ICs, we have observed in our numerical experimentations that edge and corner charge singularities do not need to be included in our templates, hence reducing the complexity of our solver even further.

Electromagnetic Simulation of 3D ICs, Some Novelties Related to 3D Problems in Stratified Media

Vassilis Kourkoulos and Roberto Suaya
Mentor Graphics, Montbonnot, France

Abstract— Industry is rapidly moving towards deploying 3D IC's based on through silicon vias (TSV's) technology, with limited understanding of the Electromagnetic behavior of the TSV's. The Electromagnetic modeling of TSV's demands non negligible extensions to what is incorporated on planar ICs. We demonstrate that treating the TSV's as lumped elements leads to substantial errors.

In this talk we present a 3D quasi-magneto static treatment to study the interaction among TSV's, as well as the interaction with horizontal currents in the different layers of a 3D IC. We use a Layered Media Green's Function formulation. We show significant results in terms of Impedance matrices for the 3D interconnect introducing a novel method for accurately describing the TSV's in the presence of general interconnect. We accurately compute the net impedance for wires that traverse two or more chip layers as function of frequency as needed for mm wave applications, and we compare to 2D treatments. We follow ITRS roadmap parameters to assess the numerical relevance of our results on the quantitative changes from 2D chips to 3D multi chips.

One of the most striking modifications affecting the impedance is the presence of magnetic coupling among orthogonal currents, one of them along the vertical direction. The effect on the resulting impedance of wires is significant. We present a methodology for taking this effect into consideration that is both accurate and efficient.

Compact AC Modeling and Performance Analysis of Through-silicon Vias (TSVs) in 3-D ICs

Chuan Xu[1], **Hong Li**[1], **Roberto Suaya**[2], **and Kaustav Banerjee**[1]

[1]Department of Electrical and Computer Engineering, University of California
Santa Barbara, CA 93106, USA
[2]D2S Division, Mentor Graphics Corporation, 38334 St. Ismier, France

Abstract— Three-dimensional integration to create multi-layer chips (3-D ICs) is a most promising vehicle to integrate dissimilar technologies (digital, analog, RF circuits, etc) on different active layers and contribute to reduce latency. High aspect ratio vertical interconnects, called through-silicon vias (TSVs), provide the connectivity between active layers, as such they constitute a key technology for 3-D ICs. While fabrication approached for TSVs are progressing, there is a need to accurately and efficiently evaluate the admittance/impedance of TSVs in a broadband frequency regime for performance analysis and design.

The TSV cross section incorporates metal (usually Cu) at the center, surrounded by a dielectric (usually SiO_2) for DC isolation. Depending on the voltage bias condition, interface charge density, material properties of surrounding Si, the isolation dielectric may or may not be surrounded by a depletion region, which is ignored by previous modeling approaches. For middle-frequencies (~ 1 MHz) its contribution to capacitance can also be substantial. We find that significant errors O(40)% in capacitance will be induced if the depletion region is not considered.

The high-frequency behavior of a TSV (signal ground) pair is obtained using a compact RLGC transmission line model, incorporating a parallel AC conductance, substrate eddy currents and skin effect. Both CG and RL models are developed separately. From the distributed RLGC model, the input impedance or admittance of the TSV pair can be obtained. The results are compared with a full-wave electromagnetic simulation in the broadband interval (1–100) GHz. The results indicate that the CG model is quite accurate, while the RL model is not as good. The deviation is explained by the limitation of the 2-D approximation when analyzing the 3-D structure. It should be noted that the AC model validity extends naturally to carbon nanotube (CNT) bundles used as TSV conductor. To do so, a complex effective conductivity of the CNT bundle is used from both DC resistivity and kinetic inductance.

The RLGC model for a TSV pair can be treated as a unit cell for more complicated systems. As an example, we compute the inverter to inverter delay and rise time with TSVs insertion at the 22 nm technology node. We demonstrate that the performance difference among TSV types (Cu, W or CNT) is negligible. We analyze the impact of accuracy of C, G, R and L on performance analysis. Coupling capacitance is the most important parameter. This indicates that our compact RLGC model, which is pretty accurate in CG, is sufficient in certain circuit applications.

REFERENCES

1. Xu, C., H. Li, R. Suaya, and K. Banerjee, *Tech. Dig. IEDM*, 2009.
2. Li, H. and K. Banerjee, *IEEE Trans. Elect. Dev.*, Vol. 56, No. 10, 2202–2214, 2009.

Passive Reduced Order Modeling of Multiport Interconnects via Semidefinite Programming

Z. Mahmood, **B. Bond**, **T. Mosehly**, **A. Megretski**, **and L. Daniel**
Massachusetts Institute of Technology, USA

Abstract— Automatic generation of accurate, compact, and passive models for multiport interconnect structures is a crucial part of the design process for circuits. Conventionally, interconnect structures are laid out in a field solver and simulated for frequency response in the desired frequency band. Based on the frequency samples extracted by the solver, a reduced model is developed which can be incorporated into a circuit simulator for time domain simulations of a larger system containing also nonlinear devices. A small violation of any basic property of the structure, such as passivity, can cause huge errors in the response of the overall system, and the results become completely nonphysical. Therefore, it is essential to preserve basic system properties during the model identification. To model multiport structures, the only available approach so far is to identify a stable, but non-passive, model from given frequency response samples, and then perturb the model to make it passive. However, such approaches suffer from limitations if the initial non-passive model has significant passivity violations.

In this presentation, we describe a new technique for passive modelling of multiport interconnect structures. Given transfer function samples, we identify a rational transfer function reduced model that minimizes the mismatch at the given frequencies subject to a global passivity constraint. After a convex relaxation this problem is formulated as a semidefinite optimization problem, which can be solved efficiently using existing techniques. Numerical results are presented for a power distribution grid and an array of inductors having 8 and 4 ports respectively. Comparisons with standard rational fitting algorithms are also provided, where transfer functions are identified individually, and then combined in a matrix. Although for the same model-complexity, alternative methods available in literature identified quite accurate models, passivity was not preserved, which was evident from the negative-real eigenvalues of transfer matrices at certain frequency points.

Session 3P4b
Microwave Devices, Propagation

An Energy Efficient Node Deployment Strategy for Wireless Sensor Network

G. Ahmed[1], **N. M. Khan**[1], **and R. Ramer**[2]

[1]Muhammad Ali Jinnah University, Pakistan
[2]University of New South Wales, Australia

Abstract— Wireless sensor networks (WSNs) are used in many different application areas including defense and military applications. Due to their resource constraint nature, researchers are trying to solve many different challenging issues. Energy-hole problem is one of such issue. In this paper, we are going to find out the answer to the question: Is it possible to avoid the energy-hole problem in WSNs. A normal distribution strategy for node deployment is proposed in order to avoid the energy-hole problem in WSNs. Results show that after using the proposed strategy, lifetime and throughput of the whole network is increased considerably.

Introduction: There are many different research issues and challenges. Node deployment is one of them and researchers are trying to find optimum node deployment strategy. The famous energy-hole problem is defined as in a multi hop environment nodes near the sink are heavily utilized as they forward heavy traffic to the sink. Due to this reason their energies are depleted faster and die earlier than the nodes far away from the sink. This leads to a reduction in network lifetime even though the far away nodes exist in the sensor field. Based on the normal distribution a.k.a. Gaussian distribution, a strategy is proposed which states that the number of sensor nodes should be normally distributed with a mean of zero distance from the sink. This results in an extension of network lifetime.

Assumptions and 68-95-99.7 Rule:

- All the nodes are constantly reports data to the sink, homogeneous and have same starting battery level.
- Only the energy consumed in communication is being considered. Other energy depletion factors like energy consume in processing and due to different environmental factors as discussed in [1] are not considered.
- Sink is located at the center of the sensor field and has no energy limitations.

68-95-99.7 Rule rule is also known as empirical rule or 3-sigma rule. According to this rule, 68% of the nodes are deployed near the sink within one standard deviation from the mean i.e., between $-\sigma$ and $+\sigma$; 95% of the nodes are deployed near the sink within two standard deviations from the mean i.e., between -2σ and $+2\sigma$; and 99.7% of the nodes are deployed near the sink within three standard deviations from the mean i.e., between -3σ and $+3\sigma$ [2].

Proposed Strategy: As discussed before the proposed non-uniform distribution strategy of sensor nodes is based on normal distribution and the distribution is followed the 68-95-99.7 rule. In this approach there is a high density of nodes near the sink which may leads to congestion near the sink. In order to reduce this congestion, sleep-wake up policy is used. It means not all the nodes simultaneously send the data. Instead of it after the deployment, nodes start sending and receiving the data in such a manner that after a certain period of time, a node goes to sleep for a short period of time. Thus a certain number of nodes work simultaneously which reduce the congestion considerably.

REFERENCES

1. Ahmed, G., "Impact of spatio-temporal and environmental factors on the performance of wireless sensor networks," *5th IEEE International Conference on Intelligent Sensors, Sensor Networks and Information Processing (ISSNIP)*, Melbourne, Australia, December 2009.
2. www.wikipedia.org.

Impact of Spatio-temporal and Environemntal Factors on the Perforamnce of Wireless Sensor Networks

G. Ahmed[1], **N. M. Khan**[2], **and R. Ramer**[3]

[1]University of Texas at Arlington, USA
[2]Muhammad Ali Jinnah University, Pakistan
[3]University of New South Wales, Australia

Abstract— Wireless Sensor Networks (WSNs) are used in a number of indoor and outdoor applications. Radio propagation among the low power sensor devices can be influenced largely by environment [1–3] due to which an unexpected behavior in terms of received signal strength, link quality and data delivery is trivial. A lot of research has been done and is going around to study the spatial-temporal characteristics of packet loss, and its environmental dependence. In this paper, the impact of spatial, temporal and other environmental factors on the performance of WSNs are also investigated and analyzed. Most of the existing simulation work does not mimic the real environment. Especially spherical radio models used by these simulators do not perfectly imitate the physical reality of radio signals. In contrast, we present experimental results for investigation of impact of spatial, temporal and other environmental factors by doing extensive real experiments on running test bed of Sun Spots [4]. The results show a strong impact of the these factors on the performance of WSNs.

REFERENCES

1. Zhao, J. and R. Govindan, "Understanding packet delivery performance in dense wireless sensor networks," *Proceedings of SenSys*, Los Angeles, California, USA, November 2003.
2. Lin, S., J. Zhang, G. Zhou, L. Gu, T. He, and J. A. Stankovic, "ATPC: Adaptive transmission power control for wireless sensor networks," *Proceedings of SenSys*, Boulder, Colorado, November 2006.
3. Ganesan, D., B. Krishnamachari, A. Woo, D. Culler, D. Estrin, and S. Wicker, "Complex behavior at scale: An experimental study of low-power wireless sensor networks," University of California, Los Angeles (UCLA), California, Los Angeles, CSD-TR 02-0013, 2002.
4. "Educational discounts," www.sunspotworld.com/proposals.

Miniaturized RF MEMS Switch Matrices

K. Y. Chan[1], R. R. Mansour[2], and R. Ramer[1]

[1]School of Electrical Engineering and Telecommunications
University of New South Wales, Australia
[2]Centre for Integrated RF Engineering (CIRFE), University of Waterloo, Canada

Abstract— Wireless technologies are being investigated widely in industry, universities, government and international organizations and more importantly they are being utilized increasingly in our daily living. As wireless technologies become faster, wider in bandwidth with more functionality, reconfigurable transceiver becomes crucial. One solution to handle multiple frequency bands and signals is to provide physical routing capability to the transceiver. While signal routings in low frequency could be easily achieved, this becomes progressively more complex in design as frequency increases. Switch matrices exist for many years. Due to the technology limitation provided by solid state semiconductors like FET and PIN diodes, existing switch matrices cannot support the requirements for the next generation wireless communications. Here, we proposed using RF MEMS technology. With the advantages given by MEMS, we have successfully developed switch matrices that overcome the bandwidth limitation and outmatch the RF performance that are provided by all existing technologies [1]. In this paper, we are presenting a novel type of a microwave switch matrix for the first time: a staircase switch matrix. The circuit diagram of a 3×3 staircase switch matrix is shown in Fig. 1(a). It can be seen in the same figure that the proposed switch matrix can be extended to larger switch matrix by just adding extra columns. This staircase switch matrix is constructed using our unique RF MEMS semi-T switch and it is shown in Fig. 1(b). This type of switch matrix has unique features. It has the least number of

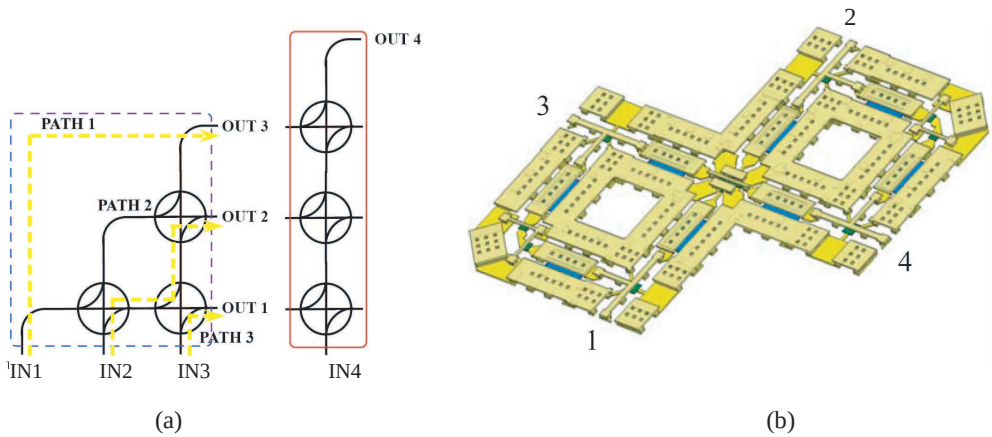

(a) (b)

Figure 1: (a) Proposed 3×3 staircase switch matrix, (b) proposed semi-T switch cell.

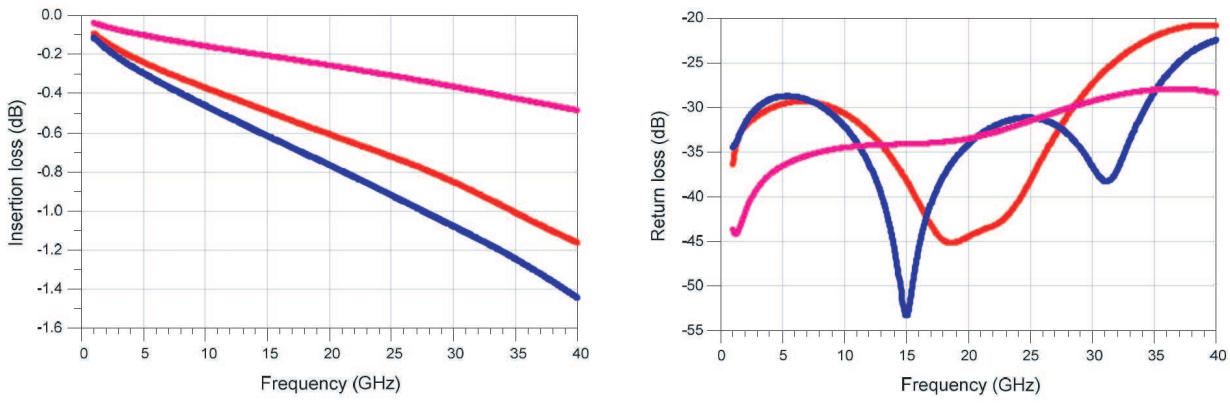

(a) (b)

Figure 2: Simulated RF performance of the 3×3 staircase switch matrix (a) insertion loss, (b) return loss.

RF MEMS switches and the size of the switch matrix is smaller compared to a traditional cross-bar switch matrix. This type of switch matrix requires special algorithm to achieve connections between input and output ports and it can be found in [2]. We have successfully simulated a 3×3 staircase switch matrix with our proposed semi-T switch and the RF performance is shown in Fig. 2 with path one in blue, path two in red and path three in violet. This set of connections shows both the worst (path 1) and best (path 3) paths in this switch matrix. The simulation results demonstrated excellent RF performance from DC to 40 GHz.

REFERENCES

1. Chan, K. Y., et al., "Scalable RF MEMS switch matrices: Methodology and design," *IEEE Transactions on Microwave Theory and Techniques*, Vol. 57, 1612–1621, 2009.
2. Yeow, T. W., et al., "Novel MEMS L-switching matrix optical cross-connect architecture: Design and analysis-optimal and staircase-switching algorithms," *J. Lightwave Technol.*, Vol. 3, 2877–2892, 2005.

RF MEMS Switchabel Bandpass Filter

King Yuk (Eric) Chan[1], **Siamak Fouladi**[2], **Rodica Ramer**[1], **and Raafat R. Mansour**[2]

[1]University of New South Wales, Sydney, NSW 2052, Australia
[2]University of Waterloo, Waterloo, Ontario N2L3G1, Canada

Abstract— For many years, planar tunable filter designs have been based on solid-state tuning elements such as varactors [1]. With the development of RF micro-electromechanical systems (RF MEMS), many different design approaches emerged. Although solid state tuning elements have a switching speed that outperforms RF MEMS switches, their loss and linearity issues have created limitations for their application at microwave frequencies. On the other hand RF MEMS switches have better performance in terms of loss and linearity and if electrostatic actuation mechanism is used within these devices, DC power consumption becomes negligible which also makes RF MEMS technology as one of the most promising replacements for the solid-state tuning elements.

In this paper, we present a novel tuning mechanism by using RF MEMS switches. This reconfiguration method is specific for edge coupled resonator filters. A minimum number of RF MEMS switches are utilized to adjust the coupling and the resonator frequency shift at the same time. As a validation of the proposed tuning method, design, fabrication and measurement results of a switchable third-order interdigital bandpass filter in coplanar waveguide (CPW) technology is presented.

A three-pole tunable filter was designed to have three distinct states at 8, 9 and 10 GHz where each state has a channel bandwidth of 1 GHz and better than 20 dB return loss over the pass band. An interdigital bandpass filter topology using quarter wavelength CPW resonators was selected which enables to achieve miniaturized dimensions. Capacitive input/output coupling was used as it has the same coupling behavior as the inter-resonator coupling in this topology unlike taped-in input/output coupling. The idea is to use RF MEMS switches to enable slow-wave structure on the resonators as well as to adjust the coupling between the resonators.

Spectrally Coded Multiplexing Based on FBG Pairs

Binbin Yan[1, 2], **Paul A. Childs**[2, 3], **Chongxiu Yu**[1], **Xinzhu Sang**[1], **Daxiong Xu**[1], **and Gang-Ding Peng**[2]

[1]Key Laboratory of Information Photonics and Optical Communications of Ministry of Education
Beijing University of Posts and Telecommunications, Beijing 100876, China
[2]School of Electrical Engineering and Telecommunications
University of New South Wales, Sydney 2052, Australia
[3]Department of Electronic Engineering, Tsinghua University, Beijing 100084, China

Abstract— Fiber-optic sensors, especially fiber Bragg grating (FBG) sensors, have been widely used in measurements of strain, temperature, pressure, dynamic magnetic field, etc. FBG sensors have many attractive attributes, such as high sensitivity, safety, immunity to electric interference, small size, capability of measuring different kinds of physical parameters, easy to be multiplexed and so on. For structural health monitoring (SHM) of large scale structures, the number of multiplexed sensors needs to be enhanced and it is also necessary to eliminate the influence of temperature on strain measurement. The conventional multiplexing techniques for FBG-based sensors are wavelength division multiplexing (WDM) and time division multiplexing (TDM). However, the maximum number of sensor that can be multiplexed is limited by the ratio of the spectral width of light source divided by the width of the spectral slot allocated to individual sensor in WDM; TDM requires the use of long delay lines which would reduce the structural integrity of host material if embedded.

In this paper, we propose a spectrally coded multiplexing (SCM) based on FBG pairs formed by two identical sub-FBGs and an interval. Each FBG pair has the same Bragg wavelength but a unique interval that determines them to have different wavelength-frequencies and allows them to be multiplexed by use of SCM. The sensing signals are demodulated by using FFT and identifying amplitudes in Fourier spectra of FBG pair sensors. The demodulation does not need complicated demodulating electronic equipments because it is carried out digitally by computer processing. Combining SCM with WDM, the number of multiplexed FBG pair based sensors can be greatly improved. The performance of proposed SCM has been demonstrated through differential strain measurements. Experimental results showed that the measurement error of the multiplexed system is within ± 8 $\mu\varepsilon$ and the crosstalk $< 40\mu\varepsilon$ for differential strain applied up to $378\mu\varepsilon$.

Session 3P5
Biomedical Electromagnetic Instruments, Electromagnetic Condensed Materials and Imaging

Bioelectrical Impedance Analysis by Multiple Frequencies for Health Care Refrigerator

Bo-Rim Ryu[1], **Haeseong Jeong**[2], **and Heung-Gyoon Ryu**[2]

[1]Seoul National University, Korea
[2]Chungbuk National University, Korea

Abstract— In this paper, we like to study the bioelectrical impedance analysis and propose a smart refrigerator for ubiquitous health care. A smart refrigerator has an additional function enabling users to keep in track of their health by the newly equipped installation. Also, it is equipped with a body fat analyzer that is used in gym and hospitals in order to receive health care in a ubiquitous environment. This proposed method is measured for body impedance and recognized for body composition by using bioelectrical impedance analysis (BIA). Also, we expect that medical center manages user's condition such as amount of body fat, muscle, body water and etc. through internet in a ubiquitous environment. This proposed method has two merits. It can be used to measure more often and much cheaper than body fat analyzer in gym and hospitals.

Simulations of Multi-Photon Absorption Spectra for Fullerene Derivatives $C_{60} > C_2H_4NH_3(Polyaniline)_n$ Based on First-principle Calculations

W.-D. Cheng and J.-Y. Wang
State Key Laboratory of Structural Chemistry
Fujian Institute of Research on the Structure of Matter, Chinese Academy of Sciences
Fuzhou, Fujian 350002, China

Abstract— Fullerene derivatives are becoming interesting nano-vehicles for imaging, diagnosis, therapy and microsurgery, and multiple-photon (2-photon or 3-photon) excitation fluorescence microscopy is an import technique in biological imaging and fluorescent probes. Accordingly, the rational designs of multi-photon absorption materials with large absorption cross section are unignoring strategy by the aid of the rapid increases in computer power. In this work, a combined method of the time-dependent density functional theory (TDDFT) and sum-over-state (SOS) formula was implemented to model multi-photon absorption spectra, including two-photon absorption (2PA) and three-photon absorption (3PA), of fullerene derivatives C_{60} >$C_2H_4NH_3$(polyaniline)$_n$ [$n = 1$: $C_{60} > C_2H_3NCH_3$ ($C_6H_4NH_2$); $n = 2$: $C_{60} > C_2H_3NCH_3$ ($C_{12}H_8N_2H_3$); and $n = 3$: C_{60} >$C_2H_3NCH_3$($C_{18}H_{12}N_3H_4$)]. It is found from Figure 1 that the multi-photon absorption cross sections are increasing in the order of C_{60} >$C_2H_4NH_3$(polyaniline)$_n$ ($n = 1 < 2 < 3$). The electronic origin of multi-photon absorption has been identified with respect to the molecular orbitals involved in charge transfer process. It shows that the increases of donor polyaniline extent result in a large multi–photon absorption cross section in C_{60} >$C_2H_4NH_3$(polyaniline)$_n$.

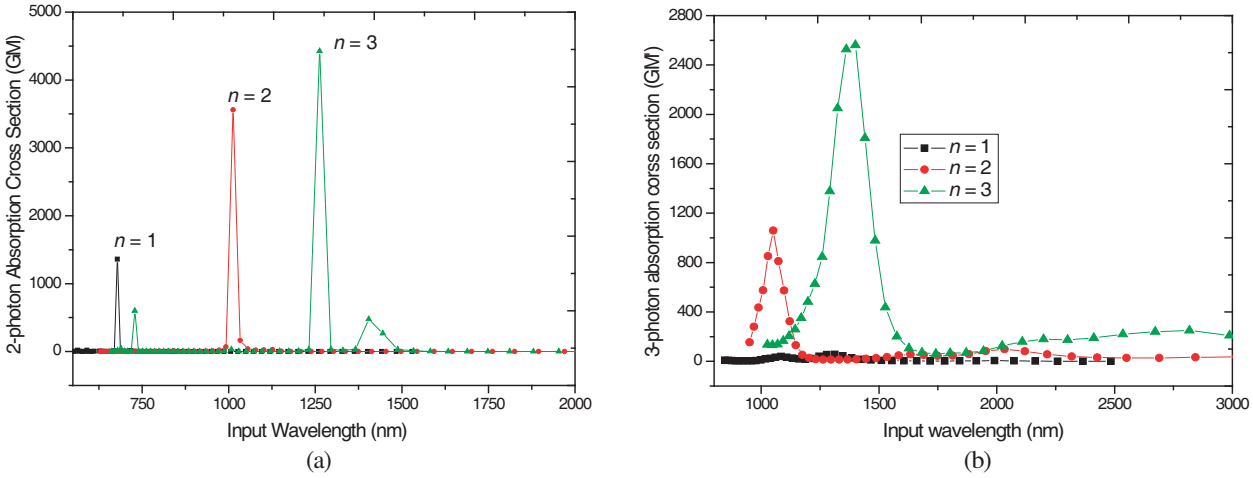

Figure 1: Multiple absorption cross sections of wavelength-dependences. (a) 2-photon, (b) 3-photon.

Modeling Induced Current in Active Medical Implants Exposed to Uniform Magnetic Fields

Juliano Katrib[1], **Mustapha Nadi**[1], **Pierre Schmitt**[1], **Djilali Kourtiche**[1], **and Isabelle Magne**[2]

[1]L.I.E.N., Nancy University, 54506 Vandoeuvre les Nancy, France
[2]EDF, R & D, Site des Renardières, Ecuelles 77250 Moret sur Loing, France

Abstract— This paper presents a numerical modeling study of electromagnetic interference on implantable medical devices (implantable cardiovertor defibrillator (ICD)), exposed to uniform magnetic fields. An analysis of the standards regarding interferences in ICD is carried out to determine the level of induced voltage which may cause the malfunction of such devices.

A uniform magnetic field at 50 and 60 Hz was generated by a Helmholtz coil. Two orientations of field exposure were considered, the vertical position (from up to down) and the horizontal position (front to back).

In the first approach we use a homogenous model for this study. In further detail, our model is composed of a human torso (cylinder), a heart (sphere) and a housing defibrillator (parallelepiped geometry) with 2 electrodes (2 spheres). We selected field strengths based on the recommendations of ICNRP and also selected fields exceeding these limits. Results show strong agreement with the literature for the induced electric field and current in a circular disc, therefore we investigate the induced electric field and current density in ICDs with bipolar detection (2 electrodes for sensing and stimulating). These results made a good base to investigate the induced electric field and current in a real human body.

In a second study we used a human model based on the MRI scan of a 34 years old male, 1.74 m in height. It is composed of more than 70 tissues thus the inhomogeneity of the human body is taken into account. Induced current density and electric field have been calculated on each organ based on the finite integral method. The next step will be to insert the ICD with the help of a scanner to provide a more realistic configuration. The induced EMF will be calculated using bipolar detection where the electrode arrives to the heart passing the aorta, with the return conductor located in the aorta. Investigations are underway to determine the role of the interface between the electrodes and human tissues when they are exposed to such magnetic fields. The magnetic field distribution near the medical implant and its probe were simulated and the results will be discussed according to the different parameters of influence.

Computational Modeling of Electromagnetically Induced Heating of Magnetic Nanoparticle Materials for Hyperthermic Cancer Treatment

L. Rast and J. G. Harrison
Department of Physics, University of Alabama at Birmingham, Birmingham, Alabama 35294, USA

Abstract— We present work on the computational modeling of electromagnetically induced heating in the hyperthermic treatment of cancer using fluid-dispersed magnetic nanoparticles. Magnetic nanoparticle hyperthermia can be used as a complement to chemotherapy or for direct targeting and destruction of tumors through heat treatment. The ability of nanoscale materials to provide an extremely localized therapeutic effect is a major advantage over traditional methods of treatment. When an AC magnetic field is applied to a ferrofluid, Brownian rotation and Néel relaxation of induced magnetic moments result in power dissipation. In order to achieve appreciable volumetric heating power, while maintaining safe values of frequency and magnetic field strength, and reduce the risk of spot heating healthy tissue, it is necessary to determine an ideal range of input parameters for the driving magnetic field as well as the complex susceptibility of the ferrofluid. We do this by the coupling of the solution of Maxwell's equations in a model of the tumor and surrounding tissue as input to the solution to the Pennes' bioheat equation. In this study, we solve both sets of equations via the Finite Difference Time Domain (FDTD) method as implemented in the program SEMCAD X (by SPEAG, Schmid & Partner Engineering). We use a multilayer model of the human head made up of perfused dermal and skeletal layers and a grey-matter region surrounding a composite region of tumor tissue and the magnetic nanoparticle fluid. The tumor/ferrofluid composite material properties are represented as mean values of the material properties of both constituents, assuming homogeneity of the region. The AC magnetic excitation of the system (within 100 kHz–2 MHz frequency range) is provided by square Helmholtz coils, which provide a uniform magnetic field in the region of interest. The power density derived from the electromagnetic field calculation serves as an input term to the bioheat equation and therefore determines the heating due to the ferrofluid. Results for several variations of input parameters will be presented.

The Effects of Breast Tissue Heterogeneity on Data-adaptive Beamforming

D. Byrne, M. O'Halloran, E. Jones, and M. Glavin
Bioelectronic Cluster, National Centre for Biomedical Engineering and Science (NCBES)
College of Engineering and Informatics, National University of Ireland Galway
University Road, Galway, Ireland

Abstract— Ultrawideband (UWB) Microwave Imaging is an emerging technology for breast cancer detection which is based on the dielectric contrast between normal and cancerous tissues at microwave frequencies. The breast is illuminated by a UWB pulse and reflected signals are used to determine the presence and location of significant dielectric scatterers, which may be representative of cancerous tissue within the breast. Beamformers are used to spatially focus the reflected signals and to compensate for pathdependent attenuation and phase effects. These beamformers can be divided into two distinct categories: data-independent and data-adaptive beamformers. Data-independent beamformers typically use an *assumed* channel model to compensate for path-dependent propagation effects. Conversely, data-adaptive beamformers attempt to directly estimate the *actual* channel based on signals reflected from the breast. Recent studies by Lazebnik et al. indicate that the range of dielectric properties of normal breast tissue is much greater than reported previously. This presents a much more difficult imaging problem due to dielectric heterogeneity. Difficulties encountered by data-independent beamformers in locating tumors within dielectrically heterogeneous breasts have been documented previously. In this paper, the effects of heterogeneity on data-adaptive beamformers is investigated. 2D MRI-derived breast models with varying levels of dielectric heterogeneity are used to evaluate the data-adaptive beamformers.

Numerical Simulation of Inductive Phase Shift Due a Brain Hematoma

R. Rojas and A. O. Rodriguez
Centro de Investigacion en Imagenologia Medica, Universidad Autonoma Metropolitana Iztapalapa
Av. San Rafael Atlixco 186, Mexico DF 09340, Mexico

Abstract—

Introduction: The presence of blood accumulated (hematoma) or extracellular fluid accumulated (edema) in brain, due a trauma, is a very dangerous condition for the patient. This accumulation of blood occurs gradually, over a period of time, hours or even days, and has severe consequences, including death. Because the electric and magnetic properties of hematomas are substantially different from the normal tissue, various measurements of those properties of the brain was proposed to non-invasively detect the changes in the brain. Conventional medical imaging modalities such as MRI and PET, are expensive, large and available to a small part of the prospective patient population in danger of developing edema and hematomas. An important part in the medical treatment of hematomas is the detection of their progressive occurrence with an inexpensive detection tool, after which the patient could be transported through a more central medical facility. We have suggested that measuring induction phase shift throughout the bulk of the brain tissue in time and over a broad range of frequencies. Our idea is design an inexpensive and mobile device using a radiofrequency transmitter and receiver coil. Here we evaluated the use of circular coil and a magnetron coil.

Theoretical Background: We proposed a spherical model and two coil configurations (Figure 1). Consider an alternating current $Ie^{j\omega t}$ flowing trough the inductor coil. The presence of the hematoma represents volumetric changes in electric properties. Thus, the induced sensor coil current could be separated in their complex coefficients given by:

$$I(t) = I(\cos(\omega t + \phi) + j\sin(\omega t + \phi)) \quad (1)$$

$$\omega t + \phi = \tan^{-1}\frac{\mathrm{Im}I(t)}{\mathrm{Re}I(t)} = \tan^{-1}\frac{\sin(\omega t + \phi)}{\cos(\omega t + \phi)} \quad (2)$$

The basal induced current argument in the sensor coil as $(\omega t + \phi)$ and the argument influenced by the hematoma presence as $(\omega t + \phi_1)$. To estimate the inductive phase shift $(\Delta\phi)$ we use argument differences at specific frequency and time: $\Delta\phi = (\omega t + \phi_1) - (\omega t + \phi) = \phi_1 - \phi$.

Method: The electric and magnetic fields produced by the coil, were calculated. Before the induced complex currents in the sensor coils were calculated by post-processing options available in COMSOL Multiphysics. Those values were used to estimate spectra of inductive phase

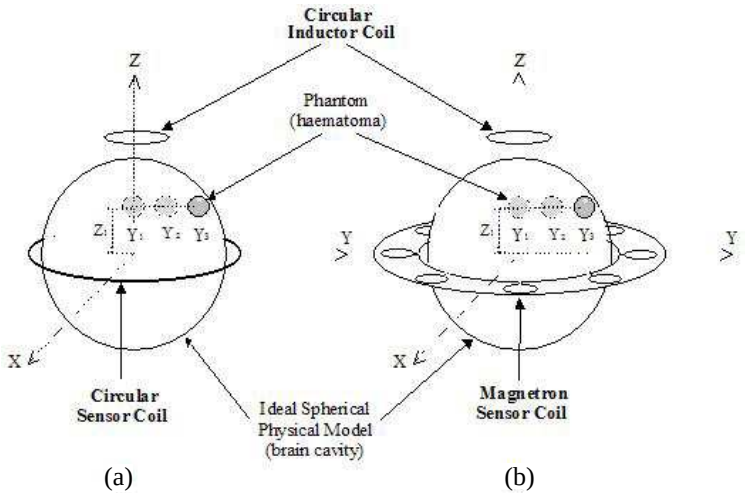

Figure 1: (a) Model with single circular coil. (b) Model with magnetron coil.

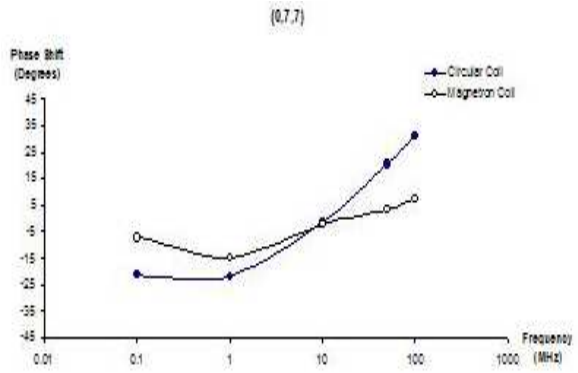

Figure 2: Spectra of inductive phase shift.

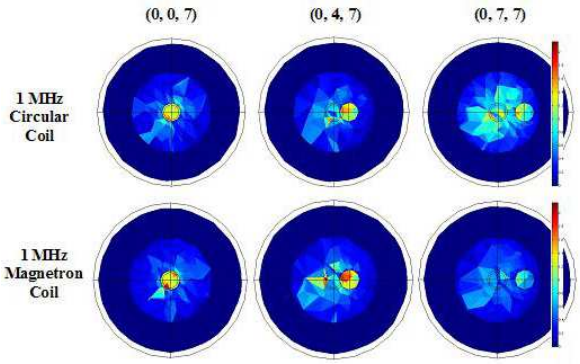

Figure 3: Induced current density maps.

shift in the bandwidth of 100 kHz to 100 MHz. Inductive phases shift simulations without the edema/hematoma presence were taken as the basal values.

Results and Discussion: Figure 2 shows spectra of inductive phase shift at one hematoma positions evaluated. The circular and magnetron sensor coil measurements are compared. The magnetron coil has a higher sensitivity than the circular coil at low frequencies. At frequencies higher than 10 MHz both sensor coils have a similar sensitivity response. Figure 3 shows the induced current density maps inside a spherical brain model influenced by circular/magnetron sensor coil configurations and three hematoma positions evaluated at 1 MHz.

Microstrip Antennas for Direct Human Skin Placement for Biomedical Applications

Sudhir Shrestha, **Mangilal Agarwal**, **Joshua Reid**, **and Kody Varahramyan**
Integrated Nanosystems Development Institute (INDI)
Department of Electrical and Computer Engineering
Indiana University — Purdue University Indianapolis (IUPUI), Indianapolis, IN 46202, USA

Abstract— Every year, thousands of individuals in the United States and around the world suffer from breast cancer. Early detection of breast tumor through a regular screening helps increase the survival rate of the breast cancer patients. Despite this fact, many women of 40 years age and older do not conduct regular mammogram screening. This has been particularly due to the health risk associated with the X-ray used in mammography and its lower accuracy rate in detecting the early breast tumors. Recently, the U.S. Preventive Services Task Force has updated its guidelines recommending regular mammogram screening at the age of 50 and above, once every two years. This is a change from its previous recommendation of yearly screening at the age of 40. This change has fueled additional debates on the health risk of X-ray mammography, its accuracy, and the merits of using it as the primary screening modality. The development of safer and more accurate breast scanning and imaging modalities has been pursued for a relatively long period with microwave breast imaging being one of the most viable technologies.

Microwave breast imaging uses low power and longer wavelength signals (compared to X-ray mammography) to obtain information about breast tissues. In this technique, an antenna transmits a microwave signal to the breast and the scattered signal is received and analyzed to extract dielectric properties of the tissues. One of the major impediments of this technology has been a large signal reflection from the breast skin. Most of the approaches that have been recently developed use an intermediate medium (semi-liquid) between the antenna and the breast, but no significant success has been achieved in reducing the signal reflection from the breast skin.

In this paper, we present a new technique for reducing the signal reflection from the breast skin by the placement of the antenna in-contact with the breast skin. In the reported antenna design, the skin is considered as a layer of the antenna substrate, and the effect of having the antenna in contact with the skin is included in the antenna design itself. Thus, the design allows the antenna to be placed on the breast skin and the skin constitutes a part of the antenna. The antenna and breast layers designed in Ansoft Designer are shown in Figure 1(a) and the voltage standing wave ratio (VSWR) plot of the antenna is shown in Figure 1(b). This design results in the radiation of the signal from the surface of the breast skin, eliminating a significant reflection problem from the skin. Design, simulation, and preliminary experimental results of the antenna are presented. While the antenna is discussed in the context of microwave breast imaging, the application of a microstrip antenna that can be directly placed on human skin has wide range of biomedical applications, some of which will also be introduced in the paper.

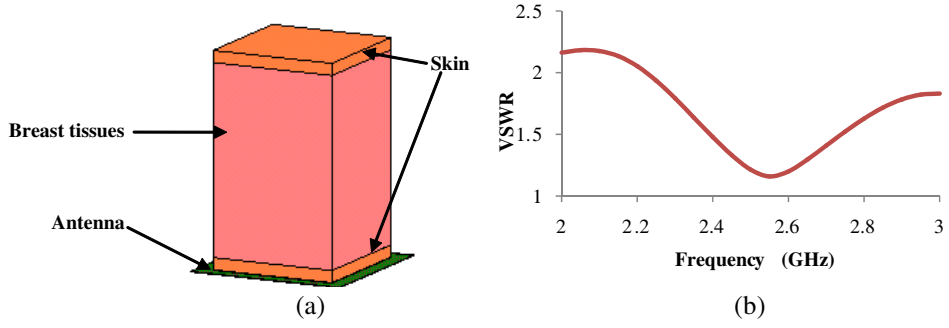

Figure 1: (a) Antenna and breast layers designed in Ansoft Designer. (b) VSWR vs. frequency plot of the antenna system (including breast layers) as shown in (a).

Design of Small-sized and Low-cost Front End to Medical Microwave Radiometer

O. Klemetsen[1], **Y. Birkelund**[1], **P. F. Maccarini**[2], **P. Stauffer**[2], **and S. K. Jacobsen**[1]

[1]University of Tromso, Norway
[2]Duke University Medical Center, USA

Abstract—

Background: Early breast cancer diagnosis is a motivation to keep on with passive sensing using microwave radiometry. National Cancer Institute reports 192 thousand new cases of breast cancer and around 40 thousand deaths caused by breast cancer in US alone during 2009. Microwave radiometry for breast cancer diagnosis has almost no interest outside academia. There might be several reasons for this lack of interest in the medical society, both technical, financial and practical limitations for sure limits the applicability of this cancer diagnosis technique. The most common methods, such as mammography and ultrasound, are active methods, where you submit X-rays or ultrasound through the breast tissue. Active methods can in rare cases lead to breast cancer, while, in contrast, passive methods as microwave radiometer does not use external radiation effects provided non-invasive and safe examination method.

Methods: We have investigated the possibility of creating a user-friendly radiometer that is cheap, small in size and consist of readily available microwave components. Our technical approach to solve this is: 1. Find a suitable frequency band that is better than others in relation to breast cancer diagnosis. 2. Find and evaluate RF components in term of noise figures, adequate amplification, size, availability and price. 3. Design, simulate and test RF frontend and checking the s-parameters, stability parameters for oscillation and gain drift. For these three points we have decided to concentrate on frontend, i.e., RF section of radiometer, since this is the most critical part.

Results: A optimal frequency bands from 3–4 GHz is suggested based on the high spatial resolution in the breast using a small size antenna and the lowest possible interference from common external sources. Hittite low noise amplifier HMC593LP3E satisfies our requirement for amplification in the band 3.3–3.8 GHz, with a moderate noise figure and a small physical size. Simulations show that we need three amplifiers in the cascade with a band pass filter, where the latter is made from a combination of low pass and high pass filters from Mini-Circuits. Prototype testing shows that we can use this system as stable and inexpensive frontend to our radiometer.

The Application of the Hilbert-Huang Transform in Through-wall Life Detection with UWB Impulse Radar

Zijian Liu[1], **Lanbo Liu**[1, 2], **and Benjamin Barrowes**[2]

[1]School of Engineering, University of Connecticut, Storrs, CT 06269-2037, USA
[2]USACE Engineer Research and Development Center
Cold Regions Research and Engineering Laboratory, Hanover, NH 03755, USA

Abstract— To support the study of numerical simulation of the electromagnetic wave propagation with the multi-regional (MR) pseudo-spectral time domain (PSTD) method, a dataset using an ultra-wide (UWB) impulse radar system with central frequency of 1 GHz was collected for life motion detection behind a cinder block wall. We first collected a radar background record without human beings present behind the wall, then with a human present at 1 meter behind the wall. The window length for each recording trace is 16 ns while the temporal spacing for consecutive traces is 0.1 sec. We have collected data with human in 3 statuses: normal breathing, holding their breath, and repeatedly speaking the words "one, two, three". For the first and the third status the total number of recording traces is well above 1024, for about 2 minutes. For the status of holding breath the number of recording traces is less than 512, i.e., generally less than 1 minute. To extract the information of life motions such as breathing and heartbeats from the raw data, we first applied the empirical mode decomposition (EMD), also known as the Hilbert-Huang transform (see Huang and Wu, 2008) to decompose the signal (background signal included) into a family of the intrinsic mode functions (IMFs). We then apply the Fourier transform to get the frequency spectra of different IMFs. After dividing by the spectrum of the background radar record (equivalent to de-convolving the background record in the time domain), we found that breathing appear as a spectral peak at 0.3–0.4 Hz, associated with intrinsic mode functions 3 and 4 (IMF3 and IMF4), while the heartbeats appear to be closely associated with the second and third mode of the intrinsic mode functions (IMF2 and IMF3), with the spectral peak appears round 1.1–1.5 Hz. High harmonics are also found for breathing and heartbeats in the intrinsic mode functions. In general, the spectral pattern in the background-eliminated IMF2 to IMF5 of the remotely detected radar records matches very well with typical bio-signals of heartbeats and breathing, as usually detected by the contact rheocardiographic instruments. Our preliminary results show that the EMD analysis provides significant assistance in signal processing for the detection of human targets behind opaque obstacles.

Session 3P6
Inverse Scattering Problems: Open Problems and New Challenges

Compressive Through-focus Imaging

Oren Mangoubi[1] and Edwin A. Marengo[2]

[1]Yale University, USA
[2]Northeastern University, USA

Abstract— Optical sensing and imaging applications often suffer from a combination of low resolution object reconstructions and expensive or bulky sensors. In traditional analog imaging, images are only acquired in focus, discarding additional information present in out-of-focus images. But it is known that one can use pictures acquired at multiple focal lengths to increase the number of information-carrying samples collected per detector [1]. If, in addition, the object under investigation is known to be sparse when represented in a given basis or dictionary, then one can additionally implement compressive sensing inversion algorithms [2, 3] to increase the resolution per sample ratio through L1-norm minimization. We propose a method that treats the information in multiple through-focus images as projective measurements for compressive sensing, allowing a greater resolution per detector ratio than possible with either conventional through-focus imaging or compressive sensing (of conventional in-focus data) alone. The proposed compressive through-focus imaging is illustrated in the reconstruction of canonical two- and three-dimensional objects, from either coherent or incoherent light. The obtained results illustrate the combined use of through-focus and compressive sensing techniques, and shed light onto the nature of the information that is present in in-focus and out-of-focus images. It is found that information about sparse objects is most highly concentrated in completely out-of-focus planes for coherent light and in near-focus planes for incoherent light.

ACKNOWLEDGMENT

This research is supported by the National Science Foundation under grant 0746310.

REFERENCES

1. Attota, R., T. Germer, and R. Silver, "Through-focus scanning-optical-microscope imaging method for nanoscale dimensional analysis," *Optics Letters*, Vol. 33, 1990–1992, 2008.
2. Candes, E. J., J. Romberg, and T. Tao, "Robust uncertainty principles: Exact signal reconstruction from highly incomplete frequency information," *IEEE Trans. Inform. Theory*, Vol. 52, 489–509, 2006.
3. Donoho, D. L., "Compressed sensing," *IEEE Trans. Inform. Theory*, Vol. 52, 1289–1306, 2006.

3D Inversion of Fresnel Database with 3D Markov Random Field

R. Autieri[1,3], **M. D'Urso**[2], **C. Eyraud**[3], **A. Litman**[3], **V. Pascazio**[1], **and T. Isernia**[4]

[1]Dipartimento per le Tecnologie, Università di Napoli Parthenope, Italy
[2]Giugliano Research Center, Large System Unit, SELEX Sistemi Integrati, Italy
[3]Institut Fresnel UMR CNRS 6133, Université Paul Cézanne Aix-Marseille III
Ecole Centrale de Marseille, Université de Provence Aix-Marseille I, Marseille
[4]DIMET, Università Mediterranea di Reggio Calabria, Italy

Abstract— The inverse scattering problems deal with the estimation of physical parameters and features (position, form, size and complex permittivity) of unknown objects [1, 5] from a limited set of measurements of scattered field data. Generally, the unknown of these inverse problems is the contrast function (related to the complex equivalent permittivity of the object) which depends on the data of the problem (i.e., the scattered field samples) through a non-linear mapping.

The wide range of applications of inverse scattering techniques, spreading from non-invasive medical diagnostics to detection of buried structures, has stimulated the development of a large number of different approaches. Traditionally, the adopted solutions consist of minimizing (or maximizing), with respect to the unknowns, a proper defined cost functional involving the mismatch between the measured and expected scattered fields. Since these problems are ill-posed, the adoption of proper regularization strategies is mandatory. In Tikhonov-like regularization techniques, the cost functional to be minimized involves the choice of the tuning parameter adopted to weight the regularization term through empirical ad-hoc techniques. Its choice affects the accuracy of the global solution of the imaging problem. Bayesian approaches [2, 3] have recently been adopted to obtain unsupervised inversion procedures, where the unknowns are modelled by means of random process and the regularization parameters are estimated starting from the (corrupted) scattered fields data without using any a priori information on the unknown targets to reconstruct.

In particular, we formulate the solution of the inverse problem in terms of a Maximum a Posteriori (MAP) estimation and we adopt a Gaussian Markov Random Fields (GMRF) as an a priori model for the unknown image. Moreover we have introduced in the inversion procedure the knowledge of the real noise disturbing the scattered field measurements, as discussed in [5]. To define the a priori function, we have to estimate two hyper-parameter maps (for the real and imaginary part of the overall unknowns of the imaging problem) before actually performing the inversion. Notably, the regularization parameters values are very high in presence of discontinuities in the image to be retrieved, while they are low in homogeneous regions. Accordingly, the estimated parameters maps return an estimation of the edge of the unknown contrast profile, thus allowing for a preliminary estimate of the targets shape and size. Once these parameters have been estimated, they are exploited in the inversion procedure to retrieve the unknown contrast profile, i.e., the permittivity and conductivity profiles of the system of obstacles located in the region under test. Note that the joint action of the ML estimation of the hyper-parameters to be included in the MRF a priori model, and of the MAP estimation of the permittivity profiles allows reconstructed profiles that follow the actual shape of the permittivity profiles better that the ones that can be obtained without regularization. Numerical results will be presented during the conference to highlight such effects. Then, since the Bayesian regularization schemes are characterized by a computational complexity which rapidly increases when the inverse scattering problem has to be solved in its full non-linearity, we adopt an extended range linear approximation [2] derived from the CS-EB model [4] to invert the measured data and solve the imaging problem.

We tested the developed algorithm on three-dimensional targets, by considering experimental multiple-frequency data measured in the anechoic chamber of the Institut Fresnel of Marseille [6]. In order to take into account the random noise which is present in the experiment, we also considered an adequate cost functional appropriately weighted by coefficients which change with the frequency, the incident angle and the receiving angle [5]. In particular, each scattered field measurement is balanced with the noise disturbing the data.

The obtained results prove the effectiveness and usefulness of the method. In particular, as it will be discussed during the conference, by processing the three-dimensional experimental data of [6], it is possible to achieve nice results in terms of shapes and permittivity values of the unknown objects.

REFERENCES

1. Bucci, O. M., L. Crocco, T. Isernia, and V. Pascazio, "Inverse scattering problems with multi-frequency data: Reconstruction capabilities and solution strategies," *IEEE Transaction Geoscience and Remote Sensing*, Vol. 38, 1749–1756, 2000.
2. Autieri, R., M. D'Urso, V. Pascazio, and T. Isernia, "Exploiting markov random field and an extended range linear approximation for 2D inverse scattering problems," *3rd European Conference on Antennas and Propagation*, 757–760, Berlin, Germany, Mar. 2009.
3. Autieri, R., G. Ferraiuolo, and V. Pascazio, "Bayesian regularization in non-linear imaging: Reconstructionfrom experimental data in microwave tomography," accepted on *IEEE Transaction Geoscience and Remote Sensing*.
4. Crocco, L., M. D'Urso, and T. Isernia, "New tools and series for forward and inverse scattering problems in lossy media," *IEEE Geoscience and Remote Sensing Letters*, Vol. 1, 327–331, 2004.
5. Eyraud, C., A. Litman, A. Hérique, and W. Kofman, "Microwave imaging from experimental data within a Bayesian framework with realistic random noise," *Inverse Problems*, Vol. 25, 024001, 2009.
6. Geffrin, J. M. and P. Sabouroux, "Continuing with the Fresnel database: Experimental setup and improvements in 3D scattering measurements," *Inverse Problems*, Vol. 25, 024001, 2009.

Evolutionary-based Optimization Techniques for Inverse Scattering — A Review

P. Rocca and A. Massa
ELEDIA Research Group at DIT, University of Trento, Via Sommarive 14, I-38050 Trento, Italy

Abstract— The use of stochastic global optimizers has had a non-negligible impact on several areas of research and industry and they have been effectively applied to several problems in engineering and sciences [1]. Thanks to the availability and growing of computational resources with the large diffusion of modern computers, optimization techniques based on Evolutionary Algorithms (EAs) have received a wide attention because of their attractive features. As a matter of fact, EAs are hill-climbing algorithms and do not require the differentiation of the cost function, which is a "must" for gradientbased methods. They are based on stochastic iterative procedures where a pool of trial solutions is used to sample the solution space at each iteration thus improving the search capability as compared to single-agent techniques (e.g., Simulated Annealing). A-priori information can also be easily introduced in terms of additional constraints on the actual solution or the boundaries of the solution space. Moreover, they can directly deal with real values as well as with coded representations of the unknowns (e.g., binary coding). Their main drawback (i.e., the convergence rate) has been also further contrasted by exploiting their implicit and explicit parallelism thanks to modern computer clusters [2].

Since EAs have shown to effectively deal with complex functionals characterized by large, complex, and nonlinear problems, they have been also profitably applied to the solution of electromagnetic inverse scattering problems for microwave imaging [3, 4]. The class of Genetic Algorithms (GAs) have been the first population-based EAs used as inversion procedures for electromagnetic diagnostic problems. Several versions of GAs have dealt with the shape reconstruction of perfectly conducting objects as well as the reconstruction of penetrable scatterers [5]. Successively, other evolutionary-based algorithms has been introduced to overcome the main drawback of GAs, namely the low convergence rate. In such a framework, the Differential Evolution (DE) algorithm [6, 7] has been used for the optimization of real-coded unknowns. Moreover, approaches inspired by the cooperative behaviour of swarms have been used. More specifically, the Particle Swarm Optimizer (PSO) [8] and the Ant Colony Optimizer (ACO) have also been successfully applied [3]. In order to exploit the high converge rate of gradient-based minimization techniques, several hybrid approaches has been implemented to improve the efficiency of EAs [9], as well.

In such a contribution, a review of the evolutionary-based techniques for inverse scattering problems is presented pointing out potentialities and limitations of state-of-the-art solutions also discussing the current trends of the research in such a field.

REFERENCES

1. Haupt, R. L. and D. H. Werner, *Genetic Algorithms in Electromagnetics*, John Wiley & Sons, Hoboken, Ney Jersey, 2007.
2. Massa, A., et al., "Parallel GA-based approach for microwave imaging applications," *IEEE Trans. Antennas Propag.*, Vol. 53, 3118–3127, Oct. 2005.
3. Pastorino, M., "Stochastic optimization methods applied to microwave imaging: A review," *IEEE Trans. Antennas Propag.*, Vol. 55, No. 3, 538–548, Mar. 2007.
4. Rocca, P., et al., "Evolutionary optimization as applied to inverse scattering problems," *Inverse Problems*, Vol. 25, 1–41, 2009.
5. Caorsi, S., A. Massa, and M. Pastorino, "A computational technique based on a real-coded genetic algorithm for microwave imaging purposes," *IEEE Trans. Geosci. Remote Sens.*, Vol. 38, 1697–1708, 2000.
6. Qing, A., "Electromagnetic inverse scattering of multiple two-dimensional perfectly conducting objects by the differential evolution strategy," *IEEE Trans. Antennas Propag.*, Vol. 51, 1251–1262, 2003.
7. Massa, A., M. Pastorino, and A. Randazzo, "Reconstruction of two-dimensional buried objects by a differential evolution method," *Inverse Problems*, Vol. 20, 135–150, 2004.
8. Donelli, M. and A. Massa, "Computational approach based on a particle swarm optimizer for microwave imaging of two-dimensional dielectric scatterers," *IEEE Trans. Microwave Theory Tech.*, Vol. 53, 1761–1776, 2005.

9. Caorsi, S., et al., "Detection of buried inhomogeneous elliptic cylinders by a memetic algorithm," *IEEE Trans. Antennas Propag.*, Vol. 51, 2878–2884, 2003.

Subspace-based Optimization Method in the Framework of the Contrast-source Extended Born Model

Krishna Agarwal[1], **Xudong Chen**[1], **and Miche D'Urso**[2]

[1]Department of Electrical and Computer Engineering
National University of Singapore, 117576, Singapore
[2]SELEX Sistemi Integrati, Via Circumvallazione Esterna di Napoli
zona ASI, I-80014 Giugliano, Napoli, Italy

Abstract— Recently the subspace-based optimization method (SOM) has been proposed to solve the inverse scattering problem of reconstructing the relative-permittivity profiles of scatterers [1–3]. In SOM, the contrast source is decomposed into two orthogonally complementary parts: the deterministic part and the ambiguous part. The deterministic part is determined by the singular value decomposition (SVD), whereas the ambiguous part is determined by optimization methods. Reference [2] compares the SOM with the contrast course inversion (CSI) method and finds that they share some properties. In particular, a special case of SOM is close in spirit to the CSI method. It is worth noting that the adopted CSI alternate update scheme in the optimization process is not the only possibility. Other schemes, such as the Contrast Source Extended Born (CS-EB) method [4–6], are good candidates.

The aim of this paper is to investigate a modified version of the subspace-based optimization method for solving inverse scattering problems working in the framework of the CS-EB model. The CS-EB equation, derived *without any approximation* from the traditional one, exhibits different and interesting properties with respect to traditional formulations. As a matter of fact, the CS-EB model has allowed introducing new and convenient solution methods (based on simple 'fixed-point' iterative methods) for both 2D and 3D forward scattering problems [4–6]. In this paper, we investigate 2-D transverse magnetic (TM) inverse scattering problems. In SOM, the deterministic part of the contrast source is determined from the spectrum analysis without using any optimization, whereas the ambiguous part is determined by an optimization method. This feature significantly speeds up the convergence of the inversion algorithm. Another important characteristic of the proposed CS-EB based SOM is its ability to deal with scatterers with high permittivity, due to the fact that the CS-EB does not directly uses the contrast but instead a function of contrast that does not goes up as the contrast does. The proposed inversion method has been found to be rapidly convergent, robust against noise, and able to reconstruct scatterers with arbitrary shapes.

REFERENCES

1. Chen, X., "Application of subspace and optimization methods in reconstructing extended scatterers," *Journal of the Optical Society of America, A*, Vol. 26, 1022–1026, 2009
2. Chen, X., "Subspace-based optimization method for solving inverse scattering problems," *IEEE Transactions on Geoscience and Remote Sensing*, 2009, accepted.
3. Zhong, Y. and X. Chen, "Twofold subspace-based optimization method for solving inverse scattering problems," *Inverse Problems*, Vol. 25, ID: 085003 (11 pages), 2009.
4. Isernia, T., L. Crocco, and M. D'Urso, "New tools and series for forward and inverse scattering problems in lossy media," *IEEE Geoscience and Remote Sensing Letters*, Vol. 1, October 2000.
5. Catapano, I., L. Corcco, M. D'Urso, and T. Isernia, "A novel effective model for solving 3D inverse scattering problems in lossy scenarios," *IEEE Geoscience and Remote Sensing Letters*, Vol. 5, July 2006.
6. D'Urso, M., T. Isernia, and A. F. Morabito, "On the solution of 2D inverse scattering problems via source type integral equation models," *IEEE Trans. Geosci. Remote Sensing*, 2009, in print.

Subspace-based Optimization Method with Initial Guess through a Multipole-expansion Based Linear Sampling Method

Yu Zhong, Krishna Agarwal, and Xudong Chen
Department of Electrical and Computer Engineering, National University of Singapore
Singapore 117576, Singapore

Abstract— Recently, a new multipole-expansion based linear sampling method (MELSM) was proposed [1] to estimate the support of the extended scatterers from the measured scattering data. It is found that the new MELSM outperforms the traditional LSM [2, 3] by introducing a new regularization, which is the assumption that the fields are only expanded by the monopoles and dipoles. Since the MELSM is able to provide good estimation of the support of the extended scatterers, one would intuitively expect to use this method firstly to shrink the domain of the interest for the traditional optimization method, and, secondly, to supply a good initial guess, so that the optimization could converge faster. For the first point, it is granted. However, for the second point, it may depend on the optimization scheme used. To verify this we try to use the MELSM to give a support of the scatterers, and use this support to calculate the dielectric profile distribution inside the support, which is accomplished by the least squares-based method [4], and finally, use the obtained dielectric profile as the initial guess for the subspace-based optimization method (SOM), which uses the CG-type optimization scheme [5].

The numerical example shown here is the "S" shape dielectric scatterers with relative permittivity $\varepsilon_r = 2$, which is the same as the first numerical example in [1]. For the detailed numerical experimental set up, the readers are referred to [1]. In Fig. 1, the estimated dielectric profile obtained from the support is depicted. This estimated result is used as the initial guess of SOM, and then we obtain the optimized result as shown in Fig. 2. If we use the same domain of interest, and use the background medium, air, as the initial guess of SOM, we obtain the optimized result as shown in Fig. 3. From Figs. 2 and 3, we clearly see that, due to the CG-type optimization scheme, the current distribution obtained from the estimated result affects the final optimized result, which shows not as smooth as the one obtained when using air as the initial guess. In both cases the optimization takes almost the same number of iterations to converge. From this simulation, we see that the CG-type optimization scheme dose not benefit from the initial guess obtained by the MELSM.

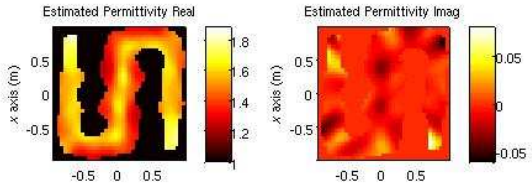

Figure 1.

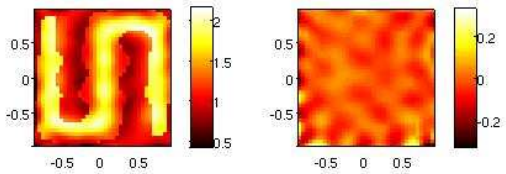

Figure 2.

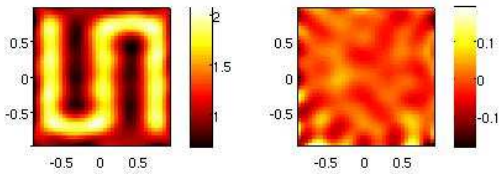

Figure 3.

REFERENCES

1. Agarwal, K., X. Chen, and Y. Zhong, "A multipole-expansion based linear sampling method for solving inverse scattering problems," *Optics Express*, 2009, submitted.

2. Kirsch, A., "Characterization of the shape of a scattering obstacle using the spectral data of the far field operator," *Inverse Problems*, Vol. 14, 1489–1512, 1998.
3. Kirsch, A. and S. Ritter, "A linear sampling method for inverse scattering from an open arc," *Inverse Problems*, Vol. 16, No. 1, 89–105, 2000.
4. Chen, X. and Y. Zhong, "A robust noniterative method for obtaining scattering strengths of multiply scattering point targets (L)," *Journal of the Acoustical Society of America*, Vol. 122, 1325–1327, 2007.
5. Chen, X., "Subspace-based optimization method for solving inverse scattering problems," *IEEE Transactions on Geoscience and Remote Sensing*, accepted, 2009.

Application of the Adaptive Cross Approximation for the Regularized Gauss-Newton Inversion Approach

Maokun Li, **Aria Abubakar**, **and Tarek M. Habashy**
Schlumberger-Doll Research, Cambridge, MA, USA

Abstract— In this abstract, we propose an approach to improve the efficiency of the regularized Gauss-Newton inversion algorithm by using an adaptive cross approximation (ACA) technique for geophysical low-frequency electromagnetic data inversion. In our approach the inversion domain is described by using pixels formed by the Cartesian grid. The conductivity of each pixel is reconstructed and the result is an image describing the conductivity distribution. In gradient-based inversion algorithms such as the Gauss-Newton method, the Jacobian matrix, whose elements describe the derivative of the simulated data with respect to the pixel conductivities, plays a key role in providing the update direction of the optimization process. Its size is equal to the number of measurement data times the number of unknown pixels. In our geophysical applications, the size of the data set and the inversion domain can be very large. Hence, the storage of the Jacobian matrix requires a huge amount of memory. Moreover, because the Jacobian matrix is a dense matrix, the arithmetic operation of a matrix-vector multiplication of this Jacobian matrix with other vector can be very expensive. These are the bottlenecks of using gradient-type inversion approaches. To reduce the size of the Jacobian matrix, we usually invert a subset of the data at the risk of missing important data points. An alternative way is to compress the Jacobian matrix based on the fact that the electromagnetic field has a limited spatial bandwidth. We can either use physics-based techniques that rely on the field kernel or use pure numerical methods that tend to be very expensive to compute. In this work, we use the adaptive cross approximation (ACA) technique introduced by Bebendorf to compress the Jacobian matrix. The ACA technique converts the Jacobian matrix into smaller rectangular matrices. This approach reduces both memory storage and CPU time of the Gauss-Newton inversion approach as well as stabilizes the inversion process. The improvement increases when we deal with large data sets with a large number of transmitters, receivers and frequencies. To demonstrate the improvements introduced by this method we present results of both synthetic and field data inversions for geophysics low-frequency electromagnetic applications. We will show that the compressed Gauss-Newton inversion approach shows a great potential for handling large data sets.

3-D Microwave Imaging in a Non-Canonical Inhomogeneous Background

Mengqing Yuan and Qing Huo Liu
Department of Electrical and Computer Engineering, Duke University, USA

Abstract— 3-D microwave imaging has important applications in breast cancer diagnosis and screening, nondestructive evaluation, and many other areas. Effective methods have been developed for both forward and inverse scattering problems in recent years. For example, recently a special section has been devoted to the nonlinear inverse scattering from a set of measured 3-D data for dielectric objects in a homogeneous background medium [1].

The next level of complexity arises in the inverse scattering problem from objects embedded in multilayered media. Recently, both the Born iterative method and distorted Born iterative method [2] and contrast source inversion method [3] have been developed for 3-D dielectric objects in layered media. Experimental data and its inversion have been reported recently for objects in such layered media [4].

However, the homogeneous background and multilayered medium background have a canonical background medium whose Green's function is relatively easy to obtain. To our knowledge, 3-D nonlinear inverse scattering in a non-canonical background medium remains an open problem and is very challenging to solve. We propose to extend the diagonal tensor approximation to such non-canonical background media [5, 6]. In this presentation, we report our progress toward solving such a noncanonical problem for 3-D forward and inverse scattering.

REFERENCES

1. *Inverse Problems*, Feb. 2009.
2. Li, F., Q. H. Liu, and L.-P. Song, "Three-dimensional reconstruction of objects buried in layered media using Born and distorted Born iterative methods," *IEEE Geosci. Remote Sensing Lett.*, Vol. 1, No. 2, 107–111, 2004.
3. Song, L.-P. and Q. H. Liu, "GPR landmine imaging: 2D seismic migration and 3D inverse scattering in layered media," *Radio Science*, Vol. 40, RS1S90, 2004.
4. Yu, C., M. Yuan, Y. Zhang, J. Stang, R. T. George, G. A. Ybarra, W. T. Joines, and Q. H. Liu, "Microwave imaging in layered media: 3-D image reconstruction from experimental data," *IEEE Trans. Antennas Propagat.*, in press.
5. Song, L.-P. and Q. H. Liu, "Fast three-dimensional electromagnetic nonlinear inversion in layered media with a novel scattering approximation," *Inverse Problems*, Vol. 20, No. 6, S171–194, Dec. 2004.
6. Song, L.-P. and Q. H. Liu, "A new approximation to three-dimensional electromagnetic scattering," *IEEE Geosci. Remote Sensing Lett.*, Vol. 2, No. 2, 238–242, Apr. 2005.

A Krylov Subspace Approach to Parametric Inversion of Electromagnetic Data Based on Residual Minimization

E. Balidemaj and R. F. Remis
Laboratory of Electromagnetic Research
Faculty of Electrical Engineering, Mathematics and Computer Science
Delft University of Technology, Mekelweg 4, 2628 CD Delft, The Netherlands

Abstract— Many iterative inversion methods use forward solutions in every inversion step and may therefore be computationally very expensive. For homogeneous objects, however, forward problems can be solved efficiently by exploiting the shift-invariance property of Krylov subspaces. To be specific, solving a forward problem for a homogeneous object using an integral equation approach essentially amounts to evaluating a matrix resolvent in which the inverse of the contrast coefficient acts as the resolvent parameter. The action of this resolvent function on a given vector can be evaluated very efficiently by exploiting the shift-invariance property of a Krylov subspace. After only a single run of a Krylov subspace method, field approximations can be constructed for a whole range of contrast coefficients. In previous work [1], we constructed these field approximations using the Arnoldi algorithm in combination with a Full Orthogonalization (FO) approach. The drawback of this FO approach is that, for a given contrast, the norm of the residuals corresponding to successive field approximations is not necessarily a nonincreasing function. In this paper, we remedy this problem by constructing field approximations for which the Euclidean norm of the corresponding residual is minimum (similar to the well known Generalized Minimum Residual or GMRES method). For a whole range of contrast parameters, we only need to solve small-scale least-squares problems and for a given contrast coefficient, the Euclidean norm of the residual is guaranteed to be nonincreasing as the number of iterations increases. Since all Krylov basis vectors need to be stored in the Arnoldi algorithm, we may run into storage problems especially for electrically large objects. A restarted version of the above method as proposed by Frommer and Glässner [2] may then be applied.

Given the Krylov field approximations, the scattered field at specified receiver locations can be computed in a straightforward manner and the inverse scattering problem can actually be solved by inspecting a (possibly nondifferentiable) objective function which measures the discrepancy between the true and modeled scattered field data. For inhomogeneous objects we can still try to match the scattered field due to a homogeneous object to the scattered field generated by an inhomogeneous object. This topic is very important in many different areas most notably in effective medium theory. To what extent it is possible to nd effective homogeneous scatterers using our method will be investigated as well and numerical experiments will illustrate the performance of the method.

REFERENCES

1. *Inv. Problems*, Vol. 20, No. 6, S17–S26, 2004.
2. *SIAM J. Sci. Comput.*, Vol. 19, No. 1, 15–26, 1998.

Multi-static Radar Through-the-wall Imaging with Time Reversal MUSIC Algorithm

Wenji Zhang and Ahmad Hoorfar
Center for Advanced Communications, Villanova University, Villanova, PA 19085, USA

Abstract— The capability of electromagnetic wave to penetrate through the building walls has made through-the- wall microwave imaging (TWMI) of increasing importance in many civilian and military radar applications. The TWMI technology is particularly useful in such applications as behind-the-wall target detection, surveillance and reconnaissance, law enforcement, and various earthquake and avalanche rescue missions, to name a few [1]. Time-Reversal Multiple Signal Classification (TR-MUSIC) method for target detection and location was first proposed in [2]. The general idea of TR-MUSIC is to localize multiple scatterers by exploiting the eigenstructure of the time reversal matrix [2]. In this paper, the TR-MUSIC algorithm is extended for the imaging of point targets behind the wall.

Consider a uniform N elements array centered at the position R_j in front of the wall, where, $j = 1, 2, \ldots, N$, $R_j = (X_j, Z_j)$. A set of M point targets are located at position r_m behind the wall, where $m = 1, 2, \ldots, M$, $r_m = (x_m, z_m)$, $M < N$. The complex dielectric constant and thickness of the wall are ε_r and d, respectively.

The multi-static response matrix K, whose element K_{ij} corresponds to the scattered field detected at the i-th receiver due to the excitation of the j-th transmitter, can be derived as

$$K = \sum_{m=1}^{M} \tau_m g_m g_m^T \tag{1}$$

where, $g_m = [G(R_1, r_m, \omega), G(R_2, r_m, \omega), \ldots, G(R_N, r_m, \omega)]^T$, τ_m is the scattering strength of the m-th target, G is the three-layered medium Green's function and can be efficiently calculated with stationary phase method.

Finally, the time-reversal matrix is defined as

$$T = K^H K \tag{2}$$

Suppose there are L none-zero eigenvalues of the time reversal matrix, by performing the SVD of the matrix, the locations of the scatterers can then be determined from the time-reversal MUSIC pseudo-spectrum [2],

$$p^{MUSIC}(r_p) = \left[\sum_{i=L+1}^{N} |\langle u_i^*, g_p \rangle|^2 \right]^{-1} \tag{3}$$

where u_i is the i-th eigenvectors of the time reversal matrix corresponds to the i-th zero eigenvalue. The inner product $\langle u_i^*, g_p \rangle = 0$ when r_p matches with the true location of the target and it shows a peak at the target location.

Examples of the application of the above time-reversal MUSIC algorithm in various TWMI scenarios will be given in the presentation.

REFERENCES

1. Dehmollaian, M. and K. Sarabandi, "Refocusing through building walls using synthetic aperture radar," *IEEE Trans. Geoscience and Remote Sensing*, Vol. 46, 1589–1599, 2008.
2. Gruber, F. K., E. A. Marengo, and A. J. Devaney, "Time reversal imaging with multiple signal classification considering multiple scattering between the targets," *J. ASA*, 3042–3047, 2004.

Session 4A1
Nonlinear Inversion Approaches for Microwave Biomedical Applications

Noninvasive SAR Measurements

George G. Cheng, Yong Zhu, and Jan Grzesik
Allwave Corporation, 3860 Del Amo Blvd., #404, Torrance, CA 90503, USA

Abstract— A novel nondestructive technique is proposed for measurement of the Specific Absorption Rate (SAR), which determines the electromagnetic power density absorbed and deposited into biological tissue. In light of the time-consuming data acquisition process, and the mechanical complexity associated with the current SAR test equipment commonly used in the wireless industry to date, we devised a method of measurement utilizing a conventional spherical near-field test system. With this equipment, coupled with our unique data processing algorithm, we were able to obtain rapid SAR evaluations using near-field data over only one spherical surface, exterior to the absorbing target under test.

The test procedure is simple. First, we place the test target, for example, a phantom attached to a cell phone, on a spherical near-field test system so as to collect two tangential components (E_θ, E_ϕ) over a spherical surface exterior to the phantom, in both incident polarizations. Second, we process the measured near-field data in accordance with the Field Mapping Algorithm, which determines all three electric field components interior to the phantom. The local SAR assessment is then obtained in the form

$$\mathrm{SAR} = \sigma |E|^2 / \rho$$

where $|E|$ represents the calculated root-mean-square electric field intensity, while σ and ρ, given *a priori*, are the conductivity and density of the medium. The average SAR is then gotten by integrating the local SAR over the entire medium of the phantom.

The success of this technique lies in the data processing algorithm. The Field Mapping Algorithm (FMA), as we have called it, transforms electromagnetic fields from one surface to another in an exact sense. This algorithm determines the entire electric and magnetic field everywhere based on two tangential field components, either electric or magnetic, on a surface, say a plane, a sphere, or a cylinder. The FMA is applicable in any region, and is not limited to free space, either interior or exterior to the data surface, or in between. Moreover, the FMA is a direct, closed-form solution to Maxwell's equations, and is numerically straightforward and efficient. When applying the FMA, the data processing time normally amounts to only a few minutes in most SAR test cases.

The chief advantages of this technique are its significant reductions in cost and testing time. One among several other charms of the FMA is the high accuracy which it provides. Verification of the algorithm is carried out here in four test cases, including two analytic examples and two FDTD simulation runs. Excellent results are obtained.

REFERENCES

1. Cheng, G. G., Y. Zhu, and J. Grzesik, "Exact solutions for microwave holography — Part II: Spherical and cylindrical cases," *Progress In Electromagnetics Research Symposium Abstracts*, Beijing, China, March 23–27, 2009.
2. Cheng, G. G., Y. Zhu, and J. Grzesik, "Microwave photography," *Digest of IEEE AP-S International Symposium*, 2008.
3. Cheng, G. G., Y. Zhu, and J. Grzesik, "Full space wave construction via single near-field measurement," *AMTA Proceedings*, 2007.
4. Cheng, G. G. and Y. Zhu, "Wave diffraction phenomenon via measurement," *EuCAP Programme*, 2007.

A New Reconstruction Method for Electromagnetic Biomedical Imaging

A. Lakhal
Faculty of Mathematics and Computer Sciences, Institute of Applied Mathematics
University of Saarland, Saarbrücken D-66041, Germany

Abstract— Microwave inverse scattering has been gaining a growing interest as an imaging technique for biomedical applications. This less-invasive technique is more suitable than computerized-tomography for investigating sensitive biological tissues. Nevertheless, in contrast to X-rays, the paths of the microwaves depend upon the properties of the tissue we aim to determine. This makes the problem highly nonlinear. The modeling for electromagnetic scattering is based on the full three-dimensional time-harmonic Maxwell equations in inhomogeneous media. We aim to reconstruct the unknown constitutive parameters of some object given by the electric permittivity and the electric conductivity using exterior measurements. Data are near-field measurements of scattered waves for multiple illuminations at a fixed frequency. Thus, we have here to solve the inverse problem, which is typically ill-posed. It is under-determined and ill-conditioned. Besides the ill-posedness and nonlinearity of this problem, it is of high complexity since all components of the electromagnetic fields are coupled. We present here a decoupling-based imaging method to reconstruct the electromagnetic properties of some buried object from exterior measurements of scattered fields. For identifying current sources we introduced in [1] a new method based on recasting the intertwined vector equations in the Maxwell's system into decoupled scalar problems. We extended this decoupling procedure in [2] to derive a fast reconstruction method for inverse medium electromagnetic scattering. To stimulate the interest in the developed algorithm for biomedical imaging, we present numerical tests in 3D with simulated and experimental data.

REFERENCES

1. Lakhal, A. and A. K. Louis, "Locating radiating sources for Maxwell's equations using the approximate inverse," *Inverse Problems*, Vol. 24, 045020, 18, 2008.
2. Lakhal, A., "A decoupling-based imaging method for inverse medium scattering for Maxwell's equations," *Inverse Problems*, Vol. 26, 015007, 2010.

3D Microwave Imaging of the Breast: Preliminary Results and Challenges

Amir H. Golnabi, **Paul M. Meaney**, **Sherri D. Geimer**, **and Keith Paulsen**
Thayer School of Engineering, Dartmouth College, Hanover, NH, USA

Abstract— Microwave imaging exploits the electrical property (permittivity and conductivity) differences in materials. Microwave imaging for biomedical applications is particularly interesting because the available range of dielectric properties for different soft tissues can provide substantial functional information about their health. Breast cancer detection and treatment response monitoring are areas where microwave imaging is becoming a promising alternative technique to current imaging modalities, mainly due to the significant contrast between dielectric properties of normal and malignant breast tissues.

We have previously demonstrated that we can recover clinically useful 2D microwave images for breast cancer detection [1]. This is based on the assumption that the 3D scattering problem can be reasonably represented as a simplified 2D model. One of the most important advantages of using a 2D model to characterize a 3D phenomenon is the significant computational time reduction; nonetheless, this may impose excessive simplifications, which can introduce image artifacts. Moreover, if the region of interest is small enough to fall between two consecutive imaging slices, the 2D reconstruction algorithm may not detect the target accurately. Therefore, a viable 3D image reconstruction process, which is computationally feasible and balances the tradeoff between the accuracy and efficiency of the model, is desired.

We have developed a 3D reconstruction algorithm, which is based on the finite difference time domain (FDTD) method. This technique is particularly interesting because the modeling along with the implementation of the absorbing boundary conditions are conceptually simple and relatively easy to program. In addition, in terms of computational frameworks, the FDTD method is superior to other techniques such as the finite element (FE) and boundary element (BE) methods [2]. We have also optimized the computational complexity and user interface of our reconstruction process by using Fortran MEX-Files in Matlab. Initial simulation and phantom results show a significant enhancement in recovering the property distributions over previous 2D results.

ACKNOWLEDGMENT

This work was sponsored by NIH/NCI Grant # PO1-CA080139.

REFERENCES

1. Meaney, P. M., M. W. Fanning, T. Raynolds, C. J. Fox, Q. Fang, C. A. Kogel, S. P. Poplack, and K. D. Paulsen, "Initial clinical experience with microwave breast imaging in women with normal mammography," *Academic Radiology*, Vol. 14, 207–218, 2007.
2. Fang, Q., "Computational methods for microwave medical imaging," Ph.D. dissertation, Thayer School of Engineering, Dartmouth College, Hanover, NH, 2004.

Iterative Multi-scaling Approach for Large-scale Problems — Contrast Source and Contrast Field Formulations

P.-A. Barrière and A. Massa
ELEDIA Research Group at DIT, University of Trento, Via Sommarive 14, I-38050 Trento, Italy

Abstract— The iterative multi-scaling approach (IMSA) [1, 2] proposes a general framework aimed at efficiently exploiting the limited amount of information available in inverse scattering experiments [4]. For large-scale problems, the IMSA turns out to be very effective and useful since it allows to deal with a smaller number of unknowns than the classical "bare" approaches, thus simplifying the solution of the problem at hand.

The IMSA strategy is based on a "find and zoom" procedure where, at each step, a region of interest (or multiple regions of interest [3]) is defined and a new reconstruction is performed within this region, still using the same number of unknowns as for the previous step. This number of unknowns is chosen according the degrees-of-freedom theory [4]. The resolution of the reconstruction is then improved from one step to the other, without increasing the number of unknowns, until a stationary condition is reached.

The IMSA is *a priori* independent of both the formulation of the problem and the used inversion algorithm. However, until now, it has been assessed by using the so-called contrast field inversion (CFI) formulation, which is based on a joint estimation of both the contrast and the electrical field distributions within the investigation domain.

Otherwise, methods based on a joint estimation of currents and contrast, known as CSI methods [5], are "close relatives" of CFI approaches and seem to be of some potential in order to enhance the IMSA performances.

The objective of this paper is to compare the results obtained with IMSA-CSI and IMSA-CFI approaches as well as those obtained with "bare" approaches.

REFERENCES

1. Caorsi, S., M. Donelli, D. Franceschini, and A. Massa, "A new methodology based on an iterative multiscaling for microwave imaging," *IEEE Trans. Microwave Theory Tech.*, Vol. 51, No. 4, 1162–1173, 2003.
2. Donelli, M., D. Franceschini, P. Rocca, and A. Massa, "Three-dimensional microwave imaging problems solved through an efficient multiscaling particle swarm optimization," *IEEE Trans. Geosci. Remote Sensing*, Vol. 47, No. 5, 1467–1481, 2009.
3. Caorsi, S., M. Donelli, and A. Massa, "Detection, location, and imaging of multiple scatterers by means of the iterative multiscaling method," *IEEE Trans. Microwave Theory Tech.*, Vol. 52, No. 4, 1217–1228, 2004.
4. Bucci, O. M. and T. Isernia, "Electromagnetic inverse scattering: Retrievable information and measurements strategies," *Radio Sci.*, Vol. 32, No. 6, 2123–2197, 1997.
5. Van den Berg, P. M. and R. E. Kleinman, "A contrast source inversion method," *Inverse Problems*, Vol. 13, 1607–1619, 1997.

Three-dimensional Tomographic Microwave Medical Imaging

Tomasz M. Grzegorczyk[1], **Paul M. Meaney**[2], **Soon Ik Jeon**[3], **Shireen Geimer**[2], **and Keith D. Paulsen**[2]

[1] Delpsi, LLC, USA
[2] Dartmouth College, USA
[3] ETRI, South Korea

Abstract— Tomographic microwave biomedical imaging has been studied as an effective method for the diagnosis and monitoring of breast cancer for example, for the last decade. The difference in composition between healthy and malignant tissues induces contrast in electrical properties (permittivity and conductivity) that can be successfully captured by a microwave system operating in the frequency range between about 300 MHz and 2 GHz. A two dimensional tomographic configuration composed of a circular array of antennas [1] has been shown to achieve good specificity levels for lesions down to 1 cm [2], very close to that of more traditional magnetic resonances studies [3]. Microwave breast imaging therefore appears as a potentially powerful technique, in addition to being fast, non-invasive, non-destructive (the power levels and exposure times are both very low), and relatively low-cost.

In this work, we extend our imaging capabilities to three dimensions and discuss the main challenges involved: necessity of a fast forward solver, data acquisition system, inversion algorithm using the logarithmic transformation, and surface rendering in order to minimize the number of points at which the properties are inverted. We also examine the influence of choosing a subset of data (such as in-plane only or cross-plane data) on the final image quality. Preliminary results indicate a smooth translation of phantom measured data into 3D permittivity and conductivity profiles in significantly shorter run times compared to what we had previously achieved. These results open the prospect of using 3D microwave techniques in clinical setup.

ACKNOWLEDGMENT

This work was supported by NIH/NCI grant # PO1-CA080139 and the IT R&D program of MKE/KEIT (2007-F-043-3).

REFERENCES

1. Meaney, P. M., M. W. Fanning, D. Li, S. P. Poplack, and K. D. Paulsen, "A clinical prototype for active microwave imaging of the breast," *IEEE Trans. Microwave Theory and Tech.*, Vol. 48, 1841–1853, 2000.
2. Poplack, S. P., K. D. Paulsen, A. Hartov, P. M. Meaney, B. Pogue, T. Tosteson, M. Grove, S. Soho, and W. Wells, "Electromagnetic breast imaging: Pilot results in women with abnormal mammography," *Radiology*, Vol. 243, 350–359, 2007.
3. Bluemke, D. A., C. A. Gatsonis, M. H. Chen, G. A. DeAngelis, N. DeBruhl, S. Harms, S. H. Heywang-Kbrunner, N. Hylton, C. K. Kuhl, C. Lehman, E. D. Pisano, P. Causer, S. J. Schnitt, S. F. Smazal, C. B. Stelling, P. T. Weatherall, and M. D. Schnall, "Magnetic resonance imaging of the breast prior to biopsy," *JAMA*, Vol. 292, 2735–2742, 2004.

Prescaling of Data for Improved Parameter Sensitivity in Biomedical Nonlinear Microwave Imaging

T. Rubæk and A. Fhager
Chalmers University of Technology, Sweden

Abstract— Microwave imaging is emerging as a modality for biomedical imaging with results being reported for different areas such as brain imaging [1–3] and breast-cancer screening [4, 5]. Different approaches have been proposed for creating images from microwave systems, such as radar-based approaches and nonlinear inversion algorithms. In the nonlinear algorithms, images of the distributions of the permittivity and conductivity of the tissue under investigation is reconstructed. This is most commonly done by solving a nonlinear minimization problem similar to

$$[\underline{\epsilon}, \underline{\sigma}] = \arg\min \left\{ \left\| \underline{S}^{\text{meas}} - \underline{S}^{\text{calc}}(\underline{\epsilon}, \underline{\sigma}) \right\|_2^2 \right\} \tag{1}$$

wherein the column vectors $\underline{\epsilon}$ and $\underline{\sigma}$ hold the distributions of the permittivity and conductivity in the discretized imaging domain while $\underline{S}^{\text{meas}}$ holds the measured data and $\underline{S}^{\text{calc}}$ holds the corresponding data calculated for the parameter distributions given by $\underline{\epsilon}$ and $\underline{\sigma}$.

When using microwave imaging for biomedical applications, lossy media are often encountered. These can give rise to signal levels which span many orders of magnitude from the receiving antenna closest to the transmitter to receivers positioned further away. The large span of the level of the signals pose a significant challenge when formulating the minimization problem (1), requiring a careful weighting of the measured data to ensure that the maximum amount of information is extracted from the signals.

In this work, several different approaches for weighting the data will be presented and the effect on images reconstructed with both a time-domain and a frequency-domain inversion code will be investigated. The different approaches include a simple difference in the measured complex S-parameters, a weighting scheme based on a Fisher information analysis of the scattering problem [6], the log-phase formulation [7], and a normalization of the received signals.

REFERENCES

1. Semenov, S. Y. and D. R. Corfield, "Microwave tomography for brain imaging: Feasibility assessment for stroke detection," *International Journal of Antennas and Propagation*, Vol. 2008, 2008.
2. Trefna, H. and M. Persson, "Antenna array design for brain monitoring," *2008 IEEE Antennas and Propagation Society International Symposium*, 1–4, 2008.
3. Khorshidi, M. A., T. McKelvey, H. D. Trefna, and M. Persson, "Classification of microwave scattering data based on a subspace distance with application to detection of bleeding stroke," *The Third International Workshop on Computational Advances in Multi-sensor Adaptive Processing*, December 2009.
4. Klemm, M., I. J. Craddock, J. A. Leendertz, A. Preece, and R. Benjamin, "Radar-based breast cancer detection using a hemispherical antenna array: Experimental results," *IEEE Transactions on Antennas and Propagation*, Vol. 57, No. 6, 1692–1704, 2009.
5. Poplack, S. P., T. D. Tosteson, W. A. Wells, B. W. Pogue, P. M. Meaney, A. Hartov, C. A. Kogel, S. K. Soho, J. J. Gibson, and K. D. Paulsen, "Electromagnetic breast imaging: Results of a pilot study in women with abnormal mammograms," *Radiology — Radiological Society of North America*, Vol. 243, No. 2, 350–359, 2007.
6. Nordebo, S., A. Fhager, M. Gustafsson, and M. Persson, "A systematic approach to robust preconditioning for gradient-based inverse scattering algorithms," *Inverse Problems*, Vol. 24, No. 2, 025027, 2008.
7. Meaney, P., K. Paulsen, B. Pogue, and M. Miga, "Microwave image reconstruction utilizing logmagnitude and unwrapped phase to improve high-contrast object recovery," *IEEE Transactions on Medical Imaging*, Vol. 20, No. 2, 104–116, 2001.

Imaging of Animal Extremities Using Dedicated Microwave Tomographic System

S. Semenov[1], **B. Nair**[1], **J. Kellam**[2], **T. Williams**[2], **and M. Quinn**[2]

[1]ISTM, School of Medicine, Keele University, Stoke-on-Trent, ST4 7QB, UK
[2]Carolinas Medical Center, Charlotte, NC 28203, USA

Abstract— Microwave Tomography (MWT) is an emerging imaging modality with potentials for use in non-invasive assessment of functional and pathological conditions of biological tissues. Extremities soft tissues imaging is one of such applications. Early, in nonimaging experiments we have demonstrated the feasibility of the technology for such applications. We have recently developed a 2D microwave tomographic system dedicated for imaging of animal extremities. The system consists of two major subblocks: Electronic/microwave block and a 2D imaging chamber. The imaging chamber is a metallic cylinder with inner radius 10.75 cm with 24 ceramic waveguide antennas equidistantly located at the perimeter of the central cross-section of the imaging chamber. During an imaging procedure the chamber is filled in with matching solution. Full system electronic scanning and control allows for a multi-frame data acquisition with as minimal as 10–30 msec data acquisition per each frame at any frequency in the range of 0.9 to 2.3 GHz.

Ten Yorkshire domestic cross/farm pigs, males and females, were used in this study. Animals were cared for under an Institutional Animal Care and Use Committee approved research protocol and the NIH guidelines for laboratory research. Short blood flow reductions and compartment syndrome in animal extremities were modeled.

During an acquisition cycle when each of 24 antennas works as transmitter and the rest 23 antennas work as receiver, raw measured data (matrix 24×23) of complex scattered EM fields is obtained. Then data were pre-processed to remove artifacts, mainly caused by respiration activity of live animals and time frames of interest were chosen. For example in blood flow reduction experiments three characteristic frames were from baseline, occlusion and reperfusion time periods. Then inversion approaches were used for image reconstruction of the raw data from each frame. We used a nonlinear Newton based approaches as well as simple Born approximation. Typical reconstruction grids were 64×64. Images of extremities were obtained demonstrating a feasibility of MWT for functional imaging of extremities soft tissues.

3D Inversion Using the Multiplicative-regularized Gauss-Newton Approach

Aria Abubakar and Tarek M. Habashy
Schlumberger-Doll Research, Cambridge, USA

Abstract— In the microwave imaging one aims to retrieve the complex permittivity distribution of a domain of interest from electromagnetic wavefield measurements. The applications of this technology include the non-destructive testing, through-wall imaging, biomedical imaging and many others. The problem is very challenging since it is a non-linear and an ill-posed problem. Furthermore we deal with a large-scale electromagnetic computation especially for three-dimensional (3D) objects.

For 3D applications there are currently two popular iterative techniques that have been used quite extensively in the literature. They are the Gauss-Newton (GN) inversion method and the Contrast Source Inversion (CSI) method. The CSI method that is equipped with the multiplicative regularization (MR-CSI) has been shown to provide reliable inversion results for both synthetic and experimental data. This MR-CSI method has two main regularization features: 1) the weight of the regularization is automatically adjusted during the optimization process; 2) the weighted L2-norm regularization function provides an edge-preserving regularization effect. On the other hand the GN inversion method usually does not use any regularization function (the regularization is done by limiting the number of iterations) or one employs only a simple regularization function (hence, there is no edge-preserving effects) and the regularization weight is determined by trial and error, which makes the method rather unpractical.

Abubakar et al. proposed to use the regularization approach of the MR-CSI method for the GN inversion. They applied this so-called multiplicative-regularized GN (MR-GN) method for low-frequency geophysical applications in two-and-half dimensional geometry and 3D geometry. In this work we applied the MR-GN approach for solving 3D inverse problems at microwave frequency. By using this MR-GN inversion approach we will show that there is no need to determine the regularization weight and the approach can also preserve sharp edges by employing the weighted L2-norm regularization. To increase the robustness of the approach the minimization is constrained by using a non-linear transformation procedure and a line search approach is used to guarantee the reduction of the cost function after each iteration. As the forward solver we employed the Conjugate-Gradient Fast-Fourier Transform approach; however the integral equation is re-normalized in order to accelerate the convergence of the Krylov iterative method. In the presentation we will show inversion results from both synthetic and experimental data for biomedical.

Microwave Imaging of Bone: Initial Patient Results

Paul M. Meaney, **Tian Zhou**, **Sherri D. Geimer**, **Amir Golnabi**, **and Keith D. Paulsen**
Thayer School of Engineering, Dartmouth College, Hanover, NH, USA

Abstract— The majority of interest in biological dielectric properties has been for determining nominal property values to support studies in electromagnetic radiation exposure and microwave hyperthermia treatment. The most widely cited example of exploiting the dynamic nature of tissue properties is the microwave imaging of the high contrast between normal breast tissue and associated neoplasms. In reality, there are multiple examples where tissue property changes and differences could provide various forms of functional information that could be useful in medical diagnoses. Early work by Ken Foster and others showed a strong relationship between bulk tissue dielectric properties and water content — both free and bound water. In addition, they showed that the properties are generally a function of the bulk constituents including fat, water and proteins. In fact, numerous physiological problems often manifest in compositional changes. These signatures could be readily detected and monitored using microwave imaging. For example, new data shows that bone dielectric properties change dramatically with age and may provide valuable data about bone disease.

Using dielectric property interrogating techniques for studying bone is especially intriguing. Bone weakness affects a high percentage of the elderly population and fractures of the hip and spine can be particularly debilitating. The associated health care costs in this area are very high. Recent studies by Peyman et al. have demonstrated that the dielectric properties of cancellous bone in animals change significantly with age. This should come as no surprise because it is well known that the trabeculae within the cancellous bone demineralizes considerably over time. In addition, the hematopoietic component of the bone marrow progressively gives way to much fattier tissue in later stages of life. Each of these constituents has a different dielectric property profile such that the bulk properties of any trabecular bone sample would subsequently also change as the ratios of these parts varied. Given that the proportion of bone mineralization is the primary metric for assessing bone health, it is possible that the dielectric properties may provide important signatures that could be diagnostically valuable.

As with ongoing breast imaging studies, we plan to use our microwave imaging techniques to image bone. The earliest tests will be performed on the human heel (calcaneus) because it is often used as a surrogate for other important sites such as the hip and spine. This is primarily because these sites are fairly similar in that all are weight-bearing and are comprised of mainly trabecular bone. Other rationales include the fact that dual energy x-ray (DXA) is the current clinical standard and involves relatively high doses of radiation. We will present initial results of patient exams where microwave images of patient's heels were compared with both x-ray and density measures to assess overall correlation. Because we have access to associated CT images, we will also be able to utilize our soft prior algorithm which allows for excellent property recovery within pre-assigned regions. In these cases, we are studying volunteers who have had an injury to one leg requiring partial or full immobilization for at least 4 weeks. This is sufficient to induce noticeable bone loss for the affected trabecular bone zones. Comparison of the data from the affected and normal heels will allow us to explore how effective microwave imaging can be in this setting and set the stage for further explorations.

ACKNOWLEDGMENT

This work was sponsored by NIH/NCI Grant # PO1-CA080139.

Antenna Modeling Issues in Quantitative Image Reconstruction Using a Flexible Microwave Tomography System

Nikola Petrovic[1], **Tommy Henriksson**[1, 2], **and Magnus Otterskog**[1]

[1]School of Innovation, Design and Engineering, Mälardalen University, Box 883, 721 23 Västerås, Sweden
[2]Laboratoire des Signaux et Systèmes, SUPÉLEC
3 rue Joliot-Curie, F-91192 Gif-sur-Yvette Cedex, France

Abstract— Quantitative microwave imaging has been extensively studied in the past years as an alternative technique in biomedical imaging, with a strong potential in early stage breast cancer detection [Keith D. Paulsen and Paul M. Meaney, "*Alternative Breast Imaging*", The Springer International Series in Engineering and Computer Science, 778, 2005]. The image reconstruction involves a nonlinear inverse scattering problem, which consists to retrieve the dielectric properties of the biological object from the measured scattered field, for an applied incident field. Consequently, the solution is highly sensitive to model errors in the incident field. This paper focus on the impact of this model error on the reconstructed quantitative image using a flexible robotic microwave imaging system, developed at Mälardalen University, together with an iterative Newton-Kantorovich (NK) algorithm. This study is conducted during the development of the imaging system and the first quantitative images of a breast phantom are obtained.

The robotic microwave imaging system is developed as a flexible experimental platform for biomedical imaging, where one of the applications is breast imaging. Using a robot controlled system the scattered field can be measured with a single transmitting/receiving antenna-pair, thus avoiding the mutual coupling that occur when an antenna-array is used. The scattered field is, herein, measured around a breast phantom, along a circular arc, in the horizontal plane with vertically polarized monopole antennas, considering a two dimensional transverse magnetic case (2D-TM). The radiated field from the transmitting antenna is modeled as a vertical polarized cylindrical wave in the numerical incident field model of the NK algorithm, where images with both the real- and imaginary permittivity profile of the breast phantom are obtained.

In this study, two different monopole antenna designs are compared with the numerical incident field model. The difference between the antennas is the ground-plane design, where the first setup uses 4 wires forming a horizontal cross as a ground-plane. By varying the length of the wires and angel between the transmitting and receiving antenna the incident electromagnetic field is changed and could be modified to best fit the simulated field. The second setup uses a circular ground plane which will give a more rotational symmetric radiation pattern in the horizontal plane and a better match when comparing measured fields with computed values. The comparison is done directly with the numerical incident field model, as well as the computed and measured scattered field, and finally the impact on the reconstructed images by the NK algorithm are compared, using measured data from both antennas.

The results show how the antenna selection impacts the error between the measured incident field and the numerical model, and how the quantitative image of an inhomogeneous object is affected by this model error.

Session 4A2
Forward and Inverse Algorithms for Microwave Remote Sensing of Soil Moisture with SMAP

A Two Layers Multi-scale Bi-dimensional SPM Model for the Study of Radar Backscatter Behavior on Semi-arid Soil Subsurfaces

L. Bennaceur Farah[1], **I. R. Farah**[2], **R. Bennaceur**[3], **I. Hosni**[1], **and M. R. Boussema**[1]

[1]LTSIRS, ENIT, Tunisia
[2]RIADI, ENSI, Tunisia
[3]LMPC, FST, Tunisia

Abstract— In this paper, we propose to simulate the polarimetric SAR response of semi-arid subsurfaces. We characterize the soil surfaces and subsurfaces by a two layer geo-electrical model. The upper layer is described by its dielectrical constant, thickness, a multi-scale bi-dimensional surface roughness model by using the wavelet transform and the Mallat algorithm, and volume scattering parameters. The lower layer is described by its dielectric constant and multi-scale surface roughness.

To compute surface, subsurface and volume scattering, we consider a two layers multi-scale bi-dimensional Small perturbations model with single and multiple scattering terms. Due to the large variability of the correlation function, backscattering models using statistical parameters like correlation length and rms height to describe roughness, often fail to predict correctly backscattering. Therefore in this study each surface of the two layers surface is considered as a band limited fractal random process corresponding to a superposition of a finite number of one dimensional Gaussian processes each one having a spatial scale.

We investigate both case of an inhomogeneous superficial layer containing no rocks clasts i.e., no volume scattering and the case of volume scattering produced by rocks.

We simulate radar backscattering for HH and VV polarizations for three upper layers thickness, for dry basalt bedrock and for a wet basaltic substratum.

We also investigate the dependence of the co-polarized phase difference on roughness multi-scale parameters and radars parameters for different incident angles and notice that multiple scattering significantly influences the copolarized phase difference which can be related to soil moisture content. We notice that radar simulation for C-band predict detection of larger depth than L band. The phase information prediction is a very important tool to map subsurface moisture in arid regions. The overall objective of this work is to predict correctly surface and volume scattering in order to be able to retrieve roughness and soil moisture parameters by inverting radar polarimetric signals.

Data Cube Representation of Vegetated Surfaces Based on Physical Scattering Model for SMAP Mission

Xiaolan Xu[1], **Shaowu Huang**[1], **Leung Tsang**[1], **Seungbum Kim**[2], **and Eni Njoku**[2]

[1]Department of Electrical Engineering, University of Washington, Seattle, WA 98195-2500, USA
[2]Jet Propulsion Laboratory, California Institute of Technology, Pasadena, CA 91109, USA

Abstract— In this paper, we present data cube representation using forward model of the microwave backscattering from a vegetated terrain at L band for application in the upcoming SMAP (Soil Moisture Active and Passive) mission. The objective of the SMAP mission is to provide global measurements of soil moisture and its freeze/thaw state. There are two options of the retrieval algorithms in the SMAP baseline, the snapshot algorithm and time-series algorithm. The data cube representation of the backscattering coefficient can be adapted into both of them. To account for the vegetation effect above the bare soil and simplify the retrieval algorithm, we use three input parameters to describe the vegetated terrain, which are vegetation water content, soil moisture and soil roughness. The physical-based forward scattering model is used to generate the data cube for both co-polarization and cross-polarization based on the description.

The radar backscattering cross section of the vegetated surface includes three kinds of mechanisms. The first one is the direct volume scattering by the vegetation components, which is solved by calculating the Maxwell Equations numerically through body of revolution method. Secondly, the rough surface scattering of the bare soil was accounted for by NMM3D (Numerical Maxwell Model of 3-dimensional simulations). The last one is the double bounce effect on the interface of the vegetation layer and soil, which is considered by modifying the rough surface reflectivity using the coherent wave as computed by NMM3D. In this paper we demonstrated two classes data cube, grassland and corn field.

Soil Moisture Retrieval Using Data Cube Representation of Radar Scattering

Seung-Bum Kim and Eni G. Njoku
Jet Propulsion Laboratory, California Institute of Technology, Pasadena, California, USA

Abstract— A time-series algorithm is investigated to retrieve surface (from surface down to 1 m depth) soil moisture using simulated 3-km resolution radar data of the Soil Moisture Active and Passive (SMAP) mission. The time-series approach uses co-polarized (VV and HH) backscattering coefficient ($\sigma 0$) values at 3-km resolution. These values are temporally averaged to reduce the measurement noise. To the extent that the surface roughness does not change within the time-series window, the reduction of the noise enables the retrieval of the roughness. With the roughness estimate, subsequently soil moisture is retrieved through least square minimization. The proposed retrieval is performed using 'data cubes'. The data cubes relate soil moisture and $\sigma 0$, and are lookup tables with the dimensions of soil moisture, roughness, and vegetation water content (VWC). The cubes were generated by an empirical radar scattering model. The roughness estimate has an error of 10–20%. Soil moisture may be retrieved within the error bounds of $0.06\,\mathrm{cm}^3/\mathrm{cm}^3$ up to $3\,\mathrm{kg}/\mathrm{m}^2$ VWC with the following experiment setup: same scattering models for the forward and retrieval processes, 13% radar measurement error at the outer edge of the swath (Kp, 1 sigma), 10% error in VWC, and 24 time-series. The magnitude of the radar measurement error, the number of the time-series record, and the fidelity of the radar scattering model are the most important in determining the performance of the retrieval. Future plans include the error assessment with in situ records.

Radar Retrieval of Subcanopy Soil Moisture Using Simulated Annealing

A. Tabatabaeenejad and M. Moghaddam
Radiation Laboratory, Department of Electrical Engineering and Computer Science
University of Michigan, Ann Arbor, MI 48109, USA

Abstract— Soil moisture is of fundamental importance to many hydrological and biological processes. Soil moisture information is vital to understanding the cycling of water, energy, and carbon in the Earth system. Knowledge of soil moisture is also critical to agencies concerned with weather and climate prediction, runoff potential and flood control, soil erosion, agricultural productivity, drought monitoring, and human health. The need to monitor soil moisture on a global scale has motivated missions such as NASA's Soil Moisture Active and Passive (SMAP).

Due to the challenging inverse problem associated with estimation of soil moisture, the previous works on subcanopy soil moisture retrieval have mostly modeled the vegetation cover with only one parameter such as an effective dielectric constant, vegetation water content, or vegetation biomass, assuming other parameters of the vegetation are known a-priori. This type of approach neglects the fact that radar response to vegetation is sensitive to several parameters such as vegetation height and other geometrical properties, density, and component dielectric constants, and not simply a function of a single equivalent parameter. This problem is addressed in this paper, by increasing the number of parameters used to describe the vegetation canopy covering the soil.

We have previously shown that simulated annealing is a powerful inversion scheme that can retrieve several model parameters in a nonlinear inverse problem. In this work, we use a numerical forest scattering model combined with an SPM solution for scattering from layered rough surfaces to develop a subcanopy soil moisture estimation method with synthesized radar data. We examine the performance of simulated annealing in retrieving subcanopy soil moisture where the vegetation cover is modeled with more than one model parameter. This approach increases retrieval accuracy by eliminating the need to assume several parameters of the vegetation are known a-priori. We also examine the capability of our inversion algorithm in retrieving deep soil moisture by modeling the soil with more than one layer. The ability to extract additional information comes at the expense of including more measurements, especially at frequencies lower than L-band. This approach is therefore intended for future airborne or spaceborne systems that may follow SMAP. We present inversion results for noise-free data, but the noise response of the inversion for some cases will also be presented.

Azimuthal Signature of Coincidental Brightness Temperature and Normalized Radar Cross-section Obtained Using Airborne PALS Instrument

Andreas Colliander[1], **Seungbum Kim**[1], **Simon Yueh**[1], **Mike Cosh**[2], **Tom Jackson**[2], **and Eni Njoku**[1]

[1]Jet Propulsion Laboratory, California Institute of Technology, USA
[2]USDA Agriculture Research Service, USA

Abstract— The airborne PALS (Passive and Active L- and S-band) instrument was used in the SMAPVEX08 (SMAP Validation Experiment 2008) campaign to measure the brightness temperature (TB) and normalized radar cross-section (NRCS) at L-band during a period of several days over an area spanning tens of kilometers in Maryland and Delaware. SMAP (Soil Moisture Active and Passive) is a NASA mission dedicated to measurement of global soil moisture and boreal land surface freeze/thaw state. The satellite will carry radar (active) and radiometer (passive) L-band instruments that will perform simultaneous and coincident measurements of the Earth's surface. The PALS instrument is a simulator for SMAP. This paper presents results obtained on one of the SMAPVEX08 campaign days when the PALS instrument measured a plowed field in 45 degree steps over the azimuth.

The field had row spacing of about 20 cm and roughness on the order of 3 to 5 cm. These surface parameters make the experiment very relevant for the L-band frequency, which is used in the study. Both TB and NRCS in the experiment show sensitivity to the azimuth angle of the measurement, which is expected for a fine resolution scale measurement of a homogeneous field surface such as the one in question. It is assumed that the azimuthal behavior arises from the Bragg scattering induced by the periodic surface. For NRCS, the resonance in the perpendicular orientation to the row structure is observed as a relative sharp spike as expected. In the TB measurement the signature is consistent in amplitude and shape with results presented in other studies of periodic field surfaces. Although it is not expected that the resolution scale of SMAP would experience azimuth effects as pronounced as the ones observed in this experiment, it is nevertheless important for the mission algorithm development to understand the fine resolution scattering and emission behavior. These results can be used, for example, for model development and validation.

Covariance Matrix for Compact Polarimetry for Soil Moisture Estimation

Joel T. Johnson
Department of Electrical and Computer Engineering and ElectroScience Laboratory
The Ohio State University, Columbus, OH, USA

Abstract— Recent studies have shown the potential advantages of the use of a "compact polarimetry" mode in active remote sensing. Compact polarimetry attempts to achieve observations similar to those in a fully polarimetric mode, but with the use of only a single transmit polarization, typically taken to be either a 45 degree linear or a circular polarization. A circular transmit polarization is preferred for systems operating at lower frequencies, due to the reduced impact of the ionosphere in this case. If a reflection symmetry assumption is invoked for the observed geophysical medium, it is possible with additional assumptions to retrieve all remaining elements of the Mueller matrix. The technique is currently being explored through post-processing of existing polarimetric SAR datasets for a variety of applications.

Further consideration of compact polarimetry is particularly relevant for NASA's SMAP mission, because the SMAP radar design provides only incoherent measurements of HH, VV, and HV cross sections, with HH and VV observed at differing frequencies so that speckle in these observations is uncorrelated. The presence of uncorrelated speckle effects in HH and VV increases errors in measurement of the HH/VV polarization ratio, potentially impacting the soil moisture retrieval accuracy. Use of compact polarimetry eliminates the use of different frequencies, producing correlated speckle noise that may be advantageous.

In order to investigate the potential of compact polarimetry for soil moisture, it is important to simulate compact polarimetry observations in a manner that models the associated speckle effects appropriately. A derivation of signal statistics for such observations is reported in this presentation. It is shown that the observed signal powers and correlations can be modeled after sufficient integration as a multivariate Gaussian random process with the mean and covariance matrix determined analytically. The use of this model in formulating appropriate weights in a soil moisture maximum likelihood estimation algorithm is also discussed.

L Band Brightness Temperature from Forests: Comparison of Approximate Techniques

Mehmet Kurum[1], **Roger Lang**[2], **and Peggy O'Neill**[1]

[1]NASA Goddard Space Flight Center, USA
[2]The George Washington University, USA

Abstract— In this paper, three approximate physical microwave radiometry models have been used to calculate brightness temperatures from a forest canopy at L-band. These models are (1) tau-omega model (zero order scattering approximation to radiative transfer equations), (2) successive order of scattering model up to first order (first order scattering approximation to the radiative transfer equations), and (3) Peak technique utilizing the active solution obtained from the Distorted Born Approximation (DBA). These models are physically-based and treat vegetation as a layer of discrete scatterers over a rough surface. Vegetation components within the canopy are represented by canonical shapes such as dielectric discs and cylinders.

The tau-omega model is based on a zero-order solution to the radiative transfer (RT) equations. The model ignores scattering except for the effect of the scatterers in the attenuation of the emission through the vegetation. Application of the tau-omega model to data acquired during airborne and ground-based campaigns over the years has solidified scientific understanding of microwave interactions with different landscapes. In particular, shrubland, grasslands, agricultural crops, and light to moderate vegetation have been investigated. Its applicability to areas with a significant tree fraction is unknown.

The first order scattering model is based on an iterative solution of the RT equation up to the first order. The first order solution is obtained by substituting the zeroth-order solution into the scattering source term and then solving the resulting radiative transfer equations. This formulation adds a new scattering term to the tau-omega model. It represents emission by particles in the layer and emission by the ground that is scattered once by particles in the layer. The resulting model represents an improvement over the standard zero-order solution (the tau-omega model) since it accounts for the scattered vegetation and ground radiation that can have a pronounced effect on the observed brightness temperature.

The third model is based on the Peake formulation in conjunction with the DBA. The procedure for calculation of forest emission is accomplished by first calculating the bistatic scattering cross section for each type of scatterer, then by using the DBA to calculate specular albedo of the ground and the diffused albedo of the layer. Once the albedos are determined, Peake's principle relating active and passive problems can be used to determine the effective emissivity of the forest layer.

This paper compares the tau omega model, the first order scattering solution to the RT equation, and the Peake formulation used in conjunction with the DBA. The applicability of these models to determine the brightness temperature in areas with a significant tree fraction will be evaluated for L-band frequencies. Contributions of the individual scattering terms and their role in contributing to forest scattering will be identified, and their dependence on angle and soil moisture will be demonstrated. Comparison to experimental data from several tree stands will be given.

Session 4A3
Novel Mathematical Methods in Electromagnetics 1

Subpixel Smoothing for Dispersive Media in the FDTD Method

Alexei Deinega[1], **Ilya Valuev**[2], **and Sergei Belousov**[1]

[1]Russian Research Centre, Kurchatov Institute, Kurchatov sq. 1, Moscow 123182, Russia
[2]Joint Institute for High Temeperatures of RAS, Izhorskaya, 13, bld. 2, Moscow 125412, Russia

Abstract— The Finite-Difference Time-Domain (FDTD) method [1] is an extensively used computational tool in electrodynamics. However, as for any other finite difference method, there exists an intrinsic problem of media properties discretization on the FDTD space grid. Any curved media interface that can not be aligned with FDTD grid is distorted by staircasing which reduces the accuracy of calculation. Subpixel smoothing [2] is an efficient method for reducing this type of the numerical error. In this method, the inverse dielectric permittivity tensor [2–4] is introduced near the interface of adjacent media. It was shown that the method leads to the quadratic convergence with increasing resolution, whereas the linear convergence is typical for staircasing [4].

So far this method has been implemented only for dielectrics. We have extended it for the case of dispersive media. Our approach consists in splitting the electric field in three auxiliary components. Additional equations should be solved for each of them. The efficiency of the suggested method has been tested by calculating the transmission spectra for various metallic photonic crystal slabs (opals). A comparison is presented between transmission spectra results, obtained by our method, staircase FDTD simulation and the layer Korringa-Kohn-Rostoker (LKKR) method [5]. It was shown that staircasing effects lead to essentially reduced accuracy when dielectric permittivity becomes negative. Therefore, taking into account non-diagonal inverse dielectric permittivity tensor elements becomes important.

REFERENCES

1. Taflove, A. and S. H. Hagness, *Computational Electrodynamics: The Finite Difference Time-Domain Method*, Artech House, Boston, 2005.
2. Lee, J.-Y. and N.-H. Myung, "Locally tensor conformal FDTD method for modeling arbitrary dielectric surface," *Microw. Opt. Technol. Lett.*, Vol. 23, 245, 1999.
3. Nadobny, J., D. Sullivan, W. Wlodarczyk, P. Deuflhard, and P. Wust, "A 3-D tensor FDTD-formulation for treatment of slopes interfaces in electrically inhomogeneous media," *IEEE Trans. Antennas Propag.*, Vol. 51, 1760, 2003.
4. Farjadpour, A., D. Roundy, A. Rodriguez, M. Ibanescu, P. Bermel, J. D. Joannopoulos, S. G. Johnson, and G. Burr, "Improving accuracy by subpixel smoothing in FDTD," *Optics Letters*, Vol. 31, No. 20, 2972, 2006.
5. Stefanou, N., N. Yannopapas, and A. Modinos, "Heterostructures of photonic crystals: Frequency bands and transmission coefficients," *Comput. Phys. Commun.*, Vol. 113, 49, 1998.

Wave Equations in Electromagnetic and Gravitational Fields

Zi-Hua Weng
School of Physics and Mechanical & Electrical Engineering
Xiamen University, Xiamen 361005, China

Abstract— In the electromagnetic field, the inferences of wave equation are believed to be correct. Until to now, this validity is confined only to one special condition that there exist only the electromagnetic fields. When there are gravitational fields, the people doubt whether the wave equation of electromagnetic field is still correct or not. The existing theories do not explain why the deductions of wave equation should keep unchanged, and then do not offer compelling reason for the unique situation. The paper attempts to find out why the deductions of wave equation keep the same in most cases, even in the gravitational field.

The algebra of quaternions was invented by W. R. Hamilton in 1843, and then was first used by J. C. Maxwell to represent field equations of electromagnetic field in 1861. O. Heaviside in 1884 recast Maxwell equation in terms of vector terminology and electromagnetic forces, thereby reduced the original twenty equations down to the four differential equations. In 1871, H. Helmholtz made clear the electromagnetic theory effectively. Helmholtz equation and boundary conditions can deduce some wave features, including the law of reflection, Snells law, Fresnel formula, etc. H. R. Hertz became famous as the first to demonstrate electromagnetic radiation.

The paper studies the inferences of wave equations for electromagnetic fields when there are gravitational fields at the same time. In the description with the algebra of octonions, the deductions of wave equations are identical with that in conventional electromagnetic theory with the vector terminology. When there are gravitational fields, the almost deductions of wave equations for electromagnetic fields keep unchanged. By means of the octonion exponential function, we can rephrase that the electromagnetic waves are transverse waves in a vacuum.

In the electromagnetic field, making use of the algebra of octonions, we can deduce the wave equation, laws of reflection and refraction, Fresnel formula, and total internal reflection. Bringing in the octonion exponential function, the wave vector and electromagnetic waves will produce two new wave components respectively. In contrast to conventional electromagnetic theory with vector terminology, the research points out that the electric components of electromagnetic waves can not be determined simultaneously with magnetic components in electromagnetic fields.

ACKNOWLEDGMENT

The author is grateful for the financial support from the National Natural Science Foundation of China under grant number 60677039.

Theory of the $\hat{L}(\hat{c},\hat{n})$ Numbers and Its Application to the Slow Wave Propagation in the Circular Ferrite Waveguide

Georgi Nikolov Georgiev[1] **and Mariana Nikolova Georgieva-Grosse**[2]

[1]Faculty of Mathematics and Informatics, University of Veliko Tirnovo "St. St. Cyril and Methodius"
BG-5000 Veliko Tirnovo, Bulgaria
[2]Meterstrasse 4, D-70839 Gerlingen, Germany

Abstract— The name L numbers has been given to the common limits of some infinite sequences of positive real numbers whose terms involve the positive purely imaginary (real) zeros of definite functions, devised through certain complex (real) confluent hypergeometric and eventually real cylindrical functions, as well [1–4]. They sprang up in the theory of azimuthally magnetized circular ferrite waveguides, sustaining normal (slow) TE_{0n} ($\hat{TE}_{0\hat{n}}$) modes, based on the functions mentioned [1–4].

In this investigation the theorem for existence and for the main features of the $\hat{L}(\hat{c},\hat{n})$ numbers — an integral part of the aforesaid class, is stated and substantiated numerically. Following the recently elaborated model [1, 3], it is structured as a composition of three lemmas. The first of them reveals the existence of quantities in question and defines them as the limits of the infinite sequences of numbers $\{\hat{K}_-(\hat{c},\hat{n},\hat{k}_-)\}$ and $\{\hat{M}_-(\hat{c},\hat{n},\hat{k}_-)\}$ in which $\hat{K}_-(\hat{c},\hat{n},\hat{k}_-) = |\hat{k}_-|\hat{\zeta}^{(\hat{c})}_{\hat{k}_-,\hat{n}}$ and $\hat{M}_-(\hat{c},\hat{n},\hat{k}_-) = |\hat{a}_-|\hat{\zeta}^{(\hat{c})}_{\hat{k}_-,\hat{n}}$ in case $\hat{k}_- \to -\infty$. The symbol $\hat{\zeta}^{(\hat{c})}_{\hat{k},\hat{n}}$ stands for the $\hat{n}$th positive real zero of Kummer confluent hypergeometric function $\Phi(\hat{a},\hat{c};\hat{x})$ in $\hat{x}$ provided $\hat{a}$, $\hat{c}$, $\hat{x}$ are real, $\hat{a} < 0$, $\hat{c} > 0$, $(\hat{n} = 1, 2, \ldots, \hat{p},\ \hat{p} = abs[\hat{a}])$ or $\hat{a} < 0$, $\hat{c} < 0$, $(\hat{c} \neq \hat{l},\ \hat{l} = 0, -1, -2, \ldots)$, $\hat{a} < \hat{c} < 0$, $(\hat{n} = 1, 2, \ldots, \hat{r},\ \hat{r} = \hat{p} - \hat{q},\ \hat{p} = abs[\hat{a}],\ \hat{q} = abs[\hat{c}],\ \hat{q} = 1, 2, \ldots, \hat{p} - 1)$, $\hat{k} = \hat{a} - \hat{c}/2$ — real, $\hat{a} = \hat{c}/2 + \hat{k},\ \hat{x} > 0$, ($[\hat{a}]$ denotes the largest integer less or equal to $\hat{a}$). The hats "$\hat{}$" are used to designate real quantities. Lemma 2 determines the numbers in case $\hat{c} = \hat{l}$ as the common limit of the sequences of numbers in the sense of Lemma 1 $\{\hat{L}(\hat{c} - \hat{\varepsilon},\hat{n})\}$ and $\{\hat{L}(\hat{c} + \hat{\varepsilon},\hat{n} + 1)\}$ for $\hat{\varepsilon} \to 0$ ($\hat{\varepsilon}$ — infinitesimal positive real number). Lemma 3 says that when $\hat{c} = \hat{l}$, it holds $\hat{L}(\hat{l},\hat{n}) = \hat{L}(2 - \hat{l},\hat{n})$ and provided $\hat{c} = 1 \pm \hat{l}$, then $\hat{L}(1 + \hat{l},\hat{n}) = \hat{L}(1 - \hat{l},\hat{n})$.

It is shown that if $\hat{c} = 3$, the zeros of $\Phi(\hat{a},\hat{c};\hat{x})$ coincide with the roots of characteristic equation of the circular waveguide of radius $\hat{r}_0$, entirely filled with azimuthally magnetized ferrite, described by a permeability tensor of off-diagonal element $\hat{\alpha} = \gamma\hat{M}_r/\omega$, ($\gamma$ — gyromagnetic ratio, $\hat{M}_r$ — remanent magnetization, ω — angular frequency of the wave), and a scalar permittivity $\varepsilon = \varepsilon_0\varepsilon_r$, for slow $\hat{TE}_{0\hat{n}}$ modes of phase constant $\hat{\beta}$. It is found out that the wave propagation may take place for negative magnetization only in two areas, corresponding to $|\hat{\alpha}| < 1$ and $|\hat{\alpha}| > 1$, resp. In the first of them for each of the modes the phase curves are restricted by an envelope line from the side of lower frequencies of equation: $\bar{\hat{r}}_0 = \hat{L}(\hat{c},\hat{n})/[|\hat{\alpha}|(1 - \hat{\alpha}^2)^{1/2}]$, $\bar{\hat{\beta}} = (1 - \hat{\alpha}^2)^{1/2}$ ($\hat{\alpha}$ is a parameter) where $\bar{\hat{r}}_0 = \beta_0\hat{r}_0\sqrt{\varepsilon_r}$, $\bar{\hat{\beta}} = \hat{\beta}/(\beta_0\sqrt{\varepsilon_r})$ and $\beta_0 = \omega\sqrt{\varepsilon_0\mu_0}$.

REFERENCES

1. Georgiev, G. N. and M. N. Georgieva-Grosse, "The $L(c,n)$ numbers and their application in the theory of waveguides," *Proc. Int. Conf. Days Diffr. 2008 DD'08*, 44–57, St. Petersburg, Russia, June 3–6, 2008.
2. Georgiev, G. N. and M. N. Georgieva-Grosse, "A property of the $L(c,\rho,n)$ numbers and its application to waveguide propagation," *Proc. XXIX URSI General Assembly*, BK.6(120), in CDROM, Chicago, IL, USA, August 7–16, 2008.
3. Georgiev, G. N. and M. N. Georgieva-Grosse, "Theorem for the $L(c,\rho,n)$ numbers," *PIERS Proceedings*, 1478–1482, Moscow, Russia, August 18–21, 2009.
4. Georgiev, G. N. and M. N. Georgieva-Grosse, "Effect of the dielectric filling on the phase behaviour of the circular waveguide with azimuthally magnetized ferrite toroid and dielectric cylinder," *Proc. Asia-Pacific Microwave Conf. APMC–2009*, WE4B-4(1680), in CDROM, Singapore, December 7–10, 2009.
5. Tricomi, F. G., *Funzioni Ipergeometriche Confluenti*, Edizioni Cremonese, Rome, Italy, 1954.

About the Specific Heat of Black Holes

Antonio Puccini
Department of Neurophysiology, Order of Malta, Naples, Italy

Abstract— If we give a certain thermic energy to a black hole (BH) it can happen that its temperature decreases and its specific heat (SH) has a negative number. At the same time its mass will increase, according to Hawking's equation: $T_{BH} = 8\pi/m$.

The mathematical formalism is easy and elegant, however we do not know the real physical checking which may explain this peculiar phenomenon.

With this paper we try to describe how heat may give a mass to the BH.

Application of Analytical Method to Weak Global Positioning System Signal

H. Babazadeh, **S. Askari**, **A. Safaian**, **and M. Razfar**
Department of Electrical Engineering, California State University Los Angeles
Los Angeles, CA 90032, USA

Abstract— The aims of the study are to analytically detect and treat the nonlinear behavior of weak indoors Global Positioning System (GPS) signal. Since analyzing nonlinear problems are of great difficulty, different numerical methods and scientists try to treat such problems. Ignoring nonlinearity is inevitable in the actual world of communications; therefore, nonlinear analysis has been of great importance to the scientists in its field. The advantages of analytical methods, specially Homotopy Perturbation Method (HPM), are that these methods are capable of solving both regular and strong non-linear equations; plus, these methods are simple to apply and will not increase complexity. The obtained results are compared simultaneously with numerical ones and as result shown in graphs and in tables; analytical solutions are in good agreement with those of the numerical method. As a strategy, chaotic oscillators, which are sensitive to periodic signal and inert to noise, possesses huge advantages in weak signal acquisition. In this paper, chaotic oscillator is employed in weak GPS signal acquisition. In the final section, the results achieved from computer simulation indicate that chaotic oscillator algorithm can acquire GPS signal at $-48\,\mathrm{dB}/2\,\mathrm{MHz}$ SNR.

Introduction: Up to this date, different numerical methods have been implemented to solve the problem of a nonlinear oscillators which this paper represents the nonlinear behavior of a Chaotic oscillator, weak GPS signal [1] but in this project, it has been attempted to propose an analytic solution for such problem, which is not only simple but also strong method for engineers to interpret and to use in their designs.

In the dynamic model of this problem, the chaotic oscillator, weak GPS signals has been modeled in the next part. The analytical methods used including Homotopy Perturbation Method (HPM), to many engineering problems by many other scientists in different fields [2–8]. This method is capable of solving highly nonlinear problems while the constant coefficients are parametrically inserted into the equation. Therefore, the obtained results can be graphically shown and analyzed for different cases, and by inserting different values for these parameters regarding each single case of study.

GPS signal indoors becomes extremely weak because of fading, refraction, reflection and multipath interference. Normally line-of-sight GPS signal is at 44 dBHz [9], while signal strength will degrade larger than 25 dB in bad case [10]. However common commercial GPS receiver can only acquire GPS signal above 38 dBHz. To achieve successful position and navigation in such challenging environment, much work has been performed, which focused on prolonging integration duration to increase SNR. Chaotic oscillator [11] is sensitive to periodic signal and inert to noise, which can be utilized to achieve successful acquisition in weak signal. Bo [12] used chaotic oscillator to detect weak linear frequency modulation (LFM) signal after decrypting. Chaotic oscillator can detect extremely weak LFM signal, even at $-27\,\mathrm{dBHz}$. In the end, a comparative study is conducted to verify the accuracy.

Oblique Incident Plane Wave Condition for Finite-difference Time-domain Simulations of Surface Plasmons Excited at Nanoscale Slits in Layered Dispersive Media

L.-X. Zhang and T. Seideman
Department of Chemistry and Physics, Northwestern University, Evanston, IL, USA

Abstract— One important method to introduce plane waves into the Finite-Difference Time-Domain (FDTD) electromagnetic simulation domain is the Total Field/Scattered Field (TF/SF) formulation in which an artificial boundary is utilized to match the fields between the TF and SF regions, such that a plane wave with arbitrary incident angle and temporal profile can be realized [1]. The TF/SF formalism has been previously extended to treat layered dielectric and conductive media and more recently to treat layered dispersive media with Debye type of poles [2, 3]. In this context, further development of the TF/SF method to treat layered media with more complex dispersiveness is attractive to the accurate description of recent experiments on surface waves — in particular, surface plasmon waves — excited under oblique plane wave illumination at nanoscale surface structures in dispersive metal films [4].

In this paper, we improve the TF/SF scheme to treat transverse electric and magnetic oblique plane waves in two dimensions upon layered dispersive media that can be described by a finite sum of Debye, Drude and Lorentz types of poles [2]. Converged FDTD results show a maximum relative error less than 5% in the free space wave impedance and the reflection and transmission coefficients from a dielectric or dispersive slab in comparison with analytical results for various incident wavelengths and angles. We then employ our method in combination with the Uniaxial Perfectly Matched Layers absorbing boundary condition to simulate a realistic experiment (currently underway in Pittsburgh) on a single slit in silver thin film under femto-second laser pulse excitation. The simulation results successfully reproduce the interference patterns between the incident wave and the excited surface plasmon waves as well as the dependence of the interference signal strength on the width of slit. Furthermore, the simulation explains the temporal evolution of the interference pattern by separating the incident and scattered fields. Field patterns in the vicinity of the slit reveal the formation of Fabry-Perot cavity mode and establish its role in enhancing the interference signal.

REFERENCES

1. Taflove, A. and S. C. Hagness, *Computational Electrodynamics: The Finite-difference Time-domain Method*, Artech House, Norwood, MA, 2005.
2. Capoglu, I. R. and G. S. Smith, "A total-field/scattered-field plane-wave source for the FDTD analysis of layered media," *IEEE Trans. Antennas Propag.*, Vol. 56, No. 1, 158–169, 2008.
3. Jiang, Y.-N., D.-B. Ge, and S.-J. Ding, "Analysis of TF-SF boundary for 2D-FDTD with plane P-wave propagation in layered dispersive and lossy media," *Progress In Electromagnetics Research*, PIER 83, 157–172, 2008.
4. Kubo, A., N. Pontius, and H. Petek, "Femtosecond microscopy of surface plasmon polariton wave packet evolution at the silver/vacuum interface," *Nano Lett.*, Vol. 7, 470, 2007.

Electrodynamics in Expanding Cavities

J. A. Grzesik
Allwave Corporation, 3860 Del Amo Boulevard, Suite 404, Torrance, CA 90503, USA

Abstract— The conventional attitude toward the electrodynamics of cavities regards the boundaries of the latter, and rightly so, as being fixed in perpetuity. There seems precious little point, evidently, in contemplating, say, the magnetron of a microwave oven in the process of undergoing any sort of deformation. This attitude, however, is turned on its head in the admittedly niche arena offered for consideration by the massive, Yin-Yang (Y-Y) coil magnets serving as particle mirrors in fusion reactors of axial type. Obviously, while no one looks forward to their possible disintegration, there intrudes nevertheless the inconvenient fact, the source of considerable safety concern, that the dilatational magnetic pressure due to the large, opposed Y-Y dc currents may trigger an unintended expansion, nay, even a violent explosion. One becomes confronted at that point with an electromagnetic field evolving amid the *bona fide* scenario of geometrically variable boundaries, a scenario enjoying moreover a modicum of both a practical and most certainly a theoretical interest.

Quite a number of years ago we had the opportunity to make some preliminary inroads on these problems in the idealized setting of two-dimensional current sheets [1, 2], separating in the first place *en masse* along their common perpendicular, and, in the second, allowing for the partial disintegration of just one of them in the form of an ejected ribbon parallel to the prevailing current flow. A measure of success was gained by treating the electrodynamic evolution in a quasi-static (QS) mode as reinforced by a moving boundary condition (MBC) requiring that one set to a null value, upon all moving material, its rest-frame tangential electric field, gotten, in lowest-order relativistic approximation, as $\sim \hat{\mathbf{v}}\times\{\mathbf{E}+\mathbf{v}\times\mathbf{B}\}$ in terms of laboratory-frame electric $\mathbf{E}$ and magnetic $\mathbf{B}$ fields, and local velocity $\mathbf{v}$. In this process, a secondary computation of $\mathbf{E}$ was bootstrapped upon a primary, QS one for $\mathbf{B}$ via Faraday's law, whereby the obligatory time derivative of the latter was tethered to the dynamic evolution of its underlying separation parameter $\eta(t)$.

We seek here to present an additional, heretofore unpublished extension of this work which brings to bear upon the separating wafer scenario the full force of Maxwell's equations undiluted by any *a priori* specializations. With due note of the intuition gained during the more heuristic, QS/MBC prelude, we go on to subject both $\mathbf{E}$ and $\mathbf{B}$ fields to Fourier transformation along the current sheet perpendicular. One is led at this point to an ordinary, simple-harmonic differential equation in time t having the sheet current density $\pm I(t)$ as its source, a source which itself implicitly depends upon the evolving field by way of a standard, perfect-conductor boundary condition. We invoke this boundary condition in its null-field form at *all* points exterior to the growing cavity, and not just immediately beyond its walls. This viewpoint liberates us, of course, from having to assemble any sort of relativistic transformation between laboratory and rest-frame fields. Then, on the one hand, there emerges from the differential equation, following Fourier inversion along the expansion perpendicular, a field structure exhibiting full retardation of the surface current source *vis-à-vis* signal crossing across a wafer cavity of net thickness $\{\eta(t)+\eta(t_*)\}/2$ that straddles an antecedent point of emission $\mp\eta(t_*)/2$ with its subsequent point of reception $\pm\eta(t)/2$ at the later time $t > t_*$, while, on the other, these surface current sources at times t and its precursor t_* are simply related via the null-field boundary condition. And, while this current relation is perfectly general, its specialization to the necessarily non-relativistic (N-R) regime of interest recovers the QS/MBC outcome which is encapsulated in maintaining invariant the product of surface current $I(t)$ by separation $\eta(t)$.

By virtue of this $I \times \eta$ N-R invariance, the dynamic evolution of $\eta(t)$ is easily gotten under the QS/MBC regime. Nevertheless, because of the physical retardation and the consequent functional mixing of both $\big\{I(t), I(t_*)\big\}$ and $\big\{\eta(t), \eta(t_*)\big\}$, such is emphatically *not* the case in a full-blown relativistic setting. We content ourselves in simply jotting down the relevant dynamical formula so as to gauge the difficulty of any further effort to attain its solution, all remaining interest at this point having been reduced to the purely theoretical.

REFERENCES

1. Grzesik, J., "Kinetic energy release in missile ejection from confining magnets," *Transactions of the American Nuclear Society Annual Meeting*, 34, New York, June 12–16, 1977.

2. Kastenberg, W. E. and D. Okrent, "Some safety studies for conceptual fusion-fission hybrid reactors," *UCLA, School of Engr. & Applied Science* (Prepared for the Electric Power Research Institute, Palo Alto, California), I-1, I-32, July 1978.

Scattering and Localization of Light in a Waveguide System with a Single Imperfection Core

Akira Komiyama
Osaka Electro-Communication University, Hatsu-cho, Neyagawa-shi 572-8530, Japan

Abstract— In a disordered waveguide system composed of randomly different cores in size mode waves are localized and are concentrated into a narrow region of several cores [1]. When one of cores is illuminated at the input end of the waveguide system several localized modes are excited and their modes propagate through the system. Outlines of the propagation properties of light can be easily known by solving numerically the coupled mode equation [2]. The coherent part of the amplitude of light decreases exponentially with increasing distance and the incoherent part of the amplitude is localized. The coherent part has been analytically derived by the perturbation method [3]. The results obtained are in good agreement with the numerical results. However, so far the analytical derivation of the incoherent part has not completely succeeded.

In this paper a scattering problem of light in a waveguide system with a single imperfection core is exactly solved in the Laplace transform domain and it is shown that the localized mode and the scattering originate from the pole and the branch cut of the scattering matrix, respectively. The amplitude of the localized mode can be calculated from the residue of the pole. The results obtained are in good agreement with the numerical results.

REFERENCES

1. Komiyama, A., *Opt. Comm.*, Vol. 151, 25–30, 1998.
2. Komiyama, A., *IEEJ Technical Report*, EMT-06-46, 2006.
3. Komiyama, A., *IEEJ Technical Report*, EMT-08-120, 2008.

Session 4A4
New Horizons in Electromagnetic Compatibility and Personal Health Protection

Electromagnetic Compatibility on Health Applications

Noemí Carranza and Victoria Ramos
Telemedicine and eHealth Research Unit, Health Institute Carlos III, Madrid 28029, Spain

Abstract— We live in a world dependent on electrical and electronic devices or equipment for our safety, security, quality of life, health and well-being. Each day, advances in technology produce new applications with added economic and social benefits to more people in more countries around the world. As this trend continues, we must be aware of unintended consequences, such as potential interaction that could affect the performance of electrical and electronic devices that permeate our lives.

One prominent concern has involved possible interference with medical devices. The electromagnetic environment in modern health care facilities can be extremely variable, particularly as a result of the growing use of emergent wireless technologies in public, health care and home areas.

As a result, electromagnetic compatibility (EMC) of medical devices cannot be specified and then forgotten. Electromagnetic Interference (EMI) problems can be expected to occur more frequently with the increasing use in health care environments of electronic medical devices, such as microprocessor-based diagnostic, monitoring, and therapeutic equipment, and portable RF sources, such as two-way radio transmitters and cellular telephones.

With the increasing use of Electromagnetic field-producing equipment in these environments, it is desirable to determine whether such fields, sometimes intense, can produce detrimental EM environmental effects in medical devices. These Medical Devices may be either implantable or externally worn by the patient. The potential for compromise of these devices's performance has been recognized for some time and specific EM interference (EMI) tests are regularly performed on such devices before they are used for humans.

There are different techniques to measure the background of electromagnetic field according to the measurement device and the width of frequency-band we want to measure. One of the options is to use a spectrum analyzer, which displays a spectral distribution of radiofrequency (RF) energy. Nevertheless, it is a complicated test and measurement tool; it is ideal for signal characterization, identification of unknown signals, signal monitoring or field strength measurements. Another option is to measure with different dosimeters. There are different options, broad-band and predefined frequency-band dosimeters. With predefined frequency-band dosimeters, the band of measurement is thinner and the origin of the EMF can be analyzed. Simulations of EMF can also be a very helpful tool, especially before designing a building.

In this work, several measurements of EMF in a healthcare environment have been taken with the different techniques explained before. In some cases, the results obtained have been different. This was the case of measurements taken with broadband and predefined frequency-band dosimeters, where we have found several peaks in the frequency-band dosimeter results which were not present in the results of the broadband dosimeter. A similar situation could occur using the spectrum analyzer. For each case, it is necessary to evaluate the measurement method together with the type of measurement we want to take, in order to obtain accurate results.

EMC Compliance on Medical Sensors and Health Risk Evaluation

Victoria Ramos, **Jorge García**, **and Noemí Carranza**
Health Institute Carlos III, Telemedicine and eHealth Research Unit
C/Sinesio Delgado 6, Pab. 6, Madrid 28029, Spain

Abstract— The quick progress in wireless technologies and their reduction in cost, together with the great mobility required by applications nowadays, will ensure that these technologies spread to and are used in many contexts. Their presence has affected almost every aspect of day-to-day living, at home, while travelling, and at school, college and work. By far, the most significant impact has been through the rapid expansion of personal mobile telecommunication and wireless network systems for voice, picture and video communication, internet access and other data transfer applications.

Other applications of EMF are found in the widespread use of electronic article surveillance, radiofrequency identification, metal detection and inductive heating devices. There is also potential for new medical applications of Ultra Wide Band (UWB) or ZigBee, for example in cardiology, detections of tumours, or the use of implantable sensors that rely on UWB communications.

Electromagnetic interference (EMI), whether intentional or not, causes a wide spectrum of difficulties including momentary, minor inconveniences to systems failures in electromedical devices. Within a health care environment (hospital, home, etc.), electronic devices must reliably perform or fail, including telecommunications infrastructure through basic instrumentation.

To quantify the risk to medical devices and electronic systems in a health care environment, on-site testing is important and the electromagnetic environment around medical devices should be checked. Electronic system characterization is also important in a controlled environment; radio wave irradiation to the medical devices, for example, aids in determining susceptibility of the device to EMI. The above scenario encourages careful investigation of the electromedical devices exposed to and used next to modern wireless systems.

This paper deals with the electromagnetic susceptibility investigation of some electromedical wearable equipment when subjected to interference generated by short-range, low-power wireless transmitters, as ZigBee and others. It is specified the test site characteristics and the procedures for verifying the immunity to radio frequency electromagnetic fields. The authors carry out a study to identify experimental conditions that allow the influence of transmitters and investigate the susceptibility of the medical sensors when interfering sources are placed in proximity to common wireless transmitters. These circumstances can occur whenever wireless sensor networks works to provide wireless remote control of monitoring health applications. To make tests that are as similar as possible to real applications, they were performed by considering real setups that are possible in practice. The results of numerous tests prove that different kinds of medical sensors can be affected by the wireless transmitters. The results obtained in this paper should be taken into account when short-range, low-power wireless technologies are used to transmit biomedical signals.

Electromagnetic Fields in Home and Public Environment and Home Care Devices

Jolanta Karpowicz
Central Institute for Labour Protection-National Research Institute (CIOP-PIB)
Czerniakowska 16, 00-701 Warszawa, Poland

Abstract— Electromagnetic fields (EMF) of radiofrequency present in the home and public environment are emitted by variety of sources, mainly RTV broadcasting stations and mobile phone base stations and handsets. Various and non-harmonizes approach to EMF exposure and limitations on the level of environmental EMF exist in guidelines, national legislations and technical requirements. Examples can be: ICNIRP'98; European resolution 519/1999 (10 MHz–10 GHz/28–61 V/m); national regulations in some European countries (3–7 V/m); Bioinitiative Report (0, 6 V/m), and electromagnetic compatibility limits for medical devices MDD EC Directive/EN-IEC60601-1-2/EMC immunity tests: IEC 61000-4-3 (80–2500 MHz/3 V/m; 10 V/m life support devices).

EMF exposure pattern was investigated many seasons in urban non-industrial environment, both indoor and outdoor, with attention to: Multi-sources EMF exposure of individual person, variability of frequency composition, variability of exposure level in daily perspective, variability of exposure level in yearly perspective, variability of exposure level in propagation perspective, variability of exposure level in perspective of technical status of EMF sources.

Frequency composition of environmental EMF is fixed by technologies used in the area, but relative level of various environmental EMF components is highly determined by location of observation point.

EMF exposure in public and home environment is in practice usually < 3 V/m. Higher exposure to EMF of > 3 V/m exist in case of wrong technical status of EMF sources or propagation difficulties for mobile phone devices or in the vicinity of EMF sources (primary sources — antennas or secondary ones — exposed metallic structures). Usually localised elevated EMF level is not marked. Investigations results do not support opinion that environmental EMF is increasing in every locations due to development of wireless systems, but EMF level is highly variable among locations.

Environmental conditions for uncontrolled electromagnetic influence on medical devices used for home care can be found in existing public and home environment but technical and administrative measures should be taken to minimize such risks.

Evaluation of Multisystem EM Dosimetry in Indoor Environments

Victor Torres[1], **Noemí Carranza**[2], **Fermín Esparza**[1], **Miguel Navarro**[1], **Miguel Beruete**[1], **Victoria Ramos**[2], **and Francisco Falcone**[1]

[1]Universidad Pública de Navarra, Spain
[2]Área de Telemedicina y Sociedad de la Información, Instituto de Salud Carlos III, Spain

Abstract— Deployment of a wide range of applications using wireless systems has been of great relevance in the last years. In the near future, the use of 4 G wireless communication systems, the use of wireless sensor networks in home automation or the popularity of personal wireless systems will increase the spectrum usage as it is known nowadays.

One of the basic concerns regarding government bodies and general public is the impact of such use of the electromagnetic spectrum in domestic areas. One of the ways to gain knowledge in this sense is to perform dosimetry measurement campaigns to analyze the effective exposure in a certain area.

In this paper, estimations of dosimetry values for different wireless systems in a domestic indoor environment are presented. To obtain such results, a three-dimensional ray tracing code has been implemented to calculate magnitude and phase of the different contributions of the electromagnetic spectrum within the indoor evaluation scenario. The indoor scenario is a domestic household within a dense population area in Madrid. The morphology (distribution of walls, windows and furniture) as well as basic material properties (loss tangent and dielectric constant) are introduced in the code, where reflection, refraction and diffraction mechanisms are calculated. Measured values from a personal dosimeter have also been obtained and are compared in order to gain insight in the exposure values.

The use of estimations of the exposure values are a helpful tool not only for dosimetry purposes, but also in preliminary planning stages of dedicated indoor wireless systems, in order to reduce radiated power as well power consumption.

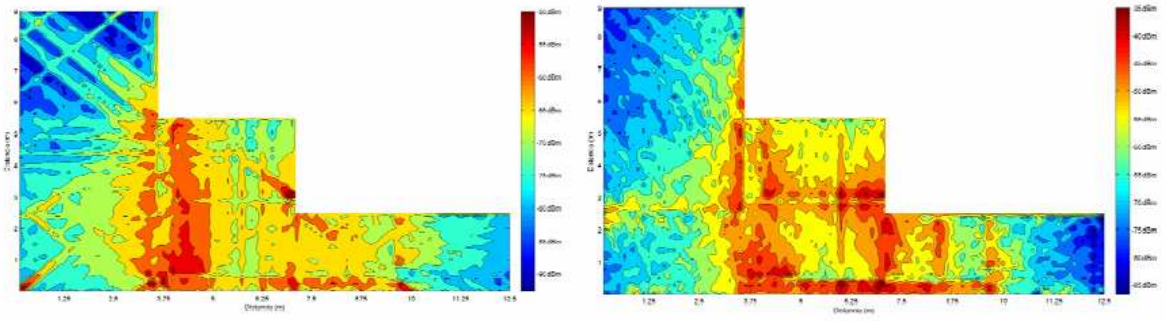

Figure 1: Simulation results for an indoor power density plot. The left plot is for UMTS, whereas the right hand side is for WLAN WiFi.

Analysis of EM Field Exposure in Future 4G Mobile System Environments

Victor Torres[1], **Noemí Carranza**[2], **Fermín Esparza**[1], **Miguel Navarro**[1], **Miguel Beruete**[1], **Victoria Ramos**[2], **and Francisco Falcone**[1]

[1]Universidad Pública de Navarra, Spain
[2]Área de Telemedicina y Sociedad de la Información, Instituto de Salud Carlos III, Spain

Abstract— Wireless communication systems have gained relevance in recent years, due to their wide implantation around the globe. In order to increase transmission bandwidth and intersystems connectivity, future fourth generation mobile systems are being proposed and the first field trials are already being conducted. 4G systems usually employ adaptive modulation schemes and certain power control mechanisms in order to decrease system interference and optimize battery lifetime.

Initial radioplanning considrerations indicate that densification of 4G base stations (macro stations as well as e-nodeB minicell, microcell and picocell configurations) is mandatory in order to fulfull coverage-capacity requirements. There is also a health issue of concern of international, national and local government bodies regarding exposure to RF non-ionizing EM fields and the fulfilment of exposure level thresholds.

In this paper, the estimation of power density in indoor environments will be analyzed. Field estimation is performed with the aid in-house 3D ray tracing code, simulating the exposure levels of possible future e-nodeB deployments within the indoor scenario.

These results aid in the planification process of the network, as well as in assessment of future exposure scenarios, especially in indoor environments, of great importance in 4G deployments.

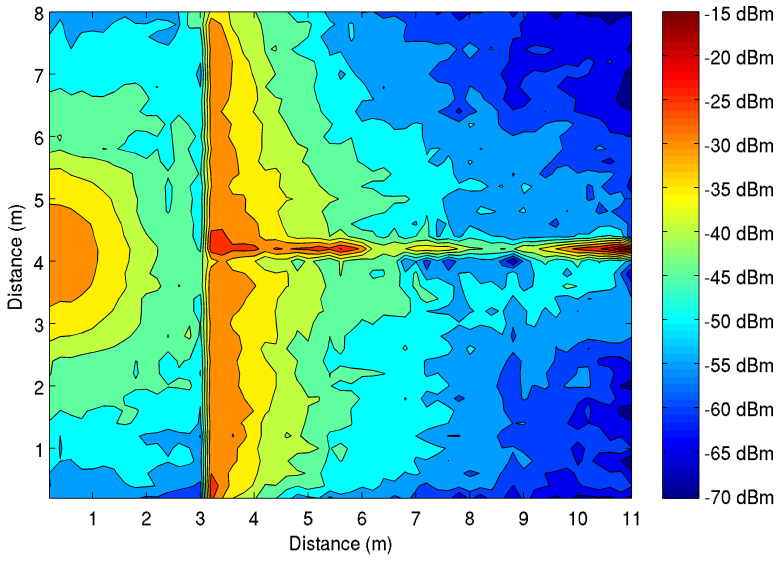

Figure 1: Power Density for a multi-antenna indoor environment using 64-QAM modulation scheme at an operating frequency of 2 GHz, within future LTE framework.

Numerical Simulation of EM Environment and Human Exposure When Using RFID Devices

Aránzazu Sanchis[1], **Javier Espinosa-García**[2], **and Agustín Martín**[2]

[1]Centro Nacional de Sanidad Ambiental (ISCIII), Majadahonda, Madrid, Spain
[2]Instituto de Física Aplicada (CSIC), Madrid, Spain

Abstract— Radio frequency identification (RFID) systems have been widely used recently to identify merchandise, materials, and personnel for the purpose of security, theft prevention, tracking, inventory control, and medical care. They continue receiving growing attention from all these domains due to their potential applications. Depending on that application and the task to be performed, a distinction is made between more or less highperformance systems (low-end through high-end). Among the highest rising uses, the real time locating systems (RTLS) — currently used in schools and hospitals — reach a range of up to 200 m, and the electronic passports — issued in the last years by many countries — can be read from more than 10 m away. Thus, it becomes essential that the implementation of RFID technology — electromagnetic (EM) field-producing equipments — takes place under a legal framework that affords citizens effective safeguards for fundamental values, health, environment, data protection, privacy and security [1, 2]. Moreover, the expected deployment of RFID in our daily lives through current and future uses, makes desirable to asses whether above applications of this technology could generate any adverse effect on health, or could even produce any detrimental EM environmental effects in medical devices [3].

In this work, RFID readers and active tags, operating at 2.4 GHz and 5.8 GHz, are simulated to calculate the electromagnetic field distribution generated in their surroundings, considering the presence of possible scattering obstacles, and including the analysis of the specific absorption rate (SAR) in human models (which can be very close to the tag). The finite-diference time-domain (FDTD) method and the finite elements (FE) method are used. Results show that significant field level can be found in regions far from the tagreader direction. This fact could constitute a risk because of the possible presence of general public and eventual eavesdroppers. Nevertheless, the calculated values of SAR are always below the basic restrictions.

ACKNOWLEDGMENT

This work has been supported by the Spanish Ministry of Science and Innovation, Projects SPY 1416/09 and TEC2009-13964-C04-02.

REFERENCES

1. European Commission, Standarisation Mandate to the European Standarisation Organisations CEN, CENELEC and ETSI in the Field of Information and Communication Technologies Applied to Radio Frequency Identification (RFID) and Systems, M/436, December 2008.
2. IEC (International Electrotechnical Commission), *Evaluation of Human Exposure to Electromagnetic Fields from Short Range Devices (SRDs) in Various Applications over the Frequency Range 0 GHz to 300 GHz — Part 1: Fields Produced by Devices Used for Electronic Article Surveillance, Radio Frequency Identification and Similar Systems*, IEC 62369-1, Geneva, Switzerland 1-149, 2008.
3. Georgia Tech Research Corporation, *EM Environmental Effects Test Protocol for Medical Devices to Security and Logistical Systems*, Ver. 5.1, August 2007.

Magnetic Field Related to Transient Currents in Electric Power Supply System — Assessment of Human's Exposure

Krzysztof Gryz, Jolanta Karpowicz, and Wiesław Leszko
Central Institute for Labour Protection — National Research Institute (CIOP-PIB)
Czerniakowska 16, 00-701 Warszawa, Poland

Abstract— Transient electromagnetic fields (TF EMF) and human's exposure to this kind of fields can be found both in occupational and in living environment. TF are produced as the result of rapid changes of electrical current, for instance during switch on/switch off current circuit or during fast changes of power load in electric installations (eq. in power supply installations of electrical vehicles like metro, trams or trains while changing of cars drive mode). Measurement equipment dedicated to investigate harmonic fields is not useful for identification of TF level because of specific parameters of TF events (irregular repetitions, duration of wide range from tens up to hundreds milliseconds and amplitude even over 30-fold higher than steady state one).

The investigations of transient magnetic field (TF MF) produced by the different electrical power supply systems have been performed to identify pattern of such electromagnetic hazards. The measurements were conducted by specially designed isotropic MF probes and data logger with programmable frequency of sampling (1–1000 Hz).

Peak value (B_p) and time derivative of the magnetic field (dB/dt) were used to assess the level of exposure because they are metrics of hazards caused by EMF for nervous system which are dominating in the case of EMF of frequencies less than 100 kHz.

The obtained results of TF MF investigations inside electrical vehicles shown variability of MF level among different modes of drive of car (up to 30–40 dB dynamics of MF level while start and braking) but usually B_p doesn't exceed 5 μT and dB/dt is below 0.1 T/s in the area occupied by passengers and workers.

Higher TF events were found during rapid breaks of electric installations. For example the rapid break in power supply installations with current over 20 A can produce TF in their vicinity of level comparable with permissible levels defined by international criteria (e.g., following ICNIRP guidelines: 0.22 T/s permissible for workers exposure to EMF of frequencies below 820 Hz).

The use of small dimensions data logger allows archiving of long duration samples of MF for identification of TF events and assessing their parameters, even personal monitoring of such hazards.

Health Risk Perception about Wireless Communication Technologies

Maria Dolores Marcos[1] and Victoria Ramos[2]

[1]Agency "Lain Entralgo" for Education and Health Research
Regional Ministry of Health of the Community of the Madrid, Spain
[2]Research Unit of Telemedicine and eHealth, Health Institute "Carlos III", Spain

Abstract— Wireless voice transmission and digitalized data in general is the fastest growing sector within telecommunications industry. It has a widespread presence in all areas of our daily life and it has been predicted the very important role of these technologies on promoting health and controlling diseases. But the massive use of mobile phones and other wireless devices has given as a result a growing concern about negative side effects of electromagnetic emissions on health. At the same time, those devices are being used by people in such a way that risks of these technologies surely increase.

In order to explain this contradictory behaviour it is mentioned the risk perception or the subjective judgment that people make about the dangerousness of certain elements or situations, etc. Consequently, a proper definition and evaluation of this factor may be decisive when it is intended both to minimize the risk associated to radiant technologies as to avoid unexplained rejection attitudes.

But the knowledge and proper characterization of this psychological phenomenon has not to be restricted to electromagnetic emissions. Risk perception can be accommodated in any action which focuses on people's safety and security, and mainly on those ones that have been designed to manage and communicate health risks to citizens.

2.4 GHz EMP Protection Circuit with Micro Strip Filter Configuration

Liann-Be Chang[1], **Atanu Das**[1], **Ching-Chi Lin**[1], **Ji-Chyun Liu**[2], **Yi-Cherng Ferng**[1], **Chien-Fu Shih**[1], **and Sheng-You Liao**[1]

[1]Department of Electronic Engineering & Green Technology Research Center
Chang Gung University, Taiwan, R.O.C.
[2]Department of Electrical Engineering, Ching Yun University, Taiwan, R.O.C.

Abstract— This article focuses on Electromagnetic pulse (EMP) protection circuit design and fabrication. In modern days the compact components have low operational power and small area and hence are insufficient to withstand EMP induced surges. Once the surge introduced into electronic devices, the internal low noise amplification circuit, memory circuit, integrated circuit and logic circuit, may be burnt due to transient overload, leading to system failure. The purpose of this circuit is to suppress the fast or slow introduced high voltage spikes. The aim of this study is to design and fabricate a cascade EMP protection circuit that can suppress fast introduced over voltage surges. The basic configuration of this circuit is composed of three element, a traditional surge arrester gas discharge tube (GDT), a micro strip filter (MSF) and a fast response electrostatic discharge (ESD) handling device (we used metal oxide varistor (MOV) varistor here). The present structure discloses a cascade EMP protection configuration, which comprises a slow response but heavy duty GDT surge arrester and a fast-response ESD protection MOV, wherein a micro strip filter (MSF) element is cascaded to the path of signal transmission. The conventional series resistor on the path of signal transmission will cause heat and reduce the output power. Thereby, the present configuration can protect next stage electronic devices from a fast introduced EMP released surges more effectively than the conventional configuration and avoid the heat issue. In the future we can also exchange the substrate from PCB to Al_2O_3 or AlN to increase heat dissipation and to improve operational power.

Session 4A5
Extended/Unconventional Electromagnetic Theory, EHD (Electro-hydrodynamics)/EMHD (Electro-magneto-hydrodynamics), and Electro-biology 1

Distributed Transverse Orientation (DiTO) in Maxwell's Equations

J. E. Carroll
Centre for Advanced Photonics and Electronics, University of Cambridge, CB3 0FA, UK

Abstract— This paper will highlight a remarkable but apparently little known property of Maxwell's equations that allows a change in the rotational phase reference of transverse vector fields and transverse vector operators provided that the same change is applied to both fields and operators. This property will have significant implications for (a) the possible connections between classical and random electrodynamics, (b) the formation of classic two frequency plane wave-packets that may be normalized and consequently may form a paradigm for the photon (c) the potential development of a classical understanding of Schrödinger number states $(N + 1/2)$, N integer, in photon theory.

It is well known that a 90° change of *temporal* phase can be given by an operator 'i' . This can form an operation $\exp(\mathrm{i}q)$ acting on the phasor fields to give a change in phase of an angle q. In this paper a 90° change of *rotational* phase of the transverse orientation of transverse vectors is represented by 'j' giving a unitary operation $R = \exp(\mathrm{j}Q)$ that can rotate the reference phase of *both* the transverse vectors and the transverse vector gradient operator $\mathbf{grad_t}$ through an angle Q. The presentation will give more detail of how this change applies to the complete set of Maxwell's equations while this abstract gives only one example using the divergence of the magnetic field. The divergence may be split into transverse and axial parts and written symbolically as: $\mathbf{grad_t}\cdot\mathbf{B_t} = -d_z B_z$. The operator R acting on the transverse gradient operator '$\mathbf{grad_t}$' gives (R $\mathbf{grad_t}$) and also operates on the transverse fields '$\mathbf{B_t}$' to give ($R\mathbf{B_t}$). The transverse vectors and gradient operator are helpfully represented by 2-element by 1-column matrices with R formed by a 2×2 matrix. A superscript solidus implies transposition of rows and columns so that the divergence operation may be written as

$$(R\mathbf{grad_t})'(R\mathbf{B_t}) = \ \mathbf{grad}_t' R' R\mathbf{B_t} = \ \mathbf{grad}_t'\mathbf{B_t} = -d_z B_z \tag{1}$$

Consequently the operator R make no difference to the axial fields B_z. If the angle Q in the operation R remains constant then there is little that is remarkable. However Q can also be an arbitrary function of the transverse position without changing the axial fields, Eq. (1) shows that $\mathbf{grad_t}$ never operates on R, it is only$R$ operating on $\mathbf{grad_t}$. It is suggested that any such operator R is called a *DiTO* (*Distributed Transverse Orientation*). The paper speculates if such operations give the connection between random electrodynamics and Maxwell's classical deterministic equations.

The paper continues with an account of how the angle Q can also be a function of time and distance provided that any space-time changes within the function Q propagate at the group velocity of the underlying modal fields to which the operation R is applied. As a further extension, when the operation R is applied to circularly polarised fields, the two different phase operators 'i' and 'j' are interchangeable, subject to a sign change that is dependent upon the sign of the circular polarisation. It is then found that it is possible to define closed packets of two circularly polarised plane waves beating together with two different frequencies yet having a Gaussian transverse profile forced on such a packet by choosing appropriate DiTOs. Such a packet can be made to have a field distribution such that the energy may be normalized. This is argued to offer a paradigm for the ground state of a photon. Appropriate DiTOs can create internal structure that might form paradigms for the excited states of a photon revealing how Schrodinger quantum numbers such as $N + 1/2$ may arise from internal distributions of the transverse fields inside a packet.

Detection of Partial Discharge inside of HV Transformer, Modeling, Sensors and Measurement

P. Fiala, **T. Jirku**, **P. Drexler**, **and P. Dohnal**
Brno, FEEC BUT, UTEE, Kolejní 2906/4, Brno 612 00, Czech Republic

Abstract— The aim of this paper is to present the particulars of result research in the HF measurement method and modeling of starting process partial discharge inside of high voltage transformer. The numerical analysis of the electromagnetic wave attenuation helped to set up conditions to decrease it and get of information for sensors conception preparing and detection apparatuses construction and measurement methods.

Introduction: One of the problematic conditions in the field of high-voltage technology, apparatuses and devices (machines) consists in the emergence of partial discharges [1]. At this point, let us also note that several other effects have combined with this notion over time [2–4]. In consequence of these effects there emerge short electromagnetic pulses with a defined and measurable spectre in the characteristic frequency band [5]. The group of end products attributable to the emergence of interfering signals involves, for example, displacement current in a dielectric, pulse current on the interface between dielectrics, or the dielectric/metal interface owing to high electric field intensity and structure of the dielectric. In HV and VHV transformers (Fig. 1) the dielectric is mineral or synthetic oil.

Large distribution transformers are constructed in such a manner as to have structural measures facilitating oil purification. Also, these transformers are equipped with sensors indicating the initial stage of increase in pulse activity. In the course of this activity, as is well-known, there occurs an increase in the boundary value of the of the applied dielectric breakdown value. As referred to in the above text, oil is the dielectric. Under certain conditions, however, the separation of chemical compounds incurred by decomposition of the dielectric does not have to occur. Thus, free atoms of carbon, hydrogen and oxygen develop from hydrocarbons, and there also generates a certain percentage of water, other organic compounds, and semiconductive carbon. All of these elements decrease the quality of the dielectric; in addition to that, rapid increase in pulse activity may cause the formation of a hazardous explosive compound of oxygen and hydrogen. Then, this situation may result in a local explosion, damage to the device and reduction of its ability to perform the respective functions (Fig. 2).

This work deals with an analysis of electromagnetic field distribution in a transformer dielectric region. The structural parts enable the placement of sensors, whose structure and concept must be adapted to the characteristics of the configuration in such a manner that, from all components of the device, there is a measurable (indicable) electromagnetic pulse signal.

The analysis will be realized for the minimum required level of an electromagnetic pulse for the discrete values of frequencies from the desired spectral interval. An example will be evaluated of electromagnetic field distribution in the region of critical parts of the device.

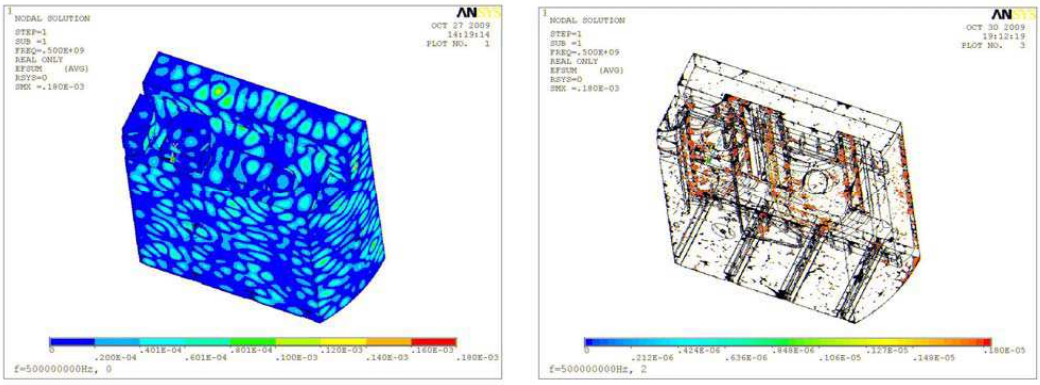

Figure 1: Typical electromagnetic field distribution, modul of electric field vector E, inside of part of transformer model, frequency $f = 500\,\mathrm{MHz}$.

Conclusion: The basic research of the numerical model HF wide band signals inside of a VHV transformer has brought a considerable sum of experience in the field of signals and possibilities of their measurement and detection. It was used for sensor design conception and construction.

ACKNOWLEDGMENT

The research described in the paper was financially supported by FRVŠ (a fund of university development) by research plan No. MSM 0021630513 ELCOM, No. MSM 0021630516 and grant Czech ministry of industry and trade MPO No. FR-TI1/001, GACR 102/09/0314.

REFERENCES

1. Kaneiwa, H., Y. Suzuoki, and T. Mizutan, "Characteristics of partial discharges, artificial simulated tree channels during in tree propagation," *IEEE Transactions on Dielectrics and Electrical Insulation*, Vol. 8, No. 1, February 2001.
2. Fiala, P., "Secondary winding model of current transformer- switchable variant," Research report, Laboratory of Modeling and Optimization Field in Electromagnetic Systems, FEI VUT and ABB EJF a.s. Brno No. 1/99, 21.1.1999, Brno, Czech Republic, 1999.
3. Fiala, P., "Transformer partial discharge modeling, minimal breakdown value set in a critical parts of transformer design," Research report, Laboratory of Modeling and Optimization Field in Electromagnetic Systems, FEI VUT and ABB EJF a.s. Brno No. 2/99, 18.3.1999, Brno, Czech Republic, 1999.
4. Fiala, P., "Optimization of two-pole voltage transoformer design $U_{max} = 25\,kV$, new variant 2000," Research report, Laboratory of Modeling and Optimization Field in Electromagnetic Systems, FEI VUT Brno No. 1/00, 20.2.2000, Brno, Czech Republic, 2000.
5. Sarathi, R., A. J. Reid, and M. D. Judd, "Partial discharge study in transformer oil due to particle movement under DC voltage using the UHF technique," *Electric Power Systems Research*, Vol. 78, 1819–1825, Elsevier, 2008.
6. Manuals ANSYS, v.8.1, USA.
7. Fiala, P., "Coupled electromagnetic model of smoothing choke," *AMTEE'01 Fifth International Conference*, 10.9–12.9.2001 Plzeň, str.C05, ISBN 80-7082-756-4.

EMHD Model Used for Linear Moving Objects Analysis

Pavel Fiala, Zoltán Szabó, Tibor Bachorec, and Premysl Dohnal
Brno, FEEC BUT, UTEE, Kolejní 2906/4, Brno 61200, Czech Republic

Abstract— The paper provides an insight into the issues of measurement methods for accuracy obtain information velocity objects. One of the measurement method used for its problems is based on electromagnetic field measurement. The accuracy measurement method is focused to use of EMHD effects analysis and results applied to the experimental measurement. This results and measurement method decrease lethality of wrong measurements of non-ballistics projectile velocity.

From the formal point of view, several perspectives are utilized to facilitate the topic analysis, and these aspects of evaluation can be identified within the regions of legal ethics, medicine, or military tactics as well as engineering and technology. In relation to the problem of protection against undesirable phenomena like terrorism, it is necessary to mention the fact that there exists long-term research focused on the institution of NATO and its member armies; this research mainly pertains to the determination and practical use of non-lethal or wounding methods and means in all constituent parts of protection and defence. The armies of European countries participate systematically in the process of non-lethal weapons development and integration within the respective armament systems.

ACKNOWLEDGMENT

The funding of the project was supported by the Ministry of Defence of the CR and Ministry of Industry and Trade of the CR (Diagnostics of superfast objects for safety testing, FR-TI1/368), Ministry of Education, Youth and Sports of the CR, and by insitutional resources from the Research Design — Electronic Communication Systems and New Generation Technologies (ELKOM) MSM0021630513, GAČR 102/09/0314.

REFERENCES

1. Krüger-Sprengel, F., "Legal adaptation of non-lethal capabilities in new conflict scenarious," *2nd European Symposium on Non-Lethal Weapons*, Ettlingen, SRN, May 13–15, 2003.
2. Kim, B., "Between principles and absolutes: Non-lethal weapons and the law of armed conflict," *2nd European Symposium on Non-Lethal Weapons*, Ettlingen, SRN, May 13–15, 2003.
3. Janssen, W. J. H and E. J. M. Jansen, "Decision-making processes: The choice between lethal an non-lethal force," *2nd European Symposium on Non-Lethal Weapons*, Ettlingen, SRN, May 13–15, 2003.
4. David, E., "A effectiveness and risk during application of NLW from the medical point of view," *4th European Symposium on Non-Lethal Weapons*, Ettlingen, SRN, May 10–12, 2005.
5. David, E., A. Fretz, and J. Reissenweber, "Mortality following taser exposure," *4th European Symposium on Non-Lethal Weapons*, Ettlingen, SRN, May 21–23, 2007.
6. Wolf, F., "Multi-spectral measurement of NLW effects," *4th European Symposium on Non-Lethal Weapons*, Ettlingen, SRN, May 21–23, 2007.
7. Fiala, P., "Finite element method analysis of a magnetic field inside a microwave pulsed generator," *2nd European Symposium on Non-Lethal Weapons*, Ettlingen, SRN, May 13–15, 2003.
8. Fiala, P. and P. Drexler, "Measurement methods of pulsed power generators," *4th European Symposium on Non-Lethal Weapons*, Ettlingen, SRN, May 21–23, 2007.
9. Groll, J. H. and C. Pick, "Assessment of non-lethal-weapons (NLW)," *4th European Symposium on Non-Lethal Weapons*, Ettlingen, SRN, May 21–23, 2007.
10. Stratton, J. A., "Teorie elektromagnetického pole," STNL, Praha, 1961.

Tuned Periodical Structures — Model, Experiments in THz Band Applied in Safety Application

Pavel Fiala, Radim Kadlec, Petr Drexler, and Premysl Dohnal
Brno, FEEC BUT, UTEE, Kolejní 2906/4, Brno 61200, Czech Republic

Abstract— The paper provides an insight into the issues of integration and application of nonlethal weapons and devices in the field of protection against special-type weapons. The structures like a metamaterials, left-handed type models were analysed and prepared to the experimental measuremnts.

Both the basic and the applied types of research on optoelectronic systems and numerical modelling of wideband signals have led to conclusions in the field of multilayer and periodic structure optical materials.

The entire project was systematically guided by theoretical discussion and consideration, the results of modelling realized by the help of numerical models, and a large number of experiments. The main asset of the materialized work consists in the field of numerical modelling, in the proposed variants of models, and in the overall verification and calibration of the designed solutions using unique experiments. The activities have contributed significantly to the field of model design by proposing a combination of complementary yet different types of numerical models; these models then enabled marked acceleration of the calculation process while achieving and maintaining a satisfactory degree of accuracy. A valuable aspect consists in the methodology of a numerical model application and handling, where the correctness of the numerical analysis was verified by the experimental results.

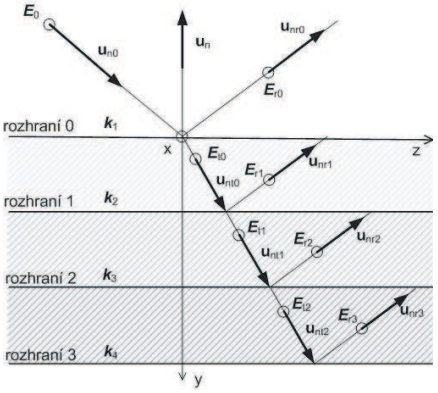

Figure 1: Multilayer environment of heterogeneous material.

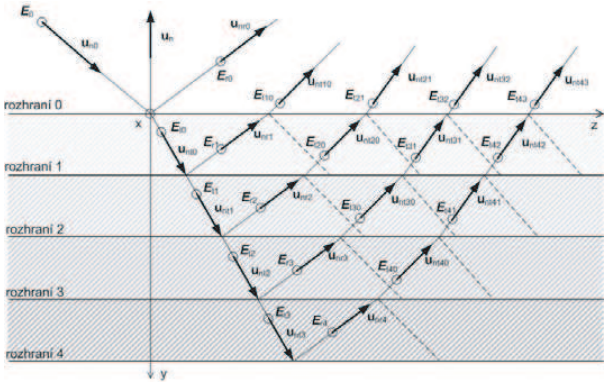

Figure 2: Waves on the surface of a heterogeneous material after the a reflection from several layers.

ACKNOWLEDGMENT

The funding of the project was supported by the Ministry of Defence of the CR and Ministry of Industry and Trade of the CR (Diagnostics of superfast objects for safety testing, FR-TI1/368), Ministry of Education, Youth and Sports of the CR, and by insitutional resources from the Research Design — Electronic Communication Systems and New Generation Technologies (ELKOM) MSM0021630513, GAČR 102/09/0314.

REFERENCES

1. Krüger-Sprengel, F., "Legal adaptation of non-lethal capabilities in new conflict scenarious," *2nd European Symposium on Non-Lethal Weapons*, Ettlingen, SRN, May 13–15, 2003.
2. Kim, B., "Between principles and absolutes: Non-lethal weapons and the law of armed conflict," *2nd European Symposium on Non-Lethal Weapons*, Ettlingen, SRN, May 13–15, 2003.
3. Janssen, W. J. H. and E. J. M. Jansen, "Decision-making processes: The choice between lethal an non-lethal force," *2nd European Symposium on Non-Lethal Weapons*, Ettlingen, SRN, May 13–15, 2003.

4. David, E., "A effectiveness and risk during application of NLW from the medical point of view," *4th European Symposium on Non-Lethal Weapons*, Ettlingen, SRN, May 10–12, 2005.
5. David, E., A. Fretz, and J. Reissenweber, "Mortality following taser exposure," *4th European Symposium on Non-Lethal Weapons*, Ettlingen, SRN, May 21–23, 2007.
6. Wolf, F., "Multi-spectral measurement of NLW effects," *4th European Symposium on Non-Lethal Weapons*, Ettlingen, SRN, May 21–23, 2007.
7. Fiala, P., "Finite element method analysis of a magnetic field inside a microwave pulsed generator," *2nd European Symposium on Non-Lethal Weapons*, Ettlingen, SRN, May 13–15, 2003.
8. Steinbauer, M., P. Drexler, and P. Fiala, "Measurement of vircator ultra-short solitary electromagnetic pulses," *3rd European Symposium on Non-Lethal Weapons*, Ettlingen, SRN, May 10–12, 2005.
9. Fiala, P., M. Steinbauer, and R. Kubasek, "High power generator test, PGP-II," *4th European Symposium on Non-Lethal Weapons*, Ettlingen, SRN, May 21–23, 2007.
10. Fiala, P. and P. Drexler, "Measurement methods of pulsed power generators," *4th European Symposium on Non-Lethal Weapons*, Ettlingen, SRN, May 21–23, 2007.
11. Groll, J. H. and C. Pick, "Assessment of non-lethal-weapons (NLW)," *4th European Symposium on Non-Lethal Weapons*, Ettlingen, SRN, May 21–23, 2007.
12. Kozyrev, V., V. V. Selivanov, V. V. Leonov, and A. A. Zverev, "Analysis of critical levels of physical effects on localized masses of people (CROWD)," *4th European Symposium on Non-Lethal Weapons*, Ettlingen, SRN, May 21–23, 2007.
13. Langhans, D. and D. Meisterhans, "Sniper locating system," *2nd European Symposium on Non-Lethal Weapons*, Ettlingen, SRN, May 13–15, 2003.
14. Kadlec, R., E. Kroutilová, and P. Fiala, "Improving of ray-tracing method for numerical modeling of lighting systems," *PIERS Proceedings*, 156–159, Beijing, China, March 23–27, 2009.
15. DěDek, L. and J. Dědková, *Elektromagnetismus*, Students Book, 232, 2, vyd., Vutium, Brno, 2000, ISBN 80-214-1548-7.
16. Stratton, J. A., "Teorie elektromagnetického pole STNL," Praha, 1961.

The Instruments for Noise Spectroscopy

P. Drexler, P. Fiala, R. Kadlec, and R. Kubásek
Dept. of Theoretical and Experimental Electrical Engineering, Brno University of Technology
Kolejní 2906/4, Brno 612 00, Czech Republic

Abstract— In the complicated material structure for the micro-wave application (tensor and composite character) is its material properties study by classical single frequency methods connected with a difficulty [1]. In boundary changes with the size close to wave-length can occurs fake information about the examined objects [2]. One possible way to suppress the negative sources of signals is use of wide-band signals, as white noise, and study absorption in the examined material.

The article describes base study of wide-band noise signal use for material study [3]. The aim is find the metrology method for metamaterial study in the frequency range about 100 MHz to 10 GHz.

ACKNOWLEDGMENT

The research described in the paper was financially supported by the research programs MSM 0021630516 research plan MSM 0021630513, Ministry of Defence of the CR and Ministry of Industry and Trade of the CR (FR-TI1/001) and AČR 102/09/0314.

REFERENCES

1. Maslovski, S., S Tretyakov, and P. Alitalo, "Near-field enhancement and imaging in double planar polariton-resonant structure," *J. Appl. Phys.*, Vol. 96, 1293, 2004.
2. Freire, M. and R. Marques, "Near-field imaging in the megahertz range by strongly coupled magnetoinductive surfaces: Experiment and ab initio analysis," *J. Appl. Phys.*, Vol. 100, 063105, 2006.
3. Machac, J., P. Protiva, and J. Zehentner, "Isotropic epsilon-negative particles," *2007 IEEE MTT-S Int. Microwave Symp. Dig.*, Honolulu, USA TH4D-03, June 2007.

Electromagnetic Wave Propagation in Heterogeneous Structures

R. Kadlec, **P. Fiala**, **and D. Nešpor**
Department of Theoretical and Experimental Electrical Engineering
Brno University of Technology, Kolejni 2906/4, Brno 612 00, Czech Republic

Abstract— Paper presents usage numerical modeling of propagation high frequency electromagnetic waves in inhomogeneous materials. For this method a numerical model was prepared. The numerical model was created in the MatLab program environment and program COMSOL. For layered heterogeneous medium is deduced algorithm for reflection on several layers. Several layers are in form of periodical structures which are composite of homogenous material. Reflection and refraction on heterogonous material is solving by numerical method. The main are refractions and reflection on boundary of materials with different properties. This method is suitable for design application of the metamaterial. Deduced algorithm was project for the visible spectrum.

ACKNOWLEDGMENT

The research described in the paper was financially supported by the research programs MSM 0021630516 research plan MSM 0021630513, Ministry of Defence of the CR and Ministry of Industry and Trade of the CR (Diagnostics of superfast objects for safety testing, FR-TI1/368) and GAČR 102/09/0314.

REFERENCES

1. Dedek, L. and J. Dedkova, *Elektromagnetismus. 2*, 232, VITIUM, Brno, 2000.
2. Moss, C., *Numerical Metods for Electromagnetic Wave Propagation and Scattering in Comlex Media*, 240, 2004. Available from www: http://portal.acm.org/citation.cfm?id=1023429.
3. Stratton, J. A., *Teorie elektromagnetickeho pole*, STNL, Praha, 1961.
4. Fiala, P., "Finite element method analysis of a magnetic field inside a microwave pulsed generator," *2nd European Symposium on Non-Lethal Weapons*, Ettlingen, SRN, May 13–15, 2003.
5. Nespor, D., *Electromagnetic Wave Propagation Study in Heterogeneous Structures*, 20, Supervisor Doc. Ing. Pavel Fiala, Ph.D., 2009.

Errors in Diffusion Coefficients Measurement

P. Marcon[1] and K. Bartusek[2]

[1]Department of Theoretical and Experimental Electrical Engineering, Brno University of Technology
Kolejni 2906/4, 612 00 Brno, Czech Republic
[2]Institute of Scientific Instruments, Academy of Sciences of the Czech Republic
Kralovopolska 147, 612 64 Brno, Czech Republic

Abstract— The magnetic resonance (MR) imaging techniques of tomography and spectroscopy are exploited in many applications. The quality of dynamic behavior of the gradient magnetic fields is one of the important properties of devices exploiting the phenomenon of magnetic resonance (MR) for imaging or diffusion measurement [5]. For the MR instruments to function properly it is necessary to maintain a high quality of homogeneity of the fundamental and gradient magnetic field [1, 4]. Gradient changes induce eddy currents in the surrounding conducting arrangement, potentially causing an image artifacts, localization errors, and signal distortion. While the use of actively shielded gradients has greatly reduced the magnitude of eddy currents, significant distortion often still remains, in particular in the short time interval after the gradient is switched off. Residual eddy currents may require further reduction. This is frequently achieved by pre-emphasis correction in the relevant gradient channel and in the homogeneous Bo shim [2], or by active shielded gradient coils [3]. The rise time of the impulse of a magnetic field or its decrease to the level of non-homogeneity of the basic magnetic field should be as short as possible ($< 100\,\mu s$).

The experiments were carried out on an MR tomograph system 4.7 T/ 120 mm (i.e., 200 MHz for ^{1}H nuclei). Actively shielded gradient coils yield a maximum gradient field magnitude of 180 mT/m. The data measured were processed in the MAREVISI and MATLAB programs.

The software for b-factor calculation was created to characterize the device artifacts on accuracy of measurement. It is possible to determine the diffusion measurement errors for changes of gradient field magnitude and inaccuracies of time parameters settings by this software. There were characterized probable diffuse measurement errors and especially the effect of gradient decay time to the accuracy of diffusion constants measurement of the chosen samples. The results of the simulation were experimentally tested and compared with analytical model. The determination of the device artifacts effects with diffusion constants measurement is useful above all for biological samples with short relaxation times.

Measuring of Temperature Fields Using MR Tomography

M. Cap[1], **P. Marcon**[1], **and K. Bartusek**[2]

[1]Dept. of Theoretical and Experimental Electrical Engineering, Brno University of Technology
Kolejní 2906/4, 612 00 Brno, Czech Republic
[2]Institute of Scientific Instruments, Academy of Sciences of the Czech Republic
Královopolská 147, 612 64 Brno, Czech Republic

Abstract— Magnetic resonance imaging is in medicine commonly used method for human body structures imaging. Progresses in imaging methods allow figure different parameters of the specimen then mere structural image. If we are able to image function of the human body then we can improve diagnosability of diseases. This article deal with noninvasive method for imaging of temperature distribution in required volume of specimen using MR tomography. Method is based on diffusion measurement [1, 4]. Temperature dependence of diffusion of materials makes possible measure temperature distribution in specimen [2].

As a specimen is used water solution of nickel sulfate ($NiSO_4$). This solution was chosen for similar properties to physiological solution. Pulsed Field Gradient Spin-Echo (PFG SE) method is used for measurement of self diffusion coefficients D [3]. Results of measurement are compared with other materials measured in [2] to improve method for human body temperature fields measurement. The experiments were carried out on an MR tomograph system 4.7 T/120 mm (i.e., 200 MHz for ^{1}H nuclei). Actively shielded gradient coils forms a maximum gradient field magnitude of 180 mT/m. The measured data were processed in the MAREVISI and MATLAB programs.

REFERENCES

1. Vlaardingerbroek, M., *Magnetic Resonance Imaging*, Springer-Verlag, 2000.
2. Holz, M., S. R. Heil, and A. Sacco, "Temperature-dependent self-diffusion coefficients of water and six selected moleculer liquids for calibration in accure ^{1}H NMR PFG measurement," *Chem. Phys.*, Vol. 2, 4740–4742, 2000.
3. Bartusek, K. and E. Gescheidtova, "Measurement technique of the rapidly switched gradient magnetic fields in MR tomograph," *Acta Polytechnica*, Vol. 4, 30–35, 2003.
4. Johansen-Berg, H. and T. E. J. Behrens, "Diffusion MRI: From quantitative measurement to in vivo neuroanatomy," *Elsevier*, 490, China, 2009, ISBN 978-0-12-374709-9.

3D Reconstruction in Magnetic Resonance Imaging

J. Mikulka[1] and K. Bartusek[2]

[1]Department of Theoretical and Experimental Electrical Engineering
Brno University of Technology, Kolejni 2906/4, 612 00 Brno, Czech Republic
[2]Institute of Scientific Instruments, Academy of Sciences of the Czech Republic
Kralovopolska 147, 612 64 Brno, Czech Republic

Abstract— This article deals with three-dimensional reconstruction methods of nuclear magnetic resonance images. The testing images were observed by tomograph with basic magnetic field of 4.7 T at the Institute of Scientific Instruments (Academy of Sciences of the Czech Republic). There were acquired 10 slices of the testing phantom. There were found methods with the aim of getting utmost information about the shape of the testing phantom. One possible way is to increase the count of the sensed slices, but it implies decreasing of the signal to noise ratio. The second approach is finding the compromise between the effective count of slices and the following interpolation of other slices between the sensed ones. The both approaches were compared. The resultant images were segmented by the active contour methods which are based on partial differential equations solution [1, 2]. The advantage of these methods is that the images may not be preprocessed before segmentation. The appropriate segmented slices were compared. The following image processing leading to 3D model creation is proposed.

REFERENCES

1. Li, C., C. Xu, C. Gui, and M. D. Fox, "Level set evolution without re-initialization: A new variational formulation," *Proceedings of the 2005 IEEE Computer Society Conference on Computer Vision and Pattern Recognition CVPR'05*, 430–436, San Diego, Washington, DC, USA, 2005, ISBN 0-7695-2372-2.
2. Aubert, G. and P. Kornprobst, *Mathematical Problems in Image Processing: Partial Differential Equations and the Calculus of Variations*, 2nd Edition, 377, Springer Science + Business Media, LLC, New York, 2006, ISBN 0-387-32200-0.

Magnetoinductive Lens for Experimental Mid-field MR Tomograph

K. Bartusek, **P. Drexler**, **P. Fiala**, **R. Kadlec**, **and R. Kubasek**
Department of Theoretical and Experimental Electrical Engineering, Brno University of Technology
Kolejni 2906/4, Brno 612 00, Czech Republic

Abstract— The growing interest of scientific community in the field of synthetic single/double negative materials has brought the effort to exploit their unique properties in various technical areas. One of the possible applications of these metamaterials is their utilization in subwavelength imaging. The recent work of some research teams deals with the application of single negative metamaterials with negative permeability for magnetic resonance imaging [1]. The concepts of the magnetoinductive lens have been proposed and realized [2]. The lens components are based on non-ferromagnetic materials. In spite of their insignificant response in the DC magnetic field, they exhibit magnetic response at certain resonant frequency. The resonant frequency approaches to the frequency of the excitation RF pulse [3]. By suitable configuration of the components the imaging effect can be observed and the device behaves like a magnetic lens. The dimension of the magnetoinductive lens is small in compare to RF pulse wavelength. Most of the published papers describe the analysis of magnetoinductive lenses and the experiments in relatively low field medical MRI devices with the excitation frequency of tens of MHz [4]. This paper presents the design and development of magnetoinductive lens for application in the experimental mid-field MRI device which has a smaller field aperture and high resolution narrowband detection system. These prerequisites appoint the properties of the designed lens in view of components resonant frequencies accuracy and lens dimension, which is limited to 40×40 mm, as shown in Fig. 1.

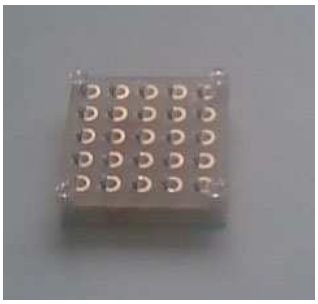

Figure 1: A double layer magnetoinductive lens for mid-field experimental MR tomograph.

ACKNOWLEDGMENT

The work described in the paper was financially supported by the research project GA102/09/0314 and research plan MSM 0021630513.

REFERENCES

1. Wiltshire, M. C. K., J. B. Pendry, and J. V. Hajnal, "Sub-wavelength imaging at radio frequency," *Journal of Physics: Condensed Matter*, Vol. 18, No. 22, 2006.
2. Wiltshire, M. C. K., J. V. Hajnal, J. B. Pendry, D. J. Edwards, and C. J. Stevens, "Metamaterial endoscope for magnetic field transfer: Near field imaging with magnetic wires," *Optic Express*, Vol. 11, No. 7, 2003.
3. Solymar, L., O. Zhuromskyy, O. Sydoruk, E. Shamonina, I. R. Young, and R. R. A. Syms, "Rotational resonance of magnetoinductive waves: Basic concept and application to nuclear magnetic resonance," *Journal of Applied Physics*, Vol. 99, No. 12, 2006.
4. Freire, M. J., R. Marques, and L. Jelinek, "Experimental demonstration of a $\mu = -1$ metamaterial lens for magnetic resonance imaging," *Applied Physics Letters*, Vol. 93, No. 23, 2008.

Session 4A6
Homogenization and Constitutive Parameter Extraction of Metamaterials

Magnetism and Homogenization of Microresonators

Robert V. Kohn[1] **and Stephen P. Shipman**[2]

[1]Department of Mathematics, Courant Institute of Mathematical Sciences
New York University, USA
[2]Department of Mathematics, Louisiana State University, USA

Abstract— Periodic arrays of cylindrical metal micro-resonators embedded in a dielectric matrix were proposed by Pendry, et al., in 1999 as a means of creating a microscopic structure that exhibits strong bulk magnetic behavior at frequencies not realized in nature. This behavior arises for magnetically polarized fields in the quasi-static regime, in which the scale of the microstructure is small compared to the wavelength of the electromagnetic fields. We model the resonator as a closed surface on which a complex conductivity relates the electric current to the tangential electric field. The emergence of effective magnetism is a result of an extreme conductivity, specifically, when the conductivity tends to infinity as the inverse of the cell-to-wavelength ratio. We carry out both formal and rigorous two-scale periodic homogenization analyses, paying special attention to the appropriate method of averaging, which is consistent with the treatment of the E, D, H, and B fields as differential forms. We prove that the resulting effective magnetic and dielectric coefficients characterize a bulk medium that, to leading order, produces the same scattering data as the micro-structured composite when a sample of the composite makes contact with the air only at the dielectric matrix.

Sub-wavelength Plasmonic Crystals: Dispersion Relations and Effective Properties

S. P. Fortes, **R. P. Lipton**, **and S. P. Shipman**
Louisiana State University, USA

Abstract— Plasmonic crystals are representative of a class of micro structured dielectrics known as meta-materials. The period of the meta-material crystal lies below the wavelength of illumination and the propagation of light is influenced by local electromagnetic field resonances on the length scale of the period. Since the crystal period lies below the wavelength of interest the notions of effective dielectric and magnetic properties have been introduced for describing electromagnetic wave propagation inside these materials.

In this talk, we report on recent work that develops a new type of power series expansion for the first branch of the dispersion relation for plasmonic crystals. The expansion parameter is given by the product kd where k is the wavenumber and d is the period of the crystal. Explicit error estimates show that a good approximation to the true dispersion relation is obtained using only a few terms of the expansion. The explicit power series for the dispersion relation is used to define a dynamic effective index of refraction. For wave propagation associated with the first passband the explicit formula shows that the plasmonic crystal behaves like a meta-material with positive index of refraction in which both the effective permittivity and permeability are positive.

REFERENCES

1. Fortes, S. P., R. P. Lipton, and S. P. Shipman, "Sub-wavelength plasmonic crystals: Dispersion relations and effective properties," arXiv:0910.0889v3 [math.AP], Submitted to *Proc. Roy. Soc. A*, Nov. 13, 2009.

Homogenization of Arrays of Nanorods

D. Felbacq[1], **G. Bouchitté**[2], **A. I. Cabuz**[1], **F. Zolla**[3], **and A. Nicolet**[3]

[1]University of Montpellier 2, 34090 Montpellier, France
[2]University of Toulon, La Garde Cedex, France
[3]University of Aix-Marseille 3, Marseille, France

Abstract— A metamaterial made of nanorods arranged periodically in two directions of space is considered in the low frequency regime. The materials constituting the nanorods can be a dielectric or a metal. The effective permittivity and permeability tensors are derived. It is shown that a magnetic activity is possible for dielectric rods while the effective medium is non-local for metallic rods.

Introduction: A lot of efforts have been made to describe the effective properties of metamaterials [1–3]. However, the complexity of these structures is generally an obstacle to a rigorous theory. In the present work, we consider a structure that is a bidimensional periodic array of finite length nanorods. Using a multiple scale approach, we derive rigorously the effective behavior of the metamaterial. The domain of validity of the results is precised by numerical experiments.

Homogenization: The behavior of dielectric rods is the same as the one obtain for infinitely long rods [3]. Let us simply describe here the behavior of ohmic nanorods. In that case, the medium has a strong spatial dispersion, the displacement field $\mathbf{D}$ being given by [4]: $\mathbf{D} = \varepsilon_0(\mathbf{E} + i\mathbf{P}e_3)$, where $\mathbf{P}$ is a polarization field satisfying a propagation equation, with the vertical component of the electric field as a source term:

$$\frac{\partial^2 J}{\partial x_3^2} + \left(k^2 + \frac{2i\pi\gamma}{\kappa}\right) J = 2i\pi\gamma E_3, \tag{1}$$

here $\kappa\varepsilon_0\omega$ is the total conductivity of the wires over the entire medium and $1/\gamma = d^2 \log\left(\frac{d}{2\pi a}\right)$. To these relations one should add the boundary condition: $\frac{\partial J}{\partial x_3} = 0$ on the top and bottom of the structure. Clearly, in that case it is not possible to define an effective local permittivity.

Conclusion: Very different behaviors can be obtained for arrays of nanorods according to the filling ratio and materials used. In the near future, we shall investigate the role of plasmons in the effective properties.

ACKNOWLEDGMENT

This work was realized in the framework of the ANR contract POEM PNANO 06-0030. Support from the Institut Universitaire de France is gratefully acknowledged.

REFERENCES

1. Belov, P. A., R. Marques, S. I. Maslovski, I. S. Nefedov, M. Silveirinha, C. R. Simovski, and S. A. Tretyakov, "Strong spatial dispersion in wire media in the very large wavelength limit," *Phys. Rev. B*, Vol. 67, 113103, 2003.
2. Shvets, G. and Y. A. Urzhumov, "Electric and magnetic properties of sub-wavelength plasmonic crystals," *J. Opt. A: Pure Appl. Opt.*, Vol. 7, S23–S31, 2005.
3. Urzhumov, Y. A. and G. Shvets, "Optical magnetism and negative refraction in plasmonic metamaterials," *Solid State Communications*, Vol. 146, 208–220, 2008.
4. Felbacq, D. and G. Bouchitté, "Theory of mesoscopic magnetism in photonic crystals," *Phys. Rev. Lett.*, Vol. 94, 183902, 2005.
5. Bouchitté, G. and D. Felbacq, "Homogenization of a wire photonic crystal: The case of small volume fraction," *SIAM J. Appl. Math.*, Vol. 66, 2061–2084, 2006.

Random Dielectric Inclusions and Artificial Magnetism

G. Bouchitté, C. Bourel, and L. Manca
Institut de Mathématiques IMATH, Université de Toulon, BP 20132, 83957 La Garde Cedex, France

Abstract— In [1–4] , a theory for artificial magnetism in two-dimensional photonic crystals was developed for large wavelength (homogenization) and more recently in a full three dimensional setting in [5], where a rigorous justification for effective tensors of negative permeability was given. This suggests that designing periodic bulk dielectric inclusions could be an efficient alternative to the very popular metallic split-ring structure proposed by Pendry [6].

Here we would like to present random models in which spherical inclusions are randomly disposed, each of them having, up to a large scaling factor, a random permittivity $\varepsilon^r(\omega)$ whose law is represented by a density on a window $\Delta_\delta = [a, b] \times [0, \delta]$ of the complex plane.

The key point is that, when the photonic crystal is illuminated at a given frequency, it happens that some values in interval $[a, b]$ are associated with internal resonances of the inclusions. The homogenization process is therefore difficult to handle if one starts with a law of ε^r concentrated on the real axis (i.e., $\delta = 0$).

In this work we determine conditions on the probability law of ε^r on Δ_δ under which the homogenization process can be identified and leads to a deterministic effective permeability of the same kind as the one found in [1, 5]. Subsequently a limit analysis is performed when the law for ε^r depends on δ and concentrates on the real axis as $\delta \to 0$.

REFERENCES

1. Bouchitté, G. and D. Felbacq, "Homogenization near resonances and artificial magnetism from dielectrics," *Acad. Sci. Paris*, No. 5, 339, 377–382, C. R. Math, 2004.
2. Felbacq, D. and G. Bouchitté, "Left handed media and homogenization of photonic crystals," *Optics Letters*, Vol. 30, 10, 2005.
3. Felbacq, D. and G. Bouchitté, "Homogenization of wire mesh photonic crystals embdedded in a medium with a negative permeability," *Phys. Rev. Lett.*, Vol. 94, 183902, 2005.
4. Felbacq, D. and G. Bouchitté, "Negative refraction in periodic and random photonic crystals," *New J. Phys.*, Vol. 7, 159, 10.1088, 2005.
5. Bouchitté, G., C. Bourel, and D. Felbacq, "Homogenization of the 3D Maxwell system near resonances and artificial magnetism," *Comptes Rendus Mathematique*, Srie A 347, 9–10, 571–576, 2009.
6. OBrien, S. and J. B. Pendry, "Magnetic activity at infrared frequencies in structured metallic photonic crystals," *J. Phys. Condens. Mat.*, Vol. 14, No. 6383, 6394, 2002.

Contribution of Higher-order Multipole Radiation to Spatial Dispersion and Radiation Losses in Metamaterials

Andrea Alù
Department of Electrical and Computer Engineering, The University of Texas at Austin, USA

Abstract— Simplified homogenization techniques that neglect the complex interaction among neighboring cells in complex metamaterial geometries may produce largely erroneous and over-simplified homogenization models, which do not satisfy basic constraints of power conservation, reciprocity and causality. A classic example is the anti-resonance behavior of the extracted effective permittivity in various classes of magnetic metamaterials, which is evidently non-physical and a symptom of neglected strong spatial dispersion in the homogenization model. An analytical approach to the problem based on multipolar expansion at the unit cell level may shed some light into some of the issues involved in strong spatial dispersion effects associated with higher-order multipole radiation non-negligibly excited in complex metamaterial geometries. Relevant examples in this sense are provided by regular circular arrays or densely packed linear arrays of plasmonic nanoparticles, which may form optical metamaterials with exotic light interaction properties. If properly designed, a subwavelength plasmonic loop may resonantly respond to the gradient of the electric field on the inclusion, inducing a weak spatial dispersion that is responsible for artificial magnetism [1]. However, specific configurations may or may not suppress unwanted higher-order multipole response, which reflects in radiation loss and strong spatial dispersion in the homogenized metamaterials. On the other hand, linear arrays of nanoparticles may be characterized by a strong spatial dispersion effect [2], producing an effective permittivity factor that depends on the square of the wave vector. Such dependence, usually undesirable, may play a relevant role in the possibility to achieve negative index of refraction without negative permeability, if properly tailored. In the talk, we will discuss the general relationship between spatial dispersion at the unit cell level and homogenized metamaterial effective parameters, providing specific examples for which these effects may provide a beneficial or detrimental effect in metamaterial applications.

REFERENCES

1. Alù, A. and N. Engheta, *Phys. Rev. B*, Vol. 78, 085112, 2008.
2. Alù, A. and N. Engheta, *Phys. Rev. B*, Vol. 75, 024304, 2007.

Spatial Dispersion and Effective Constitutive Parameters of Electromagnetic Metamaterials

Gennady Shvets and Chris Fietz
Department of Physics, The University of Texas at Austin, Austin, Texas 78712, USA

Abstract— A current-driven homogenization (CDH) approach to calculating all 36 linear constitutive parameters of a metamaterial crystal is presented. Spatial dispersion is accounted for by evaluating the constitutive parameters as a function of frequency and wavenumber. For two-dimensional centrosymmetric crystals spatial dispersion is shown to result in bianisotropy. The accuracy of the CDH constitutive parameters is verified by comparing the radiation efficiencies of a simple directional antenna embedded inside the homogenized and un-homogenized metamaterial slabs.

Optical properties of metamaterials are conceptually different from those of the natural materials. Two factors make spatial dispersion in metamaterials much more important than in the natural materials. First, a typical unit cell of a metamaterial is less than one tenth of the wavelength. Therefore, from the standpoint of their optical response, one can view metamaterials as *mesoscale* materials: their unit cell is much larger than that of natural materials yet somewhat smaller than the wavelength of light. Second, because unit cells of many metamaterials contain resonant elements (such as magnetic and electric split ring resonators, etc.), it is not unusual for a metamaterial to have an effective refractive index of order 10 or higher. Therefore, spatial dispersion is very important in most metamaterials. Spatial dispersion can lead to extraordinary phenomena such as, for example, effective optical magnetism (i.e., magnetic permittivity μ different from unity) and bianisotropy (contribution of the electric field to the magnetic inductance vector), as well as somewhat confusing effects such as anti-resonances.

We will use the CDH procedure to investigate optical properties of several 2D metamaterials. One example of the CDH result is shown in Fig. 1 for a recently introduced [1] negative index metamaterial comprised of a 2D array of squares with length $a/2$ where a is the lattice constant. The squares are composed of a high-permittivity material with $\epsilon = 200-5i$. They are surrounded by a hypothetical material with the dielectric permittivity $\epsilon = -1$. Note that the un-physical anti-resonances of ϵ obtained using the standard S-parameter extraction procedure are clearly consequences of the strong spatial dispersion. Anti-resonances disappear when ϵ is extracted at $\mathbf{k} = 0$. We will also demonstrate how the CDH procedure can be useful for practical applications, such as predicting radiation by arbitrary directional antennas embedded inside a metamaterial cloak.

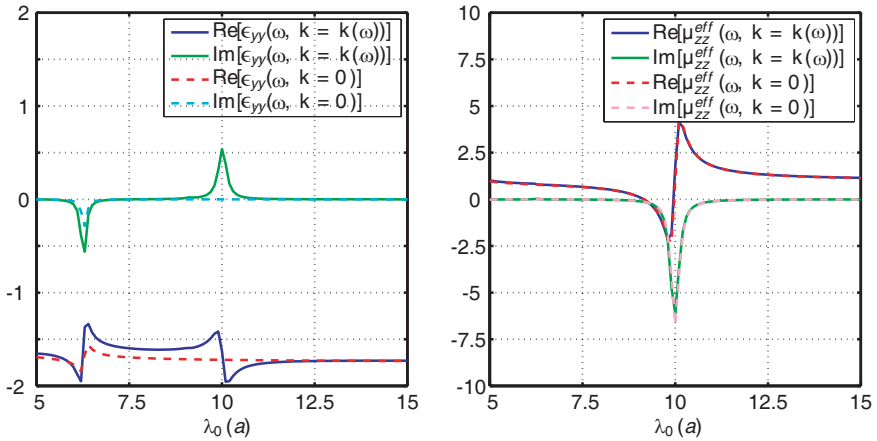

Figure 1: **Left Side**: Constitutive parameters ϵ_{yy} and μ_{zz} extracted from a a negative index metamaterial with a high-index inclusion. The square unit cell is comprised of the inner square with $\epsilon = 200 - 5i$ and the surrounding shell with $\epsilon = -1$ [1]. Solid lines: S-parameter extraction, which is in full agreement with the CDH on the dispersion curve $\mathbf{k} = k_x(\omega)\hat{x}$. Dashed lines: CDH extraction off the dispersion curve (at the Γ point $\mathbf{k} = 0$).

REFERENCES

1. Felbacq, D. and G. Bouchitte, " Left-handed media and homogenization of photonic crystals," *Opt. Lett.*, Vol. 30, No. 10, 1189–1191, 2005.

Limitations in Homogenization of Thin (Meta)material Slabs

Henrik Kettunen, **Jiaran Qi**, **Henrik Wallén**, **and Ari Sihvola**
Department of Radio Science and Engineering
Aalto University School of Science and Technology, Finland

Abstract— It is often convenient to model metamaterials and other composite materials with complex microscopic structure as macroscopically homogeneous materials by finding their corresponding effective material parameters. One of the most common methods for solving the effective permittivity and permeability is based on the S parameter retrieval technique [1–3]. In other words, the material parameters are solved by studying the reflection and transmission of an electromagnetic wave incident on a material slab. This technique is used even for very thin slabs with thickness of only few unit cells and even when the electrical size of the unit cell is not very small [4].

On the other hand, in order to consider a material effectively homogeneous, its intrinsic inhomogeneities must be very small compared with the wavelength of the impinging field. Also, the constitutive material parameters should not depend on the amount of the material. Moreover, it has even been questioned, whether the parameters obtained by the S parameter retrieval technique correspond to any physical constitutive material parameters [5]. In this presentation, we study the limitations of the material parameter retrieval with respect to the electrical size of the unit cell and the thickness of the slab.

We computationally study the homogenization of a geometrically simple composite material that consists of a periodical lattice of infinitely long dielectric cylinders. The incoming wave is normally incident to the slab and the polarization of the electric field is chosen perpendicular to the axes of the cylinders. The geometry is modelled in 2D using Comsol Multiphysics 3.5 software which is based on the finite element method.

Since the material is non-magnetic, only the effective permittivity is sought. The electrostatic permittivity of such bulk material can be analytically approximated using different mixing formulas [6]. Our results show that extra care should be taken when retrieval techniques are applied. The retrieved permittivity converges to a quasistatic value only when the unit cell size becomes very small. For instance, a cell size $\lambda/10$, which usually is considered a safe choice, is not small enough at all. When the unit cell size increases, the retrieved permeability also begins to deviate from unity. Furthermore, for very thin slabs, the permittivity becomes dependent on the thickness of the slab indicating that a slab too thin, consisting only of a couple of layers of consecutive unit cells, should not be treated as a bulk material.

These limitations can be significant even for ordinary dielectric composites. However, for metamaterials with resonant inclusions, the retrieval can fail to produce physically reasonable results instead of being only inaccurate.

REFERENCES

1. Nicolson, A. M. and G. F. Ross, "Measurement of the intrinsic properties of materials by time-domain techniques," *IEEE Trans. Inst. Meas.*, Vol. 19, No. 4, 377–382, 1970.
2. Smith, D. R., S. Schultz, P. Markoš, and C. M. Soukoulis, "Determination of effective permittivity and permeability of metamaterials from reflection and transmission coefficients," *Phys. Rev. B*, Vol. 65, No. 19, 195104, 2002.
3. Chen, X., T. M. Grzegorczyk, B.-I. Wu, J. Pacheco, Jr., and J. A. Kong, "Robust method to retrieve the constitutive effective parameters of metamaterials," *Phys. Rev. E*, Vol. 70, No. 1, 016608, 2004.
4. Smith, D. R., D. C. Vier, T. Koschny, and C. M. Soukoulis, "Electromagnetic parameter retrieval from inhomogeneous metamaterials," *Phys. Rev. E*, Vol. 71, No. 3, 036617, 2005.
5. Simovski, C. R., "Material parameters of metamaterials (a review)," *Opt. Spectrosc.*, Vol. 107, No. 5, 726–753, 2009.
6. Sihvola, A., *Electromagnetic Mixing Formulas and Applications*, IEE, London, 1999.

Magnetoelectric Coupling Effects in Metamaterials

David R. Smith
Center for Metamaterials and Integrated Plasmonics and Electrical and Computer Engineering
Duke University, Box 90291, Durham, North Carolina 27708, USA

Abstract— An electromagnetic metamaterial can be modeled as a periodic array of one-dimensional slabs having electric, magnetic, or simultaneously electric and magnetic response. When only electric or magnetic response is present — but not both — the transfer matrix method can be applied to obtain simple analytical expressions for the Bloch constitutive parameters. The technique involves taking a limit such that the slab thickness tends to zero while the slab permittivity (or permeability) tends to infinity. The analytical expressions consist of a Lorentzian multiplied by a function that depends only on the Bloch phase advance. These derived formulas, found by Liu et al. using a different analytical approach [1], exhibit all of the artifacts that have come to be associated with numerical retrievals, including distorted, non-Lorentizan line-shapes. By choosing appropriate values for the Lorentzian values, the analytically determined constitutive parameters can be made to coincide with the Bloch constitutive parameters found from numerical retrievals.

The described analytical approach used to study electric or magnetic Bloch lattices fails when both electric and magnetic response are simultaneously present in each slab. As has been shown by Simovski [2], such lattices are characterized by magnetoelectric coupling between unit cells, resulting in a nonlocal description of the slab system. For these systems, an alternative analytical approach must be employed to obtain sensible definitions for the effective index and Bloch impedance.

It is also possible that electric and magnetic elements within a unit cell may exhibit magnetoelectric coupling, resulting in a bi-anisotropic medium with characteristic features in the retrieved effective index. A variety of metamaterial elements can be used — including split ring resonators and electric "LC" resonators — to illustrate the coupling effects. For intercell magnetoelectric coupling, additional analytical formulas can be derived which, again, exhibit excellent agreement in terms of line-shapes with the index found from numerical simulations. Arrangements of resonators can be found that allow the entire range of coupling — from very weak to very strong — to be explored. The results indicate the inherent difficulty associated with forming a metamaterial with arbitrary electromagnetic properties.

REFERENCES

1. Liu, R., et al., *Phys. Rev. E*, Vol. 76, 026606, 2007.
2. Simovski, C. R., *Metamaterials*, Vol. 1, 62, 2007.

Session 4P1
Dimensionality Reduction of Large Scale forward and Inverse EM Problems

A Parametric Level Set Method for Image Reconstruction

A. Aghasi[1], **M. E. Kilmer**[2], **and E. L. Miller**[1]

[1]Department of Electrical and Computer Engineering, Tufts University, Medford, MA, USA
[2]Department of Mathematics, Tufts University, Medford, MA, USA

Abstract— A common problem in imaging is the reconstruction of one or more oddly shaped regions of interest, or hot spots, distinct from the background. In diffuse optical tomography for breast tissue imaging, for example, the goal is to recover 3D images of absorption and diffusion of light in tissue with anomalous regions of absorption and diffusion possibly indicating the presence of cancer. Unfortunately, many such image reconstruction problems are severely underdetermined when each voxel value is independently considered to be an unknown. Noise in the measured data makes reconstruction of useful images impossible without additional regularization.

We propose a parametric level-set model for the underlying images of interest. Specifically, we introduce a general formulation of a level-set description of the space-varying perturbation defined through a linear combination of basis functions. The basis functions may consist of, for example, polynomials or compactly supported radial basis functions. Our approach is different from traditional level set approaches in that the inverse problem requires the reconstruction of the expansion coefficients in the basis, as well as a few auxiliary parameters describing the background and intensity of the anomaly(ies). This eliminates the need to evolve the level sets through auxiliary differential equations. Further, some degree of regularization is provided through the model itself. The inverse (i.e., image reconstruction) problem requires the solution of a non-linear least squares problem for the unknown parameters. Since the number of parameters is significantly less than the number of voxels in the 3D image, this makes the reconstruction problem better determined, reduces the computational complexity of the nonlinear optimization problem, and helps to address the sensitivity to noise. We present computational results for applications in diffuse optical tomography and electrical resistance tomography that show the promise of our approach.

Efficient Multigrid Methods for the Time-Harmonic Maxwell's Equations on Stretched Grids

Thomas Benson and Scott MacLachlan
Tufts University, USA

Abstract— We consider the solution of the time-harmonic Maxwell's Equations, reduced to a single vector equation for the electric field, $\mathbf{E}(x,y,z,t) = \hat{\mathbf{E}}(x,y,z)e^{-\imath\omega t}$,

$$\nabla \times \frac{1}{\mu}\nabla \times \hat{\mathbf{E}} - \imath\omega\hat{\sigma}\hat{\mathbf{E}} = \imath\omega\hat{\mathbf{J}}, \tag{1}$$

where $\mathbf{J}(x,y,z,t) = \hat{\mathbf{J}}(x,y,z)e^{-\imath\omega t}$ is the known (time-harmonic) external current density, and μ, σ, and ϵ are known symmetric positive semi-definite tensor coefficients describing the electrical permeability, conductivity, and permittivity, respectively, with $\hat{\sigma} = \sigma - \imath\omega\epsilon$. We consider only the case where $\|\omega\epsilon\| \ll \|\sigma\|$ in some suitable norm.

Equation (1) is posed on a three-dimensional domain, Ω, which we take to be a cube that encloses the region of interest. Zero tangential boundary conditions are applied on the boundary of Ω. We are particularly interested in the case where the vector field, $\mathbf{E}$, is of interest only on a small portion of Ω, but the larger domain is necessary to mitigate the effects of unphysical boundary conditions. In this setting, grid adaptation is necessary in order to lead to acceptable computational costs.

A popular strategy in the recent literature is to consider so-called "stretched" grids [1, 5], using a threedimensional tensor-product mesh, where the grid points in each direction are chosen to give fine resolution (and good accuracy) around the region of interest, with progressively coarser resolution out to the computational boundary. This approach is attractive because it leads to highly structured matrices for the discretization, along with control over the accuracy of the solution.

As noted in [5], a significant disadvantage of this approach is the sharp degradation in the performance of standard multigrid solvers for Equation (1) when the stretching of the grid leads to elements with particularly large or small aspect ratios. A standard approach to address this degradation is the use of so-called line or plane smoothers and semicoarsening techniques, as was investigated in [4]. While this approach does lead to scalable iteration counts, it does so at a significant cost in CPU time; experiments in [4] show a reduction in iteration counts by factors as large as 20, but the best improvements in total CPU time are only 30%.

We consider two alternative approaches, one that mimics the BoxMG algorithm for Poisson-type problems [2, 3], and one based on the novel coarsening strategy introduced in [6]. In both cases, we adapt the coarsening phase of a standard, geometric multigrid V-cycle to account for the anisotropies in the mesh as well as the variation in the coefficient $\hat{\sigma}$. In this talk, we discuss progress to date in extending these established approaches for scalar real-valued PDEs to the complex-valued curl-curl system of Equation (1).

REFERENCES

1. Davydycheva, S., V. Druskin, and T. Habashy, "An efficient finite-difference scheme for electromagnetic logging in 3D anisotropic inhomogeneous media," *Geophysics*, Vol. 68, 1525–1536, 2003.
2. Dendy, J. E., "Black box multigrid," *J. Comput. Phys.*, Vol. 48, 366–386, 1982.
3. Dendy, Jr., J. E., "Two multigrid methods for three-dimensional problems with discontinuous and anisotropic coefficients," *SIAM J. Sci. Statist. Comput.*, Vol. 8, 673–685, 1987.
4. Jönsthövel, T. B., "Improvement of a multigrid solver for 3D EM diffusion," Master's thesis, Delft University of Technology, 2006.
5. Mulder, W., "Geophysical modelling of 3D electromagnetic diffusion with multigrid," *Comput. Visual. Sci.*, Vol. 11, 129–138, 2008.
6. Zubair, H. B., S. MacLachlan, and C. Oosterlee, "A geometric multigrid method based on l-shaped coarsening for pdes on stretched grids," *Numer. Linear Alg. Appl.*, to Appear, 2009.

A Butterfly Algorithm for Synthetic Aperture Radar Imaging

Laurent Demanet
Stanford University, USA

Abstract— The butterfly algorithm is a robust alternative to the FFT for computing all sorts of oscillatory integrals in a fast and accurate manner. It is an approach based on local low-rank expansions and hierarchical recursive partitioning. Discovered by Michielssen et al., and popularized by Rokhlin et al., the butterfly is a proud child of the line of work that started with the fast multipole method. Some of its applications are reviewed: fast special function transforms, fast wave computations, and radar imaging.

An Equivalence Theorem for Iterated Rational- and Vector-fitting

D. Vasilyev[1], **M. Tsuk**[2], **and J. White**[1]

[1]Massachusetts Institute of Technology, USA
[2]Ansoft Corporation, USA

Abstract— The problem of finding efficient and reliable techniques for generating state-space time-domain representations from measured or simulated frequency-domain scattering-parameter data has been extraordinarily persistent; perhaps surprising given its equivalence to finding good algorithms for rational interpolation. There are many reasons for this persistence. Fundamentally, rational interpolation is a non-convex optimization problem in most error metrics, but there are also application associated difficulties. It is not uncommon for the frequency range to span as many ten decades, and typical data can be both noisy and have sharp features due to resonances. In addition, there are often constraints on the interpolation, such as enforcing stability or passivity.

Two widely used strategies for generating state-space representations from scattering parameter data are the iterated rational fitting methods, whose underlying unknowns are coefficients of numerator and denominator polynomials, and the vector-fitting methods, whose underlying unknowns are poles and residuals [1, 2]. The two methods are different in more than just the unknowns, they also differ in the computation performed on each iteration. Both methods solve a linear system to find a least-squares fit to data, but then iterated rational fitting performs an update by dividing by a polynomial, whereas vector-fitting performs an update by computing the roots of a polynomial. Given these differences between the two methods, one might expect the resulting interpolations to be different. In this paper we will prove that in exact arithmetic, and given equivalent initial guesses, the two methods produce *exactly* the same interpolation, iteration by interaction. Therefore, differences between these two popular methods must stem from numerical issues or differing implementation-specific heuristics.

REFERENCES

1. Coelho, C. P., J. R. Phillips, and L. M. Silveira, "Robust rational function approximation algorithm for model generation," *Proceedings of DAC'99*, 207–212, New Orleans, 1999.
2. Gustavsen, B. and A. Semlyen, "Rational approximation of frequency domain responses by vector fitting," *IEEE Trans. on Power Delivery*, Vol. 14, No. 3, 1052–1061, 1999.

Optimal Grids for Anisotropic Problems

Shari Moskow, **Vladimir Druskin**, **and Sergey Asvadurov**
Schlumberger Doll Research, Cambridge, USA

Abstract— Spectral convergence of optimal grids for anisotropic problems is both numerically observed and explained. For elliptic problems, the gridding algorithm is reduced to a Stieltjes rational approximation on an interval of a line in the complex plane instead of the real axis as in the isotropic case. We show rigorously why this occurs for a semiinfinite and bounded interval. We then extend the gridding algorithm to hyperbolic problems on bounded domains. For the propagative modes, the problem is reduced to a rational approximation on an interval of the negative real semiaxis, similarly to in the isotropic case. For the wave problem we present numerical examples in 2-D anisotropic media.

Characterization and Synthesis of the Response Function of Elastodynamic Networks

F. Guevara Vasquez, G. W. Milton, and D. Onofrei
University of Utah, USA

Abstract— An elastodynamic network is a network of springs and masses; its response function is a matrix valued function $\mathbf{W}(\omega)$ of the frequency ω, mapping displacements to forces at some accessible or terminal nodes. The first step towards understanding the inverse problem of finding the springs and masses from the response function of such networks is to give necessary and sufficient conditions for a given function $\mathbf{W}(\omega)$ to be the response function of an elastodynamic network. We present such conditions and show how to construct an elastodynamic network with a given response function $\mathbf{W}(\omega)$. We also discuss some ideas indicating it is possible to recover the spring constants in the static $\omega = 0$ case.

Resistor Networks and Optimal Grids for Electrical Impedance Tomography with Partial Boundary Measurements

Liliana Borcea[1], **Vladimir Druskin**[2], **Alexander Mamonov**[1], **and Fernando Guevara Vasquez**[3]

[1]Rice University, USA
[2]Schlumberger-Doll Research, USA
[3]University of Utah, USA

Abstract— The problem of Electrical Impedance Tomography (EIT) is to determine the electric conductivity inside a body from the simultaneous measurements of direct currents and voltages on its boundary. In the case of partial boundary data the measurements are restricted to a subset of the boundary.

Even in the case of full boundary measurements the non-linear inverse problem is known to be exponentially ill-conditioned. Thus, any numerical method of solving the EIT problem must employ some form of regularization. We propose to regularize the problem by using sparse representations of the unknown conductivity on adaptive finite volume grids known as the optimal grids. The use of optimal grids allows us to discretize the elliptic equation for the electric potential on the same grid as we do inversion on, which may not be the case with the more traditional inversion schemes. Then the discretized partial data EIT problem can be reduced to solving the discrete inverse problems for resistor networks. We propose two distinct approaches implementing this strategy for the partial data EIT problem in two spatial dimensions.

The first approach uses the results obtained by the authors for the EIT problem with full boundary measurements, which relies on the use of resistor networks with circular graph topology. The optimal grids for such networks are essentially one dimensional objects, and under some assumptions they can be computed explicitly. We solve the partial data problem by reducing it to the full data case using the theory of extremal quasiconformal (Teichmuller) mappings.

The second approach is based on resistor networks with the pyramidal graph topology. Such network topology is better suited for the partial data problem, since it allows for explicit treatment of the inaccessible part of the boundary. We present a method of computing the optimal grids for the networks with general topology (including pyramidal), which is based on the sensitivity analysis of both the continuum and the discrete EIT problems.

We present extensive numerical results for the two approaches. We demonstrate both the optimal grids and the reconstructions of smooth and discontinuous conductivities in a variety of domains. The numerical results show two main advantages of our approaches compared to the traditional optimization-based methods. First, the inversion based on resistor networks is orders of magnitude faster than any iterative algorithm. Second, our approaches are able to correctly reconstruct the conductivities of very high contrast, which usually present a challenge to the iterative or linearization-based inversion methods.

Extended Krylov Subspace Methods for Transient Wavefield Problems

R. F. Remis
Laboratory of Electromagnetic Research
Faculty of Electrical Engineering, Mathematics and Computer Science
Delft University of Technology, Mekelweg 4, 2628 CD Delft, The Netherlands

Abstract— In this paper we present an Extended Krylov Subspace method [1] to efficiently simulate (electromagnetic) wavefield propagation in complex media. In particular, we apply the EKS method to time-domain multiconductor transmission line problems and transient electromagnetic wavefield problems are considered as well.

Starting point for both types of problems is a first-order finite-difference state-space representation obtained after discretizing the transmission line equations or Maxwell's equations in space using standard two-point finite-differences on a nonuniform staggered grid. The finite-difference representation is written in terms of a so-called system matrix and the field solution for transmission lines or Maxwell's equations is essentially given by a temporal convolution of the source vector and the system matrix evolution operator (matrix exponent).

For problems encountered in practice, the order of the system matrix can be very large and direct evaluation of the evolution operator is simply not feasible. Fortunately, we do not need the evolution operator on its own; only its action on the source vector is required. We therefore approximate the wavefield quantities by elements taken from an extended Krylov subspace. Such a space is generated by the source vector, the system matrix, and an inverse of the system matrix. Loosely speaking, the idea is that by appending a standard Krylov basis with vectors consisting of powers of an inverse of the system matrix, we approximate early- and late-time responses simultaneously.

To generate a basis of the extended Krylov space, we obviously need an inverse of the system matrix. For transmission line problems we can show that this inverse exists if (part of) the transmission line contains some loss mechanism. Moreover, we have found an explicit expression for this inverse which shows that its action on a vector can be computed in an $O(n)$ amount of work, where n is the total number of unknowns. For electromagnetic wavefield problems the inverse of the system matrix does not exist in general. Here, however, we can work with its so-called group inverse. We have found an explicit expression for this inverse as well and its action on a given vector can be computed at "FFT speed."

Having the necessary inverses available, we still need to generate a basis of the extended Krylov space. We show that this can be done very efficiently by exploiting the J-symmetry property of the system matrix and its (group) inverse. In particular, a J-orthogonal basis of the extended Krylov subspace can be generated via short Lanczos/CG-type recurrence relations. The system matrix (and its inverse) are J-symmetric, since the (discretized) wavefield quantities satisfy reciprocity. The expansion coefficients follow from a Galerkin procedure and with these coefficients we have arrived at our EKS field approximations. Numerical experiments will be presented illustrating the performance of the method.

REFERENCES

1. Druskin, V. and L. Knizhnerman, "EKS method," *SIAM J. Matrix Anal. Appl.*, Vol. 19, No. 3, 755–771, 1998.

A Thick-restart Krylov Subspace Method for Dimension Reduction of Large-scale Linear Descriptor Systems

Roland W. Freund and Efrem B. Rensi
Department of Mathematics, University of California, Davis, One Shields Avenue, Davis, CA 95616, USA

Abstract— In recent years, Krylov subspace techniques have proven to be powerful tools for dimension reduction of large-scale linear descriptor systems. These are systems of algebraic-differential equations that arise in a number of important applications, including the simulation of electrical circuits, computational electromagnetics, microelectromechanical systems (MEMS), structural dynamics, and computational acoustics. In particular, the need for efficient reduction of the ever-increasing dimension of the linear networks arising in VLSI circuit simulation motivated much of the development of Krylov subspace-based dimension reduction techniques.

Krylov subspace-based dimension reduction is intimately related to Padé approximation of the large-scale descriptor systems transfer function in frequency domain. In their basic form, these techniques are restricted to Padé approximants associated with a single expansion point in frequency domain, and they cannot be employed directly with multiple expansion points. On the other hand, for many classes of descriptor systems, the use of multiple expansion is unavoidable in order to obtain a reduced system of sufficiently small dimension.

In this paper, we present a new Krylov subspace-based dimension reduction method that employs *thick-restart Krylov subspace techniques* to generate reduced models characterized by multi-point Padé approximation properties. The key feature of the method is that it extracts the dominant eigenvector information obtained from each cycle of single-point Krylov subspace iterations and then retains these vectors in the next restarted cycle while simultaneously changing the single expansion point. We present some theory for this new dimension reduction method, and we show numerical results from VLSI circuit simulation that illustrate the viability and efficiency of this new approach.

Adaptive Rational Krylov Subspace Reduction for Solution of Time-domain Electromagnetic Problems

Mikhail Zaslavsky[1], **Vladimir Druskin**[1], **Leonid Knizhnerman**[2], **and Chad Lieberman**[3]

[1]Schlumberger Doll Research, 1 Hampshire Str., Cambridge, MA 02139, USA
[2]Central Geophysical Expedition, 38/3 Narodnogo opolcheniya Str., Moscow 123298, Russia
[3]Massachusetts Institute of Technology, Cambridge, MA 02139, USA

Abstract— We present a fast and robust algorithm for solution of the 3D time-domain Maxwell's equations in diffusive regimes typical for controlled source electromagnetic (CSEM) problems. It is based on ideas of rational Krylov subspace reduction [1]. A key question in the construction of the RKS is how to choose interpolating Laplace frequencies. We develop a priori and adaptive frequency optimization algorithms. Our a priori approach is derived from a classical Zolotaryov problem and proved to yield an asymptotically optimal solution with real Laplace frequencies for the cases with uniform spectral distributions. The adaptive approach is based on a recursive greedy algorithm for choice of real frequencies taking into account non-uniformity of the spectrum. This algorithm uses an explicit formula for the residual in the frequency domain allowing adaptive frequencies optimization at negligible cost. Real frequencies in both the algorithms lead to real symmetric frequency domain problems, that can be solved significantly more efficiently than the conventional complex frequency domain problems.

The theory is illustrated by numerical examples for the 3D CSEM problems arising in marine geophysical exploration. Both algorithms has shown the theoretically proven optimal convergence rate for low contrast media, but adaptive algorithm becomes superior for models with high conductivity contrasts. Both algorithms significantly overperform existing rational Krylov subspace algorithms for solution of evolutionary problems.

REFERENCES

1. Druskin, V., L. Knizhnerman, and M. Zaslavsky, "Solution of large scale evolutionary problems using rational Krylov subspace optimized shifts," *SIAM J. Sci. Comput.*, Vol. 31, No. 5, 3760–3780, 2009.

Solution of Time-convolutionary Maxwell's Equations Using Krylov Subspace Reduction

Vladimir Druskin and Mikhail Zaslavsky
Schlumberger Doll Research, 1 Hampshire St., Cambridge, MA 02139, USA

Abstract— We suggest a new algorithm for the solution of the time domain Maxwell equations in dispersive media. After spacial discretization we obtain a large system of time-convolution equations. Then this system is projected onto a small subspace consisting of the Laplace domain solutions for a preselected set of Laplace parameters. This approach is a generalization of the rational Krylov subspace approach for the solution of non-dispersive Maxwell's systems [1]. We prove that the projected system is structure preserving and obtain a convergence estimate by extending analysis of [1]. As an example we con- sider the 3D quasistationary induced polarization problem with the Cole-Cole conductivity model important for geophysical oil exploration. Our numerical experiments show, that the introduction of the induced polarization does not have significant effect on convergence.

REFERENCES

1. Druskin, V., L. Knizhnerman, and M. Zaslavsky, "Solution of large scale evolutionary problems using Rational Krylov Subspaces with optimized shifts," *SIAM J. Sci. Comput.*, Vol. 31, No. 5, 3760–3780, 2009.

Session 4P2a
Optics, Fiber and Optical Waveguide

Interaction Dynamics of Solitons in a Linearly Coupled Ginzburg-Landau Equation with Cubic-quintic Nonlinearity

Daniel R. Neill and Javid Atai
School of Electrical and Information Engineering, The University of Sydney, NSW 2006, Australia

Abstract— Solitary pulses play an important role in the physical systems that are described by various forms of the Ginzburg-Landau equation. Models based on complex Ginzburg-Landau (CGL) equations have been used extensively to study pattern formation and solitary pulse dynamics in various physical systems [1].

In the theoretical modeling of such pulses, the issues involved are the stability of the pulses, the interactions between them and the physical applications of the model. In [2] a model based on linearly coupled CGL equations was put forward that admitted exact stable soliton pulses. The model describes a doped dual core nonlinear optical fiber, with one core being passive and lossy and the other being active with dispersive losses, dispersion, and cubic nonlinearity.

In this paper, we investigate the interaction of solitons in a model similar to that of Ref. [2] but with cubic-quintic nonlinearity. It should be noted that cubic-quintic nonlinear response has been experimentally observed in chalcogenide glasses [3] and some organic transparent materials [4]. Addition of quintic term to the model of Ref. [2] results in the following system of equations:

$$\begin{aligned} iu_z + \left(\frac{1}{2} - i\gamma_1\right) u_{\tau\tau} + \sigma\left(|u|^2 - \delta\,|u|^4\right) u - i\gamma_0 u + v = 0 \\ iv_z + i\,\Gamma_0 v + u = 0 \end{aligned} \tag{1}$$

where u and v are the amplitudes of the pulses traveling in the active and lossy cores and z and τ correspond to the propagation distance and retarded time, respectively. Dispersion is accounted for by σ, with normal dispersion being $\sigma = -1$ and anomalous dispersion being $\sigma = +1$. γ_1, γ_0 and Γ_0 are coefficients of the dispersive losses, the gain in the active core and the loss in the passive core, respectively. δ is the strength of the quintic nonlinearity.

The interaction dynamics of solitons in the model of Eq. (1) is found to be quite complex and rich. The outcomes of interactions are dependent upon the initial separation of the pulses, the initial phase difference and dispersion regime. For example, in anomalous dispersion regime, below a certain critical value of separation the in-phase soliton pulses attract and both become destabilized. On the other hand, if the initial separation is greater than the critical value the pulses repel each other until they reach a separation that the interaction becomes negligible and thereafter they propagate in parallel.

REFERENCES

1. Malomed, B. A., "Complex Ginzburg-Landau equation," *Encyclopedia of Nonlinear Science*, 157–160, A. Scott Ed., Routledge, New York, 2005.
2. Atai, J. and B. A. Malomed, "Exact stable pulses in asymmetric linearly coupled Ginzburg-Landau equations," *Phys. Lett. A*, Vol. 246, No. 5, 412–422, 1998.
3. Smektala, F., C. Quemard, V. Couderc, and A. Barthelemy, *J. Non-Cryst. Solids*, Vol. 274, 232, 2000.
4. Zhan, C., D. Zhang, D. Zhu, D. Wang, Y. Li, D. Li, Z. Lu, L. Zhao, and Y. Nie, *J. Opt. Soc. Amer. B*, Vol. 19, 369, 2002.

Modal Dispersion Characteristics of Different Cross Sectional Optical Waveguides

Y. K. Prajapati[1], **Vivek Singh**[2], **J. P. Saini**[1], **and Alka Verma**[1]

[1]Dept. of E & C, BIET, Jhansi 284128, U.P., India
[2]Banaras Hindu University, Varanasi 221005, U.P., India

Abstract— Optical waveguides are particularly used for communication purposes or as integrated optical devices. Over the past three decades, considerable research has been performed in the areas of optical waveguides and communication systems in view of their various applications. In both the cases the knowledge of the modal propagation characteristics of the waveguide to be used is essential. The study of electromagnetic wave propagation through conventional optical waveguides like circular core optical fibers or planar guides does not involve much difficulty, and the modal properties are known. Light wave propagation through non-symmetrical core cross-sectional waveguide, however, constitutes an important area of investigation. Using numerical and analytical approach, some of the noncircular cross-sectional guides have been investigated. In this article an analytical treatment of electromagnetic wave propagation having two different cross-sections based on a boundary matching condition and cutoff values (V_c) of a waveguides are computed and compare with standard circular optical waveguide. The boundary of waveguides can be described by equations $r = \xi \exp(1 + \sin\theta)$ for optical waveguide with a core slightly flattened on one side, where ξ is a size parameter and $x^N + y^N = a^N$, where N takes the values 1 and 4. For $N = 1$, we have a circular boundary (standard fiber), for $N = 4$, the boundary is a Piet-Hein curve. At the core-cladding boundary, we will put its value equal to a, where a is a fixed constant. In the equation first, we show that propagation characteristics of the guided wave are affected when the circular waveguide is deformed and when the circular symmetry no longer exists. And we found that when the value of the V-parameter increases, the number of sustained modes also increases. In the case of standard circular fiber, the first cutoff occurs at $V = 0$, and successive cutoffs occur at $V = 2.09$ etc. We observe that the first cutoff shifts from $V = 0$ to $V = 0.785$ approximately when we have a slightly flattened waveguide. The second and third shifts in the flattened waveguide follow closely. Thus, the first cutoff is shifted slightly toward higher values of V, whereas the next cutoff V-values occur at slightly lower values than those of the standard V-values for a circular waveguide. Finally, we get five modes when $V = 10.5$. And in the second equation, it is found that the Piet-Hein shape combines the desirable characteristics of the circular and the rectangular waveguide. Piet Hein cross section, we find that these curves have the standard shapes and for $V = 10.3$ there are four modes. The lowest order mode in this case has a cutoff V-value nearly $V = 2.0$. For practical use the Piet Hein waveguide is therefore more acceptable than the slightly flattened waveguide.

Decline of Quantum Redundancy in a Thermal Environment

Srinivasa Chemudupati[1] and Vladimir Tsifrinovich[2]

[1]Department of Electrical and Computer Engineering, Polytechnic Institute of NYU, USA
[2]Department of Physics, Polytechnic Institute of NYU, USA

Abstract— We study redundancy of quantum information first introduced by W. Zurek. We propose the model of a "thermal Universe", which is described by the density matrix rather than the wave function. We show that the redundancy of quantum information in a thermal environment decreases with increasing the environment temperature. We have calculated the mutual information as a function of the number of qubits in the environment. Partial information plots demonstrate that the quantum redundancy vanishes at $k_BT > 10\hbar\omega$, where ω is the characteristic energy of the environmental qubits. This provides an insight how the transition of the quantum information to the classical world can be controlled by varying temperature of the environment.

The Transition between Superluminal and Subluminal for Optical Resonant Cavity

Yundong Zhang[1], **Jing Zhang**[1], **Xiangchun Ju**[1], **Ping Yuan**[1], **Yuhua Zhang**[2], **and Sheng Qiang**[1]

[1]Harbin Institute of Technology, Harbin 150080, China
[2]Art College, Harbin Normal University, Harbin 150080, China

Abstract— Generally, for two microspheres (or even number of) optical resonators mode splitting and destructive interference lead to a cancellation of absorption and narrow symmetrical transmission peak occurs at resonant frequency following with normal dispersion. On the specific case of doping the gain medium, the phenomenon of transition between superluminal and subluminal is investigated by adjusting the amplitude loss ratio and the amplitude coupling ratio of the outermost high-Q microsphere. The inherent loss that stems from the backward scatter and absorption is compensated by introduced active dielectric. The coupling strength is associated to the spacial distance between microspheres and straight waveguide. It isn't only applied to the even number resonant systems which is composed of microspheres coupling with a fiber taper but also odd number structures respectively under the under-coupled condition. The fast and slow light propagating of optical pulse has been analyzed theoretically at time domain and frequency domain. To explain the novel problem further, we extend to phase space in complex plane to discuss several typical coupled conditions with gain. From the application of view, gain-assisted coupled resonant structures have been applied for light amplifications, optical delay lines and micro-lasers.

Observation of the Phase Shift and Group Delay in Nested Optical Fiber Ring Resonator

Yundong Zhang[1], **Jinfang Wang**[1], **Xiangchun Ju**[1], **Ping Yuan**[1], **Yuhua Zhang**[2], **and Sheng Qiang**[1]

[1]Harbin Institute of Technology, Harbin 150080, China
[2]Art College, Harbin Normal University, Harbin 150080, China

Abstract— We demonstrate theoretically and experimentally the transmission characteristics and time delay performance in a nested fiber ring resonator. The nested ring resonator is composed with a U-shaped fiber loop and a fiber ring nested together. With proper design of the coupling coefficient between the ring and the loop, the device is capable of generating a double-Fano spectral response. And the maximal group delay that it can be induced depends on the value of the coupling coefficient. In this paper we measure the transmission properties of our nested fiber ring resonators with different coupling coefficients, using a Mach-Zehnder fiber interferometer. By inserting the nested fiber ring resonator into one arm of the fiber Mach-Zehnder interferometer we are able to optically measure the intensity transmission factor and the phase shift produced by the coupled resonators as a function of the optical frequency. The group delay can be deduced from this information. This theoretical and experimental demonstration shows the potential of nested ring resonators for the slow-light applications.

Single-mode Waveguide Optical Isolation Based on Direction-dependent Mode Cut-off

Lingling Tang, Samuel M. Drezdzon, Pantana Tor-Ngern, and Tomoyuki Yoshie
Electrical and Computer Engineering, Fitzpatrick Institute for Photonics
Duke University, Durham, NC 27708-0291, USA

Abstract— An optical isolator is a component that transmits light efficiently in one direction but prevents backward propagation. Integration of optical isolators with other optical devices would improve on-chip optical systems and reduce device size and cost. In the past years a new generation of isolators have been developed that operate on the magneto-optical phenomenon of a nonreciprocal phase shift, rather than polarization conversion as for Faraday rotation based isolators.

Our isolator designs use nonreciprocal band diagrams where isolation is produced by cutoff of backward propagating modes; and the simplicity of single waveguide isolator design, rather than a rotator or interferometer. We propose a novel isolator design that both: (1) operates via backward propagating modecutoff, and (2) employs a simple dielectric waveguide design. Furthermore, we achieve single mode, unidirectional propagation in simulation. Non-reciprocal material is included to break time-reversal symmetry, but the spatial inversion symmetry needs to be broken as well. This is accomplished by distributing magnetic material non-uniformly in the waveguide's cross-section. In our isolator designs, we choose appropriate modes and an inhomogeneous distribution of non-reciprocal materials so that only the forward propagating mode(s) is guided. Single mode isolation is realized between the cut-off frequencies of the lowest forward and backward modes. It should be noted that our designs use neither the phase shift nor a difference in propagation loss between guided forward and backward modes to achieve isolation.

We use non-degenerate perturbation theory at propagation constant $\beta = \beta_0$ to understand the correlation between the inhomogeneity of nonreciprocal materials and nonreciprocal dispersion shifts $\Delta\beta(\omega)$ [1]. This knowledge will help us optimize the isolation bandwidth $\Delta\omega$. The dispersion shift is given by

$$\Delta\beta = 2\omega^2 \left(I_{yx} + I_{xz} + I_{zy}\right) / \left(c^2\beta_0\right) \propto \Delta\omega \tag{1}$$

where

$$I_{ij} = \iint u_{ji}(x,y)\mathrm{Im}\left[E_i^*(x,y)E_j(x,y)\right] dxdy, \tag{2}$$

u_{ji} is an off-diagonal component of the permittivity, and $E_i(x,y)$ is the i-th component of electric field profile in xy plane, assuming that z is propagation direction. Figure shows $\mathrm{Im}[E_i^*(x,y)E_j(x,y)]$ profiles calculated from the lowest TE and TM mode profiles. For the TE mode shown in Figure 1(a), the largest component $\mathrm{Im}[E_z{}^*E_y]$ is odd about $y = 0$, but is almost even about a waveguide mid-plane parallel to the substrate. Therefore, it is desired that the function u_{yz} is odd about $y = 0$, i.e., the "right-left" anti-parallel magnetization is appropriate, and the "right-left" configuration produces a larger isolation for the lowest TE mode than for the lowest TM mode. Two components $\mathrm{Im}[E_i{}^*E_j]$ of the lowest TM mode are shown in Figure 1(b). The largest component $\mathrm{Im}[E_x{}^*E_z]$ is almost odd about waveguide mid-plane, but is even about $y = 0$. Therefore, it is desired that the function u_{zx} is odd about the waveguide mid-plane, i.e., the "up-down" anti-parallel magnetization is appropriate. This perturbation approach is a powerful tool to design magneto-optic isolators. We analyze isolation of singlemode waveguides for bismuth-substituted iron garnet (BIG) on GGG substrate, and clearly see the isolation based on this direction dependent mode cut-off [2]. We also fabricate BIG waveguides on GGG substrates.

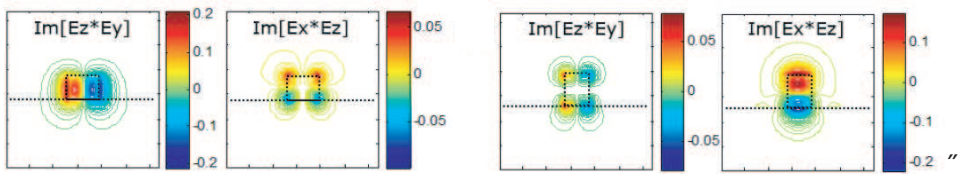

Figure 1: $\mathrm{Im}[E_z{}^*E_y]$ and $\mathrm{Im}[E_x{}^*E_z]$ profiles. (a) TE mode, $h/a = 0.6$ and $w/a = 0.8$. (b) TM mode, $h/a = 0.8$, $w/a = 0.6$.

ACKNOWLEDGMENT

Lingling Tang and Samuel M. Drezdzon equally contribute to the work.

REFERENCES

1. Tang, L., S. M. Drezdzon, and T. Yoshie, "Single-mode waveguide optical isolator based on direction-dependent cutoff frequency," *Opt. Express*, Vol. 16, No. 20, 16202–16208, 2008.
2. Drezdzon, S. M. and T. Yoshie, "On-chip waveguide isolator based on bismuth iron garnet operating via nonreciprocal single-mode cutoff," *Opt. Express*, Vol. 17, No. 11, 9276–9281, 2009.

Session 4P2b
RF Biological Effect, Bioelectromagnetics

Use of Pulse-driven Pico-Tesla Magnetoimpedance Sensor to Detect Cardiac Magnetic Activity on the Surface of the Human Chest

Shinsuke Nakayama[1], **Kenta Sawamura**[1], **Kaneo Mohri**[2], **and Tsuyoshi Uchiyama**[3]

[1]Graduate School of Medicine, Nagoya University, Japan
[2]Aichi Micro Intelligent Co., Japan
[3]Graduate School of Engineering, Nagoya University, Japan

Abstract— Numerous biological electric activities simultaneously induce magnetic field. So far, super-conducting quantum interference device (SQUID) has been applied to detect biomagnetic field, such as magnetoencephalogram and magnetocardiogram. However, SQUID sensors require liquid nitrogen and helium to maintain super-conductivity, and is therefore mounted in a liquid container, separating from biological systems at least several centimeters.

In the present study, in stead of SQUID, we employed a pulse-driven pico-Tesla (pT) magnetoimpedance (MI) sensor with the sensitivity of 0.11 V/A/m [1] to measure cardiac magnetic activity. Electric pulse (5 V in amplitude, 100 ns in duration) were applied to CoFeSiB amorphous wire (7 mm in length, 30 m in radius) at 1 s intervals, and changes in the impedance of the wire was simultaneously measured using a solenoid coil (1 mm in radius, 500 turns) and a sample-and-hold circuit. Since MI sensors work at body temperature, magnetic activity was measured on the surface of the thoracic wall. Respiration was hold at a submaximal inspiration state to rule out the effect of altering the position of the heart and diaphragm. The cardiac magnetic activity perpendicular to the thoracic wall clearly synchronized with electrocardiogram (I lead) simultaneously measured. The power of the magnetic activity was maximal near the V2 point (4th intercostals on the left lateral sternal line), and reduced to less than 50% with the distance of 3 cm.

REFERENCES

1. Uchiyama, T., S. Nakayama, K. Mohri, and K. Bushida, "Biomagnetic field detection using very high sensitive MI sensor for medical application," *Physica Status Solidi A*, Vol. 206, 639–643, 2009.

Differentiation of Human LAN-5 Neuroblastoma Cells by Electronically Trasmitted Retinoic Acid (RA)

Alberto Foletti[1] and Settimio Grimaldi[2]

[1]Independent Researcher, Lugano, Switzerland
[2]Institute of Neurobiology and Molecolar Medicine, CNR, Rome, Italy

Abstract— Previous studies suggest that the electromagnetic molecular signal (EMS) can be digitally recorded and replayed [1]. We electronically captured, and transmitted the specific EMS of Retinoic acid (a potent chemical human cells differentiating agent) to a biological system constituted by human neuroblastama cells line (LAN-5). LAN-5 neuroblastoma cells is one of the most common paediatric solid tumors originating from the sympathoadrenal lineage of neural crest. This tumor shows extremely different clinical phenotypes such as spontaneous regression on one hand and aggressive growth on the other hand. Undifferentiated neuroblastoma cell line (LAN-5) represent a good model to study neuronal differentiation induced by a variety of stimuli such as retinoic acid treatment.

Retinoic acid were placed at room temperature on one coil attached to an oscillator (VEGA select 719), while LAN-5 neuroblastoma cells were placed on another coil and incubate under controlled condition. The oscillator was then turned on for 12 hrs a day for 3 days, after which cells were counted and morphology studied by contrast microscopy. In a control experiment the effect of the differentiating agent directly added to the cell culture could be observed by a decrease in cell growth and the protrusion of neurite like structure typical of the differentiated cells. In a preliminary set of experiments when Retinoic acid where electronically transmitted to the cell culture we could detect an impairment in cell growth (but not in survival) followed by a tendency in cones formation where cones are known to be the precursor of neurite formation. These preliminary results suggest that Retinoic acid molecules emit signals that can be transferred to LAN-5 neuroblastoma cells by artificial physical means in a manner that seems related to the chemical structure of the source molecules.

REFERENCES

1. Thomas, Y., et al., "Activation of human neutrophils by electronically transmitted phorbol-myristate acetate," *Medical Hypotheses*, Vol. 54, 33–39, 2000.

A New Approach to Investigate Long-term Effects of RF Radiation on Cells

Andreas Daus[1], **Michael Goldhammer**[2], **Ulrich Bochtler**[2], **and Christiane Thielemann**[1]

[1]BioMEMS and Bioelectronics Laboratory, University of Applied Sciences Aschaffenburg, Germany
[2]Laboratory for EMC, Faculty of Engineering Sciences, University of Applied Sciences Aschaffenburg Germany

Abstract— Electrogenic cells and their origin tissues are since long target of research focusing on possible biological effects associated with radio frequency electromagnetic fields (RF-EMF). Although there is only little evidence of major health risk arising from the exposure of the human body to EMF at mobile phone frequencies, some of the published results are inconsistent and obviously knowledge gaps remain. In vitro studies are widely established to investigate possible interactions between biological tissue and EMF in a controlled environment. Therefore, explant cultures or cells grown in monolayer on Petri dishes are considered as an appropriate paradigm to mimic in vivo-like conditions. However, explanted slices or organs are typically several millimetres in size and suffer from reduced nutrient supply to central regions and poor viability. Monolayer cultures are afflicted with a highly artificial cellular environment because cell-cell and cell-ECM interactions are limited to a two-dimensional architecture. This results in less physiological relevance of monolayer experiments.

As a novel approach in electromagnetic exposure studies, we use a scaffold-free three-dimensional cell culture system for the investigation of long-term effects in vitro. Induced by permanent rotation, dissociated chick cardiac myocytes aggregate into spheres, so called spheroids. Spheroids are self-contractile up to 45 days in vitro (div), whereas cardiac myocytes grown in monolayers irreversible discontinue contractions after 12 div. We believe that these spheroids combine two striking advantages: (i) Cells within spheroids are grown in a three-dimensional architecture and resemble tissues better in terms of structural and functional properties than monolayer cultures. (ii) Cardiac spheroids are suitable to study long-term effects over several weeks, which is not feasible with monolayer or slice cultures.

For electromagnetic exposition of spheroids, we contribute a flexible, easy-to-use TEM-cell based setup integrated in a CO_2 incubator. This setup is not based on standing waves and thus suitable for a large range of sample bins, frequencies and field strengths, respectively SAR levels. Conditions in the so-called stripline are simulated at 900 MHz by finite element calculation and the setup is optimized in terms of SAR homogeneity and temperature stability. Since all experiments are performed inside a CO_2 incubator, long-term exposures are possible.

In further studies we intent to use spheroids to investigate basic developmental processes during EMF exposition. It has been shown, that fully dissociated cells of the embryonic avian retina can reconstitute spheroids with a complete arrangement of retinal layers. This allows analysis of basic principles of neural layer formation, including key-events in the life circle of cells, such as proliferation, migration or apoptosis. In conclusion, spheroids are a promising approach to investigate in vitro long-term effects as well as developmental processes due to RF radiation in a controlled environment. The presented exposition setup is integrated in a CO_2 incubator and exhibits physiologic cell culture conditions during the experiments indispensable for long-term exposures.

REFERENCES

1. Pampaloni, F., E. G. Reynaud, and E. H. K. Stelzer, "The third dimension bridges the gap between cell culture and live tissue," *Nature Reviews Molecular Cell Biology*, Vol. 8, 839–845, 2007.
2. Layer, P. G., A. Rothermel, and E. Willbold, "From stem cells towards neural layers: A lesson from re-aggregated embryonic retinal cells," *Neuroreport*, Vol. 12, 39–46, 2001.

Effects of Extremely Low Frequency Electromagnetic Fields on the Antioxidant Enzymes Activity of C3 and C4 Plants

Azita Shabrangi[2], **Ahmad Majd**[1], **Masoud Sheidai**[3], **Mohammad Nabyouni**[1], **and Davoud Dorranian**[4]

[1]Department of Biological Science, Faculty of Science, Tarbiat Moalem University, Tehran, Iran
[2]Department of Biology, Tehran North Branch, Islamic Azad University, Tehran, Iran
[3]Biology Faculty, Shahid Beheshti University, Tehran, Iran
[4]Physic Plasma Research Centre, Science and Research Branch, Islamic Azad university, Tehran, Iran

Abstract— This experimental study was dedicated to the possible oxidative stress induced by electromagnetic field accumulation in the living tissues. In this research two states of seeds (wet, dry) of *Brassica napus L* (canola)and *Zea mays L* (maize) were exposed to pulsed EMFs (15 min on, 15 min off) by magnitude of 1 to 7 mT in steps of 2 mT and the highest intensity was 10 mT for 1 to 4 hours in steps of 1 h. Exposure to EMFs was performed by a locally designed EMF generator (1). Three replicates, with 30 seeds in each one were used. Activity of stress enzymes were carried out by spectrophotometer. Our investigation was focused on root and shoot of 7 days seedlings, which showed the most and the least growth comparing to control. Based on statistical analysis, these results were observed in seedlings grown from dry pretreated seeds by 10 mT for 4 h and wet pretreated seeds by 10 for 2 h in canola, and seedlings grown from wet pretreated seeds by 10 and 3 mT both for 4 h exposure in maize. Activity enzymes were expressed based on absorbance against mg fresh weight of root and shoot tissues separately. Both treatment caused significantly decreased in Catalase (CAT) activity in root tissue of maize. But we observed significant increase activity of CAT in shoot. Ascorbate Peroxidaes (APX) activity increased significantly in both treatment and both root and shoot tissues. We observed increase of Superoxide dismutase (SOD) activity in root tissue of maize in both treatment, but 3 mT intensity did not show significant difference. In shoot tissue of maize, we observed significantly increase of SOD activity by 3 mT treatment and significantly decrease by 10 mT treatment. On the other hand, We observed significantly increase in CAT activity in root tissue of canola and significantly decrease of this enzyme activity in shoot tissue of canola. APX activity results were similar to CAT activity in both tissues of this species. Activity of SOD showed increase in both treatment of root tissue of canola. In contrast, SOD activity decreased in shoot tissue of canola in both treatments. But treatment by 10 mT intensity did not cause significant difference of this enzyme activity in both tissues of canola ($P < 0.05$).

In general, activity of all stress enzymes in root tissue of canola increased and in shoot tissue of this species decreased. In contrary, activity of the same stress enzymes in the same tissue of maize showed opposite results, except APX activity in the root tissue, which showed similar result in both species. All results suggested that antioxidant system of canola as a C3 plant and maize as a C4 plant react differently against EMFs.

REFERENCES

1. Shabrangi, A., et al., "Comparing Effects of Electromagnetic Fields (60 Hz) on Seed Germination and Seedling Development in Monocotyledons and Dicotyledons," *Progress In Electromagnetics Research Symposium Abstracts*, Moscow, Russia, August 18-21, 2009.

WI-FI Signal Exposure Effects on Developing Immune System of Young Mice

Saliha Aït-Aïssa[1, 2], Bernard Billaudel[1], Florence Poulletier De Gannes[1], Annabelle Hurtier[1], Emmanuelle Haro[1], Murielle Taxile[1], Axel Athané[2], Gilles Ruffié[3], Tongning Wu[4], Joe Wiart[4], Bernard Veyret[1, 2], and Isabelle Lagroye[1, 2]

[1]IMS laboratory, UMR CNRS 5218 Bioelectronics Group, ENSCPB-IPB, University Bordeaux 1, France
[2]Bioelectromagnetics Laboratory — EPHE/ ENSCPB IPB, University Bordeaux 1, France
[3]IMS Laboratory, IMS Transfert-A2M, ENSCPB, Pessac, France
[4]Orange Labs, Research & Development, Issy les Moulineaux, France

Abstract— In the present work, we investigated the potential effects of Wi-Fi exposure on the developing immune system of young mice. Pregnant C57BL/6 mice were exposed or sham-exposed to a 2.45 GHz Wi-Fi signals. We evaluated the effects on immature immunity of mice by assessing splenocytes phenotype and functionality. The results of this study will provide useful data for health risk assessment by WHO related to RF fields.

Pregnant C57 BL/6 mice, obtained 3 days *post coitum* were acclimated for 4 days. Dams and newborn mice were exposed or sham exposed at three SAR levels (whole-body specific absorption rate: 0.08, 0.4, and 4 W/kg) in a reverberation chamber. This free-running exposure system, specially designed for this study, emits a Wi-Fi signal in a cubic chamber with 6 antennas and mixing of the modes for a symmetrical and uniform exposure of the animals. Daily exposure lasted 2 hours. The groups were exposed for 2 weeks *in utero* and 5 weeks after birth for a total of 7 weeks of exposure. We performed three series of exposure. All experiments were performed blind. Temperature and humidity were controlled during the experiments. At the end of exposure, the 5-week-old mice were sacrificed and spleen collected. Single-cell suspensions were obtained after mechanical dissociation, isolation using a 40 µm cell strainer, and spleen erythrocyte lysis. Natural Killer (NK) cell isolation was performed using magnetic cell separation. Briefly, NK cells were labelled with specific monoclonal antibodies conjugated to paramagnetic particles. NK cells were separated from Tand B-cells using a column. YAC-1 cells derived from mouse lymphoma (ECACC, Salisbury, UK) were used as target cells for the NK cytotoxicity assay.

The number of splenocytes and the cell sub-populations distribution were determined. Evaluation of CD45, CD3, CD4, CD8, CD19, and NK1.1 expression was done by flow cytometry analysis allowing for comparison between exposed and sham-exposed splenocyte phenotypic profiles. We also performed *ex-vivo* stimulation of T and B cells using specific monoclonal antibodies (anti-CD3 and anti-CD28) or LPS for testing their proliferation ability. The functionality of splenocytes was also tested through evaluation of cytokine production (IL-2, TNF and IFN-γ) and expression of activation markers (CD25 and CD69). Finally, NK cell cytotoxic activity was analyzed using flow cytometry. This test was based on YAC-1 target cell labelling with 5-(6)-carboxy-fluorescein succinimidyl ester (CFSE) and subsequent DNA-labelling with 7AAD for identification of target cells with compromised cell membranes. The results are expressed as percentage of dead targets on a cell-to-cell basis.

The ongoing analysis of sub-population phenotype, functionality and responsiveness of lymphocytes will be completed and presented at the meeting.

Session 4P3
Novel Mathematical Methods in Electromagnetics 2

Precursory Electric- and Magnetic-field Variations Analysed in Natural Time

E. S. Skordas, N. V. Sarlis, M. S. Lazaridou, and P. A. Varotsos
Solid State Section and Solid Earth Physics Institute, Physics Department, University of Athens
Panepistimiopolis, Zografos 157 84, Athens, Greece

Abstract— It has been recently shown that novel dynamical features hidden behind time series in complex systems can emerge upon analyzing them in a new time domain, termed natural time [1–6]. In a time series comprising N events, the natural time $\chi_k = k/N$ serves as an index for the occurrence of the k-th event [1, 2], and it is smaller than, or equal to, unity (cf. the symbol χ originates from the ancient Greek word $\chi\rho\acute{o}\nu o\varsigma$ (chronos) which means "time"). In natural time analysis the evolution of the pair of two quantities (χ_k, E_k) is considered, where E_k denotes in general a quantity proportional to the energy of the individual event. The natural time analysis enables the study of the dynamical *evolution* of a complex system and identifies when the system enters a critical stage. Hence, natural time plays a key role in predicting impending catastrophic events in general. Relevant examples of data analysis in this new time domain have been presented in a large variety of fields including earth sciences, biology and physics. As a first example, natural time improves the wavelet analysis of precursory electric and magnetic field variations, termed Seismic Electric Signals (e.g., [7–11]), which lead [1, 2, 5, 6] to the prediction of an impending strong earthquake. Secondly, the analysis of the electrocardiograms, which may herald a cardiac arrest [12–15]. Finally, as a third example we mention that the data of the avalanches of the penetration of magnetic flux into thin films of type II superconductors as well as those of a three dimensional pile of rice getting progressively closer to the critical state (which are typical examples of the so called Self Organized Criticality systems), conform to [16] the features suggested, on the basis of natural time, to describe critical dynamics. Here, we present in detail the prediction of the three major earthquakes that occurred in Greece during 2008 that was achieved and publicized in advance by using natural time analysis [17, 18].

REFERENCES

1. Varotsos, P. A., N. V. Sarlis, and E. S. Skordas, *Practica of Athens Academy*, Vol. 76, 294, 2001.
2. Varotsos, P. A., N. V. Sarlis, and E. S. Skordas, *Phys. Rev. E*, Vol. 66, 011902, 2002.
3. Varotsos, P. A., N. V. Sarlis, and E. S. Skordas, *Phys. Rev. E*, Vol. 67, 021109, 2003.
4. Varotsos, P. A., N. V. Sarlis, and E. S. Skordas, *Phys. Rev. E*, Vol. 68, 031106, 2003.
5. Varotsos, P. A., N. V. Sarlis, H. K. Tanaka, and E. S. Skordas, *Phys. Rev. E*, Vol. 72, 041103, 2005.
6. Varotsos, P. A., N. V. Sarlis, E. S. Skordas, H. K. Tanaka, and M. S. Lazaridou, *Phys. Rev. E*, Vol. 73, 031114, 2006.
7. Varotsos, P. A., K. Alexopoulos, K. Nomikos, and M. S. Lazaridou, *Nature*, Vol. 322, 120, London, 1986.
8. Varotsos, P. and K. Alexopoulos, *Thermodynamics of Point Defects and Their Relation with Bulk Properties*, North Holland, Amsterdam, 1986.
9. Varotsos, P. A., N. V. Sarlis, and E. S. Skordas, *Phys. Rev. Lett.*, Vol. 91, 148501, 2003.
10. Varotsos, P., *The Physics of Seismic Electric Signals*, TerraPub, Tokyo, 2005.
11. Varotsos, P. A., N. V. Sarlis, and E. S. Skordas, *Appl. Phys. Lett.*, Vol. 86, 194101, 2005.
12. Varotsos, P. A., N. V. Sarlis, E. S. Skordas, and M. S. Lazaridou, *Phys. Rev. E*, Vol. 70, 011106, 2004.
13. Varotsos, P. A., N. V. Sarlis, E. S. Skordas, and M. S. Lazaridou, *Phys. Rev. E*, Vol. 71, 011110, 2005.
14. Varotsos, P. A., N. V. Sarlis, E. S. Skordas, and M. S. Lazaridou, *Appl. Phys. Lett.*, Vol. 91, 064106, 2007.
15. Varotsos, P. A., N. V. Sarlis, and E. S. Skordas, *CHAOS*, Vol. 19, 023114, 2009.
16. Sarlis, N. V., P. A. Varotsos, and E. S. Skordas, *Phys. Rev. B*, Vol. 73, 054504, 2006.
17. Uyeda, S., and M. Kamogawa, *Eos Trans. AGU*, Vol. 89, 363, 2008.
18. Sarlis, N. V., E. S. Skordas, M. S. Lazaridou, and P. A. Varotsos, *Proceedings of the Japan Academy, Ser. B*, Vol. 84, 331–343, 2008.

Zero Reflection from a PEC Plate Coated by Double Zero (DZR) Metamaterials

Homayoon Oraizi[1], **Ali Abdolali**[1], **and Noushin Vaseghi**[2]

[1]Department of Electrical Engineering, Iran University of Science and Technology
Tehran 1684613114, Iran
[2]Department of Electrical and Computer Engineering, K. N. Toosi University of Technology
Tehran 16315-1355, Iran

Abstract— We consider a perfect electric conductor (PEC) plate covered by a layer of DZR metamaterial coatings under an oblique plane wave incidence of TM polarization. Several analytical formulas are derived for the realization zero reflection from such structures. Exact formulas will be derived for zero reflection from a DZR coated PEC plate. Then several examples of the applications of DZR metamaterials as zero reflection coatings are provided.

CIP-BS Method for Solving Maxwell's Equations

A. Noba, **S. Murakoshi**, **and Y. Ando**
The University of Electro-Communications, Tokyo, Japan

Abstract—

Introduction: The constrained interpolation profile (CIP) method is the numerical method using field values and their spatial derivatives, and is originally developed in the area of fluid dynamics. The application of the CIP method to electromagnetic dynamics acquires many attention, and related papers have been published [1, 2]. Recently, another CIP method, which is called as CIP — basis set (CIP-BS) method, is developed to solve general hyperbolic equations [3]. In this paper, we consider the CIP-BS method for solving Maxwell's equations.

Formulation: As an example, here we present formulation of the CIP-BS method for the one-dimensional case where E_z and H_y are nonzero components. E_z and H_y are expanded into the series of the basis functions defined in the computational region R, with unknown coefficients and the inner product between the fields and test functions yields the linear equations for the coefficients.

Basis functions, $\phi_0(x)$, $\psi_0(x)$, which satisfy the following conditions can be defined.

$$\phi_0(x) = 0 \text{ at } x = \pm\Delta x, \ = 1 \text{ at } x = 0, \ \frac{d\phi}{dx}(x) = 0 \text{ at } x = \pm\Delta x, 0 \tag{1}$$

$$\psi_0(x) = 0 \text{ at } x = \pm\Delta x, 0, \ \frac{d\psi}{dx}(x) = 0 \text{ at } x = \pm\Delta x, \ = 1 \text{ at } x = 0, \tag{2}$$

The explicit form of the basis functions are given in terms of piecewise cubic polynomials by

$$\phi_0(x) = \pm\frac{2}{\Delta x^3}x^3 - \frac{3}{\Delta x^2}x^2 + 1, \ (-\Delta x \le x \le 0, \, 0 < x \le +\Delta x), \ = 0 \ (|x| > \Delta x) \tag{3}$$

$$\psi_0(x) = \pm\frac{1}{\Delta x^2}x^3 \mp \frac{2}{\Delta x}x^2 + x, \ (-\Delta x \le x \le 0, \, 0 < x \le +\Delta x), \ = 0 \ (|x| > \Delta x). \tag{4}$$

The basis function set for electric fields is defined as $\{\phi_i(x) = \phi_0(x - i\Delta x)\}$ and $\{\psi_i(x) = \psi_0(x - i\Delta x)\}$. The set for magnetic fields is defined as the same functions but with staggered grids. Therefore, the electric fields at $t = n\Delta t$ and magnetic fields at $t = (n+\frac{1}{2})\Delta t$ are represented by

$$E_z^n(x) = \sum_i^N \left\{ E_i^{0,n}\phi_i(x) + E_i^{1,n}\psi_i(x) \right\}, \quad H_y^{n+\frac{1}{2}}(x) = \sum_i^N \left\{ H_{i+\frac{1}{2}}^{0,n+\frac{1}{2}}\phi_{i+\frac{1}{2}}(x) + H_{i+\frac{1}{2}}^{1,n+\frac{1}{2}}\psi_{i+\frac{1}{2}}(x) \right\}. \tag{5}$$

Note that the electric field $E_z(x)$ and its derivative at $i\Delta x$ are E_i^0, and are E_i^1, respectively.

Here we adopt the leap-frog scheme to obtain the update equations in vacuum:

$$E_z^n(x) = E_z^{n-1}(x) = \frac{\Delta t}{\epsilon_0}\left(\frac{dH_y}{dx}\right)^{n-\frac{1}{2}}, \quad H_y^{n+\frac{1}{2}} = H_y^{n-\frac{1}{2}} + \frac{\Delta t}{\mu_0}\left(\frac{dE_z}{dx}\right)^n. \tag{6}$$

Taking the inner product with test functions (we use the basis functions for the present case), which means multiplication with the basis functions and integration over R, gives linear equations, for example,

$$\sum_{l=i-1}^{i+1}\sum_{m=0}^{1} S_l^m E_l^{m,n} = \sum_{l=i-1}^{i+1}\sum_{m=0}^{1} S_l^m E_l^{m,n-1} + \sum_{l=i-2}^{i+1}\sum_{m=0}^{1} L_l^m H_{l+\frac{1}{2}}^{m,n}, \tag{7}$$

$$S_l^0 = \langle\phi_i|\phi_l\rangle, \ S_l^1 = \langle\phi_i|\phi_l\rangle, \ L_l^0 = \left\langle \phi_i|\frac{d\phi_{l+\frac{1}{2}}}{dx}\right\rangle, \ L_l^1 = \left\langle \phi_i|\frac{d\psi_{l+\frac{1}{2}}}{dx}\right\rangle. \tag{8}$$

By solving the equasions, we can obtain time-varying electromagnetic fields.

ACKNOWLEDGMENT

This work is partially supported by "R&D promotion scheme funding international joint research" promoted by NICT(National Institute of Information and Communications Technology).

REFERENCES

1. Ando, Y. and M. Hayakawa, "Implementation of the perfect matched layer for the CIP method," *IEICE Trans. Electron.*, Vol. E89-C, No. 5, 645–648, May 2006.
2. Ando, Y., H. Saito, and M. Hayakawa, "A nearly perfect total-field/scattered-field boundary for the one-dimensional CIP method," *IEICE Trans. Electron.*, Vol. E91-C, No. 10, 1677–1683, October 2008.
3. Utsumi, T., T. Yabe, et al., "Solutions of hyperbolic equations with the CIP-BS method," *JSME Int. J., B*, Vol. 47, No. 4, 768–776, 2004.

Analysis of Electromagnetic Guided Waves on Curved Conducting Biological Surface by Conformal Mapping Method

Yasumitsu Miyazaki
Department of Media Informatics, Aichi University of Technology
50-2 Manori, Nishihasama-cho, Gamagori 443-0047, Japan

Abstract— High frequency signal transmissions using human body sensors and transmission antennas have been studied, as biomedical communication systems of high frequency electromagnetic guided waves on biological surfaces of lossy conducting media for medical diagnosis and information communication. In these biomedical systems, the first section of transmission is consisting of human body medical sensor and transmission antenna on the body surface that is signal transmission source, and receive terminal antenna that is receiver, through transmission waveguide with body surface boundary of body media. The second section of transmission is consisting of transmission source output that is receiver of the first section, and usual information transmission line of pair cables or coaxial and optical cables and further, transmission antenna.

In this paper, electromagnetic eigen characteristics of high frequency fields in lossy waveguides consisting of lossy human body with conducting bio-medical body surface that is boundary surface of waveguide are discussed.

In the first section of this paper, electromagnetic characteristics such as permittivities and conductivities of human tissues of bloods, muscles and bones are discussed for several frequencies. In the second section, electromagnetic eigen fields in lossy waveguides consisting of human bodies, such as arms and legs, with bio-medical body surfaces are studied by approximate sub-stationary analysis and exact hybrid field analysis for high frequencies. Propagation constants with phase and attenuation characteristics of hybrid modes are derived by eigen-equations for lossy waveguides consisting of conducting human body with skin surfaces. Green's dyadic functions for lossy hybrid fields in the human body are studied by vector wave equations and boundary conditions of electromagnetic fields on skin surfaces.

In the last section, by using conformal mapping method with Greens dyadic functions for straight lossy waveguides of human body with skin surfaces, electromagnetic fields in curved lossy waveguides of curved arms and legs corresponding to human elbows and knees are discussed as shown in Fig. 1. Curved lossy waveguide in physical space (X, Y, Z) is transformed to straight lossy inhomogeneous waveguide in mapped (x, y, z) space by conformal mapping with analytic function. By using conformal mapping method and integral equation with Green's function that can be applied to analysis of complicated electromagnetic field boundary problems developed by the author 1-5), electromagnetic guided characteristics of electromagnetic fields on curved conducting biological body surfaces are investigated. Fundamental properties of medical application of high frequency signal transmission on human body surfaces are shown.

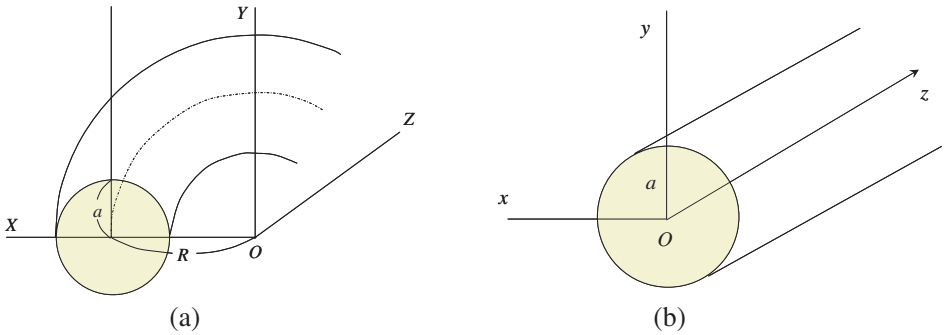

Figure 1: Curved lossy waveguide and conformal mapping. (a) Curved lossy waveguide in (X, Y, Z) space, (b) straight lossy waveguide in mapped (x, y, z) space.

REFERENCES

1. Udagawa, K. and Y. Miyazaki, *I.C.M.M.I*, Vol. M-2-2, 21–22, Tokyo, 1964.
2. Udagawa, K. and Y. Miyazaki, *Jour. of IECE*, Vol. 47, No. 8, 1186–1195, 1964.

3. Miyazaki, Y., "Opical meeting on integrated optics," *OSA, IEEE*, Vol. A-2, Las Vegas, 1972.
4. Miyazaki, Y., *Opt. and Quantum Electron.*, Vol. 9, 153–165, 1977.
5. Miyazaki, Y., *Electromagnetic Waves & Electronic Systems*, Vol. 5, No. 1, 32–45, 2000.

Signal Analysis of Electromagnetic Wave Propagation for RFID Systems in In-door and Out-door

Yasumitsu Miyazaki[1], **Tadahiro Hashimoto**[2], **and Koichi Takahashi**[1]

[1]Department of Media Informatics, Aichi University of Technology
50-2 Manori, Nishihasama-cho, Gamagori 443-0047, Japan
[2]Broadband Technology Department, Synclayer, Inc., 1-20 Himegaoka, Kani 509-0249, Gifu, Japan

Abstract— In recent years, RFID systems have received much attention in information management and security. For evaluation of RFID systems, study of electromagnetic wave propagation and scattering of UHF wave and microwave transmitted from tag antenna to reader antenna in in-door and out-door is indispensable. In this paper, we describe the characteristics of electromagnetic wave scattering, diffraction and interference by obstacles in propagation channel and show the distribution of received level using FDTD method [1, 2]. In transmitting and receiving points of the weak electromagnetic wave, receiving characteristics are influenced by the propagation environment. We have considered high-speed data communication by microwave in urban area using parallel FDTD computation [3]. In RFID systems, receiving characteristics are strongly influenced by the structure of roads and buildings for out-door environment and rooms, doors and windows for in-door environment. Three-dimensional analysis is studied by numerical simulation for the optimum design of RFID system. Comparing the results of two dimensional analysis and three dimensional analysis, the effects of the earth of roads and building with finite heights for out-door application and effects of ceil and floor of buildings for in-door application can be evaluated.

As an in-door propagation model, a building including several rooms with doors is considered. For out-door propagation model, a road model with buildings as shown in Fig. 1 is considered. RF tags are carried by human on the road and readers are installed on the electric pole. Evaluation of out-door propagation characteristics of RFID is necessary to develop high performance antenna system of readers [4–6]. Figs. 1(a) and (b) show several rooms and the T-type road. Road parameters with the earth are width W_1 and width W_2, and the height of building walls H. Here,

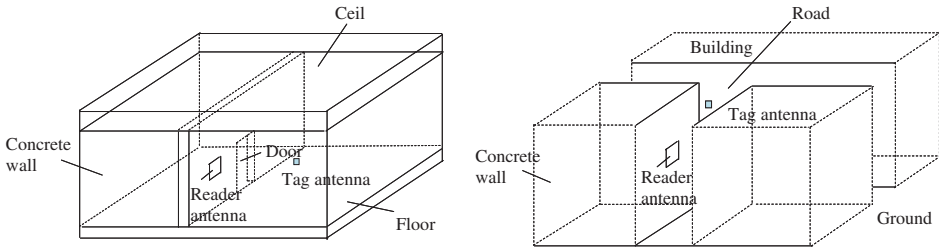

(a) RFID for in-door application (b) RFID for out-door application

Figure 1: Propagation model for RFID system.

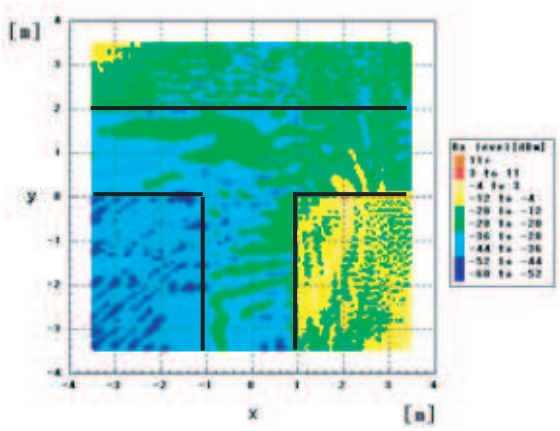

Figure 2: Received level by threedimensional FDTD analysis ($z = 1\,\mathrm{m}$).

building walls are considered as concrete whose relative dielectric constant is ε_r. The received levels of two dimensional analysis with tag position $(x, y) = (2\,\text{m}, 0\,\text{m})$ and $f_c = 426\,\text{MHz}$ are studied with road parameters $L_1 = 8\,\text{m}$, $L_2 = 4\,\text{m}$, $W_1 = W_2 = 2\,\text{m}$ and $\varepsilon_r = 6$. Received level along the street is strong due to the multiple reflection between the building walls. There are shadow regions with weak received level in vertical street when tag is in horizontal street. Fig. 2 shows the received level at $z = 1\,\text{m}$ by three dimensional analysis. The wave source is half wavelength antenna with feed point $(x, y, z) = (2\,\text{m}, 0\,\text{m}, 1\,\text{m})$. The height of walls $H = 5\,\text{m}$ and road parameters are corresponds to Fig. 2.

These simulations are very useful to obtain the fundamental data for optimum position system design of readers. We are also studying parallel FDTD computation for three dimensional wide area analysis and results by three dimensional analysis and two dimensional analysis are compared precisely.

REFERENCES

1. Masuda, T. and Y. Miyazaki, *Trans. IEE Japan*, Vol. 118-C, No. 1, 112–117, 1998.
2. Miyazaki, Y. and K. Takahashi, *Proc. Asia-Pacific Conference on Environmental Electromagnetics*, 251–256, Shanghai, China, 2000.
3. Rodriguez, G., Y. Miyazaki, and N. Goto, *IEEE Trans. Antennas & Propag.*, Vol. 54, No. 3, 785–796, 2006.
4. Taki, K. and Y. Miyazaki, "Input impedances and current distributions for meander line antennas with planar coupled parasitic meander element," *PIERS Proceedings*, 1700–1703, Beijing, China, March 26–30, 2007.
5. Masuda, T., Y. Miyazaki, and Y. Kashiwagi, "Analysis of electromagnetic wave propagation in out-door active rfid system using FD-TD method," *PIERS Online*, Vol. 3, No. 6, 937–939, 2007.
6. Cao, Y. and Q. Zhang, "High-speed I/O buffer modeling for signal-integrity-based design of VLSI interconnects," *PIERS Proceedings*, 1383–1386, Beijing, China, March 23–27, 2009.

Dimensional Effects on Electric Potentials and Fields in High-permittivity Thin Films and Interfaces

Rainer Dick
Physics & Engineering Physics, University of Saskatchewan
116 Science Place, Saskatoon SK S7N 5E2, Canada

Abstract— An effective Lagrange density for electromagnetic fields in the presence of a high-permittivity thin film or interface yields an analytic expression for electromagnetic potentials which interpolates between the two-dimensional logarithmic Coulomb potential at short distances and the three-dimensional Coulomb potential at large distances. The dimensionally hybrid potential turns out to be the Green's function which also describes density of states and electron scattering in the presence of an interface of different effective electron mass [1–3].

It is also shown that the analytic expression for the dimensionally hybrid electromagnetic potential is a very good approximation to the infinite series solution from image charges.

ACKNOWLEDGMENT

This research was supported by NSERC Canada.

REFERENCES

1. Dick, R., "Hamiltonians and Green's functions which interpolate between two and three dimensions," *Int. J. Theor. Phys.*, Vol. 42, 569–581, 2003.
2. Dick, R., "Dimensionally hybrid Green's functions and density of states for interfaces," *Physica E*, Vol. 40, 524–530, 2008.
3. Dick, R., "Dimensionally hybrid Green's functions for impurity scattering in the presence of interfaces," *Physica E*, Vol. 40, 2973–2976, 2008.

Mixed-impedance Boundary Conditions

I. V. Lindell, A. Sihvola, and H. Wallén
Department of Radio Science and Engineering
School of Science and Technology, Aalto University, Finland

Abstract— The classical impedance boundary condition defines a linear relation between time-harmonic electric and magnetic field components tangential to the boundary surface. Denoting the outer normal unit vector by $\mathbf{n}$, the tangential component of the electric field is obtained as

$$\mathbf{E}_t = \overline{\overline{\mathbf{Z}}}_s \cdot \mathbf{n} \times \mathbf{H}, \tag{1}$$

where $\overline{\overline{\mathbf{Z}}}_s$ is the two-dimensional surface-impedance dyadic.

Recently, boundary conditions in terms of field components normal to the boundary have been considered [1, 2] and two conditions dubbed as DB-boundary and D'B'-boundary conditions were respectively defined for the planar boundary $z = 0$ with $\mathbf{n} = \mathbf{u}_z$ as

$$\mathbf{u}_z \cdot \mathbf{D} = 0, \quad \mathbf{u}_z \cdot \mathbf{B} = 0, \tag{2}$$

and

$$\partial_z \mathbf{u}_z \cdot \mathbf{D} = 0, \quad \partial_z \mathbf{u}_z \cdot \mathbf{B} = 0. \tag{3}$$

The DB conditions (2) were introduced already in 1959 by Rumsey, but applications were suggested only very recently [2–4].

It has been shown that the planar DB boundary acts as a PEC plane for fields polarized TE with respect to the normal of the plane and PMC plane for the TM field. Similarly, the planar D'B' boundary acts as PMC and PEC planes for the TE and TM fields, respectively. The purpose of this paper is to study a novel more general set of boundary conditions which follow by assigning separate impedance boundary conditions for the TE and TM components of the field. The resulting conditions have the form

$$\mathbf{E}_{TE} = Z_{TE}\mathbf{u}_z \times \mathbf{H}_{TE}, \tag{4}$$

$$\mathbf{H}_{TM} = -\frac{1}{Z_{TM}}\mathbf{u}_z \times \mathbf{E}_{TM} \tag{5}$$

and they define what will be called the mixed-impedance conditions for the planar boundary. It turns out that from (4) and (5) it follows that the normal components of the total field satisfy the boundary conditions

$$jk\eta\mathbf{u}_z \cdot \mathbf{H} - Z_{TE}\partial_z \mathbf{u}_z \cdot \mathbf{H} = 0, \tag{6}$$

$$jkZ_{TM}\mathbf{u}_z \cdot \mathbf{E} - \eta\partial_z \mathbf{u}_z \cdot \mathbf{E} = 0. \tag{7}$$

Obviously, (6) and (7) generalize the DB and D'B' boundary conditions (2), (3) for isotropic media. The paper discusses the extension of (6) and (7) to more general boundaries and considers scattering from a mixed-impedance sphere.

REFERENCES

1. Lindell, I. V. and A. Sihvola, "Electromagnetic boundary condition and its realization with anisotropic metamaterial," *Phys. Rev. E*, Vol. 79, No. 2, 026604, 2009.
2. Lindell, I. V., A. Sihvola, P. Ylä-Oijala, and H. Wallén, "Zero backscattering from self-dual objects of finite size," *IEEE Trans. Antennas Propag.,* Vol. 57, No. 9, 2725–2731, September 2009.
3. Zhang, B., H. Chen, B. I. Wu, and J. A. Kong, "Extraordinary surface voltage effect in the invisibility cloak with an active device inside," *Phys. Rev. Lett.*, Vol. 100, 063904 (4 pages), 2008.
4. Yaghjian, A. and S. Maci, "Alternative derivation of electromagnetic cloaks and concentrators," *New J. Phys.*, Vol. 10, 115022 (29 pages), 2008. "Corrigendum," *ibid.*, Vol. 11, 039802 (1 page), 2009.

A Model for Electromagnetic Wave Scattering by Small Ferrite Particles with Magnetostatic-Vortex Resonances

E. O. Kamenetskii
Department of Electrical and Computer Engineering, Ben Gurion University of the Negev
Beer Sheva, Israel

Abstract— The problem of electromagnetic (EM) scattering established by Mie theory indicates that a small transparent particle can lead to the energy localization in the area below the diffraction limit. Based on the Mie solutions, it was pointed that in small particles with plasmon (quasielectrostatic) resonances one has anomalous light scattering characterized by giant optical resonances with enhanced scattering cross sections [1]. Recently, it was shown that a small ferrite-disk particle with magnetic-dipolar (quasimagnetostatic) oscillations excited by microwave EM fields can be represented as a rotating magnetic dipole [2]. This gives a very peculiar mechanism of scattering of microwave EM fields by small ferrite particles with magnetostatic (MS) resonances. Analytical and numerical studies show that small ferrite disks with MS resonances are characterized by vortex behaviors [2, 3]. For incident EM waves, these vortex topological singularities act as traps, providing purely subwavelength confinement of the microwave fields. A fascinating effect of symmetry breaking for the fields was found in the vicinities of the MS resonances [4]. The aim of this paper is to develop an analytical model for electromagnetic wave scattering by small ferrite particles with MS-vortex resonances.

In small ferrite samples, the electromagnetic boundary problem cannot be formally reduced to the complete-set Maxwell-equation representation. The spectral properties of a quasi-2D ferrite disk were analyzed based on the Walker equation for MS-potential wave function $\psi(\vec{r}, t)$ [5]. For the scattering problem, proper integrable solutions can be obtained from an analysis of the MS-wave propagation in a helical coordinate system [6]. It was shown [7] that for a quasi-2D ferrite disk, the helical MS-mode solutions can be separated into azimuthally rotating cylindrical and "thickness" modes.

Helical MS waves are generating scalar wave functions for eigen electric and magnetic fields in a ferrite disk. There are rotating fields with amplitude variations along a disk axis [3]. In the suggested model for electromagnetic wave scattering by ferrite-disk particles with MS-vortex resonances, an analysis is made both in the rotating and laboratory frames. In the rotating coordinate system, the fields are expanded by cylindrical harmonics taking into account amplitude variations along a disk axis for every mode. Further transformation for the fields from the rotating to laboratory coordinate systems gives the scattering problem solution.

REFERENCES

1. Tribelsky, M. I. and B. S. Luk'ynchuk, *Phys. Rev. Lett.*, Vol. 97, 263902, 2006.
2. Kamenetskii, E. O., M. Sigalov, and R. Shavit, *J. Appl, Phys.*, Vol. 105, 013537, 2009.
3. Sigalov, M., E. O. Kamenetskii, and R. Shavit, *J. Phys.: Condens. Matter*, Vol. 21, 016003, 2009.
4. Kamenetskii, E. O., M. Sigalov, and R. Shavit, "Magnetic-dipolar-mode vortices and microwave subwavelength metamaterials," http://arxiv.org/abs/0908.4383, 2009.
5. Kamenetskii, E. O., *J. Phys. A: Math. Theor.*, Vol. 40, 6539, 2007.
6. Kamenetskii, E. O., *J. Magn. Magn. Mater.*, Vol. 302, 137, 2006.
7. Kamenetskii, E. O., "Space-time symmetry violation of the fields in quasi-2D ferrite particles with magnetic-dipolar-mode oscillations," http://arxiv.org/abs/0909.4920, 2009.

Solution of Axisymmetric Potential Problem in Spherical Coordinates Using Exodus Method

O. D. Momoh, M. N. O. Sadiku, and C. M. Akujuobi
College of Engineering, Prairie View A&M University, Prairie View, TX 77446, USA

Abstract— The Monte Carlo Methods have been applied with great success to the solution of electromagnetic and heat conduction problems in both Cartesian and cylindrical coordinates systems, but have not been widely used in the solution of same problems in spherical coordinates system. Specifically, the authors have not come across any literature in which the Exodus method has been used to solve problems in spherical coordinates system.

In this paper, we implement the use of Exodus method for numerically computing the potential distribution in a conducting spherical shell. The Exodus method like other Monte Carlo techniques, compute the solution of a problem at a point in time thereby greatly saving computational resources. However, unlike the conventional Monte Carlo methods the Exodus method is not dependent on a random number generator. Thus, it has been found to yield more accurate results with less computing time as compared to the conventional Monte Carlo methods.

The singularities encountered at the poles ($\theta = 0, \pi$) of the sphere are treated by taking a quarter of the conducting spherical shell. This resulted in two lines of symmetries along $\theta = 0$ and $\theta = \frac{\pi}{2}$ respectively. On these lines of symmetries, a Neumann boundary condition $\frac{\partial V}{\partial \theta} = 0$ is imposed, while Dirichlet boundary conditions are imposed on the constant spherical surfaces. This strategy led to the elimination of the singularity causing term ($\frac{\cot(j\Delta\theta)}{2i^2\Delta\theta}$) at the spherical poles. Based on these boundary conditions, the dispersed particles are absorbed at the constant spherical surface boundaries while they are totally reflected at the two lines of symmetry.

The transition probabilities for the movement of the dispersed random walking particles in the solution region are obtained from the finite difference scheme (central difference) transformation of the Laplace equation in spherical coordinates. The transition probabilities are modified appropriately along the two lines of symmetry to account for the eliminated singularity causing term. In order to obtain a highly accurate result, a large number of particles need to be released for dispersion. In this work a million (10^6) was released.

The computed results obtained using this method perfectly match those obtained from the exact solution approach.

Exactly Solvable High-frequency Model of a Coil

Dierk Bormann
ABB Corporate Research, Sweden

Abstract— In the present paper a simple, analytical high-frequency model of a long, homogeneous coil, with or without iron core, is formulated and analyzed. A practical realization of this model is the high-voltage winding of a voltage measurement transformer. Typical high-voltage windings of power transformers are similar but present additional complications due to the disk structure of windings and to interleaving.

Our model is essentially a transmission line model, extended by adding homogeneously distributed stray capacitances which connect different sections of the line ("series capacitances") as well as mutual inductances between different sections. Deviations from homogeneity as well as coil-end effects can be handled at a later stage by perturbation theory, which is also briefly addressed.

It has been pointed out repeatedly in the literature (see for instance Ref. [1], p. 344) that adding series capacitance to a transmission line model (as a means to describe a transformer winding) leads to an upper limit frequency for propagating modes. At frequencies above that limit, the winding essentially behaves as a capacitance network. Surprisingly, as we show here using our model, this effect is reversed (i.e., the limit frequency is moved back to infinity) by the presence of mutual inductance.

We also report measurements on a real voltage transformer and show that they are in excellent agreement with the predictions of our model. The measurements display a characteristic deviation from the simple transmission line behavior, affecting the location of poles and zeros of the winding admittance function relative to each other, which is explained by our model in a natural way.

In conclusion, we believe that our simple analytical model will be a powerful tool for further assessing the transient and high-frequency response of real voltage transformers and other simple coils in electrical machines. Moreover, it may be a useful starting point for modeling and understanding more complex types of coils.

REFERENCES

1. Greenwood, A., *Electrical Transients in Power Systems*, 2nd Edition, John Wiley, New York, 1991.

Perturbation Theory and FRA Sensitivity Analysis

Dierk Bormann
ABB Corporate Research, Sweden

Abstract— Reliable assessment of damages to transformer or machine windings by measurement of their electric frequency response (so-called Frequency Response Analysis, or FRA) requires detailed knowledge about how these response functions depend on changes of local stray inductance and capacitance parameters. In theoretical studies, this dependence is usually inferred from computer simulations of detailed models reflecting the geometrical design of the winding in question, in which one then introduces the same types of damages as expected in reality. This kind of approach does not usually lead to any deeper understanding of the connection between geometrical change and change in the response, so that for any new design (or any new type of damage) the simulations essentially have to be repeated, an approach which can become computationally very expensive and thus is dissatisfactory.

In this paper, we attempt to arrive at a more general understanding of this connection, by applying concepts of perturbation theory [1] to transformer or machine windings viewed as electromagnetically resonating systems. A theoretical framework is developed for treating for instance damping, inhomogeneities, interactions between sub-systems, boundary conditions, etc. as small perturbations.

This new approach is illustrated on the magnetic couplings between different phase limbs in a three-phase transformer, where specific features ("resonances") of measured response spectra are explained in terms of mode hybridization and resonance level splitting by symmetry-breaking interactions. Furthermore, we show how the approach can be used to analyze the sensitivity of the FRA method with respect to typical damages of transformer windings. It is argued that the method has great potential for tackling the FRA interpretation problem [2].

REFERENCES

1. Morse, P. M. and H. Feshbach, *Methods of Theoretical Physics*, Parts I and II, Mc Graw Hill Inc., New York, 1953.
2. Picher, P., et al., "Mechanical condition assessment of transformer windings using frequency response analysis (FRA)," Final Report of Cigré WG A2.26, *ELECTRA*, No. 237, 35–45, April 2008. *CIGRE Technical Brochure*, No. 342, 67, April 2008.

Session 4P4
Circuits and Devices, CAD

Behavioral Modeling of Asymmetric Intermodulation Distortion of Nonlinear Amplifier

A. H. Yuzer[1, 2] and S. Demir[1]

[1]Electrical and Electronics Engineering, Middle East Technical University, Ankara, Turkey
[2]Electrical and Electronics Engineering, Zonguldak Karaelmas University, Zonguldak, Turkey

Abstract— Amplifier characterization is an important issue especially in the design of amplifiers and systems involving amplifiers such as linearizers and wireless communication systems. Behavioral modeling is one of the characterization techniques where a mathematical relation between input and output is constructed. Conventional power series expansion is one of the methods of behavioral modeling of an amplifier. A sample power series expansion (GPSA) to model the fifth order nonlinearity is as follows:

$$V_o(t) = a \times V_i(t) + c \times V_i^3(t) + e \times V_i^5(t) \tag{1}$$

where V_i and V_o represents the input and output signal respectively, and "a", "c" and "e" are coefficients to be found. These coefficients can be taken as real numbers for AM/AM distortion modeling and as complex numbers to include AM/PM distortion. When an amplifier is excited with a two-tone signal, inter-modulation distortion (IMD) appears as in-band distortion. Representation of the two-tone input signal and the response of the amplifier to this input signal are shown in Figure 1. Two-tone input signal and lower band IMD (IMDL) and upper band IMD (IMDU) equations are given in (2) and (3).

$$V_i(t) = V_1 \cos \omega_1 t + V_2 \cos \omega_2 t \tag{2}$$

$$\begin{aligned} V_{1MDL} &= \frac{3}{4} c V_1^2 V_2 + e \frac{5}{4} \left[V_1^4 V_2 + \frac{3}{2} V_1^2 V_2^3 \right] \\ V_{1MDU} &= \frac{3}{4} c V_2^2 V_1 + e \frac{5}{4} \left[V_2^4 V_1 + \frac{3}{2} V_2^2 V_1^3 \right] \end{aligned} \tag{3}$$

If equal amplitude excitation is assumed, IMD components will be of equal amplitude; $V_{1MDL} = V_{1MDU}$. This means that there is no asymmetry in the IMD expression given in (3). However, there is an inherent asymmetrical distribution of magnitude and phase of IMD components in measurement, which means that (1) require correction.

In the current study, asymmetry in magnitude and phase is modeled by introducing time delay to the power series components in (1). Namely, a power series with time delay (PSwTD) is introduced. According to our proposed model input-output relation and resultant IMD components for equal excitation tone are found as given in (4) and (5). "$\dot{a}$", "$\dot{c}$", "$\dot{e}$", "$\dot{g}$", and "$\dot{k}$" are real numbers and different than the coefficients given in (3). 9th order model polynomial is used to widen validity range instead of fifth order.

A sample fabricated amplifier is used to construct its behavioral model. Gain is greater than 43 dB around working frequency. Two-tone input signal is applied to the amplifier at 2.5 MHz and 2.501 MHz.

In order to constitute and then compare the PSwTD model estimation and, measured result "$\dot{c}$", "$\dot{e}$", "$\dot{g}$", "$\dot{k}$", "τ_3", "τ_5", "τ_7" and "τ_9" coefficients are found by using optimization as given in Table 1. After finding the coefficients, the PSwTD model is constituted and compared with

Table 1: Model Coefficients.

a	c	e	g	k
139,4	$-257,3$	$2,508E+3$	$1,161E+4$	$-1,803E+4$
τ_1 (n sn)	τ_3 (n sn)	τ_5 (n sn)	τ_7 (n sn)	τ_9 (n sn)
$-5858,3$	$-9023,3$	$-12252,7$	$-9776,85$	$-8967,97$

measurement results. Comparison between model estimation and measurement results for magnitudes of ImdL, ImdU, lower band Fundamental component (FL) and upper band Fundamental component (FU) is given in Figure 2. Also comparisons of model estimation and measurement results for phases of ImdL, ImdU, FL and FU are given in Figure 3.

$$V_o(t) = \dot{a} \times V_i(t-\tau_1) + \dot{c} \times V_i^3(t-\tau_3) + \dot{e} \times V_i^5(t-\tau_5) + \dot{g} \times V_i^7(t-\tau_7) + \dot{k} \times V_i^9(t-\tau_3) \quad (4)$$

$$\begin{aligned} V_{IMDL} =& \frac{3}{4}\dot{c}V_1^3\angle(-(2\omega_1-\omega_2)\tau_3) + \frac{25}{8}\dot{e}V_1^5\angle(-(2\omega_1-\omega_2)\tau_5) \\ &+ \frac{735}{64}\dot{g}V_1^7\angle(-(2\omega_1-\omega_2)\tau_7) + \frac{1323}{32}\dot{k}V_1^9\angle(-(2\omega_1-\omega_2)\tau_9) \\ V_{IMDU} =& \frac{3}{4}\dot{c}V_1^3\angle(-(2\omega_2-\omega_1)\tau_3) + \frac{25}{8}\dot{e}V_1^5\angle(-(2\omega_2-\omega_1)\tau_5) \\ &+ \frac{735}{64}\dot{g}V_1^7\angle(-(2\omega_2-\omega_1)\tau_7) + \frac{1323}{32}\dot{k}V_1^9\angle(-(2\omega_2-\omega_1)\tau_9) \end{aligned} \quad (5)$$

Error is always lower than 2.5 dB for magnitude of IMDL and IMDU and maximum error is 2dB for magnitude of FL and FU for lower than 3 dBm input power as seen is Figure 2.

Error is always lower than 10° for magnitude of IMD components and error is always lower than 1° for phase of FL and FU for lower than 3 dBm imput power level.

Simultaneous and Synchronous Measurement of Even and Odd Order Nonlinear Distortion Terms

S. K. Remillard
Physics Department, Hope College, 27 Graves Place, Holland, MI 49423, USA

Abstract— Nonlinear distortion is usually measured at different frequencies, such as $2f, 3f, \ldots$ for harmonic distortion and $f_1 + f_2, 2f_2 - f_1, \ldots$ for two-tone intermodulation distortion (IMD). This limits the physical insight available from these measurements because the distortion products are generated at different frequencies and different spatial locations in a distributed element device sample. This paper will describe a new technique to characterize nonlinear distortion in which products of even and odd order are generated at the same frequency and the same location in the driving field region [1]. The sample under test is exposed to three tones. Two probing tones at frequencies f_1 and f_2, which are very similar in frequency, are introduced at a specific location with a small probe. This determines the location of the nonlinear generation. A third driving tone at f_3, which is much higher in frequency than f_1 and f_2, determines the frequency of the nonlinear generation. With the three tones, 2nd order intermodulation occurs at $f_3 + f_2$ and 3rd order intermodulation occurs at $f_3 + (f_2 - f_1)$, among other mixing terms. By setting f_3 much higher than f_1 and f_2 by at least two orders of magnitude, the 2nd and 3rd order nonlinearity are generated at virtually the same frequency.

The technique was developed first in order to study the spatially dependent nonlinearity currents in high temperature superconducting thin film microstrip microwave resonators. f_3 was set to the 910 MHz resonant frequency of the microstrip. Because current is distributed throughout a resonator, the measured harmonics at $2f_3$ and $3f_3$ are weighted averages over the resonator, and give no useful spatial information. Instead, probing with f_1 and f_2, which are non-resonant, produces three-tone IMD terms which are generated locally in the vicinity of the probing tones. Because the 2nd and 3rd order IMD are within the resonant band of the microstrip, they then couple into the resonance and are detected by a stationary coupling probe. This technique can work in principle with samples that do not support a convenient microwave resonance by introducing the driving tone, f_3, through a resonating structure and allowing the generated nonlinearity to couple into that resonance. This concept and its potential for use in the scanning of any nonlinear surfaces will also be presented.

ACKNOWLEDGMENT

Supported by a grant from the Research Corporation.

REFERENCES

1. Pease, E. K., B. J. Dober, and S. K. Remillard, "Synchronous measurement of even and odd order intermodulation distortion at the resonant frequency of a superconducting resonator," Submitted to *Review of Scientific Instruments*, November 15, 2009.

YIG Thin Film Used to Fabricate a Coplanar Waveguide Circulator

Bassel Abdel Samad[1, 2]

[1]Laboratoire DIOM (Dispositifs et Instrumentation en Optoélectronique et Micro-ondes)
TELECOM Saint-Etienne, École Associée de L'Institut TELECOM
Université de Saint-Etienne, F-42000, Saint-Etienne, France
[2]Université de Lyon, F-69000, Lyon, France

Abstract— The requirements of mobile communication devices are today invariably associated with the miniaturization of microwave components. The development of Yttrium iron garnet (YIG) is of great interest to miniaturize these devices. The present work deals with the integration of YIG ferrite sputtered films of 10 µm thick for coplanar circulators, working at frequencies near 10 GHz. A small circulator with a coplanar structure is designed and analysed using a three dimensional finite element method. Aimed at this objective, we work on the development of a miniature planar circulator/isolator. The circulator is designed with coplanar waveguides. The structure is analysed by using a three dimensional finite-element method. The circulator is then fabricated, and its properties in the microwave range are characterised using a network analyzer and a probing system. A circulation is obtained around 10 GHz, the measured insertion loss and isolation giving interesting perspectives for the device.

Study of High Frequency Input Interference for Buck Converter

Mao Zhang[1], **Weiping Zhang**[2], **and Zheng Zhang**[2]

[1]School of Computing, Engineering and Physical Sciences, University of Central Lancashire, UK
[2]North China University of Technology, Shijingshang District, Beijing, China

Abstract— By applying the ideal analog signal sampling-recovery model, the high frequency input noise of Buck converter has been analyzed and a new type of noise, called as beat frequency noise, has been first revealed in this paper. The main contributions are as the followings: (1) Due to the switch network in Buck converter operates like a sampler, some high frequency noise can be shifted to the lower frequency — Beat frequency, which could not filter out by original LPF in Buck converter; (2) A more accurate model has been proposed to predict the output beat frequency noise; (3) A novel method to reduce the beat frequency noise has been put forward by adding a new pre-filter in the input port of Buck converter; (4) A useful designing theory and approach of the pre-filter has been investigated.

In this paper, we employ the ideal analog signal sampling-recovery model to analyze the input high frequency noise of Buck converter (DC/DC) and some following valuable conclusions have been arrived:

(1) If $|\omega_s - \omega_N| < \omega_c$, where ω_s, ω_N and ω_c repress switching frequency and noise signal frequency as well as the cutoff frequency of LPF respectively, there exist beat frequency noises which can not be eliminated by the original LPF in Buck converter.

(2) The beat frequency noise can be accurately predicted by the formula derived in this paper.

(3) A best way of reducing the beat frequency noise is to add a low pass or band pass pre-filter between the input voltage source and the input port of Buck converter.

(4) Butterworth filter has been chosen to implement the ideal low pass pre-filter and the relationship of the noise frequency, switch frequency, cut-off frequency of the original LPF as well as the cut off frequency of pre-filter has been illustrated to make one to easily select a reasonable pre-filter cutoff filter.

(5) According the designing approach and procedure given out in this paper, the parameters of pre-filter can be easily calculated.

By the way, the analyzing methods and conclusions can be easily extended to investigate the other kind of converter although we only apply Buck converter as an example.

A Novel Approach for Changing Bandwidth of FSS Filter Using Gradual Circumferential Variation of Loaded Elements

S. M. Choudhury, **M. A. Zaman**, **M. Gaffar**, **and M. A. Matin**
Bangladesh University of Engineering and Technology, Dhaka, Bangladesh

Abstract— A novel approach for varying bandwidth of Frequency Selective Surface (FSS) microwave filters has been discussed. The filter studied was a four-legged-loaded element FSS filter. The center-frequency of such filters depends on the circumference of the four-legged-loaded element of the unit cell; the wavelength corresponding to the center frequency is equal to the circumference of the loaded element. So the center frequency can be changed by varying circumference. But since the center-frequency is inversely proportional to the wavelength, the variation to the circumference will change linearly with the center frequency. Since each of the filters with a particular center frequency will allow a certain frequency range to pass, the parallel combination of these filters will result a wider bandwidth. The unit cell of a conventional loaded element FSS filter contains only a single loaded element. The novel approach requires the unit cell to contain multiple loaded elements. The circumferences of the loaded elements of the unit cell are altered utilizing a factor named *circumferential variability*; d. Unit cells consisting of 2×2 and 3×3 four-legged-loaded elements are studied. The unit cell of the 2×2 filter consists of four four-legged-loaded elements, and their circumference are scaled with factors: $1 + d$, $1 - d$, $1 + 3d$, $1 - 3d$ respectively. The unit cell of the 3×3 filter consists of 9 four-legged loaded elements and the circumferences are scaled with factors $1 - 3d$, $1 + 4d$, $1 - 2d$, $1 - d$, 1, $1 + d$, $1 + 2d$, $1 - 4d$ and $1 + 3d$. The conventional loaded-element filter thus corresponds to $d = 0$. The reflection coefficient of the filter has been simulated for different values of d with the help of parametric sweep. The simulation results show that the bandwidth can be appreciably varied by changing the value of d. For the simulated 2×2 filter with center frequency at 14 GHz, the bandwidth could be changed from 2.668–4.548 GHz by changing the value of d from 0.015–0.04. For the simulated 3×3 filter, which also had center frequency at 14 GHz, the bandwidth could be changed gradually from 1.886–2.931 GHz by changing the value of d from 0.011–0.02. The 2×2 filter gives wider bandwidth compared to the 3×3 filter. The 3×3, at small values of d, gives smaller bandwidth compared to the single four-legged loaded element FSS filter. This novel technique of creating filters with wider bandwidth gives designers the flexibility to choose a particular bandwidth, specific to the application of the microwave filter.

A Compact Substrate Integrated Waveguide Band-pass Filter

Changjun Liu and Kama Huang
School of Electronics and Information Engineering, Sichuan University, Chengdu 610064, China

Abstract— A substrate integrated waveguide (SIW) filter with compact size compared to traditional SIW filters are presented in this work. A band-pass filter for general purpose is designed at 5.8 GHz with relative bandwidths of 5%. The fabricated filter is on F4B-2 substrate and about $0.5\lambda g$ by $1\lambda g$, which is about 50% of a conventional SIW dual-mode band-pass filter. Simulation and measurements agree well over a frequency band of 3–10 GHz. The empirical design formulae are presented as well.

CAD of Resonant Circular Iris Waveguide Filter with Dielectric Filled Cavities

Uma Balaji
Electrical Engineering Technology, Farmingdale State College, Farmingdale, NY 11735, USA

Abstract— Resonant Iris bandpass filters form compact structures. These filters are composed of circular or rectangular irises formed as a junction between two rectangular or circular waveguides. Closed form solutions for the susceptance of rectangular and circular apertures in transverse plane of circular waveguide are available in literature. Based on these solutions and relevant theory such filters are designed. Mode matching method is an elegant tool to analyze discontinuity present in this filter. By using generalized scattering matrix method all the discontinuities that compose the filter can be cascaded and hence its performance is obtained. The design based on equivalent network theory approach may yield filters whose performance may not meet specifications very well. Based on the analysis from MMM the filter can further be optimized to meet specifications more precisely. Computer aided design based on MMM of circular resonant iris filters in circular waveguide is available in literature. The present work is to further compact the structures by using dielectric material in the coupled cavities. The radius of the circular cavities is reduced as dielectric material has been used in the cavities.

The analysis of any discontinuity using MMM involves the following steps. The fields on both sides of the discontinuity are expanded in terms of a series of modes of incident and reflected waves. The magnitude of power carried by each of the modes is set to unity. The continuity conditions for the tangential components of electric and magnetic fields are imposed. Using the principle of orthogonality of modes, the equations of continuity conditions are transformed into matrices relating the expansion coefficients of incident and reflected waves at the discontinuity. The matrices are rearranged and inverted suitably to obtain the generalized scattering matrix which describes the discontinuity in terms of the dominant and higher order modes. Theoretically the generalized scattering matrix is of infinite dimension corresponding to the infinite number of modes. The matrix is truncated to a finite size for numerical computations after testing the convergence of the S-parameters. While analyzing a discontinuity from larger to smaller circular waveguide (placed with axes along z-axis) for dominant mode TE_{11} excitation it is sufficient to consider only TE_{1m} and TM_{1m} modes, where m is an integer, alone to be excited at such a discontinuity due to rotational symmetry.

A program based on MMM was developed to analyze the discontinuity from larger circular waveguide to smaller one was developed. It was observed that inclusion of a maximum of 40 TE and TM modes in the analysis was sufficient for the convergence of S-parameters. This analysis was extended to incorporate the dielectric material in the cavities of the filter. A filter has been designed and analyzed using MMM and further optimized. The performance filter in for a bandwidth of 200 MHz in X band has been found to have good selectivity.

On-chip Impedance-optimized Microstrip Transmission Line for Multi-band and Ultra-wide-band Microwave Applications

Wayne Woods[1], **Guoan Wang**[1], **Hanyi Ding**[1], **and Shurong Dong**[2]

[1]IBM Microelectronics, USA
[2]Zhejiang University, China

Abstract— This paper presents a novel on-chip passive device that provides a more constant characteristic impedance over a wide frequency band from compared to conventional microstrip transmission lines. This device is designed for applications whose frequencies span the range of the microwave frequency region from 1 GHz to 30 GHz up to the millimeter-wave (MMW) frequency bands greater than 30 GHz. The novel, impedance-optimized, microstrip transmission line presented is well suited to reduce the effects of characteristic impedance mismatch in high-performance on-chip analog circuits where it is desirable for the transmission line characteristic impedance to remain relatively constant in all operating frequency bands. This new device utilizes the frequency-dependent nature of silicon substrate capacitance to reduce variation in transmission line characteristic impedance with frequency. Using specially designed metal-to-silicon substrate capacitance structures designed in "windows" that perforate a bottom grounded microstrip return line provide additional capacitance to the signal path at lower frequencies which compensates for the higher DC inductance of the thick metal signal lines at low frequencies caused by the resistance/inductance skin-effect. The proposed structure is ideal for multi-band and ultra-wide band applications, for example, analog circuits that operate in both the WCDMA range (2.11–2.17 GHz) and also in the MMW range ($f > 30$ GHz). An impedance-optimized transmission line is designed and studied in a 130 nm BiCMOS technology. The proposed device exhibits significantly improved characteristic impedance behavior versus frequency compared to conventional microstrip lines and can be implemented in any silicon-based analog technology.

Wideband, High-linearity Low-noise Amplifier Design in Sub-micrometer CMOS Technology

Mousa M. Othman, **Shuhei Amakawa**, **Noboru Ishihara**, **and Kazuya Masu**
Integrated Research Institute, Tokyo Institute of Technology, Japan

Abstract—

Background: Recently, radios for multistandard applications have been emerging, ultimately striving toward cognitive radio solutions. The wideband low-noise amplifier (LNA) is a critical circuit in the implementation of such systems. CMOS, which is the dominant technology in today's IC industry, is susceptible to scaling down, and so new circuit design techniques are needed with each technology node especially for the analog/RF circuit design.

Problems in Wideband CMOS LNA: Shunt-shunt negative feedback shown in Fig. 1(a) has appealing features in the implementation of wideband LNA, where besides the bandwidth widening and input/output matching, sufficient noise performance can be achieved along with small chip area. However, the circuit suffers from poor linearity performance due to the active feedback through the transistor M3.

Linearity Enhancement: To enhance the linearity, harmonic cancelling techniques have been studied. MOS transistors produce second-order harmonic signals. Third-order harmonic signals are produced by MOS transistor mixing operation of fundamental input and second-order harmonic signals. Therefore, a circuit technique for reducing the second-order harmonic in the feedback loop has been clarified. M4 in Fig. 1(b) is used to subtract the second-order harmonic at node X. To efficiently generate second-order harmonic from the fundamental signal output of M1, M4 has a long gate length and exhibits the long-channel "square law" behavior.

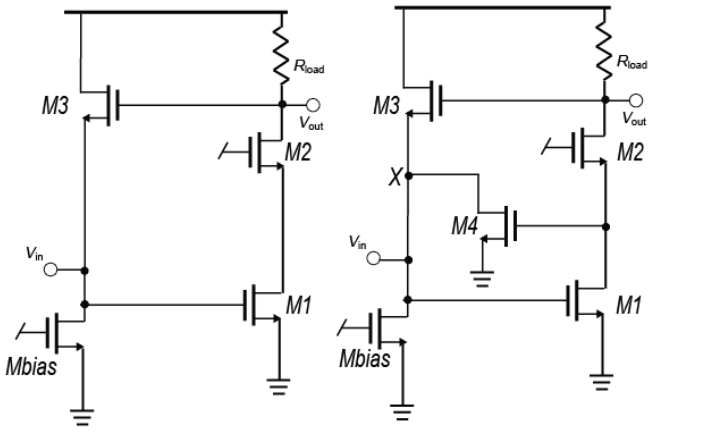

Figure 1: Circuit schematics.

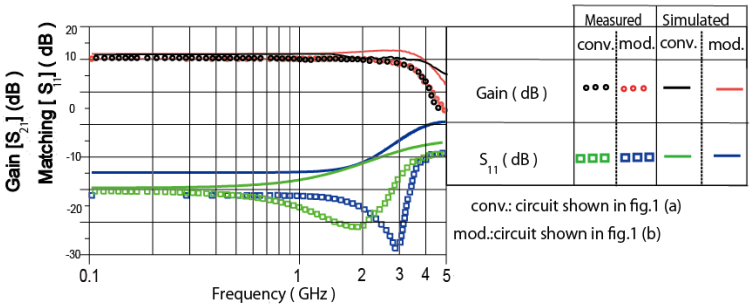

Figure 2: Frequency response.

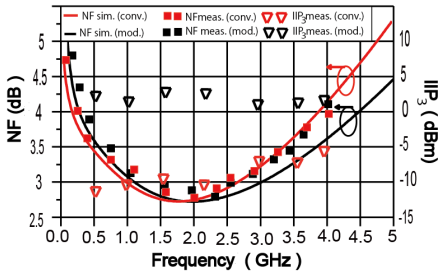

Figure 3: NF and expected IIP3.

Results of LNA Chip Fabrications: To examine the validity of the proposed technique, two LNAs were designed and fabricated by using TSMC 0.18 m CMOS technology. The expected input third-order intercept point (IIP3) estimated from single-tone measurement for both LNAs is shown in Fig. 3. An average IIP3 improvement of +8 dB is expected. Minimum noise figure of 2.8 dB was achieved at 2 GHz in the proposed circuit. 3 dB down bandwidth is about 3.7 GHz. Each of the fabricated LNAs consumes a current of 7.8 mA from 1.8 V power supply and occupies 0.007 mm^2.

Microstrip Resonator as a Measuring Device for a Single Molecule Magnet

Thomas Fan[1], **Vladimir I. Tsifrinovich**[1], **and Andrew D. Kent**[2]

[1]Department of Physics, Polytechnic Institute of NYU, 6 Metrotech Center, Brooklyn, NY 11201, USA
[2]Department of Physics, New York University, 4 Washington Square Place, New York, NY 10003, USA

Abstract— A single molecule magnet (SMM) could be used as a qubit in quantum information processing. In this work, we suggested a method for the measurement of the SMM state with a microstrip resonator. In our method the frequency of the electron spin resonance adiabatically approaches to the fundamental frequency of the microstrip resonator. The shift of the resonator frequency is maximal near the crossing point. This shift depends on the initial state of the SMM and can be used for the measurement of the initial state. We have used the classical approach for description of the SMM dynamics and the interaction between the microstrip and SMM. We have obtained an analytical expression for the resonator frequency shift at the crossing point and performed numerical analysis in the vicinity of the crossing point.

Modified Design of Branch-line Coupler for Harmonic Suppression

Jong-Sung Kim[1] **and Ki-Bok Kong**[2]

[1]Dep. Multimedia Engn., Kyungsung University, Pusan 608736, South Korea
[2]Informat. & Commun. University, Taejon, South Korea

Abstract— This paper presents the modified design that can reject the nth harmonic signals in the branch-line coupler. After modifying quarter-wavelength lines of the traditional design, a solution of the proposed branch-line coupler can be determined by network equivalence.

The branch-line coupler splits an input signal into two output ports with 90° phase difference at an operating frequency and its odd harmonics. It can also perform a division within arbitrary restrictions, i.e., port mismatches and incomplete isolation, at its even harmonics. The key concept in the modified design for harmonic suppression is to substitute the conventional quarter-wavelength branch lines with center-tapped sections as shown in Fig. 1, where Z_a, Z_b, θ_a and θ_b represent the characteristic impedances and the electrical lengths of the series and shunt open-stub sections. Since the proposed structure is intended to be equivalent to a quarter-wavelength transmission line ($Z_c = Z_0$ or $Z_0/\sqrt{2}$), the ABCD matrix of the structure should be equal to that of a conventional $\lambda/4$ line, so leading to two equations as follows,

$$\frac{Z_b}{Z_a} = \frac{\tan\theta_b \tan 2\theta_a}{2} \quad \text{and} \quad Z_a = \frac{Z_c}{\tan\theta_a}. \tag{1}$$

For the purpose of harmonic suppression, the electrical length of the open stub should be fixed to $\theta_b = \pi/(2n)$ by the desired harmonics to be rejected. Fig. 2 shows the variations of Z_a and Z_b versus the electrical length of the series section (θ_a) for three suppression cases (2nd, 3rd, and 2nd & 3rd). Note that Z_a is independent of the harmonic terms suppressed, so capable of simultaneously rejecting two terms (for example, 2nd and 3rd terms) by more adding an open stub in Fig. 1, in which $\tan\theta_b$ should be replaced with $\tan\theta_{b1} + \tan\theta_{b2}$ in (1) due to the addition of rejection term. As a numerical verification using ADS circuit design, the S-parameters for

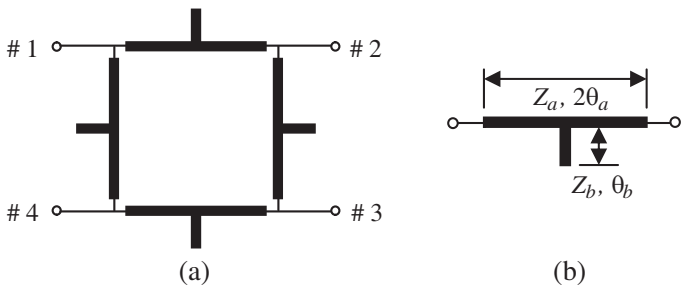

Figure 1: (a) The proposed branch-line coupler, (b) the proposed T-shaped line equal to quarter-wavelength lines.

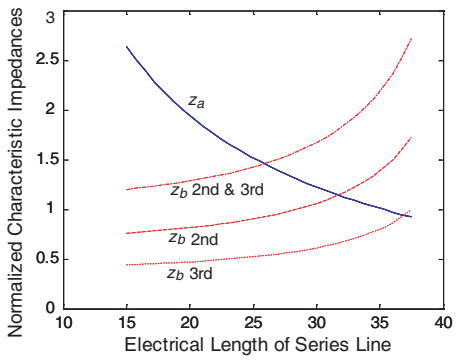

Figure 2: Characteristic impedances versus an electrical length (θ_a).

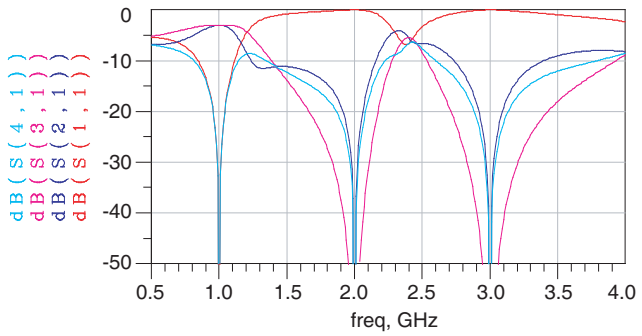

Figure 3: S-parameters of the modified branch-line coupler for 2nd and 3rd harmonic suppression.

2nd and 3rd harmonic suppression are shown in Fig. 3. For vertical quarter-wavelength lines ($Z_c = Z_0$), Z_a is 86.6 Ω for $\theta_a = \pi/6$ chosen and Z_b are 118.3 Ω for two open stubs ($\theta_b = \pi/4$ and $\pi/4$) from the above equations. The characteristic impedances of the horizontal lines can be reduced from multiplying 0.707 times those of the vertical lines ($Z_c = Z_0/\sqrt{2}$). It is observed that the proposed design can produce the function of the conventional coupler at 1.0 GHz and suppress its harmonic terms at 2.0 and 3.0 GHz.

We will explain the proposed design in detail, implement it and discuss our results.

Session 4P5a
Extended/Unconventional Electromagnetic Theory, EHD (Electro-hydrodynamics)/EMHD (Electro-magneto-hydrodynamics), and Electro-biology 2

On Motional Emf

Anamitra Palit
Motijheel Housing Cooperative Society, P-154 Motijheel Avenue, Flat C4, Kolkata 700074, India

Abstract— Motional-Emf is a well discussed topic in elementary courses on electromagnetism. A conductor moving transversely in a magnetic field which is perpendicular to its length and also to the direction of its motion develops an emf along its length. We may call this the axial emf. Interestingly we could deduce the existence of an emf existing along the direction of motion of the conductor a fact that is not highlighted in texts in relation to the topic of motional emf. When the axial emf is being developed a transient current flows between the ends of the conductor and this should be deflected by the existing magnetic field. This should create another emf which is perpendicular with respect to the axial emf. We may call this the transverse emf. Apart from this we have another interesting issue to explore. If investigations are being carried out from the moving frame for example by a person sitting in the aircraft, the magnetic force on the electron as calculated from the Lorentz force formula is zero since the average velocity of the electron as observed from the moving frame is zero. Of course from the ground frame the velocity of the electron is equal to the velocity of the aircraft or the velocity of the moving conductor for that matter. Though the magnetic force on the electron as observed from the moving frame is zero the electric force is not zero. This is due to the effect of relativistic transformations. The above mentioned ideas have been rigorously investigated in this article.

Electromagnetic Sources and Observers in Motion III — Derivation and Solution of the Electromagnetic Motional Wave Equation

S. E. Wright
ECASS Technologies Ltd., Moor Lane Laboratory, Kirkburton, Huddersfield, HD8 0QS, UK

Abstract— The considerable evidence for the existence of the propagation medium (ether) for the transmission of light (EM waves), and the fact that Einstein's relativity appears not to be supported by causality and the medium based Lorentz transform, has motivated the development of the electromagnetic (EM) motional wave equation, based on the propagation medium. Einstein believed that there was no medium, he considered that there was an unidentified mechanism that allowed light to cross space. He therefore developed his special relativity (SR) based on no medium. However, it appears that SR without a propagation medium cannot be based on the solution of the wave equation. Without the medium's reference or means to transmit light, SR appears unable to predict an ordered sequence of observed events (time). It is therefore considered to be irrational (non-causal), creating the absurdity that the observed event could occur before the source event. Thus time travel, where the future can be observed/engaged in before it occurs, appears untenable. For over a century it has been assumed that the medium did not exist, preventing the derivation and solution of the EM motional wave equation relative to its medium.

The existence of the propagation medium [1] and the lack of credibility of Einstein's relativity [2] have been considered in the Xi'an Conference. In this third paper the derivation, solution and properties of the electromagnetic (EM) motional wave equation are derived. To predict events, according to cause and effect, the classical wave equation should be derived and solved with respect to its propagation medium. This applies whether it's vibrations in structures or sound propagation in the air. Similarly, in predicting observed events, the electromagnetic wave equation should be derived relative to its propagation medium. The only difference between EM and classical solutions, is that time and space contract through motion. In the development of the EM wave equation, its derivation and solution is treated as two separable motional transforms. A general Galilean solution for sources and observers moving relative to a propagation medium is applied to the medium based Maxwell equations. The kinematic effect of moving systems is included through the Lorentz contraction of time and space in the moving frame relative to the medium. This new motional wave theory, an extension of Lorentz's medium based theory, describes observations of systems in motion. This is unlike Einstein's special relativity, which is capable of describing only relative motion between moving objects, not the *observations* of individual motions relative to the propagation medium. The new theory gives the observed source events for source and observer flight paths through the universe, for arbitrary motion relative to the medium.

The solution results in three time scales; the source and observer time compared to the time in the stationary propagation medium. Therefore, time is an observed effect, relying on waves passing through the medium, between the source and observer. Solving the motional wave equation with respect to the medium establishes causality, a definite direction of time, future and past. Time can be quickened, slowed and reversed, according to the speed and direction of the source and observer relative to the medium. The new medium based theory distinguishes clearly between source and observer motion, and between stationary and constantly moving systems, which special relativity cannot do. It predicts the complete radiation, propagation and reception processes of systems in motion, removing ambiguity and paradox in Einstein's SR. Restoring the medium forbids material time travel, allowing causally only *visual* time travel to the past. However, effective speeds greater than the speed of light are possible across hybrid reference frames, without exceeding light speed in the propagation medium. This allows distant galaxies to be reached in a fraction of the time normally associated with space travel. However, this is not a form of time travel; it is just ageing less and getting there quicker.

REFERENCES

1. Wright, S. E., "Electromagnetic sources and observers in motion I — Evidence supporting the EM propagation medium for the transmission of light," *PIERS Proceedings*, 71–76, Xi'an, China, March 22–26, 2010.
2. Wright, S. E., 'Electromagnetic sources and observers in motion II — Einstein's Ether-less relativity versus Lorentz's medium based theory," *PIERS Proceedings*, 77–81, Xi'an, China, March 22–26, 2010.

Electromagnetic Sources and Observers in Motion IV — The Nature of Gravity and Its Effect on the Propagation Medium

S. E. Wright
ECASS Technologies Ltd., Moor Lane Laboratory, Kirkburton, Huddersfield, HD8 0QS, UK

Abstract— The evidence for the propagation medium (ether) for the transmission of electromagnetic (EM) waves (light) has been considered [1]. It appears that Einstein's ether-less special relativity (SR) is not supported by the medium based Lorentz transform [2]. The motional wave equation for source and observer motion relative to the medium has been developed [3]. This paper IV investigates the effect of gravity, based on the propagation medium. The medium provides a link between the Lorentz transform, accelerating systems and gravity. They all appear to be connected with expansion or compression of space and time, either through motion relative to, or gravitational compression of the propagation medium. In the presence of a gravitational field the medium compresses in the direction of the field. Here space contracts and time slows, bending a light ray perpendicular to the field, in the direction of the field. If now an observer frame is accelerated in the direction of the field, again time slows and space compresses at the observer. However, this makes the stationary medium appear to expand relatively, and its time quicken, making the light ray appear to bend away from the direction of motion, in the moving observer frame. Thus, gravity compresses the stationary medium and observer motion effectively expands it.

Therefore, gravity can be made to decrease (time quickened), disappear (time neutralized, normal ageing) or be reversed (time advanced, ageing faster, relatively), through observer motion. This is the physical explanation of the Equivalence Principle based here on the propagation medium. The principle depends on distinguishing clearly between source and observer motion relative to the propagation medium, which special relativity cannot do. It is not that gravity attracts light; it is the medium through which the light travels that is compressed. If there was no medium there could be no gravitational medium compression or accelerating frame expansion of the medium. Newton claimed that accelerative motion was with respect to absolute space. Mach claimed that it was with respect to the distant matter of the universe. It appears that they were both right, Newton's claim of absolute acceleration, can be now confirmed, and extended to all forms of motion, including constant motion with respect to the medium and its residual gravity field from the total matter of the universe. This enables absolute motion, to be measured relative to free space and the medium at rest with in it.

The paper considers the nature of gravity where it recognises the finite structures of atoms and molecules and how they generate finite fields, avoiding singularities in their field equations. How gravity appears to be a residual difference, comb like alternate polarity, electrical field from dissimilar charges within these distributed atomic structures. This field then appears to provide a link between the electric field, large scales of gravity and the small scales of atomic structures. These fields attract similar alternate polarity fields, explaining why gravitational matter always attracts itself. Also distinction is made between binding mass, corresponding to the energy required in constructing the atomic structures, and gravitational matter, composed of complete atoms and molecules, capable of generating atomic residual difference fields (gravity) (ARDF). It therefore appears possible to have mass without gravity. It also appears that the propagation medium is attracted by these local gravitational fields, surrounding and moving with gravitational bodies. The total gravitational field, from all matter in the universe, then appears to create a net zero field intensity but a finite scalar universal gravitational reference field (UGRF). This field potential appears to contribute to dark energy, provide an absolute reference for the medium at rest in space and create the inertia for mass in motion.

REFERENCES

1. Wright, S. E., "Electromagnetic sources and observers in motion I — Evidence supporting the EM propagation medium for the transmission of light," *PIERS Proceedings*, submitted, Xi'an, 2010.
2. Wright, S. E., "Electromagnetic sources and observers in motion II — Einstein's Ether-less relativity versus Lorentz's medium based theory," *PIERS Proceedings*, submitted, Xi'an, 2010.
3. Wright, S. E., "Electromagnetic sources and observers in motion III — Derivation and solution of the electromagnetic motional wave equation," *PIERS Proceedings*, submitted, Xi'an, 2010.

Recent Advances on Interior Permanent Magnet Motor Drives for Hybrid Electric Vehicles

M. A. Rahman
Faculty of Engineering and Applied Science, Memorial University of Newfoundland
St. John's, Newfoundland A1B 3X5, Canada

Abstract— Past thirty years have been an exciting period with tremendous advances in the development of interior permanent magnet (IPM) electrical machines. Over the course of this period, permanent magnets consisting of hard neodymium iron boron (NdFeB) materials have been widely used in synchronous machines. The interior permanent magnet (IPM) machines, in which NdFeB materials are inserted in the rotor having different magnet orientations, have expanded their presence in specialized niche automotive markets for modern energy-efficient electric traction drives for the latest generation of hybrid-electric vehicles (HEV),namely Toyota Prius for ground transportation. Power ratings of available IPM traction motors and self-charging IPM generators for charging the storage batteries have dramatically increased by approximately few orders of magnitude during the last dozen years. Closer examination reveals that several different power electronics-based technological advancements and market forces have combined, sometimes in fortuitous ways, to accelerate the development of the impressive IPM synchronous motor drives technology. The purpose of this paper is to provide a broad explanation of the various factors that lead to the current state-of-the-art IPM technology, and to illustrate its application success in the automotive industry and future electric locomotives for mass transportation.

Matrix Converter Induction Motor Drive Employing Direct Torque Control Method

J. Lettl and D. Kuzmanovic
Faculty of Electrical Engineering, Czech Technical University in Prague, Czech Republic

Abstract— The presented paper deals with Takahashi direct torque control method applied on the matrix converter induction motor drive. Matrix converter belongs to the group of direct AC/AC converters, i.e., converters that transform energy from one AC power system into another one without an intermediate DC link with an energy storage. The absence of the DC link makes the control of the converter much more complex comparing to indirect converters. Instead of the constant DC link voltage the matrix converter generates output voltages by combining three input phase voltages that are not of constant values. Direct torque control is a modern control technology that uses a simple control algorithm. It directly controls motor torque and flux values without using a modulator and without the need of precise output voltage vectors generating like in the case of field oriented control. That makes it a good candidate for the use in drives fed by the matrix converter.

The concept of the matrix converter lies in direct switching of the input phases to the output phases. That is achieved by using a 3×3 matrix of bidirectional switches. Bidirectional switches enable energy flow in both directions. Anti parallel diodes increase the reverse blocking capability of the switches. There are two main tasks that the matrix converter performs in normal operation: a) generating the required output voltages by combining the input phase voltages, b) directing the converter output phase currents into the input phases in such a way to provide the sinusoidal input current with a required power factor (usually 1). Since it is easier to analyze these tasks separately the matrix converter is often observed as a combination of a virtual current source rectifier and a virtual voltage source inverter connected by a virtual DC link. Every switching combination of the virtual rectifier/virtual inverter configuration has a corresponding switching combination of the real matrix converter.

Owing to the "independent" operation of the virtual rectifier and virtual inverter stages, indirect space vector modulation can be applied to the matrix converter. This modulation method enables generation of desired voltage vectors at the output and at the same time generation of the input current vector that rotates at the same speed like the converter input voltage vector and with the constant angle displacement towards it.

A principle of the Direct Torque Control (DTC) is very simple. The estimated torque and flux values are constantly compared to their set points and if they are out of the tolerance bands an adequate switching combination is applied to the converter output that will drive the torque and flux to their set values. There are several types of DTC: Depenbrock DTC, Takahashi DTC, DTC using the space vector modulation, DTC using the discrete space vector modulation, neuro-fuzzy DTC, etc. The Takahashi DTC operates on a six sectors flux vector circle. In each sector four active and two zero voltage vectors are employed in order to keep the torque and flux values within their limits. For example in the first sector voltage vector V_2 will increase torque and flux, V_3 will increase torque but decrease flux, V_5 will decrease torque and flux, and V_6 will decrease torque but increase flux. By applying the zero vector, flux will remain constant ant torque will slowly decrease.

As the first step in application of the Takahashi DTC to an induction motor drive fed by the matrix converter a model in MATLAB Simulink was designed and simulation results of the drive dynamic behaviour were obtained. Finally, the Takahashi DTC was applied to a real system consisting of the matrix converter supplying the 4 poles 6 kW induction machine with 22 Nm rated torque. The gained experimental and simulation results presented in the paper prove that the Takahashi DTC can be successfully applied to the induction machine drive fed by the matrix converter. The torque control achieved with the matrix converter using this type of DTC is comparable to the classical indirect AC/AC converters.

Some Consequences of the Non-constancy of the Speed of Light in Vacuum for Different Galilean Reference Systems

Namik Yener
Technology Faculty, Umuttepe Campus, Kocaeli University, Izmit, Kocaeli 41380, Turkey

Abstract— Having established in previous articles that the principle of the constancy of speed of light of Special Relativity Theory is false in general, we examine some consequences of the non-constancy of speed of light in vacuum for different Galilean reference systems. We consider the modified Lorentz transformation incorporating different speeds of light for different inertial frames and which is a result of the non-constancy of speed of light in vacuum for different Galilean reference systems, i.e. reference systems in uniform rectilinear motion with respect to each other. Some consequences of this transform including the limit speed concept, transformation of lengths, summation and transformation of velocities are considered. Results of the transformation of the electromagnetic field are given. Also discussed are some consequences of the relativity of the electromagnetic field, all under the modified Lorentz transformation. These include variance of the electric charge, transformation of the potentials, transformation of the force.

Some of the highlights of these consequences are as follows. The transformation of lengths abide by the same rule as in Special Relativity Theory, at least in form. Transformation of time intervals and velocities now involve the speeds of light in vacuum for both inertial frames in distinction from Special Relativity Theory. The invariance of charge no longer applies and charge measured depends on the reference frame the measurement is made from. Force acting on a charge q in an external electromagnetic field has the same form as in Special Relativity Theory, but now because charge is no longer invariant, the force transformation also has to be modified accordingly.

Session 4P5b
Propagation of Millimetre and Sub-millimetre Waves

New Approach to Modeling of Diffuse Reflection and Scattering for Millimeter-wave Systems in Indoor Scenarios

L. Subrt, P. Pechac, and S. Zvanovec
Department of Electromagnetic Field, Czech Technical University in Prague, Czech Republic

Abstract—

Introduction: At present, users of modern mobile radio communications systems request higher and higher data rates available for their applications. One possible way to achieve high network capacity is to use large bandwidth and therefore to situate systems into millimeter-wave band. For future applications, the indoor high-speed systems working at the frequencies about 60 GHz are supposed [1]. Different approach need to be utilized for electromagnetic wave propagation predictions in millimeter band [1, 2] when compared with lower frequencies up to 10 GHz (present personal wireless communications systems).

At the very high frequencies, dimensions of common obstacles (e.g., furniture) in indoor scenarios are comparable or even smaller than the wavelength and therefore the obstacles which are normally neglected need to be taken into account [3]. Very high level of free space loss and strong attenuation caused by walls usually limits the size of the area covered by a transmitter to a single room. On the other hand, this feature helps to avoid interference among more transmitters in a building. The last significant feature of propagation within millimeter band is that the surface roughness has a substantial effect on the impinging wave. The roughness of common surfaces is not negligible in comparison with the wavelength of the impinging wave, i.e., the wave is scattered much more than at lower frequencies. The main motivation for this work arose from the above mentioned propagation issues connected with diffuse reflection and scattering phenomena.

Modeling: Many works implementing different approaches for solving the wave-obstacle interaction were published. Some of them uses principle of Gaussian beams [4] or classical ray-tracing techniques [5].

We have proposed a new 3D semi-deterministic model based on the modified ray-launching technique and stochastic approach. The model, in contrast to most of classical deterministic models, can consider all significant phenomena (reflection, absorption, penetration and scattering) using fast and simple algorithms (by implementing so called Probability radiation pattern — PRP — see in Fig. 1(b) and therefore complex and time-consuming calculations can be avoided. Classical information about obstacles (material constants, surface roughness and width) which are usually unknown is replaced by only three probabilistic parameters. The parameters are calibrated by measurements [6] Fig. 1(a) and their representing values have a direct connection with the physical reality. Furthermore, the model is able to predict both narrowband and wideband channel parameters.

The paper will focus on the simulations of wireless communication system working within a room inside a building at 60 GHz. The influence of position of the transmitter, receiver and obstacles as well as surface roughness on the channel parameters will be examined. The signal coverage, impulse response and angle of arrival predictions will be compared to each other and dominant paths between transmitter and receiver will be determined (since multipath behavior of the channel is expected).

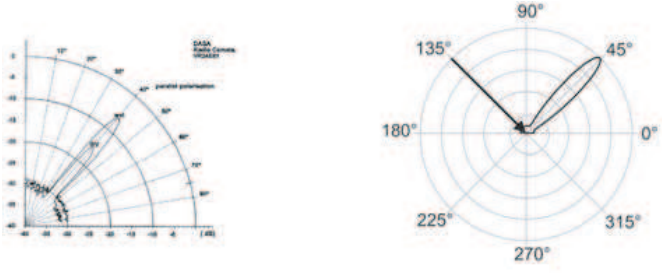

(a) (b)

Figure 1: Measured scattering profile [6] and example of its representation by PRP method.

REFERENCES

1. Smulders, P. F. M. and L. M. Correia, "Characterisation of propagation in 60 GHz radio channels," *Electronics & Communication Engineering Journal*, Vol. 9, 73–80, 1997.
2. Suiyan, G., J. Kivinen, Z. Xiongwen, and P. Vainikainen, "Millimeter-wave propagation channel characterization for short-range wireless communications," *IEEE Transactions on Vehicular Technology*, Vol. 58, 3–13, 2009.
3. Collonge, S., G. Zaharia, and G. El Zein, "Influence of the furniture on 60 GHz radio propagation in a residential environment," *International Symposium on Signals, Circuits and Systems, SCS*, 413–416, Vol. 2, 2003.
4. Fluerasu, A. and C. Letrou, "Gaussian beam based simulations of indoor radio propagation channels," *IEEE Antennas and Propagation Society International Symposium*, Vol. 2, 102–105, 2003.
5. Piesiewicz, R., T. Kleine-Ostmann, N. Krumbholz, D. Mittleman, M. Koch, J. Schoebel, and T. Kurner, "Short-range ultra-broadband terahertz communications: Concepts and perspectives," *IEEE Antennas and Propagation Magazine*, Vol. 49, 24–39, 2007.
6. Langen, B., G. Lober, and W. Herzig, "Reflection and transmission behaviour of building materials at 60 GHz," *5th IEEE International Symposium on Personal, Indoor and Mobile Radio Communications, Wireless Networks — Catching the Mobile Future*, Vol. 2, 505–509, 1994.

A Measurement System for Propagation Measurements at 300 GHz

S. Priebe[1,3], **C. Jastrow**[2,3], **M. Jacob**[1,3], **T. Kleine-Ostmann**[2,3], **T. Schrader**[2,3], **and T. Kürner**[1,3]

[1]Institut für Nachrichtentechnik, TU Braunschweig, Schleinitzstraße 22, 38106 Braunschweig, Germany
[2]Physikalisch-Technische Bundesanstalt, Bundesallee 100, 38116 Braunschweig, Germany
[3]Terahertz Communications Lab (TCL), Braunschweig, Germany

Abstract— The demand for higher data rates in indoor wireless communications is steadily growing. For future systems operating with data rates of tens of Gbps and beyond carrier frequencies above 300 GHz will be envisaged. In the past years the feasibility of wireless communications at 300 GHz has been shown by Terahertz Communications Lab (TCL) using a 300 GHz transmission system. Additionally, propagation measurements based on THz-Time Domain Spectroscopy have been applied successfully to gain insights into basic propagation phenomena like reflection and transmission focussing on the impact of the material parameters. However, in order to be able to derive the complex channel models obligatory for system simulations of a wireless communication system, more detailed measurements in realistic operation environments are required. For that purpose a 300 GHz measurement system has been set up at TCL using the components of the 300 GHz transmission system. The measurement system consists of a R & S ZVA40 Vector Network Analyzer and external 300 GHz transmitter (T_x) and receiver (R_x) front ends. The core component of both T_x and R_x is a subharmonic schottky diode mixer. In this paper the capabilities of the measurement system are characterized and results from first propagation measurements will be shown. The focus will be on measurements of a set-up corresponding to the application for THz communication systems for wireless interconnection of different electronic devices operated on a desktop.

An Evaluation of Approaches for Modeling of Terrestrial, HAP and Satellite Systems Performance during Rain Events

S. Zvanovec, L. Subrt, and P. Pechac
Department of Electromagnetic Field, Czech Technical University in Prague, Czech Republic

Abstract— The proper choice of the modeling approaches for electromagnetic wave propagation within the millimeter wave band is crucial. This is particularly due to the high cost of millimeter wave equipments associated with transmitting power. Considerably high attenuation can be caused by interaction of transmitted waves with rain drops. There can be found several approaches to enumeration and compensation of signal fades caused by rain [1, 2]. Investigations of millimeter wave propagation aspects have been conducted out within the frame of European international projects such as CRABS [3] and COST Action 280 [4] and COST Action 297 [5]. Nevertheless, due to the variability of systems' configurations, these models can be used only for investigation of alone terrestrial, satellite or High Altitude Platforms (HAPs) links. For example one of the rain fade mitigating approaches introducing a route diversity [2] (i.e., two joint links to one HAP station from two different ground localities) involves only the parameters given based on the measurements of Earth-space links within particular geographical localities.

The paper brings a comparative study of modeling approaches for propagation of millimeter waves within rain events and their adaption to HAP systems. The rain database from the period of 2002–2005 was utilized including 250 km × 250 km rain scans from Czech meteoradars (rain rate distributions with 1 km grid resolution and 1 minute time steps). Particular results of HAP system simulations performed at the frequency of 48 GHz will be discussed. Two evaluation methods were tested based on simulation results: The first following terrestrial approaches [6] and the second one from the other side utilizing a satellite approach [2].

REFERENCES

1. "Specific attenuation model for rain for use in prediction methods," *International Telecommunications Union, ITU-R Recommendation*, 838.
2. "Propagation data and prediction methods required for the design of Earth-space telecommunication systems," *International Telecommunications Union, ITU-R Recommendation*, 618-8, 2003.
3. "Report from ACTS project 215 — Cellular radio access for broadband services (CRABS)," *Propagation Planning Procedures for LMDS*, 1999.
4. Usman, I. S., M. J. Willis, and R. J. Watson, "Route diversity analysis and modelling for millimetre wave point to multi-point systems," *1st Int. Workshop of COST Action 280*, Jul. 2002.
5. "COST297 — HAPCOS high altitude platforms for communications and other services," [Online], Available: http://www.hapcos.org/.
6. "Propagation data and prediction methods required for the design of terrestrial line-of-sight systems," *International Telecommunications Union, ITU-R Recommendation*, 530-11, 2005.

Gas Absorption Measurement of Selected Stratospheric Substances by Fabry-Perot Resonator

P. Piksa[1], **S. Zvanovec**[1], **P. Cerny**[1], **J. Libich**[1], **J. Varga**[2], **and J. Koubek**[2]
[1]Department of Electromagnetic Field, Czech Technical University in Prague, Czech Republic
[2]Department of Analytical Chemistry, Institute of Chemical Technology, Czech Republic

Abstract— Observations and investigations of gas processes within the ozone layer and interaction of transmitting electromagnetic waves in the stratosphere belong nowadays to main interests of human beings. A Fabry-Perot interferometer provides an interesting tool enabling an enhancement of the sensitivity of the absorption as well as emission measurements in the region of microwave spectroscopy [1]. Measurement in the evacuated resonator allows setting particular molecular concentrations corresponding to the height above ground and adjusting concentration correspondent to the atmosphere layer. For monochromatic radiation, the Fabry-Perot interferometer can be tuned to a resonance at which the constructive interference of the multiple-reflected electromagnetic waves enables to accumulate the radiative energy. Absorption measurements in the Fabry-Perot interferometer (resonator) are then based on the measurement and subsequent evaluation of the quality factors of both the empty as well as the gas filled resonator.

The main advantage of the Fabry-Perot resonator comparing to the other laboratory measurements is its relatively higher sensitivity to weak absorptions due to an apparent lengthening of the optical path length by means of multiple reflections. The effective optical path length corresponding to the measured quality factors (according [2]) varies in our case approximately from 40 up to 83 m from the intense absorption up to the evacuated resonator, respectively. This holds true especially in cases of standing waves, where the losses caused by destructive interference processes are negligible. Therefore a precise measurement of gas attenuation can be reached. The absorption spectra of particular very short-lived (VSL) gases substances from the ozone layer were tested via the Fabry-Perot resonator. Their influences on particular millimeter wave systems, whose links intersect the stratosphere (i.e., High Altitude Platforms, Mobile to Satellite Systems), will be discussed in the paper.

REFERENCES

1. Zvanovec, S., P. Cerny, P. Piksa, T. Korinek, P. Pechac, M. Mazanek, J. Varga, J. Koubek, and S. Urban, "The use of the Fabry-Perot interferometer for high resolution microwave spectroscopy," *Journal of Molecular Spectroscopy*, Vol. 256, No. 1, 141–145, 2009.
2. French, I. P. and T. E. Arnold, "High-Q Fabry-Perot resonator for nitric oxide absorption measurements at 150 GHz," *Review of Scientific Instruments*, Vol. 38, 1604–1607, 1967.

Wave Propagation in Anisotropic Waveguides

Abdullah Eroglu
Department of Engineering, Indiana University — Purdue University, Fort Wayne, IN 46805, USA

Abstract— Waveguides have been widely used in microwave communication systems to transfer electromagnetic energy from one point to another. The operational frequency, amount of power that will be transferred, and losses depend on the structure and dielectric filling that is used in the design of the waveguide.

Anisotropic materials when used as a dielectric filling for waveguides instead of isotropic materials bring several advantages due to difference in the direction of the electric field intensity and electric flux density. Anisotropic materials can be divided into two classes depending on whether the natural mode of operation are linearly polarized or circularly polarized. In the former class, permittivity and permeability tensors are symmetric whereas in the latter class, the tensors are anti-symmetric. Gyrotrotpic materials represent the anisotropic materials with anti-symmetric tensors and uniaxial or biaxial materials represent the anisotropic materials with symmetric tensors. There are several publications [1–3] on the analysis of the wave propagation in anisotropic materials in the literature. However, literature describing their implementations in the design of microwave devices seems to be limited.

In this paper, the performance of a rectangular waveguide with perfectly conducting walls has been investigated using anisotropic materials such uniaxially anisotropic and compared with the performance of the isotropic materials. The optic axis of the unixially anisotropic material is taken to be vertically oriented and is in the direction of the stratification. The analysis has been performed on both negatively and positively uniaxially anisotropic materials with strong and weak anisotropies. The results of this work can be used in military applications where more design control parameters are needed.

REFERENCES

1. Eroglu, A. and J. K. Lee, "Wave propagation and dispersion characteristics for a nonreciprocal electrically gyrotropic medium," *Progress In Electromagnetics Research*, PIER 62, 237–260, 2006.
2. Kong, J. A., *Theory of Electromagnetic Waves*, Wiley, New York, 1975.
3. Adam, J. D., L. E. Davis, G. F. Dionne, E. F. Schloemann, and S. N. Stitzer, "Ferrite devices and materials," *IEEE Trans. Microwave Theory Tech.*, Vol. 50, 721–737, Mar. 2002.
4. Cao, M. and R. Pietig, "Ferrite coupled-line circulator with reduced length," *IEEE Trans. Microwave Theory Tech.*, Vol. 53, No. 8, 2572–2579, Aug. 2005.
5. Erickson, N. R. and R. M. Grossien, "A low-loss 74–110-GHz faraday polarization rotator," *IEEE Trans. Microwave Theory Tech.*, Vol. 55, No. 12, 2495–2501, Dec. 2007.

Session 4P6
Micro-/Nanoscale Metamaterials, Plasmonics and Other Hybrid Structures for Superresolution Imaging, Slow-light and Cloaking

Optical Superresolution Imaging Using a Metallic Nanolens Made Up of Bulk Nanowires Metamaterial

B. D. F. Casse, W. T. Lu, Y. J. Huang, E. Gultepe, L. Menon, and S. Sridhar
Department of Physics and Electronic Materials Research Institute, Northeastern University
Boston, MA 02115, USA

Abstract— We report superresolution imaging of large objects, having sub-λ features, over significant distances ($\gg \lambda$, wavelength) with a resolution well below diffraction limit in optics, using a metallic nanolens. The metallic nanolens is composed of high aspect ratio gold nanowires embedded in disordered porous alumina template matrix. This composite medium possesses strongly anisotropic optical properties with negative permittivity in the nanowire axis direction, which enables negative refraction, and transports both far-field and near-field components with very low distortions and with attenuations of the order of $< 1\,\mathrm{dB/cm}$. The long-distance image transport mechanism is not based on resonances of materials parameters and thus the subwavelength imaging occurs with low loss (Figure-of-merit (FOM) $= \mathrm{Re}(n)/\mathrm{Im}(n) \sim 12$ (much higher than existing metamaterials)) and in a broad spectral range. This nanolens not only exhibits superior optical properties over existing metamaterials-based lenses, but can also be manufactured in large scale (mm size), thereby offering significant potential for applications in optical storage devices, nanolithography and biomedical imaging.

ACKNOWLEDGMENT

This work was financially supported by the Air Force Research Laboratories, Hanscom through grant No. FA8718-06-C-0045 and the National Science Foundation through grant No. PHY-0457002.

Design of Diffractive Optical Elements for Focusing Surface Plasmon Polaritons

E. A. Bezus[1, 2], **L. L. Doskolovich**[1, 2], **and N. L. Kazanskiy**[1, 2]

[1]Image Processing Systems Institute of the Russian Academy of Sciences, Samara 443001, Russia
[2]Technical Cybernetics Department, Samara State Aerospace University, Samara 443001, Russia

Abstract— Electromagnetic modes supported by the interfaces between metal and dielectric media (surface plasmon polaritons, SPP) and by thin metal films (long-range surface plasmon polaritons, LRSPP) have attracted a lot of interest in recent years [1]. It has been shown experimentally that micro- and nanostructures located on the SPP propagation surface can be used to transform and focus SPP [2].

In this work, we design and investigate theoretically the dielectric diffractive optical elements (DOEs) for transforming and focusing SPP and LRSPP. The design of DOEs is based on phase modulation of the SPP (LRSPP) provided by the dielectric block with varying geometric parameters located directly on the interface. The problem of the SPP (LRSPP) diffraction by a dielectric block is solved using the rigorous coupled wave analysis extended to aperiodic structures [3]. It is found that the phase delay of the transmitted SPP (LRSPP) is well described by an analytical expression similar to that for the phase delay of a plane wave transmitted through a homogeneous layer. We show that the modulation can be implemented not only by changing the length of the dielectric block at fixed height, but also by changing the height at fixed length as well as by simultaneous changing of both parameters (Fig. 1(a)).

As an example, we consider the design of various diffractive elements for focusing SPP and LRSPP such as multifocus lenses (Fig. 1(b)) as well as more conventional parabolic and Fresnel lenses. It is demonstrated that combining the height and length modulations allows one to increase the diffraction efficiency by 10–20%.

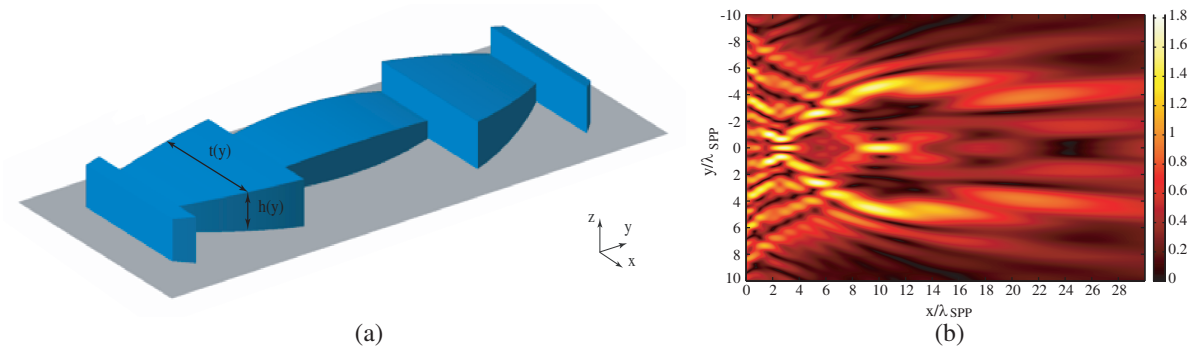

(a) (b)

Figure 1: (a) Dielectric DOE with varying height and length and (b) SPP focused to three focal spots.

ACKNOWLEDGMENT

This work was financially supported by RFBR grants Nos. 09-07-92421 and 09-07-12147, RF Presidential grant No. NSh-3086.2008.9 and Russian-American Basic Research and Higher Education (BRHE) Foundation grant.

REFERENCES

1. Ozbay, E., "Plasmonics: Merging photonics and electronics at nanoscale dimensions," *Science*, Vol. 311, No. 5758, 189–193, 2006.
2. Hohenau, A., et al., "Dielectric optical elements for surface plasmons," *Opt. Lett.*, Vol. 30, No. 8, 893–895, 2005.
3. Silberstein, E., et al., "Use of grating theories in integrated optics," *J. Opt. Soc. Am. A*, Vol. 18, No. 11, 2865–2875, 2001.

Isotropic Non-ideal Cloaks Providing Improved Invisibility

Cheng-Wei Qiu[1, 2] **and Saïd Zouhdi**[2]

[1]Department of Electrical and Computer Engineering, National University of Singapore
4 Engineering Drive 3, Singapore 117576, Singapore
[2]Laboratoire de Genie Electrique de Paris, SUPELEC, Plateau de Moulon 91192, Gif-sur-Yvette, France

Abstract— Mimicking the ideal cloak, which is anisotropic and inhomogeneous, can be achieved by alternating homogeneous isotropic materials, whose permittivity and permeability of each isotropic coating can be determined from effective medium theory. An improved two-fold method based on this classic technique is proposed by suitably discretizing the cloak and re-ordering the combination of the effective parameters of each layer designed from effective medium theory. The roles of impedance matching and index matching are investigated. Smoothing the index profile leads to better invisibility than that obtained by smoothing the impedance profile, since the forward scattering can be further diminished. Nonlinear-transformation-based spherical ideal cloaks are studied, and improved design method is explored together with different segmentation schemes. Significant improvement in invisibility is always observed for the optimal segmentation in virtual space with the proposed two-fold design method no matter how nonlinear the coordinate transformation is.

Transient Electromagnetic Field of an Electric Line Source above a Plane Drude Model Plasmonic Half-space

B. J. Kooij
IRCTR, Delft University of Technology, The Netherlands

Abstract— The enhancement of the electromagnetic field at the surface of a Drude metal is classified as the surface plasmon effect. This surface plasmon effect in a classical Drude model has been investigated extensively in the frequency domain. However, to understand what is actually happening to the electromagnetic field at the near vicinity of a Drude metal a thorough analysis in the space-time domain is needed. Once the space-time domain counterpart of the so called plasmon effect is found, one is able to describe and classify the physical phenomena that are playing a role in the occurence of this effect.

The pulsed electromagnetic radiation from a line source above a plane plasmonic half-space, which is modeled by a classical Drude model, is investigated. The modified Cagniard-de Hoop method is used to derive closed-form expressions for the space-time domain electric and magnetic field anywhere above the plasmonic half-space. In the Cagniard-de Hoop method the Laplace transform with respect to time is used, in which the Laplace parameter s is kept real and positive in order to ensure causality in the space-time domain expressions for the electromagnetic field. The derived space-time domain expressions for the reflected electromagnetic field explicitly show the special time and space dependence that exists in the reflection factor at the interface of the plasmonic half-space. Consequently, leading to a better understanding of the physical effects, that occur at the interface of classical Drude metals in the space-time domain.

Numerical results are presented for the space-time domain electric field for different points of excitation and observation above the plasmonic halfspace, as well as for different values of the plasmonic material parameters.

Two-dimensionally Isotropic Metamaterial

Abdelwaheb Ourir, **Redha Abdeddaim**, **and Julien de Rosny**
Institut Langevin, ESPCI ParisTech, UMR 7587, CNRS, Laboratoire Ondes et Acoustique (LOA)
10 rue Vauquelin 75231 PARIS Cedex 05, France

Abstract— Metamaterials are artificial composites where the anisotropy is specified through the design and orientation of subwavelength inclusions within the unit cell. For that matter, the intrinsically anisotropic properties of the planar magnetic resonators have restricted greatly the practical realization of isotropic LHM. Even so, the realization of an isotropic metamaterial has attracted much attention. In 2001, a two-dimensional isotropic LHM was realized by Shelby et al. [1] using two orthogonal arrays of split-ring resonators and wires. An isotropic 3D LHM was then proposed by Koschny et al. [2] by arranging the SRRs and the wires in a 3D orthogonal lattice. At the same time, Grbic et al. [3] studied an isotropic three-dimensional negative refractive index medium using transmission lines loaded with reactive elements. Nevertheless, these complex inclusions limit the realization of this technology, especially at very high frequency. Besides considerable progresses in the recent last years, the realization of an isotropic metamaterial exhibiting a negative refractive index remains unachieved.

In this work, we propose an original subwavelength unit cell for constructing two-dimensionally isotropic left-handed metamaterial. Numerical analyses were conducted under two different wave incidences in the microwave range. Isotropy and negative refraction in the two incidences are shown. The expected electromagnetic characteristics and the superlensing are verified experimentally.

REFERENCES

1. Shelby, R. A., D. R. Smith, S. C. Nemat-Nasser, and S. Schultz, *Appl. Phys. Lett.*, Vol. 78, 489, 2001.
2. Koschny, T., L. Zhang, and C. M. Soukoulis, *Phys. Rev. B*, Vol. 71, 121103(R), 2005.
3. Grbic, A. and G. V. Eleftheriades, *Journal of Appl. Phys.*, Vol. 98, 043106, 2005.

Slow Light in Plasmonic Metamaterials: The Double-Fano Resonance Approach

G. Shvets, Chih-Hui Wu, and Alexander Khanikaev
Department of Physics, The University of Texas at Austin, Austin, Texas 78712, USA

Abstract— A new approach to slowing light in plasmonic structures is proposed. We utilize the phenomenon of double-Fano resonance. Specific implementations of such structures based on plasmonic antennas are presented, various applications are outlined.

The ability to slow down light to extremely slow group velocities v_g compared with the vacuum light speed c while maintaining high coupling efficiency is one of the most dramatic manifestations of controlled light manipulation in optics. Apart from its fundamental significance, it has long-reaching technological applications, including enhanced nonlinear effects due to the energy density compression by as much as c/v_g; pulse delay and storage for optical information processing, optical switching, and even quantum optics. Most approaches to obtaining slow light rely on the phenomenon of Electromagnetically Induced Transparency (EIT). More recently, in response to the emerging applications, attention has shifted towards obtaining slow light using electromagnetic metamaterials which enable engineering electromagnetic resonances with almost arbitrary frequencies and with resonance symmetries. As will be discussed, the EIT approach to achieving slow light is not without limitations.

In this talk we propose a new technique to producing slow light which relies on the newly-discovered phenomenon of double-Fano resonance. We demonstrate that light propagation through a birefringent medium can be dramatically slowed down when the medium supports three electromagnetic modes: (a) two propagating modes of different polarizations strongly which are both strongly coupled to the incident electromagnetic field, and (b) a "dark" (non-propagating) electromagnetic wave which is decoupled from the incident electromagnetic field. If the frequency of the "dark" mode coincides with that of the propagating modes, then a simple symmetry breaking coupling all three modes with each other results in a dramatic slowing down of light. This phenomenon can be understood as a double Fano resonance: coupling of a single discreet state ("dark" mode) to the two sets of continuum states (two propagating modes of different polarization states). A specific implementation of such slow-light structures using metallic antennas is illustrated in Fig. 1(a). Unusual propagation bands shown in Fig. 1(a) lend themselves to exciting applications which will be discussed. One such application, adiabatic polaprization conversion, is illustrated in Fig. 1(b).

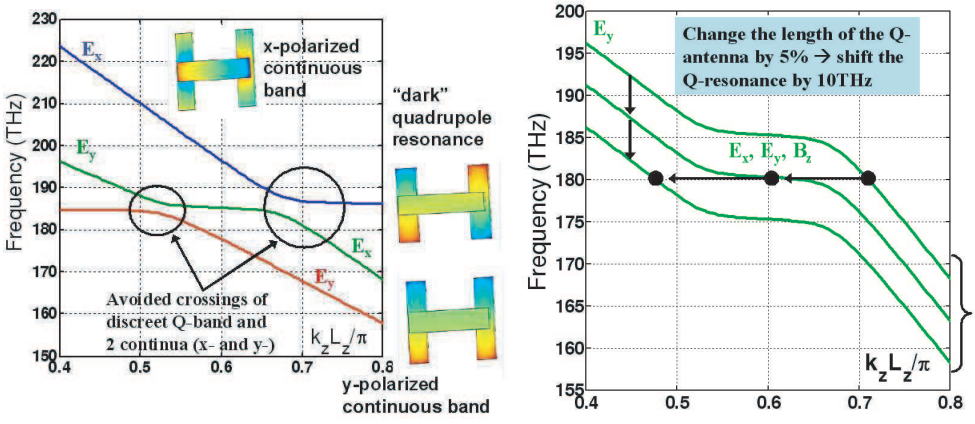

(a) (b)

Figure 1: (a) Schematic of a unit cell of a double-Fano metamaterial consisting of two vertical plasmonic antennas (forming a "dark" quadrupolar antenna) and a horizontal dipole antenna displaced in all three dimensions. Flat portion of the dispersion curve: "slow" light. (b) Conceptual schematic of adiabatic polarization conversion (from x-polarization to y-polarization) accomplished by spatially varying the frequency of the "dark" resonance between 185 THz and 175 THz.

Anti-resonant Transparency with Plasmonic Shells

Andrea Alù[1] **and Nader Engheta**[2]

[1]Department of Electrical and Computer Engineering, The University of Texas at Austin, USA
[2]Department of Electrical and Systems Engineering, University of Pennsylvania, USA

Abstract— Invisibility and cloaking are popular research topics, and various techniques have been put forward to employ exotic materials and metamaterials to reduce the visibility of various objects. Here we explore a different mechanism for achieving transparency, based on the unusual possibility presented by a metamaterial spherical shell with negative permittivity near zero, which may provide identically zero dipolar scattering, independent of its thickness and inner radius. Analyzing the problem in the quasi-static limit, this yields to the paradox of a transparency condition that depends only on the permittivity of the shell and not on its thickness, despite the material being strongly mismatched with the background. Indeed this transparency condition is also independent of the ratio between outer and inner radii of the shell. Analyzing the problem in the time-varying dynamic case, we show that this condition is produced by an anomalous anti-resonance phenomenon arising at the interior shell interface, which induces strong fields in the interior cavity, without necessarily corresponding to strong scattering. Relations and differences with respect to other invisibility and cloaking mechanisms will be discussed. In particular, we will discuss the analogies and potential applications in reference to the recent idea of a cloaked sensing device, capable of extracting a relevant signal from the background, without necessarily producing large scattering. The absence of radiation loss and the possibility to excite an anti-resonant dark mode may also be associated with electromagnetically induced transparency mechanisms and sharp frequency response, of interest for various applications in optics that require high-Q and small bandwidths of operation. We will explore these venues in our talk.

In-plane Quadrupolar Plasmon Resonance in Triangular Metallic Nano-structures

Kin Hung Fung, Pratik Chaturvedi, and Nicholas X. Fang
University of Illinois at Urbana-Champaign, Illinois, USA

Abstract— We study the "in-plane" quadrupolar resonance in triangular metallic nano-structures on top of a substrate. In general, quadrupolar resonance in a metal nanoparticle is very weak compared to dipolar resonance. When metal nanoparticles such as disk, sphere and rod are fabricated on a substrate, the "in-plane" quadrupolar resonance is impossible to be excited by a normal incident plane wave due to their geometrical symmetry (even though "out-of-plane" resonance is possible). Nanotriangle is one of the simplest nanostrucures that can support those "in-plane" quadrupolar resonances due to the broken symmetry. Such properties were observed in experiment and confirmed by numerical simulations recently. However, the physical reason for such observation was rarely discussed. We performed numerical simulations for plane wave incident on various triangular nano-structures (on substrate) that possess the same in-plane symmetry. Both single-particle scattering properties and transmission/reflection spectra through an array of particles were obtained. Near-field profiles show that "in-plane" quadrupolar resonances can be excited. Although equilateral triangle has less geometrical symmetry compared to disk and sphere, there is still no polarization dependence in its extinction cross section due to its three-fold rotational symmetry. We discuss how the broken symmetry leads to the ability of supporting "in-plane" quadrupolar resonance while keeping polarization independence. Although the far-field properties are independent of polarization, including circular polarizations, this is not true for the near-field properties (more related to surface plasmon). Since circular polarization is related to spin angular momentum of photon, we also discuss the possibility of converting the spin angular momentum of photon to higher order orbital angular momentum of plasmon using those triangular structures.

Optical Activity in Organic Metamaterials

N. Wongkasem and C. Kamtongdee
Department of Electrical Engineering, Faculty of Engineering, Khon Kaen University
Khon Kaen 40002, Thailand

Abstract— Parameters which maneuver chirality and optical activity properties in organic metamaterials are investigated. Molecular optical rotation of a four-atom chain molecule and optical rotation constant of artificial organic structures are proposed to regulate in order to control chirality and optical activity. Artificial helix DNA is presented as a case study to monitor optical activity effects in organic metamaterials. Circular polarization effect, electromagnetic parameters and index of refraction are recorded. Once chirality and optical activity can be controlled at molecular level, designed organic metamaterials can be used in electromagnetic applications at high frequencies, up to x-rays regime.

Author Index